Experimental and Kinetic Modeling Studies of Selective Catalytic Reduction of NOx with NH_3 on Fe- and Cu-Zeolite Monolithic Catalysts

A Dissertation

Presented to

the Faculty of the Department of Chemical and Biomolecular Engineering

University of Houston

In Partial Fulfillment

of the Requirements for the Degree

Doctor of Philosophy

in Chemical Engineering

by

Pranit Subhash Metkar

May 2012

Acknowledgements

I would like to thank my advisors, Professor Michael P. Harold and Professor Vemuri Balakotaiah for their guidance, strong support and motivation throughout my PhD. It was an honor and privilege to work under their supervision. They have been very generous with their time, ideas and knowledge. I thank them for giving me sufficient time and freedom in my research. Apart from the excellent tips on catalytic reaction engineering, I continue to reap the benefits from their guidance on presentation skills, technical writing and overall discussions on scientific problem solving.

I greatly acknowledge the financial support from the U.S. DOE National Energy Technology Laboratory (DE-FC26-05NT42630, DE-EE0000205) and the Texas Commission on Environmental Quality. I would like to thank BASF Catalysts LLC, Umicore Autocat USA and Sud-Chemie, Germany for providing the catalysts used in this study.

I am thankful to the other members of my dissertation committee, Prof. William Epling, Prof. Allan Jacobson and Prof. Karolos Grigoriadis, for making their time available to me, despite their busy schedules. I would also like to thank Dr. Rachel Muncrief for her valuable advice on catalyst synthesis and characterization techniques. In addition, I would also like to thank Dr. Luss for his eagerness to share his knowledge of chemical reaction engineering and catalysis research. Special thanks to Dr. James Meen and Dr. Karoline Mueller from the Chemistry Department for their assistance with the various analysis techniques. Additionally, I would like to acknowledge the faculty and staff of the Department of Chemical and Biomolecular Engineering at the University of Houston.

I would like to express my gratitude to my current and former labmates for their companionship. Yongjie Ren and Nelson Salazar walked me through many aspects of the experiments and bench-scale reactor set-up. The guidance by Sameer Israni, Saurabh Joshi, Divesh Bhatia and Ashok Kumar during the initial phase of my PhD is greatly appreciated. I am grateful to Pankaj Kumar, Arun Kota and Bijesh Shakya for their help with FORTRAN and MATLAB. I would also like to thank the other members of Dr. Harold's group – Geofrey Goldwin, Bala Nair, Hongmei An, Alejandrina Campanella, Gregory Bugosh, Prasanna Reddy, Sachi Shrestha, Richa Raj and Di Wang, who helped me during my stay at UH. It was really a great pleasure to have worked in the company of all these people. I will definitely miss working in labs S289 and S270. I wish the entire group of Dr. Harold all the very best in research.

I would like to thank all my friends and roommates: Pratik, Aditya, Ajay, Yogendra, Sameer, Abhijit, Ashutosh, Geff, Saurabh, Ashok, Vivek, Anupam, Pankaj, Arun, Robin, Ila, Rohit, Rahul, Gauarv, Ram and Udit for all the good times during my stay in Houston. I really consider myself fortunate to have become friends with these great and amazing personalities during my PhD. I wish all of them great success.

Finally, I would like to express my love and gratitude to my parents for their unconditional love, encouragement, motivation, strong support and many sacrifices. You are wonderful parents and thank you for everything! I would also like to thank my sister Pradnya and brother Prashant for all of their fruitful advice, help and support throughout my life. Talking with you always cheered me up and helped me tackle tough times.

Experimental and Kinetic Modeling Studies of Selective Catalytic Reduction of NOx with NH_3 on Fe- and Cu-Zeolite Monolithic Catalysts

An abstract

of a

Dissertation

Presented to

the Faculty of the Department of Chemical and Biomolecular Engineering

University of Houston

In Partial Fulfillment

of the Requirements for the Degree

Doctor of Philosophy

in Chemical Engineering

by

Pranit Subhash Metkar

May 2012

Abstract

The selective catalytic reduction (SCR) of NOx with NH_3 is considered to be the most promising technique for the efficient reduction of highly detrimental NOx (to N_2) emitted from diesel engine vehicles. Amongst the various catalysts available for SCR, Fe- and Cu-zeolite catalysts are found to be highly stable and efficient towards maximum NOx reduction over a wide temperature range. Cu-zeolites are more active at low temperatures ($\leq$ 350 ^{o}C) while Fe-zeolites are more active at high temperatures ($\geq$ 400 ^{o}C). We carried out a comprehensive experimental and kinetic modeling study of key SCR reactions on Fe- and Cu-zeolite catalysts and present a detailed understanding of mass transfer limitations and kinetics and mechanistic aspects of various SCR reactions on these catalysts.

Experiments carried out on monolith catalysts having different washcoat loadings, washcoat thicknesses and lengths indicate the presence of washcoat (or pore) diffusion limitations at intermediate to high temperature range in all the SCR reactions. A detailed analysis of the effect of temperature on the transitions between various controlling regimes (kinetic, washcoat diffusion and external mass transfer) is presented. Agreement in the differential kinetics studies of NO oxidation and standard SCR ($NO + O_2 + NH_3$) reactions indicates NO oxidation is the rate determining step for standard SCR. A detailed kinetic model capturing key features of all the SCR reactions is developed. This model accurately predicts the experimentally observed NOx conversions over a wide temperature range and different feed conditions.

Finally, a systematic study of various SCR reactions is carried out on a combined system of Fe- and Cu-zeolite monolithic catalysts to determine if a high NOx conversion

could be sustained over a wider temperature range than with individual Fe- and Cu-zeolite catalysts. Amongst various configurations, a dual-layer catalyst with a thin Fe-zeolite layer on top of a thick Cu-zeolite layer resulted in a very high NOx removal efficiency over a broad temperature range of practical interest. The kinetic model accurately captures the experimental data with a combined system of Fe- and Cu-zeolite catalysts and provides further insights into the catalyst arrangements for maximum NOx reduction efficiency.

Table of Contents

List of Figures

List of Tables

Nomenclature

Abbreviations

DOC	diesel oxidation catalyst
DPF	diesel particulate filter
EDS	energy dispersive spectroscopy
EGR	exhaust gas recirculation
EPA	environmental protection agency
FT-IR	Fourier transform infrared
GHSV	gas hourly space velocity
HC	hydrocarbon
ICP	inductive coupled plasma
LNT	lean NOx trap
MFC	mass flow controller
NAC	NOx adsorber catalyst
NSR	NOx storage and reduction
NOx	Nitrogen oxides ($NO + NO_2$)
PM	particulate matter
QMS	quadrupole mass spectrometer
SCR	selective catalytic reduction
SEM	scanning electron microscope
TPD	temperature programed desorption
TWC	three-way converter
XRD	X-ray diffraction

Symbols

A_{bi} reverse pre-exponential factor for step *i* (mol/m^3/s)

A_{fi} forward pre-exponential factor for step *i* (mol/m^3/s)

C_s total concentration of adsorption sites

C_{Tm} total molar concentration (mol/m^3)

D_f diffusivity of a species in fluid phase (m^2/s)

De effective diffusivity of a species in washcoat (m^2/s)

j various species (e.g., NH_3, NO, NO_2, N_2O, N_2, etc.) participating in a reaction

k_{bi} reverse rate constant of step *i* (mol/m^3/s)

$k_c(j,z)$ mass transfer coefficient of species *j* at axial position *z*

k_{fi} forward rate constant of step *i* (mol/m^3/s)

K_{eq} equilibrium constant for NO oxidation reaction

K_i equilibrium constant of step *i*

k_{mi} internal mass transfer coefficient

k_{me} external mass transfer coefficient

$k_{m,app}$ apparent mass transfer coefficient

L length of the monolith (m)

P transverse Peclet number

$P_{\Omega 1}$ channel perimeter open to flow

Q total flow rate (sccm)

$R_{\Omega 1}$ effective transverse diffusion length scale (m)

$R_{\Omega 2}$ effective washcoat thickness (m)

$R_{\Omega 3}$ radius of a single zeolite crystallite particle (m)

R_{ext} external mass transfer resistance

R_w washcoat diffusion (internal mass transfer) resistance

R_{rxn} reaction resistance

$R_{NO,oxi}$ rate of NO oxidation reaction

R_{obs} observed rate of reaction

R_v reaction rate (mol/m^3/s)

Sc Schmidt number

Sh_i internal Sherwood number

Sh_e external Sherwood number

Sh Sherwood number

$\langle u \rangle$ average velocity inside monolith channel (m/s)

Xj mole fraction of species j

Xjm dimensionless cup-mixing concentration of species j in fluid

$Xjwc$ dimensionless concentration of species j in washcoat

y length co-ordinate along radial (washcoat) direction

z length co-ordinate along axial direction

Greek letters

ε_{wc} porosity of washcoat

Ψ Weisz-Prater modulus

ν stoichiometric coefficient

θ_v fractional coverage of vacant sites S1

σ_v Mole fraction of vacant sites S2

ϕ Thiele modulus

Φ_1 generalized Thiele modulus used for plotting effectiveness factor

Λ constant used in the universal correlation for internal mass transfer coefficient

τ_e transverse diffusion or external mass transfer time (s)

τ_c convection time (s)

τ_d characteristic diffusion time in the washcoat (s)

CHAPTER 1 Introduction

1.1 Background on Emissions

Gasoline engines are commonly used in most of the passenger cars worldwide. Fossil fuels serve as the primary source of energy at present and will continue to do so in the near future. The available fossil fuel resources are limited and are being depleted very fast because of the exponentially increasing demand and consumption of energy. Passenger cars are used as a common source of commuting, while light-duty and heavy-duty vehicles are used to transport goods. Overall, all these vehicles use a major fraction of the available energy resources. With energy resources depleting fast, it has become imperative to improve the fuel efficiency of all vehicles. Diesel engine vehicles are considered to be highly fuel efficient compared to their gasoline counterparts. Hence, the recent increase in the transportation fuel prices has shifted the trend towards increasing use of diesel powered vehicles. Also, diesel engines deliver higher power compared to gasoline engines and are more durable and reliable and thus incur lower maintenance cost.

A gasoline engine is a spark-ignition engine which uses a spark plug to ignite an air fuel mixture. In contrast to the gasoline engine, a diesel engine, also known as a compression-ignition engine, uses the heat of compression to initiate ignition to burn the fuel. During the combustion of fuel, various gases like CO, CO_2, hydrocarbons (HC), NOx ($NO + NO_2$), etc. are produced and are emitted into the atmosphere. These gases are harmful to the human beings and hence must be converted into harmless gases before they are emitted into the atmosphere. Thus the US EPA (Environmental Protection Agency) has set stringent emission standards to minimize the emissions of harmful

pollutants into the atmosphere. These standards have become more and more stringent over the last few decades. These rules of minimizing emissions have resulted in the development of exhaust aftertreatment systems in both gasoline and diesel engine vehicles.

All gasoline vehicles are equipped with three way catalytic converters (TWC) in tail pipe and the TWC reduces the emissions of harmful gases. The emission standards were implemented in the United States with the introduction of the Clean Air act in 1970. Initially, precious metal catalysts containing Pt and Pd were used to meet the standards of CO and HC emissions. Over a 90% reduction in the emissions of CO and HCs was achieved with the help of these precious metal catalysts. The initial EPA standards were relaxed for NOx emissions and were met by using exhaust gas recirculation (EGR). But, the later emission standards set by US EPA required reduction in NOx emissions to less than 1 g/mile. Thus, Rh was introduced in the TWC along with Pt/Pd which were present even in the earlier catalysts. The role of Rh was to reduce NOx and it also enhanced the CO and HC oxidation. Also, it was observed that with the Pt, Pd and Rh based catalyst, if the engine could be operated around the stoichiometric air-to fuel ratio of $\lambda = 1$, all the three pollutants could be simultaneously converted. The term used to define the air-to-fuel weight ratio, lambda (λ), is defined as the actual air-to-fuel ratio divided by the air-to-fuel ratio at the stoichiometric point [1, 2]. When $\lambda=1$, it is called the stoichiometric point, representing the exact amount of air required to completely oxidize the fuel. In gasoline engines, the value of λ is kept constant at 1 and this value corresponds to the air-to-fuel ratio of 14.6. When sufficient air is not present during the combustion process, i.e., during rich ($\lambda < 1$) operation, there is incomplete combustion of fuel resulting in

higher emissions of CO and hydrocarbons with lesser NOx ($NO + NO_2$) emissions. But during lean operation ($\lambda > 1$), there is near complete combustion of fuel resulting in reduced CO and HC emissions. During lean operation, the overall operating temperatures are reduced and hence the NOx emissions are also lowered. The modern three-way catalysts are comprised of 0.1-0.15% precious metals, 10-20% CeO_2 and the remainder being the γ-Al_2O_3 washcoat [1]. Overall, the TWC technique is well developed and the catalyst configuration meets the current stringent EPA standards. But, depending upon the cost of precious metal catalyst, the amount of Pt, Rh and Pd may vary. Also, catalyst manufactures introduce some proprietary components to increase the activity and durability of the catalyst.

Diesel engines are lean burn engines which operate with an excess of air. The operating principle of diesel engines is different than that of gasoline vehicles. Unlike spark-ignited combustion in gasoline engines, the combustion in diesel engines is compression-ignited and is leaner and cooler. But this combustion process results in larger quantities of unburned fuel, lube emissions and dry soot. Even though there has been a great progress in redesigning the engine over the years to minimize these emissions, there is still a requirement for the aftertreatment system in diesel engines. This exhaust aftertreatment technology for diesel engine vehicles is still under development and is improving to meet the stringent EPA emission standards. The emissions from diesel engine vehicles are comprised of solid, liquid and gas phases. Particulate matter (PM) represents the combined solids and liquids emissions from diesel engine. Also some diesel fuel remains unconverted during the combustion process. This unburned fuel along with the lubricating oil represents the volatile organic fraction (VOF). The gaseous phase

is comprised of hydrocarbons, carbon monoxide, nitrogen oxides (NOx) and sulfur dioxide. Because of the presence of all the above components in the exhaust, the diesel engine aftertreatment system is more complicated than that of the gasoline engines. However, diesel engines hold various advantages over gasoline engines because of their high fuel efficiency, longer life, durability and reliability. Also, the lean operation in diesel vehicles results in less CO and HC emissions. The amount of NOx produced in diesel engine vehicles is also less compared to gasoline vehicles because of the leaner operation. But gasoline vehicles equipped with the TWC significantly reduce NOx and hence the overall NOx emissions are lesser in gasoline vehicles compared to diesel vehicles. The relative emissions from a gasoline engine equipped with catalyst and a diesel engine are compared in Figure 1-1.

The emission standards for diesel engine vehicles were introduced later compared to those for the gasoline vehicles. In the mid-1980s, both the EPA and California Air Resources Board (CARB) began to consider diesel emission standards. The early standards for diesel emissions were met with the help of a diesel oxidation catalyst (DOC) and EGR. Later on, catalytic devices were introduced to meet the more stricter NOx reduction standards. Table 1-1 summarizes the emission regulations for heavy-duty trucks in US [1]. All the standards are reported in the units of g/bhp-hr.

In order to meet these stringent emission standards, various technologies are being developed, commercialized and constantly improved. These technologies commonly use catalytic monoliths described in the next section.

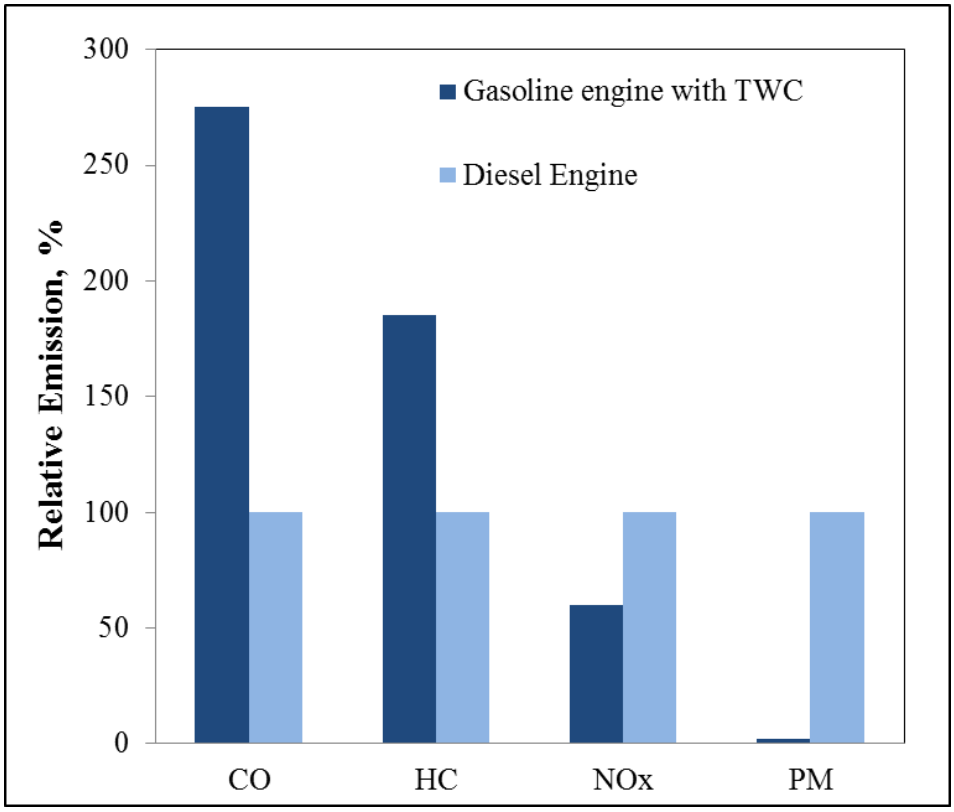

Figure 1-1: Comparison of regulated emissions-Gasoline engines vs Diesel engines.

Table 1-1: Emission regulations for heavy-duty trucks in the US.

Year	HC	NOx	PM
1994	1.3	5	0.1
1998	1.3	4	0.1
2003	0.5	2	0.1
2007	0.5	2	0.01
2009	0.14	0.2	0.01
2010	0.14	0.2	0.01

1.2 Catalytic Monoliths

Washcoated monolithic catalysts are commonly used in the exhaust aftertreatment systems of both diesel and gasoline engine vehicles. These catalysts are commonly used for reducing emissions from stationary sources like power plant applications. The other applications where monolithic catalysts are used include multiphase catalytic reactions such as hydrogenation, oxidation and bioreactions. Monoliths are proposed as suitable catalyst supports for the production of synthesis gas (CO and H_2) [3, 4]. Monolith catalysts find attractive applications in selective hydrogenations of C_2-C_4 streams e.g., from steam crackers or postreactors in selective oxidation processes. Few studies report the use of monoliths for the dehydrogenation of ethylbenzene [5-7]. Although the commercial use of monolithic catalysts is limited at present because of various challenges in terms of manufacturing cost, loading, packaging and sealing of monolithic reactors, etc., new technologies in future will broaden their commercial applications.

The monolith catalysts are in the form of a honeycomb like structure and consist of various straight parallel channels. Figure 1-2 represents typical catalytic monoliths used in automobile exhaust aftertreatment systems. The straight parallel channels have a well-defined geometry and may have a variety of cross sectional shapes, such as square, triangular, hexagonal or sinusoidal, etc. Monolithic catalysts provide the advantage of very low pressure drop compared to that of conventional packed bed reactors. The straight parallel channels have large open frontal areas and hence provide unrestricted flow. Also, these catalysts can be conveniently placed in the exhaust pipe. High flow rates of gases coming from diesel engine can pass through the monolith support with minimal pressure drop and this reduces back pressure and hence minimizes the engine

load. Further, the ceramic and cordierite monoliths (commonly used for automotive applications) can be fabricated with a large variation in cell size and geometric surface area, depending upon the application requirement. Catalyst powder can be easily deposited on these monolithic supports in the form of a thin layer. Overall, the accessibility of entire catalyst is enhanced because of this washcoating procedure. Thus the higher effectiveness of washcoated layers provides an important advantage for monolithic catalysts compared to pellets. The washcoat thickness can be optimized as per the requirements. The pore/washcoat diffusion limitations are found to be minimum in these catalysts. The thickness of the washcoat varies between 10-60 μm and the washcoat is generally porous with pores within the washcoat varying between 1-100 nm. In a typical gas-solid reaction in automotive catalysis, a reactant in the gas phase is transported in the axial direction primarily by convection and towards the catalyst's surface and within the catalyst by diffusion. The reaction takes place within the washcoat and products of reaction diffuse back to the gas phase. In an exothermic reaction, heat is generated and the amount of heat depends upon the concentrations and conversions of the reactants. This raises the overall catalyst temperature. The catalytic reactions are a strong a function of temperature giving higher conversions at higher temperatures. The catalyst temperature can go as high as 900 ^{o}C during these operations. The ceramic/cordierite material used to make these catalytic monoliths provides a significantly high mechanical strength and very high thermal resistance. Also, these materials have a low thermal expansion coefficient which offers minimal change in dimensions with varying temperatures. The uniform flow distribution in catalytic monoliths reduces the possibility of hotspot formation which is a major drawback in packed bed reactors. Also, the

monolithic structure provides high mass transfer rates. Considering all the above advantages, ceramic/cordierite monoliths are very attractive for automobile applications compared to pelleted catalysts [2]. Metallic monoliths have high conductivity and low specific heat capacity. But they are more expensive compared to that of cordierite material and hence are rarely used. Cordierite material is commonly used to manufacture monolithic supports for automotive applications and is represented by $2MgO.2Al_2O_3.5SiO_2$. Different catalysts are focused on minimizing emissions of different components. The catalyst technologies in diesel vehicles are discussed below.

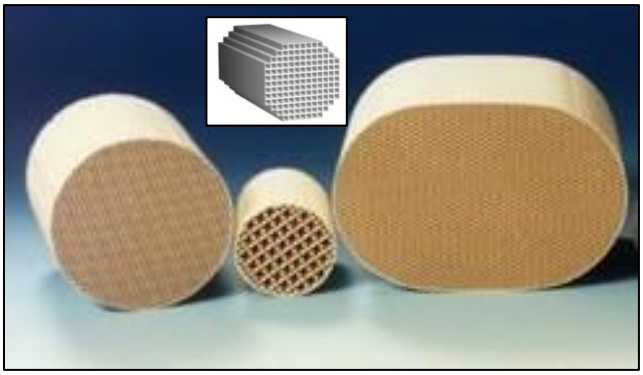

Figure 1-2: Catalytic monoliths for vehicular exhaust aftertreatment applications.

1.3 Diesel Catalysts

The three-way catalytic converter technology is now an integral part of all the spark-ignited gasoline engines which operate at stoichiometric air-to-fuel ratio. As the diesel engines operate in the presence excess air, the TWC catalyst cannot be used in diesel vehicles. Hence separate catalyst technologies have been introduced for minimizing the emissions of harmful pollutants from diesel vehicles. Table 1-2 summarizes the techniques used commercially in diesel exhaust aftertreatment systems [8].

Table 1-2: Catalyst technologies used in diesel vehicle aftertreatment system.

Catalyst Technology	Reaction Type	Reduced Emissions
Diesel Oxidation Catalyst (DOC)	Oxidation	CO, HC, PM
Selective Catalytic Reduction (SCR)	Selective catalyst reduction by urea/ammonia	NOx
Lean NOx Catalysts	Selective catalytic reduction by HC	NOx, CO, HC, PM
NOx Adsorbers	Adsorption (trapping) of NOx from lean exhaust, followed by release and catalytic reduction under rich conditions	NOx, CO, HC

The initial EPA emission standards were more stringent for CO and HC emissions compared to NOx. Hence the catalysts developed initially were designed for achieving a high removal efficiency of CO and HC. The diesel oxidation catalyst (DOC) developed during the early years successfully met the emission standards for CO and HC. The DOC technology is now well established and used commercially in all the light-duty and heavy-duty vehicles. The NOx emissions standards became more stringent over the past few years. In order to meet these strict NOx regulations, new catalyst technologies have been researched. This research has resulted in some promising catalyst technologies which are now being commercialized. Some of these NOx reduction technologies are described in the following section.

1.4 NOx Reduction Technologies

NOx is a generic term representing various oxides of nitrogen. NO and NO_2 are the major constituents of NOx. NOx is formed by the reaction between N_2 and O_2 during the combustion process. Very high temperatures (> 1100 ^oC) are required for NOx

formation. Approximately, 90% of the nitrogen oxides (emitted from diesel engine vehicles) are in the form of NO. NOx is considered as one of the major air pollutants. In the presence of sunlight, NOx reacts with volatile organic compounds leading to the ground-level ozone formation. The ground level ozone has many adverse effects on human beings since it's a cause of number of respiratory diseases like bronchitis, asthma, etc. Also it depletes the ozone layer in the stratosphere which absorbs harmful ultraviolet radiation. Reaction of NOx with water vapor leads to acid rain formation. Thus overall, NOx is highly detrimental to human beings and hence the EPA standards for NOx emissions are becoming more and more stringent. Various techniques for minimizing NOx emissions from diesel engine vehicles are being researched, developed and commercialized. These techniques are summarized below.

1.4.1 Direct Decomposition of NO

Decomposition of nitric oxide to N_2 and O_2 is thermodynamically favored under pressures and temperatures found in diesel exhaust. But the activation energy of this reaction is very high and hence the rate of the spontaneous reaction is practically zero. Various catalysts have been investigated to improve the reaction rate. But as of now, there is no catalyst available to significantly enhance the NO decomposition reaction rate. Copper based zeolite catalysts (especially Cu-ZSM-5) have shown the best activity for this reaction [9, 10]. Although this technique was found to be promising initially, it has proven difficult to realize. This reaction is significantly inhibited by H_2O and O_2. Also, the presence of SO_2 in the feed has a poisoning effect on the catalyst and thus it significantly reduces the reaction rates. The activity and selectivity of even the best

catalyst (Cu-ZSM-5) was not satisfactory. Hence this technique is not commercialized for NOx reduction in diesel engines.

1.4.2 Exhaust Gas Recirculation (EGR)

This technology is aimed at minimizing the NOx emissions by lowering the local flame temperature, which is the main reason for NOx formation. Thus a portion of an engine's exhaust is recirculated back to the engine cylinders. This results in reduction of trapped air available for combustion. Thus the engine operates at overall lower air-to-fuel ratio since the amounts of fuel and air in the inlet are constant but as some of the exhaust is being recirculated, the overall air-to-fuel ratio drops down. This results in lowering the NOx emissions. But at the same time, this technique has some other drawbacks. One major drawback is the overall increase in the engine temperature as the cooler inlet air is mixed with hot recirculated gas which results in the requirement of additional cooling system for engine to lower the harmful effects on engine durability. The other drawback is associated with the decreased efficiency of the diesel particulate filter (DPF) designed to reduce particulates. The DPF requires a regular regeneration at elevated temperatures to oxidize the accumulated soot. This avoids increased exhaust back pressure. But due to EGR, the production of soot increases and it places additional burden on the DPF. Also, the reduced temperatures may result in incomplete fuel consumption affecting the fuel efficiency of the engine. Because of all these drawbacks, EGR has very limited commercial applications and it does not provide a final solution for the stringent NOx emission regulations.

1.4.3 NOx Adsorber Catalyst

NOx adsorber catalysts have been developed to reduce NOx emissions from diesel engines. This technology is mainly used in light-duty diesel engine vehicles and also in partial lean burn gasoline engine vehicles. These catalysts are also known as the NOx Storage and Reduction (NSR) catalysts or Lean NOx Trap (LNT) catalysts. NOx storage materials were first incorporated into DeNOx catalysts to widen the temperature window of high NOx removal efficiency. The basic concept behind the working principle of these catalysts is to adsorb/store NOx during lean cycles. The adsorbed NOx is released and reduced in a subsequent fuel rich cycle by hydrocarbons present in fuel. Thus the second phase of a cycle represents the regeneration of NOx traps. The lean NOx trap is a bifunctional catalyst comprising precious metals (Pt, Pd, Rh) and alkaline earth metals (Ba, K) in the form of oxides or carbonates. The role of precious metal catalysts is to oxidize NO to NO_2 during the lean phase. The NO_2 thus formed is then stored in the form of metal nitrates. These LNT catalysts have been successfully used in stationary power, natural gas turbine aftertreatment systems for several years [11]. Toyota laboratories introduced the concept of NSR for automobile applications [12-15]. Since mid-1990s, a large amount of research and development work has been conducted worldwide to successfully adapt and commercialize this technology for diesel vehicular applications. This technique does not require any additional infrastructure in diesel vehicles as it is using the hydrocarbons which are present in fuels. But it definitely requires sophisticated, adaptive control strategies for the lean-rich diesel engine operations. One major disadvantage of this technique is a very high cost associated with the use of precious Pt/Rh/Pd metals used in NSR catalysts. The other major obstacle in

the development of diesel NOx adsorbers is their susceptibility to sulfur poisoning [16-19]. Even if ultra-low sulfur fuel is used, a regular desulfation of the catalyst is required to achieve desired NOx removal performance. This desulfation is usually carried out at higher temperatures (550-650 ^{o}C). But at these high temperatures, sintering of Pt and Pd catalysts takes place and hence the deNOx efficiency is decreased. Considering all these drawbacks, the NOx adsorber catalysts find limited applications for NOx removal in diesel vehicles.

1.4.4 Selective Catalytic Reduction

Selective catalytic reduction (SCR) of NOx by ammonia or urea is considered as the most promising technology to meet the increasingly stringent EPA standards for NOx emissions from diesel engine vehicles. The SCR of NOx with urea or ammonia as a reductant technology is well known, having been used in stationary applications like power plants for many years. This technology was initially developed in Japan in the 1970s for applications in thermal power plants. Over the years, the SCR technology has been further developed and improved and it has found widespread applications for NOx control in coal-fired power plants, refinery heaters, boilers, furnaces, coke ovens, etc. The potential of SCR for NOx removal in vehicular applications was realized in the 1990s and it has gained considerable attention in the last few years. The first commercial SCR application for a diesel truck was launched in 2004 by Nissan Diesel in Japan and by DaimlerChrysler in Europe. Now Urea-SCR has been selected by a number of catalyst and diesel engine manufacturers as the preferred technology for meeting the NOx emission regulations worldwide.

The selective catalytic reduction technique requires a reductant to reduce NOx. Various reductants have been tested for this technique. Gaseous NH_3 is found to be the best reductant for maximum NOx removal efficiency. The reductant, NH_3, needs to be injected into the flue gas stream before the catalyst. But anhydrous ammonia is highly toxic, hazardous and it is very challenging to carry anhydrous NH_3 on-board. Carrying the anhydrous ammonia onboard requires thick-shell, pressurized storage tanks and piping due to its high vapor pressure. Considering the toxicity and handling problems of anhydrous ammonia, there has been a need for an alternative reductant which is easy to handle, easy to transport and is non-toxic. Aqueous solution of urea (known as diesel exhaust fluid in the US) meets these criteria and is inexpensive. At high temperatures, urea is easily decomposed to ammonia by the following reaction,

$$CO(NH_2)_2 + H_2O \rightarrow 2NH_3 + CO_2 . \quad (1\text{-}1)$$

The urea decomposition to ammonia can be further divided into two steps. In the first step, isocyanic acid (HNCO) and one molecule of ammonia are formed by thermolysis of urea, followed by hydrolysis of the HNCO with the formation of a second NH_3 molecule:

$$CO(NH_2)_2 \rightarrow NH_3 + HNCO, \quad (1\text{-}2)$$

$$HNCO + H_2O \rightarrow NH_3 + CO_2 . \quad (1\text{-}3)$$

Thus the aqueous urea solution provides a source of ammonia and hence is the reductant of choice for use in mobile SCR applications. SCR has a number of advantages over other techniques like the lean NOx trap, discussed earlier. One major advantage of SCR over LNT is a very low cost of catalyst. This is because SCR does not use a precious metal catalyst (like Pt, Rh, Pd). Also, SCR provides a very high NOx removal efficiency over a wide temperature window. The catalysts used for SCR are stable and active over

this entire temperature window. The focus of this study is on selective catalytic reduction of NOx with NH_3 on iron- and copper-zeolite monolithic catalysts. In the following section, details about the SCR chemistry are summarized.

1.5 SCR Chemistry

The selective catalytic reduction of NOx with NH_3 has been studied in detail on various catalysts like vanadium based catalysts e.g., $V_2O_5/TiO_2/WO_3$, Fe-zeolite and Cu-zeolite catalysts [20-43]. Overall, the SCR chemistry is now well established in the literature and has been found to be very similar on all the above catalysts. This chemistry is briefly summarized as follows.

The selective catalytic reduction involves the following set of reactions which are divided into three categories.

Standard SCR Reaction: This reaction involves reduction of NO by NH_3 in the presence of O_2 and is given as

$$4\ NH_3 + 4\ NO + O_2 \rightarrow 4\ N_2 + 6\ H_2O \qquad \Delta H = -\ 4.07 \times 10^5\ J/mol\ NH_3. \qquad (1\text{-}4)$$

Thus by the stoichiometry of this reaction, equimolar amounts of NO and NH_3 are consumed in this reaction.

Fast SCR Reaction: When both NO and NO_2 in the feed react simultaneously to produce N_2 and H_2O; it is called as "fast SCR" reaction (1-5) because it is much faster than the standard SCR reaction (1-4),

$$2\ NH_3 + NO + NO_2 \rightarrow 2\ N_2 + 3\ H_2O \qquad \Delta H = -\ 3.78 \times 10^5\ J/mol\ NH_3. \qquad (1\text{-}5)$$

NO_2 SCR Reaction: When NO_2 reacts with NH_3, it is called as the NO_2 SCR reaction and is presented as

$4\ NH_3 + 3\ NO_2 \rightarrow 3.5\ N_2 + 6\ H_2O$ $\Delta H = -3.41 \times 10^5$ J/mol NH_3. (1-6)

This reaction is also known as the "slow" SCR reaction in the literature. In an historical context, the "slow" descriptor refers to the fact that its rate is typically slower than the fast SCR reaction.

Along with these main reactions, additional side reactions occur. NH_3 oxidation is a key side reaction taking place at temperatures exceeding 300 ^oC. This is an undesired side reaction as it competes with the SCR reaction for the reductant ammonia. On the Fe- and Cu-zeolite catalysts, most of the NH_3 is selectively oxidized to N_2 [44-46] by the following reaction,

$4\ NH_3 + 3\ O_2 \rightarrow 2\ N_2 + 6\ H_2O$ $\Delta H = -3.12 \times 10^5$ J/mol NH_3. (1-7)

Along with N_2 as the main product of this reaction, some byproducts like N_2O, NO and NO_2 may be produced by the following reactions:

$2\ NH_3 + 2\ O_2 \rightarrow N_2O + 3\ H_2O$ $\Delta H = -2.76 \times 10^5$ J/mol NH_3, (1-8)

$4NH_3 + 5O_2 \rightarrow 4NO + 6H_2O$ $\Delta H = -2.27 \times 10^5$ J/mol NH_3, (1-9)

$4NH_3 + 7O_2 \rightarrow 4NO_2 + 6H_2O$ $\Delta H = -2.84 \times 10^5$ J/mol NH_3. (1-10)

The other important side reaction is the oxidation of NO to NO_2 which occurs in the temperature range of interest ($T > 150\ ^oC$) and is desirable because NO_2 is more effectively reduced by NH_3 than is NO. This reaction is given by

$NO + ½\ O_2 \leftrightarrow NO_2$ $\Delta H = -5.7 \times 10^4$ J/mol NO. (1-11)

On the other hand, the existence of NO_2 complicates the reaction system where many byproducts are formed. In particular, ammonium nitrate formation occurs at lower temperatures and is given by

$2\ NH_3 + 2\ NO_2 \rightarrow N_2 + NH_4NO_3 + H_2O$ $\Delta H = -2.91 \times 10^5$ J/mol NH_3. (1-12)

If the catalyst temperature is below 170 ^{o}C, then the ammonium nitrate formed by the above reaction is deposited in the solid form on the catalyst surface. This may block the catalyst pores and active sites required for NOx reduction reactions and hence inhibit the SCR chemistry. A mechanism for the ammonium nitrate formation in the presence of NO_2 has been reported on $V_2O_5/TiO_2/WO_3$ and zeolite-based catalysts [20, 24, 31, 33, 47-50]. Koebel and coworkers [20, 22, 50] showed that the first step in this chemistry is NO_2 dimerization,

$$2\ NO_2 \leftrightarrow N_2O_4. \qquad (1\text{-}13)$$

The N_2O_4 thus formed reacts with water to form nitrous and nitric acids

$$N_2O_4 + H_2O \leftrightarrow HONO + HNO_3. \qquad (1\text{-}14)$$

HONO and NH_3 further react to form ammonium nitrite which is highly unstable and decomposes to N_2 and H_2O,

$$NH_3 + HONO \leftrightarrow [NH_4NO_2] \rightarrow N_2 + H_2O. \qquad (1\text{-}15)$$

The formation of NH_4NO_3 can be explained by reaction between NH_3 and HNO_3

$$NH_4NO_3 \leftrightarrow NH_3 + HNO_3 \qquad \Delta H = 1.84 \times 10^5 \text{ J/mol } NH_4NO_3. \qquad (1\text{-}16)$$

The reduction of nitrates by NO has been proposed to be a rate determining step in the fast SCR chemistry [36]:

$$NH_4NO_3 + NO \rightarrow NO_2 + N_2 + 2\ H_2O \qquad \Delta H = -1.75 \times 10^5 \text{ J/mol } NH_4NO_3, \qquad (1\text{-}17)$$

$$HNO_3 + NO \rightarrow NO_2 + HONO. \qquad (1\text{-}18)$$

Ammonium nitrate formed above decomposes to N_2O at higher temperatures ($\geq$ 200 ^{o}C)

$$NH_4NO_3 \rightarrow N_2O + 2\ H_2O \qquad \Delta H = -3.66 \times 10^4 \text{ J/mol } NH_4NO_3. \qquad (1\text{-}19)$$

N_2O is a greenhouse gas and therefore is not a desirable byproduct in the SCR system. Its formation may also be explained by the overall reaction,

$4\ NH_3 + 4\ NO_2 + O_2 \rightarrow 4\ N_2O + 6\ H_2O \qquad \Delta H = -\ 2.68 \times 10^5\ J/mol\ NH_3.$ (1-20)

The N_2O formed in the reaction system decomposes to N_2 and O_2 at higher temperatures:

$2\ N_2O \rightarrow N_2 + O_2 \qquad \Delta H = -\ 8.2 \times 10^4\ J/mol\ N_2O.$ (1-21)

Devadas et al. [29] studied the fate of N_2O in detail on Fe-ZSM-5. They also studied the reduction of N_2O by NH_3 separately and observed that ammonia may react with N_2O according to

$2\ NH_3 + 3\ N_2O \rightarrow 4\ N_2 + 3\ H_2O \qquad \Delta H = -\ 4.4 \times 10^5\ J/mol\ N_2O.$ (1-22)

The N_2O formed during the SCR chemistry may be reduced by NO [51-54] by

$N_2O + NO \rightarrow N_2 + NO_2.$ (1-23)

The overall SCR chemistry is summarized above. Various catalysts available for SCR of NOx with NH_3 are briefly summarized in the following section.

1.6 Catalysts for SCR

Various catalysts have been studied for the SCR of NOx with NH_3 as the reductant. This reaction was initially discovered on the platinum based catalysts [55] which are very active for the selective catalytic reduction at lower temperatures (< 250 °C) but oxidize ammonia at higher temperatures. Thus at higher temperatures, there is a very poor selectivity for NOx reduction on these noble metal catalysts. Also, the catalyst temperature must be controlled above approximately 200 °C to avoid NH_4NO_3 formation. But if the temperature exceeds 225 °C, the Pt catalyst loses its selectivity toward the NOx reduction reaction. Hence the Pt catalysts are useful only in a small temperature window (225-250 ^oC). Considering the very high cost of Pt catalysts and very small temperature window of operation, these catalysts were not commercialized for the SCR of NOx with

NH_3. But, various other catalysts were developed over the last two decades. Following, we briefly review the literature studies on these catalysts.

1.6.1 Vanadium-based Catalysts

Amongst the various investigated metal oxide mixtures, vanadia supported on titania and promoted with tungsta were found to be promising deNOx NH_3 SCR catalysts. The use of vanadia for SCR was discovered in the 1960s and the superior activity and stability of these catalysts was recognized in the 1970s [55]. Different catalyst components used in vanadia-based catalysts have different roles. V_2O_5 is responsible for NOx reduction and the oxidation of SO_2. Tungsten trioxide (WO_3) is the most frequently used stabilizer for SCR vanadia/titania formulations which improves the thermal stability up to 700 °C. The vanadia based catalysts operate best in the temperature range between 260 - 450 °C. Also, these catalysts have a significant resistance to sulfur poisoning and hence can be used for high sulfur diesel fuel [56]. Considering these different advantages of vanadia-based catalysts over Pt-based catalysts, the vanadia-based catalysts became popular deNOx SCR catalysts in diesel engine vehicles and have been used for commercial applications. A lot of research work has been carried out in the last two decades for improving these catalysts further. Many literature studies focused on the understandings of kinetics and mechanistic aspects of various reactions involved in the SCR chemistry. Key findings from some of the literature studies focused on vanadia-based catalysts are summarized below.

The industrial catalysts for the SCR process are based on TiO_2-supported V_2O_5–WO_3 and/or V_2O_5–MoO_3 oxides and many studies focus on the understanding of role of

various catalyst components in deNOx activity [57-59]. As discussed earlier, vanadia is responsible for the activity of the catalyst in the NOx reduction and WO_3 increases the catalyst activity and thermal stability [60]. A lot of research work has been carried out on understanding the SCR reaction mechanism on vanadia-based catalysts [20, 21, 24, 26, 50, 61-72]. Inomata et al. [69] proposed a reaction mechanism in which they showed that the ammonia molecule is first adsorbed as NH^{4+} at a V-OH Bronsted site adjacent to a V(5+)=O site and then reacts with gas-phase NO according to an Eley–Rideal mechanism to form N_2 and H_2O and V(IV)-OH. V(IV)-OH species are then re-oxidized to V(5+)-O by gaseous oxygen. This reaction mechanism was later confirmed by Janssen et al. [73, 74] who proposed that V=O sites are the active centers for ammonia adsorption and demonstrated that one N atom of the N_2 product comes from NH_3 and the other from NO [55]. A similar study confirming the above mechanism was carried out later using isotopically labeled reactants on vanadia based catalysts [61]. Ramis et al. [75-77] proposed a different mechanism based primarily on FT-IR studies. They suggested that ammonia is adsorbed over a Lewis acid site and is activated to form an amide species. The amide species then reacts with gas-phase NO via a radical coupling and gives rise to a nitrosamide intermediate which decomposes to N_2 and H_2O. Overall, all these different reaction mechanisms suggest that whatever is the reactive ammonia species involved in the reaction (molecularly adsorbed/protonated ammonia), a key step of the mechanism is represented by the formation of a reaction intermediate which decomposes selectively to nitrogen and water. Ciardelli et al. [63] carried out a systematic study characterizing the NH_3-SCR reactivity over a V_2O_5–WO_3/TiO_2 catalyst in a wide range of temperatures and NO/NO_2 feed ratios. Their experiments confirmed that the best deNOx efficiency is

achieved with a 1/1 NO/NO_2 feed ratio. Along with these mechanistic studies of SCR, many other literature studies focus on the kinetics and reactor modeling of these reactions on vanadia-based catalysts [25, 27, 78-81]. These studies consider both the simple empirical expressions (e.g., power law kinetics) and/or more detailed mechanistic approaches (Langmuir-Hinshelwood or Eley-Rideal models). Many authors report the reaction order with respect to NO to be fractional positive or 1 on vanadia-based catalysts [82-85]. The reaction rate was found to have negligible dependence with respect to the concentrations of O_2, NH_3 and H_2O. Tronconi and coworkers [25, 27] have derived a dual-site Mars–van Krevelen kinetic model of both the standard and the fast SCR reactions over vanadium based catalysts and it accounts for stoichiometry, selectivity and kinetics of the global NH_3-NO/NO_2 SCR process.

Overall, vanadia-based catalysts offer a number of advantages, low catalyst cost, high sulfur tolerance and higher temperature applications compared to the Pt-based catalysts and hence this catalyst has been studied extensively. Even though this catalyst has been found to be suitable for high temperature applications, the upper temperature limit of vanadia catalysts is about 450 °C which is still insufficient for mobile applications. Also, at higher temperatures (> 425 °C), the selectivity towards SCR reactions is lost as the rate of ammonia oxidation side reaction begins to dominate, causing NOx reduction efficiency to fall. These catalysts have been found to have reduced stability at higher temperatures and the toxicity of vanadia has raised public health concerns. For these reasons, recent research has focused on Fe- and Cu-exchanged zeolite catalysts, both of which are found to have a high NOx removal efficiency over a

wide temperature range. In the following section, we briefly summarize the literature findings on various zeolite based catalysts.

1.6.2 Zeolite-based Catalysts

Zeolites are crystalline, hydrated aluminosilicates containing various elements like sodium, potassium, magnesium, calcium, strontium and barium. Zeolites are represented by the empirical formula: $M_{2/n}O.Al_2O_3.xO_2.yH_2O$. They have three-dimensional network of AlO_4 and SiO_4 tetrahedra linked to each other by sharing all of the oxygen. The typical pore size of different zeolites is in the range of 3-11 Å. Zeolite-based catalysts find widespread applications in many different industries like petrochemical, nuclear, detergent, heating, refrigeration, etc. The use of zeolites for deNOx SCR applications was recognized in the last century. These catalysts provide various advantages compared to the Pt- and vanadia-based catalysts. Several metal exchanged catalysts have been investigated for the SCR of NOx with NH_3 as the reductant. They have excellent stability and selectivity for SCR of NOx with NH_3 over a wide temperature range of practical interest. Also, these catalysts have a very high selectivity for the desired SCR reactions compared to that of the other catalysts.

Various studies focused on the detailed understanding of the mechanistic aspects of NH_3 SCR reactions on different zeolite catalysts are available in the literature [31-33, 39, 47, 49, 86-95]. Recently, Brandenberger et al. [96] reviewed the NH_3-SCR reaction chemistry, mechanisms and kinetics on the metal-exchanged zeolite catalysts. The overall NH_3-SCR chemistry is summarized in the previous section. Here we provide a literature review about these mechanistic aspects of NH_3-SCR on zeolite-based catalysts.

Experiments carried out with isotopically labeled reactants have shown that N_2 is formed by taking one nitrogen atom from a molecule of NOx and the other nitrogen from ammonia [38, 97]. Many studies reported NO oxidation (to NO_2) as the first step during the NH_3-SCR reaction and proposed this as the rate limiting step on zeolite-based catalysts [29, 34, 37, 43, 98]. Thus the presence of NO_2 is must for the SCR reaction to occur and this shows that the fast SCR reaction occurs in general on these catalysts. This is evident in the fact that H-ZSM-5 shows negligible SCR activity if only NO is present, and high SCR activity after 50% NO_2 is added to the feed [96, 98]. But on metal-exchanged zeolites, NO_2 is formed first on the metal sites and is then transferred to zeolite network where SCR reactions occur. As a result, the metal-exchanged zeolites show higher SCR activities for NO only feed compared to H-zeolites. Few studies reported that the presence of metal sites accelerated the (fast) SCR reaction rates along with enhancing the NO oxidation and standard SCR reaction [29]. The NO oxidation reaction is an important step in the SCR chemistry and has been studied in detail on various catalysts [99-101]. Delahay et al. [43] suggested that the rate of the NO oxidation reaction is controlled by the desorption of NO_2 from the catalyst surface. This is in line with the experimental observations during the standard SCR reaction where adsorbed NO_2 is immediately consumed and hence no observable gas-phase NO_2 is produced. NO_2 has been shown to be a stronger oxidizing agent (compared to O_2) for Fe-zeolites than Cu-zeolites [43, 99, 102]. The presence of excess NO_2 has been reported to inhibit the NO oxidation reaction [101]. Another important reaction in this chemistry is the NO_2-SCR reaction which is slightly slower than the NO/NO_2-SCR reaction, but much faster than the NO-SCR reaction on iron-zeolite catalysts [39]. In the presence of gaseous NO_2

in the feed, nitrates are formed on the catalyst surface [103]. Some other species like NO^+, N_2O_3, N_2O_4 may also form during this process [49, 90, 104]. Many researchers proposed that the SCR reaction goes through the formation of a reactive intermediate NH_4NO_2 which immediately decomposes to N_2 and H_2O [38, 90]. NH_4NO_3 formation has been observed at low temperatures in the presence of excess NO_2 [33]. The NH_4NO_3 is decomposed to N_2O at higher temperatures (> 200 ^oC) and it may block the active sites required for SCR at lower temperatures. However, in the presence of NO, the formation of NH_4NO_3 is reduced as the NO molecule reduces the surface nitrates very fast [90, 105]. The reduction of nitrates (HNO_3/NH_4NO_3) by NO has been reported as the rate limiting step for the fast SCR reaction [36]. N_2O formation has been observed in the intermediate temperature range on both the Fe- and Cu-zeolite catalysts [87, 106-108]. The N_2O formed is further decomposed to N_2 and O_2 at higher temperatures and the rate of this reaction depends on the metal loading. At higher metal (M) loading (M/Al≈0.4), the rate constant is much higher than that compared to lower metal loading [109, 110]. All these reactions are interconnected and occur simultaneously in a real SCR unit placed in the diesel aftertreatment system. Figure 1-3 summarizes the reaction scheme of the SCR process over metal-exchanged zeolites.

Various literature studies focus on the kinetic aspects of NH_3-SCR reaction on zeolite-based catalysts. During the standard SCR reaction, the NO conversion rate is thought to depend on the concentrations of NO, NH_3, and O_2. Few literature studies proposed simplified power-law kinetics for this reaction. The reaction order with respect to NO has been found to be about unity (+ 1) on these catalysts [34, 102, 111, 112]. It has also been reported that the reaction order with respect to ammonia is about 0 [102].

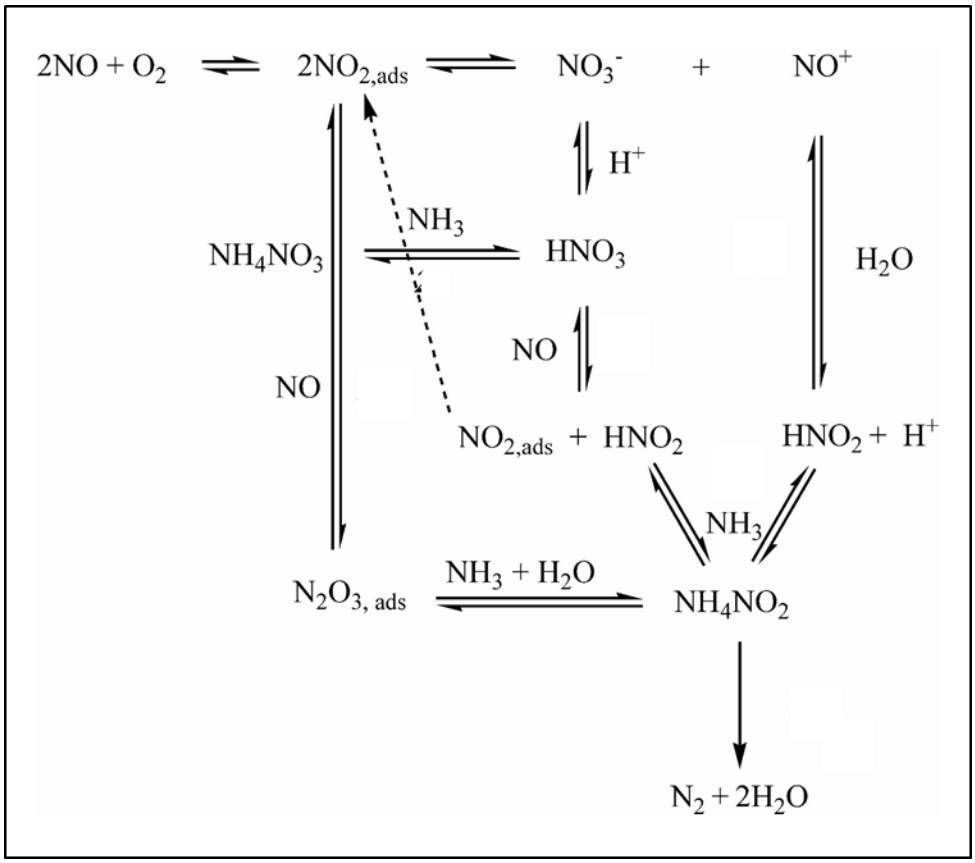

Figure 1-3: Reaction pathways for SCR over metal-exchanged zeolites [96].

However, NH_3 was found to have a slight inhibition effect on the standard SCR reaction in other literature studies [36, 103]. This inhibition is more pronounced at lower temperatures and is explained by the competitive adsorption of NH_3 and NO on the same sites [113] or by competitive consumption of adsorbed O_2 by gaseous NH_3, which decreases the NO oxidation activity and consequently the SCR activity [34]. Battiston et al. [114] observed a decrease in the oxidation state of iron from 2.9 to 2.3 after adding NH_3 to a gas feed containing exclusively NO in N_2. Thus the NH_3 inhibition can be attributed to the enhanced reduction of Fe^{+3} (to Fe^{+2}) in the presence of NH_3. The standard SCR reaction has been found to have a positive order rate dependence on the feed O_2 concentrations, where the reaction order is reported to be around 0.5 [103, 111].

Water was found to inhibit the SCR reactions slightly. The overall activation energy of the standard SCR reaction was found to be in the range of 40-60 kJ/mol [103, 115]. Based on these observations, detailed kinetic models have been proposed in the literature. The zeroth reaction order with respect to ammonia indicates a reaction between ammonia from a strongly adsorbed state and NO from the gaseous or weakly adsorbed state. Thus a few studies support an Eley-Rideal type mechanism. Along with this Eley-Rideal type mechanism, some studies proposed a Langmuir-Hinshelwood kinetic rate expression where a surface reaction between adsorbed NOx and NH_3 has been considered [36, 115]. A few other studies provided global kinetic models for the standard SCR reaction under steady-state conditions for different zeolite catalysts [102, 113, 116]. Olsson and coworkers carried out a detailed kinetic modeling study of NH_3-SCR reactions on both the Fe- and Cu-zeolite catalysts [100, 117-120]. Their kinetic model considers the effects of transients and the NO-to-NO_2 ratio. Chatterjee et al. [78, 121] presented a global kinetic model on zeolite-based catalysts. Their model can adequately describe transients and steady-state conversion and the effect of NO_2 in the feed. They combined the NOx storage and reduction catalyst (or lean NOx trap) and the catalyst for selective catalytic reduction of NOx by NH_3 (NH_3-SCR) in their modeling studies to successfully predict the performance of an actual diesel exhaust aftertreatment system [121]. Similar kinetic models have been developed by Markatou and coworkers on both the Fe- and Cu-zeolite catalysts [122, 123]. Malmberg et al. [124] presented a transient model for NH_3 SCR with NO over an Fe-zeolite. Overall, all these kinetic models predict both the steady-state and transient kinetics for various SCR reactions on the zeolite-based catalysts. These models consider global kinetic reactions for ammonia adsorption and desorption, NH_3 oxidation,

NO oxidation, standard SCR, fast SCR, NO_2 SCR and N_2O formation. Recently, Colombo et al. [51] published their results on the kinetic modeling studies of a commercial Fe-zeolite catalyst. Along with the above global reactions, their kinetic model accounts for the additional reaction of N_2O decomposition to N_2 and O_2 and the reduction of N_2O by NH_3 (i.e. N_2O SCR reaction).

1.7 Research Objectives and Outline

The overall objective of this work is to study the kinetics and mechanistic aspects of various reactions involved in the SCR chemistry on Fe- and Cu-zeolite catalysts. We carried out a comprehensive experimental and kinetic modeling study of SCR of NOx with NH_3 on various Fe- and Cu-zeolite catalysts. Different zeolite catalysts (Fe-ZSM-5, Cu-ZSM-5 and Cu-chabazite) were studied for this purpose. Some of these catalysts were synthesized in our laboratory and the performance was compared with that of the commercial catalysts. As described earlier, few studies focused on the mechanistic aspects of Fe- and Cu-zeolite (especially ZSM-5) catalysts are available in the literature. But the Cu-chabazite catalyst is a recently developed small pore zeolite catalyst and is considered as a much more active and stable catalyst compared to that of the existing Fe- and Cu-zeolite catalysts. We studied the mechanistic aspects of SCR reactions in detail on this catalyst along with the other Fe-ZSM-5 and Cu-ZSM-5 catalysts. Various reactions were considered for this purpose and these included: standard SCR, fast SCR, NO_2 SCR, NO oxidation, NH_3 oxidation, NOx and NH_3 uptake. We carried out both the steady state and transient experiments. With the help of these data, we have developed mechanistically based predictive kinetic models to accurately capture the key trends of

these reactions on both the Fe- and Cu-zeolite catalysts. All these reactions were carried out on washcoated monolithic catalysts. In a heterogeneous gas-solid reaction system on a monolithic catalyst, a molecule in the gas phase diffuses from the bulk gas phase to the gas-solid interphase and then into the catalyst deposited in the form of a washcoat on a monolithic support. The reaction takes place in the catalyst or solid phase. Thus the different processes of reaction, convection and diffusion are occurring simultaneously in a catalytic monolith. The mass transfer limitations (both external and internal) play a vital role in this reaction system. External mass transfer limitations can be important at very high temperatures. But internal mass transfer limitations are important over a wide temperature range and depend upon various parameters like washcoat thickness, reaction rates, channel dimensions, etc. These mass transfer limitations were not covered in detail in the current SCR literature. Also, the inclusion of these mass transfer limitations in a kinetic/reactor model makes the problem computationally challenging and more time consuming. Hence most of the kinetic/reactor models available in the literature neglect these diffusion limitations. We have carried out a systematic experimental and modeling study focused on the importance of these diffusion limitations. Experiments carried out on monolith catalysts having different washcoat loadings, washcoat thicknesses and lengths indicate the presence of washcoat (or pore) diffusion limitations in an intermediate to high temperature range in all the SCR reactions. A detailed analysis of the effect of temperature on the transitions between various controlling regimes (kinetic, washcoat diffusion and external mass transfer) is presented in this work. Experimental studies on Fe-ZSM-5 and Cu-chabazite catalysts are performed to study the transient and steady-state characteristics of the NO oxidation reaction. A detailed kinetic model for NO

oxidation is developed to predict the experimental data. We have developed a detailed two-dimensional, two-phase kinetic model to capture the experimental data for NH_3-SCR reactions. With the help of these fundamental understandings developed during the kinetics and mechanistic studies of SCR reactions on both Fe- and Cu-zeolite catalysts, we have designed new catalysts where Fe- and Cu-zeolite catalysts are arranged in the form of layers on the same monolith support. The NOx reduction activity on these catalysts is compared with the original catalysts and other catalyst arrangements. The specific objectives of this study are summarized below:

1. Synthesize and characterize Fe- and Cu-zeolite based powder and monolithic catalysts.
2. Conduct a comprehensive experimental study of steady-state and transient selective catalytic reduction of NOx with NH_3 on both commercial and lab-synthesized Fe- and Cu-zeolite catalysts.
3. Develop a fundamental understanding about the mass transfer limitations in various NH_3-SCR reactions on both Fe- and Cu-zeolite catalysts.
4. Elucidate the kinetics of NO oxidation using a combination of experimental and modeling studies.
5. Design new catalysts to improve the NOx removal efficiency over a wide temperature range of practical interest.
6. Develop a mechanistically based kinetic model predicting key features of various reactions involved in the SCR chemistry.

The dissertation is organized as follows: Chapter 2 describes the experimental set up, catalyst synthesis and characterization techniques. Chapter 3 focuses on the steady

state and transient kinetic studies of selective catalytic reduction of NO on Fe-ZSM-5 catalysts. The performance of lab-synthesized catalysts is compared with that of a commercial catalyst. Also, we elucidate the reaction mechanism for the standard SCR reaction. Chapter 4 describes the effect of NO_2 on the steady state and transient kinetics of various SCR reactions of Fe-ZSM-5 catalyst. Chapter 5 presents a comprehensive experimental study of steady state and transient kinetics of various SCR reactions on the recently developed small pore Cu-chabazite catalyst. The results obtained on the Cu-chabazite catalyst are compared with Fe-ZSM-5 catalyst. Chapter 6 demonstrates the importance of mass transfer limitations in SCR of NOx with NH_3 on both the Fe- and Cu-zeolite catalysts. We present an experimental study carried out on lab-synthesized monolithic catalysts having different washcoat loadings, thicknesses and lengths. The experimental results are corroborated with theoretical analysis. Chapter 7 presents a new catalyst design for the enhanced NOx removal efficiency over a wide temperature range of practical interest. Fe- and Cu-zeolite catalysts are arranged in the form of a layer on the same monolithic support. The performance of this dual-layer catalyst system is compared with single layer catalysts and other catalyst combinations including sequential brick/series arrangement and mixed waschoated catalysts. In Chapter 8, steady-state and transient experimental studies of NO oxidation are reported. A comparison is made between Fe- and Cu-zeolite catalysts. The experimental study is followed by an analysis of the microkinetic reaction mechanism and the development of the global kinetic model. Chapter 9 presents a kinetic modeling study of SCR of NOx on both the Fe- and Cu-zeolite catalysts. The kinetic model accounts for all the global reactions occurring in the SCR chemistry. Also, it accounts for the diffusion limitations in washcoat. Thus we

present a detailed two-dimensional, two-phase model. Finally, the model is used to predict the performance of combined Fe- and Cu-zeolite catalyst systems. The final Chapter (Chapter 10) of the dissertation summarizes the main conclusions of this work. In addition, recommendations are given for future research.

CHAPTER 2 Experimental

2.1 Introduction

This chapter consists of a detailed description of the experimental procedures used in this study. The catalyst synthesis and characterization techniques for different Fe- and Cu-zeolite catalysts are described in detail. All the catalysts tested were monolithic. A bench-scale reactor set-up was used to carry out the experimental procedure. Various components of this set-up are covered in this chapter. The catalyst samples and the specific experimental conditions under which they were examined are described in the respective chapters discussing them.

2.2 Catalysts

Various catalysts are available and widely used for the selective catalytic reduction (SCR) of NOx with NH_3. The focus of current study is on Fe- and Cu-zeolite based catalysts. Both the commercial and lab-synthesized catalysts were used to study the kinetics and mechanistic aspects of various reactions involved in the SCR chemistry.

The commercial Cu-zeolite catalyst was supplied by BASF (Iselin, NJ). It is a small-pore Cu-chabazite type catalyst, established in patents and communicated in recent papers to possess excellent hydrothermal stability [125-127]. The pore size of the chabazite structure is about 0.36 nm and is small compared to that of ZSM-5 with a pore size of 0.55 nm. More detail about the synthesis and structure of this Cu-chabazite catalyst can be found in [127]. This catalyst was provided in a cylindrical shaped honeycomb structure where Cu-chabazite powder was deposited on the solid support. The cell density of this catalyst was 400 cells per square inch (cpsi). A commercially used

catalyst piece with 15 cm diameter and 7.5 cm length was provided by BASF. The Cu loading was about 2.5% (by weight). The commercial Fe-zeolite catalyst was provided by Umicore Autocat USA Inc. This catalyst is commercially used in the E320 class Mercedez [128]. The zeolite used in this catalyst was ZSM-5 type and the Fe content was equal to about 3% by weight. This catalyst was also provided in a honeycomb form where Fe-zeolite catalyst powder was deposited on a monolithic support. The cell density for the commercial Fe-ZSM-5 catalyst was 400 cpsi. A large cylindrical shaped catalyst piece with dimensions of about 20 cm width and 25 cm length was provided by Umicore. The bench scale reactor (described in the following section) used in this study required a small catalyst piece. In order to obtain a catalyst piece of required dimensions, a dry diamond saw was used. The majority of experiments reported here used a catalyst sample of 2 cm length and 0.9 cm diameter. This reactor was nearly cylindrical in shape and comprised of 34 channels. The total volume of this monolithic reactor was calculated to be 1.21 cm^3 with the estimated cross sectional area of about 0.63 cm^2. In addition to the commercial catalysts, several Fe-ZSM and Cu-ZSM-5 catalysts were synthesized in-house. The next section focuses on the details of catalyst synthesis procedure.

2.3 Catalyst Synthesis

Cu-ZSM-5 and Fe-ZSM-5 catalysts were synthesized in-house. All the experimental studies were carried out on the washcoated monolithic catalysts. In order to make the washcoated monolithic catalysts, Cu-ZSM-5 and Fe-ZSM-5 catalyst powder was required. This catalyst powder was prepared by a conventional ion-exchange procedure described as follows.

2.3.1 Ion Exchange

The Cu-ZSM-5 powder was prepared by a series of ion exchange and washing steps starting with the ammonium form and ending with the copper form of a zeolite; i.e., $NH_4^+ \rightarrow H^+ \rightarrow Na^+ \rightarrow Cu^+/Cu^{2+}$. A zeolite powder in the ammonium form (NH_4-ZSM-5 type) was provided by Sud-Chemie (Munich, Germany) and it had a Si/Al ratio of 25. The NH_4-ZSM-5 was converted into the protonated form by calcining the powder at 500 ^oC for 5 hours. Exchange of H^+ with Na^+ involved contacting the H-ZSM-5 with a 0.1 M $NaNO_3$ solution. The solution contained a concentration of Na^+ that was about twice the number of Al^{3+} ions. This ion exchange was carried out for 5-6 hours in a continuously stirred solution at ambient temperature and a pH of 7. NH_4OH or acetic acid was used to adjust the pH of the solution. After the ion exchange was completed the particles were filtered and dried at 110 ^oC for about 2 hours. This ion exchange procedure was repeated twice. Thus the H-ZSM-5 powder was converted to Na-ZSM-5 by ion-exchange by continuously stirring it in a 0.1 M $NaNO_3$ solution, followed by several steps of filtration and drying.

In the final step, Na-ZSM-5 was converted to Cu-ZSM-5 by performing ion-exchange in a solution containing copper acetate (0.02M) with the pH maintained at 5 in a stirred solution for about 24 hours. The amount of Cu^{2+} was roughly 1.5 times the number of Al ions in the zeolite. When complete, the solution was filtered and the powder was dried for 2 hours at 120 ^oC. This process was repeated twice to ensure that the Cu-form of the ZSM-5 was obtained. Finally, the Cu-ZSM-5 powder was calcined at 500 ^oC for 5 hours [89].

The Fe-ZSM-5 catalyst powder was synthesized using similar procedure described above for the Cu-ZSM-5 catalyst. The NH_4^+ form was converted to protonated (H^+) form by calcination (500 ^oC for 5 hour). The H-ZSM-5 powder was then converted to Na-ZSM-5 by ion-exchange by continuously stirring it in a 0.1 M $NaNO_3$ solution, followed by several steps of filtration and drying. Na-ZSM-5 powder was then ion-exchanged with $FeCl_2$ (0.02M) solution to get Fe-ZSM-5. The Fe-ZSM-5 powder, thus obtained was calcined for 5 hours at 500 ^oC. The method used for ion-exchange was similar to described in the literature [89]. Along with the in-house synthesized Fe-ZSM-5 powder, commercial Fe-ZSM-5 catalyst powder was provided by Sud-Chemie (Munich, Germany), and it was used to synthesize majority of Fe-based washcoated catalysts used in this work. The method for washcoating monoliths is described below.

2.3.2 Monolith Washcoating

Blank cordierite monoliths with cell density of 400 cpsi and dimensions of 1 inch diameter by 3 inch length were supplied by BASF (Iselin, NJ). The catalyst powder in the form of a Fe-ZSM-5 or Cu-ZSM-5 was deposited on these blank monolith supports using a method of dip-coating. In this method, a slurry containing a mixture of zeolite catalyst, γ–alumina and water was prepared and a blank monolith piece was dipped inside the slurry to get washcoated monolithic catalysts. The particle size, viscosity, pH and slurry solids content were important parameters in achieving a uniform washcoat [129, 130]. A slurry containing a mixture of zeolite catalyst, γ–alumina and water was prepared in the proportions 32 wt.% zeolite, 8 wt.% alumina with the remainder water and a small amount of 0.1N acetic acid to obtain a pH of 3.5. Alumina served as a binder. A particle

size of 1-5μm is desirable to achieve a uniform waschoat [131]. This was achieved by ball-milling the aqueous slurry for about 20 hours. Previous studies have also shown that the slurry viscosity should be sufficiently low and therefore the solids content should not be more than 50% by weight of the overall slurry. The blank monolith piece was dipped in the slurry for 1 minute, successively from both ends. Excess slurry was removed by flowing compressed air through the monolith channels for a fixed time of 15 seconds from both the ends. The washcoated monolith catalyst was then dried at 120 ^{o}C for 2 hours and weighed to quantify the loading of the deposited washcoat. This stepwise dipping and drying process was repeated until the desired quantity of catalyst was deposited in the form of a washcoat on the monolith support. The washcoated catalyst was subjected to calcination at a very slow temperature ramp of ca. 23 ^{o}C/hr up to and maintained at 500 ^{o}C for 5 hours. The deliberate calcination reduced the likelihood of crack formation in the washcoat layer. The washcoated catalyst was then analyzed for its components using Inductive Coupled Plasma (ICP) and Energy Dispersive Spectroscopy (EDS) techniques.

2.4 Catalyst Characterization

The catalyst powder was characterized by X-ray diffraction (XRD; Siemens D5000). The Inductive Coupled Plasma (ICP) technique was used to quantify the components present in the catalyst. Scanning Electron Microscope (SEM) (JEOL JSM-6330F) was used to measure the washcoat thickness and to assess its uniformity in different channels. Energy Dispersive Spectroscopy (JEOL JSM-6330F) was used to quantify the elemental composition of the washcoated monolith catalyst. The specific

surface area of the zeolite powder was measured with a BET surface area analyzer (Coulter model 3100).

2.5 Experimental Set-up

A bench-scale reactor set-up was used to carry out the experimental study. This set-up included a gas supply system, a reactor system and an analysis system. The experimental set up used here was the same as that used and described previously [128, 132, 133]. Figure 2-1 represents the schematic diagram of the experimental set-up comprising the above major components.

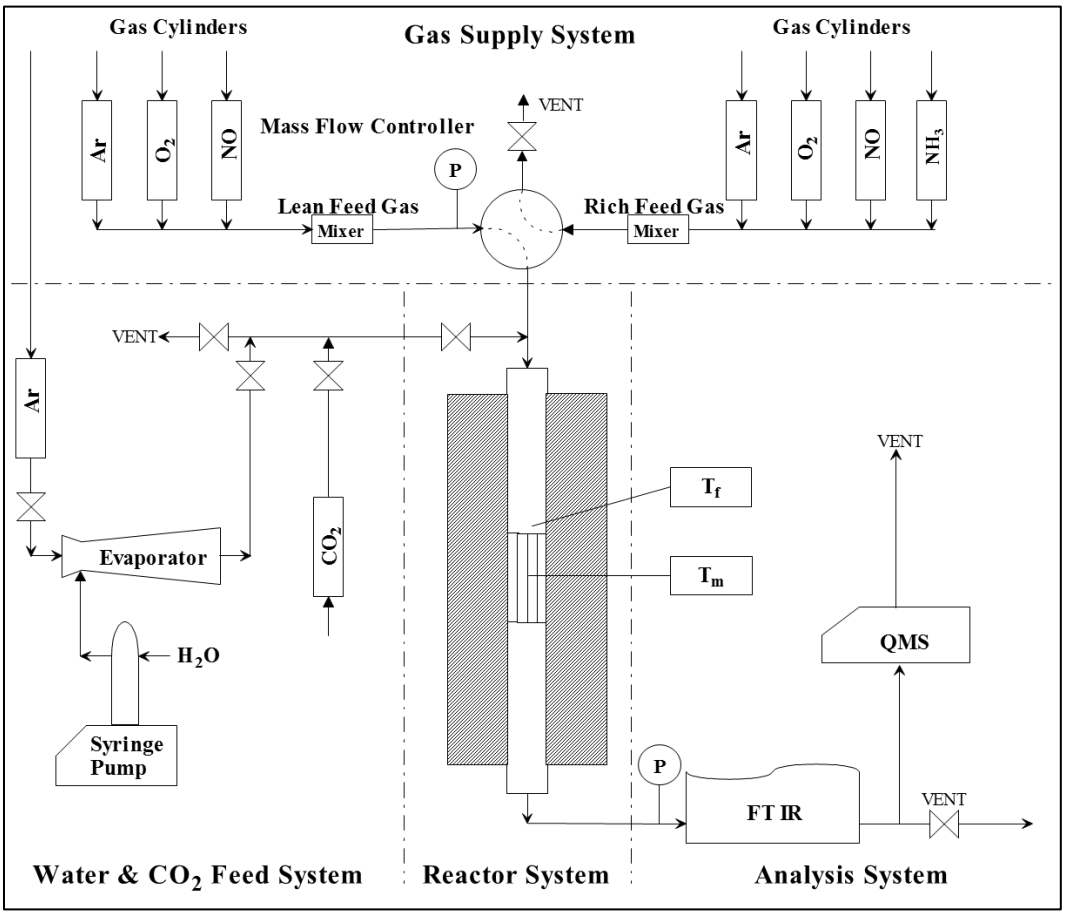

Figure 2-1: Schematic diagram of experimental set-up [133].

2.5.1 Gas Supply System

The gas supply system consisted of various compressed gas cylinders through which gases were introduced into the reactor system. The gas cylinders were supplied by Matheson Tri-Gas. Pressure regulators maintained the inlet pressure from the gas cylinders. The flow rates of the gases were controlled by mass flow controllers (MFC; MKS Inc.). Different MFCs were used to control the flow rates of different gases. Depending upon the concentration requirement of a particular gas, maximum flow rate capacity of the MFC was decided. Each MFC was calibrated for the appropriate flow range that would be used in the experiments or calibration of the analytical instruments like FT-IR or QMS. In order to calibrate the MFCs with higher flow rates (400 standard cubic centimeters per minute (sccm) and above), a bubble meter and a stop watch were used to determine the time for one bubble to move through a specific volume. For calibrating the MFCs with medium flow rates (5-400 sccm), a digital flow meter (Humonics Hewlett Packard Optiflow 250) was used. For MFCs with lower flow rates (< 10 sccm), a smaller bubble meter was used for the calibration following the same procedure as that for the MFCs with higher flow rates. Further details about the MFC calibrations procedure and the calibration curves are provided in [132]. All the gases leaving MFCs were mixed using an in-line static mixer prior to the reactor system. The specifications of all the feed and calibration gases are listed in Table 2-1 and Table 2-2.

Table 2-1: Specifications of pure gases used in the experiments.

Gas	Use	Specifications
Ar	Diluent for reactive feed gas, purge gas for reactor, QMS calibration gas	Ultra high purity: > 99.999% purity, < 1 ppm CO_2, < 1 ppm CO, < 15 ppm N_2, < 3 ppm O_2, 5 ppm H_2O
He	Pressurizing of switching valve	Ultra high purity: > 99.999% purity
O_2	Reactant gas	Ultra high purity: > 99.98% purity, < 1 ppm CO_2, < 1 ppm CO, < 15 ppm N_2, 5 ppm H_2O
H_2	Reactant gas	Ultra high purity: > 99.999% purity, < 1 ppm CO_2, < 1 ppm CO, < 7 ppm N_2, < 2 ppm O_2, 3 ppm H_2O
N_2	Adsorption gas for BET	Ultra high purity: > 99.999% purity, < 1 ppm CO_2, < 1 ppm CO, < 2 ppm O_2, 3 ppm H_2O

Table 2-2. Specifications of gas mixtures used in the experiments and calibrations.

Gas	Balance Gas	Use	Specifications
1% NO	Ar	FT-IR calibration gas, Reactant gas	Certified standard
1% NO_2	Ar	FT-IR calibration gas, Reactant gas	Certified standard
1% NH_3	Ar	FT-IR calibration gas, Reactant gas	Certified standard
1% N_2	Ar	QMS calibration gas	CP grade: > 99.5% Purity
5% N_2O	Ar	FT-IR calibration gas	CP grade: > 99.5% Purity
3% H_2	Ar	QMS calibration gas	CP grade: > 99.5% Purity

The actual exhaust coming out of vehicles contains water vapor. In order to simulate the real exhaust conditions, it was essential to have a water supply system in the

experimental set-up. For this purpose, an Isco pump (Model 5000 syringe pump) and a vaporizer were used. Before introducing the water into the evaporator, the water went through a poppet valve which was set to 100 psi and the heating tape was set at around 300 ^{o}C. The high pressure and the high temperature instantly vaporized the water as it exited the poppet valve. Around 500 sccm Ar was flowed through the evaporator to carry the steam to the reactor downstream. The total gas flow rate was kept constant at 1000 sccm in the majority of the experiments.

2.5.2 Reactor System

The reactor system consisted of a quartz tube flow reactor with dimensions of 0.32" I.D. and 0.50" O.D. The length of the quartz reactor was approximately 16". The quartz tube reactor was kept inside a 500 W Mellen single zone furnace (model SC11) and was used as a heater for the reactor. The furnace temperature was controlled by a Mellen Temperature Control System (model PS305), with an over-temperature alarm and single-zone programming option. The maximum operating temperature of the furnace was 1100 ^{o}C. A four-port, dual-actuated switching valve was placed upstream of the reactor. A switching valve was used to direct the appropriate flow stream to the reactor and was operated by Labtech software. Catalyst samples were wrapped with Fiberfrax ceramic paper that had been heat treated at 120 ^{o}C for approximately 12 hours. This prevented any bypassing around the catalyst during the experiments. The monolith temperature (T_m) was measured by K-type thermocouple (0.5 mm O.D.).

2.5.3 Analysis System

An analysis system was required for the exact measurement of the concentrations of the gases leaving the reactor system. The analysis system was thus placed downstream of the reactor system and it was comprised of a FT-IR spectrometer (Thermo-Nicolet, Nexus 470) and a quadrupole mass spectrometer (QMS; MKS Spectra Products; Cirrus LM99). All the gas lines downstream of the reactor system were kept heated to avoid condensation of any gases in the pipelines. In the FT-IR, a separate sample cell was used. It was an ultra-low volume (25 cm^3) gas cell (Axiom, Mini Linear Flow Cell) with BaF_2 windows. The path length of the cell was 0.5 m. The FT-IR was used to measure various gas species which included NO, NO_2, N_2O, NH_3, CO, CO_2, H_2O, etc. The FT-IR was calibrated for these gases using standard calibrations and some of these standards are listed in Table 2-3.

Table 2-3: Gas standards used for FT-IR [128].

Component	Concentration (ppm)	Pressure (mm Hg)	Region (cm^{-1})
NO	500	880	1871.4-1940.0
NO_2	500	880	1578.8-1613.8
N_2O	1000	880	1248.8-1325.3
NH_3	500	880	920.0-970.0
H_2O	50000	880	3750.0-3950.0

The QMS was used to measure N_2 and H_2. It was positioned 0.7 m downstream of the FT-IR. From the exit of the FT-IR, a separate line with a thin capillary tube on the inside was introduced into the QMS. The flow rate through the line was about 30 sccm.

2.5.4 Data Acquisition

The data acquisition system consisted of an ADAM 5000 TCP module and two computers. ADAM 5000 TCP module (Advanced Ind.) converted the analog signals from the thermocouples, pressure gauge and mass flow controllers into digital signals. The first computer had Labtech® software to collect these data. Also, the data from QMS was collected on this computer using Process Eye software. The FT-IR composition data was collected on the second computer using OMNIC® software (Thermo Nicolet; version 6.2). The details about the calibration procedure for the FT-IR and QMS are described in [132]. All the three software packages (OMNIC, Process Eye and Labtech) store data in the form of text files which were later converted to Excel spreadsheets to analyze. At the start of each experiment, it was attempted to start all the software simultaneously. But there was always some difference in the timing of the data recorded because different analysis systems were at different distances from the reactor. This difference in the times was considered during the data analysis. The operating, shut down and safety procedures of the bench scale reactor set-up were the same as described in [132].

CHAPTER 3 Selective Catalytic Reduction of NO with NH_3 on Iron Zeolite Monolithic Catalysts: Steady-State and Transient Kinetics

3.1 Introduction

SCR is the most efficient aftertreatment technology for converting NOx into molecular nitrogen in the presence of oxygen from the lean exhaust of stationary sources and vehicles. The two most common SCR catalysts in development for vehicular applications are Fe- and Cu-based zeolites [134, 135]. The common point-source SCR catalyst, $V_2O_5/TiO_2/WO_3$, has insufficient activity at lower temperature and inadequate durability at higher temperatures for mobile applications (>400 ^oC). Both Cu- and Fe-exchanged ZSM-5 have been of recent interest given their higher activity and lower cost. Cu-ZSM-5 has the higher of the two low temperature activities [87]. The overall SCR chemistry is generally well established and qualitatively similar for V_2O_5-WO_3/TiO_2, Cu-zeolite and Fe-zeolite catalysts. This chemistry has been summarized in Chapter 1.

The NOx emitted from diesel engines is mainly composed of NO, some of which is oxidized to NO_2 upstream of the SCR reactor. It is well established that the ammonia (obtained from urea hydrolysis) reacts with NO and NO_2 in the presence of O_2 at different rates. The reaction between NO and NH_3 involving O_2 is the "standard SCR" reaction and is given by

$$4\ NH_3 + 4\ NO + O_2 \rightarrow 4\ N_2 + 6\ H_2O \qquad \Delta H = -4.07 \times 10^5\ J/mol\ NH_3. \qquad (3\text{-}1)$$

The reaction between NO_2 and NH_3 is NO_2 SCR reaction and is given by

$$4\ NH_3 + 3\ NO_2 \rightarrow 3.5\ N_2 + 6\ H_2O \qquad \Delta H = -3.41 \times 10^5\ J/mol\ NH_3. \qquad (3\text{-}2)$$

The reaction between NH_3 and an equimolar mixture of NO and NO_2 is often referred to as the "fast SCR" reaction and is given by

$2\ NH_3 + NO + NO_2 \rightarrow 2\ N_2 + 3\ H_2O \qquad \Delta H = -\ 3.78 \times 10^5\ J/mol\ NH_3.$ (3-3)

Along with these three main reactions, several side reactions may occur in the SCR system [20, 21, 24, 29, 31, 33, 37-39, 43, 136]. An overall mechanistic picture has been proposed by Tronconi and coworkers [24, 25, 27, 33] for the reduction of NOx by NH_3 on vanadia-based catalysts. This picture explains differences in the reduction rate between the standard and fast reaction pathways. During the standard SCR reaction, the oxidation of reduced vanadia sites by gas phase O_2 is considered the rate determining step. The oxidized sites may also lead to the formation of NO_2, which is considered to react with vanadyl species, forming surface nitrates. These nitrates then react with adsorbed ammonia, forming N_2 or N_2O, the latter via NH_4NO_3. This pathway is distinctive to NO_2, and is faster than the standard pathway involving catalyst reoxidation and reaction with NH_3.

The kinetics of the V_2O_5-WO_3/TiO_2 catalyst are well established. The standard and fast SCR reactions are generally considered to involve reaction between adsorbed NH_3 and gas phase NO and/or NO_2; i.e. Eley-Rideal (ER) kinetics [57, 137]. This is because ammonia strongly binds compared to NO which has much less adsorption under similar conditions. Nova et al. [25, 27] reported an inhibiting effect of ammonia on the standard SCR rate and proposed a redox kinetic model for the NOx reduction on V-based catalysts. This feature was attributed to the blocking of active sites by spillover of NH_3 from adjacent adsorption sites. Other researchers [36, 116] have proposed a Langmuir-Hinshelwood kinetics for standard SCR reaction considering the co-adsorption of NO and NH_3 on the SCR catalyst.

Compared to the vanadia system, there have been fewer SCR kinetics studies on the Fe-based zeolite catalysts. Sjovall et al. [120, 136] presented a global kinetic model for SCR reaction over Cu-ZSM-5 and commercial Fe-zeolite monolith catalysts. Iwasaki et al. [36] reported kinetics for both the standard and fast SCR reactions on an Fe-ZSM-5 powder catalyst. Reaction orders for the standard SCR reaction were 0.81-0.88 for NO, 0.29-0.34 for O_2 and -0.21 to -0.11 for NH_3. Following earlier results for the vanadia catalyst system, they proposed NO oxidation as the rate determining step during the standard SCR chemistry. Huang et al. [34] carried out similar studies on powdered Fe-ZSM-5 catalyst and reported that the SCR reaction orders are 0.88-0.94 for NO, 0.36-0.41 for O_2 and -0.15 to -0.11 for NH_3. Similar kinds of studies reporting reaction orders on other powder catalysts are available in the literature [102, 111, 138].

This work is a part of a larger project aimed at developing steady-state and transient kinetic models of SCR reactions taking place on zeolite-based monolithic catalysts. The objective of the current study is to carry out differential and integral flow reactor experiments of NH_3 based SCR of NO on Fe-ZSM-5 monolith catalysts. As mentioned earlier, most previous studies involved powder catalysts and only a few reports of kinetics have appeared. In addition to reporting apparent reaction orders and activation energies for the standard SCR and NO oxidation reactions, we reconcile key reaction pathways and selectivity trends for both the steady-state and transient experiments. An apparently counterintuitive effect of water on the rates of NO oxidation and reduction by NH_3 is studied and elucidated. Comparisons are also made between a commercial Fe-ZSM-5 and a series of lab-synthesized Fe-ZSM-5 monolithic catalysts having different Fe loadings and washcoat thicknesses. Finally, we assess the

contributions by washcoat diffusion and external mass transport using catalysts with different lengths and washcoat thicknesses.

3.2 Experimental

3.2.1 Catalyst Preparation: Ion Exchange

The reaction studies were carried out on both the commercial Fe-zeolite and in-house synthesized Fe-ZSM-5 monolithic catalysts. For most of the experiments, commercial Fe-ZSM-5 powder provided by Sud-Chemie (Munich, Germany) was used. Cylindrical cores were cut from either a full-scale monolith (commercial catalyst) or smaller (1×3 inches) experimental cores (in-house) using a diamond saw. The in-house catalysts were prepared by dip-coating a blank cordierite monolith with a slurry comprising a mixture of the Fe-ZSM-5 and γ-alumina powder. The Fe-ZSM-5 was prepared by a series of ion exchange and washing steps starting with the ammonium form and ending with the iron form; i.e., $NH_4^+ \rightarrow H^+ \rightarrow Na^+ \rightarrow Fe^{2+}/Fe^{3+}$. The Fe-ZSM-5 powder was calcined at 500 ^oC for 5 hours [89]. The ion-exchange procedure is described in detail in Chapter 2.

3.2.2 Catalyst Preparation: Monolith Washcoating

Blank cordierite monoliths with cell density of 400 cpsi and dimensions of 1 inch diameter by 3 inch length were supplied by BASF (Iselin, NJ). The particle size, viscosity, pH, and slurry solids content are important parameters in achieving a uniform washcoat [129, 130]. A slurry containing a mixture of zeolite catalyst, γ–alumina, and water was prepared in the proportions 32 wt.% zeolite, 8 wt.% alumina, with the

remainder water and a small amount of 0.1N acetic acid to obtain a pH of 3.5. Alumina served as a binder. Nijhuis et al. [131] suggested that to obtain a uniform washcoat a particle size of 1-5μm is desirable. This was achieved by ball-milling the aqueous slurry for about 20 hours. Previous studies have also shown that the slurry viscosity should be sufficiently low and therefore the solids content should not be more than 50% by weight of the overall slurry. The blank monolith piece was dipped in the slurry for 1 minute, successively from both the ends. Excess slurry was removed by flowing compressed air through the monolith channels for a fixed time of 15 seconds from both the ends. The washcoated monolith catalyst was then dried at 120 ^{o}C for 2 hours and weighed to quantify the loading of the deposited washcoat. This stepwise dipping and drying process was repeated until the desired quantity of washcoat was deposited on the monolith support. The washcoated catalyst was subjected to calcination at a very slow temperature ramp of ca. 23 ^{o}C/hr up to and maintained at 500 ^{o}C for 5 hours. The deliberate calcination reduced the likelihood of crack formation in the washcoat layer. The washcoated catalyst was then analyzed for its components using Inductive Coupled Plasma (ICP) and Energy Dispersive Spectroscopy (EDS) techniques, described below.

3.2.3 Catalyst Characterization

The catalyst powder was characterized by XRD (Siemens D5000). The Inductive Coupled Plasma technique was used to quantify the components present in the catalyst. Scanning Electron Microscope (SEM) (JEOL JSM-6330F) was used to measure the washcoat thickness and to assess its uniformity in different channels. Energy Dispersive Spectroscopy (JEOL JSM-6330F) was used to quantify the elemental composition of the

washcoated monolith catalyst. The specific surface area of the zeolite powder was measured with a BET surface area analyzer (Coulter model 3100).

The results of characterization testing of the commercial Fe-ZSM-5 sample and representative in-house samples are shown in Table 3-1. The Fe loading in the commercial catalyst was found to be 3.5 (±0.5) (wt. %). The washcoat thickness of the commercial catalyst was 45-50 μm; this is a peripheral-averaged value since, as expected, the washcoat is considerably thicker in the corners (150 μm) than on the sides (25 μm) as shown in Figure 3-1. In-house monolith samples were prepared with a range of average washcoat thickness (30-35 μm), corresponding to a catalyst loading of 18 wt.% (2.5 g/in^3). The notation for the synthesized monoliths were given by FeZ-NN, where NN is the loading of the washcoat.

3.2.4 Bench-Scale Reactor Set-up

The experimental setup included a gas supply system, a reactor system, an analytical system and a data acquisition system, all of which were described in more detail in Chapter 2 and elsewhere [132, 139-142]. Unless otherwise stated, the monolith catalyst samples used for most of the experiments had 34 channels and were 2 cm in length. The monolith catalyst was placed inside a quartz tube reactor mounted in a tube furnace coupled to a temperature controller. The catalyst was wrapped with a ceramic fiber to seal the space between the monolith and the reactor wall in order to minimize gas bypassing. A quartz fritz was placed at a distance of 1cm upstream of the monolith catalyst for uniform mixing of gases before entering the monolith catalyst. Prior to each experiment, the catalyst was pretreated with 5% O_2 in a total flow of 1000 sccm with Ar

Table 3-1: Characteristics of the commercial Fe-zeolite monolithic catalyst and the FeZ-18 catalyst.

Properties	Commercial Fe-zeolite Catalyst	FeZ-18 Catalyst
Si/Al ratio	27	25
Fe (wt% in the washcoat)	3.5 (± 0.5)	2.5 (± 0.5)
Al (wt % in the washcoat)	13-15	15-16
Si (wt % in the washcoat)	36-38	33-35
O_2 (Balance)	46	48
BET Surface Area (m^2/gm)	-	352
Washcoat Thickness (μm)	45-50	30-35

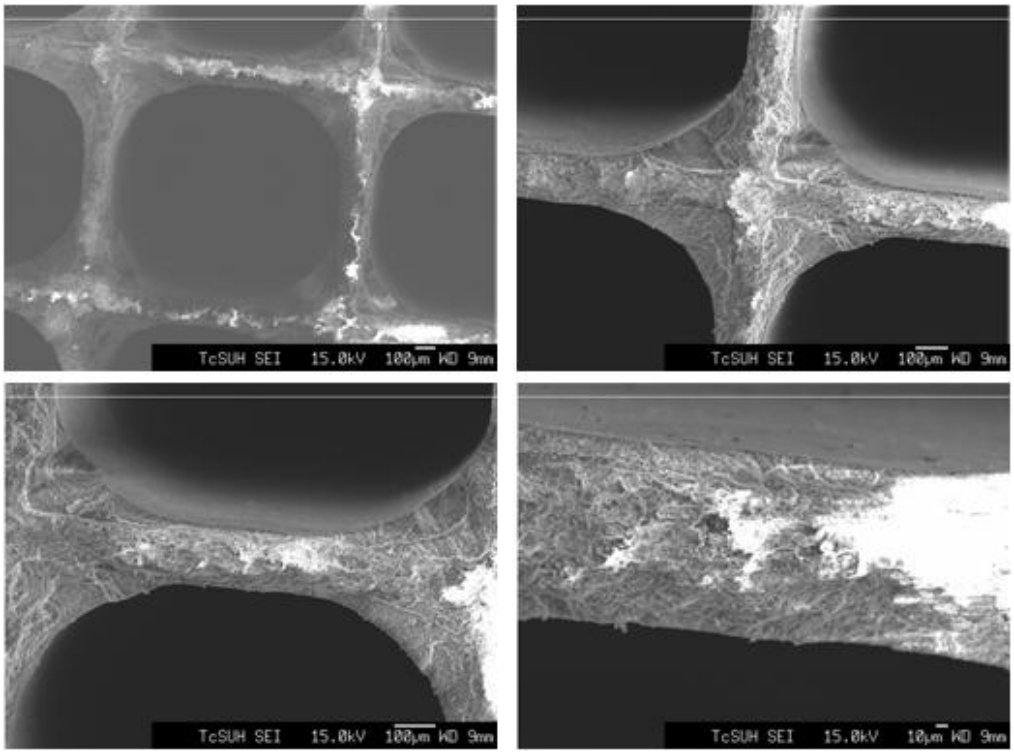

Figure 3-1: Scanning electron microscope images of the washcoated Fe-zeolite monolith catalyst are shown here. Washcoat is found to be in the circular shape with more deposition at the corners (150μm) compared to that in the center (25μm) of the channel.

(as balance gas) for 30 minutes at a temperature of 500 ^{o}C. In all the experiments Argon was the balance gas and a total flow rate of 1000 sccm was used. The total pressure was ca. 880 mm of Hg and was kept constant. A FT-IR spectrometer (Thermo-Nicolet, Nexus 470) and a quadrupole mass spectrometer (QMS; MKS Spectra Products; Cirrus LM99) were positioned downstream of the reactor to analyze the effluent gases including NH_3, NO, NO_2, N_2O and H_2O. The mass spectrometer was used to measure N_2.

Several types of experiments were carried out; (i) steady-state integral experiments (for NH_3 + NO + O_2, NH_3 + O_2, NO + O_2), (ii) steady-state differential experiments, (iii) transient ammonia uptake experiments, and (iv) sequential ammonia uptake and reaction with NO experiments. Experiment types (i) and (ii) were carried out at a constant temperature with sufficient time allowed for the system to reach steady-state. The reactor temperature was varied between 100 and 500 ^{o}C. Experiment types (iii) and (iv) were designed to measure the NH_3 uptake followed by a temperature-programmed desorption to quantify the NH_3 adsorption or by exposure to NO to carry out the transient reduction.

The ammonia uptake experiments involved the exposure of a pre-oxidized catalyst with a flowing Ar stream containing 500 ppm NH_3. After a prescribed exposure in which the effluent NH_3 concentration reached its feed value, the NH_3 was turned off (about 1 hour duration). About 30 minutes were allowed for weakly adsorbed NH_3 to desorb from the catalyst. Then a temperature ramp of 10 ^{o}C/min was applied to desorb the more strongly adsorbed NH_3. A range of inlet ammonia concentrations (50-500 ppm) were used with different initial temperatures (150-500 ^{o}C) for this study.

The oxidation of NH_3 and NO were carried out to assess the extent of these side reactions. Ammonia oxidation experiments were carried out over the commercial Fe-zeolite catalyst and results were compared with the FeZ-18 catalyst. The feed contained 500 ppm NH_3, 5% O_2 with Ar as a balance gas. NO oxidation reaction studies were also carried out on both the commercial Fe-zeolite and lab-synthesized FeZ-18 catalysts. The feed gas contained 500 ppm NO and 2-5% O_2 (with Ar as a balance gas). The above reactions were also studied in the presence of 2-5% H_2O. In order to study the inhibition of NO_2 on the NO oxidation reaction, a NOx (NO + NO_2) feed with varying NO_2/NOx (0, 0.25, 0.5, 0.75) ratios was fed to the reactor in the presence of 5% O_2.

The NH_3 + NO SCR reaction experiments were carried out on both the commercial Fe-zeolite and in-house synthesized (FeZ-NN) catalysts. The feed gas contained 500 ppm NO, 500 ppm NH_3, and 5% O_2. In order to understand ammonia inhibition in more detail, experiments were performed with different NH_3/NO feed ratios in the inlet. Here, three different NH_3/NO feed ratios (1, 2 and 3) were considered while keeping NO (500 ppm) and O_2 (5%) constant in the inlet feed. The effect of water on the SCR reaction system was also assessed by the addition of 2-5% H_2O in the inlet feed.

Differential reaction experiments were performed to quantify the kinetics (apparent reaction orders and activation energies). A shorter catalyst (4 mm) and wider range of total gas flow rates provided additional flexibility to achieve higher space velocity, and correspondingly lower conversions approaching differential conditions. Gas hourly space velocity (GHSV) as high as 285K hr^{-1} resulted in a NOx conversion below 15% for temperatures below 325 ^oC. During these experiments the feed NO concentration was varied over the range of 200-800 ppm while keeping the NH_3 concentration constant

at 500 ppm and O_2 at 5%. These data were used to determine the order of the SCR reaction with respect to NO. Similar experiments were performed to determine the reaction orders with respect to NH_3 and O_2. In the transient experiments, 500 ppm of NH_3 was introduced to the reactor along with inert gas Ar at the prescribed temperature. After the catalyst was saturated with ammonia, the feed ammonia was switched off and only Ar containing feed was flowed over the catalyst to remove loosely-bound ammonia. A feed containing NO and O_2 was then introduced to the reactor and transient response in the products and unreacted reactants were recorded with the FTIR and/or mass spectrometer.

3.3 Results and Discussion

3.3.1 Ammonia Uptake and Temperature Programmed Desorption

The strong affinity that the basic NH_3 has for the Bronsted acid sites on acidic zeolites like ZSM-5 is an important feature of the SCR reaction system. Ammonia is also known to adsorb on the Fe sites of an Fe-ZSM-5 catalyst. Zeolite catalysts have been found to have higher NH_3 storage capacity compared to the V-based catalysts [39, 87]. The adsorption capacity of the Fe-ZSM-5 catalyst was measured over the temperature range of 150-400 °C and for a range of NH_3 feed concentrations (50 – 500 ppm). The data for a typical NH_3 uptake and desorption experiment (150 ^oC) are shown in Figure 3-2. During the first 600 s, only the Ar carrier was fed to the reactor. At the 600 s time, the prescribed NH_3 concentration was fed to the reactor. NH_3 uptake occurred during the induction period preceding ammonia breakthrough. The NH_3 breakthrough time (adsorption extent) depended on both the NH_3 feed concentration and temperature. For example, the breakthrough time for a 500 ppm feed concentration at 150 °C was ca. 40 s

which was expectedly faster than the lower concentration feeds. After achieving saturation, the NH_3 inlet was shut off and the exit NH_3 concentration decreased monotonically to zero. During the 30 minute post uptake period, some physisorbed ammonia desorbed from the catalyst [128].

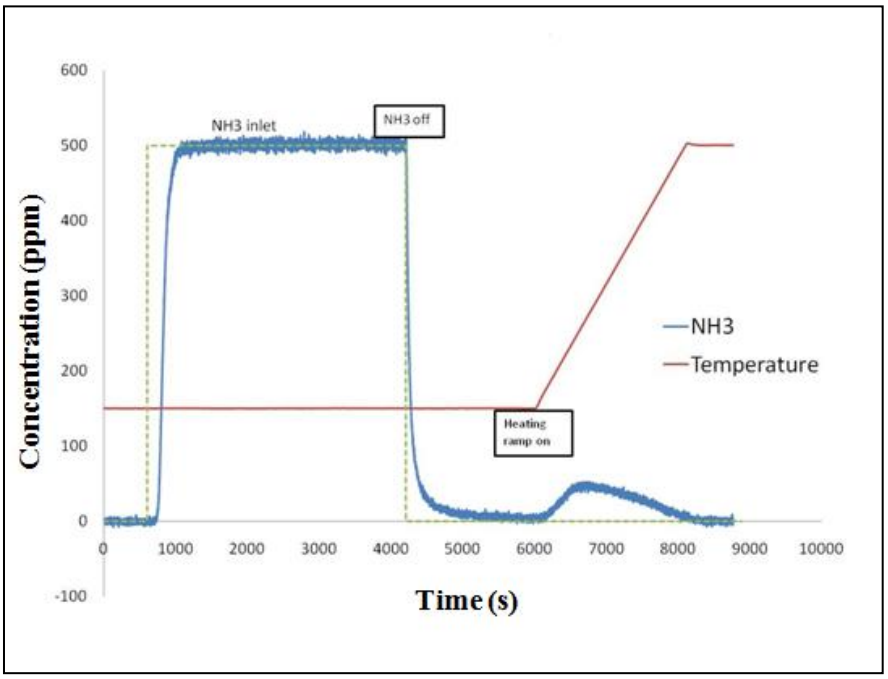

Figure 3-2: Results obtained with NH_3 TPD experiment with NH_3 adsorbed at 150 ^oC. A step change of 500 ppm NH_3 in Ar is given at 600 s; NH_3 switched off at 4200 s; temperature ramp of 10 ^oC/min at 6000 s.

The ammonia uptake is a function of both temperature and ammonia concentration. The amount of NH_3 could be quantified two ways. The first method involved the difference between the NH_3 in and the NH_3 out; the difference corresponded to the amount stored on the catalyst. The second method involved the sum of the physisorbed NH_3 and the desorbing NH_3 during the subsequent temperature ramp (10 ^oC/min). Good agreement was obtained with both methods. At higher temperatures, the ammonia uptake decreased. Figure 3-3 shows the dependence of NH_3 uptake on temperature for several NH_3 feed concentrations. Over the conditions investigated, the

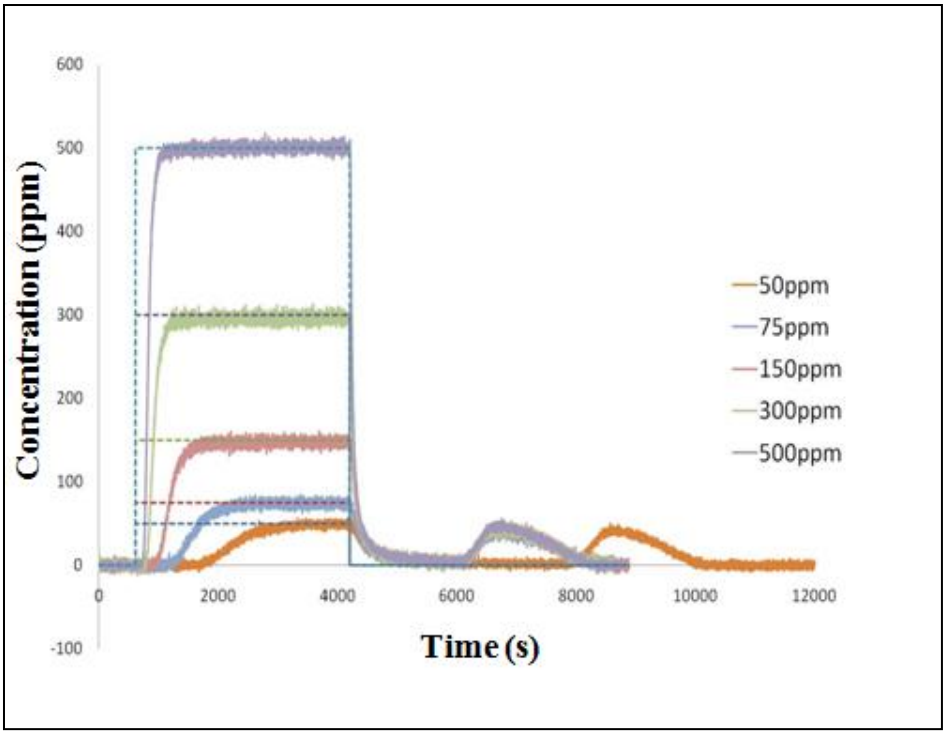

Figure 3-3: Experimental data obtained for NH_3 TPD experiments with NH_3 adsorption at 150 ^oC. A step change with various inlet concentrations of NH_3 (50, 75, 150, 300 and 500 ppm) at 600 s; NH_3 switched off at 4200 s; temperature ramp of 10 ^oC/min at 6000 s.

largest amount of NH_3 adsorbed was obtained for the 500 ppm NH_3 feed concentration at 150 °C; i.e., 0.37 moles NH_3/kg catalyst. Grossale et al.[39] reported the ammonia uptake capacity of 0.45 mol/kg catalyst under similar conditions. The data indicate that the NH_3 uptake follows a Langmuir type dependence on NH_3 feed concentration. An Arrhenius analysis of the temperature dependence gives an estimate for the heat of adsorption to be -115 kJ/mole. Recent works in the literature [25, 117, 118, 143] on various catalysts reported that the NH_3 heat of adsorption is a function of NH_3 coverage on the catalyst. The protracted desorption feature is consistent with the coverage dependence, so the -115 kJ/mole should be considered an averaged value.

The effect of H_2O on the ammonia adsorption was studied by co-feeding 5% H_2O with 500 ppm of NH_3 (with Ar balance gas) at 1000 sccm total flow rate. Water was

found to have only a negligible effect on the amount of NH_3 adsorbed. This is in line with the study of Grossale et al.[39] who did not find any effect on the NH_3 uptake capacity of the catalyst in the presence of H_2O. This result suggests that the catalyst surface acidity is not affected by H_2O over the range of temperatures considered. We return to this issue in the context of water inhibition of ammonia oxidation next.

3.3.2 Ammonia Oxidation

The oxidation of ammonia may occur in the SCR system and is detrimental because it lowers the effective NH_3 available for NOx reduction. It is critical to quantify the extent of the oxidation and product selectivities in order to fully elucidate the SCR reaction system. The oxidation of NH_3 produces N_2, N_2O, NO, and NO_2 by the following reactions:

$$4\ NH_3 + 3\ O_2 \rightarrow 2\ N_2 + 6\ H_2O \qquad \Delta H = -\ 3.12 \times 10^5\ \text{J/mol}\ NH_3, \qquad (3\text{-}4)$$

$$2\ NH_3 + 2\ O_2 \rightarrow N_2O + 3\ H_2O \qquad \Delta H = -\ 2.76 \times 10^5\ \text{J/mol}\ NH_3, \qquad (3\text{-}5)$$

$$4NH_3 + 5O_2 \rightarrow 4NO + 6H_2O \qquad \Delta H = -\ 2.27 \times 10^5\ \text{J/mol}\ NH_3, \qquad (3\text{-}6)$$

$$4NH_3 + 7O_2 \rightarrow 4NO_2 + 6H_2O \qquad \Delta H = -\ 2.84 \times 10^5\ \text{J/mol}\ NH_3. \qquad (3\text{-}7)$$

Zeolite based catalysts are highly selective towards N_2 formation. Yang et al. [44-46] reported nearly 100% selectivity to N_2 over a range of temperatures and feed ratios using a Fe-ZSM-5 catalyst.

Ammonia oxidation was studied over a wide range of temperatures (100-500 ^oC). The Fe-ZSM-5 catalyst was exposed to 500 ppm NH_3 (in Ar) for 20 minutes at 100 ^oC, after which 5% O_2 was admitted and sufficient time was allotted to reach steady state (about 25 minutes). The temperature was then increased in 50 ^oC increments. During

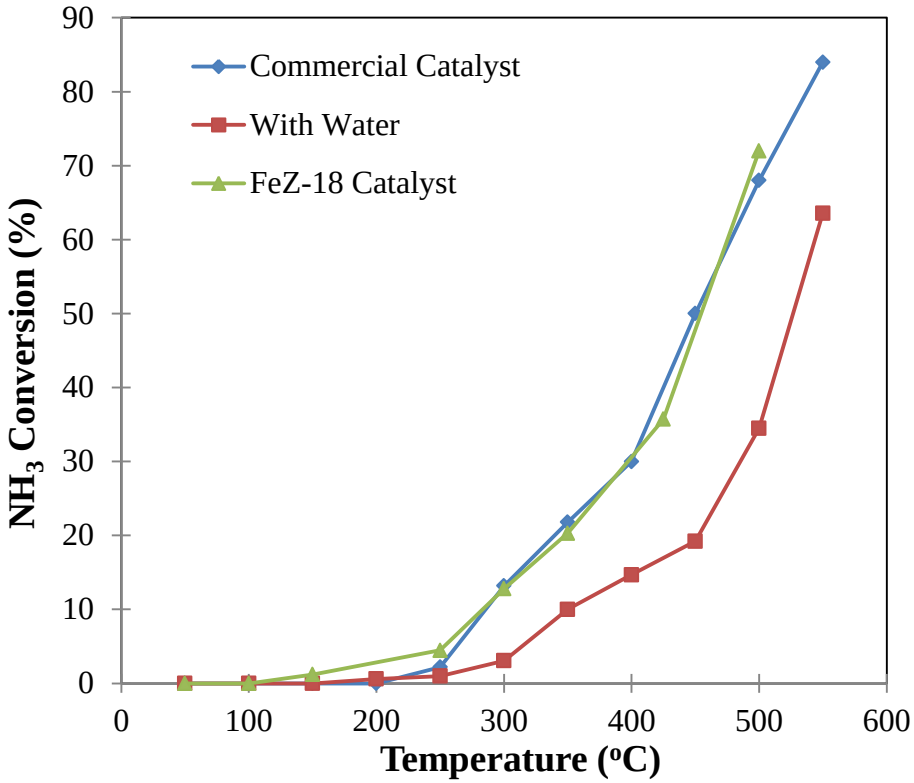

Figure 3-4: Comparison of the ammonia conversion during the ammonia oxidation on commercial and FeZ-18 catalysts. Effect of water on ammonia oxidation reaction is studied on the commercial catalyst.

each temperature rise, a transient evolution of ammonia occurred, the intensity of which decreased with increasing temperature. A similar behavior was observed in the ammonia TPD experiments. Figure 3-4 compares the steady-state NH_3 conversions obtained as a function of temperature for both the commercial catalyst and the in-house FeZ-18 catalyst. Negligible conversion was obtained for temperatures up to 250 ^{o}C. Further increase to 300 ^{o}C and higher led to significantly higher conversions with N_2 as the sole N-containing product. Only at 250 ^{o}C was a detectable amount of N_2O observed (5-10 ppm). The decrease in NH_3 concentration was complemented by a near-stoichiometric increase in N_2 concentration. In data not reported here, both NH_3 and O_2 have positive order effect on the ammonia oxidation rate. When the reaction system was studied in the presence of 2% H_2O, the NH_3 conversion dropped by about a factor of two up to 500 ^{o}C.

This decrease is attributed to H_2O blocking the active sites required for NH_3 oxidation. Since water was not found to inhibit the uptake of NH_3, this suggests that the reduction of the ammonia oxidation rate is a result of the inhibition of oxygen adsorption. We return to the effect of H_2O as it relates to the SCR reaction below.

3.3.3 NO Oxidation

Unlike the NH_3 oxidation, the oxidation of NO is desirable since NO_2 is much more reactive with NH_3 than NO [21, 22, 29, 31, 42, 68, 144]. This reaction is given by

$$NO + \tfrac{1}{2} O_2 \leftrightarrow NO_2 \qquad \Delta H = -5.7 \times 10^4 \text{ J/mol NO.} \qquad (3\text{-}8)$$

Most recent diesel aftertreatment systems include the diesel oxidation catalyst (DOC) upstream of the SCR catalyst. The Pt in the DOC serves to oxidize NO to NO_2. Here we report the NO conversion over the temperature range of 100 – 500 ^oC. In these experiments NO was initially fed to the reactor in the absence of O_2. The Fe-zeolite catalyst used in this study stored much less NO than NH_3 based on a much sharper increase in the NO effluent concentration to its inlet concentration. At that point 5% O_2 was admitted while maintaining 1000 sccm total flow rate.

Figure 3-5 reports the results for both the commercial and in-house Fe-ZSM-5 catalysts. As the temperature was increased from 100 ^oC, the NO concentration decreased to a minimum value and then increased. The maximum conversion was about 53% at 350 ^oC. During each temperature ramp, we did not observe any large peaks corresponding to NO desorption from the catalyst surface, unlike the large spikes observed for NH_3. This supports the fact that NO adsorption on the catalyst is rather weak compared to NH_3. The conversion maximum is clear evidence of an equilibrium limitation at higher

temperatures. The results obtained with the commercial Fe-zeolite and in-house catalysts are comparable.

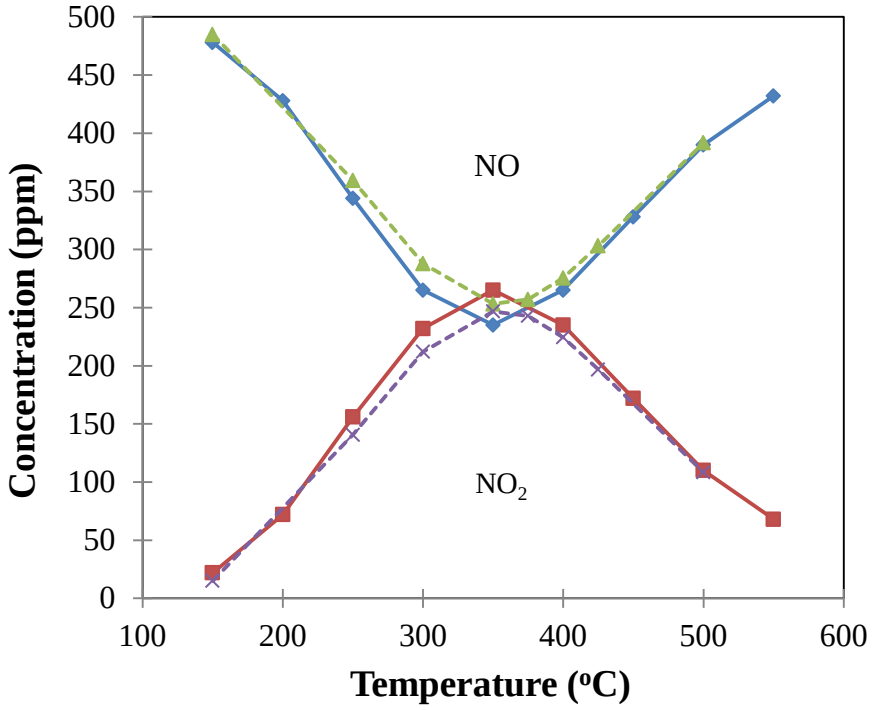

Figure 3-5: Concentrations of NO and NO_2 obtained during the NO oxidation reaction studies carried out on commercial and FeZ-18 catalysts. Feed: 500ppm NO, 5% O_2. Solid lines - commercial catalyst. Dashed lines: FeZ-18 catalyst.

Notwithstanding the upstream conversion of some of the exhaust NO to NO_2 in the DOC, NO oxidation is considered as one of the key reactions in the standard SCR chemistry and has been proposed to be the rate determining step in the literature [29, 36, 138, 145]. It is therefore appropriate to carry out the kinetic studies for this reaction system. We used a similar approach as that was used earlier for the standard SCR reaction (described later) in which a short piece of monolith catalyst was used to obtain very high space velocities up to 285K hr^{-1}. This enabled rate measurements under differential conditions (not exceeding 15%) for temperatures below 300 ^{o}C. As shown in Figure 3-5, the NO oxidation reaction is equilibrium limited for temperatures above 350 ^{o}C. Separate studies on NO_2 decomposition (not reported here) showed that this reaction

is negligible (≤ 1% NO_2 conversion) up to 300 ^oC. Thus differential kinetics for the forward reaction were obtained far from equilibrium. To determine the NO reaction order, the inlet NO concentration was varied from 200-800 ppm while keeping the O_2 concentration constant at 5%. To determine the reaction order with respect to O_2, the NO concentration was kept constant at 500 ppm while O_2 was varied from 0-5%. Based on the above differential kinetics studies, we found that the reaction was about first-order with respect to NO and positive half-order with respect to O_2.

In order to understand the individual effect of NO_2 on the NO oxidation reaction, we systematically increased the NO_2 fraction in the inlet feed from 0 to 0.75. Figure 3-6 shows the outlet NO_2/NOx ratio for various feeds with increasing NO_2 in the inlet. As mentioned for a pure NO feed, about 53% NO converted to NO_2 at 350 ^oC. The fractional NO conversion decreased for increasing NO_2/NOx ratios in the inlet feed. Figure 3-7 shows the drop in the NO conversion with increasing inlet NO_2/NOx ratios at various temperatures. NO conversions of 37% and 27% were measured at 350 ^oC for the NO_2/NOx inlet ratios of 0.25 and 0.50, respectively. For very high NO_2/NOx ratios ($\geq$ 0.75), no measurable NO conversion was detected at 350 ^oC since the NO_2 decomposition reaction was more pronounced under such conditions. These data clearly show an inhibiting effect of NO_2 on the NO oxidation reaction. The inhibition by NO_2 can be attributed to the competitive adsorption of NO_2 on the active sites available for NO oxidation reaction. NO_2 may also serve to oxidize the Fe sites, thereby preventing other species like, NO and O_2, in adsorbing and reacting on the surface [146]. We followed a similar approach of differential kinetics experiments (as described earlier) to determine the NO oxidation reaction order with respect to NO_2. Here, the feed NO_2 concentration

was systematically varied from 50-500 ppm while keeping NO (500 ppm) and O_2 (5%) concentrations constant. Figure 3-8 shows that the rate of NO oxidation is negative order (~ -0.5) with respect to NO_2 over the stated concentration range. A similar NO_2 inhibition effect on the NO oxidation reaction has been reported on both Cu-zeolite [134] and Pt/Al_2O_3 catalysts [146, 147]. In order to study the effect of feed NO_2 on the reaction orders of NO and O_2, we repeated some of the differential kinetic experiments in the presence of NO_2 (~100 ppm) in the feed. We found that the reaction orders with respect to NO and O_2 did not change in the presence of feed NO_2. Based on the differential kinetics study, the activation energy for this reaction was found to be about 39 kJ/mol.

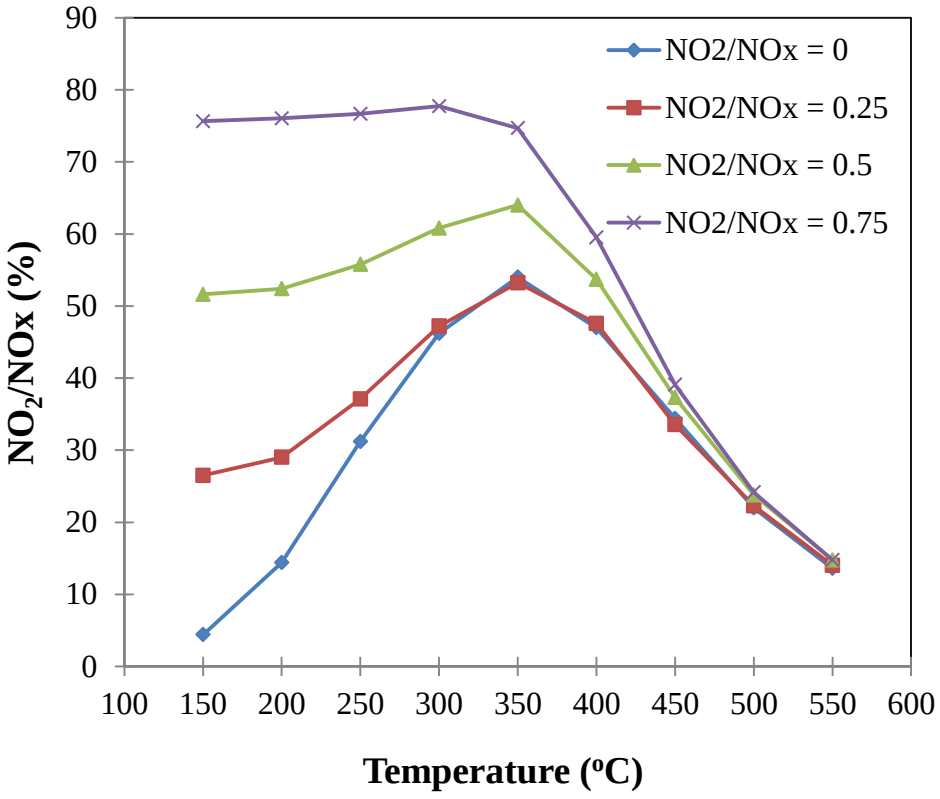

Figure 3-6: Steady state outlet NO_2/NOx concentrations obtained during the NO oxidation reaction studied with NOx feeds containing varying NO_2/NOx inlet feed ratios.

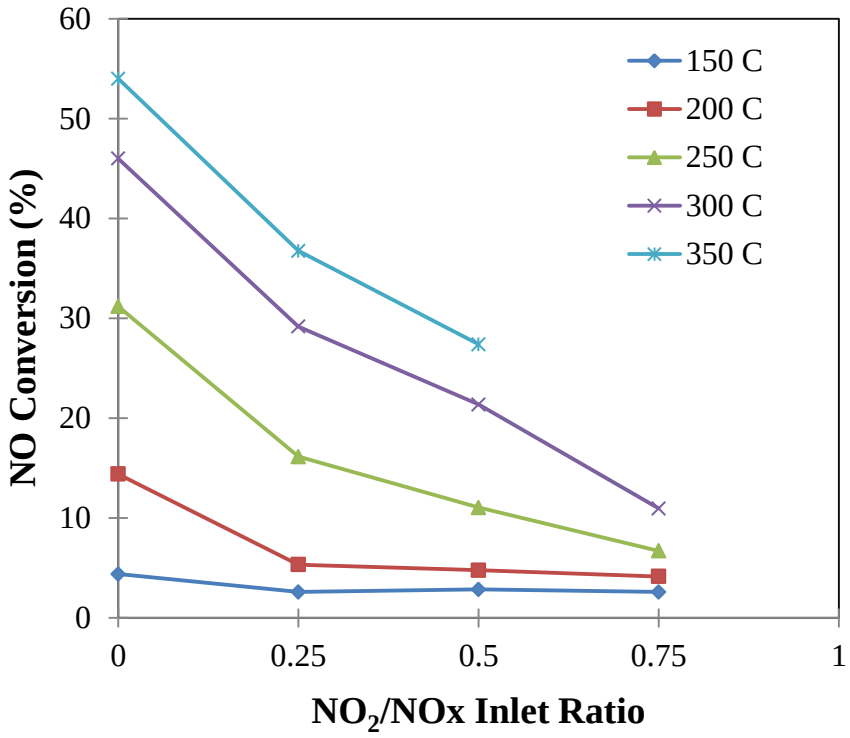

Figure 3-7: Steady-state NO conversion obtained during the NO oxidation reaction for above experiments (Figure 3-6) are shown.

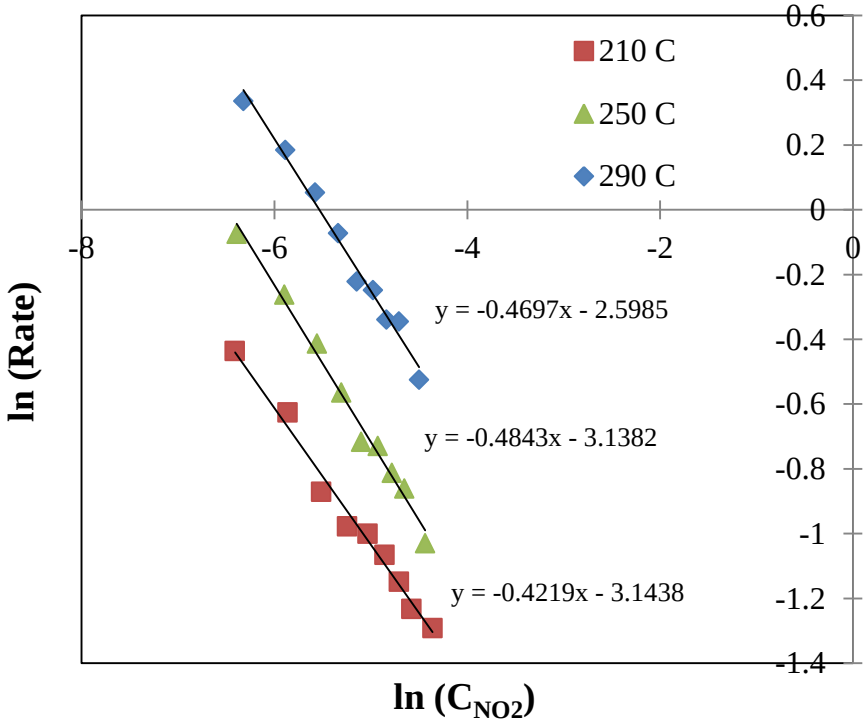

Figure 3-8: Logarithm of rate vs. average NO_2 concentration to obtain the reaction orders with respect to NO_2. Feed: 500ppm NO, 0-500ppm NO_2, 5% O_2, Ar.

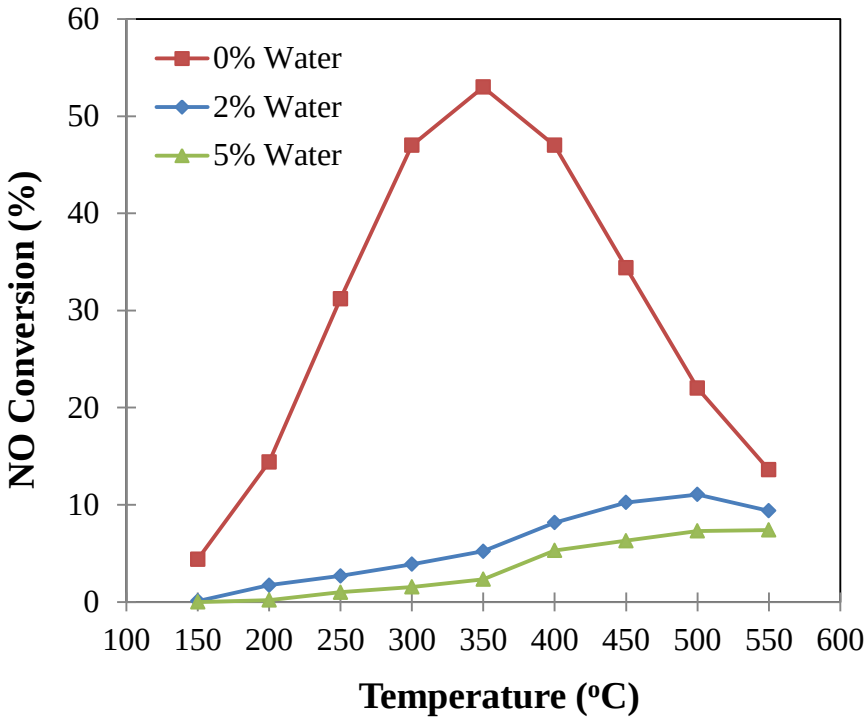

Figure 3-9: Steady state NO conversion obtained during the NO oxidation reaction with varying feed H_2O concentrations. Feed: 500 ppm NO, 5% O_2, 0-5% H_2O.

The NO oxidation reaction was also studied in the presence of water. Water is known to strongly inhibit the NO oxidation on Fe-zeolite catalysts [29, 39] as well as other catalysts [89, 99, 148]. Figure 3-9 shows the effect of water on the conversion of NO to NO_2 during the NO oxidation reaction. In the absence of water, about 53% inlet NO was converted to NO_2 at 350 ^oC. In the presence of 2% H_2O, the maximum conversion dropped precipitously to 11% and that occurred at 500 ^oC. The maximum value dropped to 7% in the presence of 5% H_2O. The strong inhibition of NO oxidation by H_2O can be attributed to the blockage of active sites for the NO oxidation reaction. Moreover, NO_2 is known to react with water to form a mixture of nitrous acid (HNO_2) and nitric acid (HNO_3) which likely remains adsorbed on the active Fe sites required for the NO oxidation reaction [36, 90]. Thus, it is likely that, NO_2, along with HONO and HNO_3, block the active Fe-sites required for the NO oxidation reaction. As a result, a

significant drop in the NO conversion is observed. The reaction orders and activation energy did not change in the presence of water.

Based on these observations, a mechanistically-based kinetic model for the NO oxidation is proposed as follows. The NO oxidation reaction is assumed to proceed through the Langmuir-Hinshelwood mechanism. Adsorption of the reactants on the catalyst surface is given by

$$NO + S_1 \xleftrightarrow{K_1} NO\text{-}S_1, \tag{3-9}$$

$$O_2 + 2\text{-}S_1 \xleftrightarrow{K_2} 2\ O\text{-}S_1. \tag{3-10}$$

[Remark: An alternative mechanism that does not require NO adsorption is described below.]

NO oxidation reaction occurs by the surface reaction,

$$NO\text{-}S_1 + O\text{-}S_1 \xleftrightarrow{k_1} NO_2\text{-}S_1 + S_1. \tag{3-11}$$

The NO_2 product appears following desorption,

$$NO_2 + S_1 \xleftrightarrow{K_3} NO_2\text{-}S_1. \tag{3-12}$$

Assuming that the overall reaction rate R_{NO} is limited by the surface reaction (3-11), a rate expression is derived as

$$R_{NO} = k_1\left(\theta_{NO}\theta_O - \frac{\theta_{NO_2}\theta_v}{k_{eq}}\right),$$

where upon substitution of the surface coverages θ_i gives

$$R_{NO} = k_1\left(K_1P_{NO}\sqrt{K_2P_{O_2}} - \frac{K_3P_{NO_2}}{k_{eq}}\right)\theta_v^{\,2}, \tag{3-13}$$

where θ_v is the mole fraction of vacant sites and is given by

$$\theta_v = \frac{1}{1+ K_1P_{NO} + \sqrt{K_2P_{O_2}} + K_3P_{NO_2}}. \quad (3\text{-}14)$$

Substitution of θ_v from (3-14) into (3-13) results in a rate expression that predicts the main trends in the NO oxidation data in the absence of water.

In the presence of water, the above reaction chemistry is complicated by reactions involving water and NO_2. NO_2 can react with water to form nitrate and nitrite (as acids) on the catalyst surface by

$$2\ NO_2\text{-}S_1 + H_2O \xleftrightarrow{k_2} HNO_3\text{-}S_1 + HONO\text{-}S_1. \quad (3\text{-}15)$$

Nitrates formed in the above reaction (3-15) are then reduced by NO into nitrites [36],

$$HNO_3\text{-}S_1 + NO\text{-}S_1 \xleftrightarrow{k_3} HONO\text{-}S_1 + NO_2\text{-}S_1. \quad (3\text{-}16)$$

Reactions (3-15) and (3-16) can be combined to give the following overall reaction

$$NO\text{-}S_1 + NO_2\text{-}S_1 + H_2O \xleftrightarrow{k_4} 2\ HONO\text{-}S_1. \quad (3\text{-}17)$$

Maintaining the assumption of surface reaction control, it can be shown that the rate expression (3-13) still applies but now the vacant site coverage θ_v is given by

$$\theta_v = \frac{1}{1+ K_1P_{NO} + \sqrt{K_2P_{O_2}} + K_3P_{NO_2} + \sqrt{k_4' K_1 K_3 P_{NO} P_{NO_2}} + \frac{k_2'(K_3P_{NO_2})^{1.5}}{\sqrt{k_4' K_1 P_{NO}}}}. \quad (3\text{-}18)$$

Here water is in excess and hence its effect is incorporated into the term k_2' and k_4' where $k_2' = k_2P_{H_2O}$ and $k_4' = k_4P_{H_2O}$. Substituting θ_v in (3-18) into (3-13) gives the modified rate expression for NO oxidation carried out in the presence of H_2O. The new rate expression has the requisite functional features to predict the inhibition by NO_2 and H_2O. The rate expression infers that the addition of water leads to the formation of two new surface

species, $HONO_{(ad)}$ and $HNO_{3(ad)}$, via reaction with NO_2 which serve to block the active sites required for the NO oxidation reaction.

The Langmuir-Hinshelwood kinetic model proposed above for the NO oxidation with and without water is based on the assumption of a surface reaction between adsorbed NO and O. It should be noted that the NO coverage, as determined by the NO adsorption measurements (not reported here), shows a lower affinity of NO than NH_3 for the Fe-ZSM-5 catalyst. This may suggest an alternative mechanism in which the rate limiting step is reaction between adsorbed O (or an oxidized Fe site) and gas phase NO through an Eley-Rideal type mechanism. The adsorbed surface concentration of NO, while small, cannot be completely ignored. However, if one neglects the adsorbed concentrations of NO, the model can be simplified to the Eley-Rideal mechanism in which gaseous NO reacts with the surface oxygen according to

$$NO + O\text{-}S_1 \xleftrightarrow{k_1'} NO_2\text{-}S_1 \ . \tag{3-19}$$

This modifies the above rate expression (3-13) as

$$R_{NO} = k_1' \left(P_{NO} \sqrt{K_2 P_{O_2}} - \frac{K_3 P_{NO_2}}{k_{eq}} \right) \theta_v \, . \tag{3-20}$$

With the assumption of negligible NO coverage, equations (3-14)-(3-20) are modified slightly and are not shown here. Both the Langmuir Hinshelwood (equation (3-13)) and Eley-Rideal (equation (3-20)) rate expressions can predict the experimentally observed NO_2 inhibition. The NO_2 concentration used in the differential study (up to 500 ppm) was insufficient to predict the higher negative orders (-1 or -2) predicted by the above two models. A complete quantitative study on the NO oxidation reaction including the discrimination between rival models is discussed in Chapter 8.

3.3.4 Selective Catalytic Reduction of NO with NH_3

In the standard SCR experiments the catalyst was exposed to an NH_3/Ar mixture for 20 minutes at 150 ^oC. This allowed sufficient time for the NH_3 to reach its inlet concentration of 500 ppm. Then NO (500 ppm) and O_2 (5%) were simultaneously fed to the reactor. The reaction system was allowed to reach steady state (about 25 minutes).

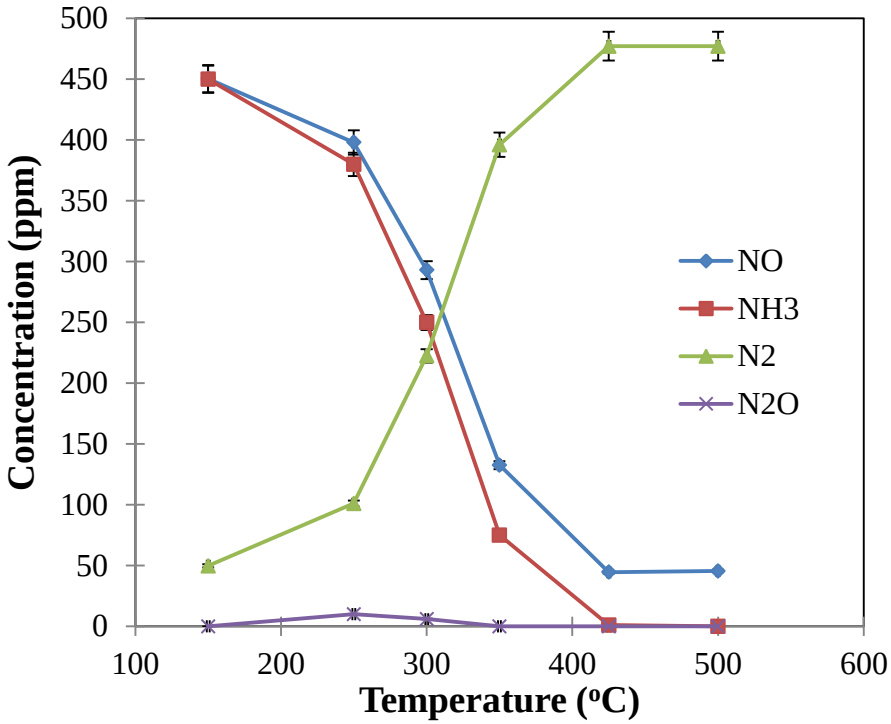

Figure 3-10: Product distribution at various temperatures obtained during the standard SCR reaction studies on the FeZ-18 catalysts are shown here. Feed: 500 ppm NO, 500 ppm NH_3, 5% O_2. Total flow rate: 1000 sccm.

As shown in a typical set of experiments in Figure 3-10 using an in-house catalyst (FeZ-18), the effluent NO concentration decreased monotonically with temperature, with the sharpest drop occurring between 250 – 350 ^oC. The ammonia concentration did as well but with a slightly steeper slope. The coincidence of the NO and NH_3 concentrations at lower temperatures combined with the nearly 100% selectivity to N_2 confirms reaction (3-1) to be the overall reaction. The departure from the 1:1 stoichiometry at higher

temperatures (≥ 300 ^{o}C) is consistent with the onset of NH_3 oxidation. Figure 3-4 shows that at 350 ^{o}C the NH_3 conversion is about 10% (50 ppm NH_3 reacted) while Figure 3-10 shows that an extra 50 ppm of NH_3 is consumed than NO at the same temperature. The NH_3 is completely consumed at 425 ^{o}C whereas about 9% of the NO remains unreacted. A further increase in temperature did not lead to any further change in the NO concentration. N_2 is the primary N-containing product of the standard SCR reaction; a minor amount of N_2O was noticed between 250 and 300 ^{o}C. Sun et al. [38] studied the standard SCR reaction mechanism over Fe-MFI catalyst by isotopic labeling (^{15}NO and $^{14}NH_3$). They found that the main product of standard SCR is $^{15}N^{14}N$ which confirms the 1:1 stoichiometry of reaction (3-1). At higher temperatures; the deviation from 1:1 stoichiometry was contributed to NH_3 oxidation with O_2 or N_2O_x (x > 3).

A comparison was carried out of two in-house synthesized catalysts of different washcoat loadings (FeZ-10, FeZ-18) and the commercial catalyst (Figure 3-11). The NO conversion achieved 95% by 425 ^{o}C on the commercial catalyst compared to 91% and 85% for FeZ-18 and FeZ-10, respectively. Except at the lowest temperature (150 ^{o}C) the order of conversion was commercial > FeZ-18 > FeZ-10. This order is the same as that for washcoat loading which is not an unexpected result. The extent of washcoat diffusion limitations is considered later.

The individual effects of NO, NH_3, and O_2 were studied on the integral conversions of NO and NH_3 were studied. As NO concentration increased, the rate of NO conversion also increased. A similar trend was observed for the effect of O_2 concentration. However higher ammonia concentration was found to have inhibiting effects on the standard SCR reaction. We expand on these trends next.

In earlier studies, water was deliberately avoided in order to isolate the effects of reacting species NO, NH_3 and O_2. In the actual exhaust, a high concentration of water is present and it is therefore important to assess its effect. This is especially relevant given the above-described inhibition of NO oxidation by H_2O. Therefore, we repeated the above experiments on the commercial catalyst in the presence of 2% and 5% H_2O in the

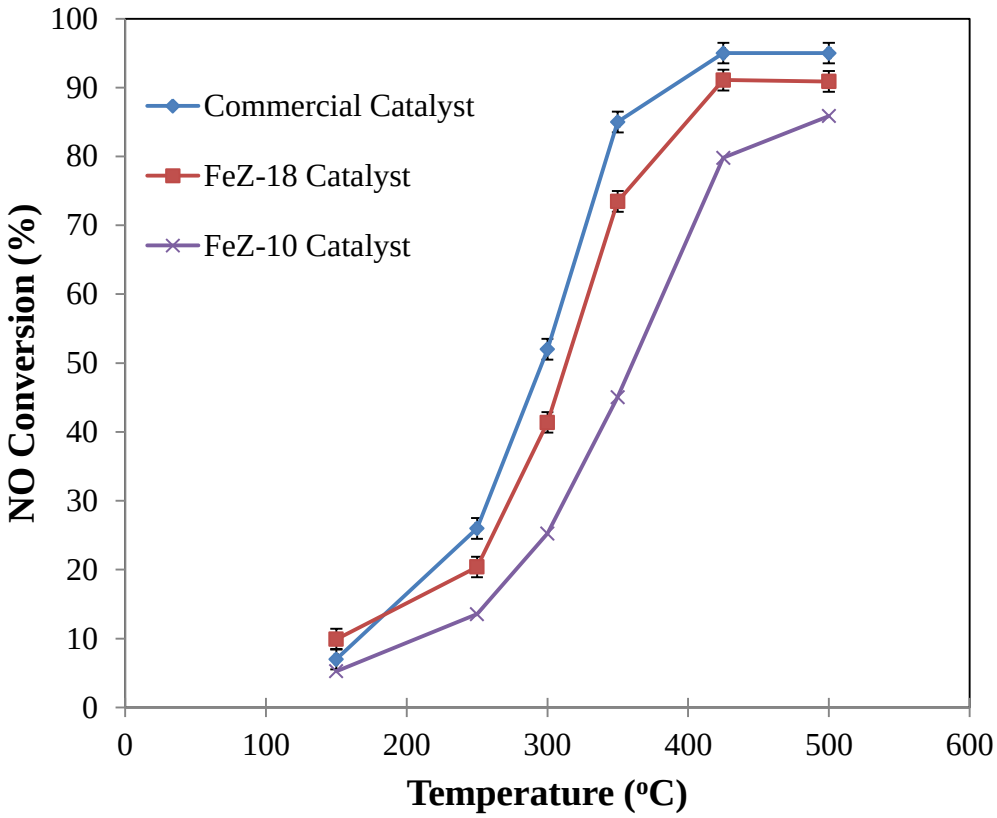

Figure 3-11: Comparison of NO conversions obtained during the standard SCR reaction studied on catalysts with different washcoat loadings is presented. Feed: 500 ppm NO, 500 ppm NH_3, 5% O_2. Total flow rate: 1000 sccm.

inlet feed. Figure 3-12 shows the results. Water has only a minor inhibition effect on the standard SCR reaction with the maximum of 7% difference obtained at 350 ^oC with a water concentration of 2%. When the H_2O concentration was increased further to 5%, very little change in the NO conversion was observed. These results are in agreement

with previous literature studies [29, 39]. One possible reason for only a minor inhibition is that water as a product of the NOx reduction is already present even when no additional water is added. Below we offer an alternative explanation for the apparent inconsistency in the water effect when comparing the NO oxidation and SCR reactions.

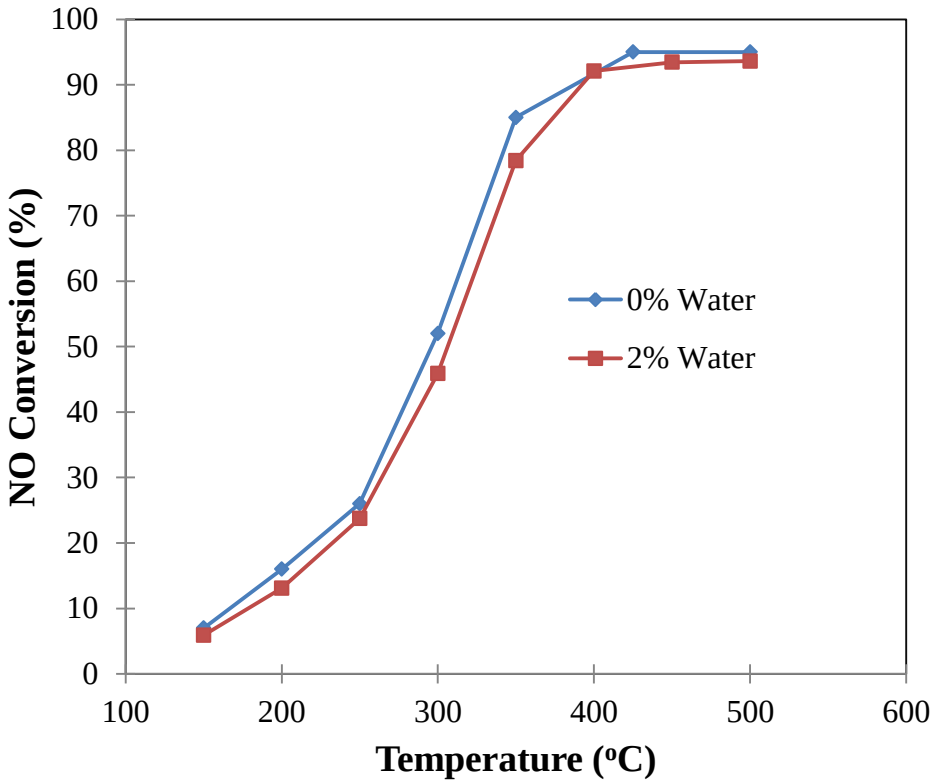

Figure 3-12: Effect of water on the standard SCR reaction carried out on the commercial Fe-zeolite catalyst. Inlet feed: 500 ppm NH_3, 500 ppm NO, 5% O_2, 0-2% H_2O. Total flow: 1000 sccm.

3.3.5 Differential Kinetics Studies of Standard SCR Reaction

A mechanistically-based intrinsic kinetic model should be able to predict key features like reaction orders and activation energies. These require experiments conducted under differential conditions as integral experiments do not provide the same functional specificity.

An initial set of experiments involved the variation of the space velocity of the feed gas comprising an equimolar mixture of NO and NH_3 in 5% O_2. This helped to identify the critical space velocity above which the conversion was less than 15%, considered here as differential. Figure 3-13 shows the dependence of NO conversion on

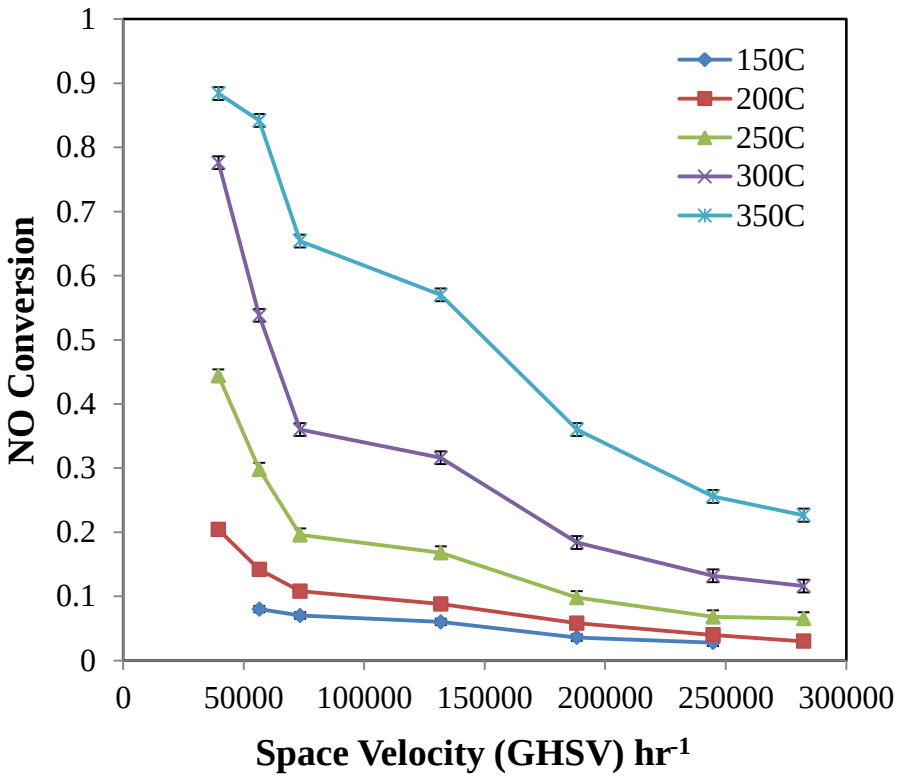

Figure 3-13: NO conversion during the standard SCR reaction as function of GHSV. Feed: 500 ppm NO, 500 ppm NH_3, 5% O_2.

space velocity for temperatures between 150 and 350 ^{o}C. The higher space velocities were attained by cutting the monolith to short lengths. The results show the expected trend of monotonically decreasing NO conversions with increasing GHSV. Subsequent kinetics measurements were made using the short monolith to ensure the differential operation over the indicated temperature range. It is noted that N_2 is the lone product of NO reduction under differential conditions. The short contact time prevented any

measurable conversion of NH_3 oxidation for temperatures $\leq 300^oC$. The extent of mass transport limitations is assessed below.

The dependence of the NO conversion rate on NO concentration is shown in Figure 3-14a. The rate (washcoat volume basis) increased linearly with the NO concentration at each temperature. From the logarithmic plot (Figure 3-14b) of rate of NO consumption vs. average NO concentration; the apparent NO order was found to be nearly linear (0.97-1.09), over the temperature range studied.

Similar experiments were carried out to determine the O_2 and NH_3 orders for the same temperature range. The results shown in Figure 3-15 reveal a fractional positive order dependence on O_2 (0.52-0.59) over the range of temperatures considered. For the NH_3 experiments the NO and O_2 concentrations were fixed at 500 ppm and 5% respectively while varying the NH_3 concentration between 200 and 800 ppm over the temperature range of 200 - 300 ^oC. As shown in Figure 3-16, the NO reduction rate decreased monotonically with increasing NH_3 concentration. Thus, the standard SCR reaction is inhibited by NH_3 with an apparent order that varies between -0.27 to -0.32. The inhibition is slightly more pronounced at higher temperatures indicating the possible emergence of ammonia oxidation side reaction. At lower temperatures, the blocking of reaction sites by the strongly bound NH_3 is the likely cause of the negative reaction order.

Finally, the apparent activation energy was determined by measuring the temperature dependence of the apparent rate constant as shown in Figure 3-17. For an equimolar feed of NO and NH_3 in O_2 the activation energy was found to be about 42 kJ/mol. To investigate the effect of water on reaction orders and activation energies, some of the above experiments were repeated with 2% H_2O in the inlet feed.

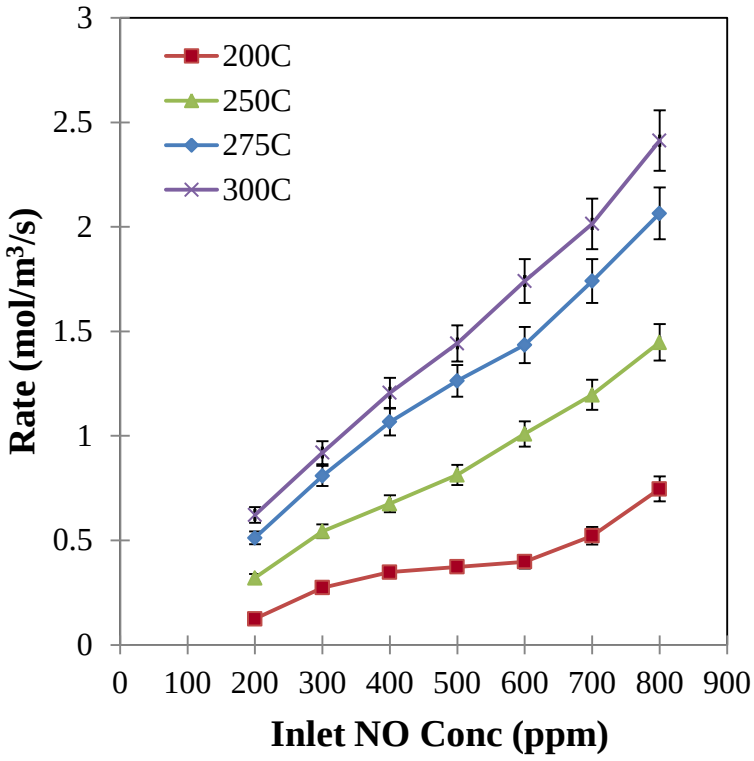

Figure 3-14: Effect of inlet NO concentration on the rate of NO consumption in the standard SCR reaction.

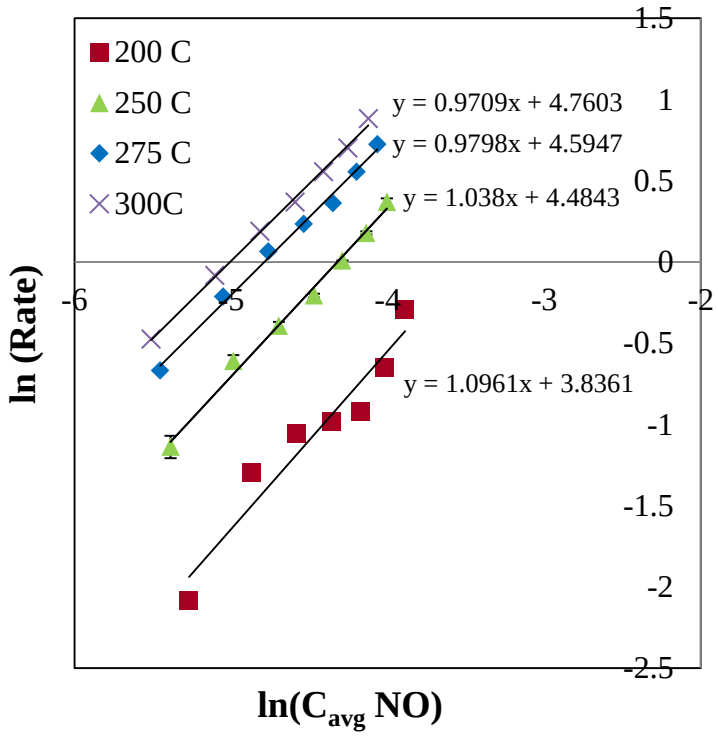

Figure 3-14b: Logarithm of rate vs. average NO concentration.

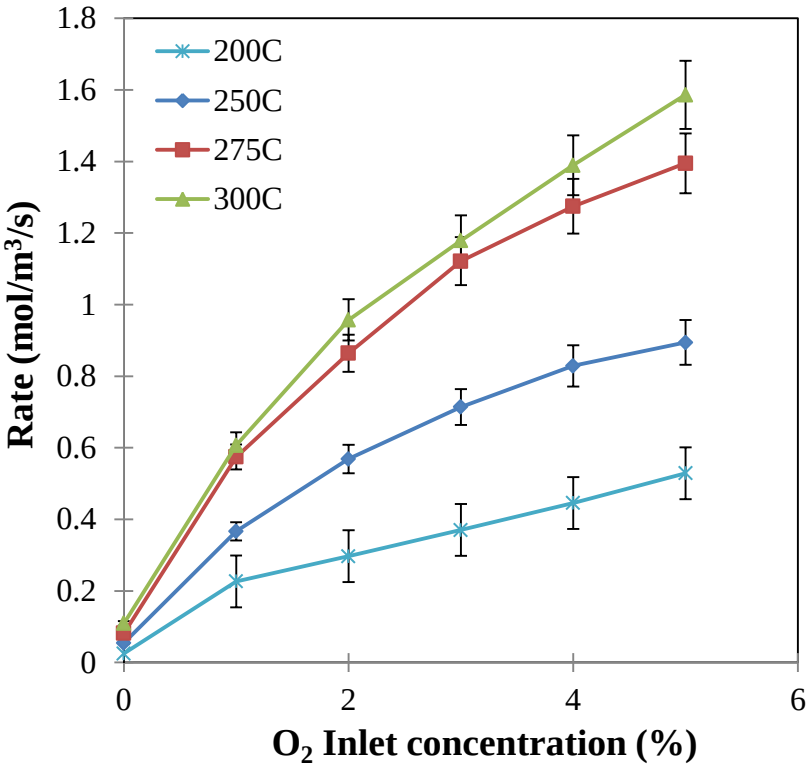

Figure 3-15a: Effect of inlet O_2 concentration on the rate of NO consumption in the standard SCR reaction.

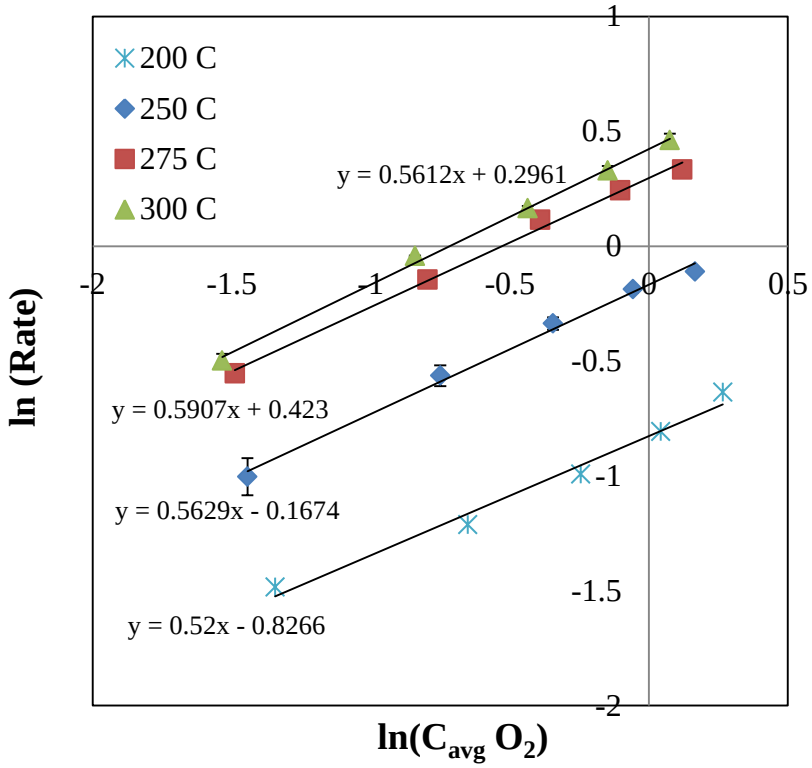

Figure 3-15b: Logarithm of rate vs. average O_2 concentration.

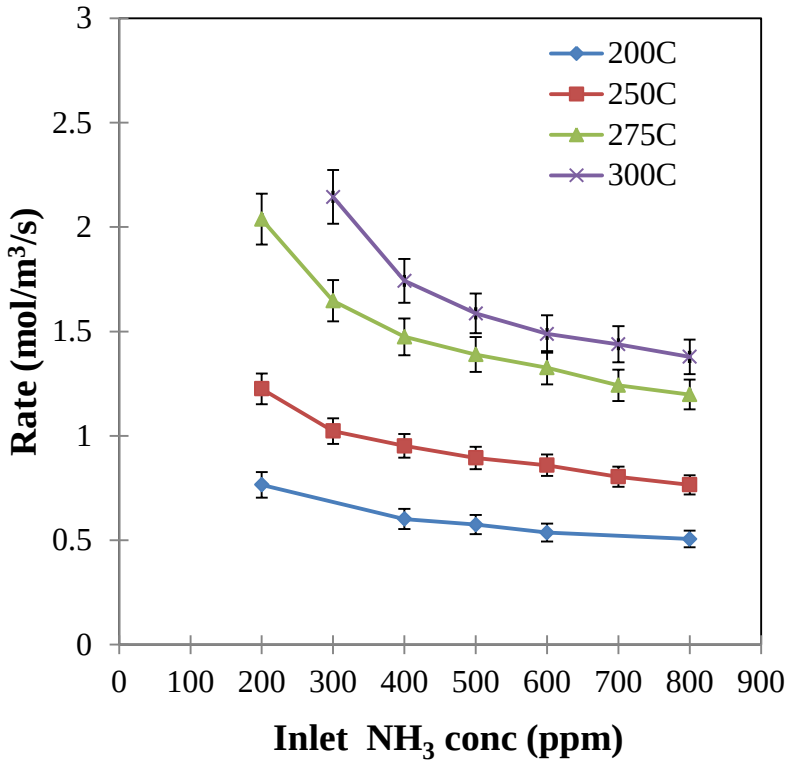

Figure 3-16a: Effect of inlet NH_3 concentration on the rate of NO consumption in the standard SCR reaction is plotted here.

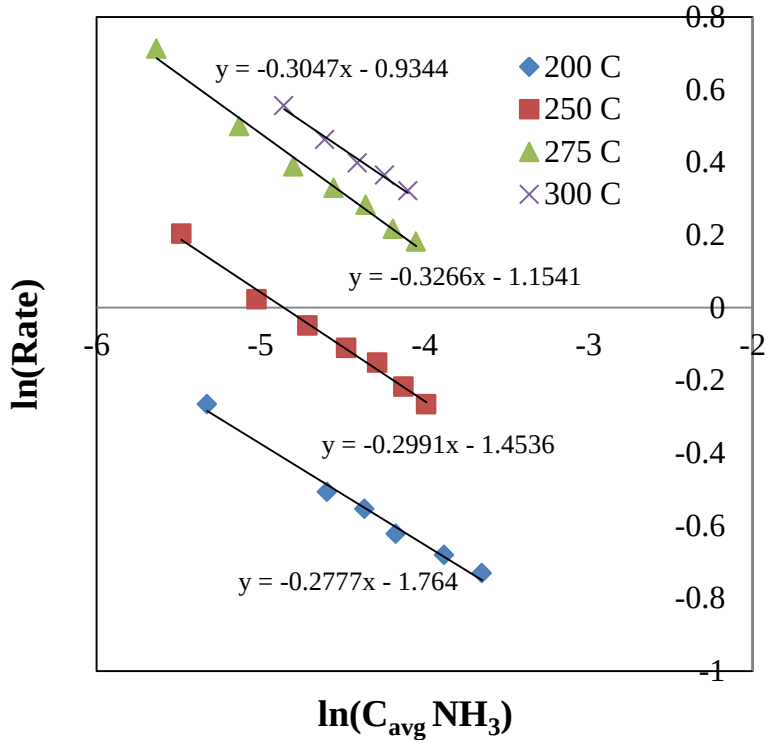

Figure 3-16b: Logarithm of rate vs. average NH_3 concentration.

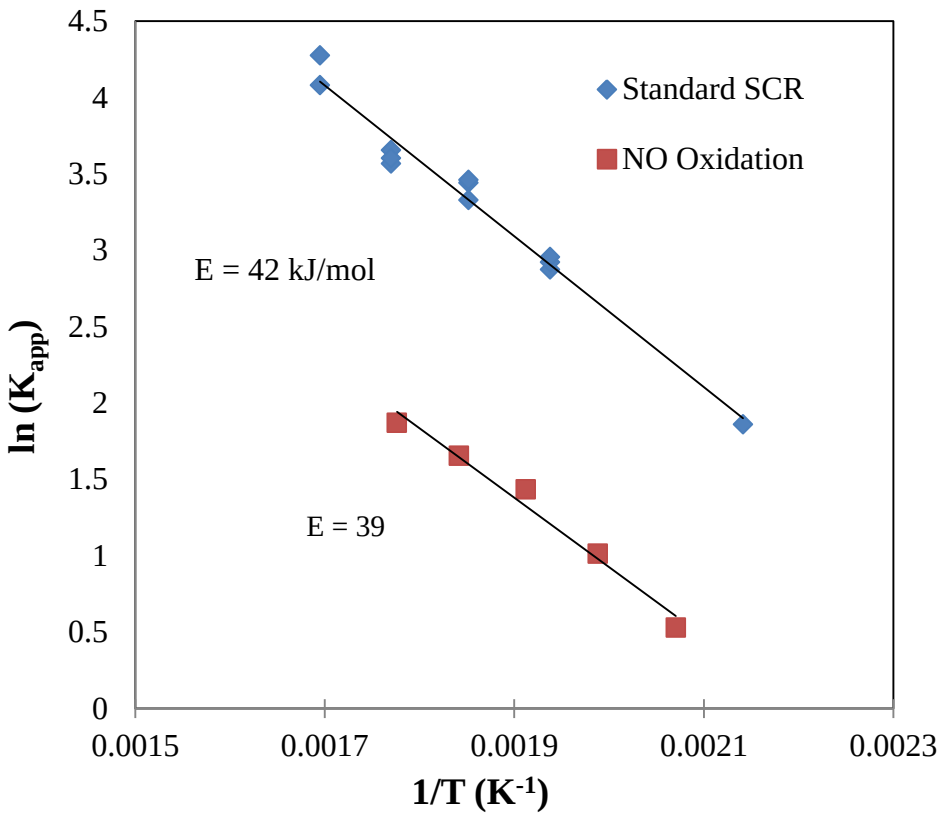

Figure 3-17: Arrhenius plot of the logarithm of apparent rate constant for NO conversion versus the inverse of catalyst temperature. Activation energies of standard SCR reaction and NO oxidation reaction are compared.

The presence of water did not make any appreciable change in both cases.

Based on the above studies of differential kinetics, following power law model is developed for the standard SCR reaction:

$$-R_{SCR} = A\exp(-\frac{E}{RT})(NO)^{\alpha}(O_2)^{\beta}(NH_3)^{\lambda}.$$

$$[\alpha = 0.97\text{-}1.09 \qquad \beta = 0.52 - 0.59 \qquad \lambda = -0.27 - -0.32 \qquad E = 42\,\text{kJ/mole}].$$

Values obtained for reaction kinetics (reaction orders and activation energy) are comparable for Fe-based zeolite catalysts in the literature. Devadas et al. [29, 30] reported an activation energy for the standard SCR reaction on an Fe-ZSM-5 washcoated monolith catalyst to be around 39 kJ/mol. Some of the experimental findings from

literature about reaction orders and activation energies on different catalysts are summarized in Table 3-2.

Table 3-2: Comparison of literature findings for standard SCR reaction orders and activation energies on different catalysts.

Catalyst	Reference	Order w.r.t. NO	Order w.r.t. NH_3	Order w.r.t. O_2	Activation Energy (kJ/mol)
Fe-ZSM-5	[34]	0.88 - 0.94	-0.11 - -0.15	0.41 - 0.36	54
Fe-ZSM-5	[36]	0.81 - 0.88	-0.11 - -0.21	0.29 - 0.34	68
H-ZSM-5	[138]	0.73	-0.61	1.06	61
Cu-Zeolite	[111]	1	0	0.5	35
Cu-FAU	[102, 149]	0.8 - 1	0	0.5-1	29
Fe-ZSM-5	This Work	0.97 – 1.09	-0.27- -0.32	0.52 – 0.59	42

3.3.6 Effect of Mass Transport Processes

The extent of mass transport limitations should be ruled out in order to claim an intrinsic rate model has been determined. In the current system there are three possible mass transport resistances. The first is external mass transfer which involves the diffusion of species from the flowing gas to the surface of the washcoat, transverse to the convective flow. The second is washcoat diffusion in the intercrystalline voids [147, 150, 151]. The third is diffusion within the pores of the zeolite crystallites, so-called intracrystalline diffusion. A comparison of the characteristic times helps to identify the rate controlling processes. These are as follows:

Washcoat diffusion time: $\tau_{d,w} = \frac{R_{\Omega 2}^2}{D_e}$;

Convection time, $\tau_c = \frac{L}{u}$;

Transverse diffusion time or external mass transfer time: $\tau_e = \frac{R_{\Omega 1}^2}{D_f}$;

Reaction time: $\tau_r = \frac{C_i}{r_i}\frac{R_{\Omega 1}}{R_{\Omega 2}}$;

Intracrystalline diffusion time: $\tau_{d,c} = \frac{R_{\Omega 3}^2}{D_{e,c}}$.

Here $R_{\Omega 1}$ denotes the effective transverse diffusion length scale ($R_{\Omega 1} = A_{\Omega 1}/P_{\Omega 1}$; $A_{\Omega 1}$ = channel cross-sectional area open to flow; $P_{\Omega 1}$= channel perimeter open to flow), $R_{\Omega 2}$ is the effective washcoat thickness (defined as the washcoat cross-sectional area $A_{\Omega 2}$ over $P_{\Omega 1}$), D_e is the effective diffusivity in the washcoat, $R_{\Omega 3}$ is the zeolite crystallite particle radius, D_f is the diffusivity of a reacting species NO in the monolith channel, $D_{e,c}$ is the effective diffusivity in the zeolite crystallite, L is the length of the monolith, u is the average velocity in the channel, and r is the rate of reaction (washcoat volume basis). Diffusion at the zeolite crystallite level has been included for completion, notwithstanding the uncertainty about the value of the diffusion coefficient in the zeolite channels and the location of the active sites within the pores or on the surface of the crystallites.

Table 3-3 provides the estimates of these parameters and the resulting values of the characteristic times and the corresponding conditions and catalysts for which they were estimated. The characteristic time for reaction (τ_r) is found to be much larger than

that for external mass transfer (τ_e), zeolite crystal diffusion ($\tau_{d,c}$), and convection (τ_c) in the temperature range of 200 - 300 ^oC.

Table 3-3: Values of characteristic times (in milli seconds), gas diffusivities of NO and Weisz-Prater modulus are reported in the temperature range of 200-575^oC.

Temperature (^oC)	D_f $\times 10^5$ m^2/s	τ_e ms	τ_c ms	$\tau_{d,c}$ ms	$\tau_{d,w}$ ms	τ_r ms	Ψ
200	4.36	1.73	5.70	0.62	5.73	184.5	0.17
250	5.19	1.45	5.15	0.62	4.83	74	0.35
275	5.65	1.33	4.92	0.62	4.42	46.25	0.53
300	6.07	1.24	4.70	0.62	4.12	37.47	0.61
325	6.35	1.19	4.50	0.62	3.94	22.3	0.97
350	7.04	1.07	4.32	0.62	3.55	16.68	1.17
425	8.5	0.89	3.86	0.62	2.94	5.54	2.92
500	10.1	0.75	3.49	0.62	2.47	3.48	3.92
575	11.8	0.64	3.18	0.62	2.12	2.865	4.34

This analysis definitively rules out any role of external mass transfer in the temperature range in which the differential kinetics data are collected. The existence of intraparticle (washcoat) diffusion limitations is evaluated by estimating the Weisz-Prater modulus defined by

$$\Psi = \frac{R_{\Omega 2}^2 \; r_{obs}}{D_e \; C_i}. \qquad (3\text{-}21)$$

The Weisz-Prater modulus (Ψ) is found to be less than unity for the temperature range of 200-300 ^oC which underscores the absence of washcoat diffusion limitations in the

differential kinetics experiments which were carried out for temperatures ≤ 300 ^{o}C. Values presented in the Table 3-3 were calculated for a single monolith channel and are based on the assumed values of effective diffusivity in the washcoat equal to 100 times lesser than that of the gas phase diffusivities. Chae et al. [137] used the value of effective diffusivity in the range of 10^{-6}-10^{-7} m^2/s. For comparison, a value of diffusivity in zeolite pores is assumed to be of the order of 10^{-8}-10^{-9} m^2/s [34].

These findings are consistent with those from the literature in the lower temperature range but present new information about the role of diffusion at higher temperatures. Chatterjee et al. [78] compared the results obtained with a zeolite monolithic catalyst and crushed monolith powder for SCR on zeolite catalysts. They found a very similar deNOx activity for both the cases up to 450 ^{o}C. From these observations, they concluded that the interphase and intraphase diffusion limitations did not play a significant role in the zeolite catalytic system. Huang et al. [34] did not find pore diffusion limitations in their experiments on Fe-ZSM-5 powder catalysts with a particle size of 0.5 μm assuming a value of pore diffusivity equal to 10^{-8} m^2/s. They performed an analysis of an effectiveness factor for standard SCR reaction in the temperature range of 240-300 ^{o}C estimating the smallest possible value equal to 0.95 at 300 ^{o}C. They concluded the absence of diffusion limitations in the SCR reaction on Fe-ZSM-5 powder catalyst under these conditions. Olsson et al. [117] performed kinetic studies of SCR on Cu-ZSM-5 washcoated monolith catalyst. They eliminated any role of diffusion limitations in the washcoat by performing experiments with catalysts of same dimensions but different catalyst loadings. The space velocity was adjusted so that the ratio between the flow rate and zeolite mass remained constant. They obtained similar

NO conversions in both the cases for the entire temperature range of 100-500 ^{o}C. But for a Cu-ZSM-5 catalyst, it should be noted that the SCR reaction proceeds faster (compared to an Fe-zeolite catalyst) and very high conversions (> 95%) are obtained even at lower temperatures (200-300 ^{o}C). It is difficult to estimate the role of washcoat diffusion limitations with such high conversions.

The calculation results shown in Table 3-3 for the characteristic diffusion times and the Weisz-Prater criterion [152, 153] indicate the emergence of washcoat diffusion limitations at higher temperatures. The Weisz-Prater modulus exceeds unity at temperatures exceeding 325^{o}C. For this reason, a more detailed experimental investigation of the extent of washcoat diffusion limitations in Fe-zeolite monolithic catalysts was carried out. To do so we synthesized monolith catalysts with different loadings and washcoat thicknesses with the intent to compare their relative activities. Specifically, we synthesized two Fe-zeolite monolithic catalysts with different washcoat loadings of 11% (FeZ-11) and 21.7% (FeZ-22). Two different sets of NO reduction experiments were performed on these catalysts. In the first set of experiments, the catalyst lengths were fixed at 2 cm. For the FeZ-11 catalyst, the total flow rate was 1000 sccm while a total flow rate of 500 sccm was used for FeZ-22 catalyst. Thus the ratio of space velocity to the washcoat loading was fixed. The standard SCR reaction was then carried out over a range of temperatures.

The data reveal no significant difference (< 2%) in the NO conversion up to 300 ^{o}C (data not reported here). However, at 350 ^{o}C the NO conversion was about 11% higher on the FeZ-11 catalyst than FeZ-22 catalyst. The difference in NO conversion on these two catalysts started decreasing at higher temperatures as the NO conversion

approached its asymptotic value of 90%. This indicated the appearance of washcoat diffusion limitations at higher temperatures for the zeolite catalysts studied.

A more sensitive approach was achieved by fixing the flow rate and varying the monolith length. Figure 3-18 shows the comparison of NO conversion obtained for a 2 cm long FeZ-11 and 1 cm long FeZ-22 samples. In both the cases, the total flow rate was fixed at 1000 sccm so that the space velocity per unit mass of catalyst was the same. Standard SCR reaction experiments were carried out on these catalysts in the temperature range of 150-500 ^{o}C which yielded the NO conversion results shown in Figure 3-18. The comparison clearly shows the separation in NO conversion in the temperature range of 350-450 ^{o}C. The difference of 12.5% in the NO conversion is seen at 350 ^{o}C. This difference decreases at higher temperatures with just 5% difference at 500 ^{o}C. Based on these observations, we conclude that the washcoat diffusion limitations do exist in Fe-zeolite washcoated monoliths at temperatures higher than 300 ^{o}C and hence must be taken into consideration. In order to further confirm this result, we determined the activation energy of standard SCR reaction for commercial Fe-zeolite washcoated catalyst at a very high space velocity of 2×10^{6} hr^{-1}in the temperature range of 350-500 ^{o}C. This high space velocity ensured that the reactor was operated in the differential kinetics regime (X < 12%). An apparent activation energy of 24 kJ/mol (±0.5 kJ/mol) was determined. This value is roughly half the value of activation energy (42 kJ/mol) obtained in the temperature range of 200-300 ^{o}C. This reduction in the activation energy ca. by a factor of two is a signature of washcoat diffusion limitations at higher temperatures.

This is an important finding which proves the existence of washcoat diffusion limitations and hence the role of mass transfer must be considered at higher temperatures (T > 300 ^{o}C).

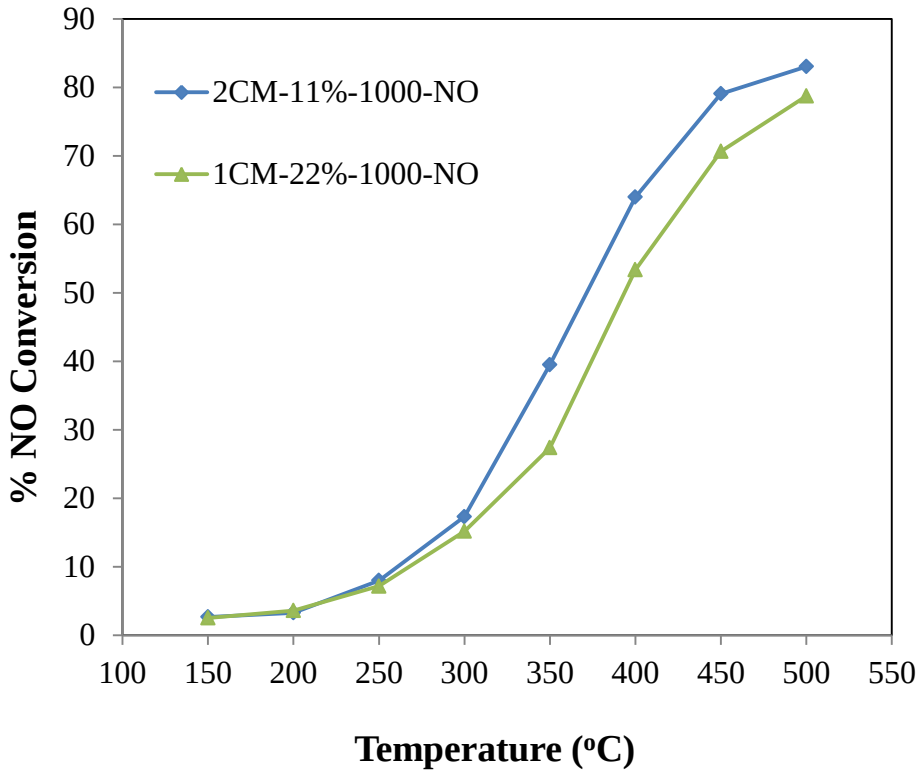

Figure 3-18: Comparison of NO conversion obtained during the standard SCR reaction for FeZ-11 (length: 1 cm) and FeZ-22 (length: 2 cm) catalysts. Feed: 500 ppm NO, 500 ppm NH_3, 5% O_2.

3.3.7 Standard SCR: Kinetic Model

A consensus has yet to emerge on the mechanism and kinetics of SCR of NO on Fe-zeolite catalysts. Some studies have proposed the oxidation of NO is the rate determining step (RDS) for the standard SCR reaction [29, 34, 36, 37]. A recent study by Iwasaki et al. [36] provided a rate expression for the standard SCR reaction that assumed NO and NH_3 adsorb on the same type of site while O_2 adsorbs on a second site. A kinetic rate expression was derived assuming that the surface reaction of adsorbed NO and O

was the RDS. Yang et al. [37] suggested that NH_3 adsorbs on acidic sites whereas NO oxidation occurs on Fe-sites. They observed a large number of Bronsted acid sites for NH_3 adsorption even on the over-exchanged Fe-ZSM-5 catalyst after hydrolysis. In their mechanism they proposed the formation of a $NO_2(NH_4^+)_2$ complex through reaction between NO_2 (formed by the slow NO oxidation step) and protonated NH_3 present on the acidic sites. This complex is reduced in a subsequent step by NO. In their mechanism, they assumed NO oxidation as being the slowest and hence the RDS for the standard SCR reaction.

In the current study, we have determined that the activation energy for the NO oxidation is nearly equal to the activation energy for the standard SCR reaction (Figure 3-17). The same is true for the apparent reaction orders with respect to NO and O_2. In the absence of feed water, the rates of NO oxidation and standard SCR reactions were found to be comparable; i.e. the NO oxidation rate only slightly higher than the standard SCR reaction rate (Figure 3-19). A direct comparison of the rates for the two different reaction systems is not possible since NH_3 has been shown to inhibit the standard SCR reaction (Figure 3-16). The difference in the rates of these two reactions clearly shows that the presence of NH_3 inhibits the NO oxidation step (and hence the SCR rate). In addition, negligible NO conversion (< 6%) was recorded at higher temperatures (> 425^{o}C) for an anaerobic feed of NO and NH_3. This underscores the important role of oxygen in the SCR chemistry. Our experimental results also indicate an enhancement of both the NO oxidation (data not reported here) and the standard SCR reaction (see Figure 3-11) with increasing Fe content and washcoat loading. These findings support the argument that the formation of NO_2 by NO oxidation on the metal site is needed for the standard SCR

chemistry to occur. Our findings are in agreement with the literature studies which showed that negligible NO conversion occurred for both reactions on H-ZSM-5 catalysts [29]. Collectively, these findings strongly suggest that the NO oxidation reaction is the rate determining step for standard SCR.

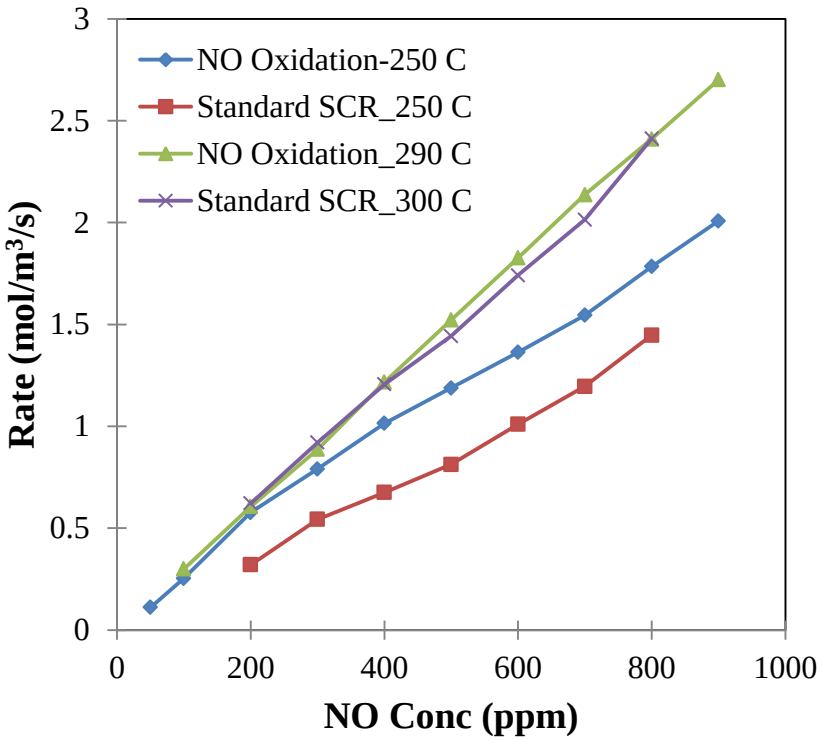

Figure 3-19: Comparison of rates of NO oxidation and Standard SCR reaction at different temperatures.

However, when the rates of NO oxidation and NO SCR are compared in the presence of water, NO oxidation was far slower compared to standard SCR. This raises doubts about NO oxidation being the RDS; otherwise a similar inhibitory effect of H_2O on SCR would seem to be necessary. In order to investigate this apparent counterintuitive finding, we carried out an experiment in which NH_3 was introduced in increasing amounts (50 ppm increments) into a feed mixture containing 500 ppm NO and 5% O_2, both in the presence and the absence of H_2O. The temperature was fixed at 350 ^oC. With

no added NH_3, the steady state outlet NO_2 concentration was ca. 255 ppm without water and 40 ppm with water. In both the cases the NO_2 concentration decreased with increasing NH_3 (Figure 3-20). The decrease was sharper in the absence of H_2O. The first 50 ppm NH_3 added resulted in ca. 90 ppm decrease in the NO_2 concentration. This disproportionate decrease in the NO_2 concentration suggests involvement of two processes. First, ammonia, in reacting with NO by the standard SCR reaction (3-1), reduces the NO that is available to oxidize by 50 ppm (i.e. stoichiometry of 1:1). Second, as shown earlier (Figure 3-19), ammonia inhibits the NO oxidation (and hence the standard SCR) reaction by blocking sites needed for NO oxidation. This would appear to cause the additional 40 ppm decrease in the outlet NO_2 concentration. These observations are in agreement with the earlier data showing NO oxidation is inhibited by NH_3 (Figure 3-19). A further increase in NH_3 concentration consumes an equal amount of NOx up to 400 ppm of NH_3 (Figure 3-20). [For example, an increase in NH_3 from 50 to 100 ppm results in a decrease in NO_2 from ca. 170 to 120 ppm. An increase in NH_3 from 200 to 250 ppm results in a decrease in NO_2 from ca. 60 to 40 ppm and there is a corresponding decrease in NO of ca. 30 ppm (data not shown here).]

When a similar experiment was carried out in the presence of H_2O, a more gradual decrease in NO_2 concentration was observed (figure 3-20). The first 50 ppm increment of NH_3 led to ca. 8 ppm decrease in the outlet NO_2 concentrations while the net NOx ($NO+NO_2$) concentration decreased by 50 ppm. Again, this shows the equimolar NO and NH_3 consumption by reaction (3-1). With water present in excess, the outlet NO_2 concentration is expectedly small due to the formation of nitrites and nitrates which are readily removed by NH_3. The chemistry is described below.

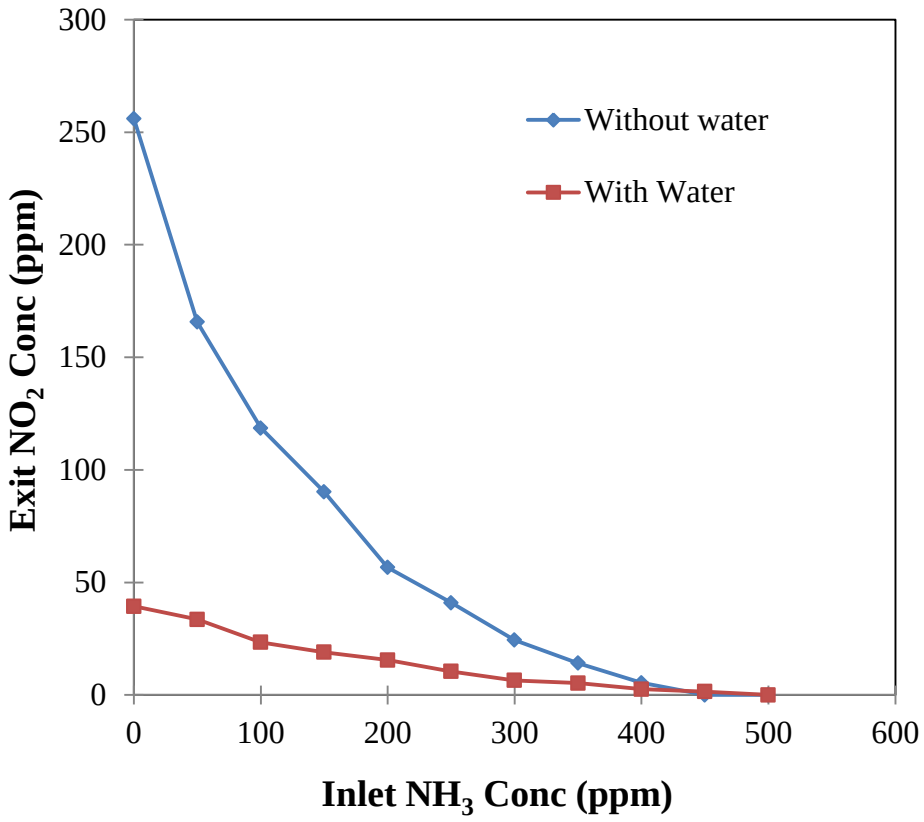

Figure 3-20: Outlet NO_2 concentration is plotted as a function of increasing NH_3 concentrations introduced in a system containing NO and O_2. Feed: 500 ppm NO, 5% O_2, 0-1.5% H_2O. Total flow: 1000 sccm. Catalyst Temperature: 350 ^oC.

On the basis of these observations a mechanism for the standard SCR reaction is proposed here that is consistent with the assertion that NO oxidation is the rate determining step. The standard SCR reaction exhibits negligible inhibition by water while the oxidation of NO is adversely affected by water. But the NH_3 uptake data showed that Fe-zeolite catalyst effectively adsorbs NH_3 in the presence of water. These observations suggest the existence of two different sites on the Fe-ZSM-5 catalyst (following literature [29, 37]): acid sites for the NH_3 adsorption and Fe-sites for the oxidation reactions. From these observations, a mechanistically based kinetic model can be constructed. NH_3 is assumed to adsorb on acidic sites represented by S_2,

$$NH_3 + S_2 \overset{K_4}{\longleftrightarrow} NH_3\text{-}S_2 . \qquad (3\text{-}22)$$

The observed inhibition effect of NH_3 on the standard SCR reaction can be attributed to NH_3 blocking the active sites. Nova et al. [25, 27] suggested a spillover process involving the transfer of NH_3 from S_2 (acidic) sites to S_1 (metal) sites in their kinetic model for V_2O_5-WO_3/TiO_2 catalyst. Here we adopt a similar approach with the spillover reaction,

$$NH_3\text{-}S_2 + S_1 \xleftrightarrow{K_5} NH_3\text{-}S_1 + S_2 . \qquad (3\text{-}23)$$

Subsequently, NH_3 adsorbed on S_1 and S_2 sites reacts with HONO formed by reaction (3-17) to give N_2 and H_2O by the following reactions [25, 36]:

$$NH_3\text{-}S_2 + HONO\text{-}S_1 \xrightarrow{k_5} N_2 + 2\,H_2O + S_1 + S_2 , \qquad (3\text{-}24)$$

$$NH_3\text{-}S_1 + HONO\text{-}S_1 \xrightarrow{k_6} N_2 + 2\,H_2O + 2\,S_1 . \qquad (3\text{-}25)$$

Reactions (3-24) and (3-25) suggest the formation of an ammonium nitrite (NH_4NO_2) intermediate which has been shown to be highly unstable at temperatures above 100 ^oC [37]. These reactions proceed very fast and free up the S_1 sites required for the oxidation of NO (steps (3-9)-(3-12)). This mechanism is consistent with negligible inhibition of the SCR reaction by water. Long et al.[37] carried out experiments in the absence of water and found that the NH_3 was present in the protonated form on acidic sites and reacted with NO_2 immediately. This also helps to explain the SCR insensitivity to added H_2O. Thus based on our experimental findings and in-line with previous literature studies, we assume that the NO oxidation is the rate limiting step for the standard SCR reaction on the Fe-zeolite catalysts.

It is instructive to note that the observed inhibition of NH_3 oxidation by H_2O is additional evidence for site blocking. Since NH_3 adsorption itself is unaffected by H_2O, the blocking is of oxygen adsorption/oxidation of Fe sites. The extent of inhibition by H_2O is not as dramatic for the NH_3 oxidation as that for the NO oxidation. That the H_2O

inhibits only one of the reactants (O_2) and not both as it does for the NO oxidation (NO and O_2), helps to explain the differences in the extent of inhibition.

Accordingly, a kinetic rate model can be derived based on this mechanism using equations ((3-9)-(3-25)). The coverage of NH_3 on S_2 and S_1 sites can be shown as

$$\sigma_{NH_3} = K_4 \, P_{NH_3} \sigma_v , \tag{3-26}$$

$$\theta_{NH_3} = K_4 K_5 P_{NH_3} \theta_v , \tag{3-27}$$

where σ_v is the mole fraction of vacant S_2 sites and θ_v is the mole fraction of vacant S_1 sites. Based on the above rate expressions, θ_v is given by

$$\theta_v = 1 - (\theta_{NO} + \theta_O + \theta_{NO_2} + \theta_{NH_3} + \theta_{HONO} + \theta_{HNO_3}). \tag{3-28}$$

In the presence of equimolar NO and NH_3, we don't see any NO_2 leaving the system as a gaseous species. Thus assuming that only the forward reaction in (3-8) is happening and is the critical step during the standard SCR chemistry, equation (3-13) can be simplified to the final rate expression for the standard SCR reaction,

$$R_{SCR} = k_1 K_1 P_{NO} \sqrt{K_2 P_{O_2}} \theta_v^2 , \tag{3-29}$$

where θ_v is given by

$$\theta_v = \frac{1}{1 + K_1 P_{NO} + \sqrt{K_2 P_{O_2}} + K_3 P_{NO_2} + K_4 K_5 P_{NH_3} + \sqrt{k_4' K_1 K_3 P_{NO} P_{NO_2}} + \dfrac{k_2' (K_3 P_{NO_2})^{1.5}}{\sqrt{k_4' K_1 P_{NO}}}} . \tag{3-30}$$

The θ_v expression can be simplified as follows. The coverage of NO_2 can be neglected in the standard SCR chemistry as it is immediately consumed ($K_3 P_{NO2} \rightarrow 0$). The N balance was closed for all the temperatures which rules out the possibility of formation of

ammonium nitrate by reaction between NH_3 and HNO_3; hence the coverage by HNO_3 can also be neglected (last term in the denominator of (3-30)). HONO formed on the surface is immediately consumed by NH_3 (to form NH_4NO_2 which is also highly unstable above 100 ^oC) and hence its coverage can also be ignored (second to last term in the denominator of (3-30)). These simplifications lead to the reduced expression of θ_v,

$$\theta_v = \frac{1}{1+ K_1P_{NO} + \sqrt{K_2P_{O_2}} + K_4K_5P_{NH_3}}. \tag{3-31}$$

θ_v in equation (3-29) can be replaced with equation (3-31) to get the overall rate of the SCR reaction. The kinetic data can be predicted very well with the proposed rate expression.

Again, the rate expression (3-29) is based on the assumed Langmuir Hinshelwood kinetics discussed earlier. Neglecting the surface coverage of NO, equation (3-29) can be modified as per the Eley-Rideal mechanism,

$$R_{SCR} = k_1' P_{NO} \sqrt{K_2 P_{O_2}} \theta_v', \tag{3-32}$$

where

$$\theta_v' = \frac{1}{1+ \sqrt{K_2P_{O_2}} + K_4K_5P_{NH_3}}. \tag{3-33}$$

A quantitative study focused on the comparison of predictive capabilities of the various models is needed to identify the efficiencies of various models.

3.3.8 Transient Experiments for Standard SCR Reaction

Transient experiments were also carried out on the SCR catalyst to understand the SCR chemistry under the more realistic conditions encountered in a vehicle [134, 135]. In

these experiments Ar was used as the gas carrier and NO was fed in the presence of 5% O_2 under isothermal conditions. In contrast to the steady state experiments, NH_3 was pre-adsorbed on the catalyst for 60 minutes and then the NO was fed as a step change from 0 to 500 ppm. A range of temperatures were considered (150 – 400 ^oC). The commercial Fe-zeolite monolith catalyst was used for these experiments. The space velocity was maintained the same as in the steady state experiments. Before each experiment the catalyst was conditioned by heating it for 30 minutes at 500 °C in 5% O_2, in order to oxidize the surface and remove any NH_3 or other species present on the catalyst. Then NH_3 was fed continuously for 3600 s at a concentration of 500 ppm and then stopped. After that, only Ar was flowed through the reactor for 1800 s, to release loosely-bound NH_3 from the catalyst; (i.e., the intention was to study only the chemisorbed NH_3 present in the sample that reacted with the NO). Once most of the weakly bound NH_3 was released, 500 ppm of NO and 5% O_2 were fed to the reactor at constant feed temperature.

As shown (Figure 3-21), for the lowest temperature experiment (150 ^oC), reaction proceeded immediately once the NO was added, and a significant increase in N_2 occurred. Even after the N_2 concentration dropped to 0, it was observed that the NO concentration never reached its inlet concentration of 500 ppm. This is attributed to the NO oxidation reaction, which produces NO_2. The amount of NO_2 produced was nearly the same as that of found during the individual NO oxidation reaction. Only N_2 was produced at this low temperature. The N_2 concentration increased to about 100 ppm and stayed relatively constant for 450-500 s. Eventually its concentration decreased and slowly approached to 0. In contrast, the NO concentration plateaued to 400 ppm for 450-500 s, and then increased to about 460 ppm where it stayed constant. At the same time

NO approached its final concentration and NO_2 was observed. This suggests that most of the NH_3 was depleted on the catalyst and that no more reductant was available to react with NO. After that point no NO was reduced since the catalyst surface was devoid of NH_3. No N_2O gas was detected during the entire reaction.

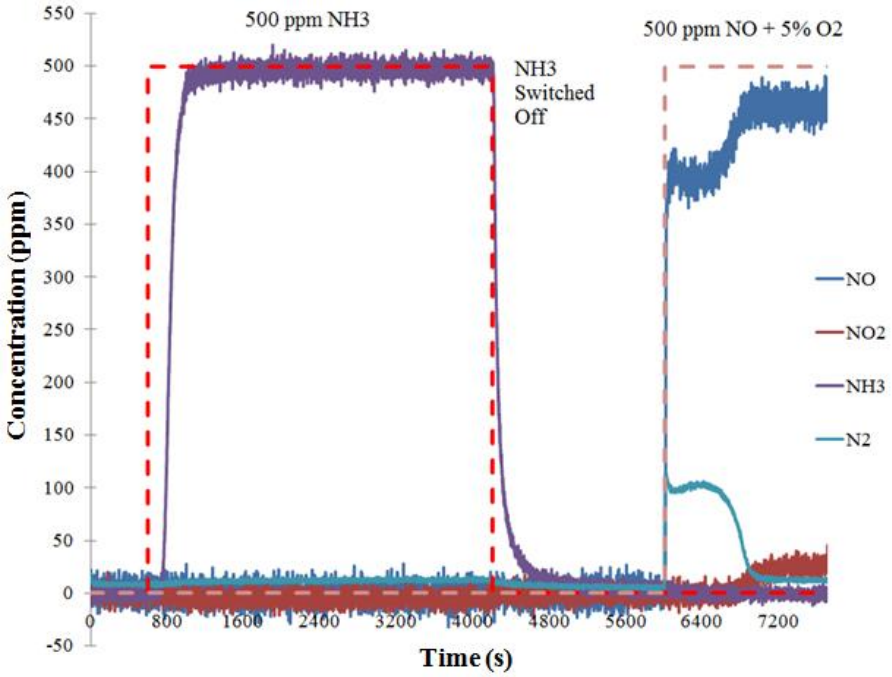

Figure 3-21: Transient experimental findings of standard SCR reaction on commercial Fe-zeolite washcoated catalyst at 150 ^oC. Feed: step feed containing 500 ppm NH_3 in Ar introduced during 600-4200 s. 500 ppm NO, 5% O_2, Ar was fed at 6000 s.

The same procedure was repeated at all the other temperatures. The results are grouped according to the different species studied (i.e., N_2, NO, and NO_2) and are presented in the Figure 3-22. At 200 ^oC, the N_2 formation showed a somewhat different trend. Contrary to the lower temperature, no temporal stationary level was achieved. After an initial fast increase in the concentration, the rate of N_2 formation increased substantially to a peak value of about 300 ppm. After that, the N_2 concentration decreased to 0 ppm. NO also exhibited a much different behavior from the 150 ^oC case. Its

concentration initially increased to about 250 ppm, and then followed a sudden drop in concentration to a relative minimum of about 200 ppm. After that, the concentration again increased towards the final stationary concentration, determined by the NO oxidation reaction (410 ppm). It is interesting to note that considerably less time was needed for NO_2 to break through for the case of 200 ^oC (190s) compared to the 150 ^oC case (790 s). In this case, the SCR reaction lasted for 200s, almost 4 times less than for the previous temperature. No N_2O was detected in all the temperatures studied. At 250 ^oC, 300 ^oC, and 350 ^oC the behavior of the different species was for the most part similar. One notable difference was the extent and duration of the N_2 production. Its peak value increased with temperature but the duration of its production decreased. The N_2 production had a steep increase up to about 400 ppm, 500 ppm and 500 ppm, respectively, for each temperature, followed by a sharp decrease in concentration. Even though the catalyst has a higher selectivity to N_2 at higher temperatures, the total amount of N_2 produced during the entire reaction is lower. This can be seen by comparing the areas of N_2 curves for each of the temperatures studied. In the case of 150 ^oC, the amount of N_2 produced was 0.048 moles compared to only 0.011 moles at 350 ^oC. The NH_3 storage capacity of the catalyst decreased at higher temperatures, as was observed in the case of ammonia TPD experiments. The NO concentration presented a similar trend at the three temperatures, showing a pronounced increase which reached immediately a stationary concentration. At higher temperatures it was observed that the amount of NO reacting decreased and the steady state concentration was achieved in a shorter period of time. The reaction time was about 140s, 80s, and 50s for 250 ^oC, 300 ^oC and 350 ^oC, respectively. These shorter durations of reaction resulted in earlier breakthroughs of NO_2.

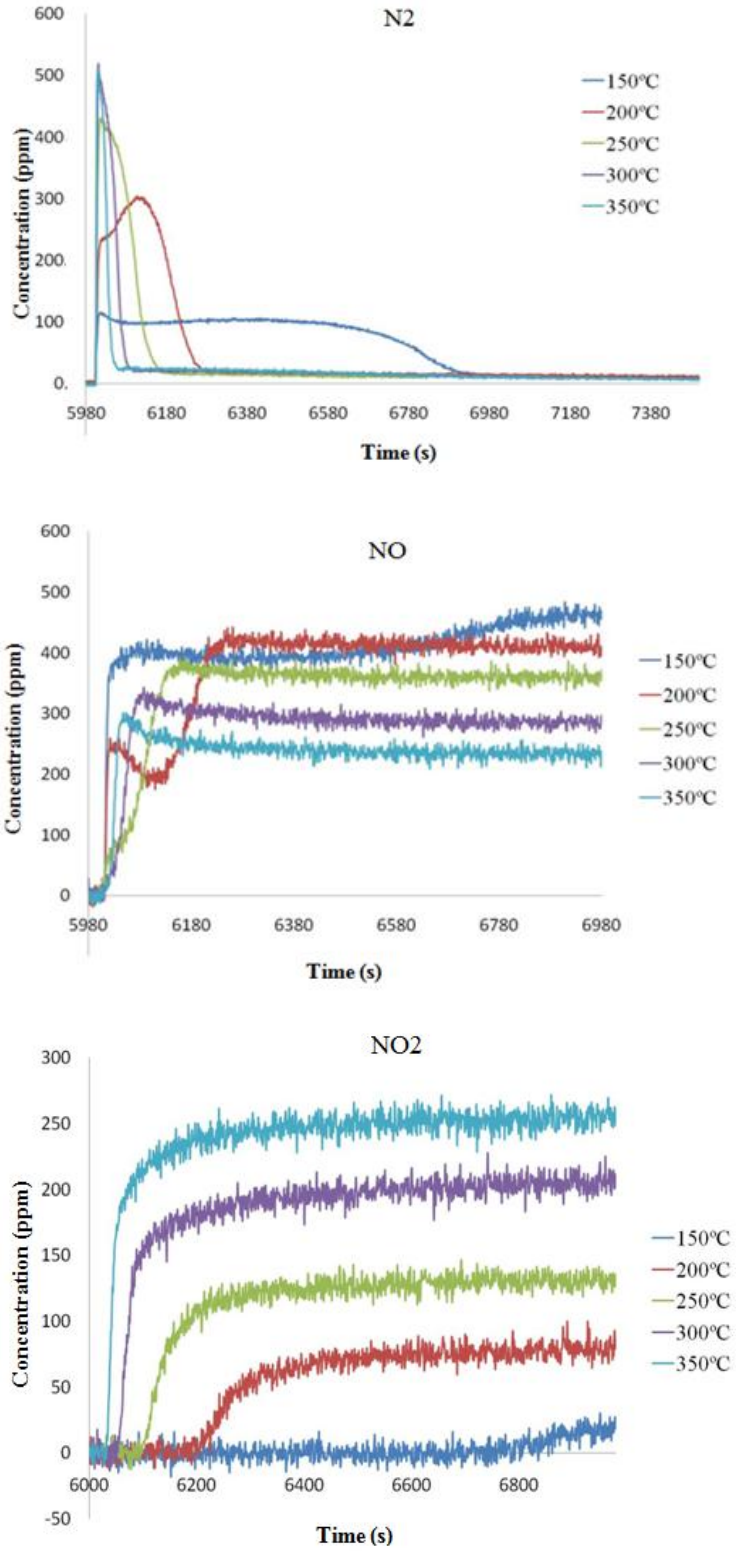

Figure 3-22: Concentrations of N_2, NO and NO_2 during the transient experiments at different temperatures with preadsorbed NH_3. Feed: step feed containing 500ppm NH_3 in Ar was fed during 600-4200s. 500 ppm NO, 5% O_2 and Ar fed at 6000s.

NO_2 was recorded only after the N_2 concentration dropped to 0 ppm. These data are consistent with the steady state integral data reported earlier which showed no measureable NO_2 in the outlet during the standard SCR reaction studies [128].

A final set of transient experiments was performed to study the NH_3 inhibition effect on the standard SCR reaction. Nova et al. [25, 27] reported transient kinetic data showing NH_3 inhibition on the standard SCR chemistry on the V-based catalysts. We followed a similar approach for the Fe-zeolite catalysts. Here, NO, NH_3 and O_2 were fed simultaneously to the reactor. After steady state concentrations of all the species were achieved, NH_3 was switched off. NO was seen to decrease immediately after ammonia was shut off. It went through a minimum and then increased, eventually reaching a new steady state with simultaneous formation of NO_2 due to the NO oxidation reaction. During the dip in NO concentration, the N_2 product transient profile was essentially a mirror image of the NO profile. NO_2 was observed only after the N_2 concentration decreased to zero. These experiments confirmed the inhibition effect of ammonia on the standard SCR reaction. That is, as the NH_3 was consumed through reaction there was a short-lived increase in the consumption of NO. Thus the transient experiments support the observations of the steady state experimental data for standard SCR and NO oxidation reactions.

3.4 Conclusions

This work reports the steady state and transient experimental findings for the NH_3 SCR reaction of NO on Fe-zeolite monolithic catalysts. Washcoated Fe-ZSM-5 catalysts (FeZ) were synthesized in our lab. A systematic study was performed to understand the

reaction systems of NO + NH_3 + O_2 (standard SCR), NO oxidation and NH_3 oxidation reactions on both the commercial Fe-zeolite and FeZ catalysts. Very comparable results were obtained on both the catalysts studied proving our catalyst synthesis capabilities.

Differential kinetics derived on standard SCR reaction showed that the reaction is nearly first order with respect to NO, positive (+0.52 to +0.59) order with respect to O_2 and negative (-0.27 to -0.32) order with respect to ammonia. Ammonia is found to have an inhibiting effect on standard SCR reaction due to ammonia blocking the active sites required for this reaction at low temperatures and due to ammonia oxidation at higher temperatures. The inhibition effect of ammonia on standard SCR reaction was further confirmed with transient experiments where NO conversion was promoted in the absence of gas phase NH_3. The NO oxidation reaction was found to be equilibrium limited for temperatures higher than 350 ^oC due to the reverse NO_2 decomposition reaction. Differential kinetics studies on NO oxidation showed close resemblance with the standard SCR reaction considering the reaction rates, activation energies and the reaction orders with respect to NO and O_2. This supports the proposed idea in the literature that the NO oxidation is the rate determining step in standard SCR reaction. The presence of water showed negligible inhibition on the standard SCR reaction while the NO and NH_3 oxidation reactions were strongly inhibited by H_2O. NO_2 along with the nitrites and nitrates formed in the presence of water appear to block the active sites for NO oxidation. However, during the standard SCR reaction, NH_3 cleans the catalyst surface by immediately reacting with the surface species to form an unstable intermediate, ammonium nitrite, which decomposes to N_2 and H_2O. The role of NH_3 serves to remove the nitrous and nitric acids, freeing up sites for adsorption of O_2 and NO. A dual-site

Langmuir-Hinshelwood kinetic model; which considers the NH_3 adsorption on acidic sites and the NO oxidation on Fe-sites; is proposed in agreement with our experimental observations. Along with the Langmuir-Hinshelwood kinetics, the Eley-Rideal mechanism can also explain the reaction mechanism.

To our knowledge, this work includes novel approach focused on the in-depth studies of washcoat diffusion limitations in the Fe-zeolite catalyst. Our findings clearly show the importance of washcoat diffusion limitations at higher temperatures which must be considered in the analysis, modeling, and design of the SCR converter.

Transient experiments performed on ammonia uptake and desorption showed that the ammonia adsorption capacity of the Fe-zeolite catalyst is strongly temperature dependent. Transient experiments carried out on the standard SCR reaction support the steady state experimental findings on the standard SCR and NO oxidation reaction. The inhibition by ammonia on the standard SCR reaction was noted at lower temperatures in the transient experiments. A quantitative kinetic analysis of these data and a follow-up study of the reduction of NO and NO_2 with NH_3 are covered in next chapters.

CHAPTER 4 Effect of NO_2 on the Reaction Mechanism and Kinetics of Selective Catalytic Reduction of NOx with NH_3 on Fe-ZSM-5

4.1 Introduction

The selective catalytic reduction of gas mixtures containing NO and NO_2 is a highly complex system involving multiple simultaneous reactions. N_2 is the main and desired product of these reactions. But a number of byproducts including N_2O, NH_4NO_3, HNO_3 etc., are formed. The overall chemistry involved in the SCR system is summarized in Chapter-2. Various catalysts are used for NH_3-SCR applications. Vanadium based catalysts have been well studied in the literature and the kinetics of SCR on this catalyst are by now well-known [20, 21, 24, 25, 50, 63, 67, 154]. This catalyst is found to have reduced selectivity at higher temperatures and vanadia which escapes to the environment can be problematic. For these reasons, recent research has focused on Fe- and Cu- based zeolite catalysts which are found to have a high NOx removal efficiency over a wide range of temperatures [87, 121, 134, 135]. In contrast to vanadia-based catalysts, far fewer studies are available on the kinetics of SCR reaction system on Fe- (or Cu-) based zeolite catalysts [34, 36, 78, 100, 117-120]. The performance of Cu- and Fe-zeolite catalysts have been reported in [89, 102, 116, 117, 120, 155, 156] and [29, 31, 33, 36-38, 41, 42, 118], respectively. In general, Cu-based catalysts have higher activity at lower temperatures (< 300 ^oC) whereas Fe-based catalysts are more active at higher temperatures (> 350 ^oC). In this chapter, our focus is on iron-based zeolite monolith catalysts.

To this end, the objective of the current study is to carry out comprehensive experiments on Fe-ZSM-5 monolith catalysts. The standard SCR reaction system was

studied in detail earlier in [103] and the results from this study are discussed in Chapter 3. We reported the results of integral and differential conversion experiments to elucidate the product distribution as a function of the main operating parameters and to quantify the kinetics in terms of apparent reaction orders and activation energies. In the current study, the effect of NO_2 is a focus. Transient experiments performed on this catalyst gives further understanding of the influence of NO_2 on the SCR system. Also, the role of NO in the presence of excess NO_2 is discussed with some transient and steady state experiments. The influence of water on the NOx reduction for various feed NO_2/NOx ratios is considered separately.

4.2 Experimental

4.2.1 Catalyst

The SCR of NOx by NH_3 reaction system was studied on both a commercial Fe-ZSM-5 catalyst and an in-house synthesized Fe-ZSM-5 monolith catalyst. Characteristics of both the catalysts are reported in Table 4-1. The in-house catalysts were prepared by dip-coating a blank cordierite monolith with slurry comprising a mixture of the Fe-ZSM-5 powder and γ-alumina particles. The Fe-ZSM-5 was prepared by a series of ion exchange and washing steps starting with the ammonium form and ending with the iron form; i.e., $NH_4^+ \rightarrow H^+ \rightarrow Na^+ \rightarrow Fe^{2+}/Fe^{3+}$. More detail about the catalyst synthesis and washcoating procedure can be found in Chapter 2 and [103].

Table 4-1: Characteristics of the commercial Fe-zeolite monolithic catalyst and the FeZ-18 catalyst.

Properties	Commercial Fe-zeolite Catalyst	FeZ-18 Catalyst
Si/Al ratio	27	25
Fe (wt% in the washcoat)	3.5 (± 0.5)	2.5 (± 0.5)
Al (wt % in the washcoat)	13-15	15-16
Si (wt % in the washcoat)	36-38	33-35
O_2 (Balance)	46	48
BET Surface Area (m^2/gm)	-	352
Washcoat Thickness (μm)	45-50	30-35

4.2.2 Bench-Scale Reactor Set-up

The experimental setup was the same one used in previous studies and is described in detail in Chapter 2 and elsewhere [103, 132, 139, 152]. A monolith catalyst with ca. 34 channels and 2 cm length was used to carry out most of the experiments. Before starting each experiment, the catalyst was pretreated by flowing 5% O_2 in Ar with total flow rate of 1000 sccm while keeping the catalyst temperature constant at 500 ^oC for 30 minutes.

Steady-state experiments were carried out using Ar as the diluent. NO_2 adsorption experiments were carried out on the commercial Fe-zeolite catalyst by flowing 500 ppm of NO_2 at several catalyst temperatures (100 ^oC, 150 ^oC and 200 ^oC) until saturation (about 1 hour). Then the feed NO_2 was stopped and 1000 sccm of Ar only was admitted for 30 minutes to desorb any loosely bound NO_2. A temperature ramp of 10 ^oC/min was then applied to desorb NO_2 from the catalyst surface. Reduction of the NO/NO_2 mixture was carried out on both the commercial Fe-zeolite and in-house synthesized FeZ

catalysts. Unless otherwise stated, 5% O_2 and an Ar gas carrier were utilized over a range of temperatures (150–500 ^oC) and various NO_2/NOx ratios (0, 0.25, 0.5, 0.75 and 1). Both 500 ppm of NH_3 and 500 ppm of NOx were present in the feed. The presence of NO_2 in the feed required the catalyst temperature to be more than 170 ^oC in order to avoid the deposition of ammonium nitrate onto the catalyst. All gas lines were kept heated for this purpose. The effect of water was studied in separate experiments by repeating some of the above experiments with 2% H_2O in the feed.

Transient experiments were carried out on the commercial Fe-zeolite monolithic catalyst to identify and understand the reaction system dynamics. The catalyst was initially pre-saturated with ammonia in the presence of Ar at a total flow rate of 1000 sccm. The NH_3 was then switched off and only Ar was flowed to remove any physisorbed NH_3 from the catalyst. Then a gas containing 500 ppm of NOx with different NO/NO_2 ratios (1/0, 1/1 and 0/1) was fed to the reactor in the presence of 5% O_2. The transient effluent composition was measured. These experiments were carried out under isothermal conditions for various temperatures in the range of 150 - 400 ^oC.

Experiments were performed on the commercial Fe-zeolite monolithic catalyst to gain further insight into the kinetics of the fast and NO_2 SCR reactions. For these experiments, a smaller piece of monolith comprising only 4 channels and 5 mm length was used. The total gas flow rate was maintained at 1000 sccm, enabling a higher space velocity (2×10^6 hr^{-1}). The effect of NO_2 concentration was examined over a range of 100-800 ppm while keeping the NH_3 concentration constant at 500 ppm. The effect of NH_3 was examined over the same range (100-800 ppm) while NO_2 was kept constant at 500 ppm. The effect of O_2 was studied by varying its concentration from 0-5% while keeping

both NO_2 and NH_3 constant at 500 ppm. These experiments were carried out at three different temperatures of 185 ^oC, 215 ^oC and 245 ^oC. A similar approach was used to perform differential kinetics studies for the fast SCR reaction.

4.3 Results and Discussion

4.3.1 NOx Adsorption Study

In Chapter 3, the uptake of NH_3 on the commercial Fe-zeolite catalyst was quantified [103]. The Fe-zeolite catalyst was found to adsorb ca. 0.37 mol NH_3/kg catalyst at 150 ^oC. Here we performed similar experiments to quantify NO and NO_2 storage on the same catalyst. In the absence of O_2, the NO concentration reached its inlet value almost immediately, indicating weak adsorption of NO on the Fe-zeolite catalyst. This was confirmed during the subsequent temperature ramp in which only very small amounts of NO were measured. Similar results on Fe-zeolite and other types of catalysts have been reported in the literature [39, 99, 100, 143, 157].

The adsorption behavior of NO_2 was quite different. Figure 4-1 shows the results obtained for NO_2 adsorption at 100 ^oC following the same procedure as for NO. Some NO was evolved upon the introduction of NO_2. This behavior is reminiscent of NO_2 storage on $Pt/BaO/Al_2O_3$ lean NOx trap (LNT) catalysts [158]. Grossale et al. [39] inferred that the NO_2 disproportionation leads to the formation of nitrates and NO,

$$3\ NO_2 + O^{2-} \rightarrow 2\ NO_3^- + NO. \qquad (4\text{-}1)$$

The temperature ramp (10 ^oC/min) resulted in two peaks; the first smaller peak at about 150 ^oC corresponds to loosely bound NO_2. This peak was not observed at higher storage temperatures. A much larger NO_2 peak was observed at higher temperatures (ca.

250-350 ^{o}C) during the ramp. The area under the desorption peak decreased with increasing temperatures of adsorption (from 100 ^{o}C to 200 ^{o}C). At higher temperatures (≥ 350^{o}C) during the temperature ramp, a small amount of NO was detected most likely due to NO_2 decomposition. The uptakes of NH_3, NO and NO_2 are obviously of interest in the overall catalyst performance and kinetics. We return to these findings in the evaluation of the steady-state and transient experiments.

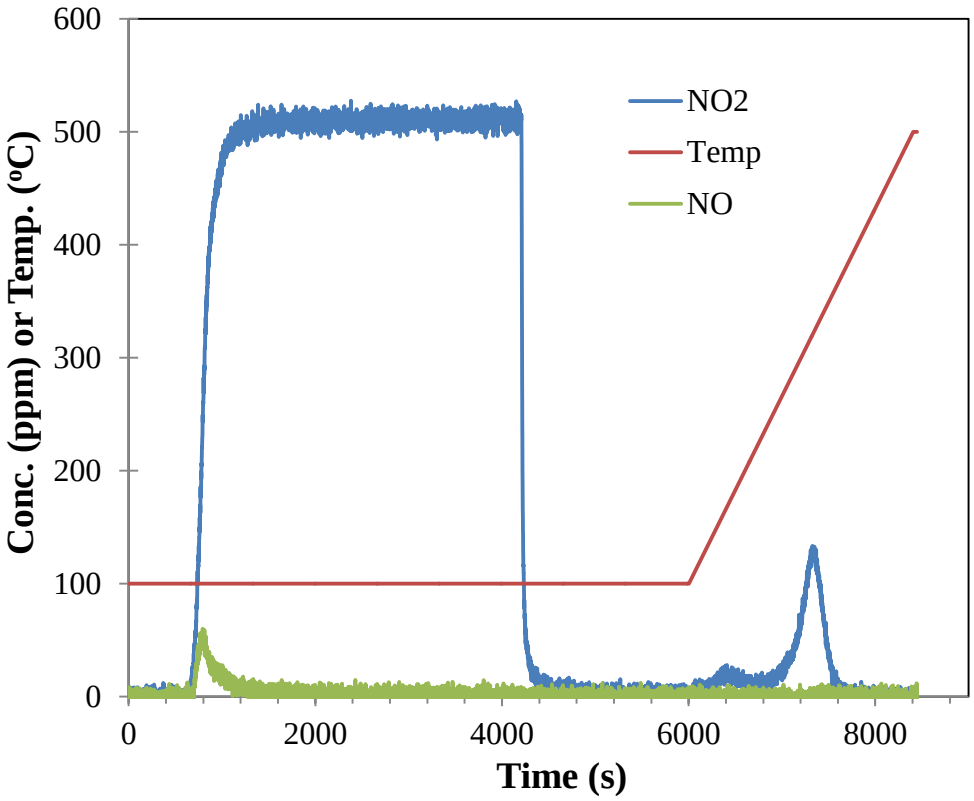

Figure 4-1: NO_2 TPD experiments performed on Fe-zeolite catalyst at 100 ^{o}C as the initial temperature of adsorption. 500 ppm of NO_2 was adsorbed on the catalyst for 1 hour. Temperature ramp of 10 ^{o}C/min was given at 6000s.

4.3.2 NO Oxidation and NO_2 Decomposition

The NO oxidation reaction was studied on both the commercial Fe-zeolite catalyst and in-house synthesized FeZ-18 catalyst. In our earlier studies, we got comparable results for the NO oxidation reaction on both the catalysts [103]. In that study the

inhibition effects of H_2O and NO_2 on the NO oxidation reaction were observed and a kinetic expression was proposed. The results indicated that NO_2 formation was the rate determining step for the standard SCR chemistry [34, 36, 37]. The reaction is kinetically limited up to about 350 ^oC beyond which it becomes equilibrium limited due to NO_2 decomposition. Additional data indicate

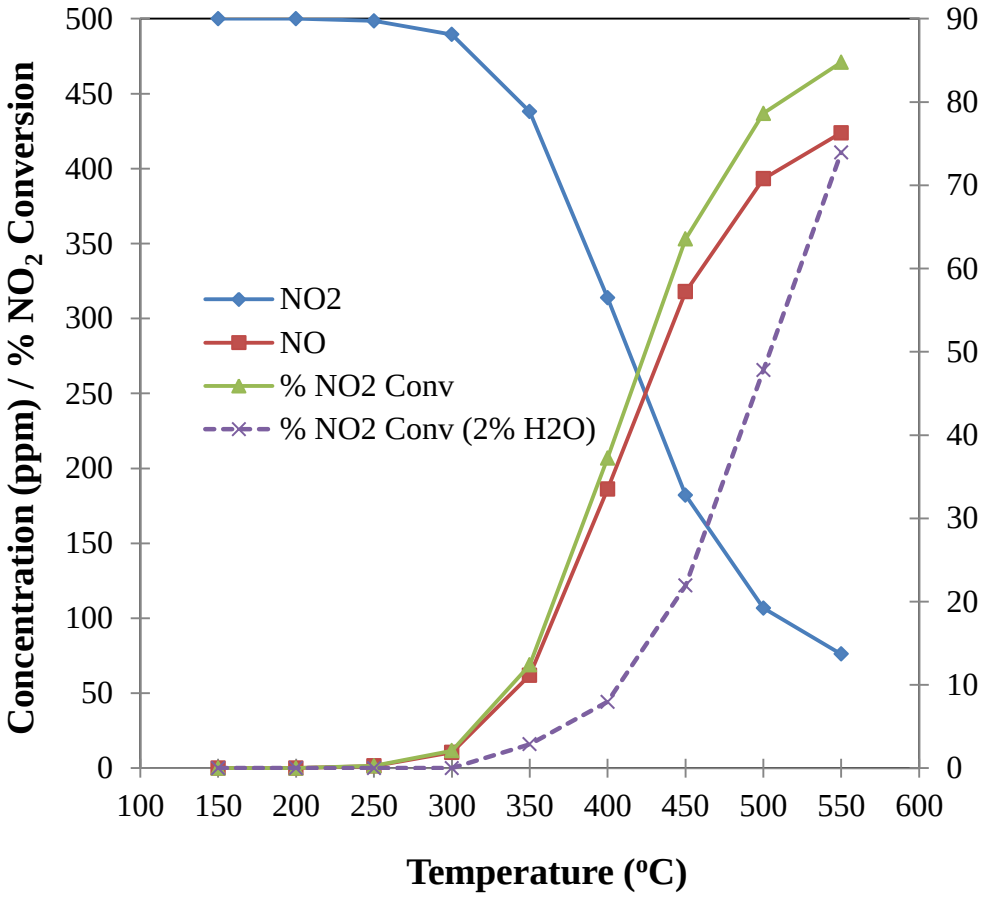

Figure 4-2: NO_2 decomposition reaction experiments carried out on Fe-zeolite catalyst in the temperature range of 150-550 ^oC. Feed: 500 ppm NO_2 , 0-2% H_2O. Total flow: 1000 sccm. Space velocity: 57,000 hr^{-1}.

that NO_2 decomposition is even more extensive at higher feed NO_2 concentrations. We studied the NO_2 decomposition reaction on the commercial Fe-zeolite catalyst, the results of which are shown in Figure 4-2. These data reveal that the NO_2 decomposition commences at 300 ^oC with about 2% NO_2 conversion. The reaction becomes more

pronounced at higher temperatures with about 85% NO_2 decomposed at a temperature of 550 ^oC. The decomposition was also studied in the presence of 2% H_2O and it was found that water significantly inhibits the reaction. This is in agreement with similar results for the forward NO oxidation reaction given by

$$NO + ½\ O_2 \leftrightarrow NO_2 \qquad \Delta H = -\ 5.7 \times 10^4\ J/mol\ NO. \qquad (4\text{-}2)$$

4.3.3 Selective Catalytic Reduction of NOx: Steady-State Experiments

The SCR of NOx by ammonia was studied on both the commercial Fe-zeolite and in-house synthesized FeZ-18 catalyst. Feeds containing various NO_2/NOx inlet ratios (0-1) were used to quantify the NOx conversion, N_2 selectivity and product distribution as a function of temperatures.

It is instructive to show selected standard SCR data before examining the effect of NO_2 in the feed. The standard SCR reaction involves NO and NH_3 reacting in presence of O_2 and is given by

$$4\ NH_3 + 4\ NO + O_2 \rightarrow 4\ N_2 + 6\ H_2O \qquad \Delta H = -\ 4.07 \times 10^5\ J/mol\ NH_3. \qquad (4\text{-}3)$$

Figure 4-3 shows the changes in the effluent concentrations as a function of temperature during the standard SCR reaction experiments carried out on the FeZ-18 catalyst. Negligible NO conversions (< 20%) were observed up to 250 ^oC. Temperatures above 300 ^oC resulted in a large increase in NO conversion, which approached 91% at 450 ^oC. The NH_3 conversion always exceeded the NO conversion (for $T \geq 300\ ^oC$) because of the NH_3 oxidation side reaction. Negligible amounts of N_2O (< 10ppm) were observed in the temperature range of 250-300 ^oC. In our earlier study in Chapter 3, separate experiments proved a positive order of NO (~ 1) and O_2 (~0.56) on the standard SCR reaction while

NH_3 showed a moderate inhibition (~ -0.3) at lower temperature. Water (2%) in the feed was observed to have only negligible effect on the standard SCR reaction. Detailed kinetic studies were carried out on the standard SCR reaction in Chapter 3.

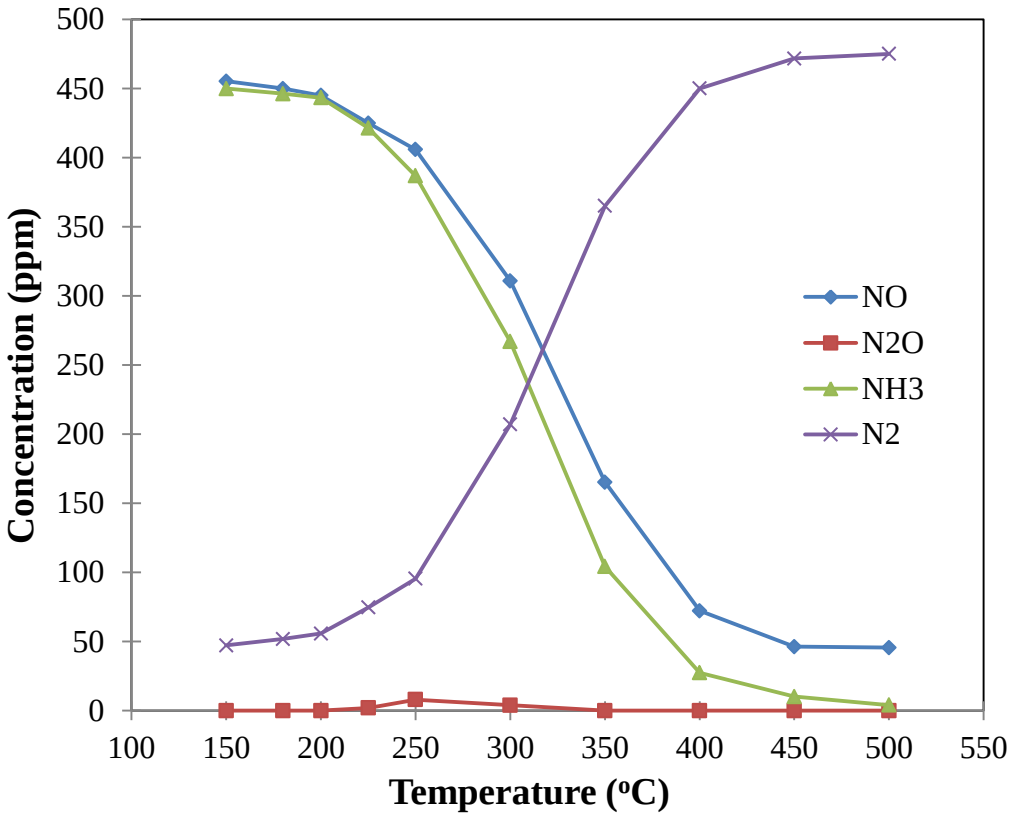

Figure 4-3: Steady state product distribution obtained for the standard SCR of NOx with NH_3 as a function of temperature. Space velocity 57,000 hr^{-1}. Total Flow rate = 1000 sccm. Feed: 500 ppm NO, 500 ppm NH_3, 5% O_2.

The effect of NO_2 on the NOx conversion was considered for this work and is described next. In the presence of NO_2, fast and NO_2 SCR reactions become important in the SCR system. The fast SCR reaction is given by

$$2\ NH_3 + NO + NO_2 \rightarrow 2\ N_2 + 3\ H_2O \qquad \Delta H = -3.78 \times 10^5\ J/mol\ NH_3. \qquad (4\text{-}4)$$

The NO_2 SCR reaction involves reaction between NO_2 and NH_3 and is given by

$$4\ NH_3 + 3\ NO_2 \rightarrow 3.5\ N_2 + 6\ H_2O \qquad \Delta H = -3.41 \times 10^5\ J/mol\ NH_3. \qquad (4\text{-}5)$$

Figure 4-4 shows the results obtained for a NO_2/NOx feed ratio of 0.25 (total NOx concentration and NH_3 at 500 ppm) in the presence of 5% O_2 carried out on the FeZ-18 catalyst. It is interesting to note that the apparent NO_2 conversion is essentially complete for the entire temperature range. At 200 ^oC, about 125 ppm of the 375 ppm NO that was fed was consumed while all of the NO_2 (125 ppm) was consumed. Thus a substantial increase in the NOx conversion was observed at lower temperatures compared to that of the standard SCR reaction. Moreover, N_2 was the only N-containing product at low temperatures. The N-balance was satisfied throughout the temperature range which rules out the formation of any undetected byproducts like ammonium nitrate (we return to this issue later). A stoichiometric consumption of NOx and NH_3 was observed up to 250 ^oC; beyond this the ammonia consumption exceeded the NOx conversion due to the ammonia oxidation side reaction, although the difference did not exceed 20 ppm. Compared to the standard SCR results, the current data indicate that the ammonia oxidation side reaction is less pronounced in the presence of NO_2. At temperatures of 250-300 ^oC, a very small but detectable amount (< 10 ppm) of N_2O was observed. No N_2O was detected at higher temperatures. Again, no NO_2 was detected at any temperature, clearly indicating the complete consumption of NO_2. These data indicate that the amount of NO consumed was comparable to the amount of NO_2 consumed up to 225 ^oC. Moreover, the consumption of equimolar amounts of NO and NO_2 suggest that the fast SCR reaction is the only reaction taking place at these low temperatures and is much faster than the standard SCR reaction. However, at temperatures above 250 ^oC, an additional quantity of NO was consumed due to the increase in the standard SCR reaction rate. Finally, when water was added to the

feed (2%), it was found to have only a negligible effect on NOx conversions at most of the temperatures.

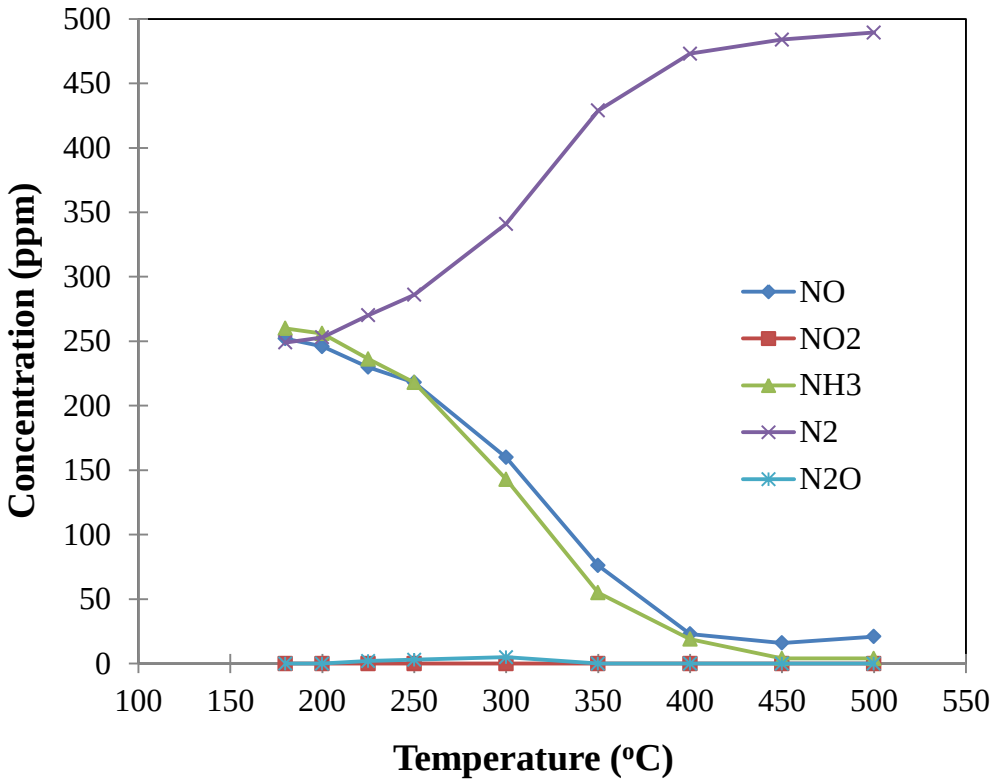

Figure 4-4: Steady state product distribution obtained for SCR of NOx with NH_3 as a function of temperature. Space velocity 57,000 hr^{-1}. Total Flow rate = 1000 sccm. Feed: 375 ppm NO, 125 ppm NO_2, 500 ppm NH_3, 5% O_2.

When the feed contains equal amounts of NO and NO_2, this is the so-called fast SCR reaction (reaction (4-4)). This reaction was studied on both the commercial catalyst and in-house FeZ-18 catalyst. Results obtained with the FeZ-18 catalyst are shown in Figure 4-5. The reaction proceeds much faster than the standard SCR reaction. Very high NOx conversions were obtained at temperatures as low as 180 ^oC; e.g., a NOx conversion of 74% was obtained at 180 ^oC. N_2 was the main product of this reaction, although at lower temperatures (< 200 ^oC) some ammonium nitrate was formed as a byproduct (discussed below). A negligible amount of N_2O (< 20 ppm) was observed in the

temperature range of 250-300 ^{o}C. The amount of NO_2 consumed exceeded the amount of NO consumed up to 300 ^{o}C. The fast SCR reaction stoichiometry involves an equimolar consumption of NO and NO_2 (reaction (4-4)). This result suggests that the additional NO_2 consumed is due to the NO_2 SCR reaction (4-5). Apart from these two reactions, some NO_2 reacts with NH_3 forming the earlier mentioned ammonium nitrate by

$$2\ NH_3 + 2\ NO_2 \rightarrow N_2 + NH_4NO_3 + H_2O \qquad \Delta H = -\ 2.91 \times 10^5\ J/mol\ NH_3. \qquad (4\text{-}6)$$

Ammonium nitrate cannot be detected by the FT-IR. The formation of ammonium nitrate was confirmed by the lack of closure of the N-balance. Specifically, there was ca. 64 and 42 ppm of N-balance missing at the temperatures of 180 ^{o}C and 200 ^{o}C respectively. Ammonium nitrate either leaves the system in gaseous form, deposits as a solid onto the surfaces or decomposes to N_2O [20, 21, 24, 29, 33, 39] via reaction

$$NH_4NO_3 \rightarrow N_2O + 2\ H_2O \qquad \Delta H = -\ 3.66 \times 10^4\ J/mol\ NH_4NO_3. \qquad (4\text{-}7)$$

The first two routes are not detectable. Analysis indicates the formation of 32 ppm and 21 ppm NH_4NO_3 at 180 ^{o}C and 200 ^{o}C, respectively, following the stoichiometry of reaction (4-6). At higher temperatures ($\geq$ 250 ^{o}C), the N-balance was closed for the equimolar feed and therefore no net ammonium nitrate formation occurred. Ammonia was consumed in nearly equimolar amounts as that of NOx. This suggests that the oxidation of ammonia by O_2 was not important in the presence of NO_2. Similar trends for the fast SCR reaction were reported in the literature on Fe-zeolite and other catalysts [20-22, 24, 29, 39, 117, 118]. The effect of 2% feed H_2O was studied separately on the fast SCR reaction system. Similar to the standard SCR reaction, water was found to have a negligible role in the fast SCR chemistry.

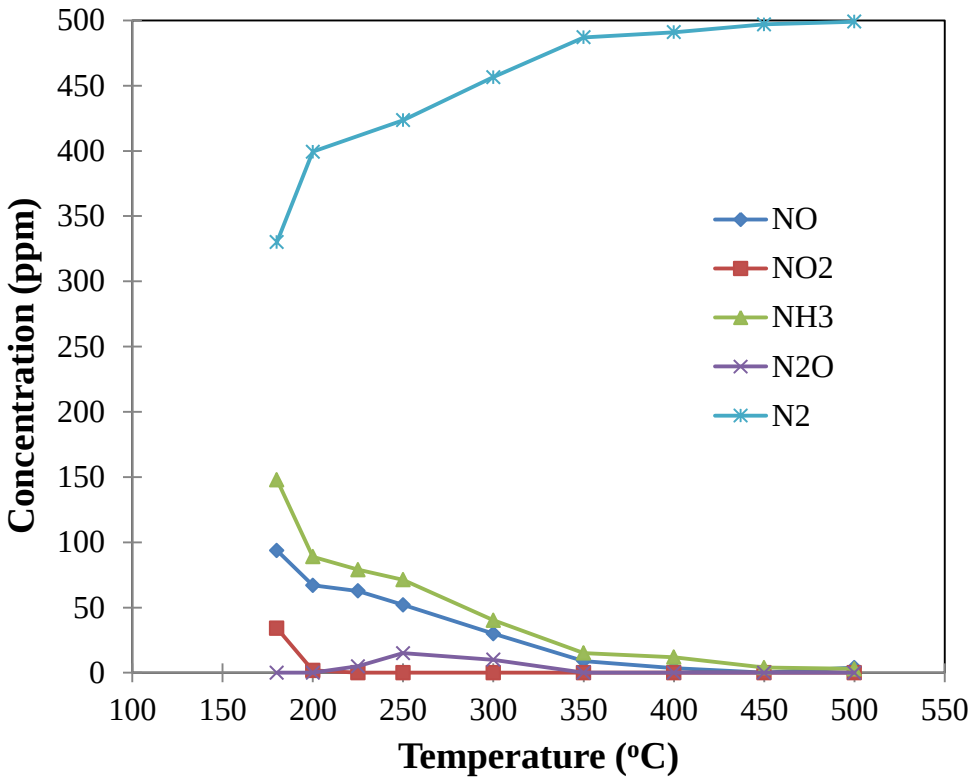

Figure 4-5: Steady state product distribution obtained for SCR of NOx with NH_3 as a function of temperature. Space velocity 57,000 hr^{-1}. Total Flow rate = 1000 sccm. Feed: 250 ppm NO, 250 ppm NO_2, 500 ppm NH_3, 5% O_2.

Similar results were obtained on the commercial Fe-zeolite catalyst. In order to decrease the NOx conversions, the catalyst length was shortened to 1 cm and the total NOx concentration was increased to 1000 ppm. The NH_3 was also adjusted to 1000 ppm in the inlet feed. Thus, in doubling the space velocity, the NOx conversion was moderately reduced for temperatures below 250 ^oC. But for higher temperatures, very high NOx conversions (same as 2 cm catalyst) were obtained. This indicated that the reaction was complete in first 1 cm length of the monolith.

The effects of a higher fraction of NO_2 in the feed was examined. Figures 4-6 to 4-8 show the results obtained with FeZ-18 catalyst for feeds containing NO_2/NOx ratios of 0.75 and 1, respectively. These data show that the NOx reduction is very fast when

NO_2 concentration exceeds the NO concentration. About 55% of the NO_2 was converted in the temperature range of 180-200 ^oC. By 250 ^oC, the NO_2 conversion increased sharply to > 98%. However, above 350 ^oC the NO_2 conversion decreased with some NO and NO_2 appearing in the outlet. At 500 ^oC the NOx conversion had decreased to about 93% and the effluent NO concentration increased to 20 ppm. Effluent NO clearly indicates the decomposition of NO_2 to NO by the backward reaction in the following NO oxidation reaction (4-2). The incompletely converted NO_2 suggests the depletion of NH_3. Indeed, at higher temperatures, the NH_3 consumption exceeded the NOx consumption due to NH_3 oxidation reaction given by

$$4\ NH_3 + 3\ O_2 \rightarrow 2\ N_2 + 6\ H_2O \qquad \Delta H = -\ 3.12 \times 10^5\ J/mol\ NH_3. \qquad (4\text{-}8)$$

An added feature was the more pronounced production of N_2O at lower temperatures. Up to 250 ^oC the N-balance did not close, which as described earlier infers the formation of ammonium nitrate. The imbalance of N, accounted to about 56 ppm of NH_4NO_3 formed at 180 ^oC. By 250 ^oC, the inferred concentration decreased to 9 ppm. At higher temperatures the N-balance closed, suggesting that ammonium nitrate was completely consumed. The maximum N_2O concentration occurred at about 275 ^oC for NO_2/NOx =0.75. The decrease in N_2O at higher temperatures can be attributed to either its decomposition to N_2 (reaction (4-9)), to its reaction with NH_3 (reaction (4-10)), to an increase in the rate of NO_2 SCR reaction (4-5), or a combination of these factors. At temperatures of 450-500 ^oC, no N_2O was detected in the effluent and therefore N_2 was the only N-containing major product.

$$2\ N_2O \rightarrow N_2 + O_2 \qquad \Delta H = -\ 8.2 \times 10^4\ J/mol\ N_2O. \qquad (4\text{-}9)$$

$$2\ NH_3 + 3\ N_2O \rightarrow 4\ N_2 + 3\ H_2O \qquad \Delta H = -\ 4.4 \times 10^5\ J/mol\ N_2O. \qquad (4\text{-}10)$$

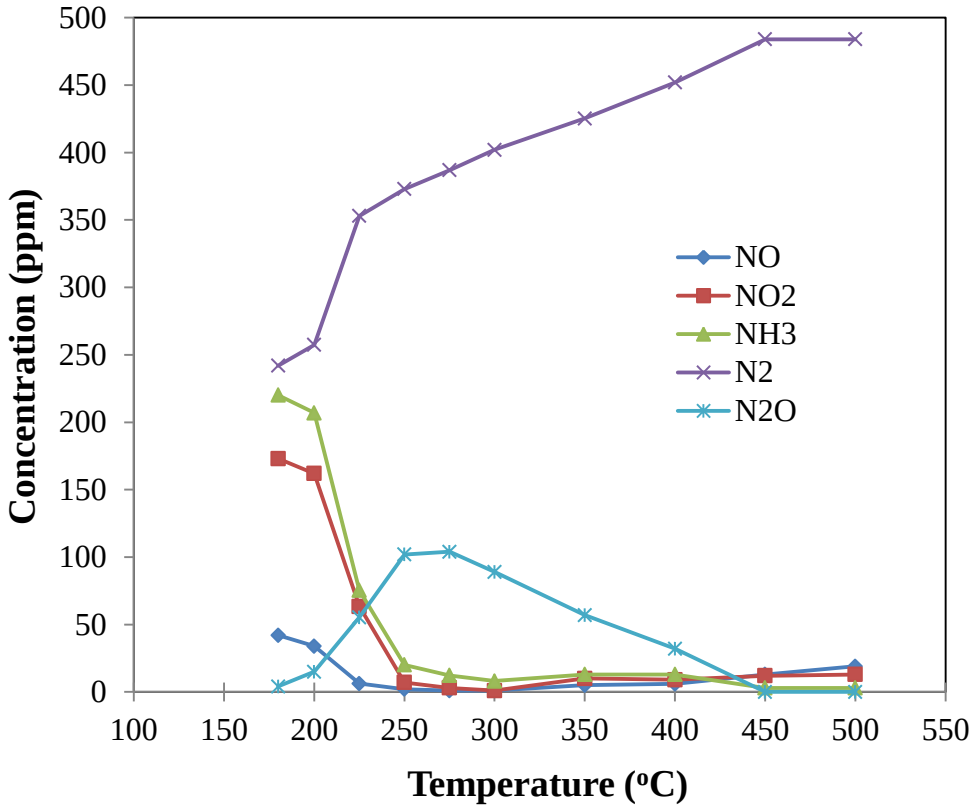

Figure 4-6: Steady state product distribution obtained for SCR of NOx with NH_3 as a function of temperature. Space velocity 57,000 hr^{-1}. Total Flow rate = 1000 sccm. Feed: 125 ppm NO, 375 ppm NO_2, 500 ppm NH_3, 5% O_2.

The above reaction system was studied in the presence of 2% water to isolate its effect. The feed composition and the catalyst temperatures were kept the same as in the above case except that the 2% H_2O stream was introduced. Water was observed to have an inhibitory effect on the NOx reduction in the temperature range of 200-250 ^oC. The product distribution for this case is shown separately in Figure 4-7. The amount of N_2O produced was less for the wet feed compared to the dry feed. These results are explained in more detail below.

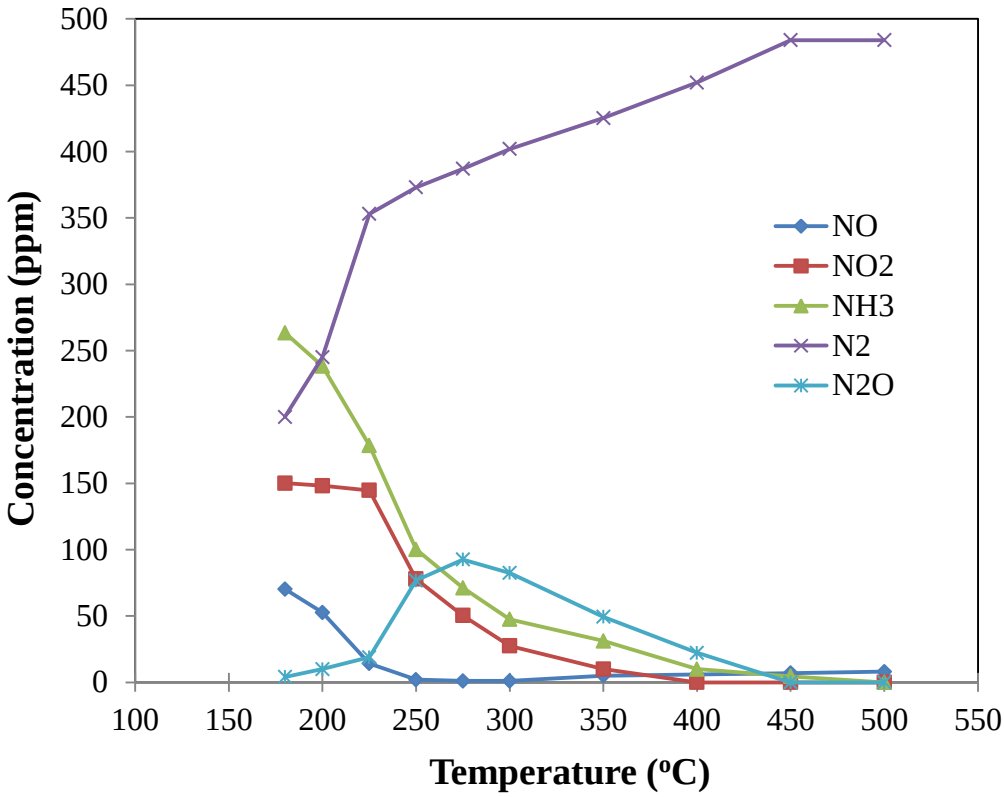

Figure 4-7: Steady state product distribution obtained for SCR of NOx with NH_3 as a function of temperature. Space velocity 57,000 hr^{-1}. Total Flow rate = 1000 sccm. Feed: 125 ppm NO, 375 ppm NO_2, 500 ppm NH_3, 5% O_2 and 2% H_2O.

A pure NO_2 feed (NO_2/NOx =1) is a special system in which the standard and fast SCR chemistries are essentially turned off, at least at temperatures below the decomposition of NO_2 (< 350 ^oC). The so-called "NO_2 SCR" reaction (4-5) becomes the dominant chemistry under these conditions. This reaction was studied on the in-house and commercial Fe-zeolite catalysts. The integral product distribution data (for dry feed) for the NO_2 feed are shown in Figure 4-8 (FeZ-18 catalyst). Approximately 60% conversion of NO_2 was observed at temperatures as low as 180-200 ^oC on the FeZ-18 catalyst. N_2 was the primary reaction product at 180 ^oC with some N_2O detected at 200 ^oC. No N_2O was detected at 180 ^oC.

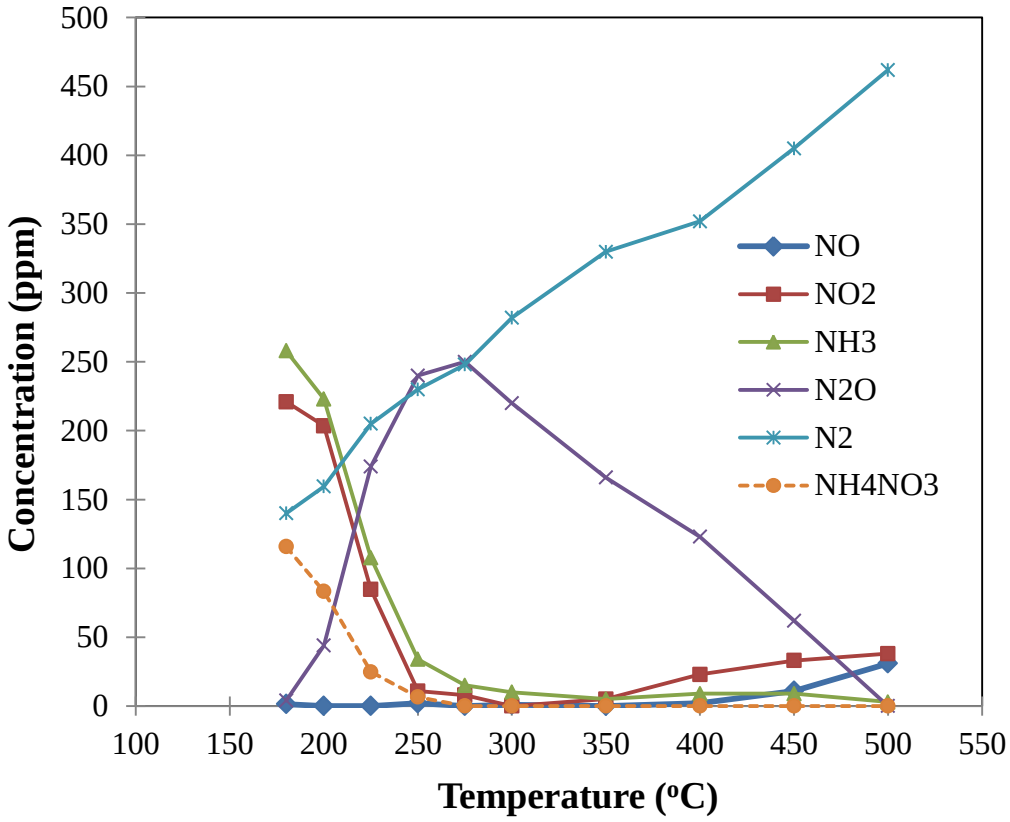

Figure 4-8: Steady state product distribution obtained for SCR of NOx with NH_3 as a function of temperature. Space velocity 57,000 hr^{-1}. Total Flow rate = 1000 sccm. Feed: 500 ppm NO_2, 500 ppm NH_3, 5% O_2.

The N-balance was not closed under these conditions (ca. 230 ppm was missing in the N-balance at 180 °C), once again indicating the formation of undetected ammonium nitrate. The N-balance inferred that about 115 and 83 ppm of NH_4NO_3 was formed at 180 °C and 200 °C, respectively. From the amounts of N_2 and NH_4NO_3 formed, this suggests that reaction (4-6) is the main reaction under these conditions. For temperatures exceeding 250 °C, the N-balance was closed which suggests that the NH_4NO_3 decomposed completely and the NO_2 SCR reaction becomes the primary one. A significant amount of N_2O was detected in the temperature range of 225-450 °C. There was a sudden increase in the N_2O concentration from 200 °C to 250 °C. The maximum amount of N_2O (ca. 250

ppm) was detected around 275 ^{o}C. The fate of N_2O at higher temperatures is discussed in more detail later.

A significant decrease in the NO_2 concentration was observed between 200 and 250 ^{o}C at which point nearly 97% conversion was achieved. This decrease is attributed to an enhanced NO_2 SCR reaction rate. Very high NO_2 conversions (~ 95%) were measured in the temperature range of 250-350 ^{o}C. The NO_2 conversion dropped below 90% at higher temperatures (T > 400 ^{o}C); again, this is attributed to NO_2 decomposition. At higher temperatures (> 350 ^{o}C), NH_3 was consumed in somewhat larger amounts compared to NO_2, the signature of ammonia oxidation. O_2 competes with NO_2 as an oxidant of NH_3. In contrast, under the fast SCR conditions (equimolar feed NO and NO_2) complete conversion of NOx was obtained at temperatures of 350 ^{o}C and higher. The difference in NO_2 and NH_3 consumption also points to the 3:4 stoichiometry of reaction (4-5).

The NO_2 SCR reaction was also carried out on commercial Fe-zeolite monolithic catalysts. Comparable results to that of FeZ-18 were obtained. In order to reduce the conversion, a shorter catalyst length (1 cm) was used. It was observed that the NO_2 conversion was reduced slightly because of the shorter residence time. The amount of N_2O detected was lower on the shorter piece of catalyst with a maximum of 193 ppm detected at 275 ^{o}C. Higher conversions of NO_2 obtained on shorter catalyst piece indicate that the reaction is fast enough to be completed in 1 cm portion of catalyst. The latter portion of the catalysts is thus not used for NOx reduction. This is comparable to the case of fast SCR reaction system studied earlier. However, when a similar study was carried out on the standard SCR reaction with a shorter (1 cm) catalyst, the NO conversion

decreased for temperatures up to 350 ^{o}C. This shows that the standard SCR requires a higher residence time (and hence catalyst length) to achieve higher NO conversions. These results are in agreement with the recent study by Luo et al. [159].

The NO_2 SCR reaction system was also carried out in the presence of 2% H_2O on the FeZ-18 catalyst. The product distribution (Figure 4-9) indicates inhibition of the NO_2 SCR reaction by water. The inhibition was more pronounced in the temperature range of

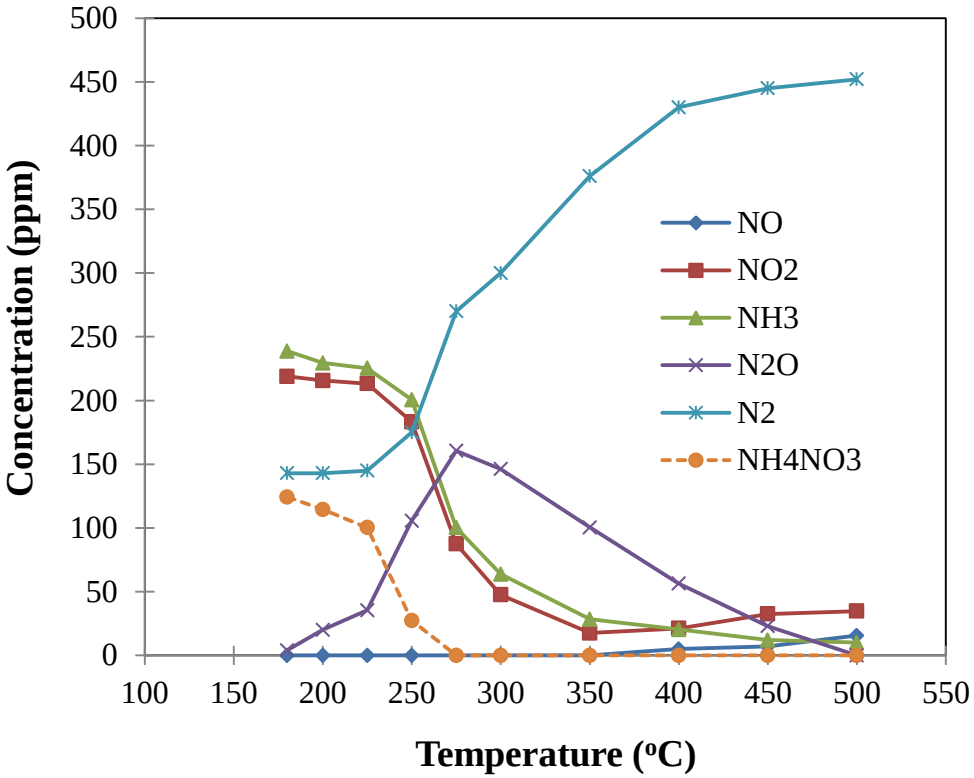

Figure 4-9: Steady state product distribution obtained for SCR of NOx with NH_3 as a function of temperature. Space velocity 57,000 hr $^{-1}$. Feed: 500 ppm NO_2, 500 ppm NH_3, 5% O_2 and 2% H_2O.

200-300 ^{o}C. Similar inhibition on NOx reduction was observed for the earlier case of NO_2/NOx = 0.75. One possible reason for this result is that water blocks active sites required for NO_2 SCR. It is also noted that the amount of N_2O, generated presumably by the decomposition of NH_4NO_3 decreased in the presence of water. This would suggest

that NH_4NO_3 decomposes to NH_3 and HNO_3 (reverse reaction (4-11)) rather than to N_2O in the presence of H_2O [29].

$$NH_4NO_3 \leftrightarrow NH_3 + HNO_3 \qquad \Delta H = 1.84 \times 10^5 \text{ J/mol } NH_4NO_3. \qquad (4\text{-}11)$$

From these studies of SCR of NOx with various NO_2/NOx inlet feed ratios, N_2O was obtained as an important byproduct because of the various side reactions taking place in the SCR chemistry. Figure 4-10 shows the effluent concentration of N_2O obtained over the temperature range of 180-500 ^oC on the FeZ-18 catalyst for several NO_2/NOx feed ratios. A negligible amount (< 20 ppm) of N_2O was detected up to NO_2/NOx = 0.5; i.e., standard and fast SCR. For higher NO_2/NOx feed ratios (> 0.5), the N_2O increased significantly. But for NO_2/NOx inlet feed ratios of 0.75 and 1, a maximum N_2O was detected at about 275 ^oC. The sharp decrease in N_2O concentration at higher temperatures is attributed to two factors:

1) The rates of the N_2 selective reactions, i.e., NO_2 SCR, fast SCR and standard SCR increase at higher temperatures, and as a result the side reactions responsible for N_2O production decrease.

2) The N_2O itself decomposes to N_2 by reaction (4-9) and hence its effluent concentration decreases at higher temperatures.

Devadas et al. [29] observed that N_2O decomposes to N_2 and O_2 starting at 350 ^oC. Our results show that there was no N_2O in the outlet at temperatures above 450 ^oC. Another possibility for N_2O consumption is reaction with NH_3 (reaction (4-10)). Devadas et al. found that the presence of NH_3 increased the N_2O decomposition. We obtained very high NOx conversions (> 90%) for dry feeds for temperatures $\geq$ 250 ^oC. NH_3 consumption was nearly 100% for these temperatures and hence it was difficult to

analyze how much NH_3 was consumed in the reduction of N_2O (reaction (4-10)) and how much NH_3 was oxidized to N_2 (reaction (4-8)). Similar trends for N_2O production on Fe-zeolite and other catalysts were reported in the literature [29, 39, 63, 118].

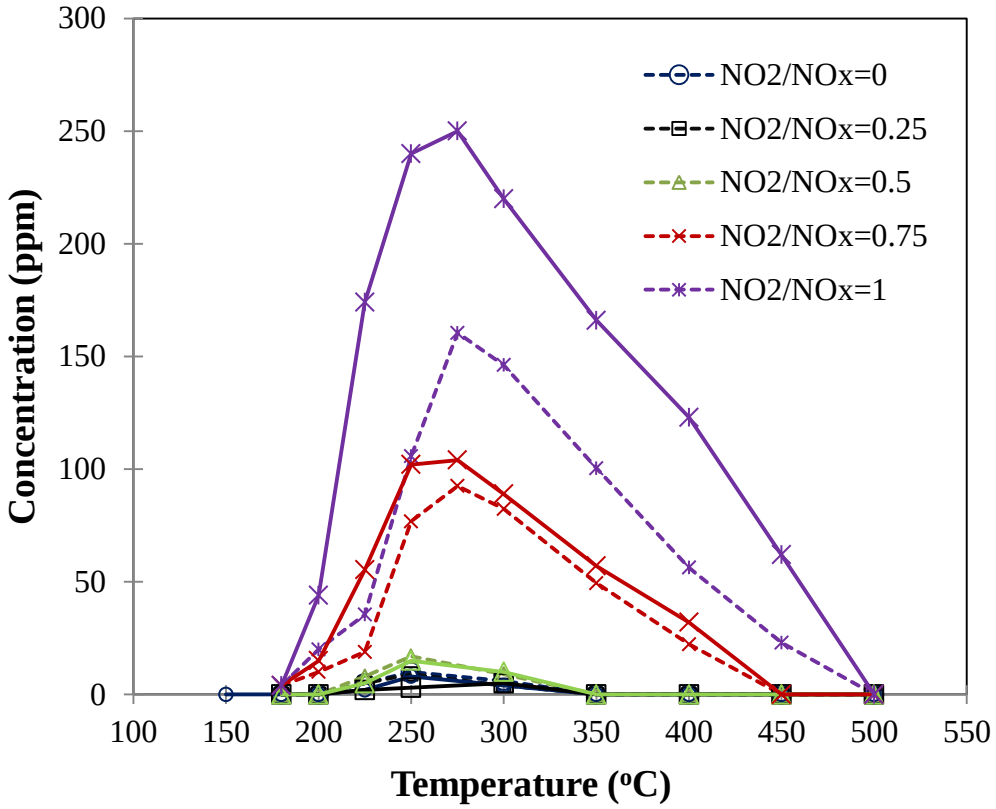

Figure 4-10: Steady state N_2O concentrations obtained during the SCR of NOx with NH_3 for feeds containing various inlet ratios of NO_2/NOx. Space velocity 57,000 hr^{-1}. Feed: 500 ppm NOx, 500 ppm NH_3, 5% O_2, 0-2% H_2O.

In results reported so far for the steady state NOx reduction studies, it is clear that the NO_2/NOx ratio is a critical parameter. The ratio has important effects on both the overall NOx conversion and the product distribution. The effect of NO_2/NOx ratio and temperature on the overall NOx conversion is shown in Figures 4-11 and 4-12. Figure 4-11 reports the results obtained for dry feed while Figure 4-12 reports the results for the wet feed. Figure 4-13 shows the effects of NO_2/NOx ratios and temperature on the N_2 selectivity.

The conversion data (Figure 4-11) show the significant enhancement effect of NO_2 on the deNOx efficiency of the catalyst at lower temperatures. At low temperature (180 ^oC), negligible NOx reduction (< 15%) occurs for the standard SCR reaction. Introduction of 125 ppm NO_2 increased this value to 50% while for an equimolar feed the conversion increased to 74%. This enhancement is attributed to the fast SCR chemistry in which NO_2 is the limiting reactant. As we have shown in our previous study, the standard SCR reaction is limited by the NO oxidation to adsorbed NO_2.

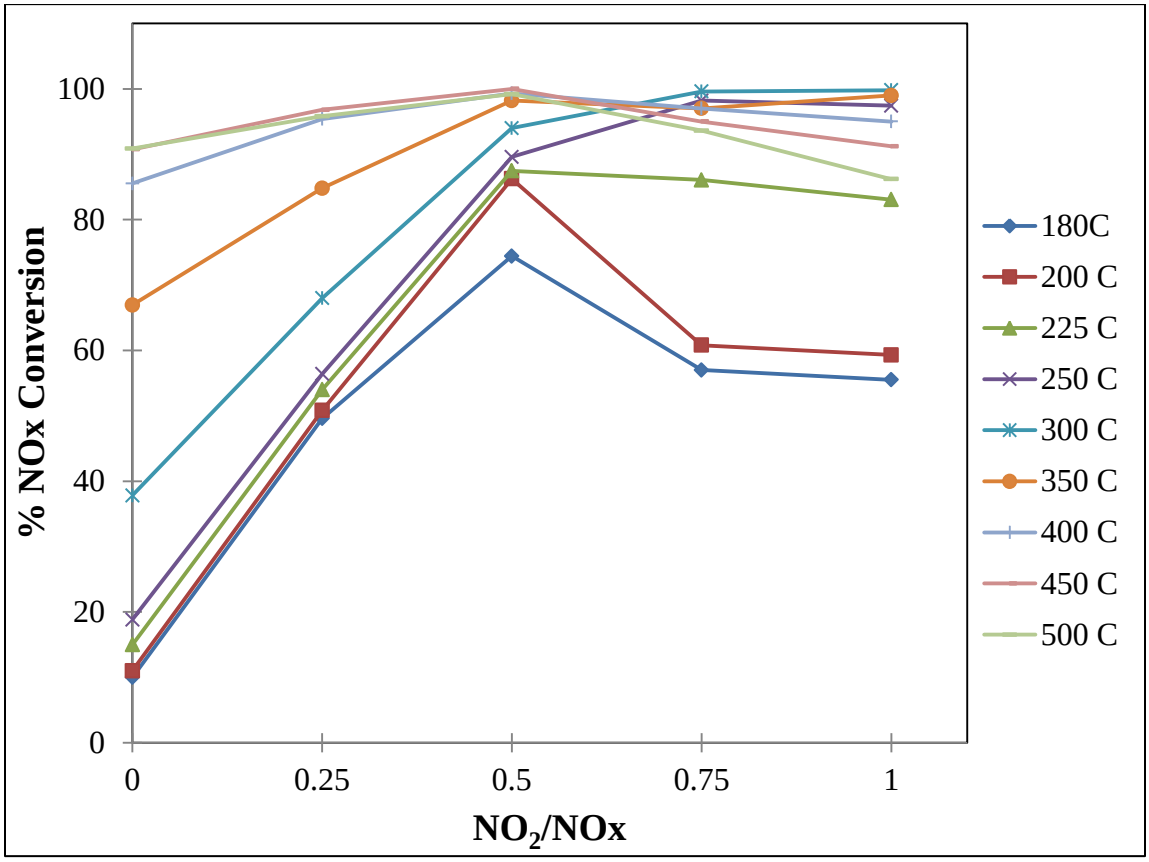

Figure 4-11: Effect of various NO_2/NOx inlet feed ratios and catalyst temperatures on the NOx conversion studied on the in-house synthesized FeZ-18 catalyst. Space velocity 57,000 hr^{-1}. Feed: 500 ppm NOx, 500 ppm NH_3, 5% O_2.

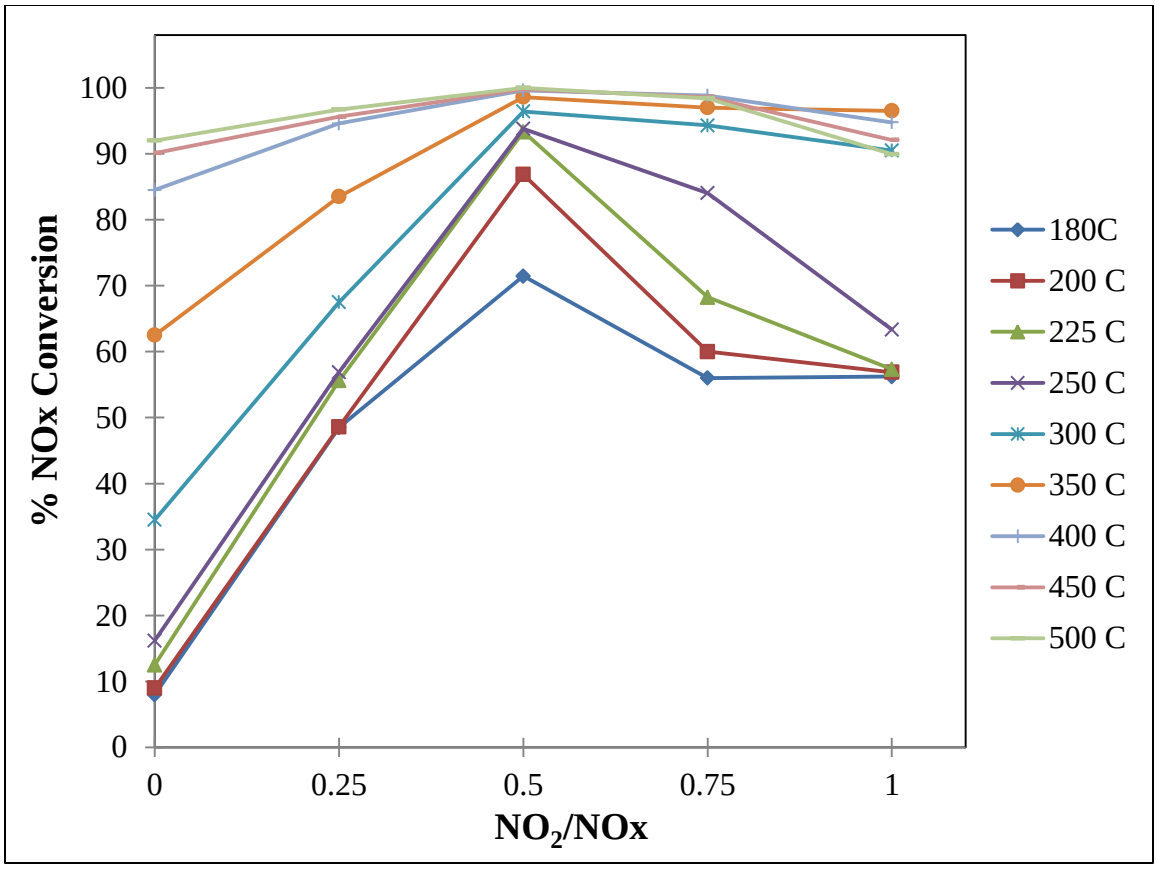

Figure 4-12. Effect of various NO_2/NOx inlet feed ratios and catalyst temperatures on the NOx conversion studied on the in-house synthesized FeZ-18 catalyst. Space velocity 57,000 hr^{-1}. Feed: 500 ppm NOx, 500 ppm NH_3, 5% O_2 and 2% H_2O.

Thus, feeding NO_2 removes this limitation. However an increase in NO_2 (NO_2/NO > 1) leads to a decrease in the NOx conversion to about 55% for the pure NO_2 feed. Similar trends were observed for 200 ^oC. At even higher temperatures, a noted conversion peak at NO_2/NOx = 0.5 shifts to ratios approaching unity. For example, between 250 and 350 ^oC, the conversion is nearly 100% for NO_2/NOx =1. A further increase in temperature to 400 ^oC and higher resulted in the conversion peak shifting back to the equimolar mixture while maintaining a peak conversion of nearly 100%. When water was introduced to the feed, it had a negligible effect on NOx reduction up to the NO_2/NOx feed ratio of 0.5. But

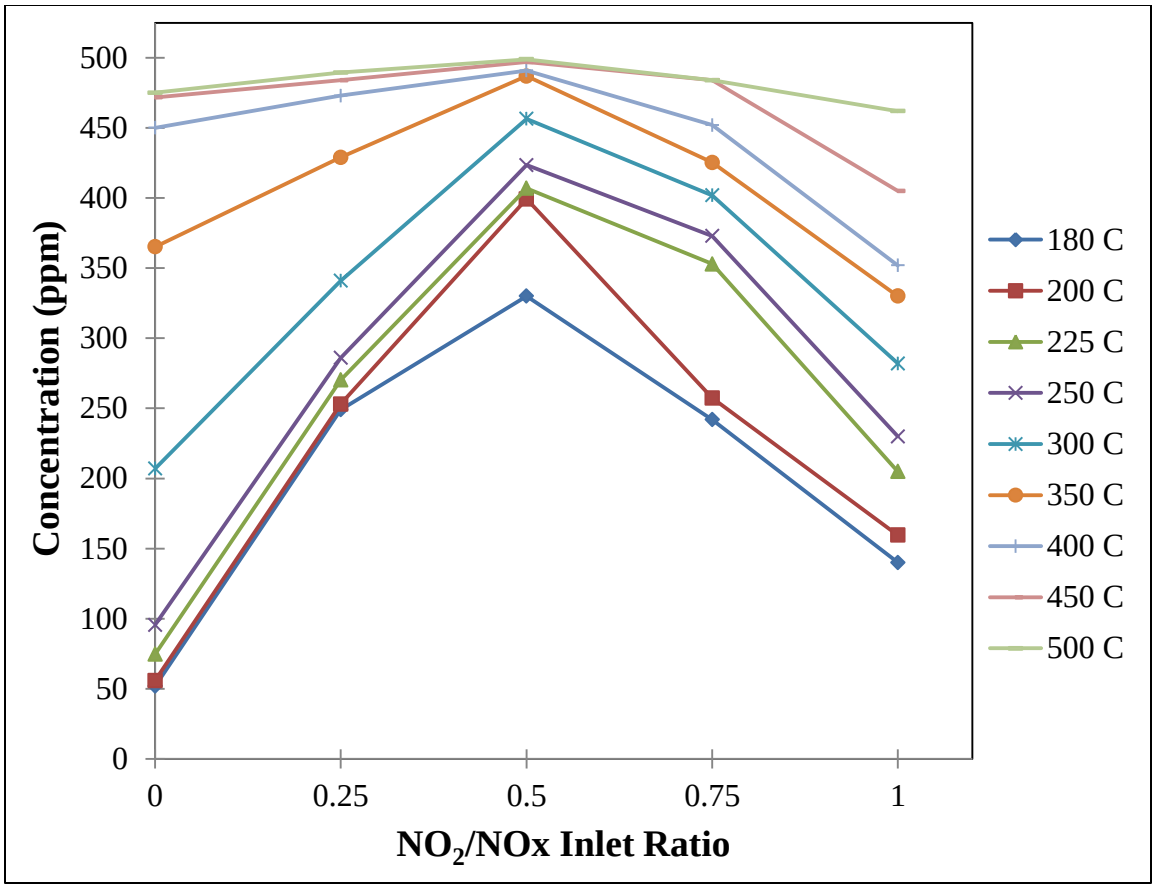

Figure 4-13: Effect of various NO_2/NOx inlet feed ratios on the N_2 selectivity obtained during the SCR studies on the in-house synthesized FeZ-18 catalyst. Space velocity 57,000 hr^{-1}. Feed: 500 ppm NOx, 500 ppm NH_3, 5% O_2.

for NO_2/NOx feed ratios exceeding 0.5, a noticeable inhibition on the NOx reduction was observed in the temperature range of 200-300 ^oC (Figure 4-12). The optimum NO_2/NOx ratio for maximum NOx reduction shifted to 0.5 (fast SCR reaction) for the wet feeds, in line with previous literature studies [29, 39].

Along with deNOx efficiency, it is important to achieve a maximum selectivity towards N_2 where the formation of byproducts should be minimum. The effluent N_2 concentrations indicate that the equimolar feed (NO_2/NOx = 0.5) is optimal in terms of selectivity over the entire temperature range for both the wet and dry feeds (Figure 4-13).

Unlike the NOx conversion, the N_2 production is a monotonic function of temperature for a fixed NO_2/NOx ratio. This feature suggests the byproduct pathways emerge for non-equimolar feeds. Thus, taken together, Figures 4-11, 4-12 (NOx conversion) and 4-13 (N_2 selectivity) show that the equimolar NO/NO_2 feed achieves both a high conversion and N_2 selectivity. For NO_2/NOx < 0.5, the conversion decreases because less NO_2 is available to react with NH_3 via the fast chemistry. As a result, the slower standard SCR chemistry takes over and the conversion declines. As NO_2 increased beyond NO_2/NOx > 0.5, the emergence of ammonium nitrate and NO_2 decomposition impact the overall NOx conversion. For temperatures less than 250 ^oC, the ammonium nitrate is not completely decomposed and inhibits NOx reduction. For higher temperatures ($\geq$ 350 ^oC) some NO_2 decomposition occurs leading to a slight reduction in the NOx conversion. Thus, for temperatures of 350 ^oC and higher, the highest deNOx efficiency was observed for the inlet feed ratio of NO_2/NOx equal to 0.5; i.e., fast SCR reaction. In addition, side reactions like ammonia oxidation only emerge at higher temperatures. This side reaction was not observed for the case of fast SCR reaction in which stoichiometric conversions of NOx and NH_3 occurred. The fast and standard SCR reactions are clearly beneficial for N_2 formation whereas the pathways to and through ammonium nitrate leads to large amounts of N_2O. Considering all these factors, a NO_2/NOx ratio of 0.5 proves to be the most ideal ratio where the SCR system should run to achieve maximum NOx removal efficiency and highest product selectivity towards N_2. Similar steady state results were reported in the literature on Fe-zeolite and Cu-zeolite catalysts [39, 86, 87].

4.3.4 Selective Catalytic Reduction of NOx: Transient Experiments

The results described thus far were under steady state conditions. In order to better understand the conditions during SCR of NOx in more detail, it is informative to evaluate the system under transient conditions. To our knowledge, no literature studies have reported transient results for the Fe-zeolite catalyst over a broad range of temperatures. In the following experiments, Ar was used as the carrier gas and the reactants NO and NO_2 were fed in the presence of 5% O_2 at isothermal conditions. The total flow rate was kept constant at 1000 sccm. In contrast to the steady state experiments, NH_3 was pre-adsorbed on the commercial catalyst for 60 minutes and then the NOx gases were introduced as a step change from 0 to 500 ppm using different NO/NO_2 ratios. Above mentioned SCR reactions were studied at various temperatures of 150 ºC, 200 ºC, 250 ºC, 300 ºC, 350 ºC and 400 ºC with three different NO/NO_2 ratios of (1/0, 1/1, 0/1). Experimental results are presented below.

4.3.4.1 NO Feed (NO/NO_2 = 1/0)

The reactivity of NO with pre-adsorbed NH_3 in the presence of O_2 was first studied under transient conditions. NH_3 was fed continuously for 3600s at a concentration of 500 ppm and then stopped. After that, only Ar was admitted to the reactor for 1800s, to release loosely bound NH_3 from the catalyst; i.e., the intention was to study only the chemisorbed NH_3 present in the sample that reacted with the NO. After that a feed containing 500 ppm of NO and 5% O_2 was fed to the reactor and the temperature was fixed at a prescribed value. An increase in N_2 was observed after the NO containing feed was introduced. This N_2 concentration remained constant for 450-500s after which it decreased to zero. After all the ammonia present on the catalyst surface was consumed by

NO, no more N_2 was detected. No N_2O was detected during these reaction studies. This study was repeated for different catalyst temperatures in the range of 150-400 ^oC and was explained in more detail in Chapter 3 and [103, 128].

4.3.4.2 Equimolar Feed (NO/NO_2 = 1/1)

The same procedure was followed for an equimolar mixture of NO/NO_2 (250 ppm each) after the initial NH_3 uptake. The presence of NO_2 in the feed led to a significantly faster consumption of preadsorbed NH_3. Peak values of N_2 obtained were always above 400 ppm for this fast SCR case. In fact, for the 350-400 ^oC temperatures, the peak value attained 500 ppm. N_2O was not detected in the entire temperature range. Figure 4-14a-c shows the trends obtained for N_2, NO and NO_2 at different temperatures.

4.3.4.3 NO_2 Feed (NO/NO_2 = 0/1)

In this set of experiments, a gas containing 500 ppm of NO_2 in 5% of O_2 (balance Ar) was fed to the catalyst after pre-adsorbing 500 ppm of NH_3. In this case the temperature had a much less significant impact on the N_2 production (Figure 4-15 a). The same sharp peak was observed for the entire range of temperatures. In addition to N_2, N_2O was detected for this system. The maximum amount of N_2O was detected in the temperature range of 250-300 ^oC in line with the steady state results (Figure 4-8). For temperatures exceeding 400 ^oC, no N_2O was detected in the system. In the inlet feed, NO was not present. But NO appeared in the effluent for T > 300 ^oC due to the decomposition of NO_2 (Figure 4-15 b-c). These results are in agreement with the steady state data (Figure 4-10).

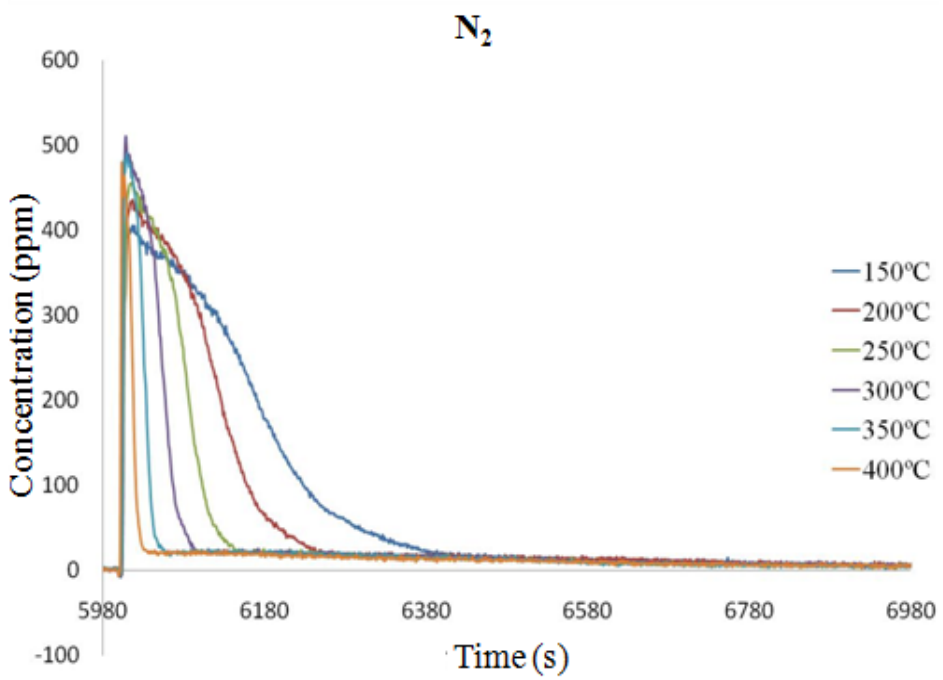

Figure 4-14a: Measured N_2 concentrations during the reaction of pre-adsorbed NH_3 (500 ppm) with NO (250ppm), NO_2 (250ppm) and O_2 (5%).

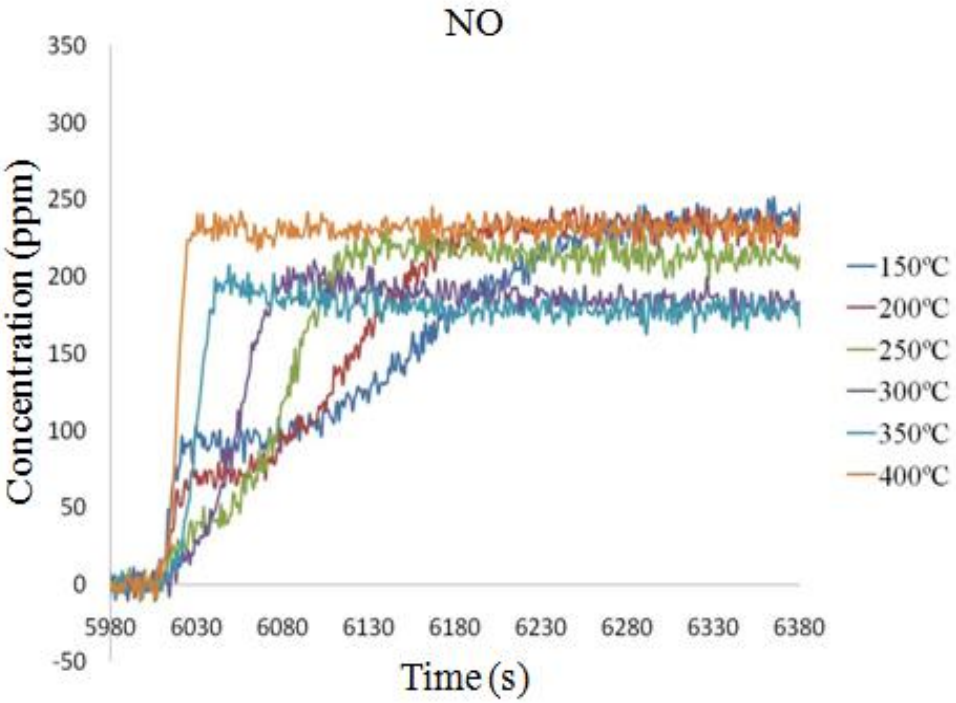

Figure 4-14b: Measured NO concentrations during the reaction of pre-adsorbed NH_3 (500 ppm) with NO (250ppm), NO_2 (250ppm) and O_2 (5%).

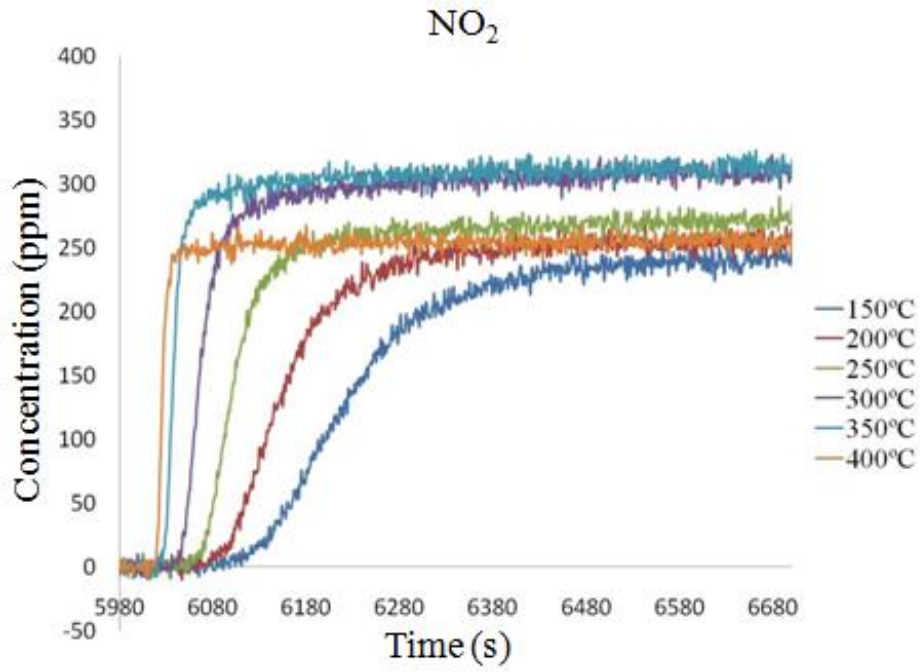

Figure 4-14c: Measured NO_2 concentrations during the reaction of pre-adsorbed NH_3 (500 ppm) with NO (250ppm), NO_2 (250ppm) and O_2 (5%).

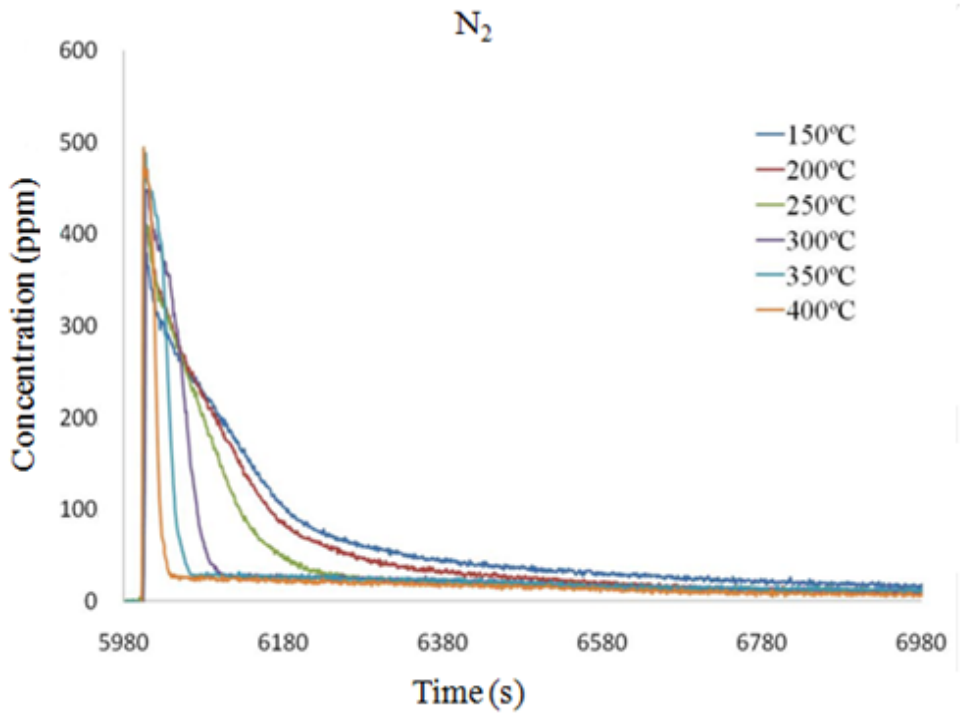

Figure 4-15a: Measured N_2 concentrations during the reaction of pre-adsorbed NH_3 (500 ppm) with NO_2 (500ppm) and O_2 (5%).

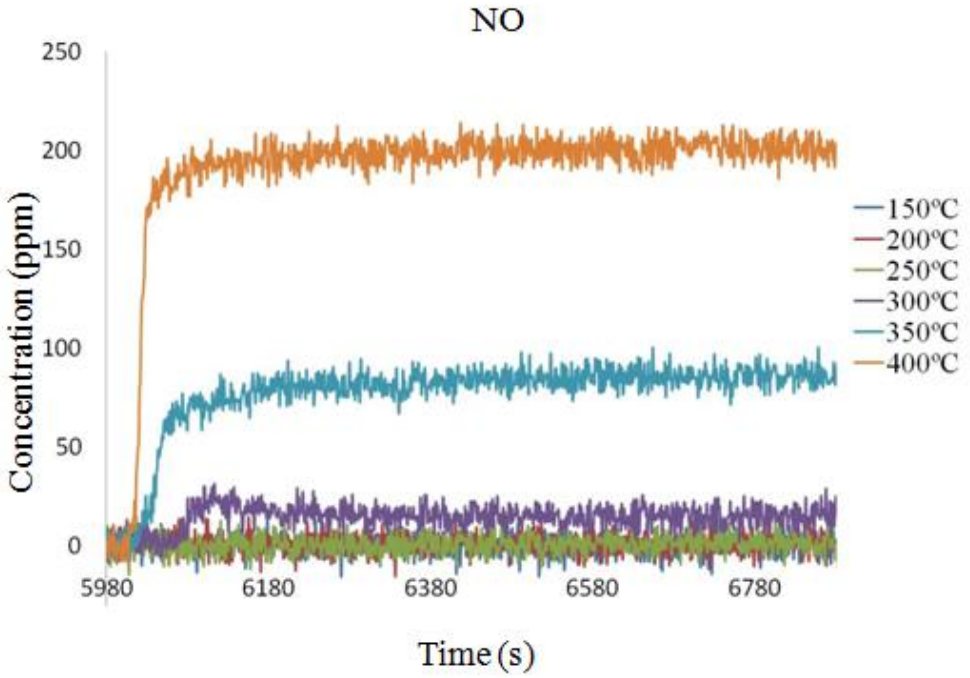

Figure 4-15b: Measured NO concentrations during the reaction of pre-adsorbed NH_3 (500 ppm) with NO_2 (500ppm) and O_2 (5%).

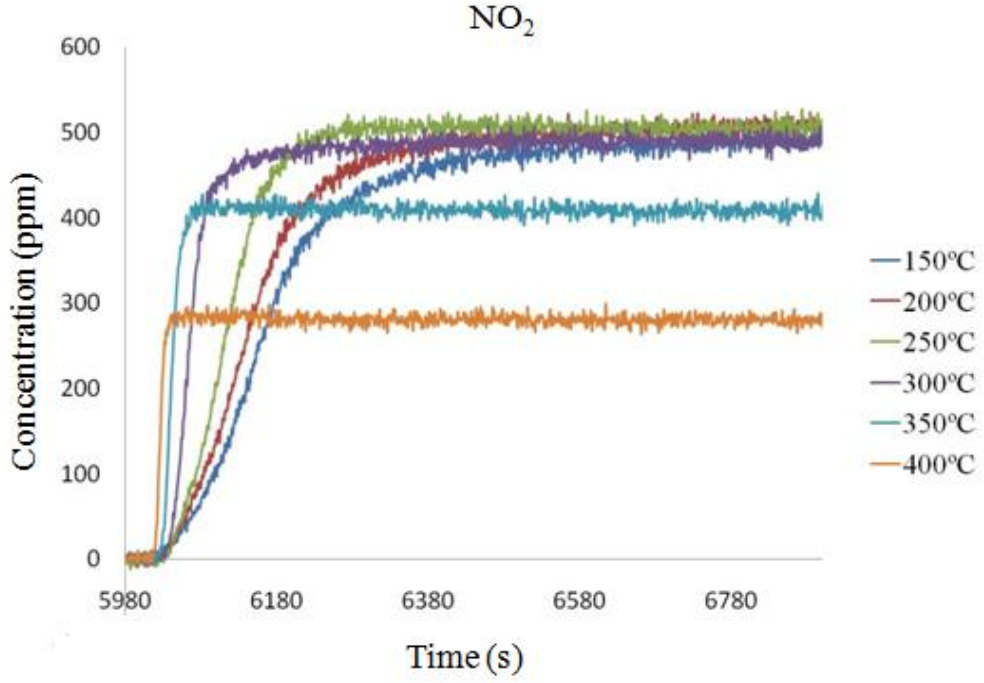

Figure 4-15c: Measured NO_2 concentrations during the reaction of pre-adsorbed NH_3 (500 ppm) with NO_2 (500ppm) and O_2 (5%).

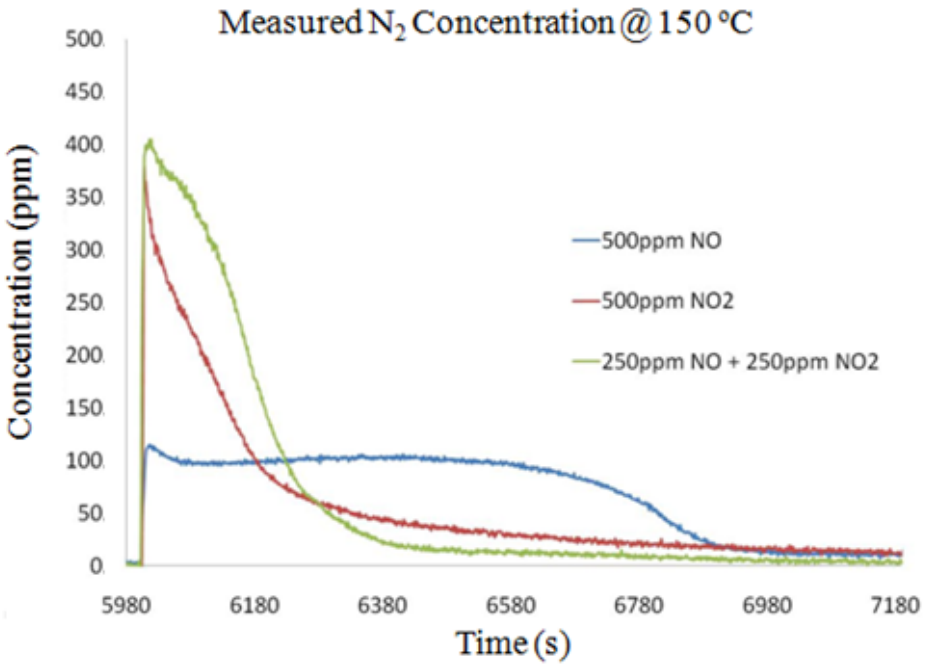

Figure 4-16: Comparison of N_2 formation on Fe-zeolite catalyst pre-saturated with NH_3 at 150 ºC after introducing feeds with different (1:0, 1:1 and 0:1) NO/NO_2 inlet ratios onto the catalyst surface.

These transient experiments convey the large difference in the SCR chemistry for the standard and fast SCR systems. For the equimolar feed corresponding to the fast SCR reaction, the rate of N_2 formation was much higher than for the standard SCR reaction. Moreover, no other byproducts were formed. Similarly, for the NO_2 SCR, the rate of N_2 formation was found to be higher than the standard SCR reaction. This reaction showed the formation of byproducts like ammonium nitrate below 250 ^oC and formation of N_2O at higher temperatures. In order to confirm the formation and deposition of ammonium nitrate at lower temperatures, a separate experiment was performed and is discussed later. The amount of N_2 generated for various NO/NO_2 ratios was measured for all the temperatures. Figure 4-16 summarizes the results obtained for the low temperature (150 ^oC). The results show that a maximum amount of N_2 was obtained for the case of fast

SCR reaction. Similar results with a maximum in the N_2 production were obtained for fast SCR up to 300 ^oC. These results are in qualitative agreement with our previous results for steady state experiments.

An additional set of experiments was performed to verify the existence of some other species like ammonium nitrate stored on to the catalyst but which could not be detected by the analyzers. This experiment involved pre-adsorbing 500 ppm NH_3 for 1 hr and then shutting off the NH_3 and flowing just Ar for 30 minutes. Subsequently, 500 ppm of NO_2 and 5% O_2 in Ar were fed for 4 minutes at a constant temperature of 150 ^oC. Then a temperature ramp of 10 ^oC/min was initiated until the monolith temperature reached 500 ^oC. During the temperature ramp, only Ar was fed to the reactor to observe any species that had accumulated on the catalyst, or their decomposition products. During the temperature ramp, the evolution of N_2O commenced at around 200 ^oC with its concentration increasing to a maximum of about 200 ppm at about 280 ^oC. Small quantities of N_2 were measured starting from 240 ^oC. This experiment proved the existence of ammonium nitrate which accumulates on the catalyst at lower temperatures and decomposes to N_2O and N_2 at higher temperatures. For this reason, we expect that the NH_4NO_3 deposition is the principle reason for the decrease in NOx conversion with higher feed NO_2 fractions.

4.3.5 Fate of NH_4NO_3

From the steady state and transient data, it is clear that the maximum NOx removal efficiency and N_2 selectivity are obtained for the NO_2/NOx feed ratio of 0.5. These results are in line with some recent studies [29, 39, 86, 87]. However, there is

some discrepancy in the literature regarding the optimal NO_2/NOx ratio that gives a maximum NOx conversion at lower temperatures (< 200 ^oC). For example, Grossale et al. [39, 86] reported this optimal ratio to be 0.5 in one study [86] but reported an optimal ratio of 1 in another study [39]. Our findings suggest that experimental complications associated with ammonium nitrate formation can cause such inconsistencies. Specifically, we found that the NOx conversion in the fast SCR reaction did not reach a steady state even after waiting for a period of 3 hours. A high NOx conversion of 85% was observed initially when a feed containing an equimolar ratio of NO/NO_2 was fed to the catalyst presaturated with NH_3. But the NOx conversion slowly decreased with time.

These transient effects inspired us to carry out some investigative experiments. Specifically, we performed some TPD experiments after the catalyst was exposed to a feed containing 1000 ppm of both NOx and NH_3 in the presence of 5% O_2 for different durations (0.5 hr, 1 hr and 2 hr). The catalyst temperature was maintained constant at 180 ^oC during this exposure. After the prescribed time had elapsed, all the gases except Ar were switched off for 30 minutes to remove any physisorbed species. A temperature ramp of 10 ^oC/min was then initiated. During the temperature ramp, N_2O (0.23 mol) was evolved, reaching a peak value in the temperature range of 250-300 ^oC. The amount of N_2O generated by integrating the N_2O peak provides a measure of the amount of N_2O evolved during the temperature ramp, and correlates to the amount of NH_4NO_3 present on the catalyst. The experimental results are shown in Figure 4-17. The amount of N_2O evolved was different for each of the cases. The largest amount of evolved N_2O (0.43 mol) was obtained for the 2 hour experiment while the smallest was obtained for the 30 minutes experiment. The amount of N_2O obtained during the 2 hr adsorption study was

slightly greater than that for 1 hr (0.37) study. This shows that the catalyst surface was getting saturated with NH_4NO_3 and further increase in adsorption time would not make any appreciable difference.

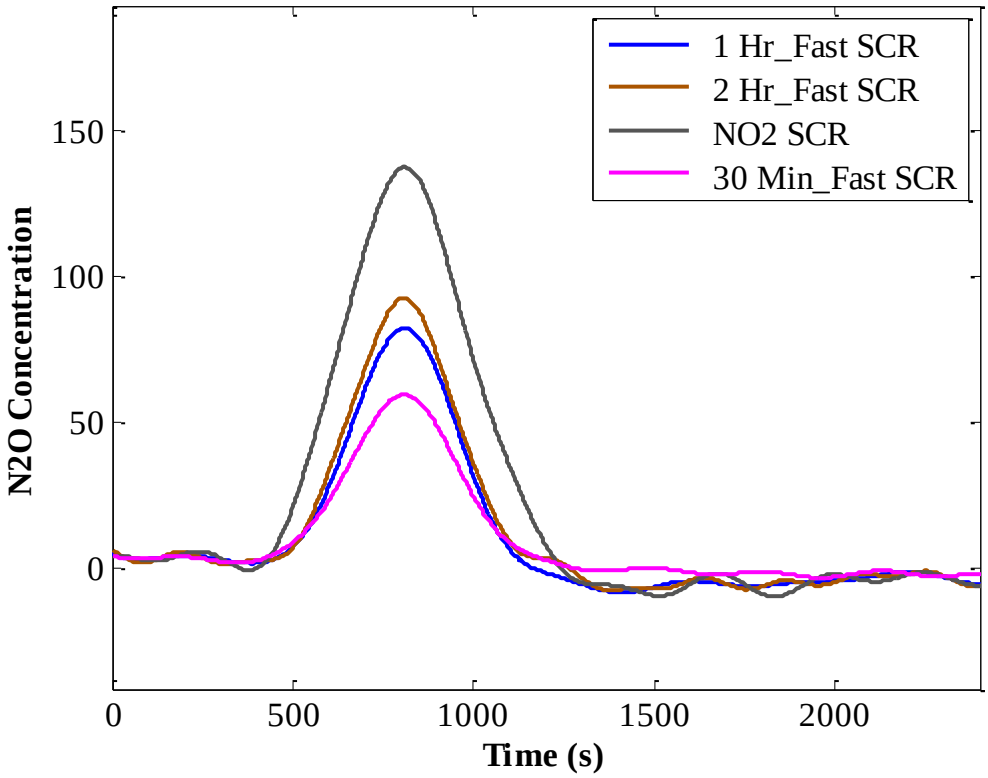

Figure 4-17: Comparison of N_2O concentration profiles obtained during the temperature programmed desorption studies carried out under different conditions of fast and NO_2 SCR reactions.

These trends clearly show that the NH_4NO_3 formed during the lower temperature SCR does indeed accumulate on the catalyst where it can block catalyst sites and/or pores. This likely reduces the catalytic activity, slows the approach to steady state and would be especially problematic at lower temperatures. To investigate further, we contacted the same FeZ-18 catalyst with a feed mixture containing 1000 ppm of both NO_2 and NH_3 and 5% O_2 in Ar for different time periods of 0.5 hr, 1 hr and 2 hr at the fixed temperature of 180 ^oC. Following the same procedure as above, similar amounts of

N_2O were obtained for all the three different times. This would suggest that the formation and accumulation of ammonium nitrate is nearly instantaneous when only NO_2 is present in the inlet feed. Presumably the NH_4NO_3 rapidly accumulates and blocks the active SCR sites. Moreover, the N_2O evolved (0.77 mol) during the temperature ramp in the NO_2 SCR was greater than the amount of N_2O (0.43 mol) obtained for the 2 hr adsorption in the fast SCR study. This shows that the amount of NH_4NO_3 formed was higher during the NO_2 SCR than in the fast SCR. These results are in line with the steady state NOx reduction experiments mentioned earlier. In addition, the fraction of NOx reduction achieved for fast SCR was higher than the NO_2 SCR at these low temperatures. Taken together, these results indicate that the formation and accumulation of NH_4NO_3 present on the catalyst is responsible for the reduction in the deNOx activity of catalyst at lower temperatures (< 250 ^oC).

In an earlier chapter, we proposed a mechanism that offers a possible explanation for why NH_4NO_3 is not encountered during the standard SCR reaction. The above described steady state experiments show that NH_4NO_3 is formed at lower temperature if the feed contains NO_2 and the amount of NH_4NO_3 formed for the fast SCR system is less compared to the NO_2 SCR system. In order to study this in more detail, we carried out a steady state experiment in which the concentration of NO was systematically increased in the feed containing 1000 ppm NH_3, 1000 ppm NOx ($NO+NO_2$), 5% O_2 and 2 % water. The total amount of NOx was held constant at 1000 ppm so that an increase in the fraction of inlet NO decreased the fraction of NO_2. Figure 4-18 shows the product distribution obtained for various inlet NO concentrations. The increasing feed concentration of NO increased the NOx conversion and the amount of N_2 formed. The N-

balance data indicated that the NH_4NO_3 formation decreased with the increase in the NO feed concentration. Thus, the increasing amount of NO enhanced the N_2 formation which is the desired product of NOx reduction and decreased the undesired NH_4NO_3 formation. The results suggest a reduction of surface nitrates, perhaps in the form of HNO_3, by NO (reaction (4-12)),

$HNO_3 + NO \rightarrow NO_2 + HONO.$ (4-12)

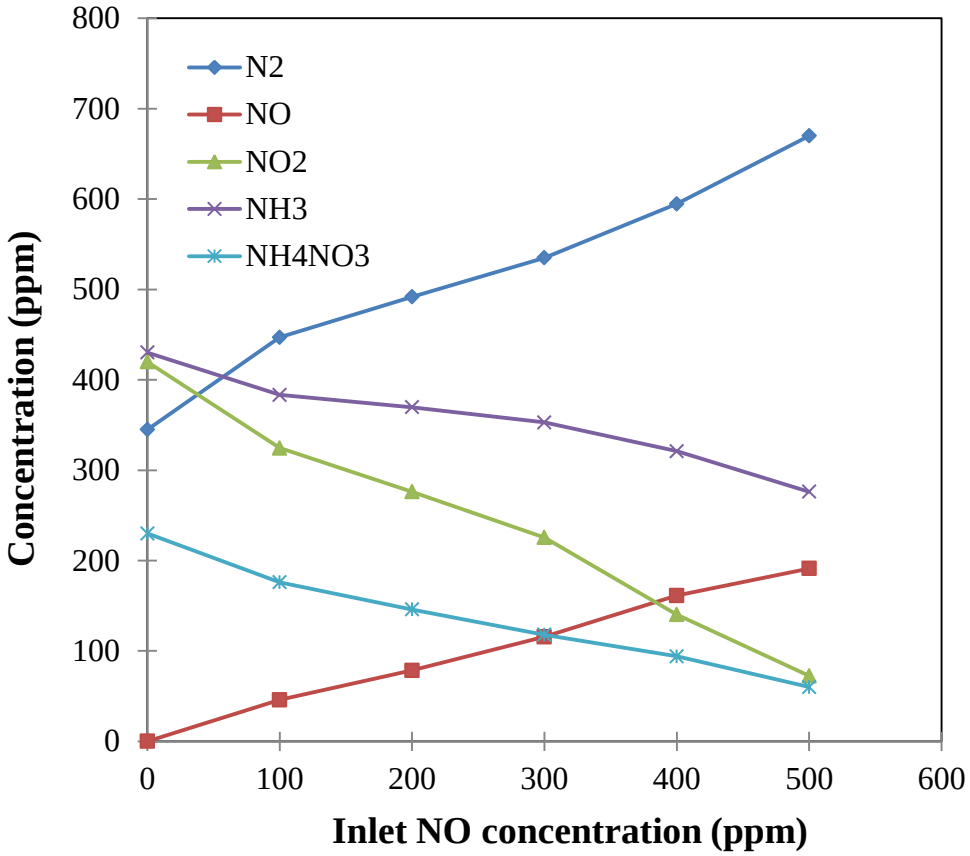

Figure 4-18: Effect of increasing NO concentrations on the product distribution obtained during the SCR of NOx on the in-house synthesized FeZ-18 catalyst. Feed: 1000 ppm NOx (NO + NO_2), 1000 ppm NH_3, 5% O_2 and 2% H_2O. Temperature studied: 185 ^oC.

As discussed earlier, it is now well established in the literature that the SCR chemistry involves the formation of HNO_2 and HNO_3 intermediates [21, 33, 90]. However, in the presence of NO, NH_4NO_3 production is lowered due to reaction (4-12) as sufficient

HNO_3 is not available to react with NH_3. Thus reaction (4-12) is considered as the key step during the fast SCR reaction [36].

Another potential pathway involves the reaction of NH_4NO_3 with NO,

$NH_4NO_3 + NO \rightarrow NO_2 + N_2 + 2\ H_2O \qquad \Delta H = -1.75 \times 10^5$ J/mol NH_4NO_3. (4-13)

In order to investigate this possibility, we carried out a transient experiment in which 500 ppm NO_2 and 500 ppm NH_3 were fed to the reactor at 185 ^oC for 30 minutes. Then both NO_2 and NH_3 were switched off and only Ar was admitted for 30 minutes in order to remove any loosely bound surface species like NO_2, NH_3 or NH_4NO_3. As we have shown earlier, some NH_4NO_3 (0.77 mol) is expected to accumulate on the catalyst. Under these conditions and after flowing Ar for 30 minutes, a feed containing 500 ppm NO was introduced. The N_2 concentration increased immediately as a sharp peak. Along with N_2, NO_2 was also detected in the FTIR. This experiment proves the existence of reaction (4-13). It also suggests a key role of NO during the SCR chemistry is to reduce HNO_3 and NH_4NO_3 present on the catalyst surface. Interestingly, Yeom et al. [90] suggested the similar role of NO for NOx reduction studies on the BaNa-Y zeolite catalyst.

4.3.6 Differential Kinetics for Fast SCR Reaction

In our earlier work, we presented the differential kinetics for the standard SCR reaction. We showed that a space velocity of 285,000 hr^{-1} was needed to keep the NO conversion below 15% in the temperature range of 200-300 ^oC. Such differential measurements enable one to directly measure apparent reaction orders and activation energies. Here we followed the similar approach. When the SCR reaction was carried out with an equimolar NO/NO_2 feed, it was much faster than the standard SCR reaction at

temperatures as low as 180 ^{o}C and much higher conversions were obtained. In order to meet the same 15% maximum conversion, we tested various catalyst sizes and gas flow rates. We found that a space velocity of 2×10^{6} hr^{-1} would ensure a NOx conversion less than 15% at temperatures as high as 245 ^{o}C. This high space velocity was achieved by reducing the size of the catalyst to 4 channels and 5 mm length. A total flow rate of 1000 sccm was used with Ar as a balance gas. This enabled us to measure the rate of NOx conversion with respect to the NO, NO_2 and NH_3 in the desired range of concentrations (0 ppm – 800 ppm). Also, since the temperature was below 300 ^{o}C, the decomposition of NO_2 should be minimal. The measured effluent NO and NO_2 were used to calculate an average rate normalized by the washcoat volume using 50 μm as the estimated thickness. The results from three experiments are shown in Figures 4-19 - 4-21. We refer to the overall NOx rate as R_{NOx}, the NO_2 rate as R_{NO2} and the NO rate as R_{NO}. Temperatures above 250 ^{o}C could not be used because differential conversion was not possible.

The rate data (Figure 4-19) show an interesting dependence on the concentrations of NH_3 during which the NO and NO_2 concentrations were each fixed at 250 ppm. The figure breaks down the individual rates of NO and NO_2 consumption. Their sums equal the overall rate, R_{NOx}. At lower temperature (185 ^{o}C), R_{NOx} exhibits a slight maximum at 200 ppm NH_3 and is constant at NH_3 concentrations exceeding 200 ppm. At the intermediate temperature (215 ^{o}C), R_{NOx} exhibits a more pronounced maximum at about 300 ppm NH_3. At the highest temperature (245 ^{o}C), the R_{NOx} maximum is less pronounced. The decrease in rate to the right of the rate maximum suggests inhibition by NH_3, a feature that was observed during standard SCR [103]. Interestingly, to the left of the overall rate maximum at 245 ^{o}C, R_{NOx} for 215 ^{o}C and 245 ^{o}C essentially coincide; i.e.

the overall rate is independent of temperature. At each temperature, the NO_2 consumption rate (R_{NO2}) exceeds the rate of NO consumption. This is not a surprising result since the standard SCR was determined to be limited by the formation of NO_2 [29].

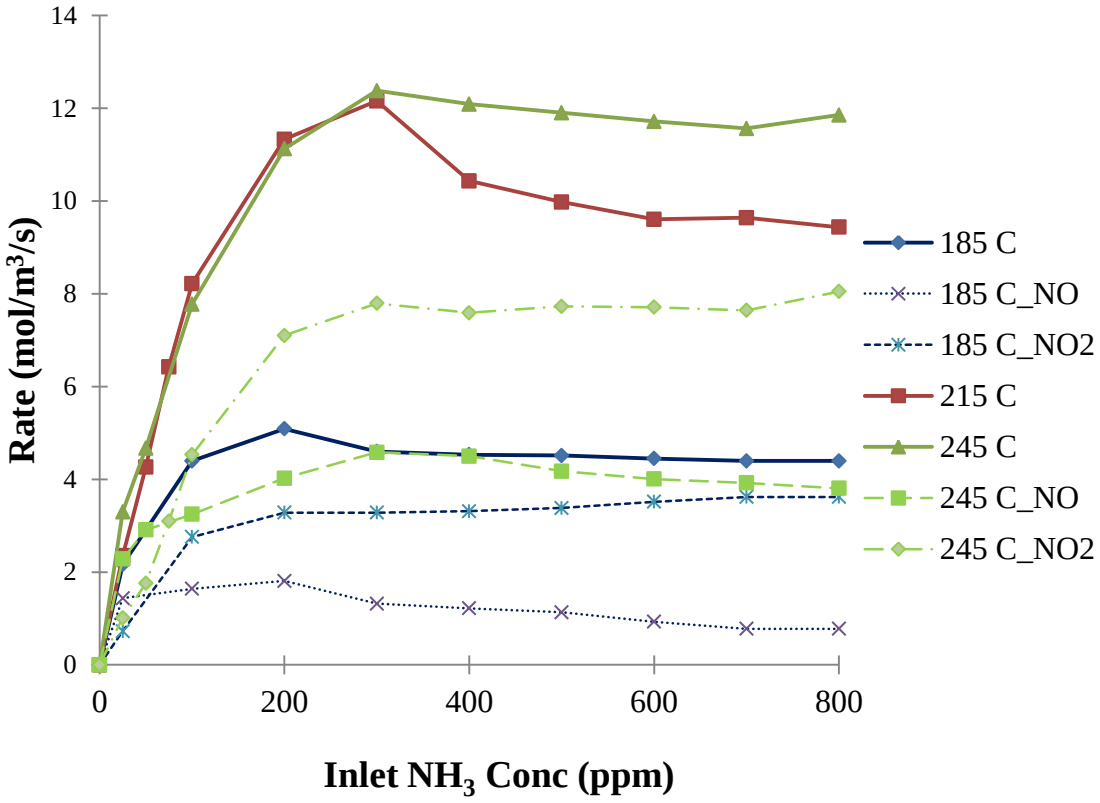

Figure 4-19: Effect of various inlet ammonia concentrations on the rate of NOx conversion during fast SCR reaction. Space velocity 2×10^6 hr^{-1}. Feed: 250 ppm NO, 250 ppm NO_2 , 0-800 ppm NH_3, 5% O_2.

A similar set of experiments was carried out for NO. Here, the feed NH_3 and NO_2 concentrations were kept constant at 1000 ppm and 500 ppm, respectively. O_2 was not fed to the reactor system to avoid any additional side reactions. The feed NO concentration was varied from 0 to 900 ppm. Figure 4-20 shows the dependence of the overall NOx reduction rate on the feed NO concentration at these temperatures. An increasing NO feed concentration increased the deNOx rate. The increase was more

pronounced at higher temperatures. This suggests a positive apparent reaction order with respect to NO that increases with temperature.

Similar studies were repeated with NO_2 by varying the inlet NO_2 concentration in the temperature range of 185-245 ^oC. NO and NH_3 feed concentrations were kept constant at 500 ppm and 1000 ppm, respectively. Again, no O_2 was present in the feed. Figure 4-21 shows that the apparent reaction order with respect to NO_2 is also positive and even had a sigmoidal shape, indicating a complex mechanism at work. The NO_2 dependence (order) is more pronounced than is for NO.

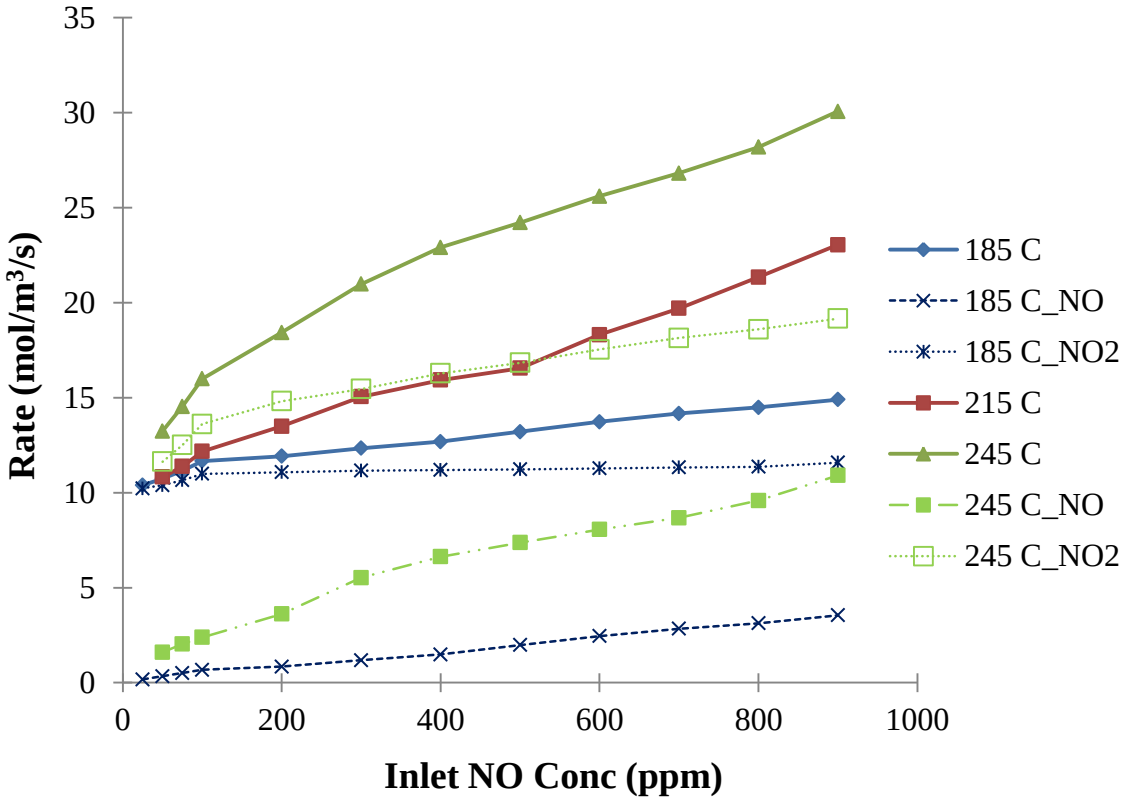

Figure 4-20: Effect of various inlet NO concentrations on the rate of NOx conversion during fast SCR reaction. Space velocity 2×10^6 hr^{-1}. Feed: 0-900 ppm NO, 500 ppm NO_2, 1000 ppm NH_3, 5% O_2.

The above experiments involved variations of either NO or NO_2 to determine their apparent positive orders. We performed one more set of experiments in which we

simultaneously increased NO and NO_2 concentrations in the inlet feed. In this case, NO and NO_2 were fed in equimolar ratio while keeping the NH_3 constant at 1000 ppm. These reactions were studied in the absence of O_2 in the temperature range of 185-245 ^oC. An increasing feed NOx concentration increased the deNOx rate over the catalyst substantially. The fraction of NO_2 converted was always greater than that of NO. This trend matches earlier results obtained for integral NOx conversion experiments.

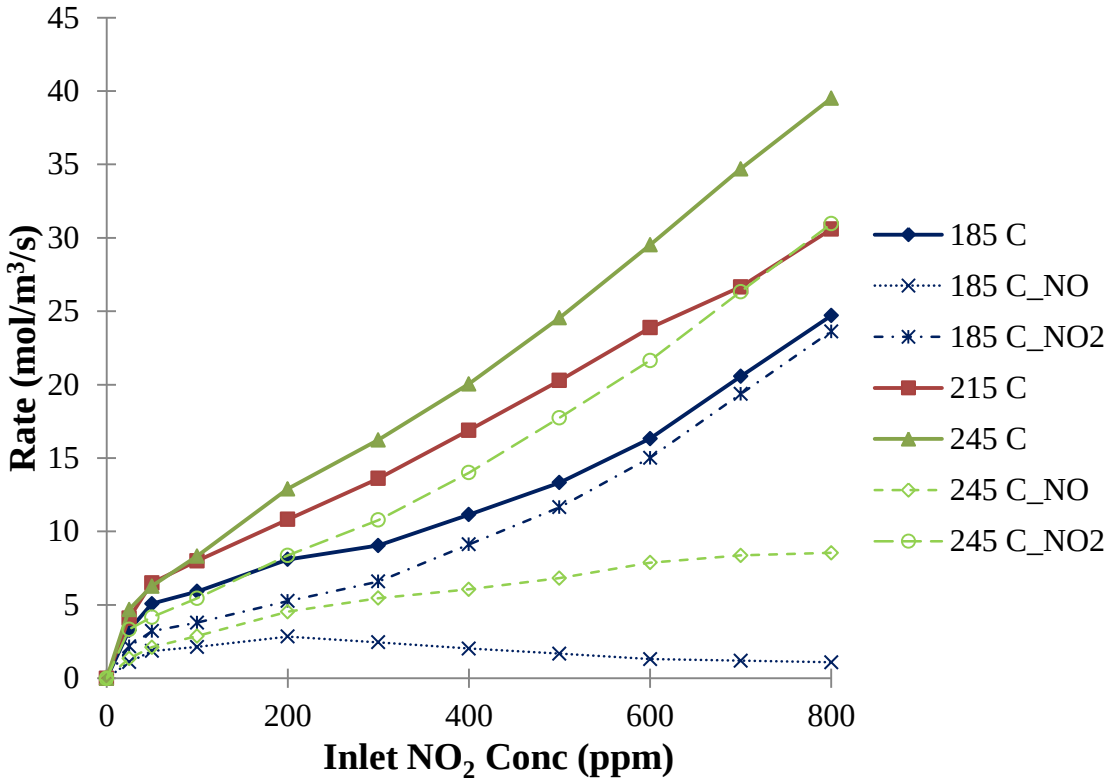

Figure 4-21: Effect of various inlet NO_2 concentrations on the rate of NOx conversion during fast SCR reaction. Space velocity 2×10^6 hr^{-1}. Feed: 0-900 ppm NO_2, 500 ppm NO, 1000 ppm NH_3, 5% O_2.

Similar experiments were carried out to determine the effect of oxygen concentration on the fast SCR reaction. For these experiments, 500 ppm NO, 500 ppm NO_2 and 1000 ppm NH_3 were kept constant in the inlet feed and Ar was used as a balance gas with 1000 sccm as the total flow rate. The inlet O_2 concentrations were varied in the

range of 0-5% for temperatures of 185 ^{o}C, 220 ^{o}C and 245 ^{o}C. The O_2 was found to have no effect on the fast SCR reaction, essentially the same NOx conversion was obtained for all O_2 concentrations for a particular temperature. Hence the apparent reaction order with respect to O_2 can be considered to be zero.

From these rate data the following conclusions can be drawn. The fast SCR reaction has apparent positive orders with respect to NO and NO_2. The apparent order for ammonia varies between positive and negative while the apparent reaction order for O_2 is nearly zero. The apparent activation energy for the fast SCR reaction with respect to the rate of NOx conversions at different temperatures was found to be 18±1 kJ/mol which is somewhat less than that of standard SCR reaction (ca. 40 kJ/mole). Devadas et al. [29] reported the value of activation energy of fast SCR reaction on washcoated Fe-ZSM-5 catalyst to be around 7 kJ/mol for temperatures up to 350 ^{o}C. But at this temperature, diffusion limitations cannot be ruled out and thus the value they have obtained may not be valid for the intrinsic kinetic regime. An examination of mass transfer is presented in the next section.

From the differential kinetics data, it appears that the NH_3 has a slight inhibition on the fast SCR chemistry. From Figure 4-19 it is clear that the increasing NH_3 reduces the R_{NO} slightly while having a negligible effect on $R_{NO2.}$ Recently, Grossale et al. [32] described the role of NH_3 inhibition on the fast SCR chemistry at lower temperatures. They concluded that the NH_3 blocking effect is due to the strong interactions between NH_3 and nitrates. Our differential kinetics results show that the inhibition due to NH_3 is negligible. The data suggest that excess NH_3 may block the NO from adsorbing and reacting with surface nitrates (reaction (4-13)) which is the rate determining step for the

fast SCR reaction. This inhibition was negligible compared to that of standard SCR reported in the earlier Chapter 3.

In order to study this effect in some more detail, we carried out some transient experiments in which a mixture containing 500 ppm each of NO and NO_2, and 1000 ppm NH_3 was fed to the reactor for 1 hour and then NH_3 was suddenly switched off and the transient response of the NO, NO_2 concentrations was monitored. The experiment was repeated for three different temperatures of 180 ^oC, 250 ^oC and 300 ^oC. At 180 ^oC, it was observed that the NO concentration dropped for a while, went through minimum and then increased; NO_2 and N_2 increased with the removal of NH_3. At 250 ^oC, the dip in NO concentration was small, while at 300 ^oC, no dip in the NO concentration was observed. This indicates that the dip in NO concentration is due to the reaction of NO with NH_4NO_3 present on the catalyst (reaction (4-13)). As observed in the steady state and transient experiments reported above, the NH_4NO_3 present on the catalyst decreased with time and at 300 ^oC, there was essentially no NH_4NO_3 present for the fast SCR case. This proves that the fast SCR reaction does not have as such a strong inhibition by NH_3 compared to the standard SCR case.

4.3.7 Kinetic Model

With all these results, we can construct a mechanistic-based kinetic model for the fast SCR chemistry. Recently, Iwasaki et al. [36] reported their results on the fast SCR chemistry in which they proposed a mechanism and corresponding kinetic model for fast SCR chemistry. Our approach is similar to their approach but includes the involvement of NH_4NO_3 formation and inhibition on the fast SCR chemistry. On Fe-zeolite catalysts,

different sites are present (Fe-metal sites and acidic zeolite sites) on which following reactions take place.

Adsorption of the reactants on the catalyst surface is given by:

$$NO + S_1 \xleftrightarrow{K_1} NO\text{-}S_1, \quad (4\text{-}14)$$

$$NO_2 + S_1 \xleftrightarrow{K_2} NO_2\text{-}S_1, \quad (4\text{-}15)$$

$$NH_3 + S_2 \xleftrightarrow{K_3} NH_3\text{-}S_2, \quad (4\text{-}16)$$

where S_1 denotes the active metal site and S_2 denotes acidic zeolite site. NH_3 spillover from sites S_2 to S_1 has been proposed in the literature [27] and is given as

$$NH_3\text{-}S_2 + S_1 \xleftrightarrow{K_4} NH_3\text{-}S_1 + S_2. \quad (4\text{-}17)$$

NO_2 can react with water to form nitrate and nitrite (as acids) on the catalyst surface by the following reaction

$$2\ NO_2\text{-}S_1 + H_2O \xleftrightarrow{k_1} HNO_3\text{-}S_1 + HONO\text{-}S_1. \quad (4\text{-}18)$$

Nitrates formed in the above reaction (4-18) are then reduced by NO into nitrites by

$$HNO_3\text{-}S_1 + NO\text{-}S_1 \xrightarrow{k_2} HONO\text{-}S_1 + NO_2\text{-}S_1. \quad (4\text{-}19)$$

Nitrous and nitric acids formed in the above reaction (4-18) can react with NH_3 by following reactions:

$$NH_3\text{-}S_1 + HONO\text{-}S_1 \xrightarrow{k_3} N_2 + 2\ H_2O + 2\ S_1\ , \quad (4\text{-}20)$$

$$NH_3\text{-}S_1 + HNO_3\text{-}S_1 \xleftrightarrow{k_4} NH_4NO_3\text{-}S_1 + S_1. \quad (4\text{-}21)$$

The NH_4NO_3 formed in the above reaction can be reduced by NO by the following reaction

$$NH_4NO_3\text{-}S_1 + NO\text{-}S_1 \xrightarrow{k_5} N_2 + NO_2\text{-}S_1 + S_1. \quad (4\text{-}22)$$

From these steps, the fractional coverage of the various species are derived as follows:

$$\theta_{NO} = K_1 P_{NO} \theta_v , \quad (4\text{-}23)$$

$$\theta_{NO_2} = K_2 P_{NO_2} \theta_v , \quad (4\text{-}24)$$

$$\sigma_{NH_3} = K_3 P_{NH_3} \sigma_v , \quad (4\text{-}25)$$

$$\theta_{NH_3} = K_3 K_4 P_{NH_3} \theta_v , \quad (4\text{-}26)$$

$$\theta_{HONO} = K_2 P_{NO_2} \sqrt{\frac{2k_1 k_2 K_1 P_{NO}}{k_3 K_3 K_4 P_{NH_3}}} \theta_v , \quad (4\text{-}27)$$

$$\theta_{HNO_3} = K_2 P_{NO_2} \sqrt{\frac{k_1 k_3 K_3 K_4 P_{NH_3}}{2k_2 K_1 P_{NO}}} \theta_v , \quad (4\text{-}28)$$

$$\theta_{NH_4NO_3} = k_4 K_2 P_{NO_2} \sqrt{\frac{k_1 k_3 (K_3 K_4 P_{NH_3})^3}{2k_2 K_1 P_{NO}}} \theta_v . \quad (4\text{-}29)$$

Here, σ_v is the mole fraction of vacant acid (S_2) sites and θ_v is the fraction of vacant metal (S_1) sites available and is obtained from the following site balance

$$\theta_v = 1 - (\theta_{NO} + \theta_{NH_3} + \theta_{NO_2} + \theta_{HONO} + \theta_{HNO_3} + \theta_{NH_4NO_3}). \quad (4\text{-}30)$$

Assuming that the reduction of nitric to nitrous acid (reaction (4-19)) is the rate determining step for the fast SCR chemistry, a complex rate expression can be derived from equation (4-31) using the above equation (4-29) for θ_v,

$$R_{fast} = k_2 \theta_{NO} \theta_{HNO_3} . \quad (4\text{-}31)$$

The resulting rate expression can predict most of the trends in the differential kinetic data.

4.3.8 Differential Kinetics for NO_2 SCR Reaction

As described above, the presence of NO_2 greatly affects the deNO_x efficiency over a range of temperatures. Here we studied the differential kinetics for the NO_2 SCR reaction in which only NO_2 was present as the NOx species in the inlet feed. In order to achieve the differential conversions ($\leq$ 15%), a small piece of monolith catalyst with 4 channels and 5 mm length was used so that a very high space velocity of 2×10^6 hr^{-1} could be achieved.

In order to determine the effect of NO_2 on the NOx removal efficiency, 500 ppm of NH_3 was kept constant in the inlet feed and the total flow rate of 1000 sccm was used with Ar as a balance gas. This system was studied in the absence of O_2 to avoid side reactions like the ammonia oxidation reaction. The NO_2 concentration in the inlet feed was varied from 0-800 ppm and corresponding changes in the NO_2 conversion were recorded. The results obtained for this study in the temperature range of 185-245 ^oC show that the NO_2 SCR reaction has a positive order dependence on the NO_2 concentration. Similar conversions were obtained in the temperature range of 185 - 215 ^oC. Similar experiments were repeated with NH_3 to quantify its role in NO_2 conversion. This was carried out by keeping the inlet NO_2 concentration constant at 500 ppm. The NH_3 concentration was varied in the range of 0-800 ppm. Again, very similar NO_2 conversions were obtained till 215 ^oC. Increasing NH_3 concentrations have a positive effect on the NO_2 removal efficiency of the catalyst. Thus the apparent order of NH_3 is also positive.

In order to study the effect of NH_3 in more detail, we carried out transient experiments in which 500 ppm of NH_3, 500 ppm NO_2 were fed to the reactor system in the presence of 2% H_2O for about 1 hour at 200 ^oC. NH_3 was then removed from the feed

and the corresponding NO_2 concentration was monitored. The NO_2 concentration was observed to increase immediately after the NH_3 was removed from the feed stream. This shows that the NH_3 inhibition effect observed for the standard and fast SCR chemistries was completely absent for the NO_2 SCR chemistry.

It was not possible to extract exact orders for the NO_2 SCR reaction using this differential kinetic data as it was not the only reaction taking place here. Hence the apparent orders were not calculated for NO_2 SCR reaction. The overall activation energy for the NO_2 reduction rate was estimated to be 12.8 (±0.5) kJ/mol of NO_2 reacted.

Recently, Grossale et al. [31] published a reaction mechanism of NO_2 SCR on an Fe-zeolite catalyst in line with that available for the BaNa-Y zeolite catalyst [90]. In the reaction mechanism, they assume that the reduction of HNO_3 by NH_3 (reaction (4-35)) is the rate determining step for the NO_2 SCR reaction. It is represented as follows:

$$6\ NO_2 + 3H_2O \leftrightarrow 3\ HNO_3 + 3\ HONO, \quad (4\text{-}32)$$

$$3\ HONO + 3\ NH_3 \rightarrow 3\ N_2 + 6\ H_2O, \quad (4\text{-}33)$$

$$3\ HNO_3 + 2\ NH_3 \rightarrow 3\ HONO + 3\ H_2O + N_2, \quad (4\text{-}34)$$

$$3\ HONO + 3\ NH_3 \rightarrow 3\ N_2 + 6\ H_2O, \quad (4\text{-}35)$$

$$3\ HNO_3 + 5\ NH_3 \rightarrow 4\ N_2 + 9\ H_2O. \quad (4\text{-}36)$$

Our results agree with the proposed reaction mechanism. Moreover, at lower temperatures, we have shown that the formation of NH_4NO_3 inhibits the NO_2 SCR reaction. This could be due to NH_4NO_3 formed on the surface blocking the HNO_3 access to NH_3.

4.4 Conclusions

This work reports the experimental findings of steady-state and transient experiments on the selective catalytic reduction of NOx with NH_3 performed on the commercial and in-house synthesized Fe-zeolite catalysts. Comparable results were obtained on both the catalysts for various reaction systems studied. NO_2 TPD experiments performed on the commercial Fe-zeolite catalyst showed that the Fe-zeolite catalyst has a good adsorption capacity for NO_2 and was found to be less than that of NH_3.

This work covers the effect of inlet NO_2 concentrations on the NOx conversion during the SCR reaction. NO_2 was found to have a promoting effect on the SCR reaction especially at lower temperatures. Water was seen to have negligible role in the SCR chemistry. Water inhibits the NOx reduction for feeds containing excess NO_2 (NO_2/NOx > 0.5) in the temperature range of 200-300 ^oC. A feed containing equimolar quantities of NO and NO_2 was found to have maximum selectivity towards N_2 production. Increasing inlet concentrations of NO_2 were found to be favorable for NOx reduction at lower temperatures. Very high NOx conversions were obtained for feeds containing NO_2/NOx ratio of 0.5 and higher for temperatures of 300 ^oC and above. Feeds containing NO_2 higher than the equimolar NO/NO_2 ratios led to a number of side reactions at lower temperatures. Excess of NO_2 in the inlet feed mainly led to the formation of byproducts like ammonium nitrate below 250 ^oC. The ammonium nitrate decomposes at higher temperatures and leads to the formation of another byproduct N_2O. Maximum N_2O was detected for a feed containing pure NO_2 in the temperature range of 250-300 ^oC. Thus, the presence of NO_2 in the inlet feed complicates the SCR reaction system with number

of reactions occurring simultaneously e.g., standard SCR, fast SCR, NO_2 SCR, ammonium nitrate formation and decomposition, ammonia and NO oxidation.

Steady state and transient experiments confirm the presence of NH_4NO_3 on the catalyst surface at lower temperatures. The ammonium nitrate reduces the NOx conversion for both the fast and NO_2 SCR reactions at lower temperatures by inhibiting the rate determining reactions. Increasing amounts of NO in the feed NOx increases the N_2 production by inhibiting the formation of undesirable byproducts like NH_4NO_3 and N_2O. The key role of NO was found to reduce HNO_3 and NH_4NO_3; present on the catalyst; to desired nitrites and thereby increasing N_2 production.

Differential kinetics studies were carried out under both the NO_2 SCR and the fast SCR reaction conditions. The NO_2 SCR reaction was found to be positive order with respect to both NO_2 and NH_3. The fast SCR reaction was found to be positive order with respect to both NO and NO_2. However, fast SCR reaction showed little inhibition with respect to NH_3 at lower temperatures. This inhibition could be attributed to NH_3 blocking the reduction of nitrates by NO by forming a layer above nitrates. Fast SCR was found to be positive order for lower NH_3 concentrations with slightly negative and then zero order at higher concentrations. Both the NO_2 SCR and the fast SCR reactions were found to be essentially zero order with respect to O_2. Based on the experimental findings, a kinetic rate expression is proposed for the fast SCR reaction which explains key trends obtained during experiments. Reduction of nitrates by NO appears to be the rate determining step for fast SCR while reduction of HNO_3 by NH_3 seems to determine the NO_2 SCR reaction mechanism.

CHAPTER 5 Experimental Study of Selective Catalytic Reduction of NOx with NH_3 on a Cu-chabazite catalyst

5.1 Introduction

The selective catalytic reduction (SCR) of NOx with NH_3 is considered as the most promising technique to meet stringent EPA NOx emission standards. The SCR of NOx with NH_3 has been commercialized for the vehicular applications in the 1990's. Since then, various catalysts have been developed and used commercially for this purpose. Initially, the focus was on the vanadia-based catalysts [21, 22, 24-27, 63, 78, 160, 161]. Catalysts like $V_2O_5/WO_3/TiO_2$ have been used extensively for the commercial applications. Recently, the focus has shifted to the metal-exchanged zeolite catalysts. Amongst the various metal-exchanged zeolite catalysts available, Fe- and Cu-zeolite catalysts are found to have a very high NOx reduction efficiency over a wide temperature range of practical interest. Fe-zeolites are found to be more active for the high temperature range applications while Cu-zeolites are more active for the low temperature range applications. The structure of zeolite catalysts is very complex and it usually consists of rings of various shapes, sizes and dimensions. Zeolites like ZSM-5 have pentasil structure with 10-membered rings. Similarly, different zeolites (e.g., beta-zeolite, chabazite, SSZ-13, Y-zeolite, etc.) have different ring sizes and hence different pore dimensions. Different zeolite structures give different selectivity and activity for a particular reaction under consideration. Also, these dimensions affect the overall stability of the catalysts. Based on these considerations, it is critical to choose the right metal-exchanged zeolite to get optimum NOx removal efficiency over the entire temperature range of practical interest. This particular study is focused on the understanding of

kinetics and mechanistic aspects of various reactions occurring during the NOx reduction chemistry on recently developed Cu-chabazite catalysts.

Cu-zeolites are found to have higher oxidation activity compared to Fe-zeolites. Because of this advantage, these catalysts give higher deNOx activity at lower temperatures. Iwamato et al. [162, 163] performed pioneering research recognizing the activity of Cu-zeolites for high deNOx efficiency. Various types of Cu-zeolites have been studied extensively in the SCR literature and these catalysts mainly include Cu-MOR, Cu-BEA, Cu-ZSM-5, Cu-Y, Cu-NaY, Cu-Ferrierite and Cu-FAU [89, 98, 102, 111, 164-171]. Even though various types of Cu-zeolites are available in the market, Cu-ZSM-5 catalyst has received a special attention because of its very high NOx removal efficiency over the temperature range of 200-400 ^{o}C [89, 172, 173]. Various studies focused on the in-depth understanding of the kinetics and mechanistic aspects of various NH_3-SCR reactions are available in the literature [87, 89, 100, 117, 119, 120]. Few literature studies described the nature of active sites present in Cu-ZSM-5 catalysts [174-178]. Even though Cu-ZSM-5 catalysts provide excellent activity for the NOx removal in presence of NH_3 as the reductant, these catalysts are not found to be very stable at very high temperatures. This issue with respect to the stability of these catalysts is more pronounced in the presence of water. Under realistic conditions, in the actual exhaust aftertreatment system, water vapor is present in sufficiently large amounts. Under these realistic conditions, i.e., in the presence of water and at sufficiently high temperatures, 700 °C and above, the catalyst deactivates rapidly and exhibits greatly diminished SCR activity. Various literature studies provide fundamental understanding about the deactivation of Cu-ZSM-5 catalyst [13, 179-182]. Overall, the deactivation of the catalyst

was found to be due to the dealumination of the zeolite framework, because, at higher temperatures, the aluminum in the zeolite framework becomes unstable and hence detaches from the zeolite framework [183, 184]. Along with the loss of zeolite framework, because of the loss of aluminum, the Bronsted acid sites within the zeolite are lost. As a result, copper migrates into the unstable zeolite structure resulting in the formation of some oxides of copper. Some copper aluminate structure also forms in this overall process of catalyst deactivation [185-187]. Thus even though the Cu-ZSM-5 catalyst gives substantially higher SCR activities, it is highly unstable under realistic conditions. Recently, Cu-exchanged beta zeolite has been reported to have excellent activity in the SCR of NOx with NH_3. In general, metal-exchanged beta zeolites are generally found to have greater hydrothermal stability than similar ZSM-5 catalysts [188]. But beta-zeolites are reported to have lower NOx reduction efficiency and hence are not used to a great extent compared Cu-ZSM-5 catalysts. Generally the pore sizes of the beta and ZSM-5 catalysts are sufficiently large and hence hydrocarbons can enter the pores of these zeolites easily. Thus hydrocarbons, if adsorbed on the catalyst surface, further reduce the deNOx efficiency of the Cu-zeolites (ZSM-5). This issue is of practical concern especially during the cold start operation. Thus considering the hydrocarbon adsorption along with the issue with the hydrothermal instability, Cu-ZSM-5 catalysts find very little scope for practical applications in the automobile industry. As a result, recent research is focused on inventing a new zeolite catalyst which gives comparable (to Cu-ZSM-5) or even better NOx removal efficiency and at the same time has sufficiently high hydrothermal stability for practical applications.

In order to overcome the earlier discussed drawbacks with the use of Cu-ZSM-5 and Cu-beta and other Cu-exchanged zeolites, researches have invented various small pore zeolite catalysts. These catalysts mainly include Cu-chabazite, Cu-SSZ-13, Cu-SSZ-16, SAPO-34, etc. A recent study by Kwak et al. [125] compared the activities of Cu-ZSM-5, Cu-beta and Cu-SSZ-13 catalysts. With the identical experimental conditions for NOx SCR with NH_3, they found that the Cu-SSZ-13 demonstrated a superior activity and N_2 formation selectivity in comparison with Cu-beta and Cu-ZSM-5 zeolites. Considering the activity and overall selectivity towards N_2 formation, their results suggest that Cu-SSZ-13 is an excellent candidate catalyst for use in practical NH_3 SCR of NOx applications. In a recent study [189], Kwak et al. discussed the effects of hydrothermal aging on the material properties and NH_3 SCR activity of Cu-ZSM-5, Cu-BEA, Cu-Y, and Cu-SSZ-13 catalysts. They reported a substantially high NH_3 SCR activity for the Cu-SSZ-13 catalyst after hydrothermal treatment at 800 °C for 16 h. Also, they reported a significant loss in the NH_3-SCR activities of other catalysts (Cu-ZSM-5, Cu-BEA, and Cu-Y) under similar conditions of hydrothermal aging. They attributed the loss in the NH_3-SCR activity to the de-alumination of the zeolite framework. With the help of XRD and H_2-TPR experiments, they found that the Cu^{2+} could be reduced to Cu^{+} and to Cu^{0} in Cu-ZSM-5 and Cu-beta, while Cu^{2+} could be reduced to Cu^{+} only in Cu-SSZ-13. After hydrothermal aging, CuO and Cu-aluminate-like species were found to form in Cu-ZSM-5 and Cu-beta, while little changes were observed for Cu-SSZ-13, consistent with the minor changes in the SCR activity of this catalyst. Thus the small pore Cu-SSZ-13 and Cu-chabazite represent highly stable and active NH_3-SCR catalysts and hold the potential of replacing the existing catalysts used commercially. This study is

focused on the detailed understanding of the kinetics and mechanistic aspects of various reactions involved in the NH_3-SCR chemistry. We used a commercial Cu-chabazite catalyst provided by BASF Catalysts LLC, for this study. In the following section, we present a comprehensive steady state and transient kinetics study of various reactions on this catalyst. This study provides an insight into the reaction mechanism of various reactions on the Cu-chabazite catalyst. These results are compared with that of Fe-ZSM-5 catalyst discussed in earlier Chapters 3 and 4.

5.2 Experimental

5.2.1 Catalyst Sample

The catalyst sample used in this particular study was a commercial Cu-zeolite catalyst and it was supplied by BASF (Iselin, NJ). It is a small-pore Cu-chabazite type catalyst, established in patents and communicated in recent papers to possess excellent hydrothermal stability [125-127]. More detail about the synthesis and structure of this Cu-chabazite catalyst can be found in [127]. This catalyst was supplied in the form of a washcoated monolithic catalyst with a cell density of 400 cpsi.

5.2.2 Catalyst Characterization

The catalyst was characterized using various characterization techniques described earlier in Chapter 2. In order to determine the loading of active metal (Cu) content in this catalyst, we scraped the washcoat containing Cu-chabazite catalyst. This powder was characterized using the Inductive Coupled Plasma-Atomic Emission Spectroscopy (ICP-AES) method. The Cu loading was found to be about 2.5% (by

weight) of the total Cu-chabazite sample used in the washcoat. Scanning Electron Microscope (SEM) (JEOL JSM-6330F) was used to measure the washcoat thickness. The washcoat thickness was found to be of the order of 45-50 μm; this is a peripheral-averaged value since, as expected, the washcoat is considerably thicker in the corners (150μm) than on the sides (25μm) as shown in Figure 5-1.

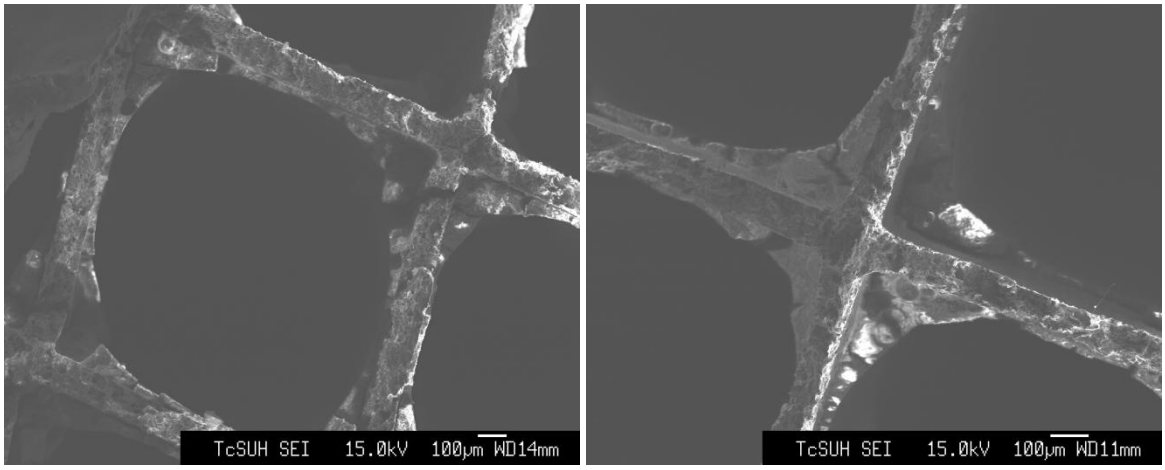

Figure 5-1: SEM images of the commercial Cu-chabazite monolith catalyst are shown here. Washcoat was found to be in the circular shape with more deposition at the corners compared to that in the center of the channel.

5.2.3 Bench-Scale Reactor Set-up

The experimental set up used to study the activity of Cu-chabazite catalyst for the SCR of NOx with NH_3 was the same as described earlier in Chapter 2. The experimental setup included a gas supply system, a reactor system, an analytical system, and a data acquisition system. A monolith catalyst wrapped with a ceramic fiber was placed inside a quartz tube reactor mounted in a tube furnace. The quartz tubes used for this study were 40.6 cm long with an internal diameter of 0.81 cm and an outer diameter of 1.27 cm. In most of the experiments, we used 2 cm length and 34 channels of the monolith piece. This corresponds to a gas hourly space velocity (GHSV) (represented as the ratio volumetric flow rate calculated at standard temperature and pressure to the monolith

brick volume) of 57,000 hr^{-1}. The typical gas linear velocity during the experiments was calculated as a function of temperatures and was found to be in the range of 0.6-1.2 m/s. The furnace temperature was adjusted with a temperature controller. A FT-IR spectrometer (Thermo-Nicolet, Nexus 470) was placed downstream of the reactor to analyze various effluent gases including NH_3, NO, NO_2, N_2O, and H_2O. A quadrupole mass spectrometer (QMS; MKS Spectra Products; Cirrus LM99) was used to measure N_2.

5.2.4 NH_3/NO/NO_2 Uptake and Temperature Programed Desorption

The initial set of experiments involved studying the adsorption capacity of the catalyst for various gas species. The uptake experiments involved the exposure of a pre-oxidized catalyst with a flowing Ar stream containing 500 ppm concentration of one of the following three gas species: NH_3, NO or NO_2. The catalyst temperature was maintained constant at 150 ^oC initially during the uptake experiments. For the NH_3 uptake experiments, after a prescribed exposure in which the effluent NH_3 concentration reached its feed value, the NH_3 was turned off (about 1 hour duration). About 30 minutes were allowed for weakly adsorbed NH_3 to desorb from the catalyst. Then a temperature ramp of 10 ^oC/min was applied to desorb the more strongly adsorbed NH_3. The desorbed NH_3 from the catalyst surface was measured with the help of an FT-IR. A similar procedure was used during the NO and NO_2 uptake and temperature programed desorption experiments.

5.2.5 Steady-state Experiments

As discussed earlier in Chapter 1, there are various side reactions taking place as part of the SCR chemistry. NH_3 and NO oxidation are two important side reactions. The oxidation of NH_3 and NO was carried out to assess the extent of these side reactions. In order to study the NH_3 oxidation, a feed containing 500 ppm NH_3 and 5% O_2 with Ar as a balance gas was introduced on the catalyst surface. NO oxidation reaction studies were also carried out on the commercial Cu-chabazite catalyst. The feed gas contained 500 ppm NO and 5% O_2 (with Ar as a balance gas). The effect of feed water was studied separately on both the oxidation reactions.

Several steady state NH_3 SCR experiments were carried out on the commercial Cu-chabazite catalyst to study the catalyst activity as a function of concentrations of various gas species. In order to study the standard SCR reaction, a feed containing 500 ppm NO, 500 ppm NH_3 and 5% O_2 was introduced on the catalyst surface. In order to understand the ammonia inhibition in more detail, additional experiments were carried out at temperatures of 200 ^oC where feed NH_3 was increased from 100 ppm to 1000 ppm by keeping the NO (500 ppm) and O_2 (5%) concentrations constant. Role of NO_2 was studied separately using feeds containing various amounts of feed NO_2. For this purpose, we used feeds containing four different NO_2/NOx (0.25, 0.5, 0.75 and 1) inlet ratios. The temperature range selected for this purpose was 180-550 ^oC. Temperatures below 180 ^oC were avoided as they lead to the formation and deposition of solid ammonium nitrate in the pipelines. Both 500 ppm of NH_3 and 500 ppm of NOx were present in the feed along with 5% O_2 and Ar as a balance gas. The effect of water was studied in separate experiments by repeating some of the above experiments with 2% H_2O in the feed.

The above experiments covered the entire temperature and conversion range. Along with these integral experiments, we carried out differential experiments where the conversions were kept below 15%. These experiments were carried out to estimate the kinetics (apparent reaction orders and activation energies). A shorter catalyst (1 cm and 4 channels) and a wider range of total gas flow rates provided additional flexibility to achieve higher space velocity and correspondingly lower conversions approaching differential conditions. Gas hourly space velocity as high as 960,000 hr^{-1} resulted in NOx conversions below 15% for temperatures below 250 ^{o}C. During these experiments the NO concentration was varied over the range of 200-800 ppm while keeping NH_3 concentration constant at 500 ppm and O_2 at 5%. These data were used to determine the order of SCR reaction with respect to NO. Similar experiments were carried out to determine the reaction orders with respect to NH_3 and O_2.

5.2.6 Transient Experiments

Transient experiments were carried out on the commercial Cu-chabazite monolithic catalyst to identify and understand the reaction system dynamics. The catalyst was initially pre-saturated with ammonia (500 ppm) in the presence of Ar at a total flow rate of 1000 sccm. The NH_3 was then switched off and only Ar was flowed to remove any physisorbed NH_3 from the catalyst. Then a gas containing 500 ppm of NOx with different NO/NO_2 ratios (1/0, 1/1 and 0/1) was fed to the reactor in the presence of 5% O_2. The transient effluent composition was measured. These experiments were carried out under isothermal conditions for various temperatures in the range of 150 - 400 ^{o}C.

5.3 Results and Discussion

5.3.1 NH_3 Uptake and Temperature Programmed Desorption

Zeolite catalysts consist of different types of sites. Mainly two types of acidic sites, Lewis acid and Bronsted acid sites, are important in these zeolites [190]. The strong affinity that the basic NH_3 has for the Bronsted acid sites on acidic zeolites like ZSM-5 is an important feature of the NH_3-SCR reaction system. Ammonia can adsorb on metal sites along with these acid sites [117].

The data for a typical NH_3 uptake and desorption experiment (150 ^oC) are shown in Figure 5-2. During the first 600 s, only the Ar carrier was fed to the reactor. At the 600 s time, the prescribed NH_3 concentration feed was introduced to the reactor. NH_3 uptake occurred during the induction period preceding ammonia breakthrough. After achieving saturation, the NH_3 inlet was shut off and the exit NH_3 concentration decreased monotonically to zero. During the 30 minute post uptake period, some physisorbed ammonia desorbed from the catalyst. In Chapter 3, we discussed this in detail on the Fe-ZSM-5 catalyst. Figure 5-3 compares the NH_3 adsorption capacity of the commercial Fe-ZSM-5 and Cu-chabazite catalysts. Under exactly identical experimental conditions, the Cu-chabazite catalyst showed higher adsorption capacity for NH_3 compared to that of Fe-ZSM-5. From Figure 5-3, it is clear that, during the NH_3 uptake, the NH_3 breakthrough occurred earlier on Fe-ZSM-5 compared to Cu-chabazite. Also, during the temperature ramp, the NH_3 released from the Cu-chabazite catalyst resulted in a higher peak area. After quantifying the area under the peak, we found that the NH_3 adsorption capacity of Cu-chabazite (0.82 mol/kg catalyst) was more than twice the adsorption capacity of Fe-ZSM-5 (0.37 mol/kg catalyst). The difference in the NH_3 adsorption capacities is

attributed to the difference in types of zeolites used. It also depends upon the amount of washcoat, active metal loading, washcoat thickness, etc. Also, the shapes of the desorption peaks are different which may indicate the role of different sites in NH_3 storage. Komatsu et al. [111] proposed the coordination of four ammonia molecules to each copper. Depending on the nature of adsorption of NH_3, various sites can be considered for NH_3 adsorption [117, 119, 120]. All the ammonia adsorbed on the Fe-ZSM-5 catalyst was desorbed at temperatures earlier than that of Cu-chabazite. Colombo et al. [87] also reported a higher NH_3 adsorption capacity for a Cu-zeolite than a Fe-zeolite catalyst.

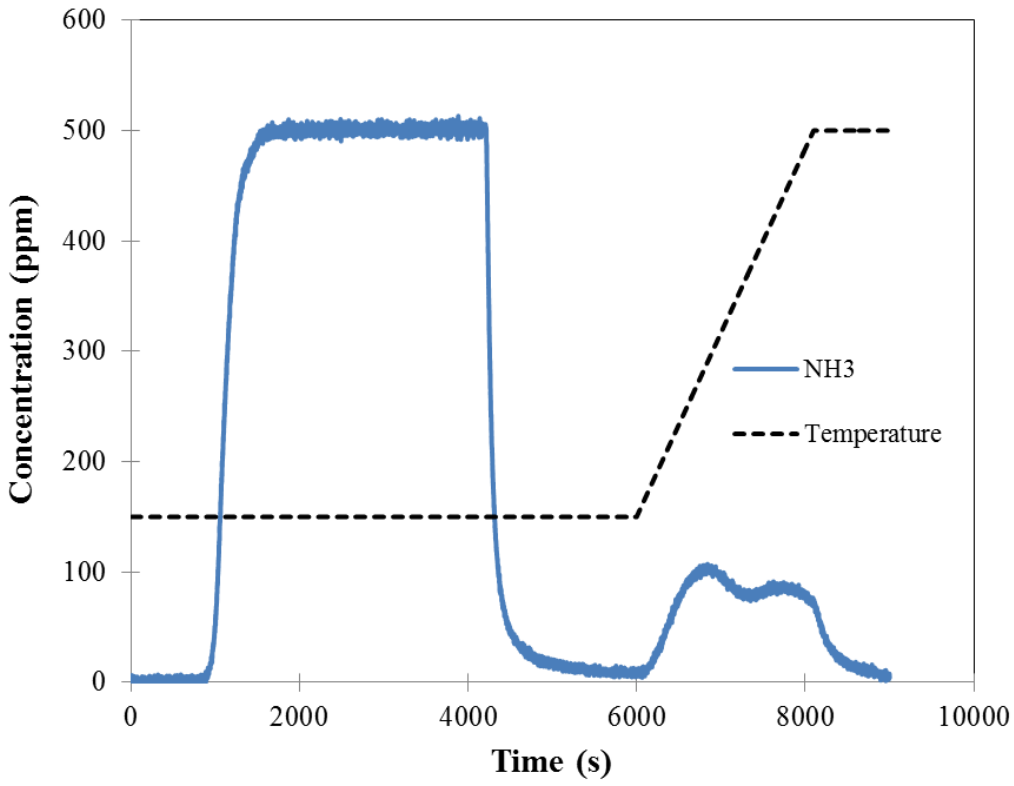

Figure 5-2: Measured NH_3 concentrations during the NH_3 TPD experiment with NH_3 adsorbed at 150 ^oC. Temperature ramp of 10 ^oC/min was given at 6000s and corresponding NH_3 concentration is recorded.

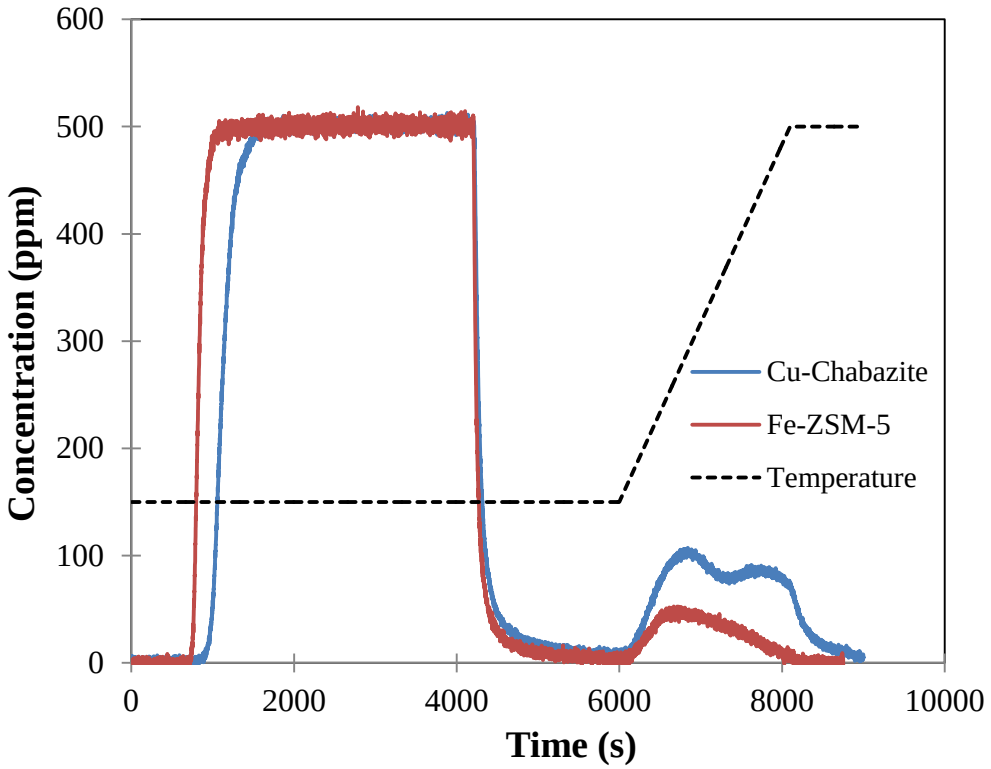

Figure 5-3: Comparison of NH_3 concentration profiles during the NH_3 TPD experiments carried out on Cu-chabazite and Fe-ZSM-5 catalysts. NH_3 was adsorbed at 150 ^oC and a temperature ramp of 10 ^oC/min was given at 6000s.

5.3.2 NOx Uptake and Temperature Programmed Desorption

We carried out similar experiments for NO and NO_2 uptake and temperature programed desorption on the Cu-chabazite catalyst. For the NO uptake experiments, a feed containing 500 ppm NO was introduced on the catalyst (at 150 ^oC) surface for 1 hour followed by switching off the NO feed and flowing Ar only feed throughout the experiment. This was then followed by the temperature ramp. The NO concentration reached its inlet value almost immediately, indicating weak adsorption of NO. This was confirmed during the subsequent temperature ramp in which only very small amounts of NO were measured.

The adsorption behavior of NO_2 was quite different. Figure 5-4 shows the results obtained for NO_2 adsorption at 150 ^oC following the same procedure as for NO. Some NO was evolved upon the introduction of NO_2. This behavior is reminiscent of NO_2 storage on $Pt/BaO/Al_2O_3$ lean NOx trap (LNT) catalysts [158]. Despress et al. [99] reported the formation of nitrates on the Cu-ZSM-5 catalyst after the introduction of NO_2 feed. They found that the presence of feed NO lowers the storage of adsorbed nitrates. Grossale et al. [39] also inferred in their experimental study that the NO_2 disproportionation leads to the formation of nitrates and NO by the following reaction

$$3\ NO_2 + O^{2-} \rightarrow 2\ NO_3^- + NO. \qquad (5\text{-}1)$$

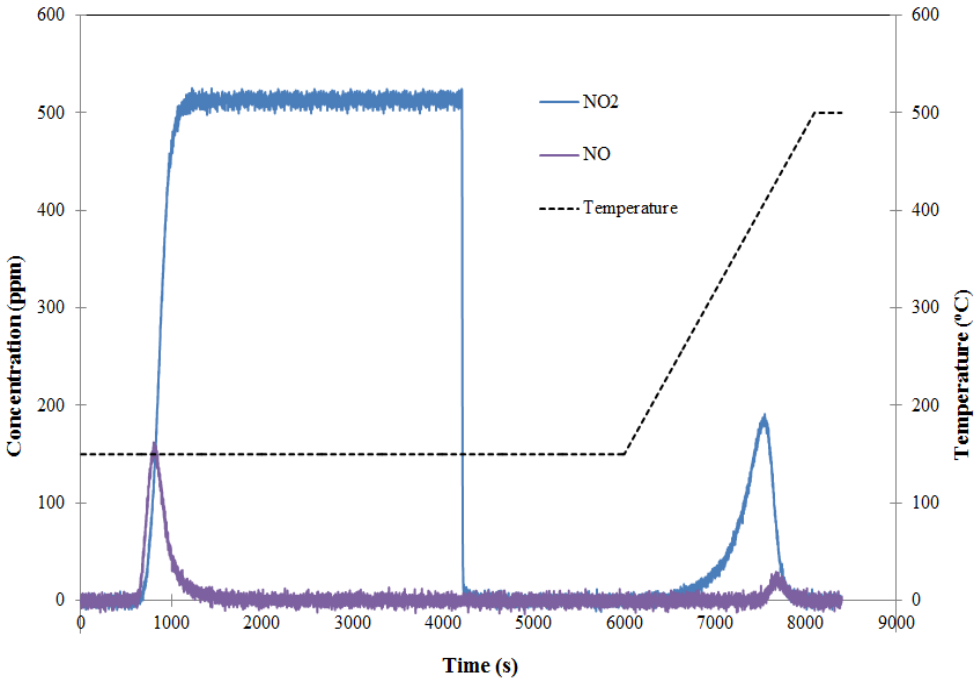

Figure 5-4: NO_2 concentration profile obtained during the TPD experiments carried out on the Cu-chabazite catalyst at 150 ^oC as the initial temperature of adsorption. Temperature ramp of 10 ^oC/min was given at 6000s.

The temperature ramp (10 ^oC/min) resulted in the evolution of NO_2 which confirms that the catalyst has sufficient storage capacity for NO_2 which can be stored in the form of nitrates. The fate of nitrate is discussed in more detail in the subsequent Chapter 8 of this

thesis. At higher temperatures ($\geq 350^{o}C$) during the temperature ramp, a small amount of NO was detected most likely due to NO_2 decomposition.

The uptakes of NH_3, NO and NO_2 are obviously of interest in the overall catalyst performance and kinetics. We use this understanding in developing kinetic models which are discussed later in Chapter 9.

5.3.3 Ammonia Oxidation

As discussed earlier, various side reactions occur during the NH_3-SCR chemistry. One of the key reactions in this chemistry is the ammonia oxidation side reaction. The oxidation of ammonia is detrimental because it lowers the effective NH_3 available for NOx reduction. It is critical to quantify the extent of the oxidation and product selectivities in order to fully elucidate the SCR reaction system. The oxidation of NH_3 produces N_2, N_2O, NO and NO_2 by the following reactions:

$$4\ NH_3 + 3\ O_2 \rightarrow 2\ N_2 + 6\ H_2O \qquad \Delta H = -3.12 \times 10^5\ J/mol\ NH_3, \qquad (5\text{-}2)$$

$$2\ NH_3 + 2\ O_2 \rightarrow N_2O + 3\ H_2O \qquad \Delta H = -2.76 \times 10^5\ J/mol\ NH_3, \qquad (5\text{-}3)$$

$$4\ NH_3 + 5\ O_2 \rightarrow 4\ NO + 6\ H_2O \qquad \Delta H = -2.27 \times 10^5\ J/mol\ NH_3, \qquad (5\text{-}4)$$

$$4\ NH_3 + 7\ O_2 \rightarrow 4\ NO_2 + 6\ H_2O \qquad \Delta H = -2.84 \times 10^5\ J/mol\ NH_3. \qquad (5\text{-}5)$$

Zeolite based catalysts are highly selective towards N_2 formation. Yang et al. [44-46] reported nearly 100% selectivity to N_2 over a range of temperatures and feed ratios using a Fe-ZSM-5 catalyst. A recent study by Kwak et al. [125] reports the steady state NH_3 oxidation activity on Cu-ZSM-5, Cu-beta, and Cu-SSZ-13 catalysts. They observed a very high selectivity for N_2 (as the main product) during the NH_3 oxidation reaction

carried out on Cu-ZSM-5 and Cu-SSZ-13 catalysts. But the Cu-beta catalyst produced noticeable amounts of N_2O during this reaction.

We studied the activity of Cu-chabazite catalyst for the NH_3 oxidation side reaction in the temperature range of 100-550 ^oC. The catalyst was exposed to 500 ppm NH_3 (in Ar) for 30 minutes at 100 ^oC, after which 5% O_2 was admitted and sufficient time was allotted to reach steady state (about 25 minutes). After steady state was reached, a temperature ramp of 25 ^oC/min was given for 2 minutes so that the next temperature which is an increment of 50 ^oC, was achieved. This procedure was repeated at all the temperatures to record the steady state NH_3 conversions. At low temperatures, the catalyst stored sufficiently large amounts of NH_3. Hence, during the temperature ramp, a clear peak of NH_3 was observed. But at higher temperatures, the NH_3 storage capacity of the catalyst goes down and hence the peak intensity observed during the temperature ramp also decreased. The NH_3 uptake experiments showed similar results. Figure 5-5 compares the steady state NH_3 conversion activity as a function of temperature in the presence and absence of feed water. In the absence of feed water, the Cu-chabazite catalyst did not show any NH_3 oxidation activity below 200 ^oC. A further increase in temperature to 250 ^oC showed a substantial NH_3 conversion activity of about 20%. Subsequent increment in temperatures lead to a very high NH_3 oxidation activity giving almost complete NH_3 conversions for temperatures above 400 ^oC. The decrease in NH_3 concentrations was complemented by a near-stoichiometric increase in N_2 concentration. N_2 was obtained as the main product of this reaction and negligible amounts (< 5 ppm) of other N-containing products such as NO and N_2O were obtained in a particular temperature range, specifically N_2O was obtained in the range of 250-350 ^oC while NO

was observed at higher temperatures (≥ 500 °C). This shows that the Cu-chabazite catalyst is highly selective towards oxidation of NH_3 to N_2.

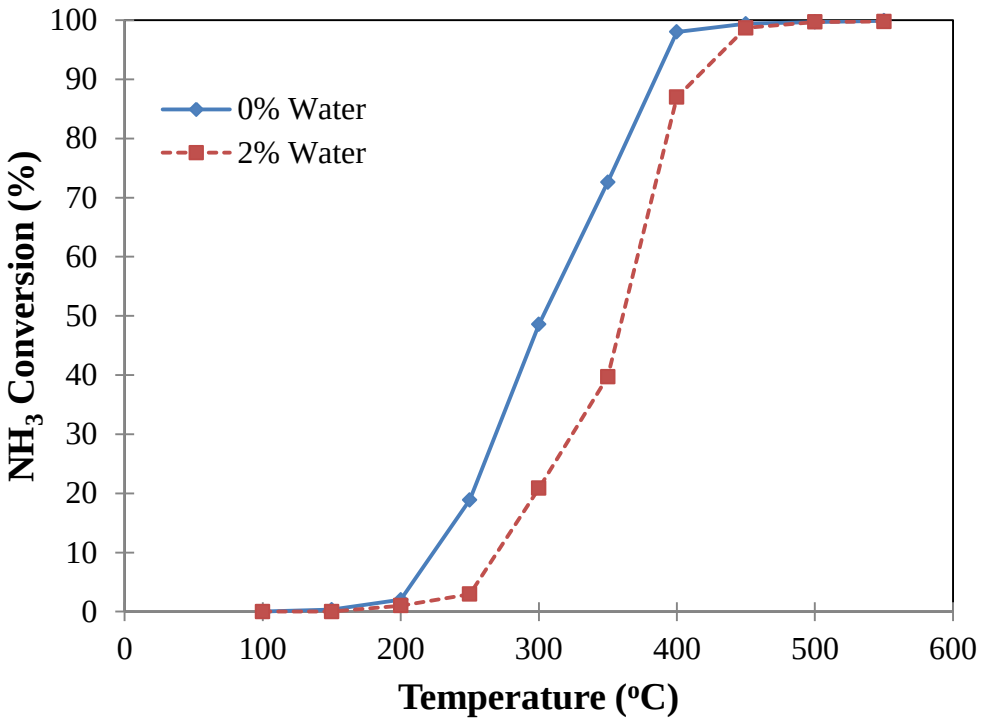

Figure 5-5: Comparison of the ammonia oxidation activity on the commercial Cu-chabazite catalyst in the presence and absence of feed water. Feed: 500 ppm NH_3, 5% O_2 and 0 - 2% water.

The NH_3 oxidation reaction system was then studied in the presence of 2% feed H_2O. Water showed a strong inhibition effect on this reaction where the NH_3 conversion dropped substantially in the temperature range of 250-400 °C. This decrease is attributed to H_2O blocking the active sites required for NH_3 oxidation. At higher temperatures (≥ 450 °C), near about complete conversion of NH_3 was obtained which shows a very high NH_3 oxidation activity for the Cu-chabazite catalyst. Overall, Cu-chabazite was thus found to be highly active towards the NH_3 oxidation side reaction compared to that of Fe-ZSM-5, discussed earlier in Chapter 3. We provide a systematic comparison of these two catalysts for various reactions later in Chapter 7.

5.3.4 NO Oxidation

NO oxidation is another important side reaction in the SCR chemistry. This is a reversible reaction which is kinetically controlled at lower temperatures and is equilibrium controlled at higher temperatures. This reaction generates NO_2 in the forward direction which is a main product at lower temperatures. At higher temperatures, reverse NO_2 decomposition (to NO) reaction becomes dominant and the NO conversions thus decrease.

$$NO + \tfrac{1}{2} O_2 \leftrightarrow NO_2 \qquad \Delta H = -5.7 \times 10^4 \text{ J/mol NO.} \qquad (5\text{-}6)$$

In the presence of NO_2, the rate of SCR increases. Hence, NO oxidation is considered to be a desirable side reaction in the SCR chemistry. A few studies propose this reaction as the rate limiting step in the standard SCR chemistry. Thus we studied this reaction separately on the Cu-chabazite catalyst.

A feed containing 500 ppm NO and 5% O_2 was introduced on the catalyst surface both in the presence and absence of 2% feed water. As discussed earlier, the NO storage capacity of the catalyst was negligible and was verified during the NO uptake and temperature programmed desorption experiments. Thus when NO was fed to the catalyst in the absence of O_2, it reached the initial feed values immediately. Sufficient time was given for the steady state to be reached. After a steady state was reached, a temperature ramp (25 ^{o}C/min) was given to reach the next temperature. Figure 5-6 reports the steady state NO conversion obtained as a function of temperature. In the absence of water, the NO conversions increased significantly with increasing temperature reaching a maximum NO conversion activity of about 36% at 400 ^{o}C after which the NO conversions decreased because of the reversible NO_2 decomposition reaction becoming more active at

higher temperatures. When the reaction was studied in the presence of water, the NO conversion activity dropped significantly. This confirmed the strong inhibition of water on this reaction. Thus, water blocked the active sites required for NO oxidation reaction. This result is in line with that of the NH_3 oxidation reaction where water showed significant inhibition.

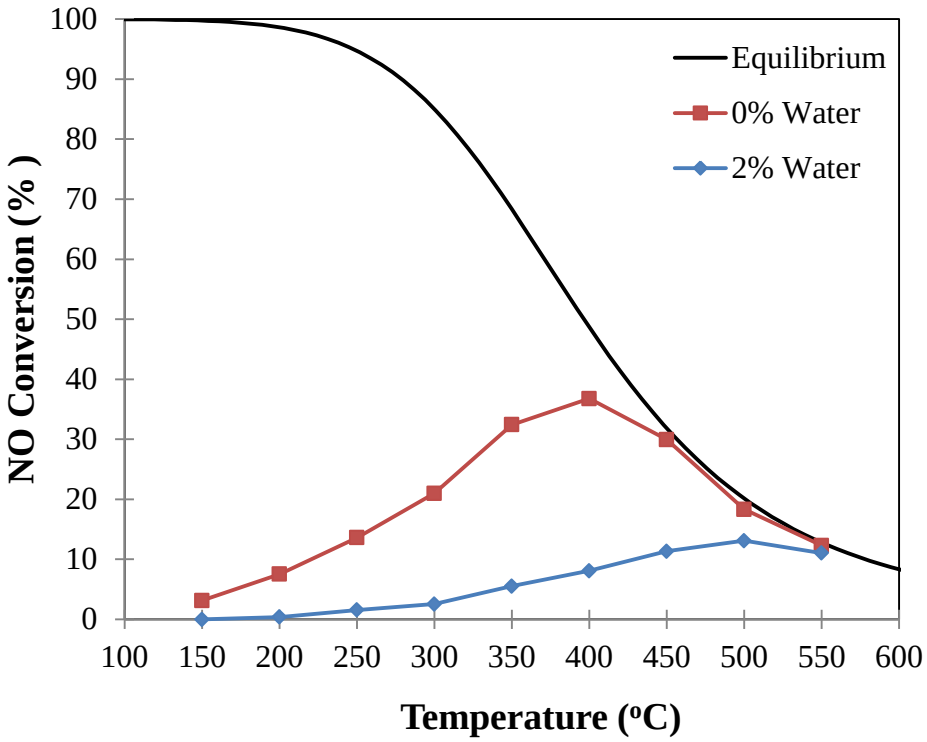

Figure 5-6: Steady state conversion of NO obtained during the NO oxidation reaction on Cu-chabazite catalyst. Feed: 500 ppm NO, 5% O_2, 0-2% H_2O.

In separate experiments, we studied the kinetics of NO oxidation using a differential reactor where maximum NO conversions were kept below 15%. We selected a temperature range of 200-290 ^oC for this purpose and used a gas hourly space velocity of 57,000 hr^{-1}. These experiments and results are discussed in more detail in Chapter 8 where we develop a predictive kinetic model to explain key features of this reaction. Here we give a brief summary of these experimental results as they are used in the analysis of

the experimental data later discussed in this chapter. In order to determine the NO reaction order, the inlet NO concentration was varied from 100-900 ppm while keeping the O_2 concentration constant at 5%. In order to determine the reaction order with respect to O_2, the NO concentration was kept constant at 500 ppm while O_2 was varied from 0-5%. Based on the above differential kinetics studies, we found that the reaction was about first-order with respect to NO and positive half-order with respect to O_2. Also, the activation energy of this reaction was found to be around 56 kJ/mol.

5.3.5 Selective Catalytic Reduction of NO with NH_3

The standard SCR reaction involves reduction of NO by NH_3 in the presence of O_2 and is given by

$$4\ NH_3 + 4\ NO + O_2 \rightarrow 4\ N_2 + 6\ H_2O \qquad \Delta H = -4.07 \times 10^5\ J/mol\ NH_3. \qquad (5\text{-}7)$$

We studied this reaction on the Cu-chabazite catalyst where the catalyst was exposed to a mixture of NO, NH_3, O_2 and 0-2% water. Initially, the catalyst was exposed to 500 ppm of NH_3 (in Ar) only feed for about 30 minutes. This allowed sufficient time for the NH_3 to reach its inlet concentration of 500 ppm. Then NO (500ppm) and O_2 (5%) were simultaneously fed to the reactor. The reaction system was allowed to reach steady state (about 25 minutes).

Figure 5-7 shows the steady state concentrations of various species obtained as a function of temperature during the standard SCR reaction carried out in the absence of water. As shown in Figure 5-7, the effluent NO concentration decreased monotonically with temperature, with the sharpest drop occurring between 150 – 250 ^oC. At 100 ^oC, the activity of the catalyst was negligible. At 200 ^oC, there was a sudden drop in the concentrations of both NO and NH_3, with NH_3 concentration slightly lower than that of

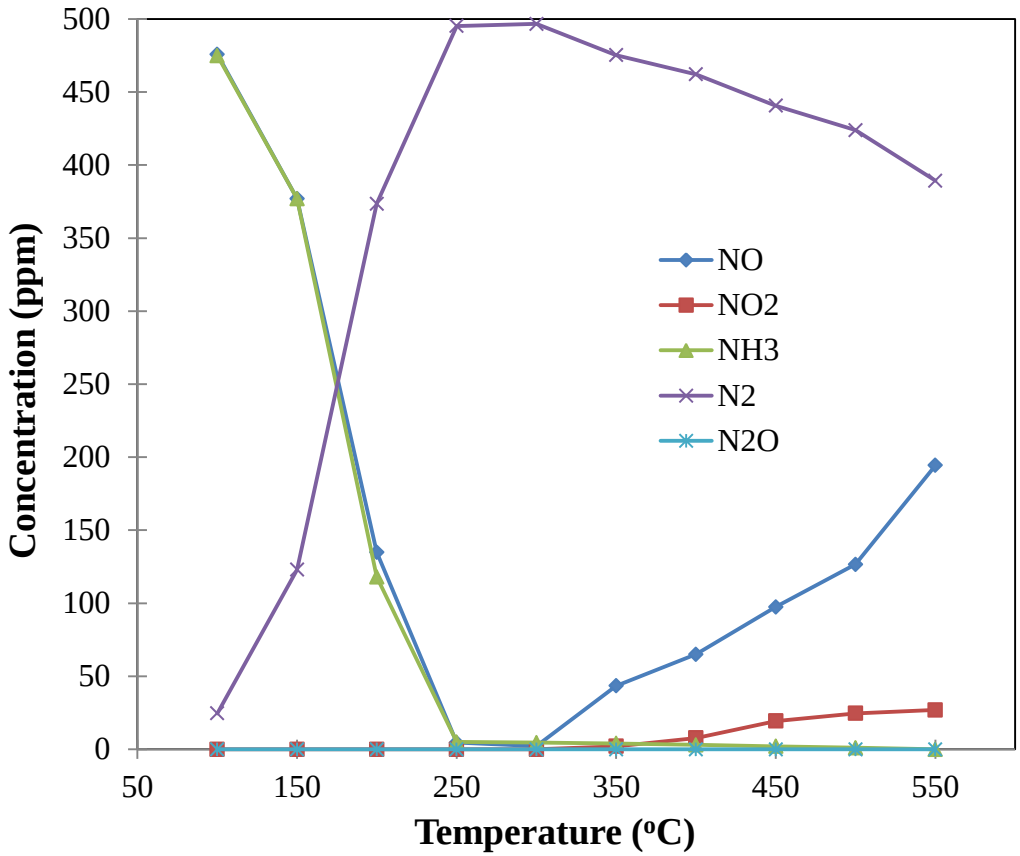

Figure 5-7: Steady state product distribution obtained during the standard SCR reaction. Feed: 500 ppm NO, 500 ppm NH_3, 5% O_2.

NO. The slight difference in the conversions of NO and NH_3 at these low temperatures has been attributed to parasitic NH_3 oxidation [134]. The Cu-chabazite catalyst gave a very high NO conversion activity in the temperature range of 250-300 ^oC where negligible amount of NOx was detected in the outlet. For temperatures above 350 ^oC, the NO concentration in the outlet started increasing while no NH_3 was observed in the outlet. This showed that the NH_3 conversions were nearly 100% and hence NH_3 was involved in the NH_3 oxidation side reaction. As discussed earlier, the NH_3 oxidation reaction was found to be very active on the Cu-chabazite catalyst where nearly complete NH_3 conversion activity was recorded for temperatures above 400 ^oC (in the absence of water). Thus, as the rate of this side reaction increased, sufficient reductant (NH_3) was

not available for the standard SCR reaction and hence the NO concentrations in the outlet started increasing. At higher temperatures, some NO_2 was detected along with NO because of the NO oxidation side reaction. Throughout the temperature range, amount of N_2O in the outlet was found to be negligible. Thus the Cu-chabazite catalyst selectively reduces NO to N_2 during the standard SCR reaction.

In the above experiments, water was deliberately avoided in order to isolate the effects of reacting species NO, NH_3 and O_2. In the actual exhaust, a high concentration of water vapor (or steam) is present and it is therefore important to assess its effect. Therefore, we repeated the above experiments on the Cu-chabazite catalyst in the presence of 2% H_2O in the feed. Figure 5-8 shows the product distribution obtained during the standard SCR reaction in the presence of water. Presence of feed water did not show a major effect on the product distribution for temperatures $\leq$ 300 ^oC. But at higher temperatures ($\geq$ 350 ^oC), the difference between the NO and NH_3 concentration decreased compared to that in the absence of feed water. Thus, in the presence of water, the NH_3 oxidation side reaction was suppressed and hence more amount of NH_3 was available to reduce NO. Figure 5-9 shows the NOx conversion activity both in the presence and absence of water. Thus these data show that the feed water has a positive effect on the standard SCR reaction where NOx conversion activity was enhanced at higher temperatures.

We considered the individual effects of NO, NH_3 and O_2 on the conversions of NO and NH_3. For this purpose, we carried out a systematic study where the inlet concentration of one particular species was varied keeping the concentrations of rest of the species the same. The temperature of the catalyst was kept constant at 200 ^oC during

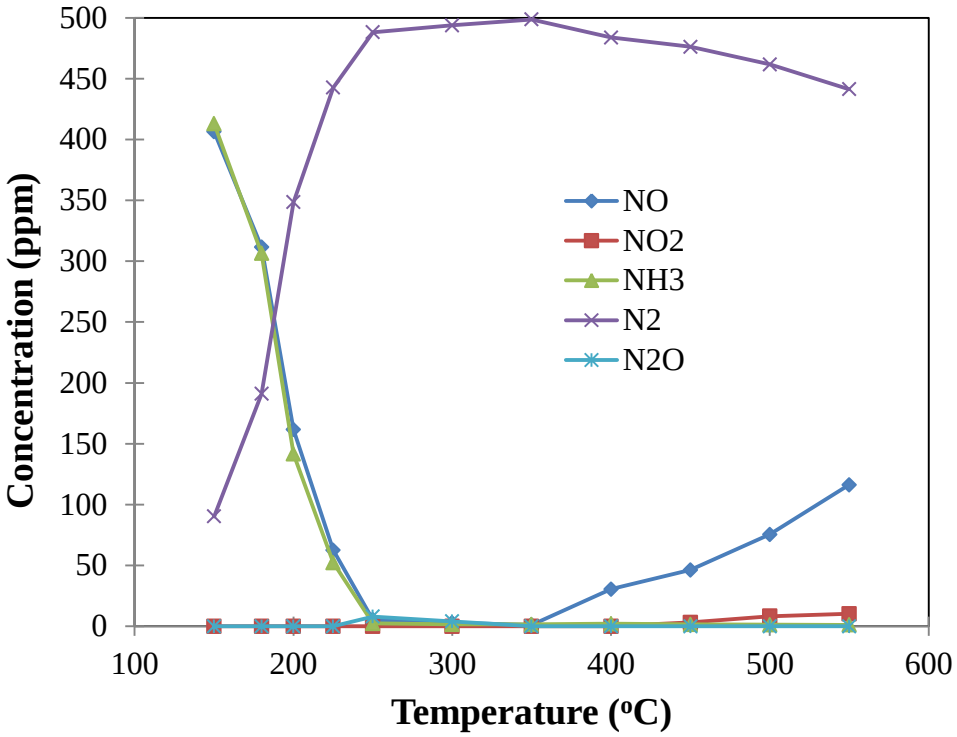

Figure 5-8: Steady state product distribution obtained during the standard SCR reaction. Feed: 500 ppm NO, 500 ppm NH_3, 5% O_2 and 2% H_2O.

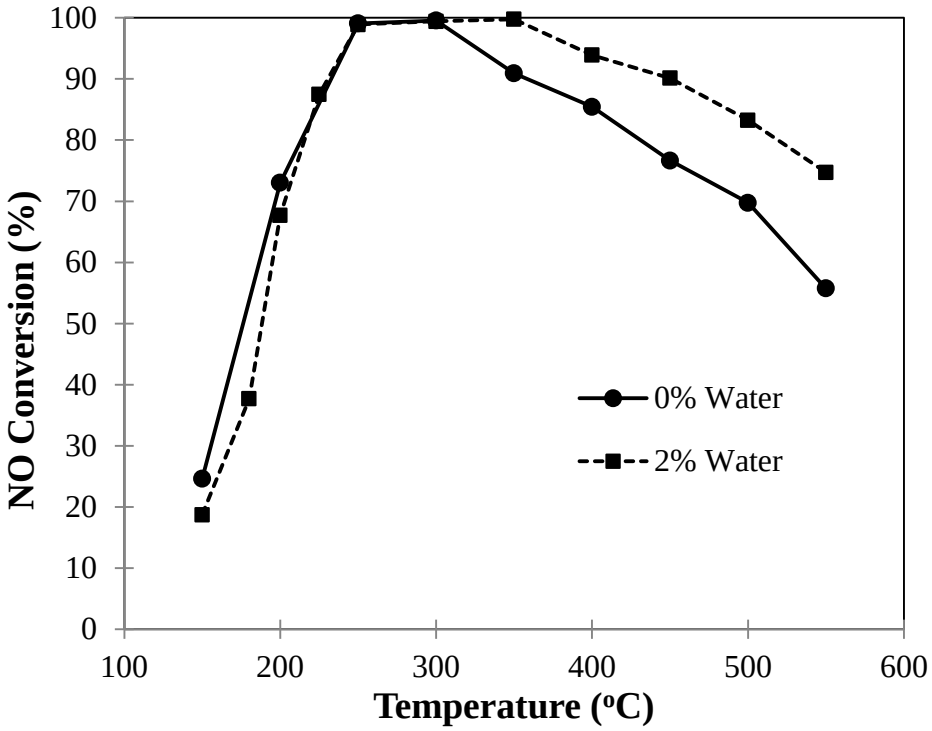

Figure 5-9: Effect of feed water on the standard SCR reaction. Feed: 500 ppm NH_3, 500 ppm NO, 5% O_2 and 0- 2% H_2O.

these studies. As NO concentration increased, the rate of NO conversion also increased. A similar trend was observed for the effect of O_2 concentration. Thus NO and O_2 showed a positive order dependence on the rate of the standard SCR reaction. A similar study with varied NH_3 concentrations did not have a fixed (either positive/negative) effect on the SCR reactions. At lower concentrations, the NH_3 showed positive order dependence while at higher concentrations, it inhibited the standard SCR reaction. The steady state data reporting the inhibition of NH_3 on the standard SCR reaction is summarized in Figure 5-10 where increasing feed NH_3 concentrations showed a positive order dependence till 400 ppm after which the NO conversion and hence the SCR activity

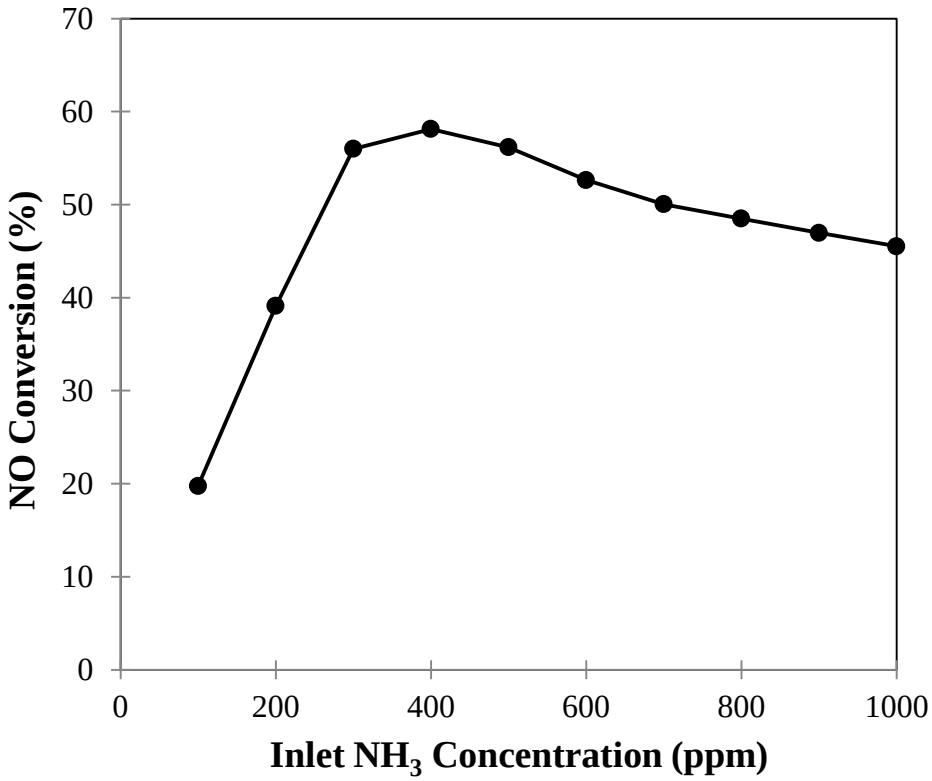

Figure 5-10: Effect of increasing feed NH_3 concentrations on the NO conversions obtained during the standard SCR reaction. Feed: 100-1000 ppm NH_3, 500 ppm NO and 5% O_2.

dropped with each incremental rise in the feed NH_3 concentration. These steady state data proved the inhibition effect by NH_3 in certain concentration range at lower temperatures.

In order to study the NH_3 inhibition in further detail, we carried out a transient experiment. The catalyst temperature was kept constant at 190 ^oC. A feed containing 500 ppm NO, 500 ppm NH_3 and 5% O_2 was fed simultaneously to the reactor. After the concentrations of all the species reached a steady state value, NH_3 was switched off. NO was seen to decrease immediately after the feed ammonia was shut off (Figure 5-11).

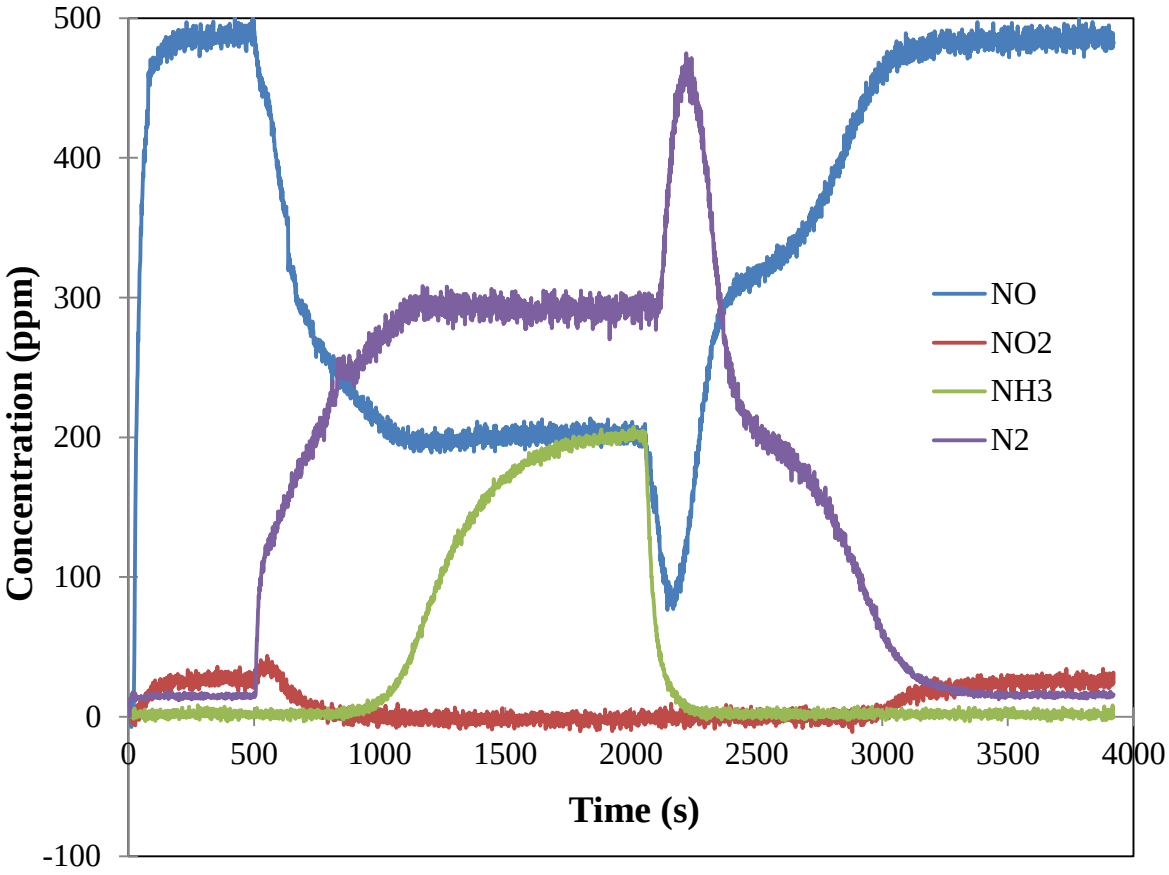

Figure 5-11: Transient experiment carried out on the Cu-chabazite catalyst to study the NH_3 inhibition effect on the standard SCR reaction.

It went through a minimum and then increased, eventually reaching a new steady state with simultaneous formation of NO_2 due to the NO oxidation reaction. During the dip in

NO concentration, the N_2 product transient profile was essentially a mirror image of the NO profile. NO_2 was observed only after the N_2 concentration decreased to zero. These experiments confirmed the inhibition effect of ammonia on the standard SCR reaction. That is, as the NH_3 was consumed through reaction there was a short-lived increase in the consumption of NO. Thus the transient experimental result supports the observations of the steady state experimental data for the standard SCR reaction proving the NH_3 inhibition effect.

5.3.6 Differential Kinetics Studies of Standard SCR Reaction

The above steady state experiments covered the entire temperature range of practical interest. The NO conversion obtained during these experiments varied from 0 to 1. This part of the study focuses on the differential kinetics studies of standard SCR reaction where we derive reaction orders of the standard SCR reaction with respect to various species participating in the reaction and also determine the overall activation energy of the reaction.

In order to decide upon the conditions for the differential kinetics where maximum NO conversions can be kept below 15%, we carried out various experiments with monoliths of different sizes and using different flow rates. Higher space velocities resulted in achieving small conversions and were achieved by cutting the monolith in short pieces. The results (not shown here) show the expected trend of monotonically decreasing NO conversions with increasing space velocities. We used a space velocity of 960,000 hr^{-1} in the temperature range of 180-240 ^{o}C. N_2 was obtained as the sole product

of the standard SCR reaction in these operating conditions. Also, the short contact time prevented any measurable conversion of NH_3 oxidation for temperatures $\leq 240^oC$

Figure 5-12 shows the dependence of the NO conversion rate on NO concentration. The rate (washcoat volume basis) increased linearly with the NO concentration at each temperature. From the logarithmic plot (Figure 5-13) of rate of NO consumption vs. average NO concentration, the apparent NO order was found to be nearly linear (0.95-1.0) over the temperature range studied. Similar experiments were carried out to determine the O_2 and NH_3 orders for the same temperature range. The results shown in Figure 5-14 and Figure 5-15 reveal a fractional positive order dependence on O_2 (0.52-0.59) over the range of temperatures considered. For the NH_3 experiments, the NO and O_2 concentrations were fixed at 500 ppm and 5% respectively while varying the NH_3 concentration between 200 and 800 ppm over the temperature range of 180 - 240 ^oC. As shown in Figure 5-16 and Figure 5-17, the NO reduction rate decreased monotonically with increasing NH_3 concentration. Thus, the standard SCR reaction is inhibited by NH_3 with an apparent order that varies between -0.20 to -0.23. For very low NH_3 concentrations (< 200 ppm), the reaction order was found be positive. But at higher NH_3 concentrations, the standard SCR reaction showed complete negative order dependence with NH_3 concentrations. The inhibition by NH_3 is attributed to the blocking of reaction sites by the strongly bound NH_3 and this behavior is similar to that observed earlier for the Fe-ZSM-5 catalyst discussed earlier in Chapter 3. Finally, the apparent activation energy was determined by measuring the temperature dependence of the apparent rate constant as shown in Figure 5-18. For an equimolar feed of NO and NH_3 in O_2 the activation energy was found to be about 54 kJ/mol. To investigate the

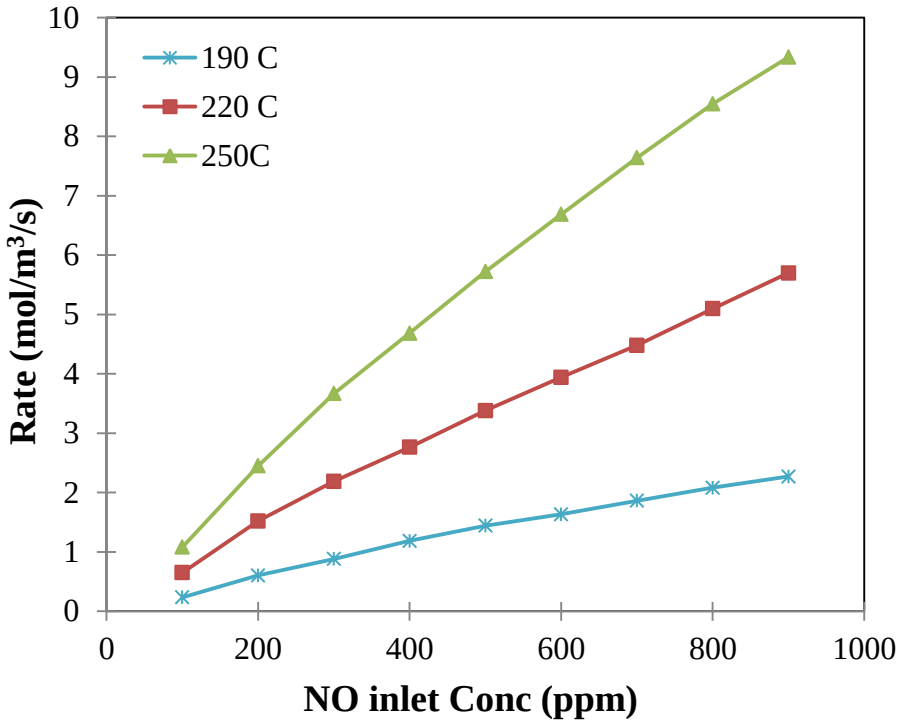

Figure 5-12: Rate of standard SCR reaction as a function of inlet NO concentration.

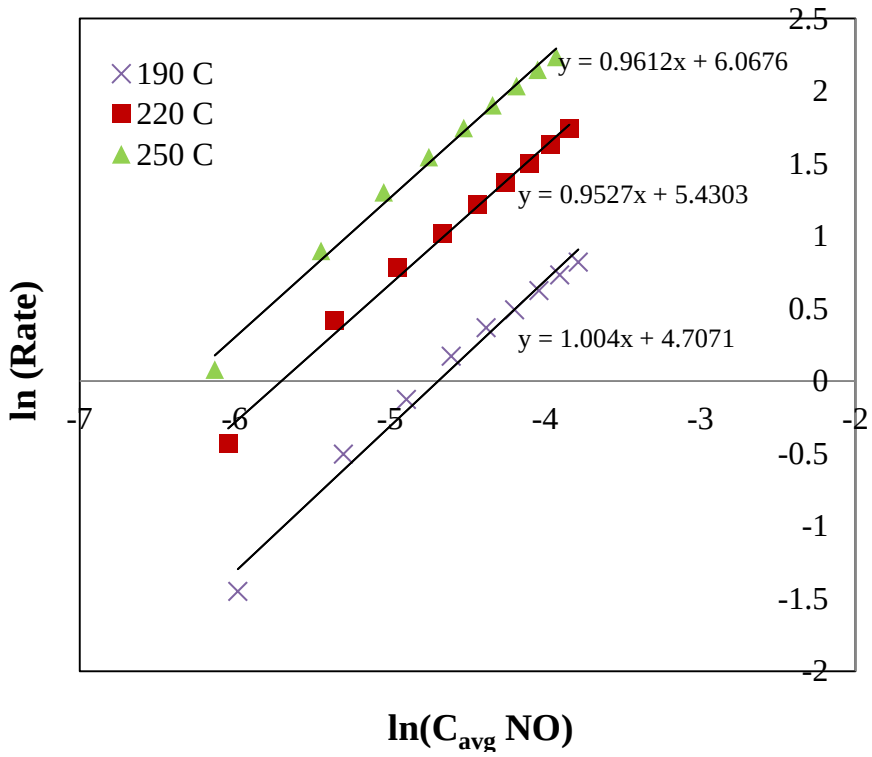

Figure 5-13: Logarithmic dependence of rate on average NO concentration.

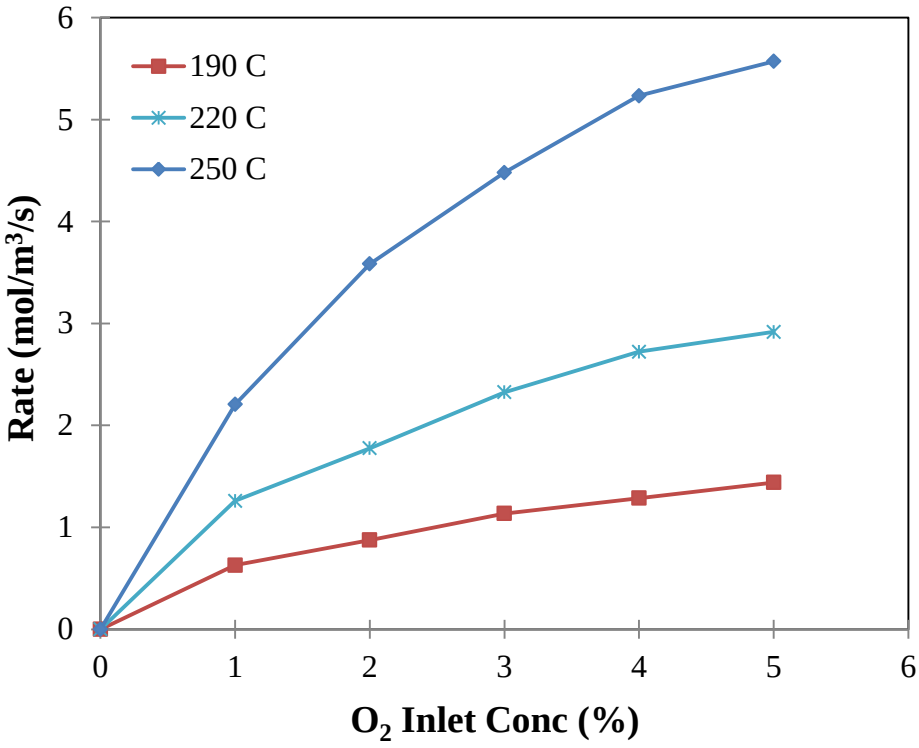

Figure 5-14: Rate of standard SCR reaction as a function of inlet O_2 concentration.

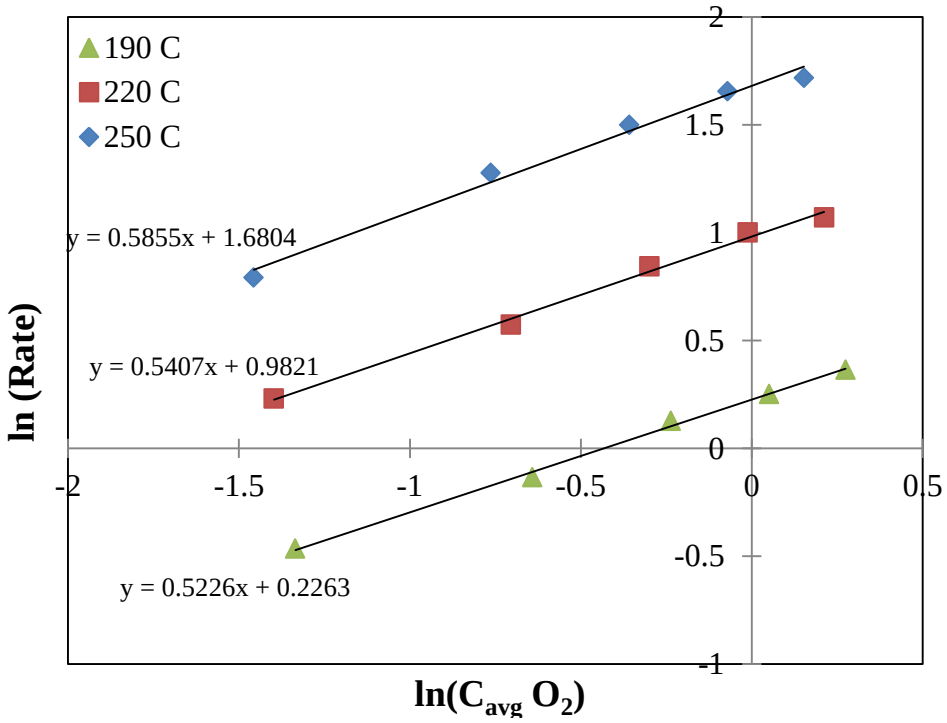

Figure 5-15: Logarithmic dependence of rate on average O_2 concentration.

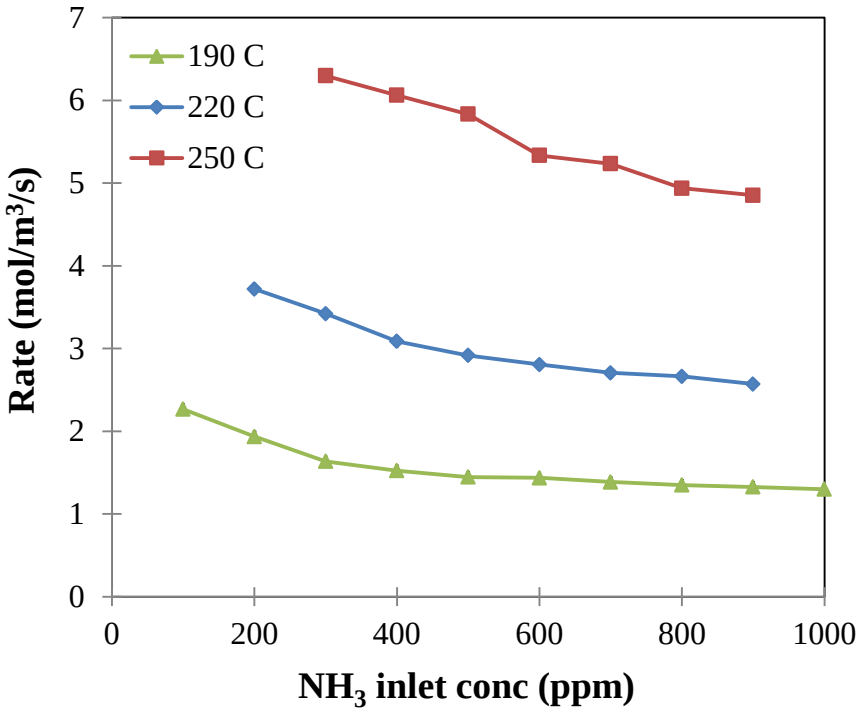

Figure 5-16: Rate of standard SCR reaction as a function of inlet NH_3 concentration.

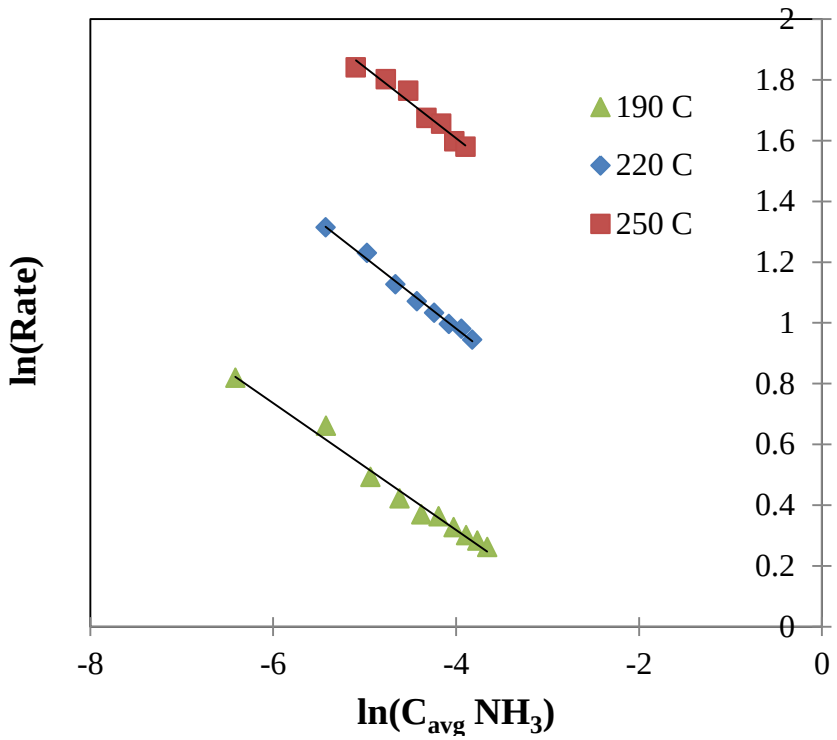

Figure 5-17: Logarithmic dependence of rate on average NH_3 concentration.

effect of water on reaction orders and activation energies, some of the above experiments were repeated with 2% H_2O in the inlet feed. The presence of water did not make any appreciable change in both the cases.

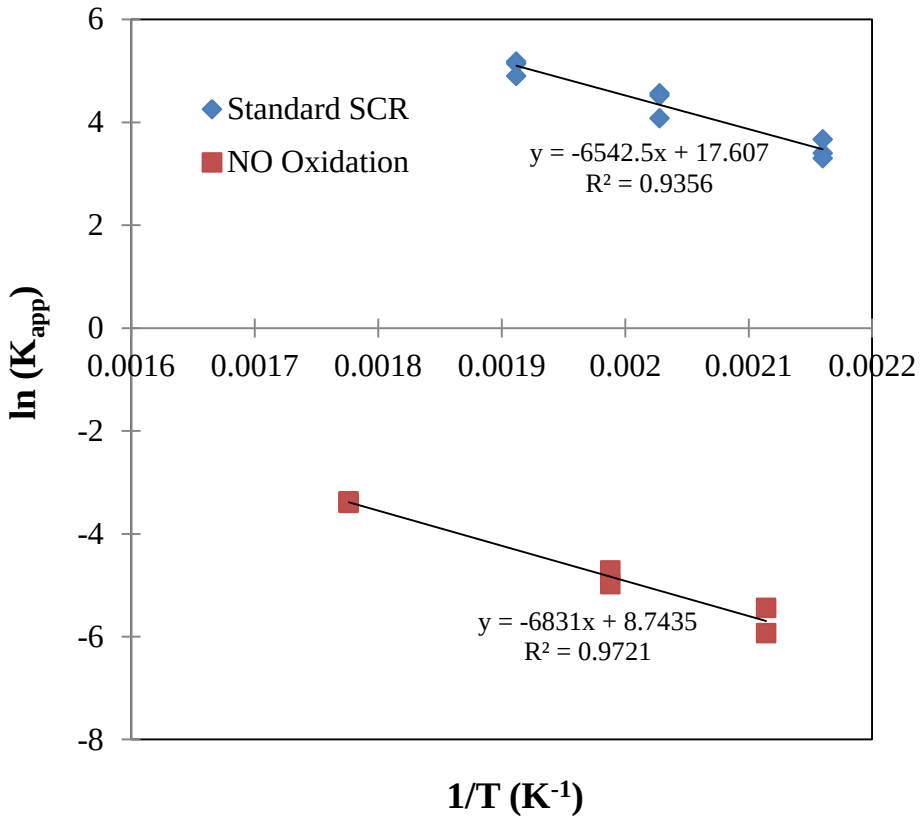

Figure 5-18: Arrhenius plot for the standard SCR and NO oxidation reaction under differential conditions.

Based on the above studies of differential kinetics, following power law model is developed for the standard SCR reaction:

$$-R_{SCR} = A\exp(-\frac{E}{RT})(NO)^{\alpha}(O_2)^{\beta}(NH_3)^{\lambda}.$$

$$[\alpha = 0.95\text{-}1.0 \qquad \beta = 0.52 - 0.59 \qquad \lambda = -0.20 - -0.23 \qquad E = 54\,kJ/mole]. \qquad (5\text{-}8)$$

The forward reaction orders with respect to both NO and O_2 along with the overall activation energy closely coincide for both the standard and NO oxidation reaction which indicate that NO oxidation could be the rate limiting step for the standard SCR reaction.

The above expression is very similar to that developed earlier for the standard SCR reaction studied on the Fe-ZSM-5 catalyst and was discussed in detail in Chapter 3. We observed a close resemblance between the power law kinetics of both these reactions earlier on the Fe-ZSM-5 catalyst. This shows that the qualitative behavior and hence the reaction mechanism of the standard SCR reaction is the same on both the Fe-ZSM-5 and Cu-chabazite catalysts. This suggests that NO oxidation could be the rate limiting step for the standard SCR on the Cu-chabazite catalyst. These results and conclusions are in line with that observed earlier for the Fe-ZSM-5 catalyst. Readers are referred to Chapter 3 for the detailed understanding of the mechanistic model of the standard SCR and NO oxidation reactions.

5.3.7 Effect of NO_2 on the SCR of NOx

In the actual exhaust after-treatment system, a diesel oxidation catalyst (DOC) unit precedes the SCR unit. A DOC unit consists of various precious metals like Pt, Pd and Rh. One of the major roles of the DOC is to oxidize various exhaust components which consist of CO, hydrocarbons and NO. Thus NO is partially oxidized to NO_2 before it enters the SCR unit. And hence the SCR feed comprises of NO_2 along with NO. Thus it is essential to consider the effect of NO_2 on the selective catalytic reduction chemistry.

The following section considers the effect of NO_2 on the NOx conversion. Figure 5-19 shows the product distribution obtained during the SCR studies for a NO_2/NOx feed ratio of 0.25 (total NOx and NH_3 concentrations were kept constant at 500 ppm each) in the presence of 5% O_2 and 2% water carried out on the Cu-chabazite catalyst. The apparent NO_2 conversion was essentially complete over the entire temperature range. At

180 ^{o}C, about 135 ppm of the 375 ppm NO that was fed was consumed while all of the NO_2 (125 ppm) was consumed. Thus there was a slight increase in the overall NOx conversion compared to that of NO only feed. As the temperature increased the amount of NO observed in the exit decreased till 350 ^{o}C, indicating an overall increase in the NOx removal efficiency. In the temperature range of 250-350 ^{o}C, about complete conversion of NOx was recorded and is similar to the standard SCR as discussed earlier. N_2 was the only N-containing product at low temperatures. The N-balance was satisfied throughout the temperature range which rules out the formation of any undetected byproducts like ammonium nitrate. A small amount (< 20 ppm) of N_2O was recorded in the temperature range of 200-350 ^{o}C. At higher temperatures, N_2O measured in the outlet was negligible. For temperatures above 350 ^{o}C, the NOx concentrations measured at the exit started rising, while NH_3 conversions were close to complete. This shows the onset of the NH_3 oxidation side reaction because of which sufficient NH_3 reductant was not available to reduce NOx and hence the NOx concentrations started increasing. A very small amount of NO_2 was detected at higher temperatures. This NO_2 could be the unreacted NO_2 leaving the system or that formed by the NO oxidation reaction. Finally, we repeated the above experiments in the absence of feed water. The absence of feed water showed a negligible difference in the NOx conversion activities at lower temperatures. But at higher temperatures (> 350 ^{o}C), the NOx conversions were found to be lower compared to that in the presence of water. These results are in line with our earlier observations for the standard SCR reaction where we observed a sharp decrease in the NOx conversion efficiencies at higher temperatures. Thus the presence of water improved the NOx removal efficiency by suppressing the NH_3 oxidation side reaction.

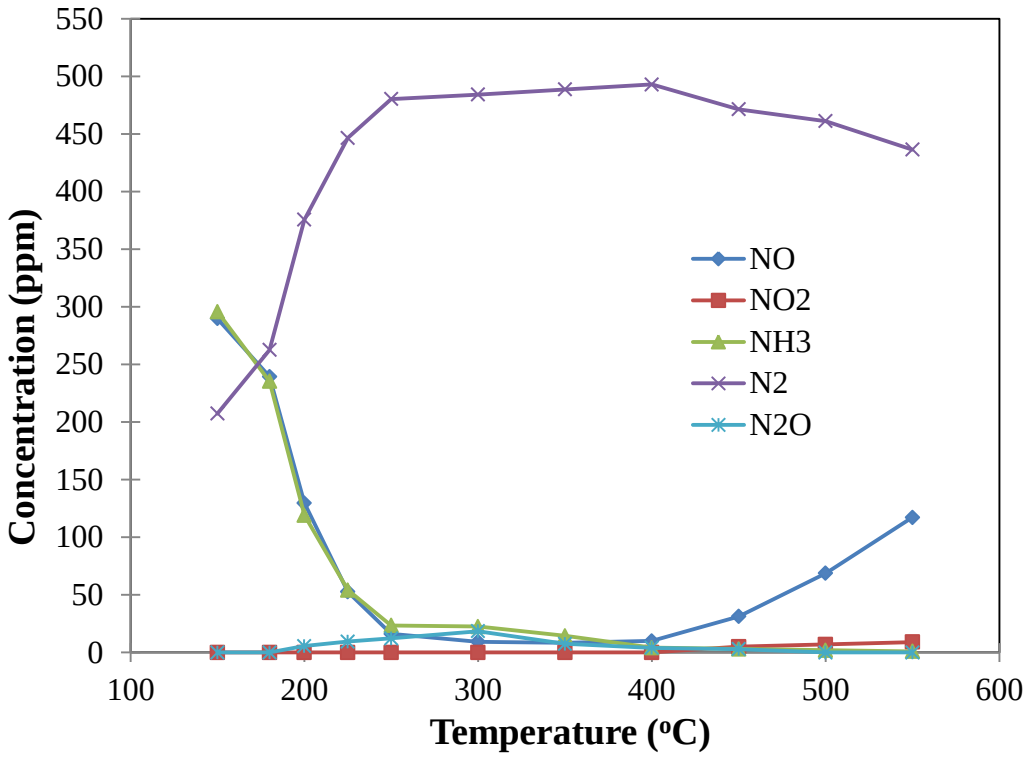

Figure 5-19: Steady state product distribution obtained for SCR of NOx with NH_3. Feed: 375 ppm NO, 125 ppm NO_2, 500 ppm NH_3, 5% O_2 and 2% H_2O.

For the next set of experiments, we increased the feed fraction of NO_2 by decreasing the feed NO. Specifically, we had equal amounts of NO and NO_2 in the feed. When the feed contains equal amounts of NO and NO_2, this is the so-called fast SCR reaction and is given by

$$2\ NH_3 + NO + NO_2 \rightarrow 2\ N_2 + 3\ H_2O \qquad \Delta H = -3.78 \times 10^5\ J/mol\ NH_3. \qquad (5\text{-}9)$$

In order to study the fast SCR reaction on the Cu-chabazite catalyst, we introduced a feed containing 250 ppm NO, 250 ppm NO_2, 500 ppm NH_3, 5% O_2 and 2% water on the catalyst surface. The product distribution obtained during this reaction is shown here in Figure 5-20. The reaction proceeded faster than the standard SCR reaction at lower temperatures and substantially lower concentrations of NOx ($NO+NO_2$) species were detected in the exit. Some N_2O was detected in the temperature range of 200-350 ^oC. At

lower temperatures (180-225 ^{o}C), the N-balance was not completely closed indicating the formation of NH_4NO_3 which cannot be detected either by FT-IR spectroscopy or mass-spectrometry. Our calculations predicted about 52 ppm and 17 ppm of ammonium nitrate formation at temperatures of 180 ^{o}C and 200 ^{o}C, respectively. The ammonium nitrate formation occurs by the following reaction:

$$2\ NH_3 + 2\ NO_2 \rightarrow N_2 + NH_4NO_3 + H_2O \qquad \Delta H = -\ 2.91 \times 10^5\ J/mol\ NH_3. \qquad (5\text{-}10)$$

This reaction mainly occurred at lower temperatures and hence the concentration of NO at the exit exceeded the NO_2 concentration for temperatures below 225 ^{o}C. This explains the occurrence of the ammonium nitrate formation side reaction which consumes both NO_2 and NH_3 leading to lower concentrations of these species than that expected by the fast SCR stoichiometry. In Chapter 4, we presented a systematic transient study to show the inhibition effect of NH_4NO_3 on the NOx reduction efficiency of the Fe-ZSM-5 catalyst. A similar inhibition effect was found here and is more important for the feeds containing excess NO_2. In the temperature range of 250-350 ^{o}C, near complete conversions of NOx and NH_3 were observed and we did not detect these species in the outlet. The NH_3 concentration was comparable to the total NOx concentration in the exit (for $T \leq 400$ ^{o}C) which shows the equimolar consumption of NOx and NH_3 in the fast SCR reaction. But at higher temperatures, the NOx concentration in the outlet started increasing which showed the onset of ammonia oxidation side reaction consuming the reductant NH_3 required for NOx reduction. We studied the fast SCR reaction in the absence of feed water and did not see any substantial difference in NOx conversion efficiency at lower temperatures (< 400 ^{o}C). But at higher temperatures, the absence of

feed water enhanced the ammonia oxidation side reaction and thus resulted in lower NOx removal efficiency as compared to that obtained in the presence of water.

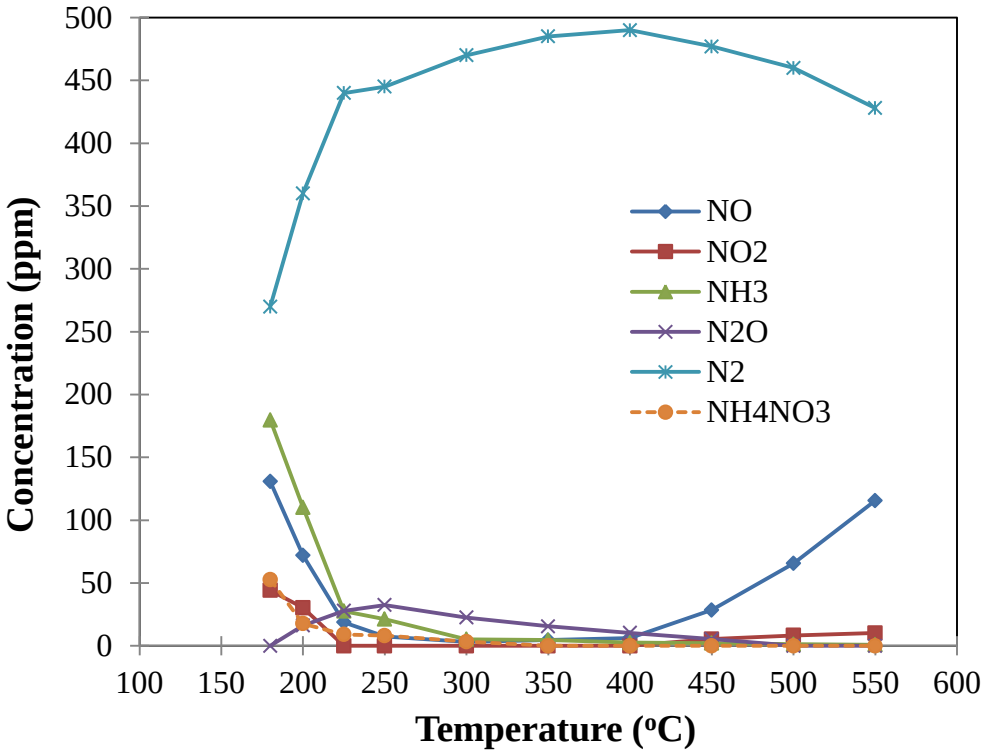

Figure 5-20: Steady state product distribution obtained during the fast SCR reaction studies. Feed: 250 ppm NO, 250 ppm NO_2, 500 ppm NH_3, 5% O_2 and 2% H_2O.

The effect of a higher fraction of NO_2 in the feed was examined. Figure 5-21 shows the results obtained with the Cu-chabazite catalyst for the feed containing a NO_2/NOx ratio of 0.75. Thus we used a feed containing 125 ppm NO, 375 ppm NO_2, 500 ppm NH_3, 5% O_2 and 2% water. About 35% of the total NOx was converted for temperatures between 180 – 200 ^oC. This activity was less compared to that of the fast SCR reaction system with equimolar mixtures of NO and NO_2 in the feed. Thus, the increasing amounts of NO_2 in the feed result in lower NOx conversions. At lower temperatures, the N-balance did not close completely, which suggests the formation of ammonium nitrate. Also, a substantial amount of N_2O was detected in the temperature

range of 200-400 ^{o}C. N_2O can be formed by the decomposition of ammonium nitrate at higher temperatures ($\geq$ 200 ^{o}C),

$NH_4NO_3 \rightarrow N_2O + 2\ H_2O$ $\Delta H = -\ 3.66 \times 10^4$ J/mol NH_4NO_3. (5-11)

The N_2O formation may also be explained by the overall reaction,

$4\ NH_3 + 4\ NO_2 + O_2 \rightarrow 4\ N_2O + 6\ H_2O$ $\Delta H = -\ 2.68 \times 10^5$ J/mol NH_3. (5-12)

At higher temperatures, N_2O disappeared completely. Also, the N-balance closed completely at higher temperatures suggesting that ammonium nitrate was consumed and N_2 was obtained as the only N-containing product of this reaction. NOx conversion activity increased substantially from 250 ^{o}C to 300 ^{o}C. About 97% of the inlet NOx was converted in the temperature range of 300-400 ^{o}C. But at higher temperatures, the NOx concentrations started increasing again which shows a decrease in the NOx conversion efficiency. Also, the NOx was observed mainly in the form of NO with negligible NO_2. This was because of the NO_2 decomposition (to NO) reaction at higher temperatures. Again, at higher temperatures the NH_3 consumption exceeded the NOx consumption due to the NH_3 oxidation side reaction and hence NH_3 was completely depleted.

The above reaction system was studied in the absence of 2% water to isolate its effect. The feed composition and the catalyst temperatures were kept the same as in the above case except that the 2% H_2O stream was not introduced. In the absence of water, higher NOx conversion activity was observed especially at lower temperatures where complete NOx got converted at 250 ^{o}C. At higher temperatures, there was not a very significant difference in the NOx removal efficiency in the presence and absence of water. Thus these results show that water inhibits the NOx reduction in the temperature range of 200-250 ^{o}C.

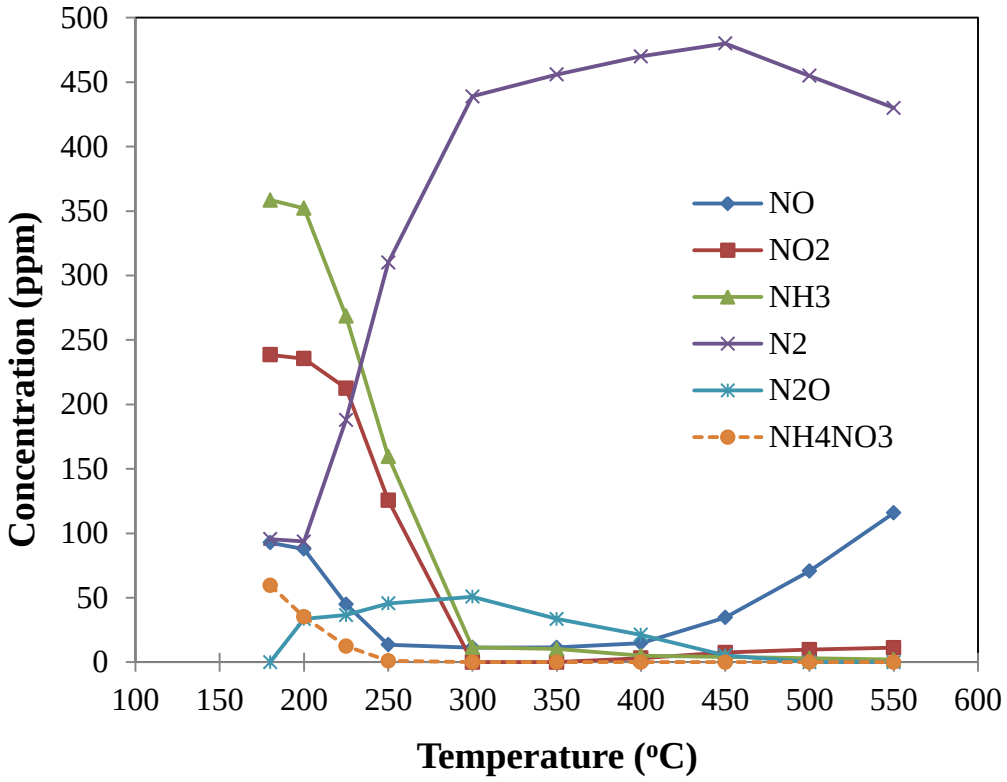

Figure 5-21: Steady state product distribution obtained during the NH_3 SCR reaction. Feed: 250 ppm NO, 375 ppm NO_2, 500 ppm NH_3, 5% O_2 and 2% H_2O.

A pure NO_2 feed (NO_2/NOx =1) is a special system in which the standard and fast SCR chemistries are essentially turned off, at least at temperatures below the decomposition of NO_2 (< 350 ^oC). The so-called "NO_2 SCR" reaction becomes the dominant chemistry under these conditions,

$$4\ NH_3 + 3\ NO_2 \rightarrow 3.5\ N_2 + 6\ H_2O \qquad \Delta H = -3.41 \times 10^5\ J/mol\ NH_3. \qquad (5\text{-}13)$$

Figure 5-22 shows the data for the exit concentrations of various species obtained as a function of temperature. The feed consisted of 500 ppm NO_2, 500 ppm NH_3, 5% O_2 and 2% water. Approximately 35% conversion of NO_2 was observed in the temperature range of 180-250 ^oC. N_2 was obtained as the main product detected by gas analyzers with a negligible amount of N_2O at 180 ^oC. The N_2O concentration in the outlet started increasing as a function of temperature and a substantial amount of N_2O was detected in

the temperature range of 200-400 ^{o}C. A Maximum N_2O concentration of 67 ppm was detected at 300 ^{o}C after which the N_2O, if formed, started decomposing to N_2 and hence the N_2O started disappearing.

$2\ N_2O \rightarrow N_2 + O_2$ $\Delta H = -\ 8.2 \times 10^4$ J/mol N_2O. (5-14)

The N-balance did not close in the temperature range of 180-250 ^{o}C (ca. 154 ppm was missing in the N-balance at 180 ^{o}C), once again indicating the formation of undetected ammonium nitrate. The N-balance inferred that about 77 ppm of NH_4NO_3 was formed at 180 ^{o}C. From the amounts of N_2 and NH_4NO_3 formed, reaction (5-10) was found to be the dominating reaction under these conditions. There was a significant increase in the NOx conversion efficiency going from 250 ^{o}C to 300 ^{o}C. About 96% of the fed NO_2 was converted at 300 ^{o}C. Also the N-balance closed for temperatures $\geq$ 300 ^{o}C. But at higher temperatures ($\geq$ 350 ^{o}C), the NOx removal efficiency again dropped because of the enhanced NH_3 oxidation side reaction. Along with NO_2, some NO started appearing at the exit at 400 ^{o}C. At higher temperatures, the concentration of NO in the outlet exceeded the NO_2 concentration as the NO_2 decomposition reaction became more dominant. The NOx conversions dropped below 90% for temperatures above 400 ^{o}C reaching about 74% at 550 ^{o}C.

The NO_2 SCR reaction was also carried out in the absence of water to isolate its effect. The product distribution (Figure 5-23) indicates a high NOx conversion efficiency in the temperature range of 225-300 ^{o}C unlike that obtained in the presence of feed water. Thus the presence of feed water inhibited the NO_2 SCR reaction and this inhibition was more pronounced in the temperature range of 200-300 ^{o}C. Similar inhibition on NOx reduction was observed for the earlier case of $NO_2/NOx = 0.75$. One possible reason for

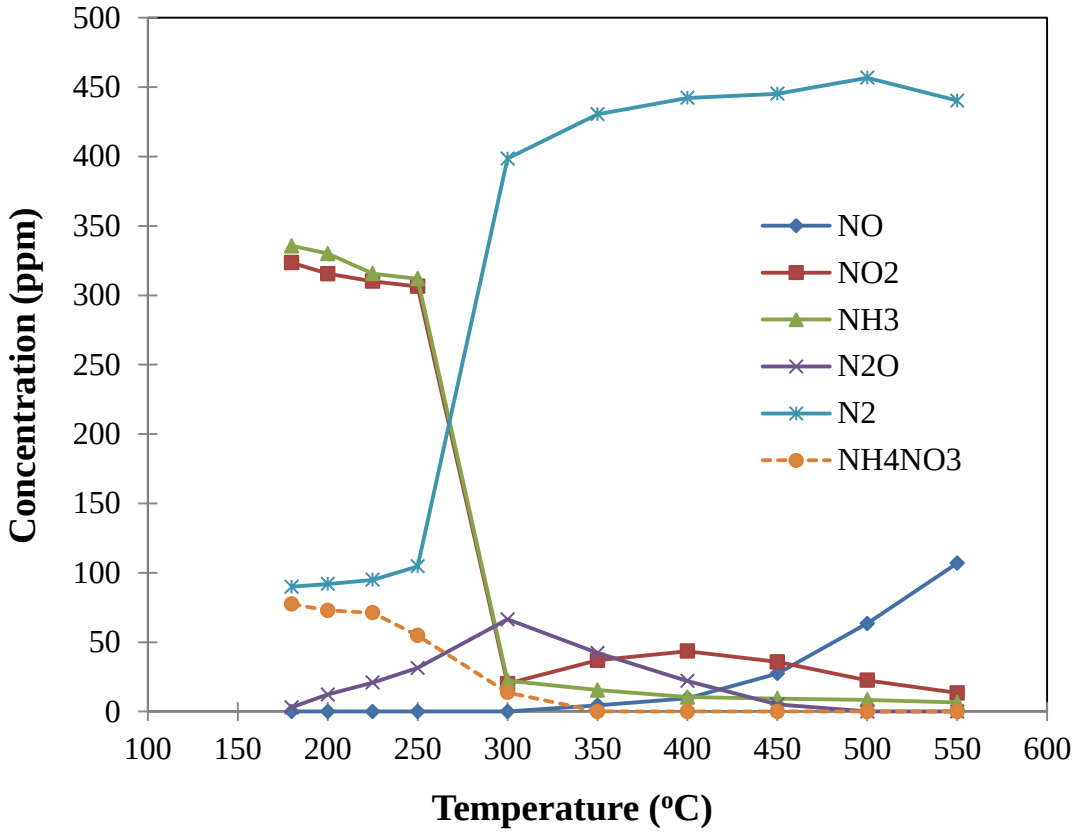

Figure 5-22: Steady state product distribution obtained during the NO_2 SCR reaction. Feed: 500 ppm NO_2, 500 ppm NH_3, 5% O_2 and 2% H_2O.

this result is that water blocks active sites required for NO_2 SCR. The amount of N_2O produced during the NO_2 SCR reaction studies carried out in the absence of water was much greater than that carried out in the presence of water. Here, the maximum amount of N_2O detected was around 135 ppm at 300 ^oC. Also, the N-balance did not close as observed earlier. But the estimated amount of NH_4NO_3 formed during this study was higher than that of the earlier study carried out in the presence of water. Thus, the presence of water reduces the formation of NH_4NO_3 and hence its decomposition to N_2O at later higher temperatures.

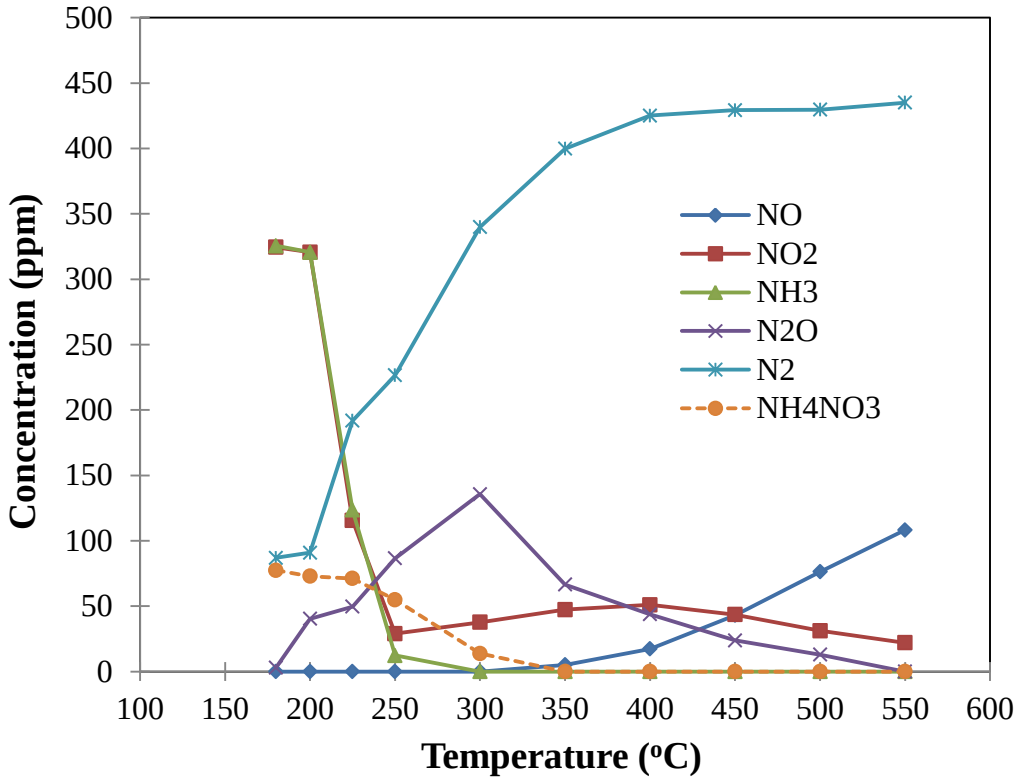

Figure 5-23: Steady state product distribution obtained during the NO_2 SCR reaction. Feed: 500 ppm NO_2, 500 ppm NH_3 and 5% O_2.

The above studies of SCR of NOx with NH_3 covered the effect of NO_2 on the product distribution and NOx conversion efficiency. This study shows that the presence of NO_2 in the feed plays a critical role in altering the NOx removal efficiency and N_2 selectivity as various byproducts (like N_2O, ammonium nitrate) are formed. Also, the overall SCR chemistry becomes complicated in the presence of NO_2 where several side reactions take place. Figure 5-24 shows the effluent concentration of N_2O obtained over the temperature range of 180-550 ^oC on the Cu-chabazite catalyst for several NO_2/NOx feed ratios, both in the presence and absence of water. Solid lines indicate the data in the absence of water while the dashed lines indicate the data in the presence of water. In the presence of water, negligible amount (< 30 ppm) of N_2O was detected up to NO_2/NOx = 0.5; i.e., standard and fast SCR reaction conditions. For higher NO_2/NOx feed ratios (>

0.5), the N_2O increased significantly. For the feeds containing NO_2/NOx inlet ratios of 0.75 and 1, a maximum N_2O was detected at about 300 ^oC.

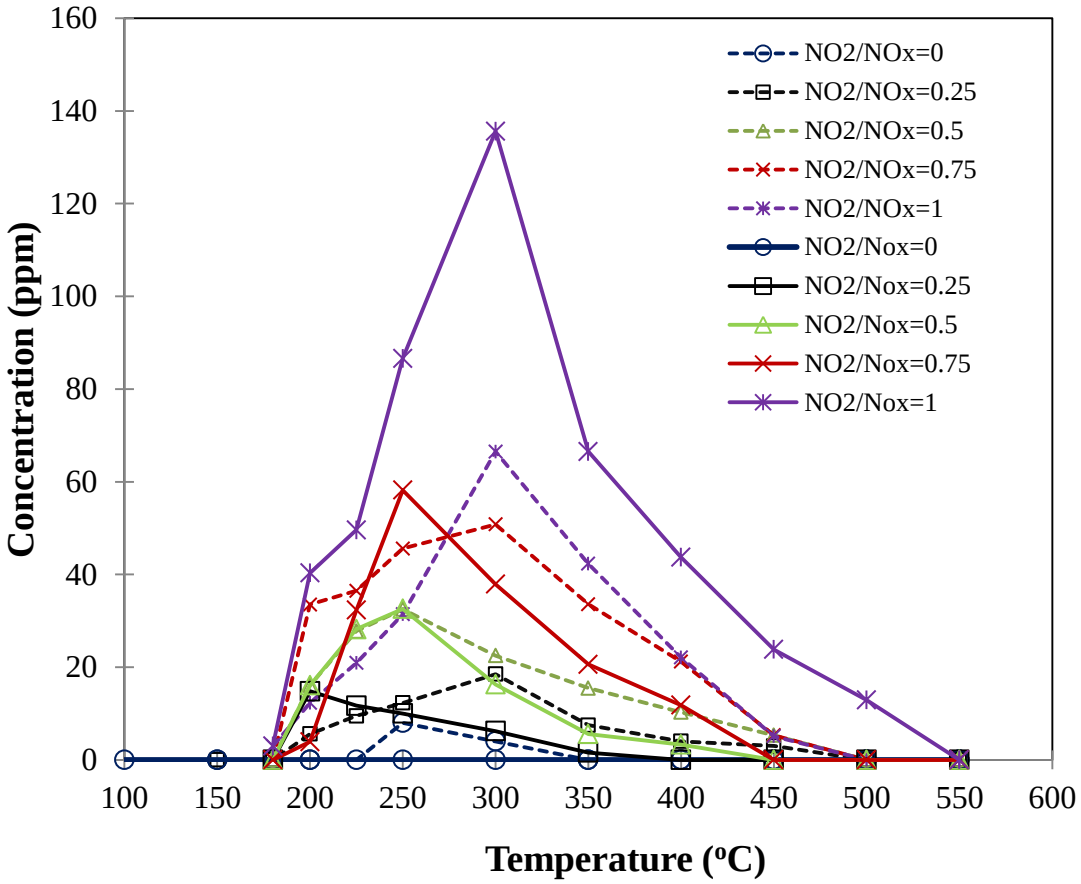

Figure 5-24: Steady state concentration of N_2O obtained as a function of temperature for various inlet ratios of NO_2/NOx.

The N_2O concentration decreased at higher temperatures and this decrease is caused mainly by:

1) the rates of the N_2 selective reactions, i.e., NO_2 SCR, fast SCR and standard SCR increase at higher temperatures, and as a result the side reactions responsible for N_2O production decrease,

2) the N_2O itself decomposes to N_2 by reaction (5-14) and hence its effluent concentration decreases at higher temperatures.

Devadas et al. [29] observed that N_2O decomposes to N_2 and O_2 starting at 350 ^oC on Fe-ZSM-5 catalyst. Another possibility for N_2O consumption is reaction with NH_3 (reaction (5-15)),

$$2\ NH_3 + 3\ N_2O \rightarrow 4\ N_2 + 3\ H_2O \qquad \Delta H = -\ 4.4 \times 10^5\ J/mol\ N_2O. \qquad (5\text{-}15)$$

Similar trends for N_2O production on other catalysts were reported in the literature [29, 39, 63, 118].

In results reported so far for the steady state NOx reduction studies, it is clear that the NO_2/NOx ratio is a critical parameter. The ratio has important effects on both the overall NOx conversion and the product distribution. The effect of NO_2/NOx ratio and temperature on the overall NOx conversion is shown in Figure 5-25.

The conversion data (Figure 5-25) show that the NOx conversion efficiency increased as a function of increasing NO_2/NOx feed ratio till 0.5. At higher feed NO_2 concentrations, NOx removal efficiency decreased significantly. This decrease in the NOx removal efficiency was more pronounced for temperatures up to 250 ^oC. This decreasing trend in the NOx conversion activity at temperatures below 250 ^oC is mainly attributed to the formation of ammonium nitrate on the catalyst surface which blocks the active sites for NOx reduction. Thus 0.5 can be considered as an ideal feed ratio to obtain a very high NOx removal efficiency in the SCR unit. Even though having equimolar amounts of NO_2 and NO increased the NOx removal efficiency, this increase was significant only for temperatures up to 225 ^oC. At higher temperatures ($\geq$ 250 ^oC), both the standard and fast SCR reactions gave very similar deNOx efficiencies. In the absence of feed water (as discussed earlier), we did not see a significant difference in the deNOx efficiencies at temperatures below 400 ^oC for the NO_2/NOx feed ratio of $\leq$ 0.5. But at

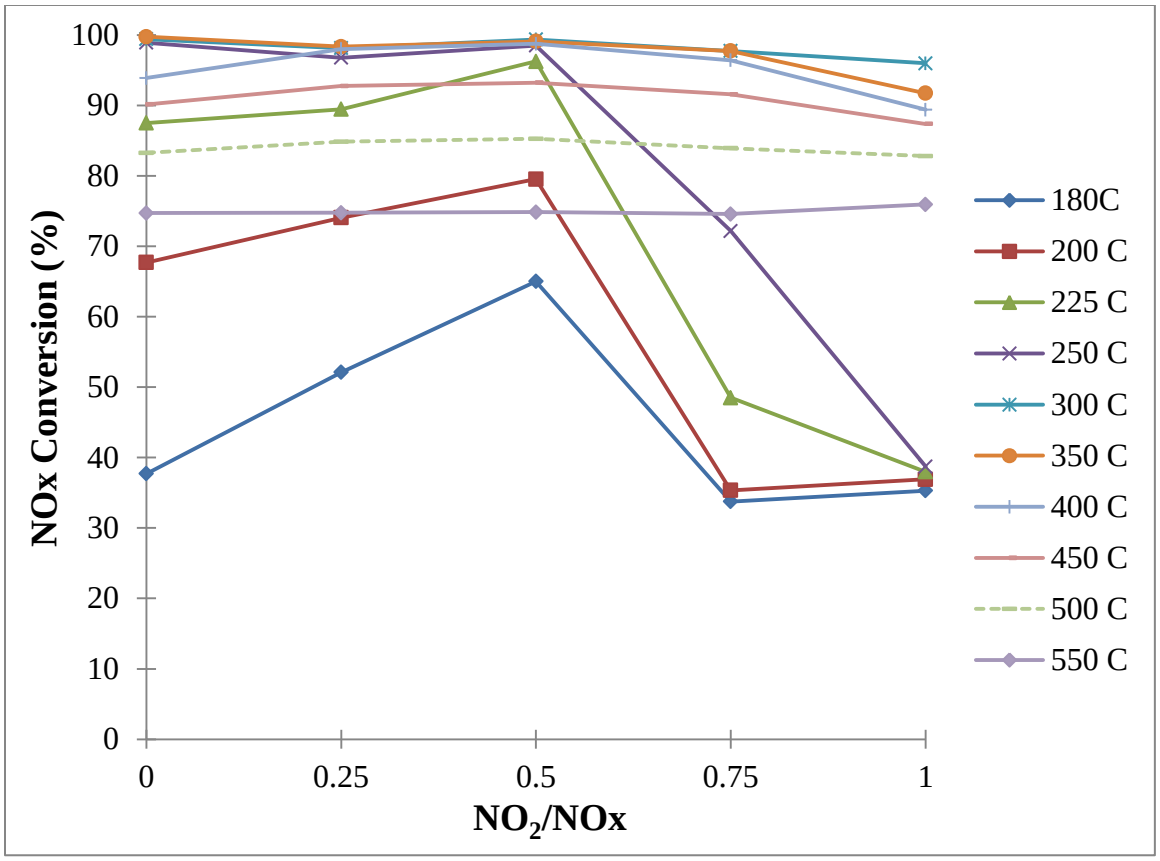

Figure 5-25: Effect of various NO_2/NOx inlet feed ratios and catalyst temperatures on the NOx conversion.

higher temperatures, the presence of water had a positive effect on increasing the overall NOx removal efficiency as the presence of water suppressed the NH_3 oxidation side reaction. For the feeds containing excess NO_2 (NO_2/NOx > 0.50), the presence of feed water inhibited the NOx reduction reaction and thus decreased the NOx removal efficiency up to 250 ^oC. Thus the above data show that the optimum NO_2/NOx ratio for maximum NOx reduction is to 0.5 (fast SCR reaction) for the wet feeds. This is in line with that observed for the Fe-ZSM-5 catalyst as discussed earlier in Chapter 4. But for the Fe-ZSM-5 catalyst, there was a significant enhancement in the NOx reduction efficiency over the entire temperature range when the feed contained equimolar amounts of NO and NO_2. For the Cu-chabazite catalyst, the enhancement in the NOx reduction

efficiency (in the presence of feed NO_2) was observed only for temperatures below 250 ^oC and it was not very significant. This shows that the NOx removal performance of the Cu-chabazite catalyst is not very sensitive to the feed NO_2 concentrations and it can give very high deNOx removal efficiency even in the absence of feed NO_2 [29, 39].

One important goal in the SCR system is to selectively reduce the maximum amount of NOx to N_2. Thus, along with deNOx efficiency, it is important to achieve a maximum selectivity towards N_2 and the formation of byproducts should be at a minimum. Figure 5-26 shows the effects of NO_2/NOx ratios and temperature on the N_2 productivity and selectivity. From Figure 5-26, it is clear that, at 180 ^oC, the maximum amount of N_2 was obtained with the feeds containing equimolar amounts of NO and NO_2. But for all the temperatures above 180 ^oC, the maximum selectivity (or concentration) of N_2 was obtained for feeds containing NO_2/NOx ratio $\leq$ 0.25. Also, the NOx removal efficiencies, obtained with the feeds do not containing NO_2 (NO_2/NOx = 0), were significantly different only for temperatures below 200 ^oC. Thus the above analysis indicates that the Cu-chabazite catalyst is not very sensitive to the amount of NO_2 present in the feed. This catalyst can give very high NOx removal efficiencies even for feeds without NO_2 (standard SCR) or with small amounts of NO_2 (NO_2/NOx $\leq$ 0.25). Considering the selectivity towards N_2 and formation of byproducts, feeds without NO_2 give optimal NOx removal performance.

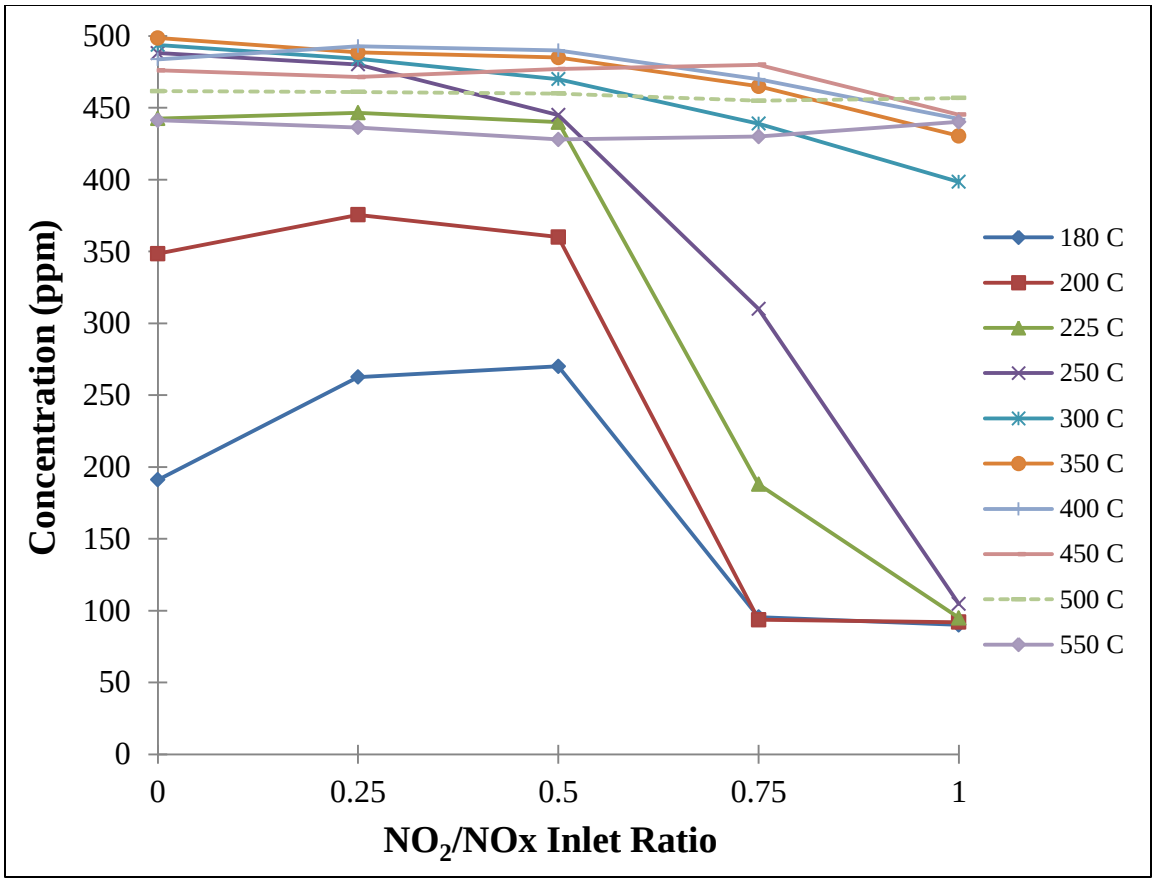

Figure 5-26: Effect of various NO_2/NOx inlet feed ratios and catalyst temperatures on the N_2 formation during NH_3 SCR reactions.

5.3.8 Standard SCR: Transient Experiments

Transient experiments were also carried out on the SCR catalyst to understand the SCR chemistry under the more realistic conditions encountered in a vehicle [134, 135]. In these experiments Ar was used as the gas carrier and NO was fed in the presence of 5% O_2 under isothermal conditions. In contrast to the steady state experiments, NH_3 was pre-adsorbed on the catalyst for 60 minutes and then the NO was fed as a step change from 0 to 500 ppm. These experiments were carried out over a broad range of temperatures (150 – 400 ^oC). The catalyst used for these experiments was the same Cu-chabazite as was discussed earlier. The experimental conditions (e.g., space velocity, catalyst dimensions, etc.) were the same as in the steady state experiments. The pretreatment method used for

the transient experiments was the same as that of the steady state experiments where the catalyst was conditioned by heating it for 30 minutes at 500 °C in 5% O_2, in order to oxidize the surface and remove any NH_3 or other species present on the catalyst. In contrast to the steady state experiments, the catalyst surface was initially saturated with that of NH_3 by continuously feeding 500 ppm NH_3 for 3600s. After that, only Ar was flowed through the reactor for 1800 s, to release loosely-bound NH_3 from the catalyst (i.e., the intention was to study only the chemisorbed NH_3 present in the sample that reacted with the NOx). Once most of the weakly bound NH_3 was released, 500 ppm of NOx and 5% O_2 were fed to the reactor at constant feed temperature. The above mentioned SCR reactions were studied at various temperatures; 150 ºC, 200 ºC, 250 ºC, 300 ºC, 350 ºC, 400 ºC and 450 ºC, and with three different NO/NO_2 feed ratios; 1/0, 1/1, and 0/1. Experimental results are presented below.

5.3.8.1 NO Feed (NO/NO_2 = 1/0)

Figure 5-27 shows the results obtained for the lowest temperature experiment (150 ºC). As described above, after the feed NH_3 was removed, we waited for 30 minutes after which 500 ppm NO and 5% O_2 were introduced. The reaction proceeded immediately once the NO was added, and a significant increase in N_2 occurred. The N_2 concentration reached a peak value of about 200 ppm and stayed constant for a while for about 100 s, after which it started decreasing. After about 2600 s, the N_2 disappeared completely at the exit. Also, the NO concentration reached close to its inlet value of 500 ppm after the N_2 concentration reached 0. We observed a very small amount of NO_2 (about 10 ppm) produced during these reaction conditions. The NO_2 was observed only after the N_2 concentration reached 0 ppm, that is, after all the stored NH_3 on the catalyst

surface was completely consumed. NO_2 was produced because of the NO oxidation side reaction. This is consistent with the results discussed earlier for the NO oxidation reaction system where we recorded negligible NO oxidation (< 2%) reaction at 150 ^{o}C. We did not see any N_2O during the entire reaction.

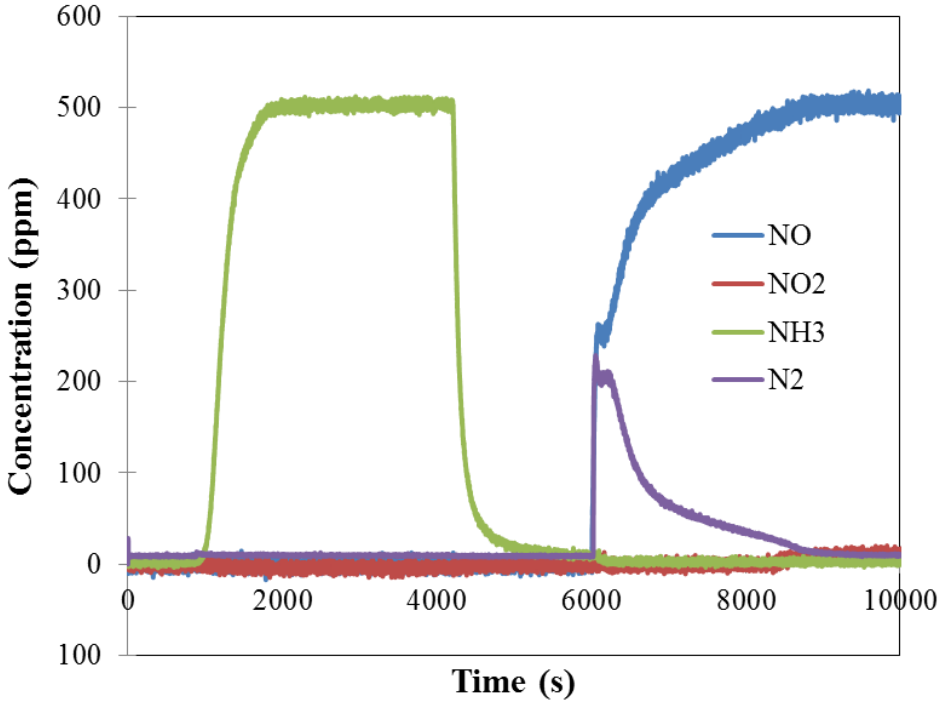

Figure 5-27: Transient experimental findings of standard SCR reaction on commercial Cu-chabazite catalyst at 150 ^{o}C.

The same procedure was repeated at the other temperatures. The results are grouped according to the different species studied (i.e., N_2, NO, and NO_2) and are presented in Figures 5-28 – 5-30. At 200 ^{o}C, the N_2 concentration showed a very similar behavior like that at 150 ^{o}C. The peak N_2 concentration reached around 366 ppm. The reaction rate was fast at this temperature and all the NH_3 was consumed within 1200 s and the N_2 concentration dropped down to 0 ppm at 7200 s. At later temperatures, the N_2 peak started becoming narrower indicating the fast consumption of stored NH_3 because of the high reaction rates at higher temperatures and as well as the decreasing storage

capacity of NH_3 at higher temperatures. Figure 5-31 shows the concentration profiles for NH_3 during its uptake for various temperatures (150-450 ^oC). As expected, the breakthrough was obtained late for the lower temperature of 150 ^oC. The time required for NH_3 breakthrough decreased at higher temperatures and thus shifted the NH_3 uptake profiles to the left. These data help in understanding the decreasing NH_3 storage capacity as a function of temperature. The peak value for N_2 (Figure 5-28) was about 400 ppm and 425 ppm for the temperatures of 300 ^oC and 350 ^oC, respectively. At higher temperatures, this value further increased to 564 ppm at 400 ^oC and 790 ppm at 450 ^oC. The NO concentration presented a similar trend at the higher temperatures, showing an immediate increase in NO concentration which reached a stationary concentration value immediately. Except at 150 ^oC, the steady state concentrations of NO and NO_2 were achieved very fast. Here we show the NO_2 concentrations profiles (Figure 5-30) for these experimental conditions. It can be seen that, substantially high amounts of NO_2 were detected after the NH_3 present on the catalyst surface was completely utilized. The amount of NO_2 observed in the outlet was consistent with that obtained during the steady state NO oxidation reactions studied separately. Also, NO_2 was recorded only after the N_2 concentration dropped to 0 ppm. These data are consistent with the steady state integral data reported earlier which showed no measureable NO_2 in the outlet during the standard SCR reaction. We did not see any N_2O formation during this transient study over the entire temperature range. Hence the data for N_2O production are not reported here.

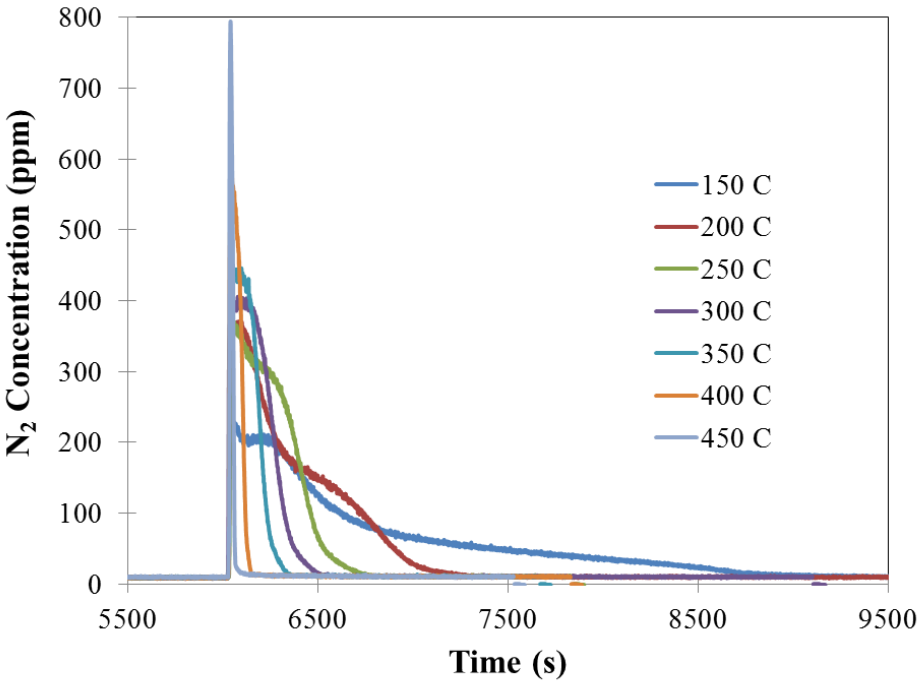

Figure 5-28: Measured N_2 concentrations during transient experiments (NO/NO_2=1/0).

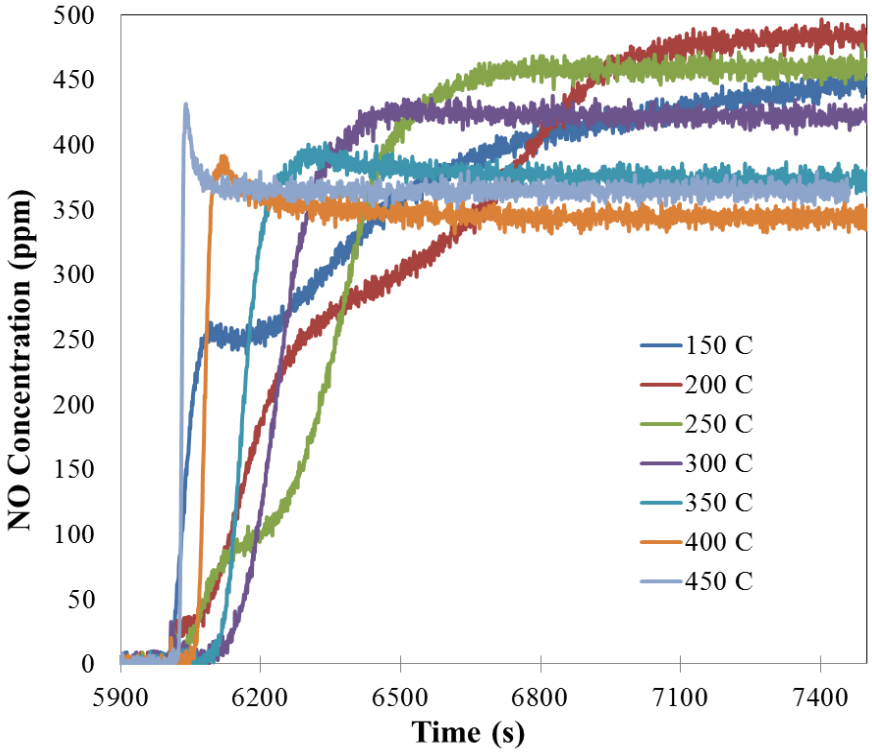

Figure 5-29: Measured NO concentrations during transient experiments (NO/NO_2=1/0).

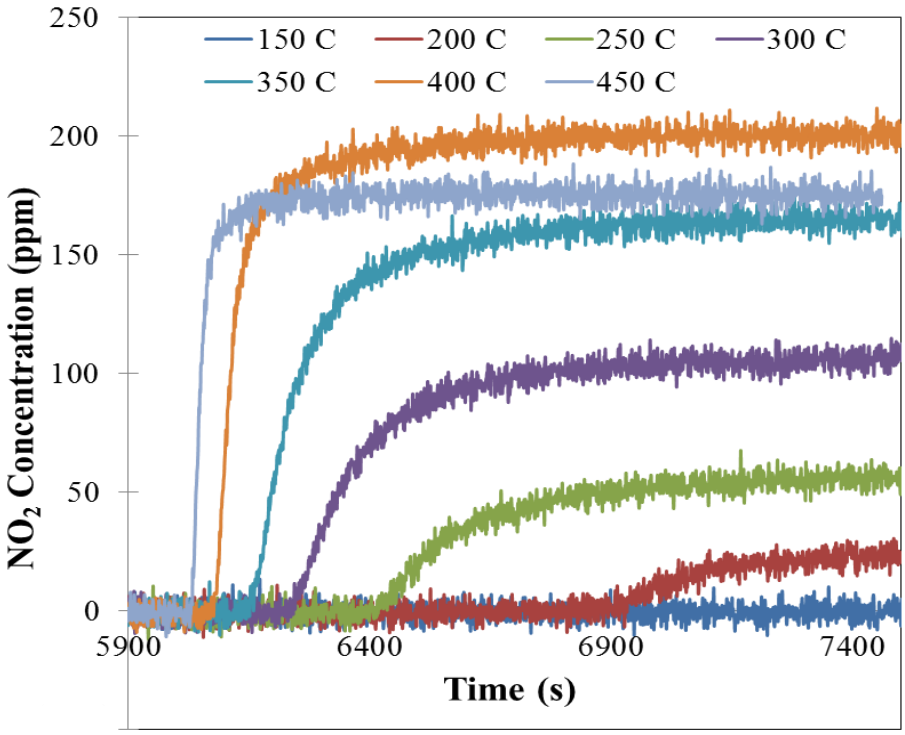

Figure 5-30: Measured NO_2 concentrations during transient experiments (NO/NO_2=1/0).

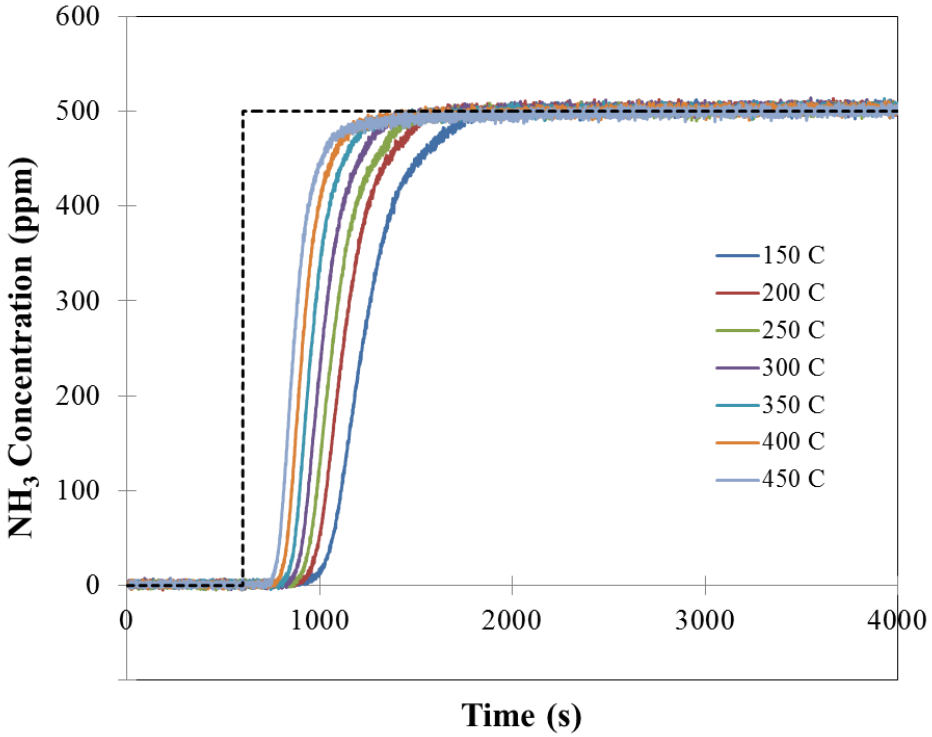

Figure 5-31: Measured NH_3 concentrations during transient experiments (NO/NO_2=1/0).

5.3.8.2 Equimolar Feed (NO/NO_2 = 1/1)

The same procedure was followed for an equimolar mixture of NO/NO_2 (250 ppm each) after the initial NH_3 uptake. This system represents the fast SCR reaction under transient conditions. The presence of NO_2 in the feed enhanced the rates of consumption of pre-adsorbed NH_3 compared to that for the NO only feeds. This effect was found to be more pronounced at lower temperatures (below 200 ^oC). The peak value of N_2 was around 300 ppm for 150 ^oC. This value increased slightly as a function of temperature but was found to be around 350-400 ppm for most of the temperatures in the range of 200-350 ^oC. Also, the N_2 peak became narrower as a function of temperature. At 400 ^oC, this value reached around 573 ppm. N_2O was not detected for the entire temperature range. Figures 5-32 – 5-34 show the trends obtained for N_2, NO and NO_2. The amount of N_2 formed during these conditions for different temperatures ($\geq$ 200 ^oC) was about the same

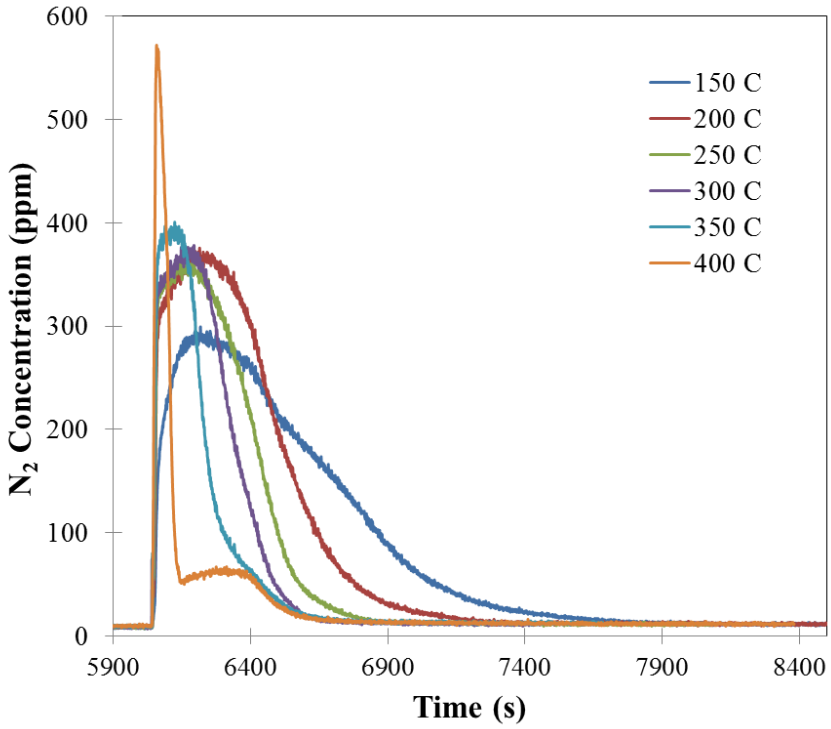

Figure 5-32: Measured N_2 concentrations during transient experiments (NO/NO_2=1/1).

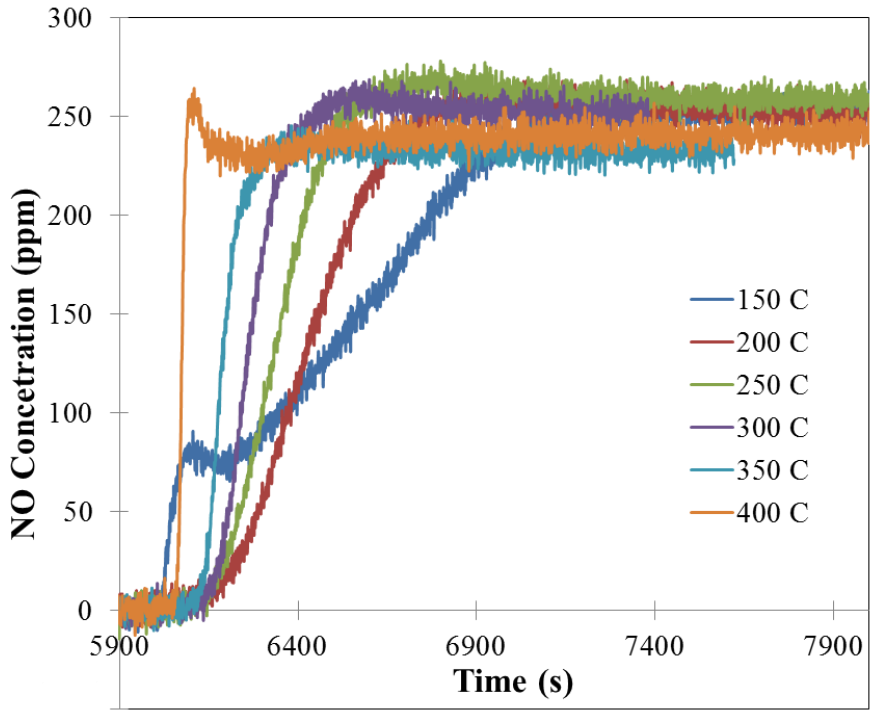

Figure 5-33: Measured NO concentrations during transient experiments (NO/NO_2=1/1).

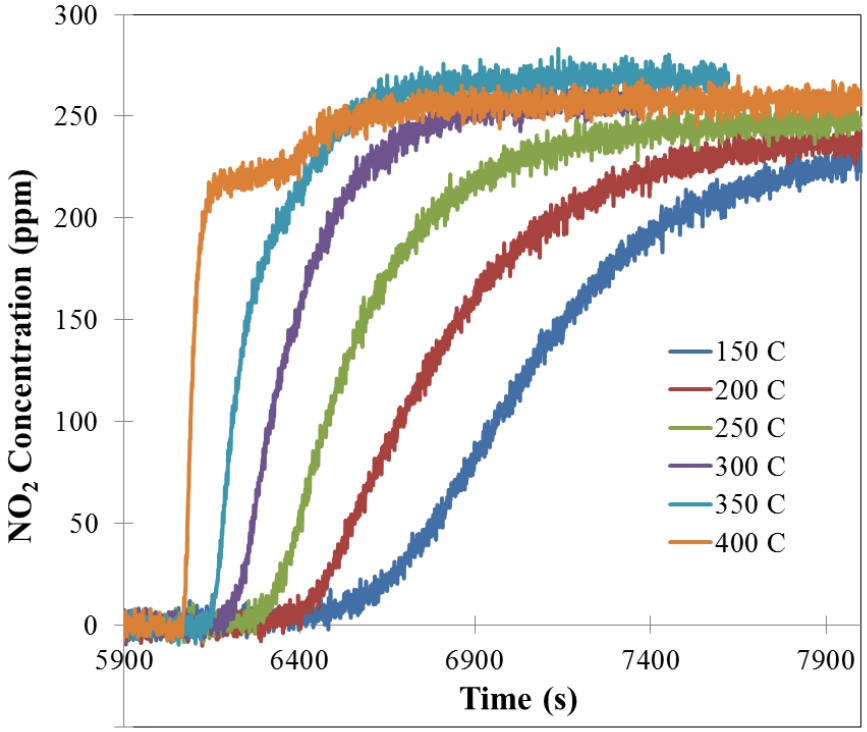

Figure 5-34: Measured NO_2 concentrations during transient experiments (NO/NO_2=1/1).

as that for the earlier case with NO only feed. Also, the reaction time was nearly the same for both the standard and fast SCR reaction at temperatures $\geq$ 200 ^{o}C. This is observed by the time required for the N_2 concentration to drop down to 0 ppm.

5.3.8.3 NO_2 Feed (NO/NO_2 = 0/1)

In this set of experiments, a gas containing 500 ppm of NO_2 and 5% of O_2 (balance Ar) was fed to the catalyst after pre-adsorbing 500 ppm of NH_3. This system presents the NO_2 SCR reaction studies under transient conditions. The concentration profiles for N_2, NO and NO_2 are shown in Figures 5-35 – 5-37. The N_2 concentration profile was very similar at both the 150 and 200 ^{o}C temperatures. When a feed containing NO_2 and O_2 was introduced to the catalyst surface pre-saturated with NH_3, a N_2O peak was also detected along with that of N_2 peak. The peak for N_2O was missing in the experiments discussed earlier for the feed containing 0-250 ppm NO_2.

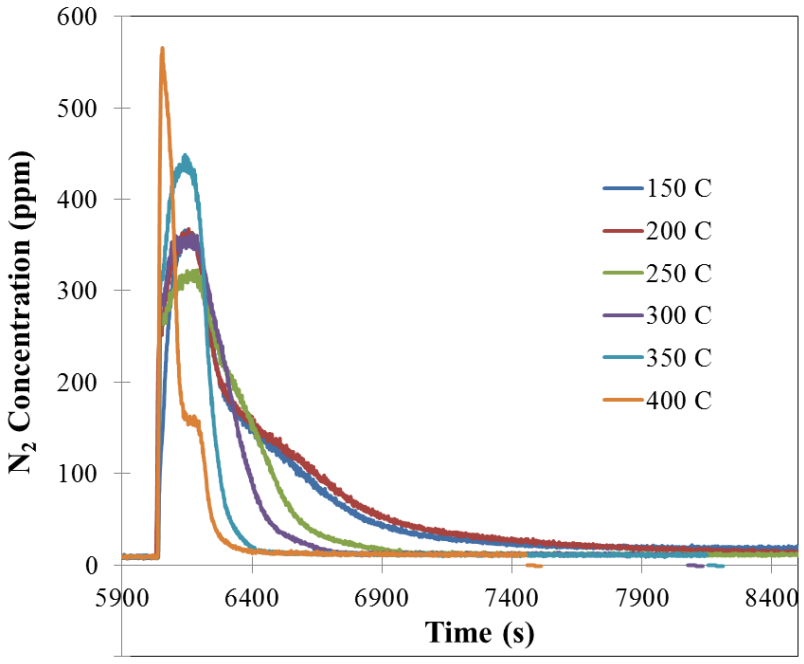

Figure 5-35: Measured N_2 concentrations during transient experiments (NO/NO_2=0/1).

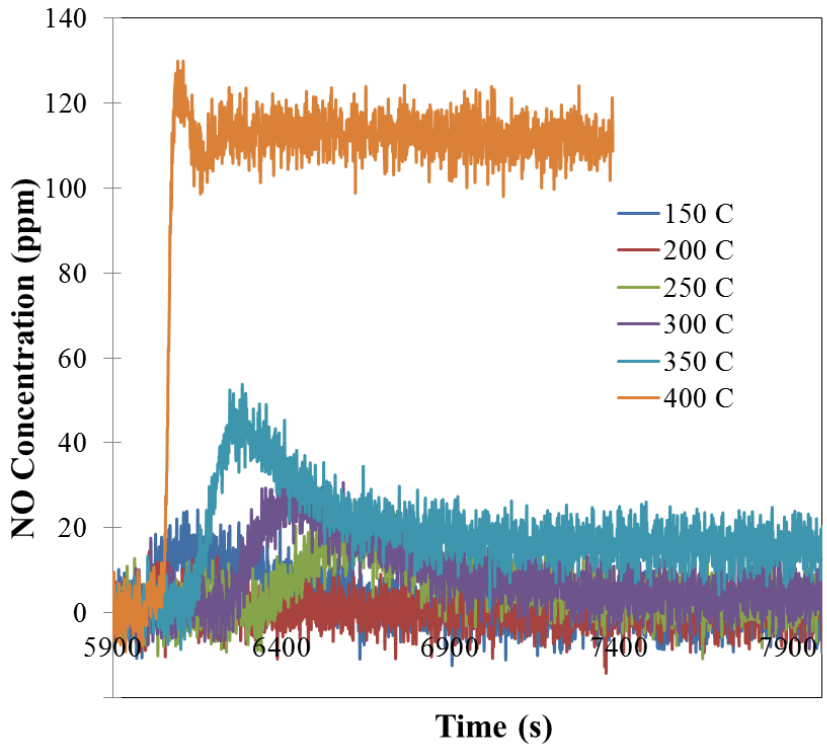

Figure 5-36: Measured NO concentrations during transient experiments (NO/NO_2=0/1).

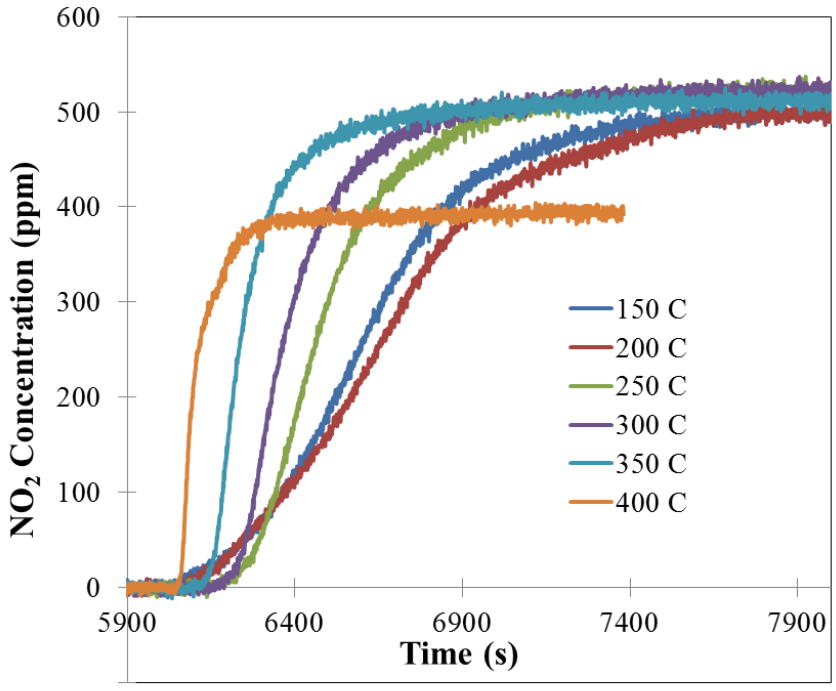

Figure 5-37: Measured NO_2 concentrations during transient experiments (NO/NO_2=0/1).

Also, the peak of N_2O was visible for the temperature range of 200-350 ^oC. At 400 ^oC, negligible N_2O was observed in the exit. The maximum amount of N_2O was detected in the temperature range of 250-300 ^oC in line with the steady state results. In the inlet feed, NO was not present. But NO appeared in the effluent for T > 300 ^oC due to the decomposition of NO_2.

Similar kinds of transient experiments were carried out and reported earlier for the Fe-ZSM-5 catalyst in Chapter 4. These results showed the difference in the SCR chemistry for the standard and fast SCR reaction systems on Fe-ZSM-5 catalyst where the rate of fast SCR reaction was found to be significantly greater than that of the standard SCR reaction. Here for the Cu-chabazite catalyst, the rate of fast SCR reaction was found to be significantly different only for lower temperatures (< 200 ^oC). But at later temperatures, the standard SCR reaction occurred at rates comparable to that of the fast SCR reaction. This is confirmed from the time required for the complete consumption of NH_3 adsorbed on the catalyst surface. Moreover, no other byproducts were formed for the standard and fast SCR reactions studied under transient conditions. Also, the amount of N_2 formed was found to be comparable for the standard and fast SCR cases. For the NO_2 SCR reaction, we detected the formation of byproducts like N_2O in the temperature range of 200-350 ^oC. Also, the amount of N_2 formed during the NO_2 SCR reaction was found to be less compared to the earlier two cases. These results are in qualitative agreement with our previous results for the steady state experiments and show that the Cu-chabazite is insensitive to the amount of NO_2 present in the feed, especially up to equimolar feeds of NO and NO_2. When excess NO_2 was present in the feed, it leads to the formation of byproducts like N_2O (and ammonium nitrate). Thus, the Cu-chabazite

catalyst can do a significant job of very high NOx reduction even with feeds do not containing NO_2.

5.4 Conclusions

We carried out a comprehensive experimental study of various reactions involved in the selective catalytic reduction of NOx with NH_3 on the commercial Cu-chabazite catalysts. A systematic study was performed to understand the reaction systems of NO oxidation, NH_3 oxidation, standard SCR ($NO + NH_3 + O_2$), fast SCR ($NO + NO_2 + NH_3$) and NO_2 SCR reactions. The experimental study involved both steady state and transient experiments aimed at understanding the kinetics and mechanistic aspects of these reactions on the Cu-chabazite catalyst. This study provides a comparison between Fe-ZSM-5 (discussed earlier in Chapters 3 and 4) and Cu-chabazite catalysts for the SCR of NOx with NH_3.

NH_3 TPD experiments showed that the Cu-chabazite catalyst has a strong affinity to adsorb NH_3. The adsorption capacity of NH_3 was found to be significantly higher than the Fe-ZSM-5 catalyst under identical experimental conditions. Cu-chabazite was found to adsorb negligible amount of NO at temperatures as low as 150 ^oC. But the catalyst adsorbs significant amounts of NO_2 some of which is stored in the form of nitrates. The catalyst has a strong NH_3 oxidation activity where complete NH_3 conversions were achieved at temperatures of 400-450 ^oC. The catalyst oxidizes significant amount of NO to NO_2 by NO oxidation reaction and NO_2 is decomposed at higher temperatures back to NO by the reverse NO oxidation reaction. Both NO and NH_3 oxidation reactions are inhibited by water and the inhibition was found to be more severe for the NO oxidation.

Standard SCR reaction carried out under steady state conditions showed a very high NOx reduction activity in the temperature range of 200-400 ^{o}C. At higher temperatures, the NOx reduction efficiency decreased because of the NH_3 oxidation side reaction. Presence of water did not have a significant effect on the NOx reduction efficiency at lower temperatures ($\leq$ 300 ^{o}C) but it significantly improved the NOx conversions at higher temperatures by suppressing the NH_3 oxidation side reaction. Presence of excess feed NH_3 inhibited the standard SCR reaction under both the steady state and transient conditions.

Differential kinetics derived under standard SCR reaction conditions showed that the reaction was nearly first order with respect to NO, positive (+0.52 to +0.59) order with respect to O_2 and negative (-0.20 to -0.23) order with respect to ammonia. Differential kinetics studies for the NO oxidation reaction showed close resemblance with that for the standard SCR reaction considering the activation energies and the reaction orders with respect to NO and O_2. This shows that the NO oxidation could be the rate determining step in the standard SCR reaction chemistry. This observation is in agreement with our earlier studies on the Fe-ZSM-5 catalyst and hence shows that both the catalyst follow similar mechanism.

This study covers the effect of inlet NO_2 concentrations on the NOx conversion during the SCR reaction both in the presence and absence of water. NO_2 was found to have a promoting effect on the SCR reaction at temperatures $\leq$ 180 ^{o}C. But at later temperatures ($\geq$ 200 ^{o}C), very similar deNOx efficiency was observed for feeds containing $NO_2/NOx \leq 0.5$. Thus the Cu-chabazite catalyst was found to be insensitive to the amount of NO_2 present ($NO_2/NOx \leq 0.5$). Considering the selectivity and NOx

reduction efficiency, NO_2/NOx ratio of 0.5 does not necessarily represent the ideal ratio for SCR operation on the Cu-chabazite catalyst unlike that on Fe-ZSM-5 (Chapter 4) and vanadium based catalysts reported in the literature. Feeds containing excess NO_2 lead to a formation of byproducts like ammonium nitrate and N_2O. Also, the NOx removal efficiency and selectivity towards N_2 decreased for feeds with excess NO_2. Water was found to have negligible role in the SCR chemistry at lower temperatures for NO_2/NOx ratio of $\leq$ 0.5. But the presence of water inhibited the NOx reduction capacity for the feeds containing excess NO_2 (NO_2/NOx > 0.5) in the temperature range of 180-250 ^oC. At higher temperatures, water favors the NOx SCR reactions by suppressing the NH_3 oxidation side reactions for all the cases.

The steady state results are supported by the transient experimental study where NOx feeds containing varied NO/NO_2 ratios were fed to the catalyst surface presaturated with NH_3. For both the standard and fast SCR reaction, we observed very similar rates for temperatures $\geq$ 200 ^oC. Also, the amount and the selectivity of N_2 was nearly the same for both of these reactions. For the feeds containing only NO_2, N_2O was observed as a byproduct.

CHAPTER 6 Mass Transfer Limitations in Fe- and Cu-Zeolite based NH_3-SCR Monolithic Catalysts

6.1 Introduction

Selective catalytic reduction (SCR) of NOx with NH_3 generated from onboard thermal decomposition of urea has gained considerable attention in the last few years and has proven to be an effective catalytic process for NOx reduction. As discussed in earlier chapters, various catalysts have been studied and researched for the ammonia-based SCR technique [29, 37-39, 42, 44, 50, 57, 63, 67, 89, 116, 155]. The overall chemistry of various SCR reactions on these catalysts (vanadia-based catalysts, Fe- and Cu-zeolites) is well established in the literature and it has been covered in Chapter-2. Very fewer studies focus on the predictive kinetic and reactor models for NH_3-SCR reactions on zeolite-based catalysts. Moreover, the extent of mass transfer limitations has yet to be resolved. The current study is focused on the understanding mass transfer limitations in Fe- and Cu-zeolite based NH_3-SCR monolithic catalysts.

In the past several years, many literature studies have focused on the performance of the emerging Cu- and Fe-based zeolite catalysts. The data from these studies have been used in the development of kinetic models for SCR reactions [78, 117]. However, in order to develop an intrinsic kinetic model, it is prudent to measure rates in a pure kinetic regime so that the impacts of external and internal mass transfer limitations on the observed kinetics are negligible. By now, the importance of mass transfer processes occurring in monolithic reactions is well understood [191, 192]. Washcoat diffusion limitations (known more generally as internal mass transfer limitations) are known to play a key role and can be rate limiting in various washcoated monolithic catalytic

reactions [150, 193]. However, washcoat diffusion along with external mass transfer have been either ignored or ruled out in the development of the existing kinetic models for SCR catalysts. Indeed, few SCR studies are available which describe the existence of diffusion limitations. In our recent study in Chapter 3 and [103], we showed the existence of washcoat diffusion limitations for the standard SCR reaction catalyzed by Fe-zeolite at higher temperatures ($\geq$ 350 ^{o}C). Olsson et al. [117] studied the standard SCR reaction on Cu-zeolite and reported NO conversion of more than 95% at temperatures of as low as 200 ^{o}C. They used catalysts with different washcoat loadings to investigate the presence of washcoat diffusion limitations. However, with very high conversions (~100%) of NO at temperatures above 300 ^{o}C, the presence of diffusion limitations was inconclusive and thus diffusional gradients were not included in their kinetic model. A recent study by Nova et al. [23] indicated the presence of mass transfer limitations for Cu-zeolite catalysts. They used monolith catalysts having different cell densities (200, 400 and 600 cpsi) but the same washcoat loadings. The NH_3 conversion was found to have a substantial difference between the 200 cpsi and 400 cpsi catalysts. The difference was negligible when comparing the 400 and 600 cpsi catalysts. The authors attributed the differences to mass transfer limitations for the SCR reaction on Cu-zeolite catalysts. Chatterjee et al. [78] found comparable NOx reduction activity on crushed monolith (zeolite) powder and washcoated zeolite catalysts while studying the standard SCR reaction. Thus they neglected the interphase and intraphase diffusion limitations in their model. Collectively, these studies convey some uncertainty of the extent of mass transfer limitations in the SCR reaction system.

Therefore, the objective of the current study is to investigate the extent of internal and external mass transfer limitations during several representative reactions occurring in the SCR reaction systems. A systematic study of various SCR reactions was carried out on both Fe-ZSM-5 and Cu-ZSM-5 washcoated catalysts. For this purpose, catalysts with various washcoat loadings, washcoat thicknesses and lengths were synthesized in our laboratory. The reactions studied included: NO oxidation, ammonia oxidation, standard SCR (NH_3+NO+O_2), fast SCR (NH_3+NO+NO_2) and NO_2 SCR (NO_2 + NH_3). For the NO_2 SCR reaction, the effect of feed water and O_2 was considered separately. A detailed analysis of characteristic times for various transport processes and of the Weisz-Prater modulus are presented to support the experimental findings. The effect of temperature and effective washcoat diffusivities on transitions between various regimes (from kinetic to washcoat diffusion to external mass transfer) is presented using simplified kinetics and related to experimental observations.

6.2 Experimental

6.2.1 Catalysts

The SCR of NOx by NH_3 reaction system was studied on Fe-ZSM-5 and Cu-ZSM-5 washcoated monolith catalysts synthesized in-house. The Cu-ZSM-5 catalyst was prepared by conventional ion exchange starting with the NH_4^+ form of zeolite (NH_4-ZSM-5, Sud-Chemie Munich, Germany) powder having a Si/Al ratio of 25. The NH_4^+ form was converted to protonated (H^+) form by calcination (500 ^oC for 5 hour). The H-ZSM-5 powder was then converted to Na-ZSM-5 by ion-exchange by continuously stirring it in a 0.1 M $NaNO_3$ solution, followed by several steps of filtration and drying.

In the final step, Na-ZSM-5 was ion-exchanged with 0.02 M copper acetate solution to get Cu-ZSM-5. The Cu-ZSM-5 powder, thus obtained, was calcined for 5 hours at 500 ^{o}C. The method used for ion-exchange was similar to described in the literature [89]. Fe-ZSM-5 powder, provided by Sud-Chemie (Munich, Germany), was used to synthesize Fe-based washcoated catalysts. The washcoated catalysts were prepared by dipping a blank cordierite monolith in a slurry comprising a mixture of either Fe-ZSM-5 powder or Cu-ZSM-5 powder and γ-alumina particles. More detail about the washcoating procedure can be found in Chapter 2 and [103]. Characterization included inductive coupled plasma (ICP) and scanning electron microscopy (SEM) to provide information about the elemental composition and washcoat thickness, respectively.

6.2.2 Bench-Scale Reactor Set-up

The experimental setup was the same one used in our previous studies [132, 139, 152] and is described in more detail in Chapter 2. It included a gas supply system, a reactor system, an analytical system and a data acquisition system. The monolith catalysts were wrapped with a ceramic paper and inserted inside a quartz tube reactor (40.6 cm long, 0.81 cm inner diameter, 1.27 cm outer diameter) which was mounted in a tube furnace coupled to a temperature controller. A FT-IR spectrometer (Thermo-Nicolet, Nexus 470) and a quadrupole mass spectrometer (QMS; MKS Spectra Products; Cirrus LM99) were positioned downstream of the reactor to analyze the effluent gases.

Monolith catalysts with different dimensions (lengths, washcoat loadings, number of channels) were used to study the washcoat diffusion limitations for various reactions. Before starting each experiment, each catalyst was pretreated by flowing 5% O_2 in Ar

with total flow rate of 1000 sccm while keeping the catalyst temperature constant at 500 ^{o}C for 30 minutes. The catalyst temperature was then brought back to the room temperature before the start of each experiment.

In order to study the diffusion limitations in various SCR reactions, several Fe- and Cu-zeolite catalyst samples were synthesized with prescribed washcoat loadings. These catalysts are named as FeZ-XX and CuZ-XX where -XX denotes the washcoat loading (weight %). Most experiments were carried out in the temperature range of 150-550 ^{o}C. We waited about 30 minutes at each temperature until steady state was reached.

For the NH_3 oxidation reaction, the catalysts had 28 channels and the total flow rate was kept constant at 1000 sccm. For the purpose of keeping the same space velocity per unit mass of catalyst (i.e., keeping the W/F, mass of catalyst/molar flow rate, ratio constant), 2 cm length of FeZ-11 and 1 cm length of FeZ-22 catalyst were used. A similar approach was used for this study on Cu-zeolite catalysts, where CuZ-10 (2 cm) and CuZ-20 (1 cm) samples were used. The feed consisted of 500 ppm NH_3, 5% O_2 and 2% water. For the NO oxidation reaction, same Fe-zeolite catalysts (2 cm long FeZ-11 and 1 cm long FeZ-22) were used. The feed consisted of 500 ppm NO and 5% O_2. For the standard SCR, using the same catalysts the feed consisted of 500 ppm NO, 500 ppm NH_3, 5% O_2 and 2% water. For the fast SCR reaction studies, catalysts with the same loadings as described above were used. But higher space velocities were required to achieve smaller conversions since this reaction is faster compared to the other reactions. For the Fe-zeolite system, shorter catalyst lengths (1 cm of FeZ-11 and 5 mm of FeZ-22) were used to achieve lower conversions. Both the catalysts had 28 channels. For the Cu-zeolite system, the number of channels was reduced from 28 to 9 to achieve higher space

velocity and lower conversion. Catalysts with 2 cm length of CuZ-10 and 1 cm length of CuZ-20 were used for this study. The feed consisted of 500 ppm NO, 500 ppm NO_2, 1000 ppm NH_3, 5% O_2 and 2% water. The reaction was studied in the temperatures range of 200-550 ^oC. The starting temperature for this set of experiments was 200 ^oC so that there was no solid state ammonium nitrate deposition on the catalyst surface. All the gas lines were kept heated (T > 150 ^oC) to avoid deposition of ammonium nitrate and minimize the adsorption of water and ammonia.

The NO_2 SCR reaction was studied using the same catalysts as described earlier for the fast SCR reaction. The feed consisted of 500 ppm NO_2, 500 ppm NH_3, 0-5% O_2 and 0-2% water. Effects of O_2 and water were studied in separate experiments and are described in following section. Again, the reaction was studied in the temperatures range of 200-550 ^oC to avoid the ammonium nitrate deposition (at lower temperatures) on the catalyst surface.

6.3 Theoretical Background: Characteristic times, Controlling regimes and Conversion analyses

6.3.1 Characteristic times

While the main focus of this work is the investigation of washcoat diffusion limitations in various SCR reactions, the potential contribution of other transport processes is also examined. In a monolith containing washcoated zeolite catalyst, four types of transport processes exist: 1) External mass transfer: this involves diffusion of species from the gas phase to the surface of washcoat. 2) Internal mass transfer (washcoat or pore diffusion): this involves diffusion of a species in the intercrystalline voids (pores)

within the washcoat. 3) Intracrystalline diffusion: this involves diffusion within the nano pores of the zeolite crystallites. 4) Convective flow: this involves the flow of the gas mixture through the monolith channels. The catalytic reaction is the fifth process, obviously a chemical process. A comparison of characteristic times of each of these individual processes gives an insight on the rate limiting process [147]. The five characteristic times were compared:

Transverse diffusion or external mass transfer time: $\tau_e = \frac{R_{\Omega 1}^2}{D_f}$;

Washcoat diffusion time: $\tau_{d,w} = \frac{R_{\Omega 2}^2}{D_e}$;

Intracrystalline diffusion time: $\tau_{d,c} = \frac{R_{\Omega 3}^2}{D_{e,c}}$;

Convection or space time, $\tau_c = \frac{L}{\langle u \rangle}$;

Reaction time: $\tau_r = \frac{C_i}{r_i}\frac{R_{\Omega 1}}{R_{\Omega 2}}$.

Here $R_{\Omega 2}$ is the effective washcoat thickness (or effective transverse diffusion length for the washcoat defined as the ratio of washcoat cross-sectional area $A_{\Omega 2}$ to the fluid-washcoat interfacial perimeter $P_{\Omega 1}$), D_e is the effective diffusivity of the reactant in the washcoat. L is the channel length, $\langle u \rangle$ is average gas velocity in the monolith channel, $R_{\Omega 1}$ is the effective transverse diffusion length (defined as the ratio of channel cross sectional area ($A_{\Omega 1}$) to $P_{\Omega 1}$), $R_{\Omega 3}$ is the zeolite crystallite particle radius, D_f is the diffusivity of a reacting species in the gas phase and $D_{e,c}$ is the effective diffusivity in the zeolite crystallite. Diffusion within the zeolite crystallite level is included for completion,

notwithstanding the uncertainty about the value of the diffusion coefficient in the zeolite channels and the location of the active sites within the pores or on the surface of the crystallites [103]. We represent a shape of a typical washcoat in a washcoated monolithic channel in Figures 6-1a and 6-1b. There are two additional important parameters. The transverse Peclet number is the ratio of characteristic times for the transverse (to convective flow) gas phase diffusion and convection processes ($P = \tau_e/\tau_c$), and is defined as

$$P = \frac{R_{\Omega 1}^2 \langle u \rangle}{L D_f}. \tag{6-1}$$

The magnitude of P determines the upper bound on conversion that can be attained in a monolith (in the external mass transfer controlled regime). The Weisz-Prater modulus (Ψ) provides an estimate of the extent of washcoat diffusion limitations and is defined as

$$\Psi = \frac{R_{\Omega 2}^2 \, R_{obs}}{D_e \, C_i}, \tag{6-2}$$

where R_{obs} is the observed rate of reaction (washcoat volume basis). If $\Psi \geq 1$, then washcoat diffusion limitations exist while if $\Psi << 1$, then diffusion limitations are negligible. Corresponding estimates of all these parameters for various SCR reactions are shown in Tables 6-1-6-3. These findings are discussed in the later section of this chapter where we discuss our experimental findings.

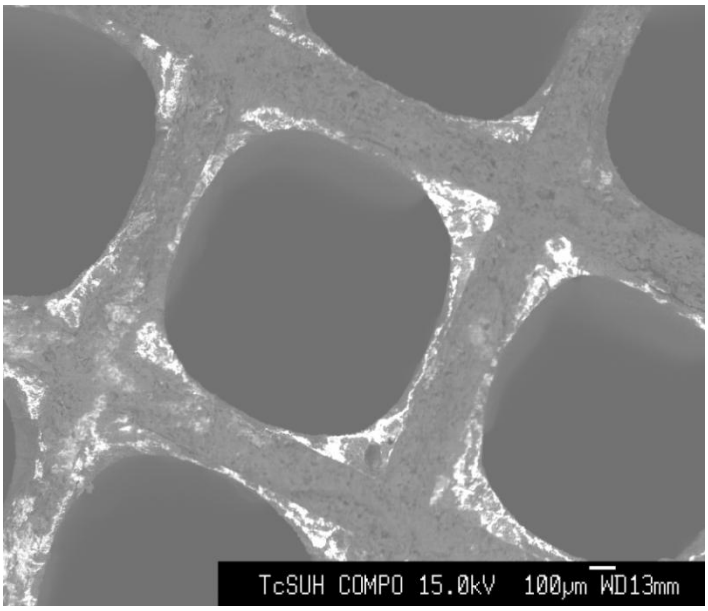

Figure 6-1a: Scanning electron microscope image of the washcoated Cu-zeolite monolith catalyst. Washcoat shape was found to be nearly circular with more deposition at the corners compared to that in the center.

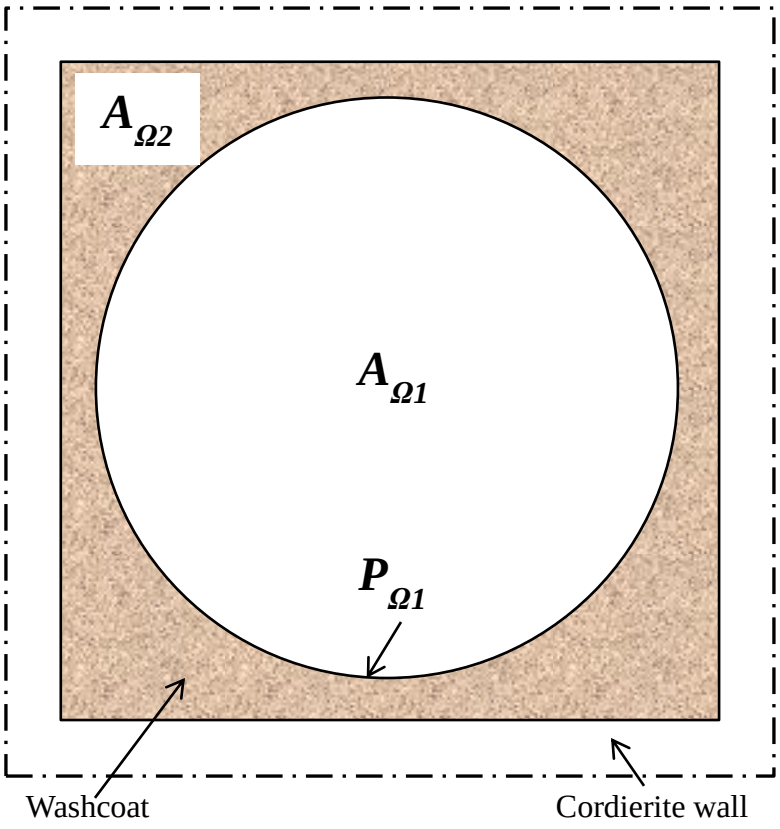

Figure 6-1b: Schematic diagram illustrating various length scales in a typical washcoated monolithic channel.

Table 6-1: Estimated values of various characteristic times (in milli seconds) and the dimensionless numbers *P* (transverse Peclet number) and Ψ (Weisz-Prater modulus) in the temperature range of 200-575 ^{o}C for the standard SCR reaction.

Temperature (^{o}C)	τ_c (ms)	τ_e (ms)	$\tau_{d,w}$ (ms)	τ_r (ms)	*P*	Ψ
200	5.70	1.73	5.73	184.5	0.30	0.17
250	5.15	1.46	4.83	74	0.28	0.35
275	4.92	1.33	4.42	46.2	0.27	0.53
300	4.70	1.24	4.12	37.5	0.26	0.61
325	4.50	1.19	3.94	22.3	0.25	0.97
350	4.32	1.07	3.55	16.7	0.25	1.17
425	3.86	0.89	2.94	5.54	0.23	2.92
500	3.49	0.75	2.47	3.48	0.21	3.92
575	3.18	0.64	2.12	2.86	0.20	4.34

Table 6-2: Estimated values of various characteristic times (in milli seconds) and the dimensionless numbers *P* (transverse Peclet number) and Ψ (Weisz-Prater modulus) in the temperature range of 200-500 ^{o}C for the fast SCR reaction (FeZ-22 catalyst).

Temperature (^{o}C)	τ_c (ms)	τ_e (ms)	$\tau_{d,w}$ (ms)	τ_r (ms)	*P*	Ψ
200	5.87	1.73	3.66	25	0.30	1
250	5.31	1.46	3.08	7.5	0.28	2.8
300	4.84	1.24	2.64	4.8	0.26	3.8
350	4.45	1.07	2.29	3.6	0.24	4.4
400	4.12	0.95	2.01	2.9	0.23	4.8
450	3.84	0.84	1.78	2.5	0.22	4.9
500	3.59	0.75	1.59	2.2	0.21	4.8

Table 6-3: Estimated values of various characteristic times (in milli seconds) and the dimensionless numbers P (transverse Peclet number) and Ψ (Weisz-Prater modulus) in the temperature range of 200-500 ^{o}C for the NO_2 SCR reaction (FeZ-22 catalyst).

Temperature (^{o}C)	τ_c (ms)	τ_e (ms)	$\tau_{d,w}$ (ms)	τ_r (ms)	P	Ψ
200	5.87	2.25	4.77	32	0.38	1
250	5.31	1.89	4.01	12.3	0.36	2.2
300	4.84	1.62	3.42	7.4	0.33	3.2
350	4.45	1.4	2.96	3.6	0.31	5.6
400	4.12	1.2	2.59	2.7	0.30	6.6
450	3.84	1.1	2.29	2.5	0.28	6.3
500	3.59	0.96	2.04	2.4	0.27	5.9

In most of our experiments, we used small lengths of monolith pieces (0.5-2 cm). For this reason, the entrance length effects associated with the development of the axial flow velocity profile need to be included in the analysis. If the flow is fully developed within a short fraction of total length, then the entrance length effect can be assumed to be negligible. Ramanathan et al. [194] presented correlations for developing flow in catalytic monoliths. Using those correlations, Clayton et al. [152] found that the flow was fully developed within the first 3% of the monolith channel used in their study. In the current study, we used the correlation for local Sherwood number as a function of axial distance for simultaneously developing flow in a circular channel. This correlation appeared in a recent study [195] and is given as

$$Sh(z) = 4.364 + \frac{0.98 Sc^{-1/6} \dfrac{P}{z}}{1 + 0.512 \left(\dfrac{P}{z} \right)^{1/2}}. \qquad (6\text{-}3)$$

where *Sh(z)* is local Sherwood number, *Sc* is Schmidt number and *z* is dimensionless coordinate along the length of the channel *(z = x/L)*. Different values of transverse Peclet number (*P*) in the range of 0.05-0.4 (Tables 1-3) have been considered as per our experimental conditions. Figure 6-2 shows the dependence of local Sherwood number on the dimensionless channel length. From the results obtained, it is seen that the flow is almost fully developed (as *Sh(z)* reaches its asymptotic value) within 5% channel length for the value of *P* up to 0.2. For high space velocity experiments (*P* values of 0.3-0.4), the length required for the complete flow development increased but did not exceed 8% of the total channel length. As the flow was found to be fully developed within a very short channel length, we neglected the entrance length effects (assuming fully developed flow) in our further calculations.

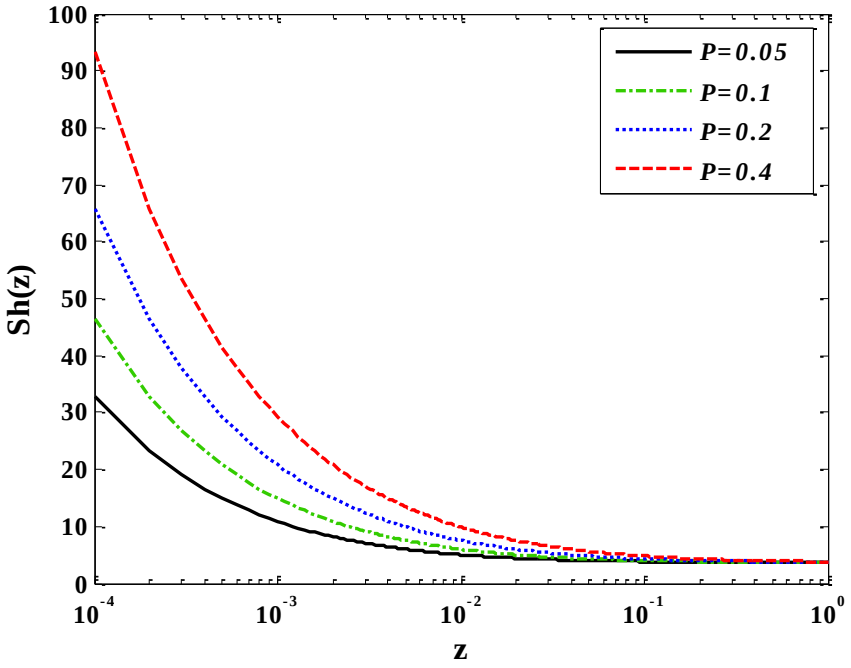

Figure 6-2: Computed diagram showing the dependence of the local Sherwood number on dimensionless axial position in a circular channel for simultaneously developing flow for different values of transverse Peclet number (*P* = 0.05-0.4).

6.3.2 Controlling Regimes in Catalytic Monoliths

Mass transfer limitations are of prime importance in all the catalytic reactions. While the experimental study on catalysts with different washcoat thickness is helpful in investigating washcoat diffusion limitations, external mass transfer limitations should also be considered. A recent study by Joshi et al. [150] showed the effect of temperature on transition between various controlling regimes in catalytic monoliths (from kinetic to washcoat diffusion to external mass transfer) for the case of an isothermal monolith. They used a resistances-in-series approach to determine the controlling regime. The following resistances were considered in their study:

- Fluid phase film or external mass transfer resistance (R_{ext})

$$R_{ext} = \frac{1}{k_{me}(z)} = \frac{4R_{\Omega 1}}{Sh_e(z)D_f}, \tag{6-4}$$

where Sh_e is external Sherwood number, k_{me} is external mass transfer coefficient (from the bulk of the fluid-washcoat interface). If the entrance effects are negligible, a constant value of $Sh_e(z)$ may be used in equation (6-4) e.g., $Sh_e(z)$ = 4.36 for a circular channel.

- Internal mass transfer (washcoat diffusional) resistance (R_w)

$$R_w = \frac{1}{k_{mi}} = \frac{R_{\Omega 2}}{Sh_i(\phi)D_e}, \tag{6-5}$$

where k_{mi} is internal mass transfer coefficient between the interior of the washcoat and the fluid-washcoat interface, Sh_i is internal Sherwood number and for linear kinetics may be expressed as

$$Sh_i(\phi) = Sh_{i\infty} + \frac{\Lambda\phi^2}{1+\Lambda\phi^2}. \tag{6-6}$$

[As we show below, we approximate the kinetics of the examined reactions as first-order.] Values of $Sh_{i\infty}$ and Λ depend upon the washcoat geometries [150]. Here, the inner boundary of the washcoat was assumed to be circular in shape and the washcoat has a constant thickness. This gives values for $Sh_{i\infty}$ = 3 and Λ = 0.32. The washcoat Thiele modulus (ϕ) is defined as

$$\phi = R_{\Omega 2}\sqrt{\frac{k(T)}{D_e}}, \tag{6-7}$$

where k is the first order rate constant (having units of inverse time) based on washcoat volume.

- Reaction resistance (R_{rxn})

$$R_{rxn} = \frac{1}{k(T)R_{\Omega 2}}. \tag{6-8}$$

The sum of all these resistances gives the total resistance (R_t) for the conversion of reactants to products

$$R_t = \frac{4R_{\Omega 1}}{Sh_e(z)D_f} + \frac{R_{\Omega 2}}{Sh_i(\phi)D_e} + \frac{1}{k(T)R_{\Omega 2}}. \tag{6-9}$$

In order to determine the controlling regime, Joshi et al. [150, 193, 196-199] designed some practical criteria described as follows:

- *Kinetic regime:* The monolith is said to be in the kinetic regime (or conversion in the monolith is mainly determined by the kinetics) if $R_{rxn} > 0.9\ R_t$.
- *Washcoat diffusion regime:* The monolith is said to be in washcoat diffusion controlled regime if $R_w > 0.9\ R_t$. In this regime, the conversion in the monolith is strongly influenced by changes in the washcoat properties.

- *External mass transfer regime:* The monolith is in external mass transfer regime if $R_{ext} > 0.9\ R_t$.

We have used these criteria along with simplified first order kinetics (Rate = *kC; k* = 1e13*exp(-11500/T) s^{-1}) to gain an insight on the controlling regimes for the Fe- and Cu-zeolite catalysts. A typical value of the activation energy for the fast and NO_2 SCR reactions of 96 kJ/mol was used [78, 117]. When both NO and NO_2 in the feed react simultaneously to produce N_2 and H_2O; it is called the "fast SCR" reaction and is given by

$$2\ NH_3 + NO + NO_2 \rightarrow 2\ N_2 + 3\ H_2O \qquad \Delta H = -\ 3.78 \times 10^5\ J/mol\ NH_3. \qquad (6\text{-}10)$$

The reaction between NO_2 and NH_3 and is known as NO_2 SCR reaction and is given by

$$4\ NH_3 + 3\ NO_2 \rightarrow 3.5\ N_2 + 6\ H_2O \qquad \Delta H = -\ 3.41 \times 10^5\ J/mol\ NH_3. \qquad (6\text{-}11)$$

An estimate of the first order rate constant (k_o) was determined using the experimentally measured rates (washcoat volume basis) obtained during the high space velocity experiments (and in the absence of transport limitations). A representative case for NO_2 SCR reaction is shown in Figure 6-3. Here, we show the effect of temperature on the transition between regimes for various values of the reactant effective diffusivity in the washcoat. From Figure 6-3, it is clear that very low values of washcoat diffusivities (D_e) are required to attain purely washcoat diffusion controlled regime. However, washcoat diffusion is seen to be practically important for most of the temperatures as the reaction system is found to be in mixed regime. Also, we show the curves that demarcate the regions in which the washcoat diffusion resistance is an important fraction of the total resistance ($R_w > 0.25\ R_t$ and $R_w > 0.5\ R_t$).

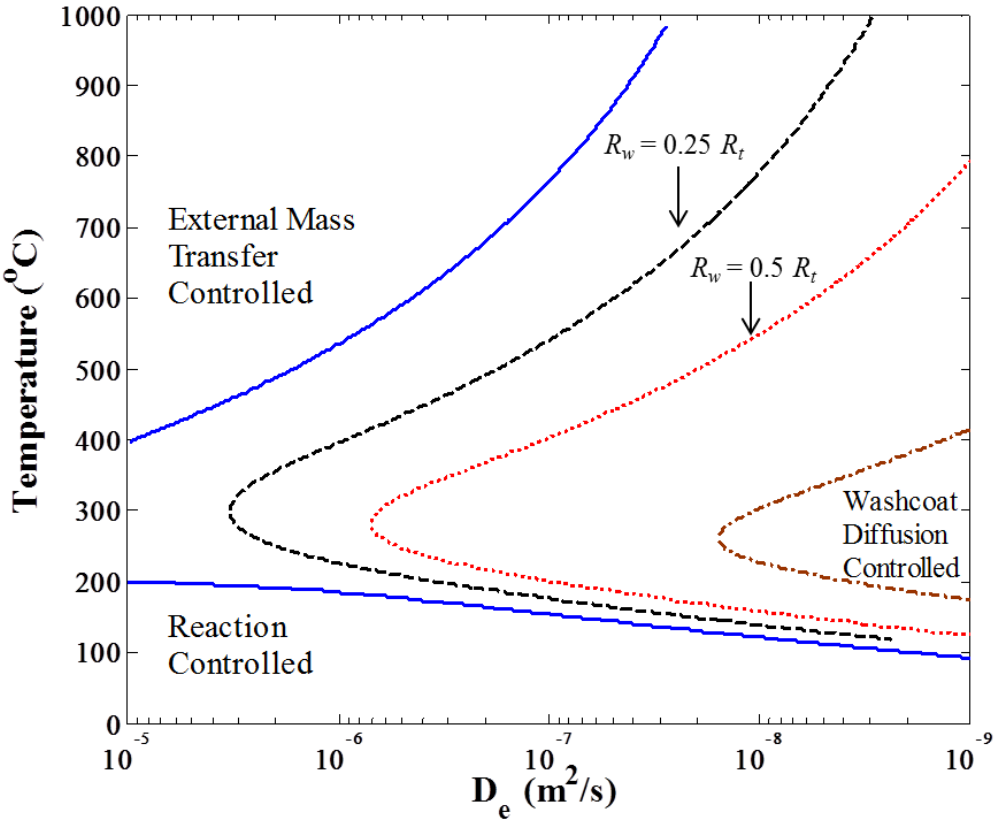

Figure 6-3: Diagram showing the effect of temperature and effective washcoat diffusivity on regime transition in a catalytic monolith.

In Figure 6-4, we show two curves for the cases when reaction resistance is a significant fraction of the total resistance (R_{rxn} = 0.10 R_t, and R_{rxn} = 0.90 R_t). For the case of R_{rxn} > 0.90 R_t (below the lower curve), the reactant conversion is controlled by the kinetics. If we want to study intrinsic kinetics, reaction should be carried out in this regime. For R_{rxn} < 0.10 R_t (above the upper curve), the reaction resistance is negligible and the reactant conversion is controlled by internal and external mass transfer. If experiments are carried out in this regime, then the data should not be used to extract kinetics. To attain purely external mass transfer controlled regime, very high temperatures are required.

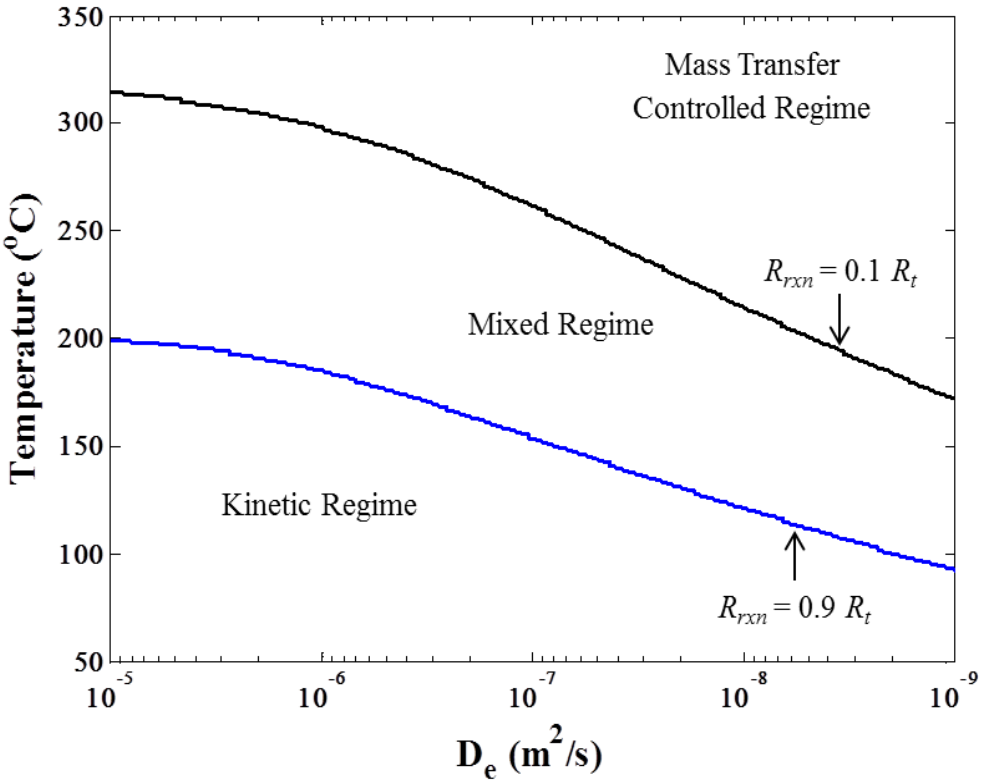

Figure 6-4: Diagram showing the effect of temperature and effective washcoat diffusivity on regime transition in a catalytic monolith. Below the lower curve (R_{rxn} = 0.9 R_t), reaction controlled (kinetic) regime is dominant. Above the upper curve (R_{rxn} = 0.10 R_t), mass transfer (external and internal) controlled regime is dominant.

6.3.3 Effect of Washcoat Properties on Conversions in an Isothermal Monolith

The value of total resistance (R_t) obtained in equation (6-9) can be used to determine the apparent mass transfer coefficient ($k_{m,app}$) in washcoated monoliths.

$$k_{m,app} = \frac{1}{R_t}. \tag{6-11}$$

For an isothermal monolith, value of $k_{m,app}$ can be used to calculate the conversion of a limiting reactant using following equation [150]

$$\chi = 1 - \alpha_1 \exp\left(\frac{-k_{m,app} L}{R_{\Omega 1}\langle u \rangle}\right). \tag{6-12}$$

Substituting for $k_{m,app}$ and writing it in terms of dimensionless parameters, equation (6-12) reduces to the following formula for conversion in an isothermal monoliths [152, 191]

$$\chi = 1 - \alpha_1 \exp\left(\frac{-\mu_1}{P(1+(\mu_1/\Phi^2))} \right), \tag{6-13}$$

where

$$\Phi^2 = \frac{R_{\Omega 1}}{R_{\Omega 2}} \frac{D_e}{D_f} \phi \tanh \phi. \tag{6-14}$$

P (transverse Peclet number) is calculated as a function of temperature and catalyst length. Values of α_1 (1) and μ_1 (1.09) depend upon the washcoat shape [Remark: Here, the washcoat is assumed to be a thin layer around a circular flow area and flow is assumed to be fully developed.] μ_1 can also be represented as $Sh_{e\infty}/4$. The Thiele modulus (ϕ) is expressed as a function of temperature by

$$\phi^2 = \phi_o^2 \exp\left[\frac{E}{RT_o} \left(\frac{T - T_o}{T} \right) \right], \tag{6-15}$$

$$\text{where} \quad \phi_o^2 = \frac{R_{\Omega 2}^2 k(T_o)}{D_e}; \tag{6-16}$$

and

$$k(T_o) = k_o e^{-E/RT_o}. \tag{6-17}$$

E is the activation energy, T_o is the reference temperature (300 K) and R is the universal gas constant.

Using equation (6-13) with $k_o = 1 \times 10^{13} s^{-1}$ *and* $E/RT_o = 38.3$, we estimated the conversion of the limiting reactant NO_2 for the NO_2 SCR reaction using above parameters. These results are summarized in Figure 6-5 where we indicate the

temperatures at which transitions occur between the kinetic regimes (R_{rxn} > 0.90 R_t), mixed (mass transfer) regime (R_{rxn} < 0.10 R_t) and the purely external mass transfer controlled regime (R_{ext} > 0.9 R_t). Three different values of the D_f/D_e ratios (10, 100 and 1000) are used. From these results, it is clear that the reaction was in kinetic regime for temperatures below 190 ^oC for all the three cases. The increasing D_f/D_e ratio shifts the reaction regime temperature towards the left even though the shift is not large.

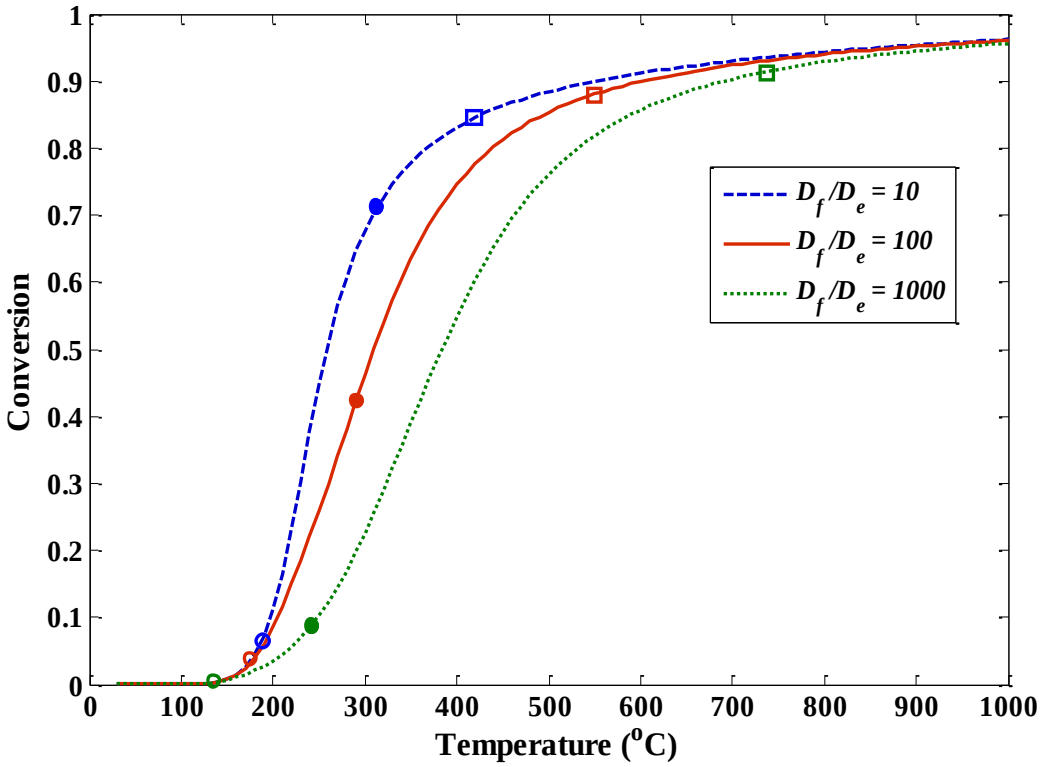

Figure 6-5: Diagram showing the effect of temperature on conversion and regime transitions in a catalytic monolith for the three values of effective diffusivities. (Hollow circle: R_{rxn} = 0.9 R_t, Dark circle: R_{rxn} = 0.1 R_t , Rectangle: R_{ext} = 0.9 R_t).

For D_f/D_e = 10, the effect of washcoat diffusion limitations is found to be negligible as the difference in transition temperatures from mixed mass transfer regime to external mass transfer regime was negligible. This temperature window increases further for the case of D_f/D_e = 100 and thus washcoat diffusion limitations become important for wide

temperature range. Also, the temperature required to attain pure external mass transfer regime shifts towards the right. For the case of D_f/D_e = 1000, the reaction is found to be in the mixed mass transfer regime for most of the temperatures and washcoat diffusion limitations become very important. The temperature required to achieve pure external mass transfer regime increases further.

The results shown in Figure 6-5 results are for a representative case of the NO_2 SCR reaction which shows the effect of effective washcoat diffusivities on the regime transition for one fixed value of catalyst loading. If the catalyst loading is varied, then the temperatures required to achieve the corresponding regimes will shift accordingly. From this figure, it is seen that the reaction is in kinetic regime for a very narrow temperature range. If the catalyst loading is decreased (metal content or washcoat loading), then the temperature range for the kinetic regime could be broadened. The above case for NO_2 SCR should be considered as a representative case of all the SCR reactions. Clearly, a more detailed kinetic model would be required for the accurate prediction of all the regimes. These theoretical calculations are revisited in the next section of this chapter where we present our experimental observations.

The experimental study on catalysts with the same washcoat loadings but different washcoat thicknesses is useful to investigate washcoat diffusion limitations. Here we use a simple isothermal monolith model based on linear kinetics to study the above representative case. The conversion of the limiting reactant (say NO for standard SCR case) is calculated using equation (6-13). The results are summarized in Figure 6-6 which shows the plots obtained for conversion vs temperature (χ vs T) for the three cases of assumed values of effective washcoat diffusivities (D_f/D_e = 10, 100 and 1000).

Following parameters were used for this study. T_o = 300 K, E/RT_o = 22.2, $R_{\Omega 1}$ = 0.275 mm. For a thin catalyst: L = 2 cm, $R_{\Omega 2}$ = 20 μm; while for a thick catalyst: L = 1 cm, $R_{\Omega 2}$ = 40 μm. The additional parameters for three different cases are as follows:

D_f/D_e = 10; Thin catalyst: ϕ_o = 0.004, Thick catalyst: ϕ_o = 0.008,

D_f/D_e = 100; Thin catalyst: ϕ_o = 0.008, Thick catalyst: ϕ_o = 0.016,

D_f/D_e = 1000; Thin catalyst: ϕ_o = 0.025, Thick catalyst: ϕ_o = 0.050.

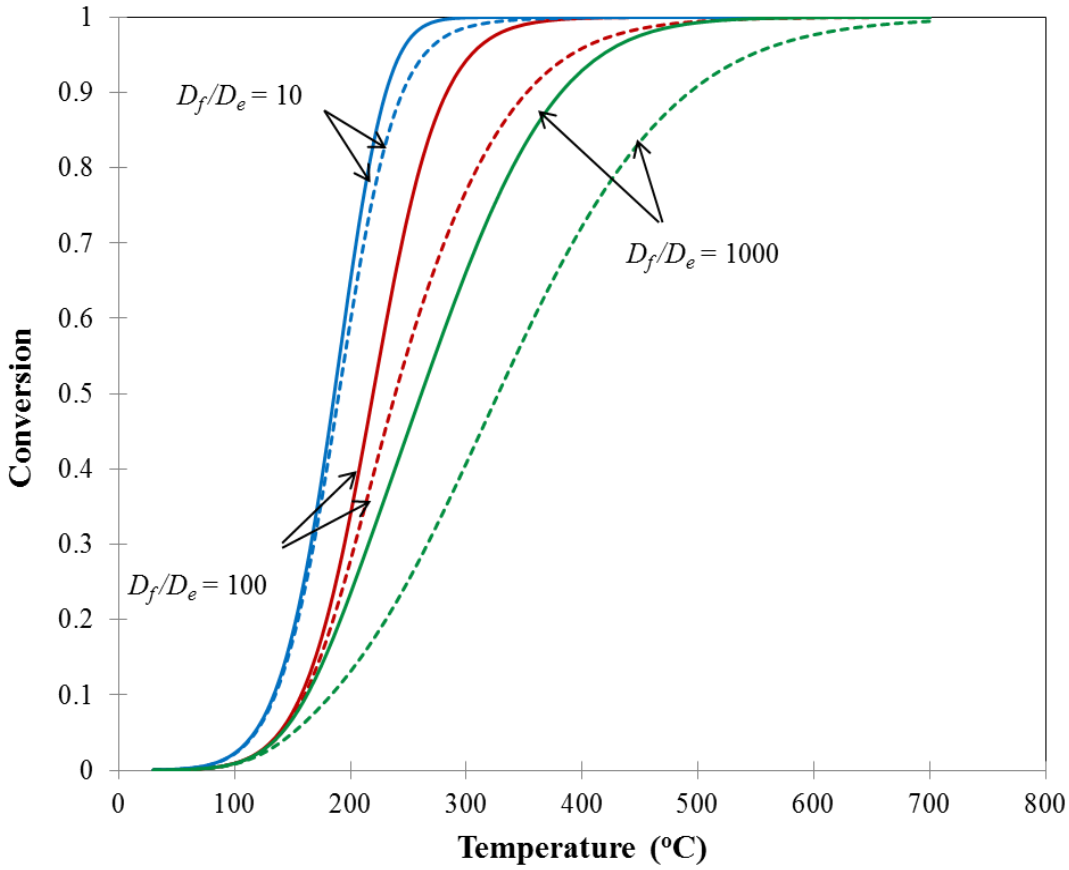

Figure 6-6: Influence of washcoat thickness on the conversions of a limiting reactant for the case of isothermal catalyst. Dashed lines: Thicker catalyst; Solid lines: Thinner catalyst.

In the above Figure 6-6, the solid lines represent catalysts with the thinner washcoat while dashed lines represent the catalysts with the thicker washcoat. For all the cases, thinner washcoated catalysts give higher conversions than the thicker washcoated

catalysts. The separation in conversions increased with increasing D_f/D_e ratios. Thus for the case of isothermal monoliths, we can test the existence of washcoat diffusion limitations by using two different catalysts with the same washcoat loadings and different washcoat thicknesses. We use a similar approach in our experimental study for all the SCR reactions. The experimental results are presented and discussed in the next section.

6.4 Results and Discussion

6.4.1 Ammonia Oxidation

Ammonia oxidation has been studied on various zeolite-based catalysts in the literature [103, 134] and is found to have nearly 100% selectivity towards N_2 [44]. This reaction is given by

$$4\ NH_3 + 3\ O_2 \rightarrow 2\ N_2 + 6\ H_2O \qquad \Delta H = -\ 3.12 \times 10^5\ J/mol\ NH_3. \qquad (6\text{-}18)$$

Here, ammonia oxidation was studied on both Fe-zeolite and Cu-zeolite catalysts with different washcoat loadings to investigate the presence and extent of washcoat diffusion limitations. Figure 6-1a shows the SEM image of a washcoated monolithic channel (CuZ-25) synthesized in our lab. The washcoat boundary was found to be nearly circular in shape with a thicker layer near the corners. The SEM analysis also showed that the effective washcoat thickness $R_{\Omega 2}$ (calculated as the ratio of the washcoat cross sectional area ($A_{\Omega 2}$) and the channel perimeter open to flow ($P_{\Omega 1}$)) was proportional to the catalyst loading, i.e., FeZ-22 with ~ 22% (by wt.) washcoat loading was found to have an average washcoat thickness (35-40 μm) which was nearly double the washcoat thickness (15-20 μm) of FeZ-11 catalyst with 11% washcoat loading.

The results obtained for the Fe-zeolite catalyst are shown in Figure 6-7. [Experimental conditions for the FeZ-11 and CuZ-10 catalysts: Length: 2 cm, No. of channels: 28. Feed: 500 ppm NH_3, 5% O_2, 2% water. Experimental conditions for the FeZ-22 and CuZ-20 catalysts: Catalyst: Length: 1 cm, No. of channels: 28. Feed: 500 ppm NH_3, 5% O_2, 2% water.] As expected, the irreversible standard SCR reaction has a monotonic dependence of conversion on temperatures. It is observed that there is clear separation in the NH_3 conversions at higher temperatures for the two catalysts. The 2 cm long FeZ-11 catalyst with the thinner washcoat gave higher conversions than the 1 cm long FeZ-22 thicker catalysts. Up to 300 ^oC, the difference was negligible (3%). But at 350 ^oC, there is 10% difference in the conversions with thinner catalyst giving higher conversion. The observed differences in the conversions remained up to 450 ^oC, after which the difference in conversion decreased as the conversion started reaching an asymptote. These findings are in line with the model calculations validating the approach of detecting transport limitations using the two catalysts of different lengths and loadings and prove the existence of washcoat diffusion limitations present at intermediate temperatures in SCR catalysts.

The same reaction was then studied on Cu-zeolite catalysts with different washcoat thicknesses. The NH_3 conversions obtained with the CuZ-10 and CuZ-20 are compared in Figure 6-7. The results obtained with the Cu-zeolite catalysts follow a similar trend as those for the Fe-zeolite catalysts. There is a clear separation in NH_3 conversions obtained with these catalysts with the thinner CuZ-10 catalyst giving higher conversions. Unlike with the Fe-zeolite, there was about 6% difference in NH_3 conversions observed at 300 ^oC. The difference in conversion widened further with

temperature and ca. 16% difference was observed at 400 ^{o}C. This difference diminished at higher temperatures as the NH_3 conversions were 100 % at 450 ^{o}C and higher temperatures. These results show that the rate of NH_3 oxidation is higher on Cu-zeolite compared to Fe-zeolites. The observed differences in NH_3 conversions further confirmed the presence of washcoat diffusion limitations for the NH_3 oxidation in zeolite catalysts.

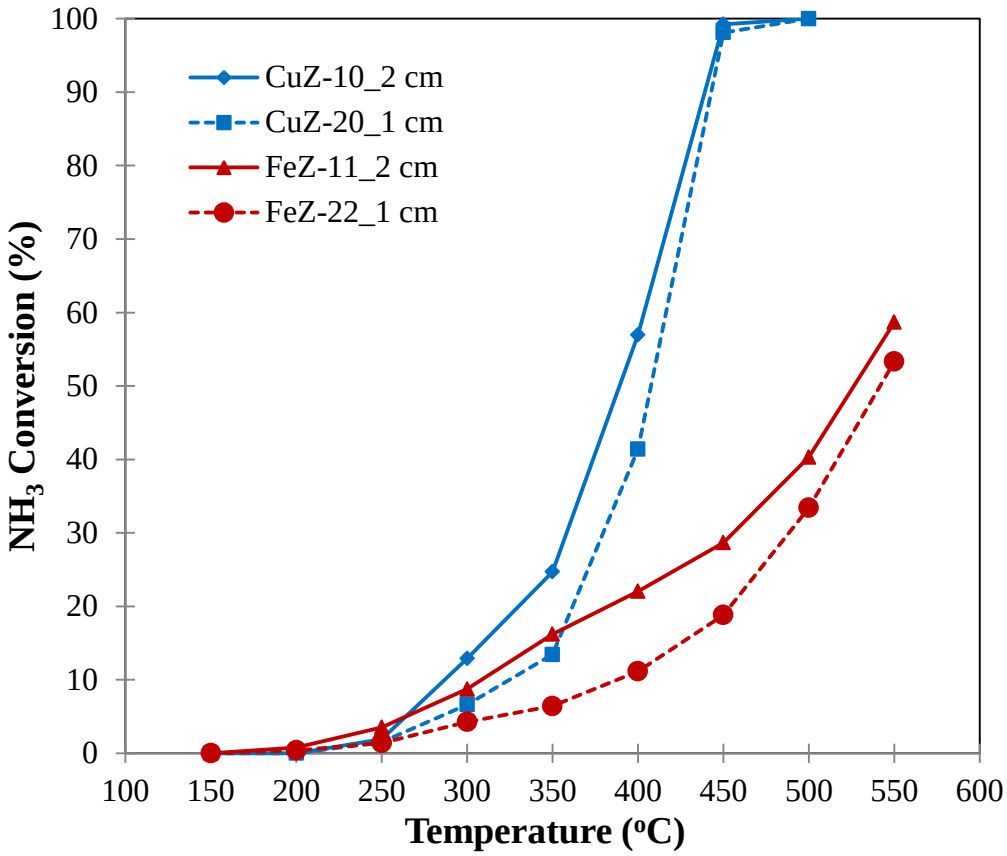

Figure 6-7: Steady state NH_3 conversions obtained during the NH_3 oxidation reaction studied on in-house synthesized FeZ-XX and CuZ-XX catalysts.

6.4.2 Standard SCR

As described earlier in Chapter 2, the standard SCR reaction involves NO, NH_3 and O_2 simultaneously present and reacting in the feed,

$$4\ NH_3 + 4\ NO + O_2 \rightarrow 4\ N_2 + 6\ H_2O \qquad \Delta H = -\ 4.07 \times 10^5\ J/mol\ NH_3. \qquad (6\text{-}19)$$

In our earlier study in Chapter 3 and [103], we showed that NO oxidation is the rate determining step for the standard SCR reaction; further, we described the mechanistic reasons for differences in these two reactions in the presence and absence of water. We also showed the differences in NO conversions obtained on the same catalysts described earlier for NH_3 oxidation. For the sake of completeness, we report the results from Chapter 3. Using the same approach, the total flow rate was kept constant at 1000 sccm while varying the catalyst length so that the space velocity per unit mass of catalyst was kept constant i.e., 2 cm long piece of FeZ-11 and 1 cm long piece of FeZ-22 were used. The results obtained from these experiments are summarized in Figure 6-8 [Experimental conditions for the FeZ-XX catalysts: Length: 1 cm-2 cm, No. of channels: 28. Feed: 500 ppm NO, 500 ppm NH_3, 5% O_2, 2% water. Experimental conditions for the CuZ-XX catalysts: Length: 1cm-2 cm, No. of channels: 28. Feed: 500 ppm NO, 500-900 ppm NH_3, 5% O_2, 2% water]. The trends obtained with NO conversions remained nearly the same up to 300 ^oC but a clear difference in NO conversion was obtained for temperatures between 350-450 ^oC. The difference was largest at intermediate temperatures and decreased at higher temperatures. Thus the results obtained during the standard SCR reaction confirm the presence of washcoat diffusion limitations in this reaction studied on Fe-zeolite catalysts.

Table 6-1 provides the estimated values of various time constants for this reaction studied at high space velocity. Here, effective diffusivity in the washcoat was assumed to be 100 times smaller than the gas phase diffusivity [116]. Also, the characteristic time constant for diffusion within the zeolite crystallite ($\tau_{d,c}$) was found to be around 0.6 ms based on the assumed value of $D_{e,c}$ to be 10^{-8} - 10^{-9} m^2/s. Huang et al. [34] used the

crystallite diffusivity values of the similar order and found that the zeolite pore diffusion was negligible. A comparison of the various time constants shows that the characteristic reaction time was much larger than other characteristic times for temperatures up to 325 ^{o}C. But at higher temperatures, the characteristic times were comparable, showing the emergence of mass transfer limitations at moderate temperatures. The value of the Weisz-Prater modulus was found to exceed unity for temperatures $\geq$ 350 ^{o}C. This corroborates our experimental observations of presence of washcoat diffusion limitations. The range over which these diffusion limitations were observed is similar to NH_3 oxidation reaction studied on the same catalysts.

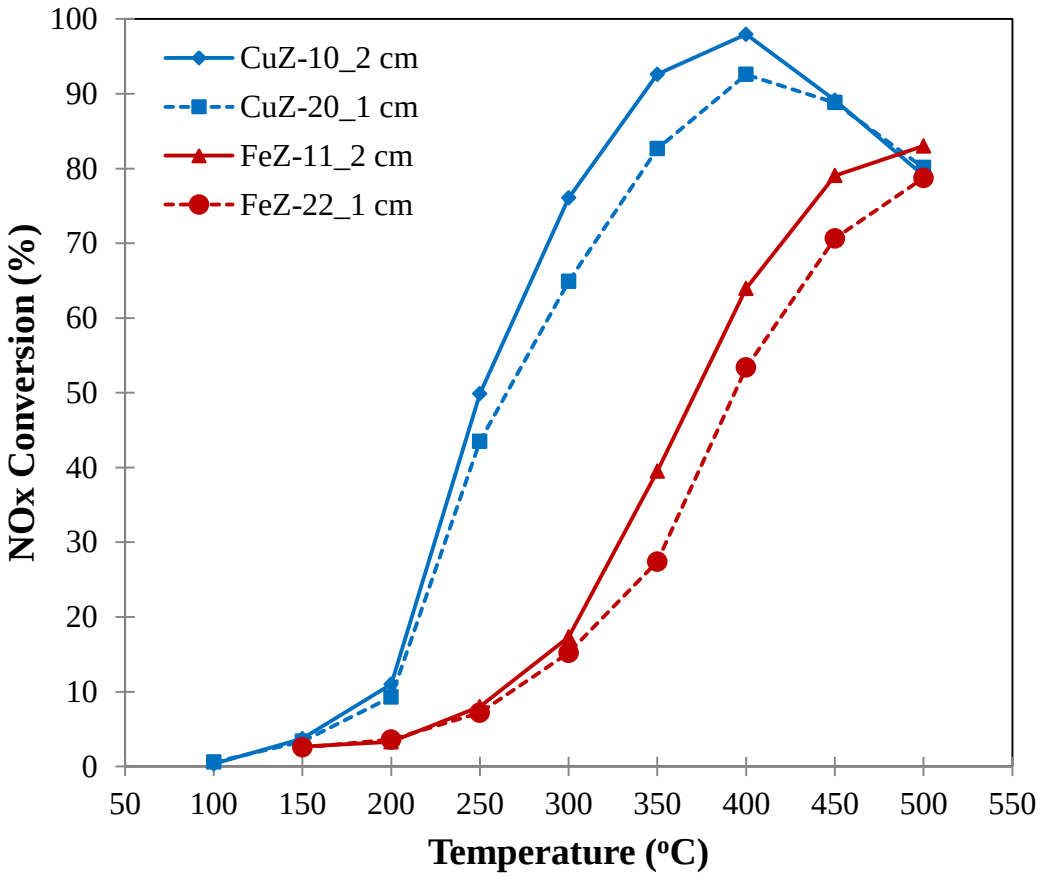

Figure 6-8: Steady state NOx conversions obtained during the standard SCR reaction studied on in-house synthesized FeZ-XX and CuZ-XX catalysts.

The standard SCR reaction was also studied on Cu-zeolite catalysts of different lengths and loadings. We used the same catalysts (CuZ-10 and CuZ-20) as described earlier for the NH_3 oxidation study. Initially, a feed containing 500 ppm NO, 500 ppm NH_3, 5% O_2 and 2% water was used. A substantial difference in NOx conversions were observed at temperatures as low as 250 ^oC. But for temperatures greater than 350 ^oC, it was difficult to analyze the NOx conversion data as NH_3 conversion started increasing due to the NH_3 oxidation side reaction as a result of which NO conversions decreased. Thus, a higher feed NH_3/NOx ratio of 1.8 was used. The NOx conversion results obtained with these experiments are summarized in Figure 6-8. A clear difference (7%) in NOx conversion was observed starting at 250 ^oC with the thinner catalyst giving higher conversion. The difference increased further (to 12%) at intermediate temperatures (300-350 ^oC) but decreased at higher temperatures. For temperatures of 450-500 ^oC, the rate of the ammonia oxidation side reaction increased and hence the ammonia conversion was 100%. Under these conditions, sufficient NH_3 was not available for the NOx reduction and as a result the NOx conversions decreased from their maxima at 400 ^oC. Comparable NOx reduction activities were obtained at these temperatures. With these data, it can be concluded that the washcoat diffusion limitations are present for the standard SCR reaction in the temperature range of 250-450 ^oC on Cu-zeolite catalysts. The range is similar for ammonia oxidation reaction discussed earlier. These data also show that the NH_3 oxidation reaction was very fast on Cu-zeolite catalysts even in the presence of NO.

6.4.3 NO Oxidation

As mentioned earlier, NO oxidation is a key step for the standard SCR reaction. It is a reversible reaction and is equilibrium controlled at higher temperatures (> 350 ^{o}C) [103]. This reaction is given by

$NO + ½ O_2 \leftrightarrow NO_2$ $\Delta H = - 5.7 \times 10^4$ J/mol NO. (6-20)

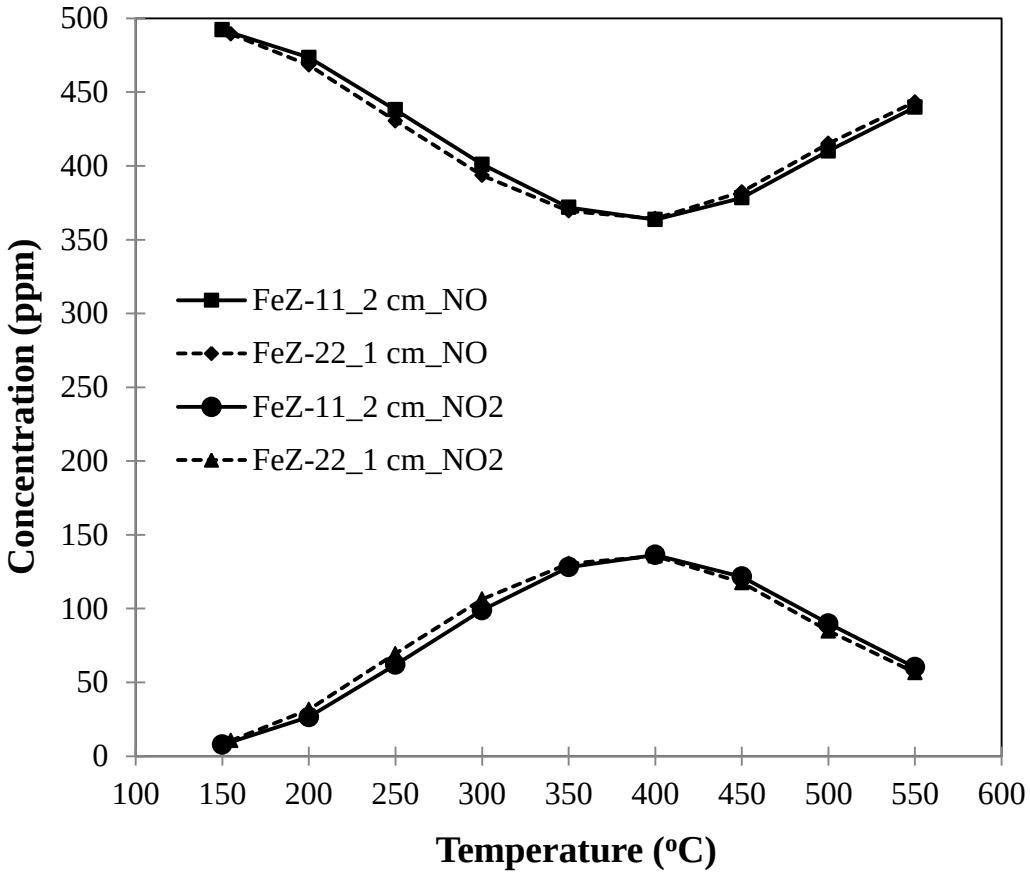

Figure 6-9: Steady state NOx concentrations obtained during the NO oxidation reaction studied on in-house synthesized FeZ-XX catalysts. Feed: 500 ppm NO, 5% O_2, 0% water. Catalyst properties: No. of channels: 28, Length: FeZ-11: 2 cm, FeZ-22: 1 cm.

We used FeZ-XX catalysts (2 cm long FeZ-11 and 1 cm long FeZ-22), described earlier for NH_3 oxidation reaction studies, to study diffusion limitations in this reaction system. The results obtained are summarized in Figure 6-9. Unlike for NH_3 oxidation and standard SCR, we did not see a clear separation in NO conversions on the two different

catalysts used for this reaction. Rather, both the catalysts showed very similar NO oxidation activities, suggesting an absence of diffusional limitations. The obvious reason is that NO oxidation is slower than other reactions considered thus far. Also, at higher temperatures (> 350 ^{o}C), the reverse NO_2 decomposition reaction becomes important. For the above two cases, the diffusion limitations were observed at intermediate to higher temperatures. For the NO oxidation, the reverse reaction starts around the same temperatures and hence the diffusion limitations were not observed.

6.4.4 Fast SCR

The fast SCR reaction (reaction (6-10)) involves a simultaneous reaction of NO and NO_2 with ammonia. The presence of NO_2 in the inlet feed enhances the NOx conversion, especially at lower temperatures. This reaction is much faster than the standard SCR reaction especially on Fe-zeolite catalysts [29, 39]. In order to study the diffusion limitations for this case, it was necessary that the reaction be carried out at very high space velocity so that lower conversions could be achieved. For the Fe-zeolite, this was achieved with the use of catalysts having lengths less than 1 cm, shorter than for the earlier experiments.

The results obtained with this reaction are summarized in Figure 6-10. Significant differences in the NOx conversions were obtained throughout the temperature range for the two catalysts studied, with thinner catalysts giving higher conversions. The data show the presence of washcoat diffusion limitations for the fast SCR reaction throughout the temperature range. We estimate the values of various time constants for all the processes

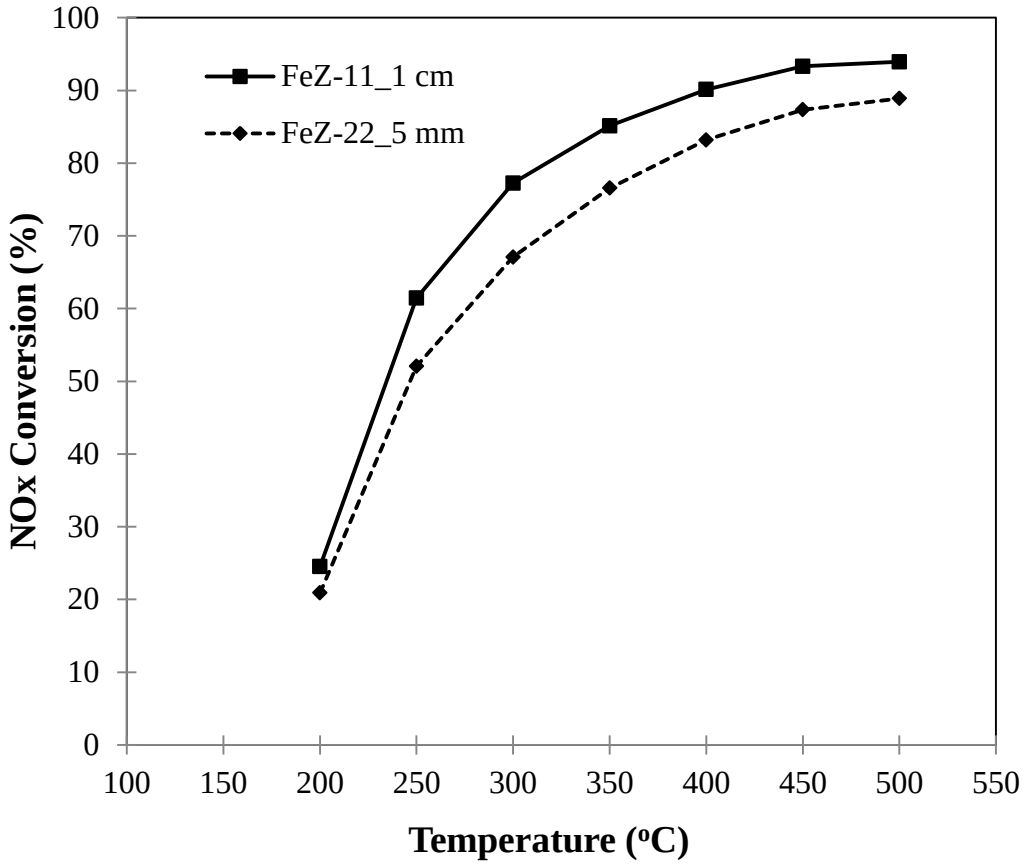

Figure 6-10: Steady state NOx conversions obtained during the fast SCR reaction studied on in-house synthesized FeZ-XX catalysts. Feed: 500 ppm NO, 500 ppm NO_2, 1000 ppm NH_3, 5% O_2, 2% water. Total flow rate = 1000 sccm. Catalyst properties: No. of channels: 28, Length: FeZ-11: 1 cm, FeZ-22: 5 mm.

occurring during this reaction and are summarized in Table 6-2. Unlike standard SCR, the reaction time was found to be comparable with other characteristic times starting at temperature as low as 200 ^{o}C. At higher temperatures, the characteristic times for reaction, internal and external mass transfer were quite comparable and hence show the co-existence of all these processes. Moreover, the value of the Weisz-Prater modulus was found to be greater than 1 for all the temperatures. These estimates are in agreement with our experimental results and hence confirm the existence of diffusion limitations throughout the temperature range. External mass limitations cannot be ruled out completely because of the comparable time constants for both the external and internal

mass transfer processes. In earlier section, we discussed about the importance of all the processes (reaction, internal and external mass transfer) for intermediate temperature range for very fast reactions. The comparable values of time constants suggest that the fast SCR reaction was in mixed regime for most of the temperatures considered for our experimental studies.

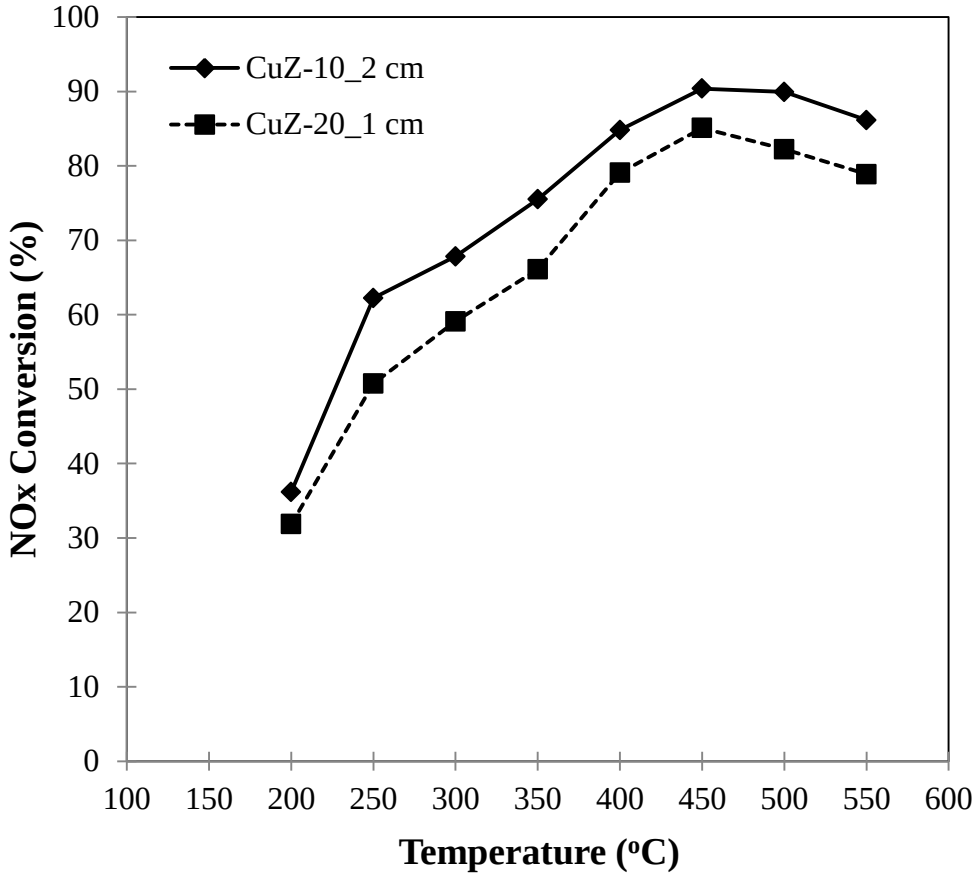

Figure 6-11: Steady state NOx conversions obtained for the fast SCR reaction studied on in-house synthesized CuZ-XX catalysts. Total Flow rate = 1000 sccm. Feed: 500 ppm NO, 500 ppm NO_2, 1000 ppm NH_3, 5% O_2, 2% water. Catalyst properties: No. of channels: 9. Length: CuZ-10: 2 cm, CuZ-20: 1 cm.

A similar approach was used to study diffusion limitations in Cu-zeolite catalysts. Catalyst dimensions and experimental conditions are mentioned in the experimental section. Results obtained with these catalysts are summarized in Figure 6-11. These

results are in line with the above results on Fe-zeolite catalysts. The differences in NOx conversions obtained over entire temperature range confirm the presence of washcoat diffusion limitations for the fast SCR reaction.

6.4.5 NO_2 SCR

The NO_2 SCR reaction (reaction (6-11)) involves NO_2 and NH_3. In Chapter 4, we have studied various SCR reactions on Fe-zeolite catalysts with feeds containing different NO_2/NOx ratios. These observations show that the presence of NO_2 enhances the overall NOx conversions (especially at lower temperatures). We have also observed that the NO_2 SCR reaction proceeds faster than the standard SCR but is slower than the fast SCR. Moreover, this reaction leads to the formation of additional byproducts like N_2O and NH_4NO_3. The effect of feed water was studied separately on these reactions. For the NO_2 SCR reaction, FeZ-18 catalyst with 2 cm length was used. The experiments were carried out in the absence and presence (2%) of water. It was observed that very high NOx conversions were achieved throughout the temperature range in the absence of water. But the presence of water inhibits the steady state NOx conversions drastically in the temperature range of 200-300 ^oC (Figure 6-12). The stability of formed ammonium nitrate could be considered to be responsible for this. The inhibition by feed water was seen only for the feeds containing excess NO_2 (NO_2/NOx > 0.5) and was absent for feeds containing lower NO_2/NOx ratios.

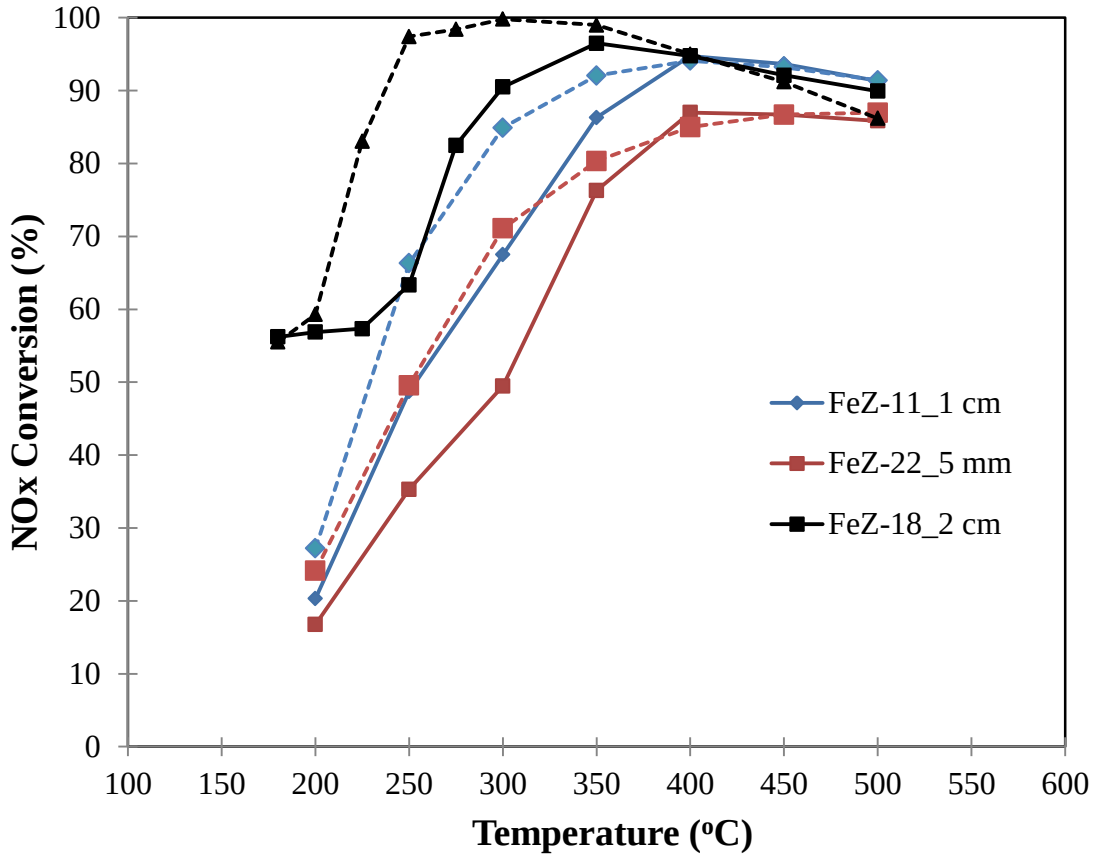

Figure 6-12: Steady state NOx conversions obtained during the NO_2 SCR reaction studied on in-house synthesized FeZ-XX catalysts. Feed: 500 ppm NO_2, 500 ppm NH_3, 5% O_2, 0-2% water. (Dashed lines: 0% water).Catalyst properties: No. of channels: 28; Length: FeZ-11: 1 cm, FeZ-22: 5 mm, FeZ-18: 2 cm.

In order to examine the importance of washcoat diffusion limitations, we used similar catalysts system as described earlier for the fast SCR studies. This study was carried out both in the presence and absence of water. The results obtained are summarized in Figure 6-12. Dashed lines show the results in the absence of water. Again, the inhibition effect of water is clearly evident here. Also, the difference in the NOx conversion was seen throughout the temperature range for catalysts with different washcoat loadings. The thinner catalyst gave the higher NOx conversion throughout the temperature range for both the cases (0 and 2% water). These results thus confirm the presence of washcoat diffusion limitations for Fe-zeolite catalysts for all the SCR

reactions discussed earlier. Following a similar approach for the standard and fast SCR reactions, we estimated the values of characteristic time constants for various processes occurring during the NO_2 SCR reaction and are summarized in Table 6-3. Like fast SCR, characteristic times for all the processes were found to be comparable. Also, the Weisz-Prater modulus was found to be greater than 1 starting at 200 ^oC. This is in line with our experimental findings where we detected the washcoat diffusion limitations for all the temperatures studied (200-550 ^oC).

We used equation (6-13) to estimate the NOx conversions obtained for the above catalysts. The rate parameters (k_o and E) used were similar to that mentioned in equation (6-17). Values of the remaining parameters were based on experimental conditions (L = 5 mm-1 cm, $R_{\Omega 2}$ = 20-40 μm, $R_{\Omega 1}$ = 0.275 mm, D_f/D_e = 100). The model can predict the experimentally observed differences in NOx conversion activities on the two catalysts (Figure 6-13). For reaction at 250 ^oC, the model predicts a difference of 21% in the NOx conversions on the two catalysts. This compares favorably with the 16% difference measured experimentally. Thus, the model satisfactorily captures the experimentally observed trends; i.e., different NOx conversion activities on two catalysts with the same washcoat volume but different washcoat thicknesses. However, a simple (linear) kinetic model could predict the data only qualitatively and not quantitatively as the SCR chemistry is highly complex with the co-existence of multiple reactions. A detailed kinetic model would be required to predict the experimentally observed NOx reduction activities.

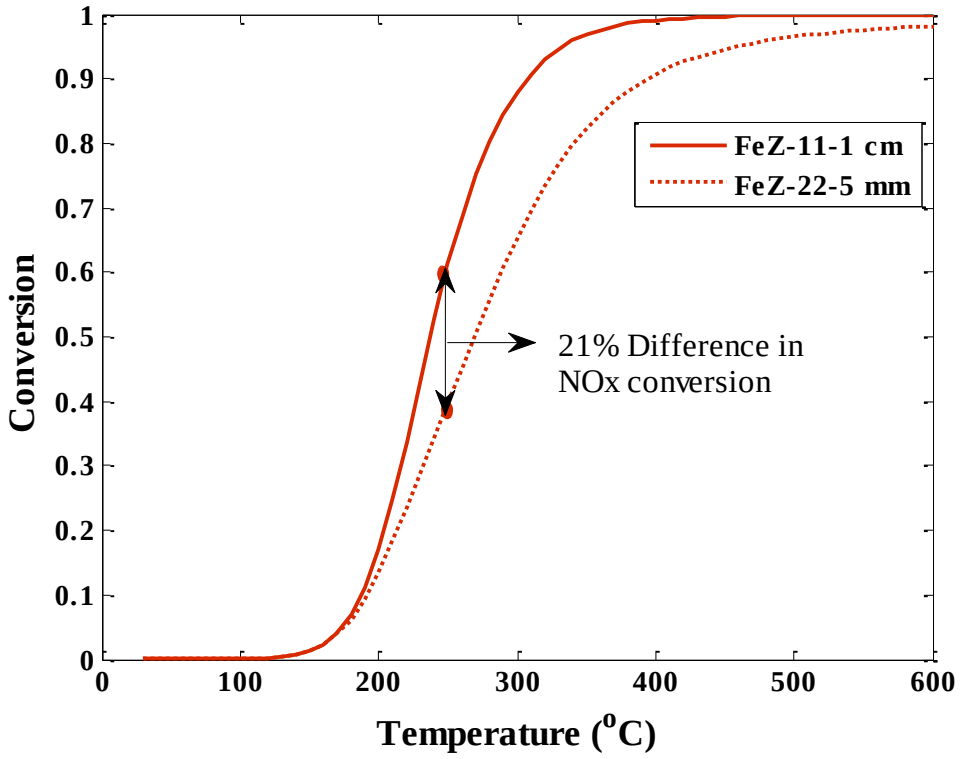

Figure 6-13: Model predictions of steady state NOx conversions for the NO_2 SCR reaction studied on in-house synthesized FeZ-XX catalysts.

The experimental study was continued on Cu-zeolite catalysts. Same catalyst system (2 cm long CuZ-10 and 1 cm long CuZ-20 catalysts, 9 channels), described earlier for the fast SCR reaction studies on Cu-zeolite catalysts, was used here. The reaction was studied in the presence of 2% water. O_2 was deliberately avoided as it does not play any role in the kinetics of NO_2 SCR reaction (findings from our current ongoing study). If O_2 is present, it leads to the NH_3 oxidation side reaction at higher temperatures ($\geq$ 400 ^oC) which results in decreasing NOx conversions and hence was not included as a feed. The results obtained with Cu-zeolite catalysts are summarized in Figure 6-14. These results follow similar trends as that of Fe-zeolite catalysts and show the presence of diffusion limitations throughout the temperature range.

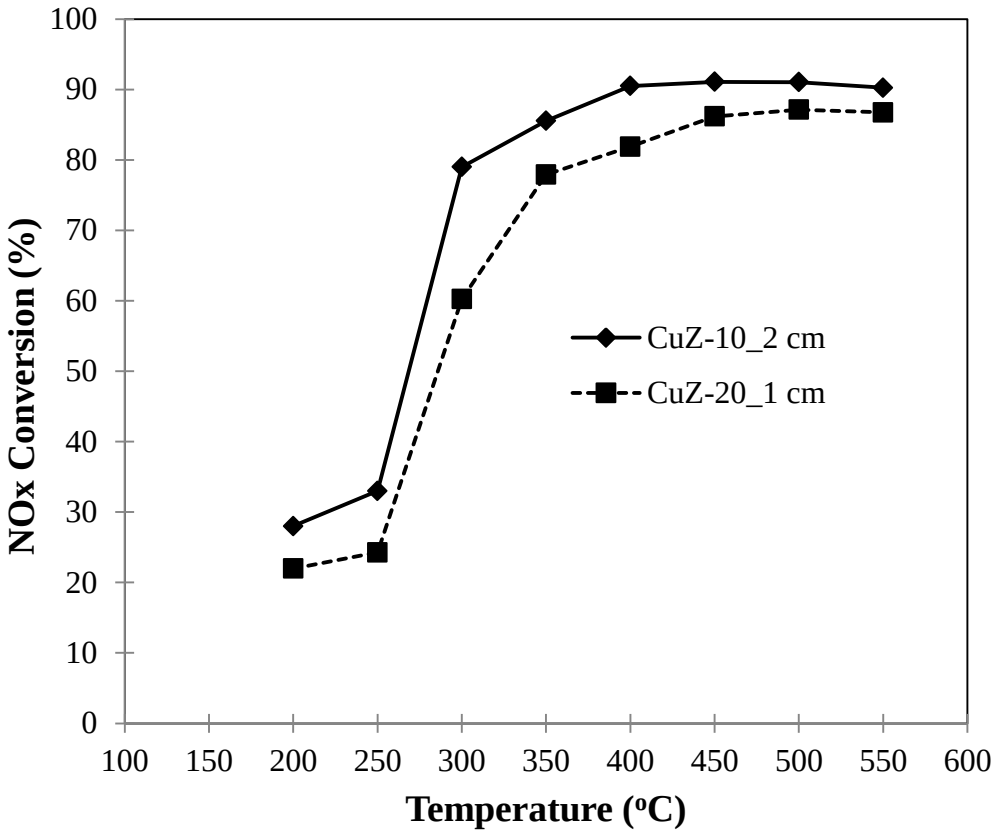

Figure 6-14: Steady state NOx conversions obtained during the NO_2 SCR reaction studied on in-house synthesized CuZ-XX catalysts. Feed: 500 ppm NO_2, 500 ppm NH_3, 2% water. Catalyst properties: No. of channels: 9; Length: CuZ-10: 2 cm, CuZ-20: 1 cm.

All the above experimental findings clearly show the presence of internal mass transfer limitations for all the SCR reactions for intermediate temperatures. For NH_3 oxidation and standard SCR reactions, these diffusion limitations were observed for intermediate temperatures (300-450 ^oC). But for fast and NO_2 SCR reactions, these diffusion limitations were observed over a broader temperature range window (200-550 ^oC). Comparable values of characteristic time constants for reaction, internal mass transfer and external mass transfer show the importance of all these process in the intermediate temperature range. Theoretical calculations presented in the earlier part of this chapter help in explaining the experimental findings.

These findings indicate the necessity of inclusion of mass transfer limitations in SCR modeling, catalyst design and optimization. A commercial catalyst used as a catalytic converter is about 15 cm long. If catalyst deposition is increased on a fixed length of catalytic converter to enhance the NOx reduction (or CO or hydrocarbon oxidation (in diesel oxidation catalyst (DOC) unit)) rates, then diffusion may emerge and the reactor would not meet the expected conversion. For this purpose, a longer catalyst piece with optimum washcoat thickness would be desired as the catalyst would be distributed over the entire length. This would maximize the use of catalyst present in a catalytic converter. This emphasizes on the importance of mass transfer studies during the design of commercial catalysts.

6.5 Conclusions

We carried out a systematic experimental study of various SCR (of NOx with NH_3) reactions on Fe-zeolite and Cu-zeolite catalysts in order to investigate the extent of washcoat diffusion limitations. This study is focused on an in-depth investigation of washcoat diffusion and external mass transfer limitations for various SCR reactions on both the Fe-zeolite and Cu-zeolite catalysts. A simple isothermal monolith model was used to validate our approach of using washcoated monoliths of varying washcoat loadings and lengths to check for the existence of mass transfer limitations. To this end, washcoated monolith catalysts of varying washcoat loadings, washcoat thicknesses and lengths were synthesized.

The presence of washcoat diffusion limitations for ammonia oxidation reaction are explicitly shown on both the Fe-zeolite and Cu-zeolite catalysts. Ammonia oxidation

was seen to be more pronounced on Cu catalysts and diffusion limitations become important at lower temperatures compared to Fe-zeolites. The diffusion limitations were confirmed for the standard SCR reaction on both the catalysts. For Fe-zeolite, these limitations were found to be important in the temperature range of 350-500 ^{o}C. However for Cu-zeolite, the rate of standard SCR reaction was higher compared to Fe-zeolite and the diffusion limitations were observed at earlier temperatures starting at 250 ^{o}C. A similar study on NO oxidation reaction showed that the diffusion limitations were negligible for this reaction. NO oxidation is a slower reaction than the standard SCR reaction. Moreover, it is reversible reaction and the reverse NO_2 decomposition commences at temperatures where diffusion limitations were observed for the standard SCR reaction. Both the fast and NO_2 SCR reactions, being very fast, show the presence of washcoat diffusion limitations throughout the temperature range of interest. Theoretical calculations of characteristic times for various mass transfer processes and Weisz-Prater modulus support our experimental findings. Also, a representative case of NO_2 SCR reaction is shown which predicts the effects of washcoat diffusivity and temperatures on the regime transitions (from kinetic to washcoat diffusion to external mass transfer). Fast and NO_2 SCR reactions were found to be mainly in mixed regimes where washcoat diffusion plays a significant role. A simple isothermal model qualitatively predicts the experimentally observed trends of differences in NOx reduction activities on catalysts with different lengths and washcoat loadings.

CHAPTER 7 Selective Catalytic Reduction of NOx on Combined Fe- and Cu-Zeolite Monolithic Catalysts: Sequential and Dual Layer Configurations

7.1 Introduction

Selective catalytic reduction (SCR) of NOx with NH_3 is now the preferred technology to achieve the large NOx reductions mandated for medium and heavy-duty vehicles. As discussed in earlier chapters, the recent SCR catalysis research is now focused on Fe- and Cu-based zeolite catalysts, both of which have demonstrated very high NOx reduction efficiencies at high space velocities. Cu-based catalysts are particularly effective at lower temperatures ($\leq$ 350 ^{o}C) [87, 89, 102, 111] which is desirable for vehicles that operate at low load for a large fraction of their use. Moreover, NOx removal efficiencies on Cu-based catalysts are found to be rather insensitive to the amount of NO_2 in the feed at lower temperatures [87, 117]. On the other hand, Fe-based catalysts are active at higher temperatures (> 350 ^{o}C) and give very high NOx reduction efficiencies even at very high temperatures (up to 600-700 ^{o}C) [29, 37-39, 103]. The presence of feed NO_2 accelerates the NOx conversion on Fe-zeolite catalysts, particularly at lower temperatures [29, 39, 87].

The catalytic reactions occurring during SCR have been extensively studied in the literature on the aforementioned vanadia, Fe-zeolite, and Cu-zeolite catalysts. There are three SCR reactions defined according to the composition of the feed NOx (NO + NO_2). Each is catalyzed by either Fe- or Cu-zeolite materials and are highlighted below.

Standard SCR: This reaction involves NO and NH_3 reacting in the presence of O_2,

$$4\ NH_3 + 4\ NO + O_2 \rightarrow 4\ N_2 + 6\ H_2O \qquad \Delta H = -\ 4.07 \times 10^5\ J/mol\ NH_3. \qquad (7\text{-}1)$$

Fast SCR: This reaction is called the "fast SCR" reaction (7-2) because it has a much higher rate than the standard SCR reaction (7-1) due to the presence of NO_2 in the feed,

$$2\ NH_3 + NO + NO_2 \rightarrow 2\ N_2 + 3\ H_2O \qquad \Delta H = -3.78 \times 10^5\ J/mol\ NH_3. \qquad (7\text{-}2)$$

NO_2 SCR: This involves reaction between NH_3 and NO_2 and is given by

$$4\ NH_3 + 3\ NO_2 \rightarrow 3.5\ N_2 + 6\ H_2O \qquad \Delta H = -3.41 \times 10^5\ J/mol\ NH_3. \qquad (7\text{-}3)$$

An important side reaction is the oxidation of NH_3 by O_2. This reaction is undesirable since NH_3 is the reductant of NOx. Both Fe- and Cu-zeolites catalyze the NH_3 oxidation to N_2,

$$4\ NH_3 + 3\ O_2 \rightarrow 2\ N_2 + 6\ H_2O \qquad \Delta H = -3.12 \times 10^5\ J/mol\ NH_3. \qquad (7\text{-}4)$$

Ammonia oxidation has been well studied on various zeolite catalysts in the literature [44, 134]. Fe- and Cu-zeolite catalysts have been found to be highly selective in oxidizing NH_3 to N_2. For Fe-zeolite catalysts, NH_3 oxidation starts at higher temperature (300 ^oC) and is slower compared to that on Cu-zeolite (ca. 250 ^oC). The consumption of NH_3 on Cu-zeolites is significant and leads to a sharp decrease in NOx conversion activity at high temperatures [87, 89]. In contrast, NH_3 oxidation is less pronounced on Fe-based zeolites, becoming important only at very high temperatures. Other side reactions like NO oxidation, ammonium nitrate formation and its decomposition to N_2O also take place on these catalysts [33].

Given the differences in activities of the Cu- and Fe-based catalysts, it seems plausible that a combination of Fe-zeolite and Cu-zeolite catalysts might achieve high NOx conversions over a broader temperature range than the individual catalysts. A few literature studies considered such combined Fe- and Cu-zeolite systems [200, 201]. Krocher et al. [200] studied various combinations of Fe-zeolite, Cu-zeolite and

V_2O_5/WO_3-TiO_2 and found that a Fe-zeolite section followed by a Cu-zeolite (in series) gives higher NOx conversion efficiencies. Girard et al. [201] carried out similar studies on combinations of Fe- and Cu-zeolite monolith catalysts and came to the same conclusion. In their study, they found that the series combinations of (33%) Fe-zeolite followed by (67%) Cu-zeolite give the highest NOx reduction efficiency throughout the temperature range. Similar studies of a series arrangement of Fe- and Cu-zeolite catalysts with different individual catalyst lengths were carried out by Theis et al. [202]. In an actual diesel engine exhaust aftertreatment system, an SCR unit is preceded by a diesel oxidation catalyst (DOC) unit, which had the function of oxidizing hydrocarbons to CO_2 and H_2O and NO to NO_2. The NO oxidation generated the NO_2 needed to increase the effectiveness of the downstream SCR. However, the high cost of Pt is a major issue for the DOC unit. It is therefore of practical interest to develop alternative, more cost-effective SCR catalysts that can achieve high NOx removal efficiencies with a reduced reliance on NO_2 generation using expensive precious metals (e.g., Pt).

The approach of combining two or more distinct catalysts to achieve improved performance has been considered in other reaction systems [203-205]. Xu et al. [204] used a physical mixture of zeolites with Na-rich Fe-Cu Fischer-Tropsch catalysts to get improved activity for the hydrogenation of carbon dioxide. A few other studies [205-208] reported the use of so-called dual-layer monolithic catalysts for the SCR of NOx with hydrocarbons (e.g., propene) as reducing agents. The particular catalyst had a Pt/Al_2O_3 or Pt/SiO_2 in the bottom layer and H- or Cu-zeolite (ferrierite or ZSM-5) in the top layer. The idea was to use the precious metal (e.g., Pt/Pd) in the bottom layer to oxidize NO to NO_2 which then diffuses back to get reduced by hydrocarbons (e.g., propene) in the upper

layer containing a zeolite. The dual layer catalysts were found to be superior for NOx reduction compared to the single layer catalyst (e.g., Pt/SiO_2). To our knowledge no literature study has focused on such dual layer catalyst configurations using NH_3 as a reductant.

The objective of the current study is to determine if a dual-layer Fe/Cu zeolite catalyst can exhibit improved performance for lean NOx reduction. To this end, we examine in detail various combinations of sequential brick and dual-layer catalysts. Our approach is to systematically vary the lengths of the Fe- and Cu-zeolite monoliths in order to identify superior axial configurations, along the lines of the aforementioned pioneering studies at Ford [201]. Various catalysts are then tested in terms of NOx removal efficiencies during the standard SCR reaction. Several dual layer catalysts having different washcoat loadings of Fe- and Cu-zeolite catalysts are compared for the standard and fast SCR reactions. The findings are interpreted in terms of the current understanding of lean NOx reduction on zeolite-based catalysts.

7.2 Experimental

7.2.1 Catalyst Preparation: Ion Exchange

We used both commercial and in-house synthesized Cu- and Fe-zeolite monolithic catalysts. The commercial Cu-zeolite catalyst was supplied by BASF (Iselin, NJ). It is a small-pore Cu-chabazite type catalyst, established in patents and communicated in recent papers to possess excellent hydrothermal stability [125-127]. More detail about the synthesis and structure of this Cu-chabazite catalyst can be found in [127]. The Cu loading was about 2.5%. The commercial washcoated Fe-zeolite (ZSM-5

type) catalyst was supplied by Umicore Autocat USA Inc. The sample had a Fe loading of about 3 wt.% in the monolith washcoat. Both the commercial samples had a cell density of 400 cpsi and effective washcoat thickness of about 45-50 microns. Additional washcoated monolith catalysts were synthesized in-house using catalyst powder. Fe-zeolite (ZSM-5) powder with Fe-content of about 3% (by wt.) was provided by Sud-Chemie (Munich, Germany) while the Cu-zeolite (ZSM-5) powder was synthesized by a conventional ion-exchange process briefly described below. Cordierite monolith cores (400 cpsi) were used as the support.

For the in-house synthesized Cu-ZSM-5 catalysts, the NH_4^+ form of zeolite (NH_4-ZSM-5, Sud-Chemie Munich, Germany) powder with a Si/Al ratio of 25 was used as the starting material. The NH_4-ZSM-5 powder was calcined in a box furnace at 500 ^oC for 5 hours to convert it to H-ZSM-5. The H-ZSM-5 powder was then ion-exchanged with 0.1 M $NaNO_3$ solution by continuously stirring for several hours. The Na-ZSM-5 powder, thus obtained, was filtered and dried. The ion-exchange with the Na^+ solution was repeated twice. The Na-ZSM-5 powder was then ion-exchanged with 0.02M copper acetate solution. This step was carried out by continuous stirring of the solution for 24 hours followed by filtration and drying. This step was repeated twice to get the final Cu-ZSM-5 powder which was then calcined for 5 hours at 500 ^oC [89]. The Cu content of the in-house synthesized Cu-ZSM-5 powder was found to be about 2% (by wt) with inductive coupled plasma- atomic emission spectroscopy (ICP-AES) analysis. The basic zeolite type (ZSM-5) was the same for all the above Fe- and Cu-zeolite catalysts (except Cu-chabazite) used in this study and these catalysts have a BET surface area of about 350 m^2/g .

7.2.2 Catalyst Preparation: Monolith Washcoating

Catalysts prepared and evaluated in this study are summarized in Table 7-1. We used a dip-coating method to deposit catalyst on the monolith pieces. Blank cordierite monolith samples with cell density of 400 cpsi and dimensions of 1 inch diameter by 3 inch length were supplied by BASF. In Table 7-1 the CuZ-XX and FeZ-XX nomenclatures are used to define catalyst properties. "–XX" denotes the weight % of zeolite loading on the blank monolith support after drying. The monolith washcoating technique was the same as described in our earlier study [103]. A catalyst slurry consisting of a mixture of zeolite powder, γ–alumina and water was prepared in the proportions 32 wt.% zeolite, 8 wt.% alumina, with the remainder water with a small amount of 0.1 N acetic acid added to obtain a pH of 3.5. Alumina served as the binder. The catalyst slurry was ball milled for 20 hours to obtain a particle size in the range of 1-5 μm, a necessary step to obtain a more uniform washcoat. Multiple dip coating steps were needed to achieve a prescribed loading (based on weight %). After each dipping, air was blown through the monolith channels to remove excess slurry, and then the washcoated monolith piece was dried at around 120 ^{o}C for 1 hour. Drying removes the water and gives an idea about the catalyst loading. After the desired catalyst coating/loading was achieved, the washcoated monolith sample was calcined at 500 ^{o}C for 5 hours.

Table 7-1: Following catalysts were used to study the standard and fast SCR reaction.

Catalyst	Catalyst Description	~ Cu-Zeolite loading (wt. %)	~ Fe-Zeolite loading (wt. %)
A	Commercial Cu-zeolite (BASF)	23	0
B	Commercial Fe-zeolite (Umicore)	0	24
C	CuZ-12 on Catalyst B	12	24
D	FeZ-12 on Catalyst A	23	12
E	CuZ-25	25	0
F	FeZ-24	0	24
G	Combined FeCuZ-24 catalyst	12	12
H	CuZ-13 on FeZ-12	13	12
I	FeZ-16 on CuZ-8	8	16
J	FeZ-12 on CuZ-12	12	12
K	FeZ-8 on CuZ-16	16	8
L	FeZ-15 on CuZ-15	15	15
M	FeZ-10 on CuZ-20	20	10

Dual-layer catalysts were prepared as follows. The same Cu-ZSM-5 and Fe-ZSM-5 slurries were used to synthesize all the CuZ-XX and FeZ-XX catalysts (Table 7-1). To obtain the Cu-ZSM-5 layer on the commercial Fe-zeolite catalyst (Catalyst B), Cu-ZSM-5 slurry was deposited using the dip-coating technique. This resulted in Catalyst C comprising a CuZ-12 layer on the commercial Fe-zeolite. Similarly, in order to deposit a Fe-ZSM-5 layer on the commercial Cu-zeolite (catalyst A), Fe-ZSM-5 slurry was deposited in the prescribed number of times and the same 12 wt.% loading of the top layer was achieved; this was Catalyst D. Catalysts E and F were obtained by repeating the

dip coating till the desired 24-25 wt.% loading was achieved. For catalyst H, first the FeZ-12 layer was deposited on a blank monolith support followed by the deposition of the CuZ-13 layer. For the rest of the dual layer catalysts (I-M), first a CuZ-XX layer was deposited on the blank monolith support followed by the deposition of a FeZ-XX layer. In order to avoid the possible leaching of metal from the underlying layer during the coating of a second layer, we dried and calcined the catalyst with the first layer completely at 500 ^{o}C. Only then was the second layer was deposited. Finally, the washcoated catalysts were subjected to calcination at a very slow temperature ramp of ca. 23 ^{o}C/hr up to and maintained at 500 ^{o}C for 5 hours. This deliberate calcination reduced the likelihood of crack formation in the washcoat layer.

The hydrothermal stability of the dual-layer catalysts (L and M) was evaluated. The catalysts were subjected to two different temperatures of 600 ^{o}C and 700 ^{o}C for 6 hours in the presence of 5% feed water and Ar as a balance gas. These are typical catalyst degreening (or aging, if for very long time) conditions. The standard SCR experiments were then repeated on catalysts L and M and results were compared to that obtained before the catalyst aging/degreening.

In order to investigate the issue of possible migration and hence mixing of the Fe and Cu metals from one layer to another at higher temperatures, we carried out energy dispersive spectroscopy (EDS) (JEOL JSM-6330F) analysis of both the fresh and the degreened (or aged) samples. For this purpose, we selected six different points along the corner of the washcoated monolithic catalyst channel where the washcoat was thicker and two different points near the center of the channel where the washcoat was thinner. At these points we investigated the presence of various metal elements using EDS analysis.

7.2.3 Bench-Scale Reactor Set-up

The experimental setup included a gas supply system, a reactor system, an analytical system and a data acquisition system. Details of the apparatus are described elsewhere [139]. A monolith catalyst wrapped with a ceramic fiber was placed inside a quartz tube reactor mounted in a tube furnace. The quartz tubes used for this study were 40.6 cm long with an internal diameter of 0.81 cm and an outer diameter of 1.27 cm. In most of the experiments, we used 2 cm length and 34 channels of the monolith piece. This corresponds to a gas hourly space velocity (GHSV) (represented as the ratio volumetric flow rate calculated at standard temperature and pressure to the monolith brick volume) of 57,000 hr^{-1}. The typical gas linear velocity during the experiments was calculated as a function of temperatures and was found to be in the range of 0.6-1.2 m/s. The furnace temperature was adjusted with a temperature controller. A FT-IR spectrometer (Thermo-Nicolet, Nexus 470) was placed downstream of the reactor to analyze various effluent gases including NH_3, NO, NO_2, N_2O and H_2O. A quadrupole mass spectrometer (QMS; MKS Spectra Products; Cirrus LM99) was used to measure N_2.

7.2.4 Steady State Experiments

Several steady-state experiments were carried out on the catalysts described in Table 7-1. The experiments included NH_3 oxidation, standard SCR and fast SCR reactions. The space velocity was fixed at the same 57,000 hr^{-1} unless otherwise noted; Argon (Ar) was used as a balance gas and the total flow rate was maintained constant at 1000 sccm. Prior to reaction, each catalyst was exposed to 5% O_2 in Ar at 500 ^oC

temperature for 30 minutes. The catalyst temperature was then reduced down to ambient temperature before each experiment was started. All the experiments were carried out in the temperature range of 150-550 ^{o}C and sufficient time was given to reach the steady state effluent concentrations.

The NH_3 oxidation reaction was studied on catalysts A and B of different lengths. The feed consisted of 500 ppm NH_3, 5% O_2 and 2% water. The standard SCR reaction was studied on all the catalyst samples listed in Table 7-1. For catalysts A and B, different lengths in the range of 4 mm to 2 cm were used to examine the effect of contact time. The space velocity was 57,000 hr^{-1} for the shorter catalyst piece (1 cm) and 114,000 hr^{-1} for the longer catalyst piece (2 cm). This helped in obtaining conversion data as a function of catalyst length. The standard SCR feed consisted of 500 ppm NO, 500 ppm NH_3, 5% O_2 and 2% water for all the experiments.

The effect of feed NO_2 was studied on catalysts A, F and K by using a feed consisting of an equimolar mixture of NO and NO_2 (250 ppm each), 500 ppm NH_3, 5% O_2 and 2% water in the temperature range of 180 – 550 ^{o}C. Finally, we used Fe-zeolite catalysts of different washcoat loadings, different washcoat thicknesses and lengths to study the existence and extent of mass transfer limitations during the standard and fast SCR reactions.

7.3 Results and Discussion

Before presenting the data for the dual layer catalysts, representative results are reported for the single-layer commercial catalyst to establish conversion trends with

temperature and space velocity. These data were also useful for justifying and interpreting the subsequent sequential Fe/Cu monolith configurations.

7.3.1 Ammonia Oxidation: Catalyst Type and Length Effects

NH_3 oxidation reaction was carried out on both the Fe- and Cu-zeolite commercial catalysts using two different catalyst lengths (1 and 2 cm). These experiments identified the conditions (temperature, space velocity) needed to achieve a prescribed conversion. Figure 7-1 clearly shows that the commercial Cu-zeolite (Cu-Z) is more active than the commercial Fe-zeolite (Fe-Z). While the metal loadings are not the same and the zeolites are different types, the trends are nevertheless consistent with those reported in previous studies [87, 89, 103]. On the 2 cm long Cu-Z (Fe-Z) catalyst the reaction commenced at about 200 ^{o}C (250 ^{o}C). Nearly complete NH_3 conversion was achieved at about 450 ^{o}C for Cu-Z (catalyst A), while only 88% conversion was achieved on Fe-Z (catalyst B) at 550 ^{o}C. On Cu-Z, a length of 2 cm provided sufficient contact time to achieve a high NH_3 conversion by 400 ^{o}C. The results show that for temperatures exceeding 400 ^{o}C up to half of the catalyst (A) was unused.

The results for the commercial Fe-zeolite catalyst (B) using pieces of two different lengths (1 and 2 cm) exhibited somewhat different behavior (Figure 7-1). Unlike Cu-Z, the conversion never reached 100% for temperatures up to 550 ^{o}C. A noted difference in conversion was observed for the catalysts of 1 and 2 cm length for temperatures below 550 ^{o}C. At 550 ^{o}C, there was a slight difference in conversions obtained on the two catalysts with different lengths.

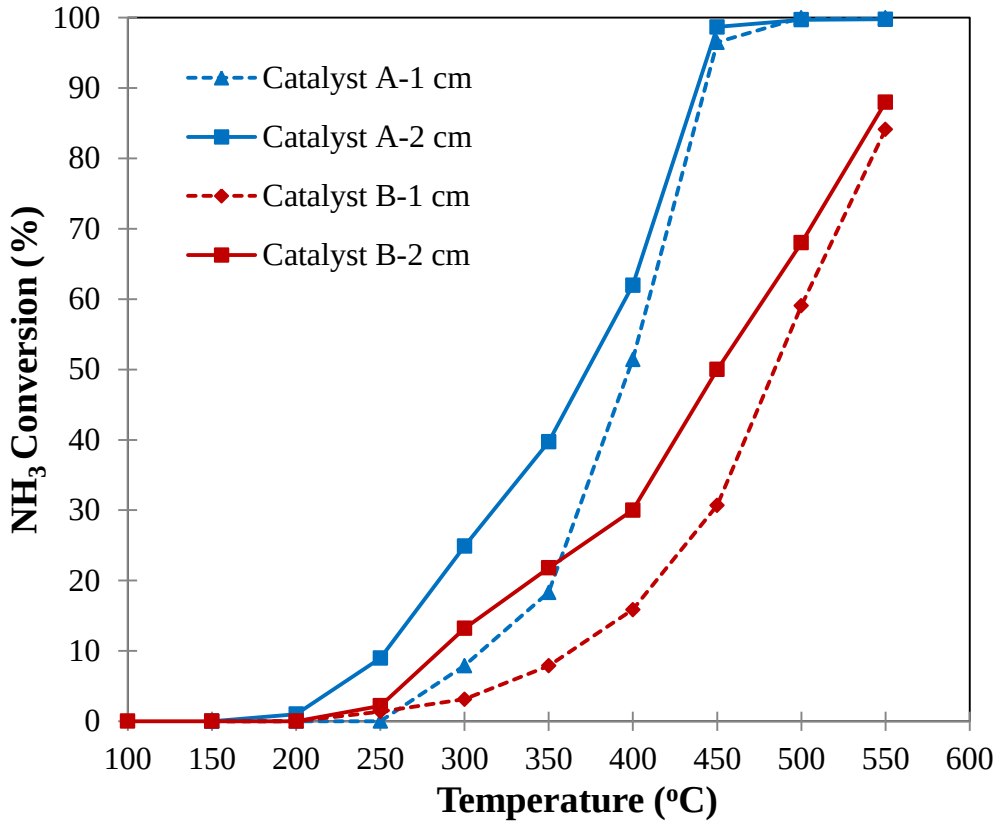

Figure 7-1: Steady state NH_3 conversions obtained during the NH_3 oxidation reaction studied on Cu-(catalyst A) and Fe-zeolite (catalyst B) catalysts. Space velocity: 57,000 hr^{-1} (2 cm) and 114,000 hr^{-1} (1 cm). Feed: 500 ppm NH_3, 5% O_2, 2% water.

7.3.2 Standard SCR: Catalyst Type and Length Effects

The standard SCR reaction (reaction (7-1)) utilized NO, NH_3 and O_2 in the feed stream. All of the catalysts listed in Table 7-1 were used in this part of the study. First we compared the effect of monolith length on the NOx conversion for the commercial Cu- and Fe-zeolite catalysts (A and B). The steady state NOx conversions obtained on Cu-zeolite catalysts with two different lengths of 1 and 2 cm are compared in Figure 7-2a. The data indicate that the Cu-zeolite shows very high NOx reduction activity even at low temperature. For example, the NOx conversion approached 68% for the 2 cm long catalyst at 200 ^oC and was essentially 100% in the temperature range of 250-350 ^oC.

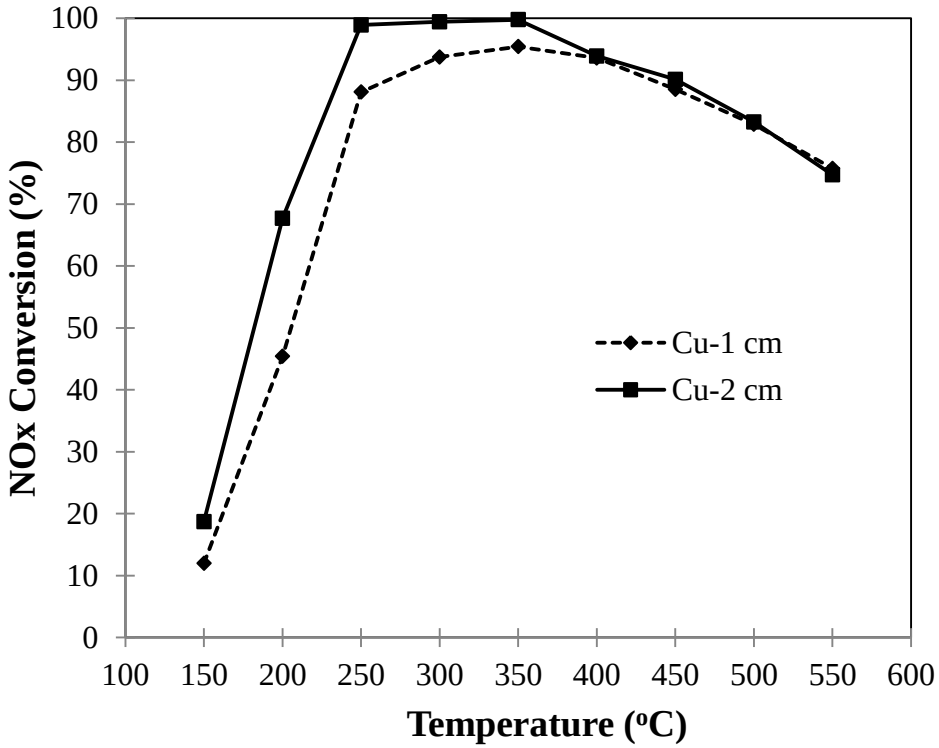

Figure 7-2a: Steady state NOx conversions obtained during the standard SCR reaction studied on commercial Cu-zeolite catalyst (A). Space velocity: 57,000 hr^{-1} (2 cm) and 114,000 hr^{-1} (1 cm). Feed: 500 ppm NO, 500 ppm NH_3, 5% O_2, 2% water.

Beyond this range the NOx conversion decreased. This decrease is attributed to the oxidation of the reductant NH_3, which we have shown in earlier experiments achieve a high conversion at these conditions (Figure 7-1). Figure 7-2b shows that there is an absence of NH_3 in the effluent for the 2 cm Cu-Z catalyst (A) (100% conversion at $T \geq 250\ ^oC$) and confirms the complete consumption of feed NH_3 by the NH_3 oxidation side reaction. The same standard SCR experiments on the shorter, 1 cm long Cu-zeolite catalyst resulted in lower NOx conversions for temperatures below 250 ^oC. However, for temperatures beyond the conversion maximum, there was little effect of the catalyst length. This clearly indicates that a 1 cm catalyst provides sufficient residence time to obtain the high NOx conversion at that temperature and that a large fraction of the 2 cm catalyst was not needed. The depletion of NH_3 (by oxidation) is undoubtedly responsible

for the near coincidence in the conversions for the two catalysts beyond the conversion maxima.

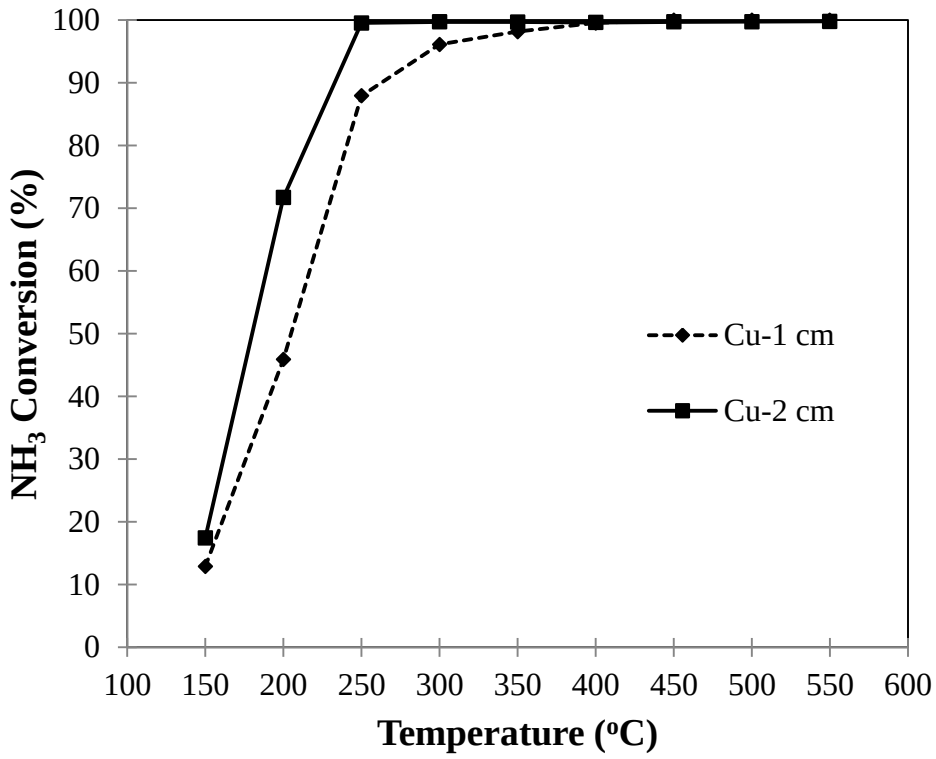

Figure 7-2b: Steady state NH_3 conversions obtained during the standard SCR reaction studied on commercial Cu-zeolite catalyst (A). Space velocity: 57,000 hr^{-1} (2 cm) and 114,000 hr^{-1} (1 cm). Feed: 500 ppm NO, 500 ppm NH_3, 5% O_2, 2% water.

The consumption of NH_3 by oxidation increases the reactor length needed to achieve complete NOx conversion. Balakotaiah et al. [191] derived various correlations to estimate the limiting reactant conversion in various catalytic monoliths of arbitrary shapes and found that the conversion depends mainly on the transverse Peclet number (*P*) when the flow is fully developed and the reaction is fast. An estimate of the *P* enables one to determine the upper bound of the conversion for a single irreversible reaction operated in the mass transfer controlled regime. That is, the upper bound value approaches 99^+ % as *P* decreases. *P* is defined as

$$P = \frac{R_{\Omega 1}^2 \langle u \rangle}{L D_f}, \qquad (7\text{-}5)$$

where $R_{\Omega 1}$ is the effective transverse diffusion length scale, $\langle u \rangle$ is the average velocity inside monolith channel, L is the length of the monolith channel and D_f is the diffusivity of a species in fluid phase. A typical value of P is about 0.06 for most of our experiments using monolithic catalyst of 2 cm length. The value of P increases with decreasing catalyst length or increasing space velocity. According to the correlations provided by Balakotaiah et al. [191], nearly complete reactant conversion can be achieved even with a P value of 0.4. Using these correlations, we estimated that 2 mm of catalyst length (for a monolith with 34 channels) would be sufficient to approach complete NOx conversion on

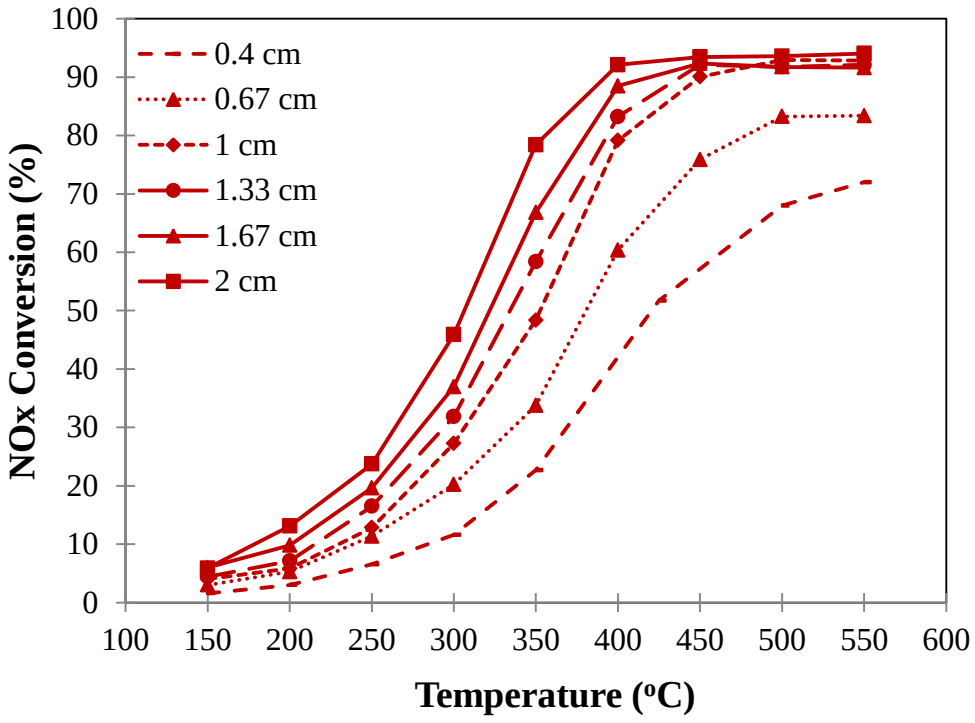

Figure 7-3a: Steady state NOx conversions obtained during the standard SCR reaction studied on the commercial Fe-zeolite catalyst (B) with different lengths in the range of 0.4 – 2 cm. Feed: 500 ppm NO, 500 ppm NH_3, 5% O_2, 2% water.

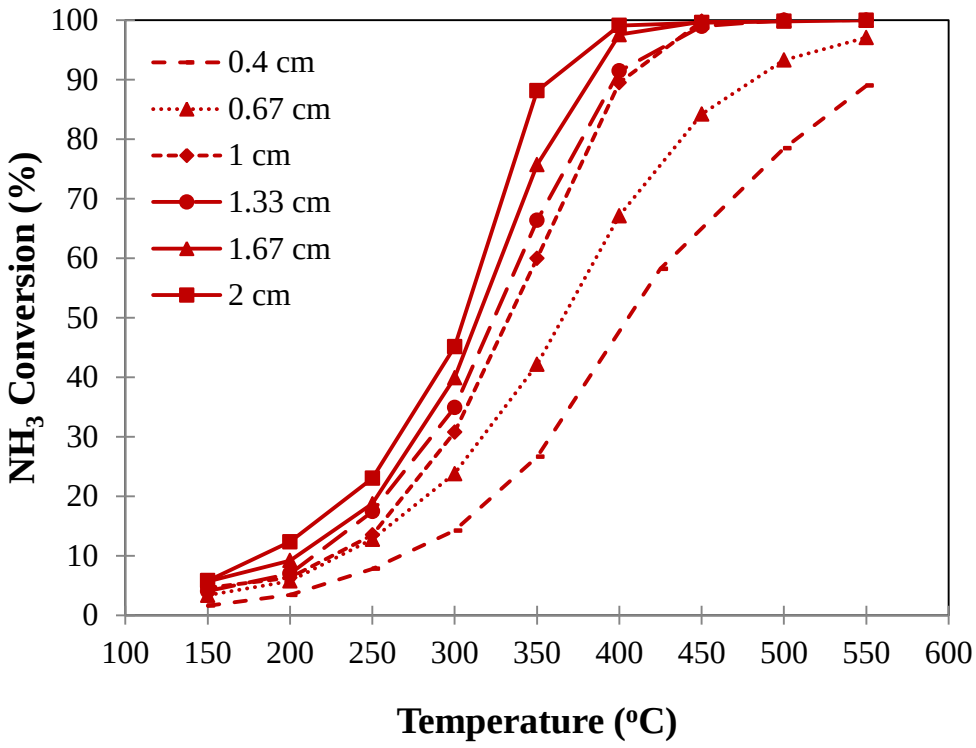

Figure 7-3b: Steady state NH_3 conversions obtained during the standard SCR reaction studied on the commercial Fe-zeolite catalyst (B) with different lengths in the range of 0.4 – 2 cm. Feed: 500 ppm NO, 500 ppm NH_3, 5% O_2, 2% water.

both the Cu- and Fe-zeolite catalysts as the reaction is very fast at these temperatures (at $T \geq 450\ ^{o}C$). This further confirms that the presence of the NH_3 oxidation side reaction reduces the NOx conversion (i.e., NH_3 is depleted) on both the catalysts.

The performance of the commercial Fe-zeolite catalyst was examined by measuring the NOx conversion during the SCR reaction for several different lengths (Figure 7-3a). Unlike the commercial Cu-zeolite, the activity of the Fe-zeolite was quite low for temperatures below 350 ^{o}C. There was also a substantial difference in the NOx conversion on catalysts with different lengths between 0.4 and 2 cm. At higher temperatures ($\geq 400\ ^{o}C$), the NOx conversions reached an asymptotic value of ~93% for the catalysts with lengths 1 cm and above. The data indicate that a 1 cm long Fe-zeolite catalyst would provide sufficient catalyst amount and contact time required to achieve the

desired NOx conversion at higher temperatures (> 350 ^{o}C) as the entire 2 cm length was not utilized. The NOx conversions never reached 100% because of the NH_3 oxidation side reaction which consumed the reductant NH_3. Figure 7-3b shows the steady state NH_3 conversions obtained during the above standard SCR experiments studied on Fe-zeolite catalysts of different lengths.

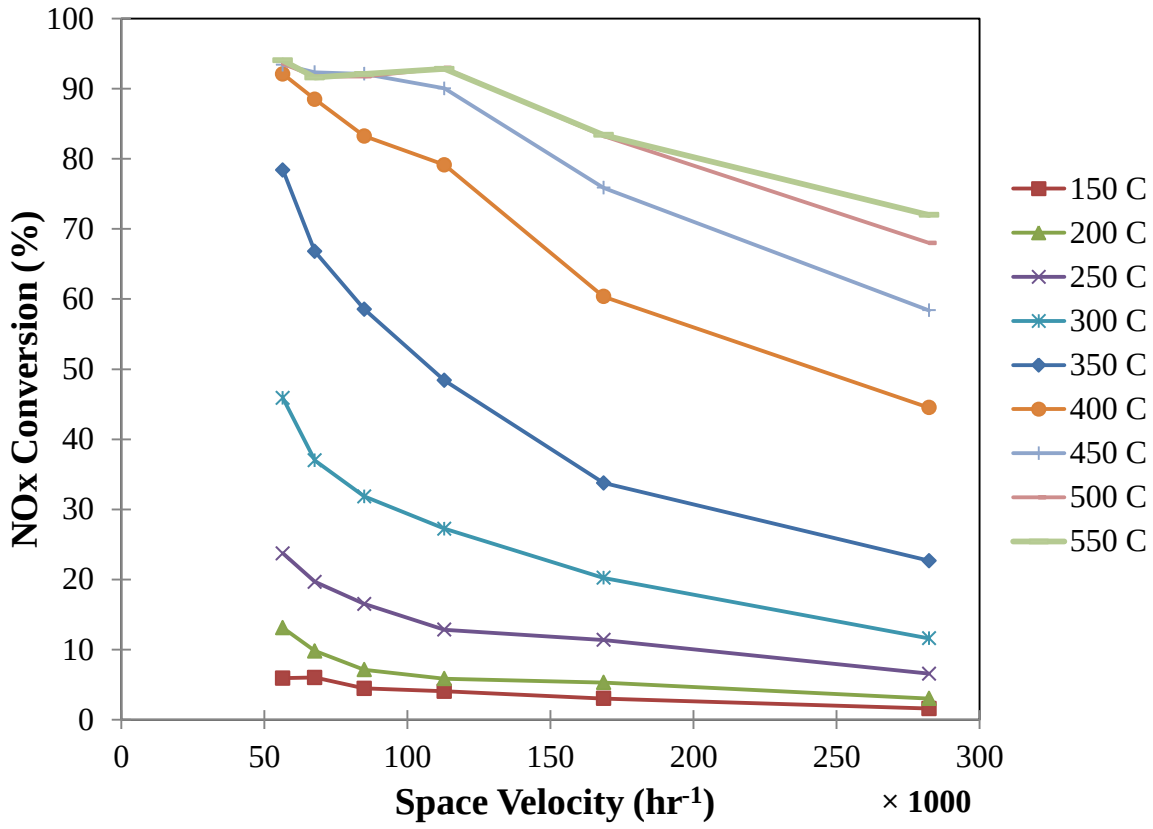

Figure 7-4: Steady state NOx conversions obtained during the standard SCR reaction studied on the commercial Fe-zeolite catalyst (catalyst B) as a function of space velocity (hr^{-1}).

In Figure 7-4, we represent the NOx conversion as a function of the space velocity for several catalyst temperatures. These results show that the NO conversion decreases with increasing space velocity and comparable NOx reduction activities were achieved for space velocities below 110,000 hr^{-1} at higher temperatures.

7.3.3 Fe- and Cu-Zeolite Series Arrangement

The data presented thus far show that the commercial Cu-zeolite catalyst is an effective NOx reduction catalyst at lower temperatures ($\leq$ 350 ^{o}C) while the commercial Fe-zeolite is superior at higher temperatures ($\geq$ 400 ^{o}C), in agreement with the literature studies [87, 117]. A Cu-zeolite catalyst of 1 cm length is sufficient to achieve a NOx conversion exceeding 90% at lower temperatures (250-350 ^{o}C). For the commercial Fe-zeolite catalyst, 1 cm length is sufficient to achieve 90% conversion in the higher temperature range (400-550 ^{o}C). These conversion versus volume performance data are utilized in the next set of experiments in which we examine series combinations of the two catalysts.

The first series monolith configuration considered was a Cu-zeolite followed by a Fe-zeolite. Specifically, a 1 cm long piece of the commercial Cu-zeolite (Catalyst A) was followed by a 1 cm long piece of commercial Fe-zeolite (B). The experimental conditions used previously for the individual catalysts were repeated here for the sequential configuration. The results provided in Figure 7-5 compare the 2 cm long Cu (1 cm)/Fe (1 cm) monolith series combination with the 2 cm long individual Cu-zeolite (A) and Fe-zeolite (B) samples. The sequential configuration exhibited behavior very similar to that of the Cu-Z (A) catalyst: a sharply increasing NOx conversion at low temperature (< 300 ^{o}C), a maximum NOx conversion exceeding 95% at intermediate temperature (300-350 ^{o}C) and a decreasing conversion at high temperature (> 400 ^{o}C). These data clearly indicate that, at low temperature, most of the NOx reduction occurs in the Cu-Z (A) section and that the Fe-Z (B) catalyst is not utilized. At higher temperature there is nearly

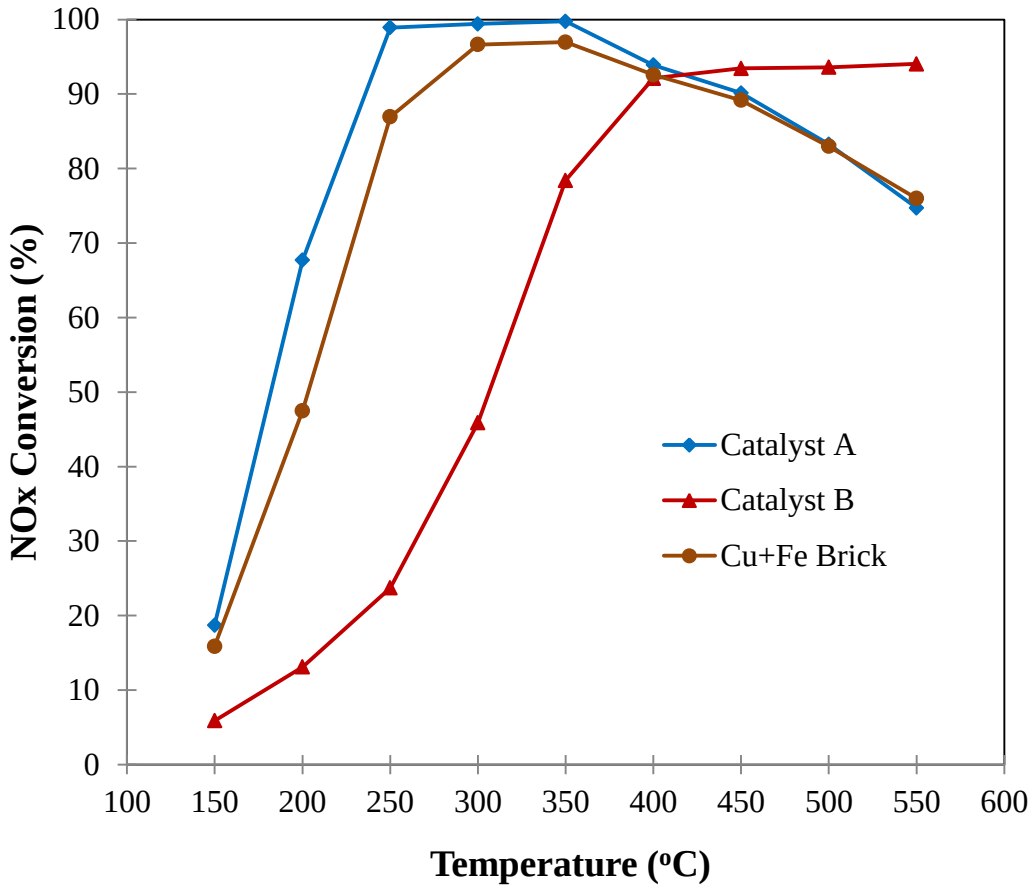

Figure 7-5: Steady state NOx conversions obtained during the standard SCR reaction studied on catalysts A, B and combined system of series arrangement of catalyst A (1 cm Cu brick in front) followed by catalyst B (1 cm Fe brick). Feed: 500 ppm NO, 500 ppm NH_3, 5% O_2, 2% water.

complete overlap of the conversions obtained for the Cu-Z/Fe-Z monolith and the Cu-Z (A) monolith. This suggests that the high rate of NH_3 oxidation on the Cu-zeolite prevents utilization of the Fe-zeolite section for NOx reduction. Thus, in effect, the Fe-zeolite section is not utilized over the entire temperature range. Therefore, a series catalyst configuration in which Cu-zeolite is followed by the Fe-zeolite does not improve the NOx reduction performance at high temperatures. For this reason we did not consider any other Cu-Z/Fe-Z combinations in subsequent experiments.

The results are more encouraging when the catalyst arrangement is reversed and the Fe-zeolite catalyst is positioned in front of the Cu-zeolite. Here we studied three different combinations for this Fe-Z/Cu-Z series arrangement. The total catalyst length was fixed at 2 cm while varying the individual lengths of Fe- and Cu-zeolite sections. Specifically, following three Fe-Z/Cu-Z series combinations were studied:

series 1: Fe (1.33 cm/ 67% of total length) + Cu (0.67 cm/ 33%),

series 2: Fe (1 cm/ 50%) + Cu (1 cm/ 50%),

series 3: Fe (0.67 cm/ 33%) + Cu (1.33 cm/ 67%).

Results obtained with these three series arrangements are shown in Figure 7-6. For comparison, the 2 cm long Cu-zeolite (catalyst A) and Fe-zeolite (catalyst B) monolith results are also provided. For Series 1, the NOx conversions exceeded the Fe-Z only conversion at lower temperatures ($\leq$ 350 ^{o}C) although the conversion was still considerably lower than the Cu-Z only catalyst (A). At higher temperatures ($\geq$ 400 ^{o}C), the conversion obtained for Series 1 was nearly identical to the Fe-Z only sample (catalyst B). For Series 2, the NOx conversion increased significantly at lower temperatures and remained close to that of the Fe-Z only catalyst at higher temperatures. For Series 3 these trends continued. The NOx conversion at low temperature approached that of the Cu-Z only catalyst without much loss in conversion at high temperature. These results show that the overall NOx conversion can be maintained at a relatively high level over a wide temperature range by utilizing a Fe-Z/Cu-Z series configuration. The findings are in agreement with earlier results of Girard et al. [201] and suggest that there exists an optimal Fe-Z/Cu-Z configuration in terms of NOx conversion for the standard SCR reaction. By positioning Fe-Z in front of Cu-Z, the high NOx reduction activity of

Fe-Z is exploited at high temperature while avoiding the detrimental NH_3 oxidation activity of Cu-Z. At low temperature the low activity of Fe-Z shifts the bulk of the NOx reduction downstream to the Cu-Z section.

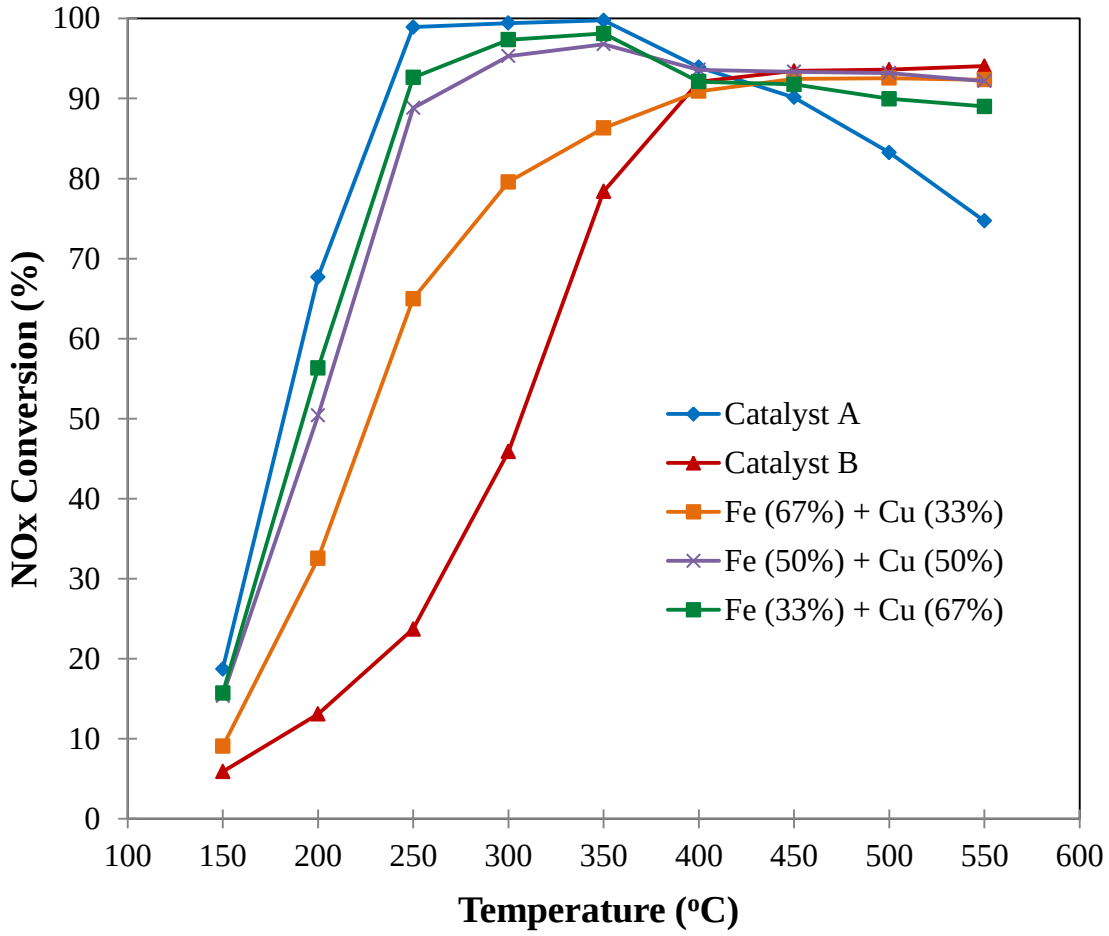

Figure 7-6: Steady state NOx conversions obtained during the standard SCR reaction studied on catalysts A, B, and combined system of series arrangement of catalyst B (in front) (1.33 cm, 1 cm and 0.67 cm bricks) followed by catalyst A (0.67 cm, 1 cm and 1.33 cm bricks).

7.3.4 Mixed Fe- and Cu-ZSM-5 Layer Monolith Catalyst

The series configuration results provided the incentive to explore a combination of the Fe- and Cu-zeolite catalysts in a layered structure. In Chapter 6, we have found that washcoat diffusion can limit the overall rate during standard-, fast- and NO_2-SCR [209]. Specifically, we have shown improved performance (conversion) when a fixed amount of

Fe- or Cu-zeolite is spread over a longer monolith. This provides incentive to pursue the dual layer strategy. In this section, we present results obtained on various in-house synthesized dual layer monolithic SCR catalysts.

In order to conduct a meaningful comparison our approach is to synthesize monolith catalysts having a fixed total washcoat loading (mass basis) and monolith length while varying the mass fractions of the Cu-ZSM-5 and Fe-ZSM-5. Then the conversion of NOx for each dual-layer catalyst is compared to the conversions obtained for the single layer Cu-ZSM-5 and Fe-ZSM-5 catalysts. The total washcoat loading was selected to be 24-25 wt.%. The metal loading for the Cu and Fe were fixed by using the same exchanged zeolite samples. All other experimental conditions were kept the same as described earlier.

First we show the results obtained for single-layer catalysts Cu-Z-25 (catalyst E) and Fe-Z-24 (catalyst F) of total length 2 cm. Figure 7-7 shows the NOx conversions obtained during the standard SCR reaction carried out on these catalysts. The NOx conversion trends obtained for catalysts E and F are comparable to the results obtained with the commercial catalysts A and B, respectively (Figures 7-2,7-3). The only difference is a slightly lower activity for the in-house synthesized catalysts. Also shown in Figure 7-7 is the NOx conversion for a mixed washcoat catalyst (G) for which the loading of Cu-ZSM-5 and Fe-ZSM-5 were identical (12 wt.%). This catalyst was prepared by coating a blank monolith with slurry containing a physical mixture of the two metal exchanged zeolites.

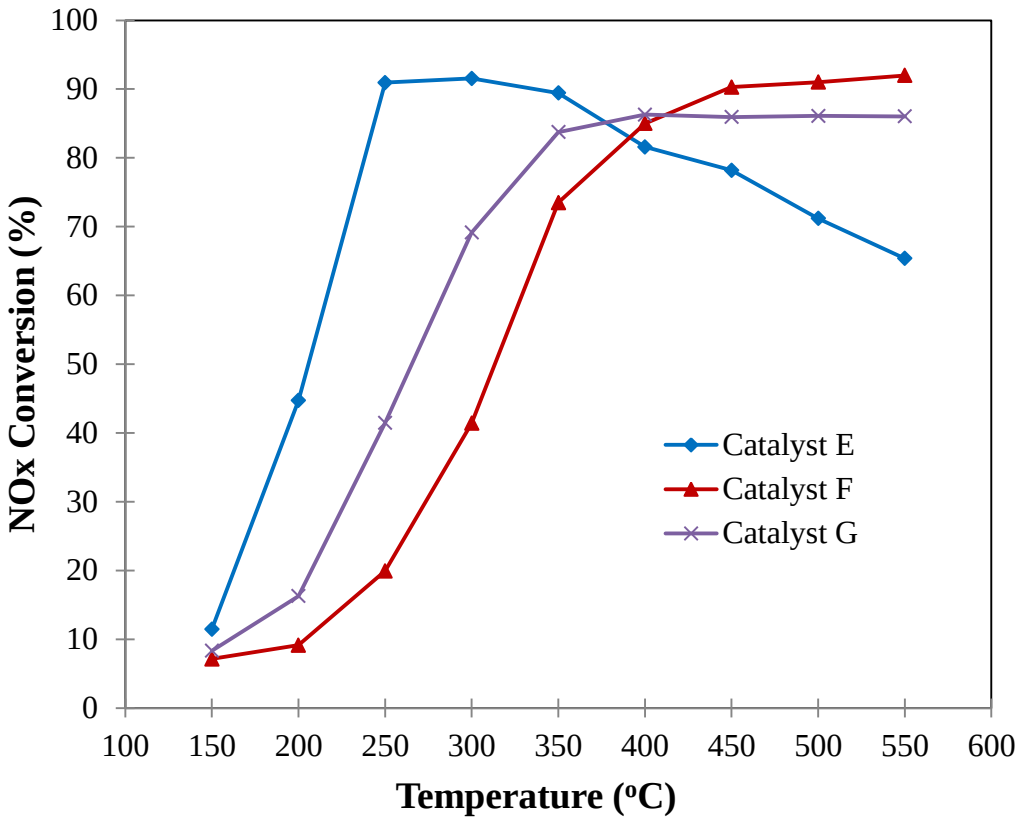

Figure 7-7: Steady state NOx conversions obtained during the standard SCR reaction studied on lab-synthesized catalysts E, F and G. Total length of the monolithic reactor: 2 cm. Feed: 500 ppm NO, 500 ppm NH_3, 5% O_2, 2% water.

The mixed washcoat catalyst G gave a NOx conversion effectively bound above and below by the conversions obtained for catalysts E and F. Thus, the NOx conversion activity obtained on this catalyst could be considered as an average of the conversions obtained on the two separate catalysts. In the lower temperature range (T < 400 ^{o}C), the conversion was bound above by the Cu-ZSM-5 and below by the Fe-ZSM-5. In the higher temperature range (T > 400 ^{o}C) the conversion was bound above by the Fe-ZSM-5 and below by the Cu-ZSM-5. Next we show that the physical mixture is not the best approach to combining the two metal-exchanged zeolites in a layered structure.

7.3.5 Dual Layer Fe-ZSM-5/Cu-ZSM-5 Monolith Catalysts

A group of synthesized dual-layer catalysts were evaluated and compared to the performance of the single-layer Cu-ZSM-5 and Fe-ZSM-5 catalysts. The properties of catalysts H-M are provided in Table 7-1.

As shown earlier, the series combination of Cu-zeolite section followed by Fe-zeolite section had similar performance to the Cu-only catalyst and did not show any improvement in the NOx conversion at higher temperatures. We carried out an experiment of a monolith with Cu-ZSM-5 as the top layer and Fe-ZSM-5 as the bottom layer to see if comparable results would be obtained. The total loading was fixed at 25 wt.% with nearly equal loadings of the Cu and Fe layers. The trends obtained with this catalyst H shown in Figure 7-8 are similar to those obtained for the Cu-Z/Fe-Z series configuration (Figure 7-5). The NOx conversion for catalyst H exceeded the conversion obtained for Fe-ZSM-5 (catalyst F) for temperatures up to 400 ^{o}C. But at higher temperatures (> 400 ^{o}C), the NOx conversion approached that of the Cu-ZSM-5 (catalyst E). In light of the Cu-Z/Fe-Z series results, these results were not surprising. With the dual-layer configuration, reactants diffuse into the washcoat, obviously encountering the top layer first. This is comparable but not equivalent to encountering the first section in a series of bricks configuration. Thus, at low temperature, the SCR reaction occurs in the more active Cu-ZSM-5 top layer while the underlying, less active Fe-ZSM-5 layer is essentially not utilized. Similarly, at high temperature, the active Cu-ZSM-5 is encountered first and catalyzes the reactions. But at the higher temperatures the ammonia oxidation activity is significant, resulting in the consumption of ammonia in the top layer. This results in a lack of availability of NH_3 for the complete NOx reduction at higher

temperatures. That the drop in the NOx reduction activity at high temperature was somewhat less compared to the Cu-only (catalyst E) catalyst suggests that some reacting species diffuse through the top Cu-ZSM-5 layer to react on the more selective Fe-ZSM-5 catalyst in the bottom. The NOx reduction occurs on catalysts present in both the layers. Thus, the dual-layer catalyst system with Cu-zeolite on top of Fe-zeolite exhibits improved performance (compared to Fe-only catalyst) at lower temperature but has the drawback of reduced NOx conversions at higher temperatures. No other compositions of the Cu-ZSM-5 on Fe-ZSM-5 were examined for this reason.

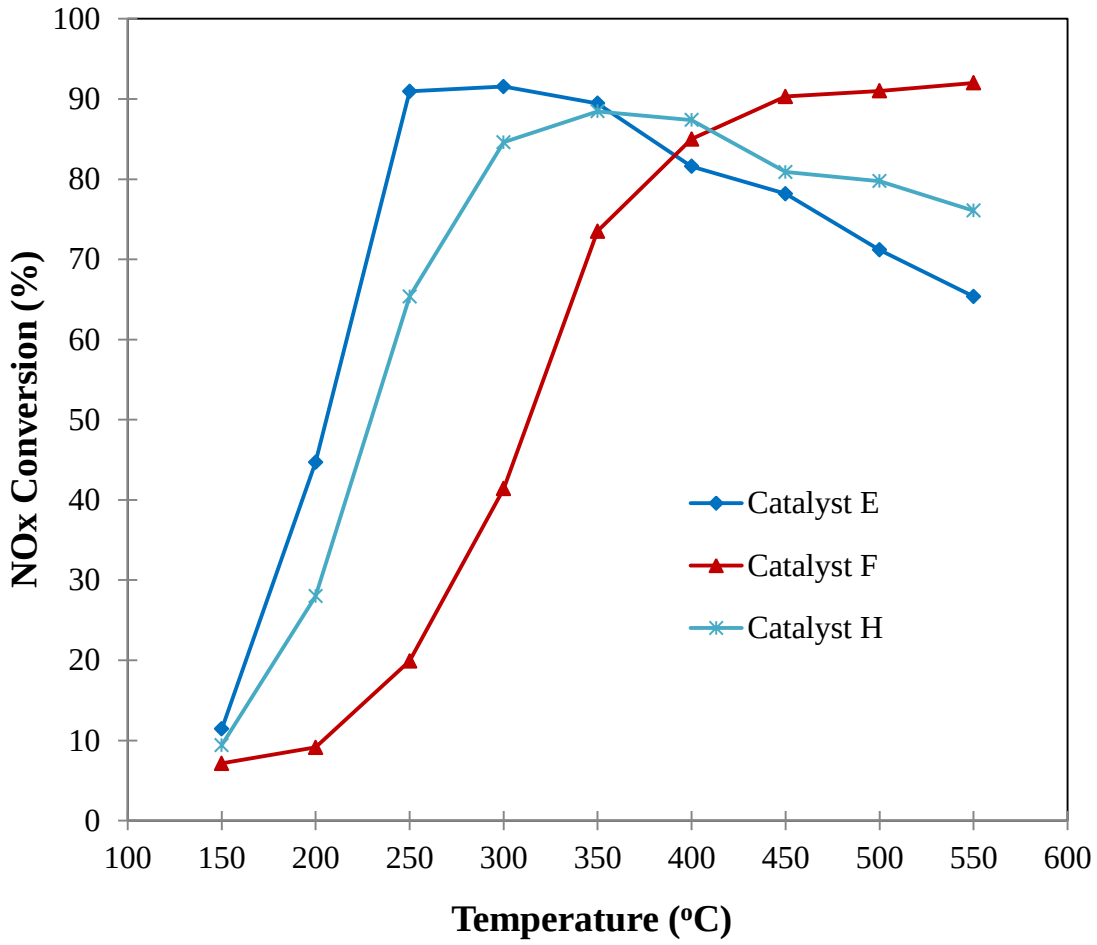

Figure 7-8: Steady state NOx conversions obtained during the standard SCR reaction studied on lab-synthesized catalysts E, F and H. Reactor length: 2 cm. Feed: 500 ppm NO, 500 ppm NH_3, 5% O_2, 2% water.

We turned our attention to dual-layer catalysts with the Fe-zeolite layer on top of the Cu-zeolite layer. Again, we fixed the total washcoat loading to 24-25% in order to conduct a meaningful comparison with the single-layer Cu-ZSM-5, Fe-ZSM-5 and mixed washcoat catalysts. Figure 7-9a shows the standard SCR results for catalysts I - K in which the fraction of Fe-ZSM-5 was decreased from 16 to 8 wt.% while maintaining a fixed total loading of 24 wt.%. The operating conditions were the same in all of the experiments (Reactor length: 2 cm. Feed: 500 ppm NO, 500 ppm NH_3, 5% O_2, 2% water). The data show that as the fraction of Fe-ZSM-5 (Cu-ZSM-5) decreases (increases) there is a progressive increase in the low temperature conversion accompanied by a much less pronounced decrease in high temperature conversion. Specifically, catalyst I showed a slightly higher NOx reduction activity than the Fe-only sample (catalyst F) for temperatures below 300 ^{o}C while at higher temperature (> 350 ^{o}C) the NOx reduction activity was nearly identical on both the catalysts. Following earlier discussion, the reason for this trend is that the thinner Cu-zeolite layer positioned underneath the thicker Fe-zeolite layer has only a small contribution to the overall conversion. That is, coupled reaction and diffusion in the top Fe-zeolite layer prevents the reacting species from penetrating the underlying Cu layer. The effect of a decrease in the Fe-zeolite top layer thickness and corresponding increase in the Cu-zeolite bottom layer thickness helps to confirm this trend. Figure 7-9a shows an enhancement in the low temperature conversion for Catalysts J and K while the high temperature conversion is largely unaffected. For example, at 250 ^{o}C the NOx conversion increases from 24 to 37 to 55% as the Fe-ZSM-5 loading is decreased from 16 to 12 to 8 wt.%, while at 500 ^{o}C the NOx conversion varies from 92 to 90 to 87%. The increase at low temperature is clearly a result of the increase

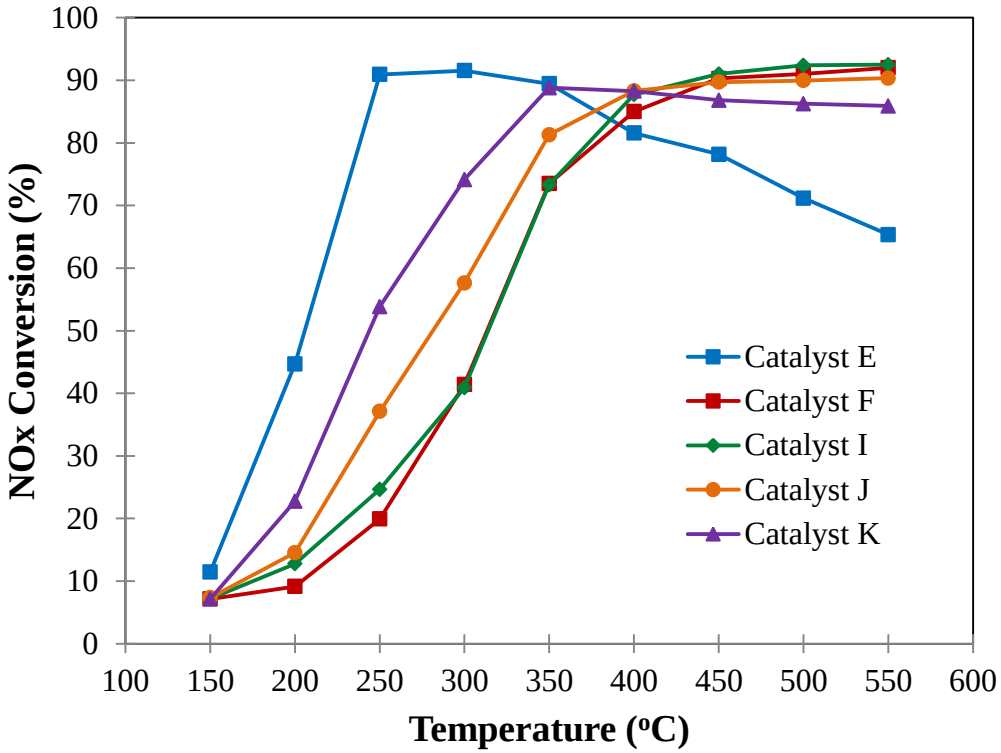

Figure 7-9a: Steady state NOx conversions obtained during the standard SCR reaction studied on lab-synthesized catalysts E, F, I, J and K.

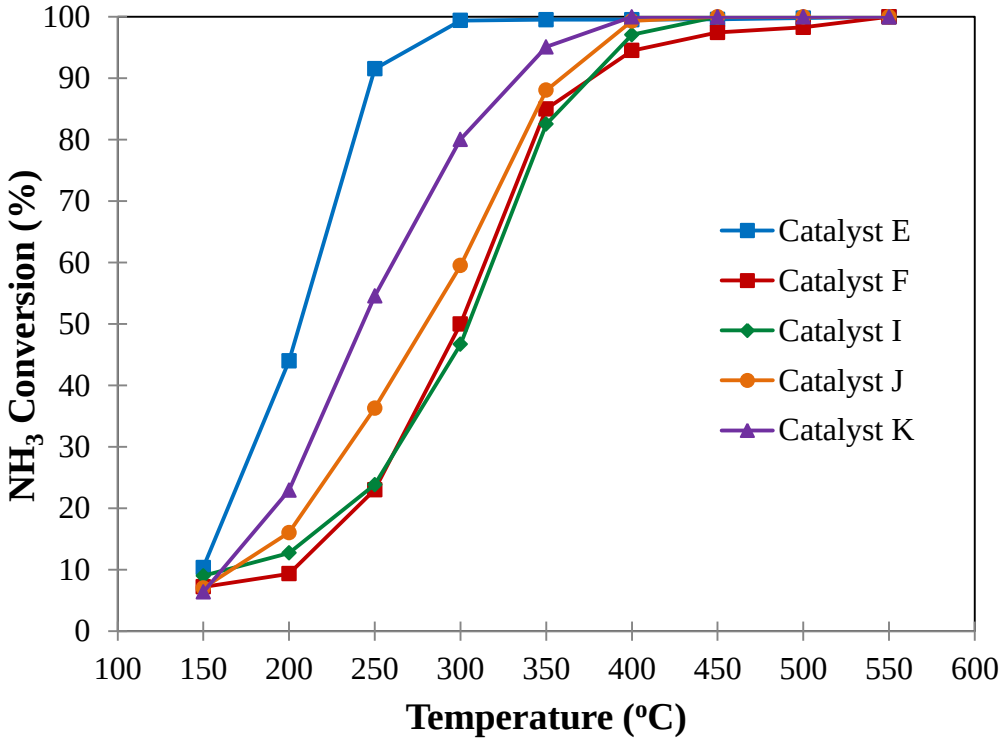

Figure 7-9b: Steady state NH_3 conversions obtained during the standard SCR reaction studied on lab-synthesized catalysts E, F, I, J and K.

in the loading of the underlying Cu-ZSM-5 and decrease in the thickness of the relatively inactive Fe-ZSM-5 layer, which serves more as a non-catalytic diffusion barrier. The small conversion decrease at high temperature indicates some penetration of reacting species, in particular NH_3, to the underlying Cu-ZSM-5 layer where it is oxidized. Again, the conversions obtained on all these catalysts never reached 100% because of the NH_3 oxidation side reaction. In Figure 7-9b, we show the steady state NH_3 conversions obtained on catalysts E-K during the above mentioned standard SCR experiments. Figure 7-9b clearly shows the complete consumption of NH_3 at higher temperatures on all the catalysts.

Comparing all the three dual layered catalysts, catalyst K (1:2 Fe:Cu-zeolite ratio) clearly gives the highest NOx reduction activity over the entire temperature range. The results indicate that for a fixed loading there exists an optimum Fe-ZSM-5 top layer thickness similar to the aforementioned series configuration.

In order to pursue the NOx enhancement with the dual-layer configuration further, we examined the effect of increasing the total washcoat loading while maintaining a smaller fraction of the Fe layer compared to the Cu layer. Figure 7-10 shows the results for catalysts with a total washcoat loading of about 30% (by wt). We intentionally focused on catalysts with mass fraction of Fe-ZSM-5 $\leq$ 0.5. Figure 7-10 shows the results for Catalysts L and M, which respectively correspond to Fe-Z(15)/Cu-Z(15) and Fe-Z(10)/Cu-Z(20). For comparison, the 24 wt.% single-layer Fe-ZSM-5 and Cu-ZSM-5 samples (catalysts E and F) are shown. The higher loading and thinner Fe-ZSM-5 top layer clearly shows further enhancement at low temperature while maintaining high

conversion at high temperature. These results further underscore the existence of an optimal loading of Fe-zeolite (top layer) and Cu-zeolite (bottom layer).

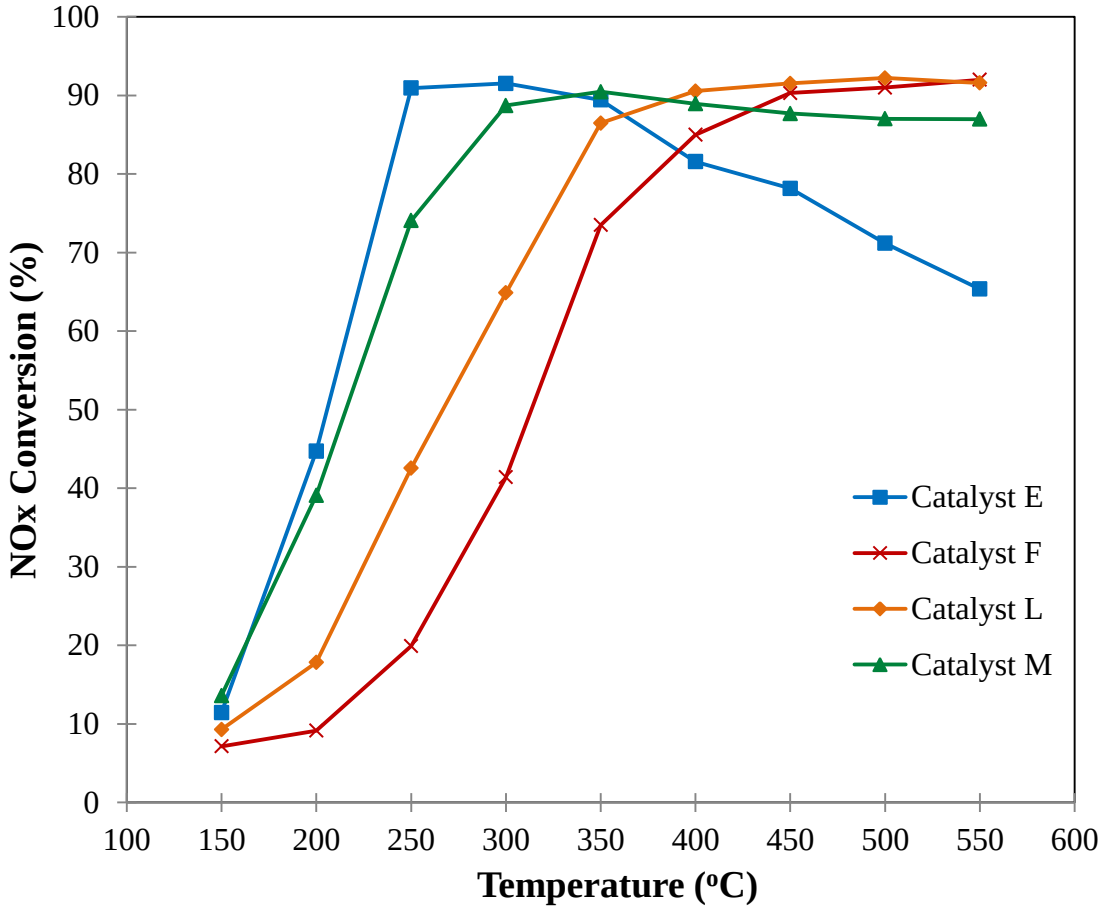

Figure 7-10: Steady state NOx conversions obtained during the standard SCR reaction studied on various in-house synthesized catalysts E, F, L and M. Reactor length: 2 cm. Feed: 500 ppm NO, 500 ppm NH_3, 5% O_2, 2% water.

7.3.6 Application to Fast SCR

In the real exhaust aftertreatment system, the SCR unit is preceded by a diesel oxidation catalyst (DOC) unit (containing a precious metal like Pt) which has the role of catalyzing the oxidation of hydrocarbons, CO and NO. As previous literature studies have shown, the reduction of NOx is enhanced significantly by NO_2 with the optimal feed ratio being $NO/NO_2 = 1$. The so-called "fast SCR" reaction system given by reaction (7-2) does not require the oxidation of NO to NO_2 in the SCR. It is now well accepted that the

rate of SCR reaction increases in the presence of NO_2 (especially at lower temperatures) on both the Fe- and Cu-zeolite catalysts [29], although the rate increment is more dramatic for Fe-zeolite compared to Cu-zeolite catalyst. In the context of the current study, it is of interest to determine the potential for the dual layer catalyst when the feed contains NO_2.

Here we show the results (Figure 7-11) of NOx conversion obtained during the fast SCR reaction on both the Fe- (catalyst F) and the commercial Cu-zeolite (catalyst A) and also on catalyst K as a representative case of the dual layer catalyst system (8 wt.% Fe-ZSM-5, 16 wt.% Cu-ZSM-5). A feed containing an equimolar mixture (250 ppm each) of NO and NO_2 was introduced in the presence of 500 ppm NH_3, 5% O_2 and 2% water. As expected, the NOx conversions increased dramatically for the Fe-zeolite (F) catalyst especially at lower temperatures compared to the case of standard SCR reaction and very high conversion of NOx was obtained at higher temperatures ($\geq$ 300 ^oC). In the presence of feed NO_2, there was an enhancement in the NOx reduction activity at lower temperatures even for the Cu-zeolite catalyst (A). But the effect was not as dramatic as that for the Fe-zeolite. The Cu-zeolite catalyst (A) exhibited similar trends in the NOx conversion at higher temperatures for both the standard and fast SCR reactions. This includes the sharp decrease in the NOx conversion at temperatures > 350 ^oC as a result of the consumption of the NH_3 reductant by oxidation.

The dual layer catalyst K exhibited remarkably high NOx conversion (> 90%) over the entire temperature range (250-550 ^oC). In fact, the NOx reduction activity of this catalyst was comparable to the Fe-only system even at higher temperatures where it showed very stable NOx reduction efficiency. These results demonstrate that the dual

layer catalyst system with thinner Fe-zeolite layer on top of a thicker Cu-zeolite layer works well even for the case of fast SCR system which is more representative of an diesel exhaust system.

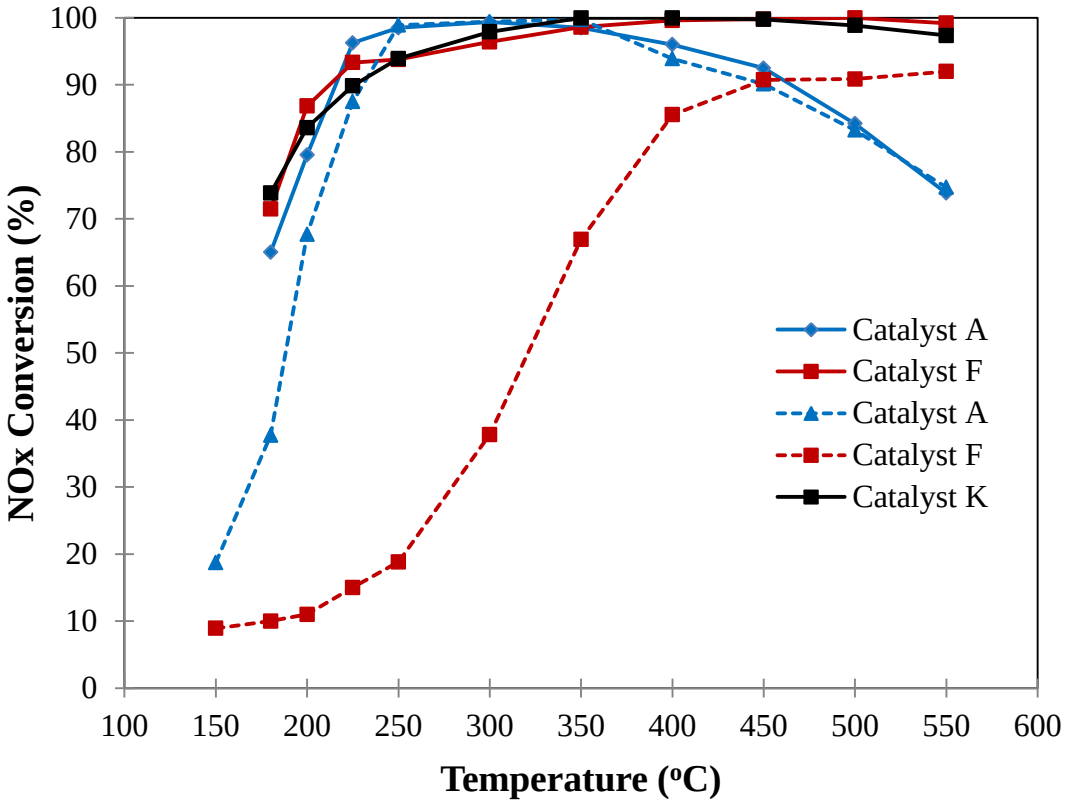

Figure 7-11: Steady state NOx conversions obtained during the fast SCR reaction studied on various catalysts. Feed: 250 ppm NO, 250 ppm NO_2, 500 ppm NH_3, 5% O_2, 2% water. (Dashed lines: NOx conversions during the standard SCR reaction.)

7.3.7 Coating Commercial Catalysts

The results shown so far establish that the dual-layer SCR catalyst system demonstrates superior performance during the standard and fast NOx reduction over a wide temperature range. Figures 7-9 and 7-10 results show that a Fe-Z/Cu-Z configuration can achieve over 90% conversion at temperatures up to 550 ^{o}C, a significant increase over the single component catalyst. As mentioned earlier, the results suggest that an optimal dual-layer catalyst composition exists that maximizes the NOx

conversion over a prescribed temperature range. A combination of additional experiments with modeling is needed to identify the optimal composition.

In order to examine the generality of the findings, we carried out an additional set of experiments in which the commercial Fe-zeolite and Cu-zeolite catalysts were coated with Cu-ZSM-5 and Fe-ZSM-5, respectively. Catalyst C was prepared by depositing a thin layer (12 wt.%) of Cu-ZSM-5 on the commercial Fe-zeolite (catalyst B), while catalyst D was prepared by depositing a thin layer (12 wt.%) of Fe-ZSM-5 on the commercial Cu-zeolite (catalyst A). The standard SCR reaction was studied on these catalysts under the same conditions as the previous experiments. Results obtained for catalysts C and D are compared in Figure 7-12 to the unmodified catalysts A and B, as well as to two of the sequential monolith configurations. The comparison reveals excellent performance for catalyst D. The NOx conversion exceeds 90% over the 250 to 550 ^{o}C temperature range. Comparable performance is achieved for the sequential monolith configuration Fe-Z(33%)/Cu-Z(67%). These results obtained with the modified commercial catalysts are in agreement with earlier results with the in-house synthesized dual-layer catalysts. The results also show that with the simple deposition of a thin layer of the Fe-exchanged zeolite the performance of a commercial Cu-zeolite can be improved significantly. The results obtained on the modified (dual layer) commercial catalysts were compared with the series arrangements of the catalyst bricks and the trends obtained with these two reaction system were found be similar.

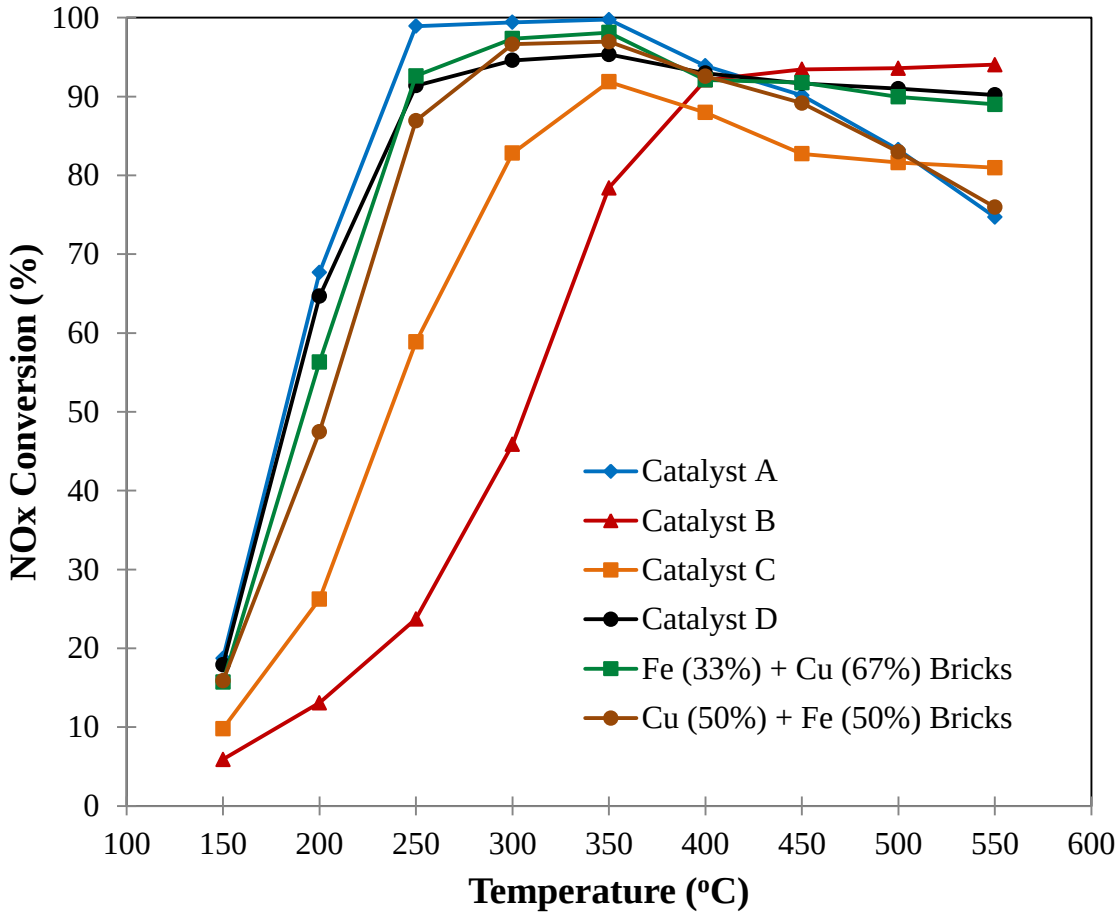

Figure 7-12: Steady state NOx conversions obtained during the standard SCR reaction studied on catalysts A, B, C and D. Additional plots for the series arrangements of catalysts A and B are also shown. Feed: 500 ppm NO, 500 ppm NH_3, 5% O_2, 2% water.

7.3.8 Dual-Layer Metals Distribution and Thermal Stability

A practical concern about the dual-layer catalyst performance is their durability at elevated temperatures. For example, were migrations of the Fe and/or Cu to occur this might compromise the enhanced performance of the segregated metal-exchanged zeolite layers. To address this concern, catalysts L and M were heated to 600 ^{o}C and 700 ^{o}C for 6 hours in a 1000 sccm feed stream containing 5% water in Ar. The temperature was then brought down to the ambient temperature and the standard SCR reaction was carried out under the same conditions as before the thermal treatment. The NOx reduction activity was found to be identical (within experimental error) to that of the previous case of

fresh/unaged samples. Thus the catalyst was found to be stable and was able to sustain very high temperatures of 700 ^{o}C without undergoing any physical/chemical changes. That said, prolonged aging that emulates sustained high load operation and/or filter regenerations may be necessary to assess whether migration eventually becomes an issue.

In order to study the distribution of Fe and Cu in the fresh and aged dual layer catalyst samples, we used energy dispersive X-ray spectroscopy (EDS) analysis. Figure 7-13 depicts the shape of a typical washcoat in washcoated monolithic channel that we synthesized in-house by the dip-coating technique. As there was more catalyst deposition near the corner of a monolithic channel, we measured the local concentration at six distinct points separated by the same distance at one of the corners of the monolith (Figure 7-13). The EDS "counts" provide a measure of the local concentration of Fe and Cu. The spatially-resolved profile provides a semi-quantitative trend in the concentrations of the metal species. The data obtained at various points for degreened catalyst L is presented in Table 7-2. The top layer of the dual layer catalyst consisted of Fe-ZSM-5, within which we made EDS measurements at three points (labeled as 1-3 in Figure 7-13). In this section of the washcoat we did not detect a clear peak for Cu while the Fe-peak was clearly visible. The bottom layer consisted of a Cu-zeolite layer. In this section no Fe peak was detected at the three labeled points 4-6 (Figure 7-13) whereas Cu was detected. Thus the EDS analysis showed that the Fe- and Cu-zeolite layers remained intact even after degreening at very high temperature and the two metals/layers did not migrate/mix. The reproducibility of SCR results obtained on catalysts even after the high temperature degreening confirm the stability of dual layer catalysts synthesized for this study.

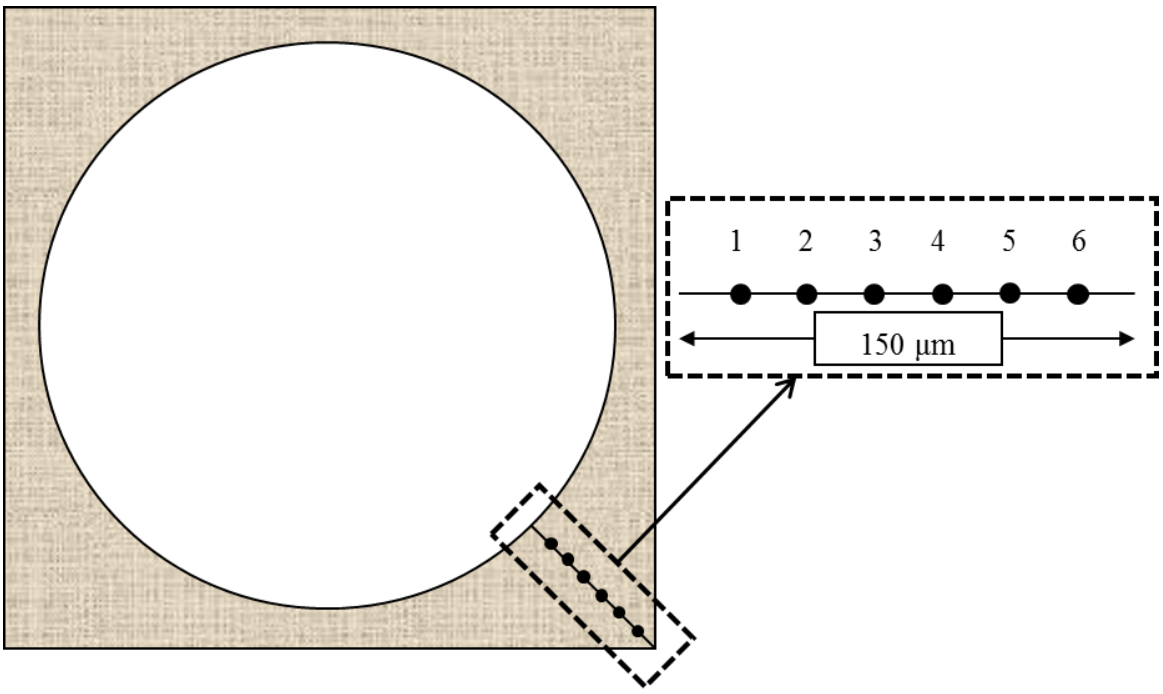

Figure 7-13: Approach used for the EDS analysis of elemental composition in dual layer washcoated catalysts.

Table 7-2: EDS analysis of the dual layer catalyst (catalyst L).

EDS Analysis Point	Fe peak	Cu peak	Fe (wt %)	Cu (wt %)
1	√	×	2.37	0.30*
2	√	×	3.81	0.01*
3	√	×	3.28	0.1*
4	×	√	0.51*	2.53
5	×	√	0.05*	1.18
6	×	√	0.16*	1.82

* below detection limit of the instrument
√ presence of peak for the particular element during EDS analysis
× absence of peak for the particular element during EDS analysis

7.3.9 Dual Layer Catalyst: Working Principle

The objective of using a dual layer SCR catalyst system was to achieve a distribution of Fe- and Cu-zeolite layers that maximizes the NOx reduction activity over a wider temperature range than achievable with the individual metal-exchanged zeolites. Figure 7-14 shows a schematic representation of the Fe- and Cu-zeolite dual layer catalyst concept. As discussed earlier, the Cu-based zeolite is an effective NOx reduction catalyst at lower temperature whereas Fe-based zeolite is relatively inactive. At low temperature the Cu-zeolite layer is needed to achieve high NOx reduction efficiency. A sufficiently thick Cu-zeolite layer coated with a thinner porous overlayer of Fe-zeolite should retain its NOx reduction activity since the Fe-layer behaves essentially as an inactive diffusion barrier. In contrast, at higher temperatures, the ammonia oxidation reaction proceeds at a much higher rate on the Cu-zeolite while NOx reduction is more effective on Fe-zeolite. The steady state experiments carried out on different lengths and thicknesses of the Fe-zeolite catalyst defined the space velocity and loading needed to achieve a high NOx conversion. As long as the thickness of the top Fe-zeolite layer is sufficient, most of the desired NOx conversion should occur in the top Fe layer with the underlying Cu layer serving as a spectator. Thus at high temperature, reacting species encounter the SCR-active Fe layer first and reduction proceeds, unlike at lower temperatures in which it served as a comparatively inactive diffusion barrier.

Our approach of combining the Fe and Cu SCR catalysts in either a sequential brick arrangement or a dual layer system capitalizes on the differences in the kinetics of the desired (SCR) and undesired (ammonia oxidation) reactions over a wide range of temperatures. The results clearly demonstrate that there exists an optimum catalyst design

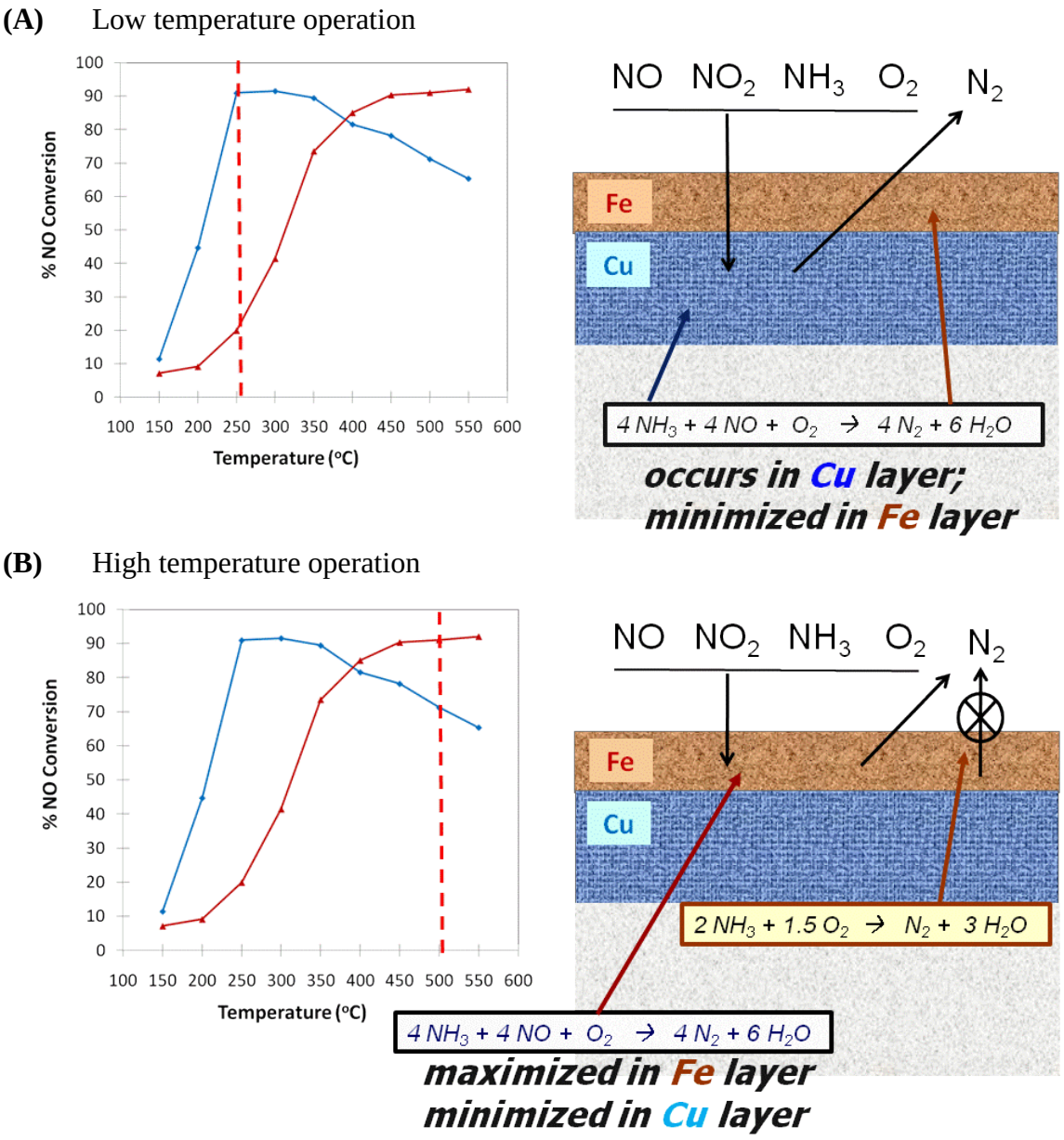

Figure 7-14: Schematic of the working principle of the dual-layer SCR catalyst (A) low temperature; (B) high temperature.

that maximizes the NOx conversion over a range of temperatures. In order to compute this maximum, the simplest model would need to include flow and reaction processes.

Only few literature studies have reported the kinetics of standard and fast SCR reaction systems on Cu- and Fe-zeolite catalysts. Komatsu et al. [111] reported the

kinetics of the standard SCR reaction on Cu-zeolite catalysts, suggesting the following power law kinetic model

$$R_{Cu\text{-}SCR} = k_{Cu}\,[NO]^{1}[O_2]^{0.5}[NH_3]^{0}, \quad (7\text{-}6)$$

where k_{Cu} is the rate constant. In Chapter 3 and in our recent study [103], we proposed the following power-law kinetics for the standard SCR reaction on Fe-zeolite catalysts

$$R_{Fe\text{-}SCR} = k_{Fe}\,[NO]^{1}[O_2]^{0.55}[NH_3]^{-0.3}, \quad (7\text{-}7)$$

where k_{Fe} is the rate constant. A few other literature studies [44, 134] showed that the NH_3 oxidation reaction has a linear dependence on the NH_3 concentration. Since O_2 is present in excess in the feed, the following simple rate expression can be used to describe NH_3 oxidation reaction on Fe- and Cu-zeolite catalysts

$$R_{NH3\text{-}oxi} = k_{oxi}\,[NH_3]. \quad (7\text{-}8)$$

Our experimental results showed a difference in NH_3 oxidation activities on Fe- and Cu-zeolite catalysts. Thus the above rate expression with different values of rate parameters (k_{oxi}) should do a reasonable job of predicting the trends in the experimental data. As observed, there is a difference in the rates and selectivities of the standard SCR and NH_3 oxidation reactions for the Fe- and Cu-zeolite catalysts. These power law kinetic rate expression incorporated into a standard two-phase monolith model should be a good starting point to conduct an optimization study of the sequential brick configuration. However, for the optimal dual layer catalyst configuration, a two dimensional two phase model would clearly be required along with the detailed kinetics of all the above reactions. This complementary modeling work is presented in Chapter 9.

7.3.10 Dual Layer Catalyst vs. Series Arrangement of Catalyst Bricks

The above findings (Figure 7-9) with the dual-layer catalyst resemble closely the results with the sequential Fe-Z/Cu-Z monolith configuration. A question of practical importance is which configuration is superior for a fixed mass of Cu- and Fe-zeolite. Given a fixed mass of the two catalysts, the dual-layer configuration spreads each catalyst over the entire length of the monolith. The series configuration concentrates the individual components over shorter lengths, necessarily resulting in thicker washcoats. Obviously, the contacting patterns of the reacting gas with the catalysts are different for the two configurations. The flow configuration and catalyst geometry directly impact the effectiveness of the transport of reactants to the catalyst sites via external mass transport and washcoat (pore) diffusion. Intuitively, if the reactions are purely kinetically limited, then there will be no effect of the transport processes and the overall conversion would simply be a function of the residence time of the flowing gas at the prescribed temperature. On the other hand, if either or both mass transport processes limit the reaction rates at least in part, then the overall conversion will obviously depend on the catalyst configuration. Thus, to answer the design question we must consider the effect of transport processes on the SCR reaction.

For this purpose, we synthesized catalysts with same washcoat volume and various washcoat thicknesses. Experiments were designed in such a way that the W/F ratio (mass of a catalyst/molar flow rate) i.e., the space velocity per unit mass of the catalyst remained the same all the experiments [103, 209]. This was achieved using different lengths of catalysts having varied washcoat loadings. For example, we used 2 cm length of FeZ-11 and 1 cm length of FeZ-22 catalysts for the standard SCR reaction.

Same catalysts were used to study the presence of mass transfer limitations in the fast SCR reaction but using shorter catalyst lengths as the fast SCR reaction rates are very high. We used 1 cm piece of FeZ-11 and 5 mm piece of FeZ-22 catalysts for this study. The number of monolith channels was kept the same (28) for all the catalysts.

Figure 7-15 shows typical results obtained for the standard and fast SCR reaction carried out on in-house synthesized Fe-zeolite catalysts. The results show separation in the NO conversion activity obtained on two catalysts with different washcoat thicknesses at higher temperatures ($\geq$ 350 ^{o}C) for the standard SCR reaction. However the difference was negligible at lower temperatures. These results indicate the presence of washcoat diffusion (internal mass transfer) limitations for the standard SCR reaction on Fe-zeolite catalysts. This is because the reaction rates increase at higher temperatures for the standard SCR reaction because of which the entire catalyst (deep inside the thicker washcoat) is not utilized. Using a similar approach for the fast SCR reaction, we found that the difference in NOx conversion activity studied on catalysts with different washcoat thicknesses emerged at temperatures lower than that for the standard SCR reaction. Our results showed a clear separation in NOx conversion activities throughout the temperature range (200-500 ^{o}C). This confirms the presence of washcoat diffusion limitations for the fast SCR reaction in the Fe-zeolite catalyst over the entire temperature range and the obvious reason of appearance of these diffusion limitations at earlier temperatures compared to the standard SCR reaction was very high reaction rates of the fast SCR reaction.

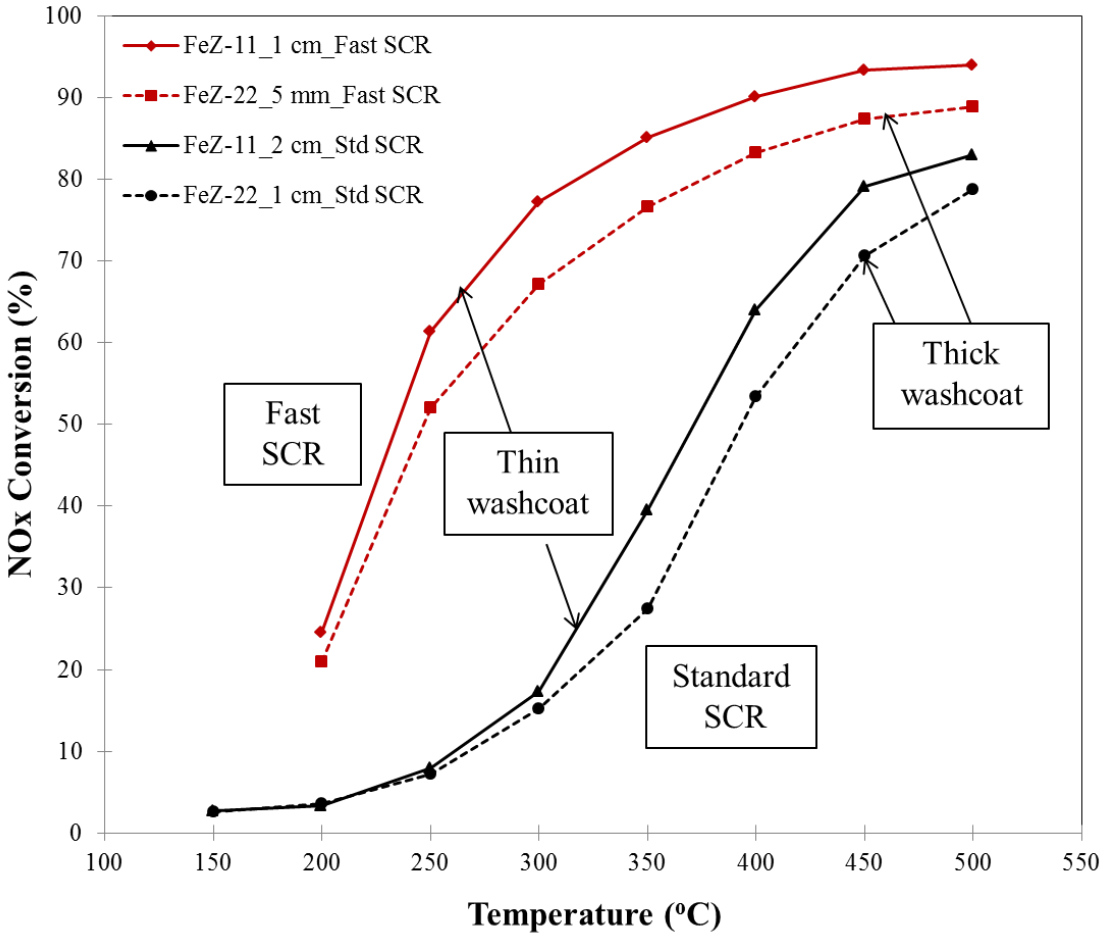

Figure 7-15: Data showing the extent of transport limitations for standard and fast SCR reactions on in-house synthesized Fe-zeolite catalysts.

The presence of internal mass transfer limitations is an important issue for the above case of a series arrangement of bricks. Were we to use a small section of Fe-zeolite brick in front of a longer Cu-zeolite brick to improve the NOx removal efficiency then diffusion limitations may inhibit the reaction in the front brick and most of the NH_3 and NOx would be transferred to the downstream Cu-zeolite catalyst. This would result in a decreased NOx conversion at higher temperatures. For this case, the dual layer catalyst system would have an advantage over the series arrangement of catalyst bricks.

We complete this study by making some final comments about the potential advantages of the dual layer catalyst system. The dual layer SCR catalyst has the advantage of very high NOx removal efficiency over a wider temperature range for standard SCR. The dual layer catalyst is especially useful for heavy-duty diesel engine vehicles as it provides the advantage of high NOx reduction efficiencies at lower temperatures compared to Fe-only catalyst as part of Fe-zeolite is replaced by Cu-zeolite. Also, at higher temperatures, very high NOx reduction efficiencies could be achieved with higher SCR reaction rates in the top Fe-zeolite layer. This may reduce the need to have NO_2 in the feed, which would otherwise be needed to achieve high NOx removal performance, especially at lower temperatures. Thus, indirectly, the dual layer catalyst reduces the need for the conversion of NO to NO_2 in the DOC unit, which is a potential savings in Pt needed to convert NO to NO_2 upstream. In addition, a recent study by Cavataio et al. [210] showed that contamination of the zeolite-based SCR catalysts can occur by precious metals like Pt, which travel from the DOC unit to the downstream SCR unit because of poor adhesion of Pt metals in the DOC washcoat. This results in a decline in the NOx removal activity of SCR unit. With the dual layer SCR catalyst system, the DOC unit may be designed with reduced loadings of Pt which would prove to be cost effective and avoid the possible contamination of SCR unit by Pt. A final point to note is that the dual layer SCR unit may serve as a good NH_3 slip catalyst since it reduces the amount of unreacted NH_3 leaving the SCR unit. This is because both Fe and Cu are good ammonia oxidation catalysts and they selectively oxidize NH_3 to N_2. Few studies [29, 134, 200] focused on the optimum NH_3/NOx ratio required to achieve high NOx removal efficiency on Fe- and Cu-zeolite catalysts. For the Cu-zeolite catalysts, high NH_3/NOx

feed ratios are required at higher temperatures compared to Fe-zeolite catalysts because of the high NH_3 oxidation activity on the Cu catalyst. For the dual-layer catalyst system, the NH_3 requirement at higher temperatures may be decreased because of the increased standard SCR reaction rates on the Fe-zeolite catalyst present in the top layer. As a result, the optimum NH_3/NOx ratio would decrease (compared to the Cu-only catalyst system) resulting in less consumption of NH_3 and hence less urea.

Amongst the different catalyst arrangement systems studied, the dual-layer catalyst system was found to give the highest NOx removal efficiency. For this dual layer catalyst system, we used Fe-ZSM-5 and Cu-ZSM-5 catalysts. Even though the metal exchanged ZSM-5 catalysts give very high NOx removal efficiencies, they are more prone to lose stability and hence NOx removal efficiency at very high temperature (> 700 ^oC) hydrothermal aging. Recently, various small pore zeolite catalysts like SAPO-34, SSZ-13, SSZ-16, etc. [125, 126] have been introduced for the NH_3 SCR studies and were found to be highly stable towards very high temperature hydrothermal aging and highly efficient towards maximum NOx reduction. The dual layer catalyst system design can be extended to these small pore zeolite catalysts to make this system more efficient.

7.4 Conclusions

A systematic study of standard and fast SCR reaction on combined Fe- and Cu-zeolite monolith catalysts was carried out to determine if a high NOx conversion could be sustained over a wider temperature range than with individual Fe- and Cu-zeolite catalysts. To our knowledge, this is the first study introducing the concept of a novel

dual-layer washcoated monolithic catalyst for widening the overall temperature window for the standard and fast SCR reactions.

Ammonia oxidation and standard SCR reactions were studied on individual Fe- and Cu-zeolite catalysts of different lengths to determine the activity of commercial and in-house synthesized Cu- and Fe-zeolite catalysts. In agreement with previous literature studies, the Cu-exchanged zeolite was found to be a very good low temperature ($\leq$ 350 ^{o}C) NOx reduction catalyst during the standard SCR reaction. Fe-zeolite was found to be a better NOx reduction catalyst at higher temperatures ($\geq$ 400 ^{o}C). A series combination of Fe-zeolite (in the front) (33-50% of the total length) followed by Cu-zeolite (50-67%) gave the highest NOx conversion over a wide temperature range. The reverse series catalyst arrangement with the Cu-zeolite in front of the Fe-zeolite catalyst had little if any effect on the NOx reduction efficiencies at higher temperatures. The results indicated that this catalyst system did not utilize the Fe-zeolite catalyst as the NOx conversion activities were similar to the Cu-only catalyst system.

Standard and fast SCR experiments were carried out on various dual layer catalysts. Amongst the various combinations of dual-layered catalyst systems with Fe-zeolite catalyst layer on top of the Cu-zeolite catalyst layer, a catalyst with thinner (33% of the total washcoat loading) Fe-zeolite layer on top of a thicker (67% of the total washcoat loading) Cu-zeolite layer at bottom gave optimum NOx reduction activities for both the standard and fast SCR reactions. The improvements in the NOx conversion were obtained by exploiting the different reactivities of the two catalysts. At low temperatures the Fe-zeolite is relatively inactive compared to the Cu-zeolite, whereas at high temperatures the Fe-zeolite top layer is effective in converting most of the NOx while

minimizing the consumption of ammonia via its oxidation on Cu-zeolite. The dual layer catalyst results clearly indicate that an optimal dual-layer catalyst composition would maximize the NOx conversion over a prescribed temperature range.

The dual layer Fe/Cu catalyst is shown to be a more effective configuration than the Fe/Cu series brick configuration because of the existence of washcoat diffusion limitations. The expansion of the temperature window is most notable for the standard SCR reaction, but performance improvement is obtained for fast SCR as well. The dual layer catalyst would be highly suitable for NOx removal in heavy duty vehicles as it gives high NOx reduction efficiencies over a wide temperature range. At high temperatures, it utilizes more selective Fe-zeolite top layer. While at lower temperatures, it utilizes highly active Cu-zeolite bottom layer which also reduces the requirements for feed NO_2 for Fe-only catalyst system. This would have the intangible benefit of reducing the precious metal requirements in the upstream diesel oxidation catalyst. Finally, comparison of fresh and hydrothermally aged catalysts indicate no noticeable reduction in catalyst performance.

CHAPTER 8 Experimental and Kinetic Modeling Study of NO Oxidation: Comparison of Fe and Cu-Zeolite Catalysts

8.1 Introduction

The current study is focused on the understanding of kinetics of NO oxidation reaction which is a key step in NH_3 SCR of NOx on Fe- and Cu-zeolite (ZSM-5 and chabazite) based monolithic catalysts. In a typical diesel exhaust aftertreatment system, SCR unit is preceded by a diesel oxidation catalyst (DOC) unit, which converts a fraction of NO to NO_2 by the NO oxidation reaction represented by

$$NO + ½\ O_2 \leftrightarrow NO_2 \qquad \Delta H = -\ 5.7 \times 10^4\ J/mol\ NO. \qquad (8\text{-}1)$$

The presence of NO_2 in the feed increases the NOx reduction capacity of the SCR unit, especially at lower temperatures [29, 87]. Cu- and Fe-zeolite catalysts also oxidize NO to NO_2 [100, 103]. In our earlier study in Chapter 3 and [103], we showed that the NO oxidation is the rate determining step for the standard SCR reaction (7-2) on Fe-zeolite catalyst. This conclusion is in agreement with literature studies on different zeolite catalysts [29, 34, 36, 113, 145, 159, 211]. The standard SCR reaction is given by

$$4\ NH_3 + 4\ NO + O_2 \rightarrow 4\ N_2 + 6\ H_2O \qquad \Delta H = -\ 4.07 \times 10^5\ J/mol\ NH_3. \qquad (8\text{-}2)$$

NO oxidation is also considered to be a key step in various hydrocarbon SCR reaction systems [205, 212]. Because of the very high costs of precious metals (e.g., Pt), there is hope that non-PGM catalysts eventually replace the existing DOC unit. In addition, recent research is focused on the combination of Lean NOx Trap (LNT) and SCR units to get optimum NOx reduction efficiency [203] and NO oxidation is a key step for the NOx reduction chemistry on both the LNT and SCR catalysts. In order to understand the

complex chemistry during the NOx reduction process, it is necessary to have a sound understanding of the NO oxidation reaction during SCR on Fe- and Cu-zeolite catalysts.

Recent literature studies have focused on both mechanistic and kinetic aspects of the NO oxidation reaction on various NOx storage and reduction (NSR) or LNT catalysts (Pt/Al_2O_3, $Pt/BaO/Al_2O_3$) and have improved the understanding of this reaction on these catalysts [146, 147, 213]. However, few studies have focused on a detailed understanding of the NO oxidation reaction on SCR (Fe/Cu-zeolite) catalysts. A recent study by Olsson et al. [100] presented a kinetic study of NOx adsorption and NO oxidation on Cu-ZSM-5 catalyst in which they proposed a microkinetic model based on the existence of three different sites in the Cu-ZSM-5 catalyst to predict their experimental data. A few other studies [78, 101, 117, 212, 214] used a simplified global kinetic model approach to describe the NO oxidation reaction on various ion-exchanged zeolite catalysts. However, NO oxidation data have not been reported on the recently developed small pore Cu-chabazite catalysts.

The objective of the current study is to carry out a comparative study of the NO oxidation reaction on the Fe- and Cu-zeolite (ZSM-5 and chabazite) monolithic catalysts and to develop a mechanistically based kinetic and reactor model that predicts the main features of this reaction system. Steady state experiments of NO oxidation are carried out on both the catalysts over a wide temperature range (150-550 ^oC) of practical interest. The effects of increasing amounts of feed NO_2 and water are analyzed and differential kinetics studies are performed for the NO oxidation reaction (on both the catalysts) to determine reaction orders and activation energies. Transient NOx uptake and temperature programed desorption experiments are also conducted that elucidate the nitrate formation

on both the catalysts. The effect of catalyst pretreatments by different oxidizing/reducing agents is considered for the NO oxidation studies. Experiments on monolithic catalysts with a fixed washcoat loading but different washcoat thicknesses coupled with theoretical analyses help in assessing the extent of mass transfer limitations. Finally, a mechanistic-based global kinetic model is developed to predict the experimental findings which include steady state NO conversions, NO_2 and water inhibition effect, experimentally observed reaction orders and the fate of nitrates.

8.2 Experimental

8.2.1 Catalyst Samples

A commercial washcoated monolithic Fe-zeolite (ZSM-5 type) catalyst was provided by Umicore Autocat USA Inc. A commercial Cu-zeolite (chabazite) catalyst sample was provided by BASF Catalysts LLC (Iselin, NJ) in monolithic form. Both the samples had a cell density of 400 cells per square inch (cpsi). Even though the two catalysts differed in the types of basic zeolite type (or framework), the qualitative behavior obtained for various Fe- and Cu-zeolite catalysts was found to be very similar and is discussed in earlier chapters. Scanning electron microscopy (SEM) and energy dispersive spectroscopy (EDS) analysis showed that the two catalysts had nearly the same washcoat loadings and loadings of active metal in the washcoat (~ 2.5-3 wt %).

In order to study the extent of washcoat diffusion limitations, we synthesized various Fe- and Cu-ZSM-5 washcoated catalysts having different lengths, washcoat loadings and washcoat thicknesses. Fe-ZSM-5 powder used for this purpose was supplied by Sud-Chemie (Munich, Germany). Cu-ZSM-5 powder was synthesized in-house using

a conventional ion-exchange technique as discussed in Chapter 2 and [209, 215]. In order to deposit the catalyst powder on blank cordierite monolith samples (supplied by BASF, Iselin, NJ), we used a dip-coating method which was the same as the one described earlier in Chapter 2 and [103]. We refer to these catalysts as FeZ-XX and CuZ-XX henceforth where –XX represents the weight % of zeolite loading on the blank monolith support.

8.2.2 Bench-Scale Reactor Set-up

The experimental setup was the same as described in our earlier studies [103, 139]. It included a gas supply system, a reactor system, an analytical system and a data acquisition system. The monolith catalyst wrapped with a ceramic fiber was placed inside a quartz tube reactor mounted in a tube furnace. The furnace temperature was set with a temperature controller. A FT-IR spectrometer (Thermo-Nicolet, Nexus 470) was placed downstream of the reactor to analyze various effluent gases including NH_3, NO, NO_2, N_2O and H_2O. A quadrupole mass spectrometer (QMS; MKS Spectra Products; Cirrus LM99) was used to measure N_2. Unless otherwise stated, monolith samples of 2 cm length with 34 channels were used for most of the experiments. Argon was used as a balance gas and the total flow rate was kept constant at 1000 sccm in all the experiments. This corresponds to a gas hourly space velocity (GHSV) of about 57,000 hr^{-1} and a linear velocity of 0.62 m/s (150 ^oC). Before the start of each experiment, each catalyst was pretreated at 500 ^oC in the presence of 5% O_2 in 1000 sccm Ar for 30 min.

8.2.3 Steady State Experiments

We carried out various steady state experiments on both the commercial Fe-ZSM-5 and Cu-chabazite catalysts. The NO oxidation steady state experiments included fixed concentrations of NO (500 ppm) and O_2 (5%) over a range of temperatures (150-550 ^oC). Sufficient time was given to achieve the steady state concentrations of NO and NO_2. The above experiments were repeated in the presence of 2-5% (by volume) water along with 500 ppm NO and 5% O_2. In order to study the effect of feed NO_2 on the NO oxidation reaction, feeds containing varied concentration of NO_2 were used (NO_2/NOx = 0.25, 0.5 and 0.75). The NO_2 decomposition reaction was studied using 500 ppm feed NO_2 in the temperature range of 150-550 ^oC, both in the absence and presence of (2%) feed water.

In order to study the extent of washcoat diffusion limitations in the NO oxidation reactions, in-house synthesized catalysts with the same washcoat volume (loading) but different washcoat thicknesses were used. For the Fe-ZSM-5 catalyst system, we used a 1 cm long FeZ-22 (22% by wt. washcoat loading) piece and a 2 cm long FeZ-11 (11% by wt. washcoat loading) piece. For the Cu-ZSM-5 catalyst system, we used a 2 cm piece of CuZ-10 catalyst and 1 cm piece of CuZ-20 catalyst. The total number of channels in a monolith piece was 28 for all these catalysts. With the different catalyst lengths but the same total washcoat volume (or mass), the W/F (mass of catalyst/flow rate) ratio and the space velocity per unit mass of catalyst were kept the same.

We carried out differential kinetics experiments on both the commercial Fe-ZSM-5 and Cu-chabazite catalysts to determine reaction orders and activation energies. In order to determine reaction orders with respect to NO, a feed containing 5% O_2 and excess NO_2 (330 ppm for Fe-zeolite and 125 ppm for Cu-chabazite) was used and NO

concentrations were varied in the range of 100-800 ppm. Similarly, in order to determine the reaction orders with respect to O_2, the NO and NO_2 concentrations were kept constant at 500 ppm and 330 ppm (125 ppm), respectively for Fe-ZSM-5 (Cu-chabazite) and while varying the feed O_2 concentration from 0-5%. In order to determine the NO_2 reaction order, the concentrations of both NO (500 ppm) and O_2 (5%) were kept constant while the feed NO_2 concentration was varied (50-500 ppm for Fe-zeolite and 50-300 ppm for Cu-chabazite) in increments of 50 ppm. For all these experiments, NO conversions were kept below 12%. The reaction orders with respect to all the individual reactants were then derived in the presence of 2% feed water using a similar approach and feed conditions.

We carried out further experiments to determine the dependence of NO oxidation reaction on NO and O_2 in the absence of feed NO_2 for temperatures in the range of 200-290 ^{o}C. Maximum NO conversions were kept below 15%. For Fe-zeolite catalyst, this was achieved using a smaller catalyst piece with 16 channels and 1 cm length. As the NO oxidation was found to be slower on the Cu-chabazite, similar catalyst dimensions as described earlier for the above steady state experiments were used to obtain data.

8.2.4 Transient Experiments

NO uptake and temperature programmed desorption (TPD) experiments were carried out on the commercial Fe-ZSM-5 and Cu-chabazite catalysts. For these experiments, the temperature of catalyst was kept constant at 150 ^{o}C and a gas mixture containing 500 ppm NO was continuously fed to the catalyst surface for 1 hour. The NO feed was then switched off and only Ar was flowed for 30 minutes to remove loosely bound NO. A temperature ramp of 10 ^{o}C/min was then applied so that the catalyst

reached 500 ^{o}C after 35 minutes. A similar approach was used for the NO_2 TPD experiments. The temperature of the catalyst was kept constant at 150 ^{o}C in the beginning and 500 ppm feed NO_2 was fed to the catalyst for 1 hr. After that, Ar was flushed for 30 minutes, followed by a temperature ramp of 10 ^{o}C/min to record the concentration of strongly bound NO_2 evolved during the temperature ramp. The NO_2 uptake experiments were repeated on Cu-chabazite catalyst for three different inlet NO_2 concentrations of 100, 300 and 500 ppm under similar conditions. The effect of catalyst pretreatments by different oxidizing/reducing agents (O_2, NO_2, H_2 and NH_3) is discussed for the transient and steady state NO oxidation studies.

8.3 Reactor Model

We used a one dimensional two phase model to predict steady-state experimental results of NO oxidation for various feed conditions and a range of temperatures. The model equations used for this study are summarized in Table 8-1. The length of reactor was rather short (2 cm). As the concentrations used were quite small, non-isothermal effects were negligible (estimated adiabatic temperature rise of about 1 K). Hence, the reactor could be treated as an isothermal reactor at a given temperature. The model is based on the following assumptions: i) steady-state conditions, ii) laminar flow, iii) isothermal operation and iv) negligible washcoat diffusional limitations (justified later). The mass transfer coefficient (k_c) of species *j* was evaluated using the asymptotic Sherwood (*Sh*) number (3.6) and its axial variation with monolith length was neglected as the flow was found to be fully developed within 5% length of the channel [195]. More detail about the model equations used in Table 8-1 can be found in various literature

studies [158, 216]. The model equations were discretized in the axial direction to solve a set of non-linear equations. Table 8-2 shows the values of various parameters and physical properties used in this study.

Table 8-1: Steady-state equations used in reactor modeling.

$$\langle u \rangle \frac{dX_{jm}}{dz} = -\frac{k_{c(j,z)}}{R_{\Omega 1}}(X_{jm} - X_{js}),$$

$$X_{jm} - X_{js} + \frac{R_{\Omega 2}}{c_{Tm} k_{c(j,z)}} \upsilon_j R_v(T, \underline{X_s}) = 0.$$

Boundary Conditions:

$$X_{jm} = X_{jm,in} \quad at \;\; z = 0; \;\; j = 1, 2, .., N \; (number \; of \; species).$$

Table 8-2: Parameters used in experimental/kinetic modeling study.

L	0.02 m
$R_{\Omega 1}$	2.75×10^{-4} m
$R_{\Omega 2}$	5×10^{-5} m
Q	1000 ml/min
ΔH_R	-57.2 kJ/mol
$D_{f,NO}$	2×10^{-5} m^2/s at 300 K
$D_{f,NO2}$	1.5×10^{-5} m^2/s at 300 K
$\langle u \rangle$	0.45 m/s at 300 K

8.4 Results and Discussion

8.4.1 NO Oxidation

In Chapters 3 and 5, we showed some of the results of NO oxidation reaction studies on the commercial Fe-zeolite and Cu-zeolite catalysts, respectively. Here, we build on the results from those studies with particular focus on a comparison between Fe- and Cu-zeolite catalysts.

The steady-state NO oxidation experiments were carried out on both the commercial Fe-ZSM-5 and Cu-chabazite catalysts with an inlet feed of 500 ppm NO and 5% O_2. The results obtained on both the catalysts are summarized in Figure 8-1a (Fe) and 1b (Cu) which show the NO conversion obtained as a function of catalyst temperature.

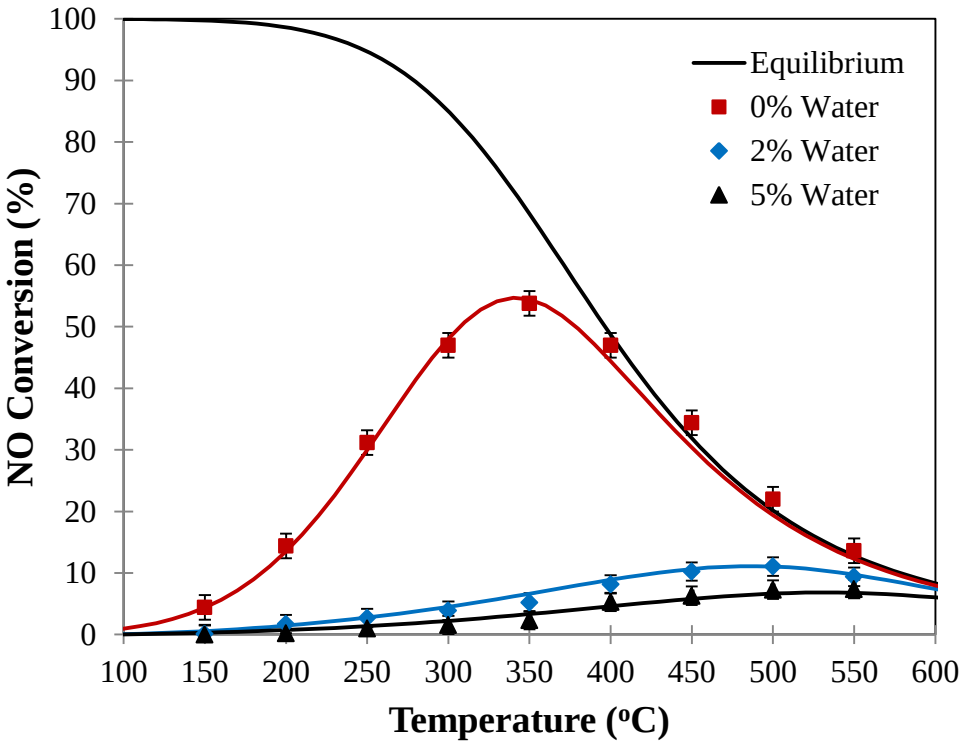

Figure 8-1a: Steady state NO conversions (symbols: experimental data, continuous lines: model predictions) obtained during the NO oxidation reaction on Fe-ZSM-5 catalysts. Feed: 500 ppm NO, 5% O_2, 0-5% H_2O.

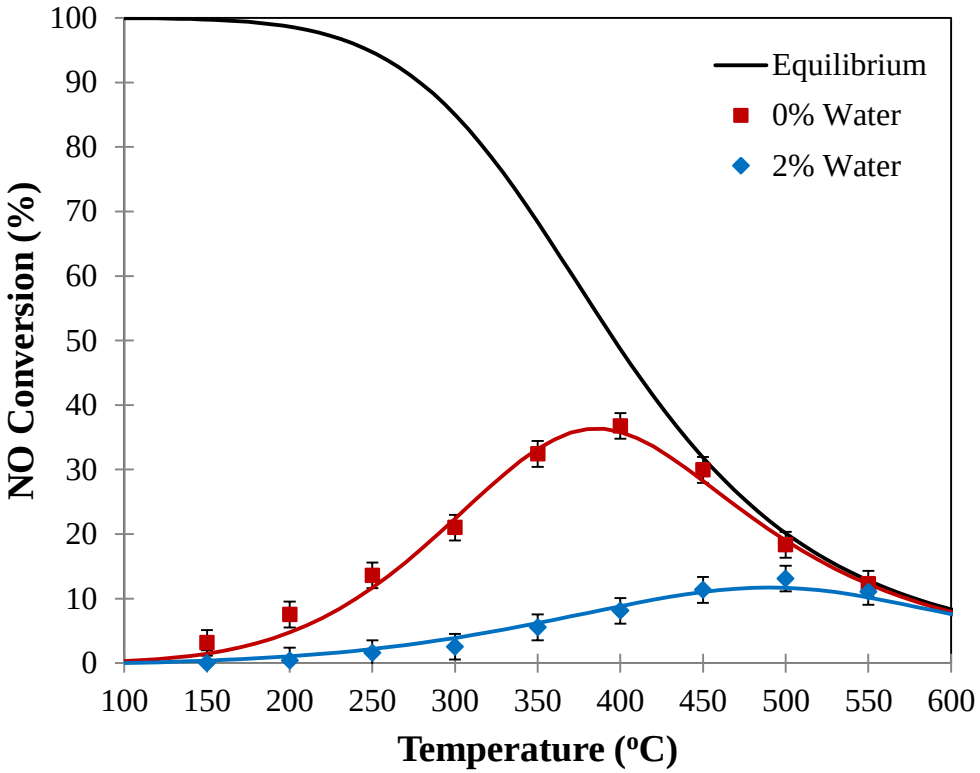

Figure 8-1b: Steady state NO conversions (symbols: experimental data, continuous lines: model predictions) obtained during the NO oxidation reaction on Cu-chabazite catalysts. Feed: 500 ppm NO, 5% O_2, 0-5% H_2O.

The model results will be described later. The trends indicate that the reversible NO oxidation reaction is kinetically controlled at lower temperatures and is equilibrium limited at higher temperatures. For both catalysts the NO conversion goes through a maximum at an intermediate temperature in the range 350-400 ^oC. After reaching the maximum, the NO conversion follows the equilibrium curve for both catalysts, conditions for which the reversible NO_2 decomposition (to NO) becomes dominant. Several literature studies reported similar trends for NO oxidation on LNT and SCR catalysts [89, 134, 147, 217]. A comparison of the Fe- and Cu-exchanged zeolites shows that Fe-ZSM-5 is a more active NO oxidation catalyst as we get a maximum NO conversion of about 53% on Fe-ZSM-5 at 350 ^oC compared to 36% at 400 ^oC on the Cu-

chabazite catalyst. Kamasamudram et al. [135] also compared the activities of NO oxidation on Fe- and Cu-zeolite catalysts and found Fe-zeolite to be a superior NO oxidation catalyst.

The NO oxidation reaction was then studied in the presence of feed water. For the Fe-ZSM-5 catalyst, the reaction was studied in the presence of 2% and 5% water. Water strongly inhibited the NO oxidation reaction as the maximum NO conversions decreased to 11% (for 2% water) and 7% (for 5% water). The presence of (2%) feed water showed a similar inhibition effect on the NO oxidation reaction on the Cu-chabazite catalyst. Few literature studies have reported similar effect of water inhibition on the NO oxidation reaction [89, 99]. The observed inhibition is attributed to water blocking the active NO oxidation sites, as we discussed later.

The NO oxidation reaction was also studied in the presence of feed NO_2. Three different feeds with NO_2/NOx inlet ratios of 0.25, 0.50 and 0.75 were considered while the total amount of inlet NOx was fixed at 500 ppm. Figures 2a (Fe) and 3a (Cu) report the measured outlet NO_2/NOx ratio as a function of temperature under these conditions. Figures 2b (Fe) and 3b (Cu) report the NO conversion as a function of NO_2/NOx inlet ratios for different temperatures. It is clear that increasing amounts of NO_2 in the feed results in decrease in the NO oxidation activity on both the catalysts. For the Fe-ZSM-5 catalyst, substantial NO oxidation activity was obtained for the feeds containing NO_2/NOx feed ratio up to 0.5. As a result, the outlet NO_2/NOx ratio was always greater than feed ratio up to 350 ^oC. But in the presence of excess NO_2 (NO_2/NOx = 0.75), NO oxidation activity was negligible. A similar study of Cu-chabazite showed a stronger inhibition of NO oxidation with increasing feed NO_2 because of which the outlet

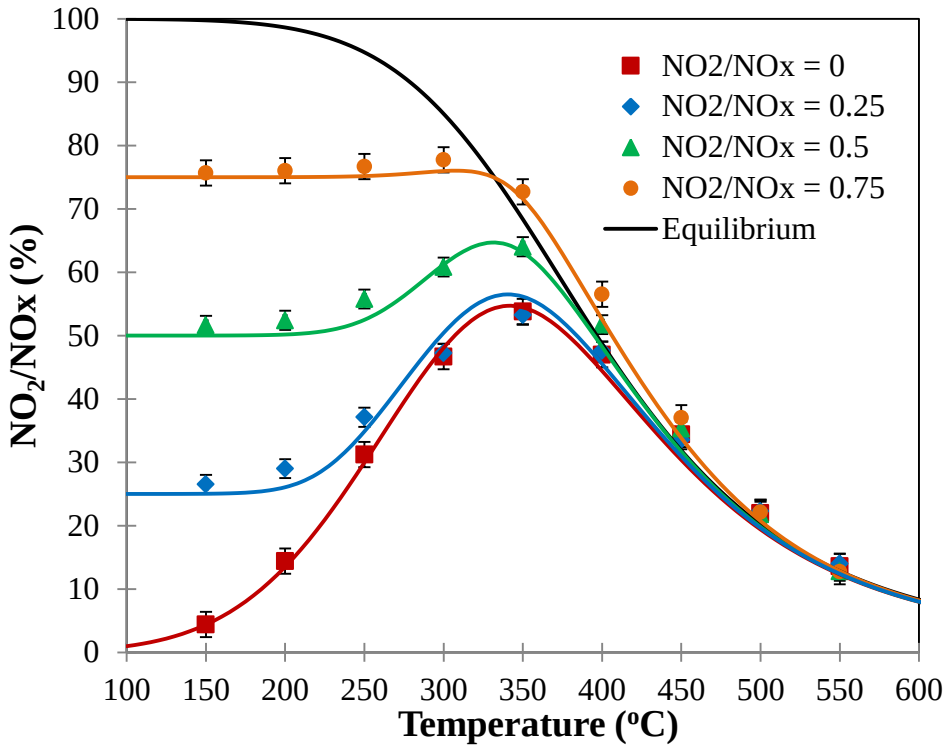

Figure 8-2a: Steady state outlet NO_2/NOx ratio (symbols: experimental data, continuous lines: model predictions) obtained during the NO oxidation reaction studied on Fe-ZSM-5 catalyst with NOx feeds containing varying NO_2/NOx inlet ratios (0-0.75).

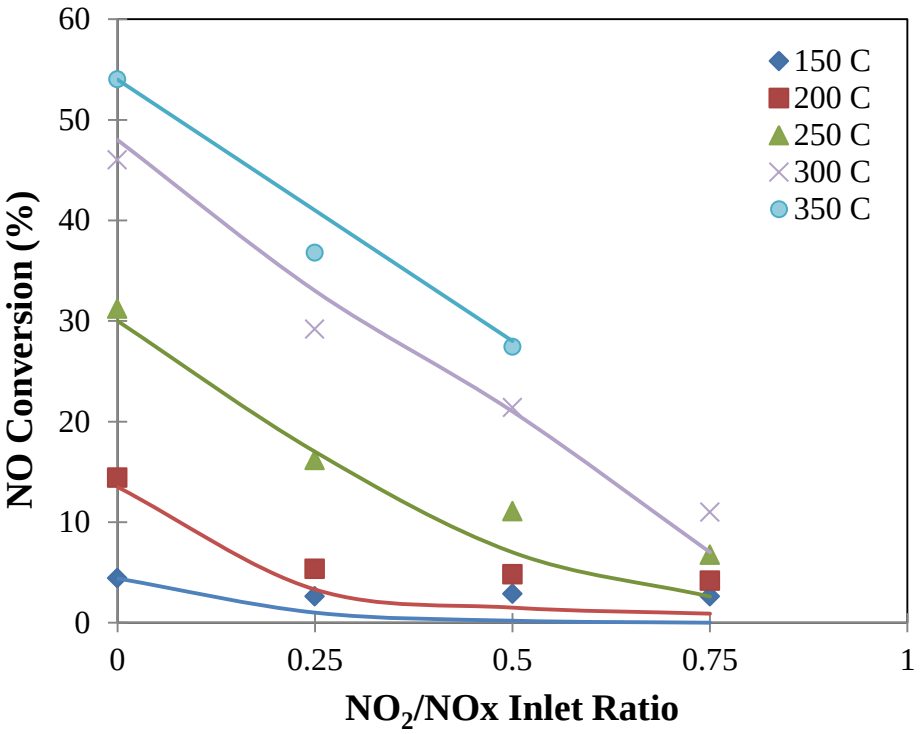

Figure 8-2b: Steady state NO conversions obtained during above experiments.

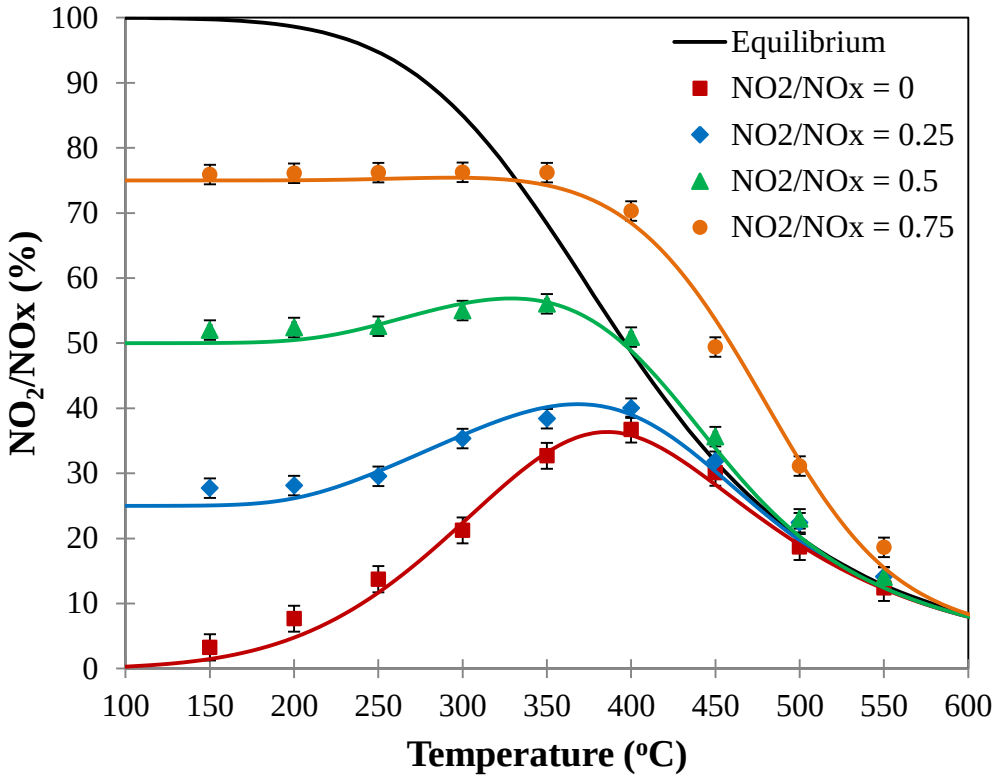

Figure 8-3a: Steady state outlet NO_2/NOx concentration ratio(symbols: experiments, lines: model predictions) obtained during the NO oxidation reaction studied on Cu-chabazite catalyst with NOx feeds containing varying NO_2/NOx inlet ratios (0-0.75).

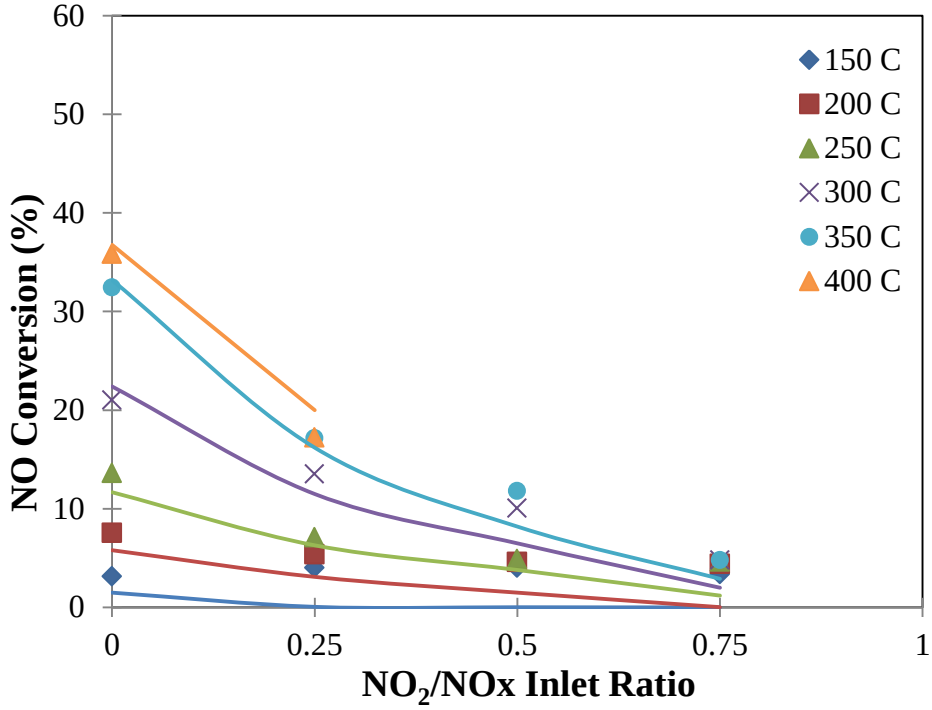

Figure 8-3b: Steady state NO conversions obtained during above experiments.

NO_2/NOx curve was nearly flat (i.e., negligible NO oxidation activity) for (NO_2/NOx $\geq$ 0.5) temperatures up to 400 ^oC after which the reversible NO_2 decomposition was dominant. In addition, the outlet NO_2/NOx ratio for Cu-chabazite was always less compared to Fe-ZSM-5 results under similar conditions. This is in line with the results discussed earlier for the NO oxidation reaction studied in the absence of feed NO_2 for which we observed higher NO oxidation activities on Fe-ZSM-5. At higher temperatures, all the curves approach the equilibrium curve. For feeds containing excess NO_2, the outlet NO_2/NOx curve deviated from the equilibrium curve at lower temperatures. The deviation was more pronounced on Cu-chabazite as the NO_2 decomposition starts at higher temperatures on this catalyst. This issue is discussed in more detail in the next section.

Figures 8-2b (Fe) and 8-3b (Cu) give a clearer picture of effect of NO_2 on the NO oxidation. As the NO_2 fraction of feed NOx increased, the NO conversion decreased. In these plots, the NO conversion is shown for temperatures up to 400 ^oC because the reverse NO_2 decomposition reaction became dominant at higher temperatures and hence no measurable NO oxidation activity was recorded. These results clearly show that the NO oxidation activity was always higher on Fe-ZSM-5. Moreover, the inhibition of NO_2 on NO oxidation was more severe on the Cu-chabazite as the introduction of NO_2 decreased the NO conversion by a larger extent.

All these results clearly show the NO_2 inhibition of the NO oxidation reaction on both the commercial Fe and Cu-zeolite catalysts. A possible reason for this could be the partial blockage of active NO oxidation sites by NO_2 because of the competitive adsorption of NO_2. Another explanation is that, NO_2, being a strong oxidizing agent,

could oxidize the metal sites and prevent the other species like O_2 to adsorb and react on the surface [148]. A similar NO_2 inhibition effect on the NO oxidation reaction has been reported on various other catalysts [101, 134, 146, 147, 212]. We return to this issue in the later part of this study.

8.4.2 NO_2 Decomposition

We studied the NO_2 decomposition reaction on both the Fe-ZSM-5 and Cu-chabazite catalysts using feeds containing 500 ppm NO_2. For Fe-ZSM-5 (Figure 8-4a),

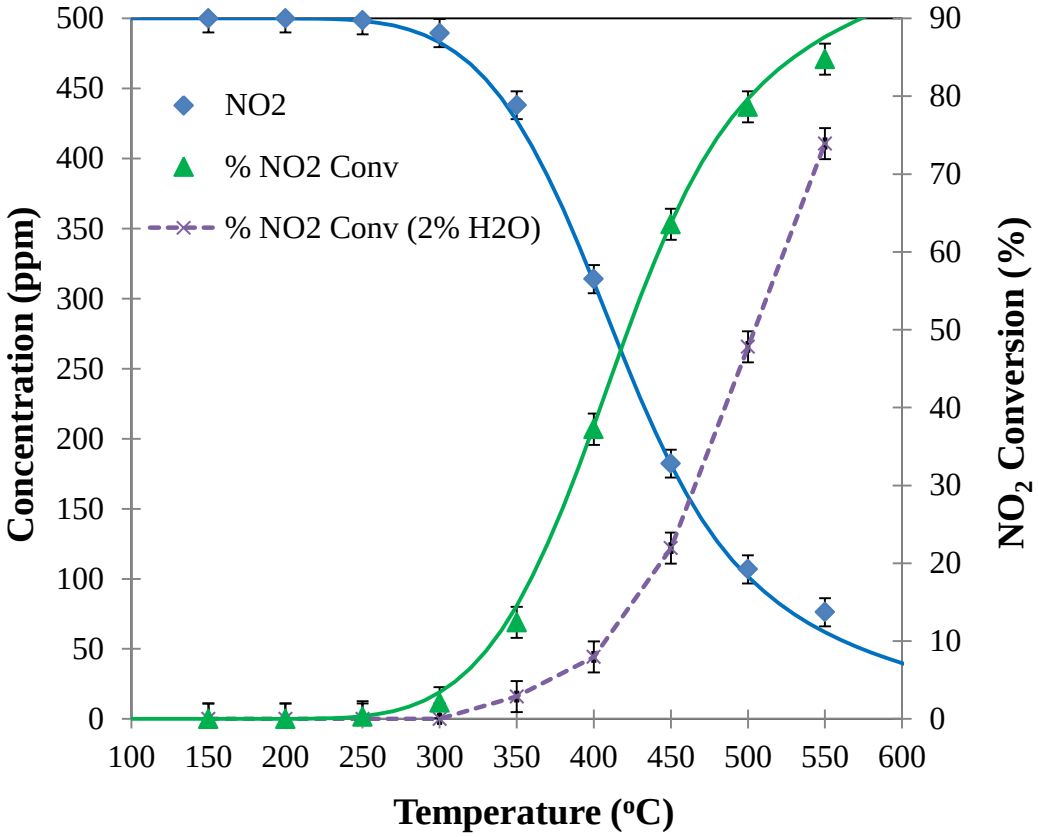

Figure 8-4a: Steady state NO_2 concentrations and conversions (symbols: experiments, continuous lines: model predictions) during the NO_2 decomposition reaction studied on Fe-ZSM-5 catalyst. Feed: 500 ppm NO_2 and 0-2% H_2O.

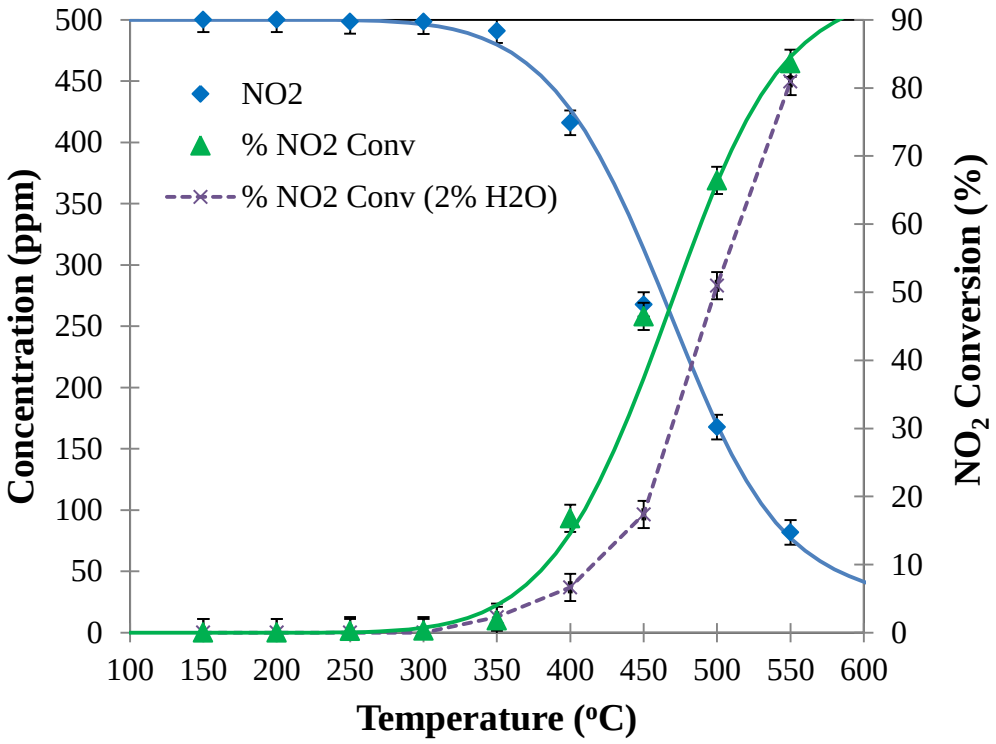

Figure 8-4b: Steady state NO_2 concentrations and conversions (symbols: experiments, continuous lines: model predictions) during the NO_2 decomposition reaction studied on Cu-chabazite catalyst. Feed: 500 ppm NO_2 and 0-2% H_2O.

NO_2 consumption started at 300 ^oC and increased with temperature, attaining about 84% at 550 ^oC. The presence of (2%) feed water inhibited this reaction to a great extent with negligible NO_2 decomposing at temperatures up to 350 ^oC. The maximum NO_2 conversion at 550 ^oC decreased to 74%. Thus water showed similar inhibition effect (as observed earlier during the NO oxidation) on the NO_2 decomposition reaction.

A similar study was carried out on the Cu-chabazite catalyst (Figure 8-4b). In the absence of water, the NO_2 decomposition reaction started at around 350 ^oC compared to 300 ^oC on the Fe-ZSM-5 catalyst. The reaction was slower on Cu-chabazite catalyst for temperatures up to 500 ^oC. The probable reason for this could be the strong adsorption of NO_2 on Cu-chabazite. Thus the reverse NO_2 decomposition reaction is slower on Cu-chabazite catalyst which also explains the observed deviation from equilibrium curve in

the presence of excess feed NO_2 (NO_2/NOx = 0.75) in Figure 8-3a. The introduction of NO_2 leads to the formation of nitrates which are more stable on Cu-chabazite compared to Fe-ZSM-5 catalysts [135]. The nitrate formation is given by

$$3\ NO_2 + O^{2-} \leftrightarrow 2\ NO_3^- + NO. \qquad (8\text{-}3)$$

We discuss this issue later in this chapter. The NO_2 conversions remained unaffected in the presence of 5% O_2 on both the catalysts. The presence of (2%) feed water inhibited the NO_2 decomposition reaction on the Cu-chabazite catalyst as well.

8.4.3 Kinetics Studies

A key objective of this study was to build a mechanistically-based predictive intrinsic kinetic model which captures the experimentally observed reaction orders and rate dependence with respect to all the participating reactant and/or product species.

Above, we discussed the inhibition effect of NO_2 on the forward NO oxidation reaction. Thus, while estimating the reaction orders with NO and O_2, it was necessary to include excess NO_2 in the feed so that the reactor could be operated in a differential manner while restricting the maximum NO conversions below 10% [146]. This was achieved with the inclusion of excess feed NO_2, 330 ppm for Fe-ZSM-5 and 125 ppm for Cu-chabazite catalysts. The amount of feed NO_2 for Cu-chabazite was less compared to Fe-ZSM-5 as the forward NO oxidation reaction was found to be slower on Cu-chabazite with stronger inhibition by feed NO_2 compared to Fe-ZSM-5. Since NO oxidation is a reversible reaction, it was necessary to choose the reaction temperature in such a way that the reverse reaction was negligible and operation was far from equilibrium. Earlier results on NO_2 decomposition showed that the reverse NO_2 decomposition reaction started at

higher temperatures (> 350 ^{o}C). Thus the temperature selected for this study was 290 ^{o}C which ensured that the differential kinetics study was carried out far from equilibrium.

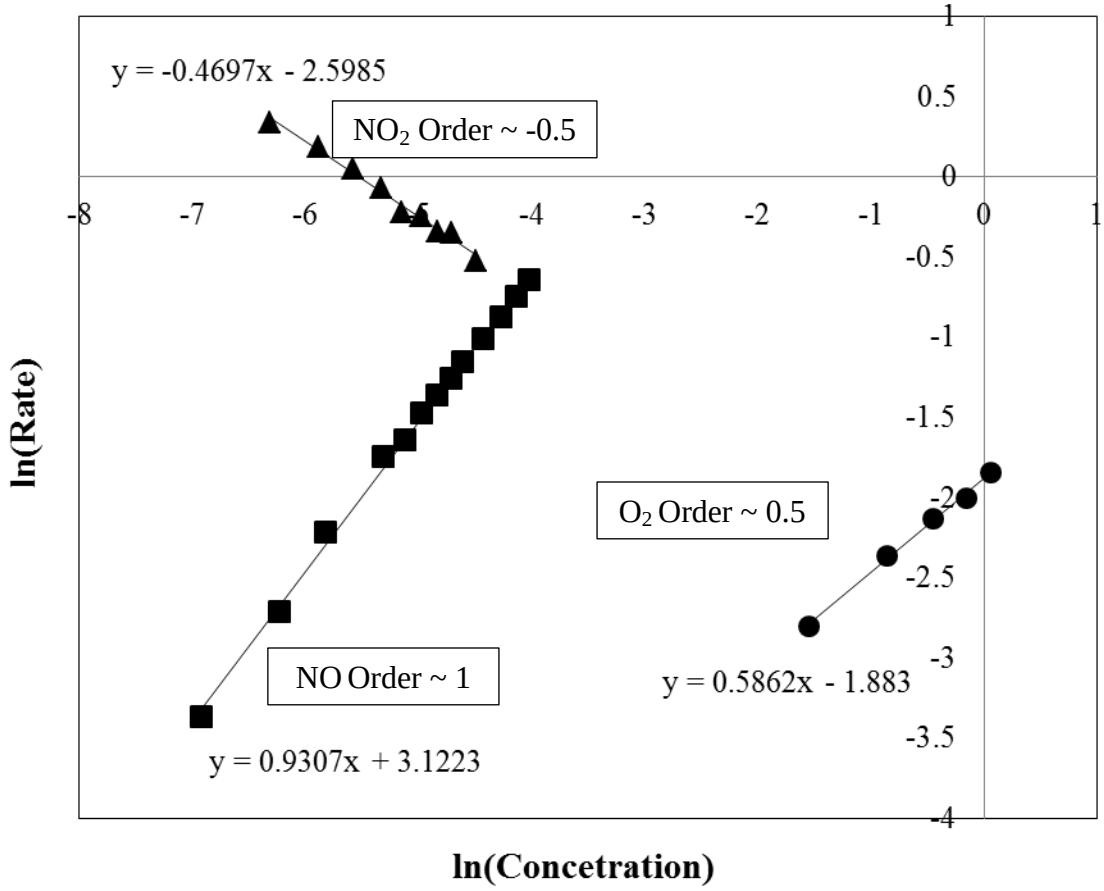

Figure 8-5: Dependence of NO oxidation rates on NO, O_2 and NO_2 at 290 ^{o}C. Feed for NO order: 5% O_2, 330 ppm NO_2, 100-800 ppm NO. Feed for O_2 order: 500 ppm NO, 330 ppm NO_2, 0-5 % O_2. Feed for NO_2 order: 500 ppm NO, 5% O_2, 50-500 ppm NO_2. Catalyst: Fe-ZSM-5. Total flow rate =1000 sccm. GHSV = 57,000 hr^{-1}.

The forward NO oxidation reaction orders were determined by independently varying the concentrations of the reacting species over the ranges: NO (100-800 ppm), O_2 (0-5%) and NO_2 (50-500 ppm). From the logarithmic plot of rate (mol/m^3/s) of disappearance of NO vs concentrations (mol/m^3) of the reacting species, Figure 8-5 (Fe-ZSM-5) and Figure 8-6 (Cu-chabazite), the reaction rate was found to have linear (+1

order) dependence with respect to NO and about positive half order dependence with respect to O_2 on both the catalysts.

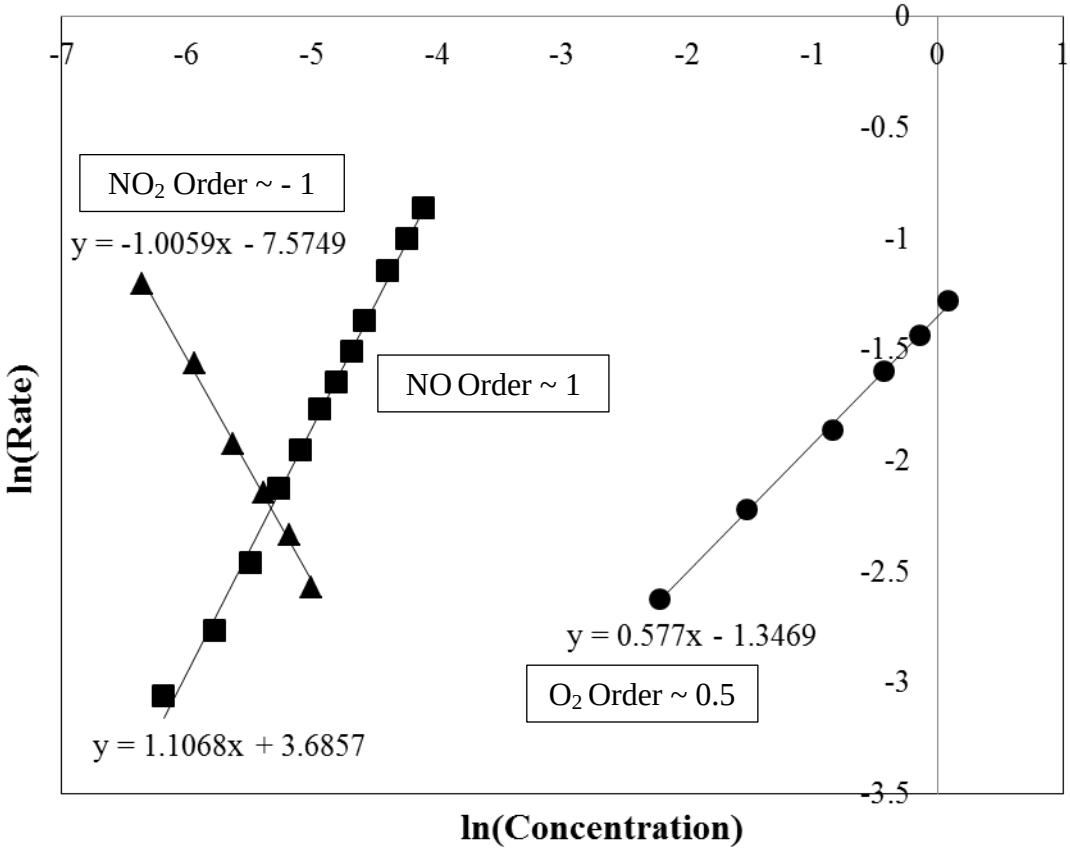

Figure 8-6: Dependence of NO oxidation rates on NO, O_2 and NO_2 at 290 ^{o}C. Feed for NO order: 5% O_2, 125 ppm NO_2, 100-800 ppm NO. Feed for O_2 order: 500 ppm NO, 125 ppm NO_2, 0-5 % O_2. Feed for NO_2 order: 500 ppm NO, 5% O2, 50-300 ppm NO_2. Catalyst: Cu-chabazite. Total flow rate =1000 sccm. GHSV = 57,000 hr^{-1}.

In order to determine the reaction order with respect NO_2, we varied the inlet NO_2 concentrations from 50-500 ppm while keeping NO (500 ppm) and O_2 (5%) concentrations the same. The NO oxidation rate decreased for each incremental rise in the inlet NO_2 concentration. The apparent NO_2 reaction order was found to be nearly -0.5 on Fe-ZSM-5 (Figure 8-5) and -1 on Cu-chabazite (Figure 8-6) catalyst. This further confirms the NO_2 inhibition on the NO oxidation reaction discussed earlier and this inhibition is found to be more pronounced on Cu-chabazite compared to Fe-ZSM-5.

We further studied the effects on NO and O_2 concentrations on the forward NO oxidation reaction by keeping the maximum NO conversions below 15% for the feeds containing no NO_2 in the feed. As discussed earlier, the rate of NO oxidation is higher on Fe-ZSM-5 compared to the Cu-chabazite catalyst. Hence, higher space velocities were required to achieve the low NO conversions (< 15%). For Fe-zeolite, this was achieved using a small monolith piece (16 channels, 1 cm length) so that a GHSV as high as 240,000 hr^{-1} could be achieved. For Cu-chabazite catalyst, we used the same catalyst dimensions (GHSV = 57,000 hr^{-1}) as discussed earlier. We selected three different temperatures (in the range of 200-290 ^oC) for this study. Figure 8-7 (8-8) shows the dependence of rate vs. inlet NO (O_2) concentrations for the Fe-ZSM-5 catalysts while Figure 8-9 (8-10) shows the dependence of rate vs. inlet NO (O_2) concentrations for the Cu-chabazite catalyst. These data again confirm that the reaction orders with respect to NO and O_2 are about the same as discussed earlier for the feeds containing excess NO_2. The reason for this could be that the NO_2 produced during the NO oxidation reaction with conversions as small as 12% is insufficient to strongly inhibit this reaction. Very small amounts of NO_2 (< 50 ppm) produced during the reaction alter the NO oxidation rates to a small extent, hence have only a negligible effect on the reaction orders.

To this end, we propose the following power law kinetic model for the forward NO oxidation reaction on Fe-ZSM-5 catalyst

$$R_{NO_{oxi}} = k_f \frac{[NO]^a [O_2]^b}{[NO_2]^c}, \tag{8-4}$$

where k_f is the forward rate constant and a = 0.9 – 1, b = 0.55 – 0.59 and c = 0.42 – 0.49.

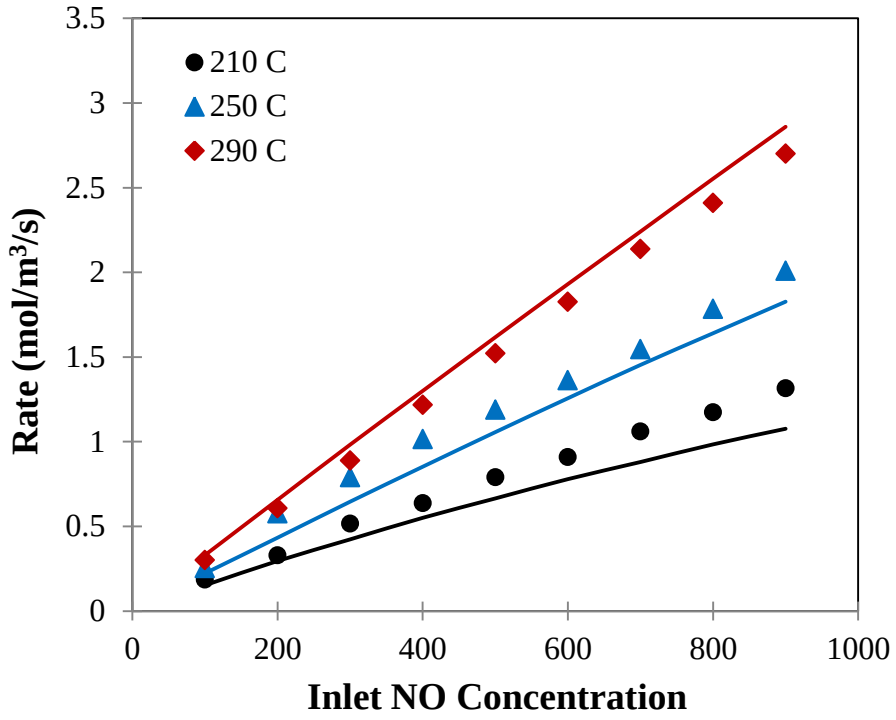

Figure 8-7: Effect of inlet NO concentration on the rate of NO consumption during the NO oxidation reaction on Fe-ZSM-5 catalyst (Symbols: experiments, Solid lines: model predictions). Feed: 100-900 ppm NO, 5% O_2, Total flow rate =1000 sccm.

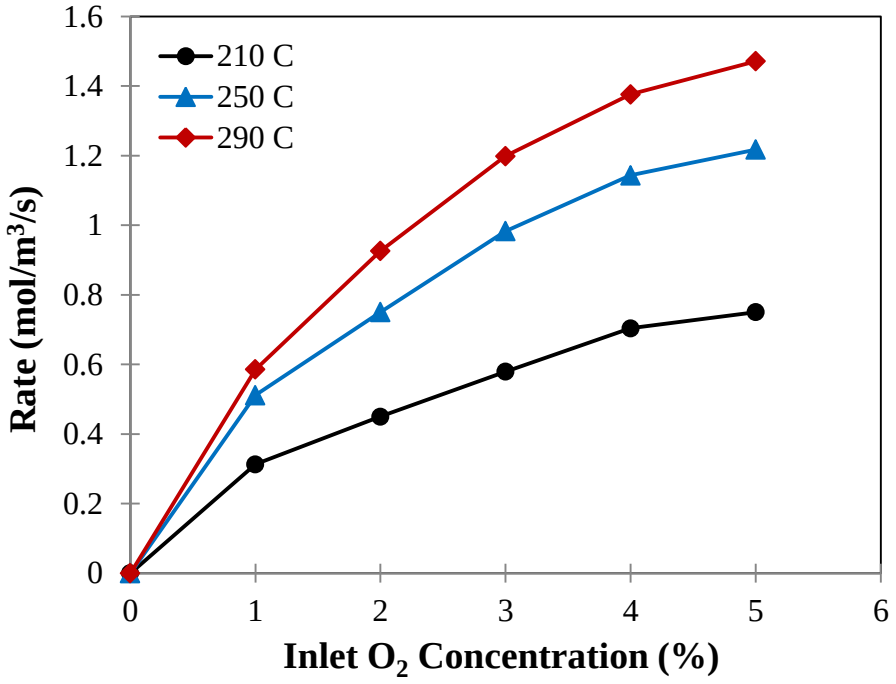

Figure 8-8: Effect of inlet O_2 concentration on the rate of NO consumption during the NO oxidation reaction on Fe-ZSM-5 catalyst. Inlet Feed: 500 ppm NO, 0-5% O_2.

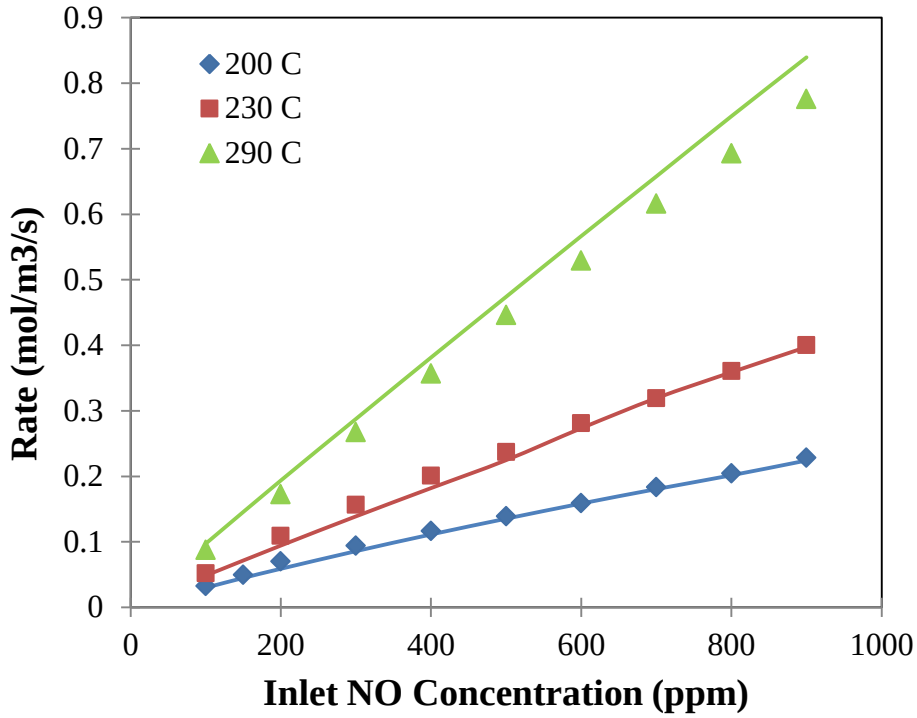

Figure 8-9: Effect of inlet NO concentration on the rate of NO consumption during the NO oxidation reaction on Cu-chabazite catalyst (Symbols: experiments, Solid lines: Model predictions). Feed: 100-900 ppm NO, 5% O_2, Total flow rate =1000 sccm.

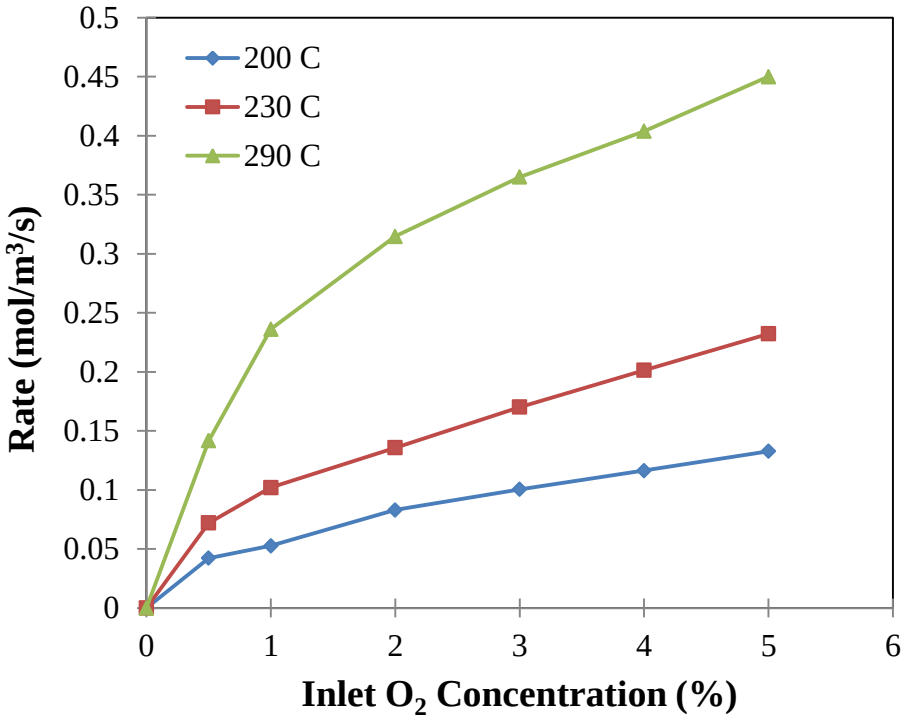

Figure 8-10: Effect of inlet O_2 concentration on the rate of NO consumption during the NO oxidation reaction on Cu-chabazite catalyst. Feed: 500 ppm NO, 0-5% O_2.

Similarly, the following power law kinetic model is proposed for the forward NO oxidation reaction on Cu-chabazite catalyst

$$R_{NO_{oxi}} = k_f^{'} \frac{[NO]^{a'}[O_2]^{b'}}{[NO_2]^{c'}}, \qquad (8\text{-}5)$$

where $k_f^{'}$ is the forward rate constant and *a'* = 0.85 - 1, *b'* = 0.47 – 0.51 and *c'* = 0.89 – 1. The activation energy of this reaction was found to be 39 kJ/mol on Fe-ZSM-5 while 56 kJ/mol on Cu-chabazite catalysts. Finally, since the real exhaust contains an excess of water, it was necessary to verify the above observed apparent reaction orders and activation energies in the presence of water. Hence, we repeated above experiments (Figures 8-5, and 8-6) in the presence of 2% feed water. Even though the presence of feed water decreased the NO oxidation reaction rate significantly, it did not have any dramatic effect on the above observed reaction parameters.

Thus, this kinetic study was useful in estimating the reaction orders with respect to all the individual reactants. The reaction orders with respect to NO and O_2 were similar on both the Fe-ZSM-5 and Cu-chabazite catalysts. However, the NO oxidation reaction rate was found to have stronger negative order dependence with respect to NO_2 on the Cu-chabazite compared to Fe-ZSM-5. These results confirm and explain the earlier reported (Figures 8-2 and 8-3) strong NO_2 inhibition on the NO oxidation reaction on the Cu-chabazite catalyst.

8.4.4 Mass Transfer Limitations

In order to derive an intrinsic kinetic model, the reaction should be carried out in a purely kinetically limited regime in which the extent of mass transfer limitations is

minimal. In Chapter 6 and [209], we described four types of transport processes of interest in the washcoated zeolite-based catalyst system: 1) external mass transfer, 2) internal mass transfer (washcoat or pore diffusion), 3) intracrystalline diffusion and 4) convective flow. In addition, there is a catalytic reaction which is a chemical process. Tables 8-3 and 8-4 summarize the estimated values of characteristic times of these individual processes for the Fe-ZSM-5 and Cu-chabazite catalysts, respectively. Comparisons of these characteristic times provide an insight in to the rate limiting process [147, 209]. The maximum temperature selected for these estimates was 350 ^{o}C as the reverse NO_2 decomposition reaction becomes important at higher temperatures. From Tables 8-3 and 8-4, it is clear that the characteristic reaction time was always much greater than the characteristic times for the other processes over the temperature range of interest. Moreover, the value of Weisz-Prater modulus (Ψ) was found to be less than unity for a value of effective diffusivity as low as 10^{-7} m^2/s [116]. This is in contrast to our earlier study [103] which focused on the standard SCR reaction in which we reported the existence of washcoat diffusion limitations at higher temperatures ($\geq$ 350 ^{o}C). NO oxidation being slower (than the standard SCR) and reversible at higher temperatures, we do not see any internal mass transfer limitations. This analysis indicate that the reaction was in kinetic regime for temperatures up to 350 ^{o}C and the reverse NO_2 decomposition reaction was negligible.

In order to study the extent of washcoat diffusion limitations in more detail, we synthesized catalysts with same washcoat volume but different washcoat thicknesses and lengths. This approach was similar to our earlier study focused on the standard SCR reaction [103]. For Fe-ZSM-5, we used 1 cm long FeZ-22 and 2 cm long FeZ-11 catalyst.

Table 8-3: Estimated values of various characteristic times (in milli seconds) and the dimensionless numbers *P* (transverse Peclet number) and Ψ (Weisz-Prater modulus) in the temperature range of 210-350 ^{o}C for the NO oxidation reaction on Fe-ZSM-5 catalyst.

Temperature (^{o}C)	τ_c (ms)	τ_e (ms)	$\tau_{d,w}$ (ms))	τ_r (ms)	*P*	Ψ
210	5.70	1.67	5.5	84.4	0.25	0.36
250	5.15	1.45	4.8	46.2	0.24	0.59
290	4.92	1.28	4.2	36.3	0.23	0.67
350	4.70	1.08	3.6	23.9	0.21	0.87

Table 8-4: Estimated values of various characteristic times (in milli seconds) and the dimensionless numbers *P* and Ψ in the temperature range of 150-350 ^{o}C for the NO oxidation reaction on Cu-chabazite catalyst.

Temperature (^{o}C)	τ_c (ms)	τ_e (ms)	$\tau_{d,w}$ (ms))	τ_r (ms)	*P*	Ψ
150	31.8	2.1	6.91	998	0.065	0.038
200	28.5	1.72	5.71	454	0.06	0.069
250	25.8	1.46	4.81	177	0.056	0.151
300	23.5	1.24	4.12	100	0.053	0.229
350	21.6	1.11	3.58	55.9	0.05	0.361

While for the Cu-ZSM-5 catalyst, we used 1 cm long CuZ-20 and 2 cm long CuZ-10 catalysts. Results obtained with this study are summarized in Figure 8-11 and show that the NO conversions obtained on catalysts with the same washcoat volume but different washcoat thicknesses were comparable for both the Fe- and Cu-zeolite catalysts. These results are in agreement with the above theoretical calculations and confirm the absence

of washcoat diffusion limitations for the NO oxidation reaction and show that the data was estimated in a pure kinetic regime.

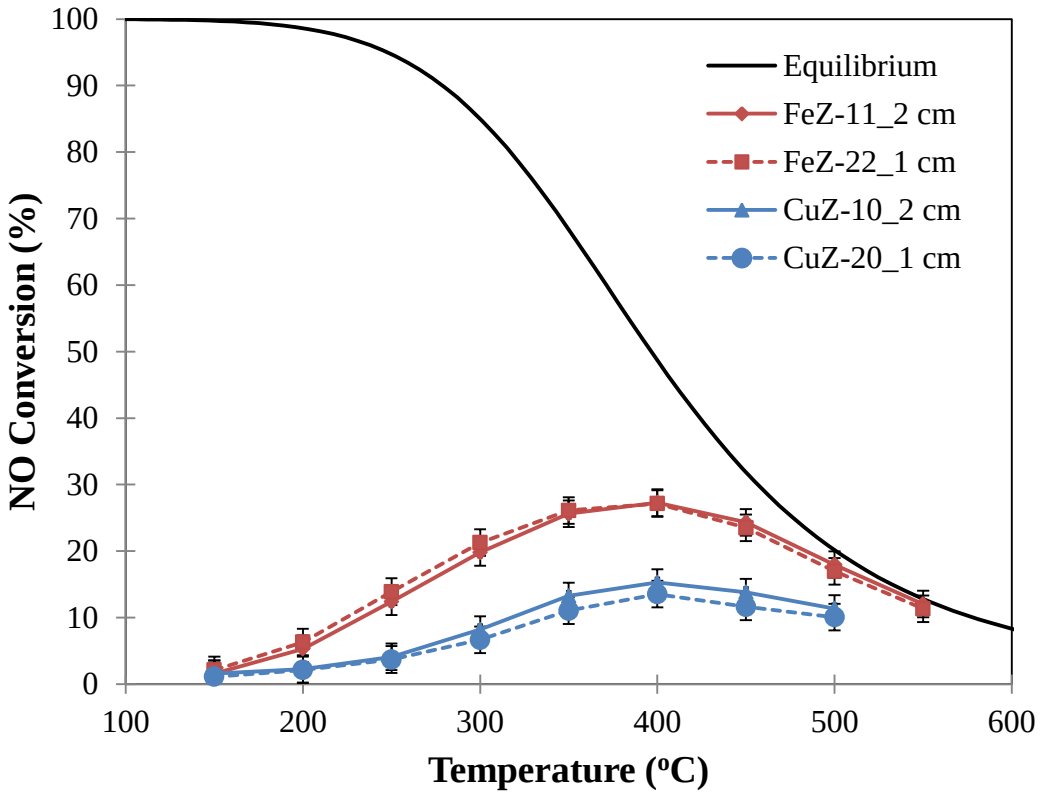

Figure 8-11: Steady state NO conversions obtained during the NO oxidation reaction studied on in-house synthesized FeZ-XX and CuZ-XX catalysts. Catalyst: No. of channels: 28. Length: 2 cm (FeZ-11 and CuZ-10); 1 cm (FeZ-22 and CuZ-20).

8.4.5 Transient Experiments

In order to get further insight into the NO oxidation chemistry, we carried out various transient experiments on the commercial Fe- and Cu-zeolite catalysts. Temperature programmed desorption (TPD) studies of NO and NO_2 were carried out. A mixture containing 500 ppm NO (in Ar) was fed to the catalyst (1 hour) followed by an Ar flush for 30 minutes, then a 10 ^{o}C/min temperature ramp was applied. Negligible amounts of NO were detected during the temperature ramp on both the catalysts. This indicates that the NO adsorption capacity of the zeolite catalysts is low, in agreement

with previous literature studies [39, 100]. A similar approach was used for the NO_2 TPD studies on both the catalysts. Figure 8-12 compares the NO_2 TPD experiments on Fe-ZSM-5 and Cu-chabazite catalysts at 150 ^oC. Unlike NO, a substantial amount of NO_2 was detected during the temperature ramp on both catalysts. In addition, during the NO_2 uptake a temporal peak of NO was detected. An analysis of the data indicated that the ratio of NO formed/NO_2 consumed was about 1/3 which confirms the NO_2 disproportionation reaction (8-3) forming NO and nitrates. Similar observations during the NO_2 uptake experiments have been reported on various catalysts [39, 99, 100, 147].

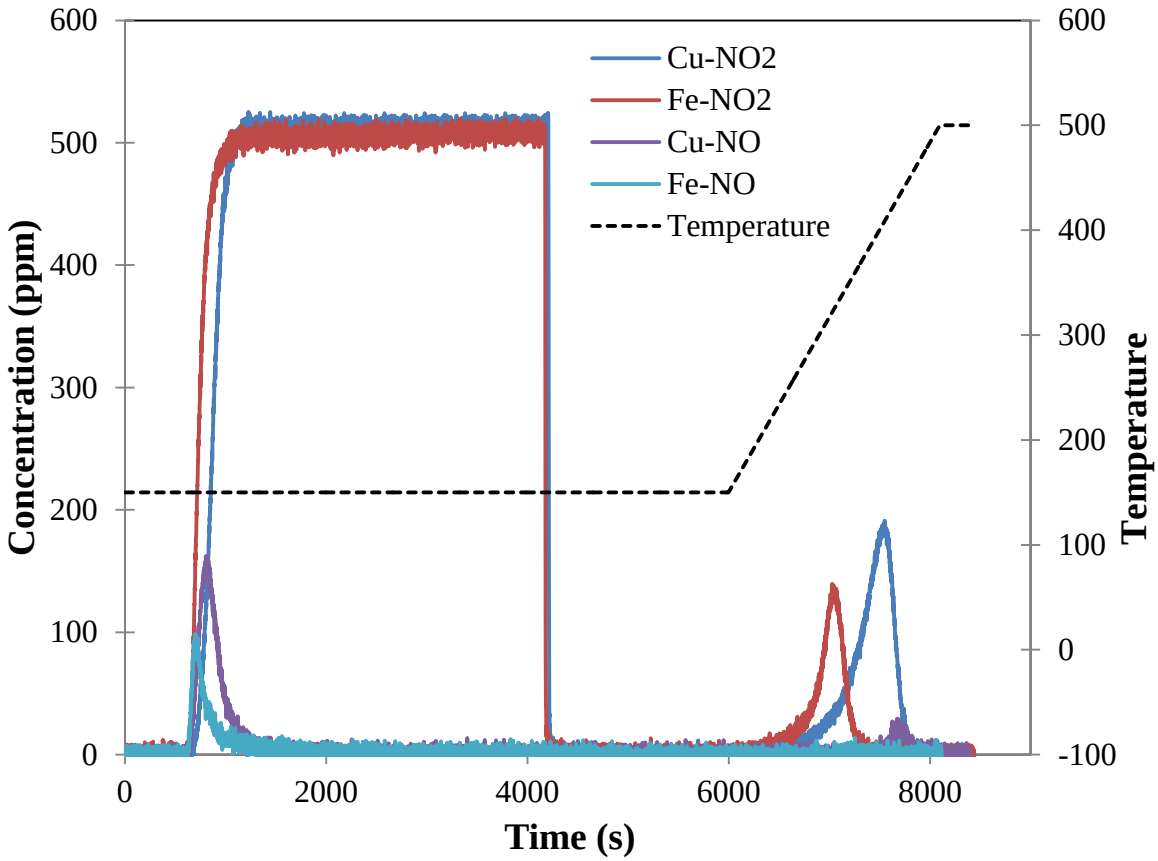

Figure 8-12: NO_2 Temperature Programmed Desorption (TPD) experiments carried out on Fe- and Cu-chabazite catalyst at 150 ^oC as the initial temperature of adsorption. 500 ppm of NO_2 was adsorbed for 1 hour. Temperature ramp of 10 ^oC/min at 6000s.

The results in Figure 8-12 reveal that a larger amount of NO_2 was evolved during the temperature ramp and was released at higher temperatures for the Cu-chabazite catalyst. These trends suggest a higher adsorption capacity of NO_2 on Cu-chabazite. Cu, being more basic than Fe, leads to the higher NOx storage [135]. Moreover, the NO_2 was more strongly adsorbed on the Cu-chabazite compared to the Fe-ZSM-5 catalyst, since it was released at higher temperatures. This may indicate that some of the NO_2 is stored in the form of nitrates [87] and copper (cuprous/cupric)-nitrates are more stable than iron(ferrous/ferric)-nitrates [218]. The higher storage capacity of NO_2 and higher stability of nitrates on Cu-chabazite help to explain the stronger NO_2 inhibition of NO oxidation on Cu-chabazite catalyst. We return to this issue later in the kinetic analysis.

Additional NO_2 uptake experiments were carried out on the Cu-chabazite catalyst at 150 ^oC in order to understand the effect of the NO_2 concentration on NO and nitrate formation. Three different feed NO_2 concentrations of 100 ppm, 300 ppm and 500 ppm were used. The catalyst was exposed to a feed of pure NO_2 (in Ar) for about 5400 s. Figure 8-13 shows the ratio of amount of NO formed to the total inlet NO_2 concentration. Again a large peak of NO was observed for each NO_2 feed during initial uptake. This confirms the NOx storage and formation of nitrates by reaction (8-3) discussed above. For each NO_2 feed concentration, the ratio of NO formed/inlet NO_2 exhibited a maxima of about 0.3 and then decreased. In each case, the ratio decreased to 0 (the noise level) in less than 3600 s. Bhatia et al. [147] and Kabin et al. [219] carried out similar studies on Pt/Al_2O_3 and $Pt/BaO/Al_2O_3$ catalysts, respectively. The experimental trends reported here are similar to those reported results, albeit a different catalyst system. But they observed higher NOx storage capacities on the Pt/Al_2O_3 catalysts compared to what we obtained

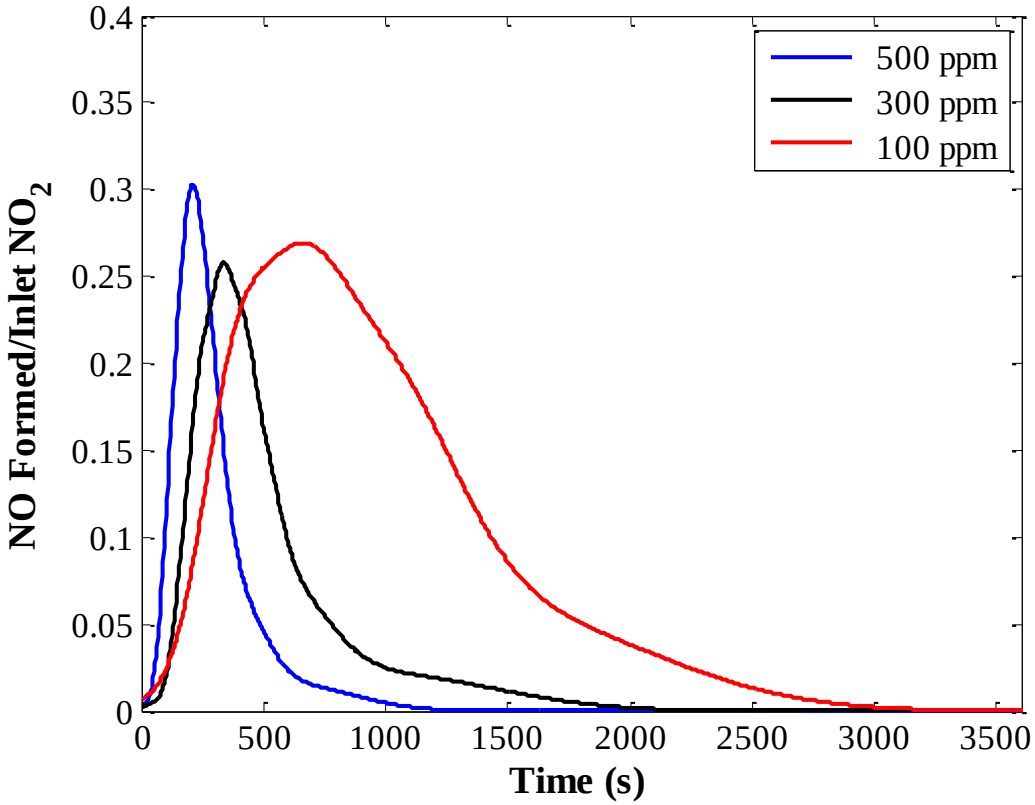

Figure 8-13: Ratio of outlet NO concentration (measured at the reactor outlet) to inlet NO_2 concentration Catalyst: Cu-chabazite, Temperature: 150 ^{o}C, Total flow rate: 1000 sccm, GHSV: 57,000 hr^{-1}.

on the Cu-chabazite catalyst. Bhatia et al. [147] called the ratio of outlet NO concentration/inlet NO_2 concentration' as the 'relative NO concentration'. The relative NO concentration decreased very fast for the feeds of 500 and 300 ppm NO_2 compared to that for the 100 ppm feed NO_2. This is because higher the feed NO_2 concentration, the more quickly the catalyst surface is saturated with nitrates. The maxima obtained for the relative NO concentration was less for the feeds with lower NO_2 concentrations (i.e., 100, 300 ppm). This was due to the higher relative amounts of NOx storage [147] for the lower inlet NO_2 feeds. Figure 8-14 shows the same results where we plot integral ratio (equation 8-6) of NO formed to NOx stored as a function of time,

$$\frac{\int_0^{t^*} C_{NO}(t)dt}{\int_0^{t^*}\left[C^0_{NO_2}(t) - C_{NO_2}(t)\right]dt}. \qquad (8\text{-}6)$$

$C^0_{NO_2}$ is the inlet NO_2 concentration, C_{NO2} and C_{NO} are the effluent gas concentrations, and t^* is the total time. The plot clearly shows that the integral ratio reaches the expected 1/3 ratio in equation (8-3) and confirm the evolution of NO because of NO_2 disproportionation.

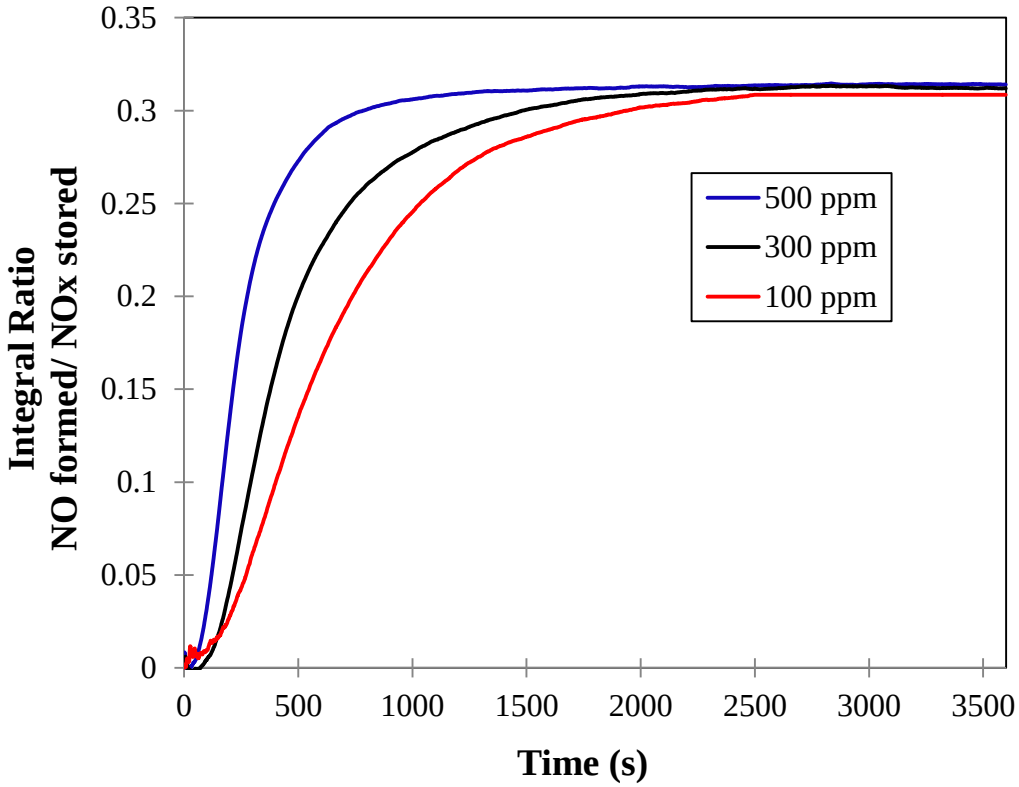

Figure 8-14: Integral ratio of NO formed to NOx stored for different feed NO_2 concentrations. Catalyst: Cu-chabazite, Temperature: 150 ^oC, Total flow rate: 1000 sccm, GHSV: 57,000 hr^{-1}.

These results emphasize on the importance of inclusion of NO_2 disproportionation (and storage) step during transient data analysis of NO oxidation reaction. However, inclusion of these steps is not required for the analysis of steady state NO oxidation data. We

discuss this issue later in this chapter. Earlier (Figure 8-4) we reported the evolution of NO from NO_2 decomposition reaction at higher temperatures (> 350 ^oC). Thus, with pure NO_2 feed, NO can be observed at the outlet by NO_2 storage and disproportionation at lower temperatures and NO_2 decomposition at higher temperatures.

In order to better understand the role of nitrate formation on the NO oxidation reaction, we pre-exposed the catalyst to a prescribed feed and duration and then carried out transient and steady state NO oxidation studies. For this purpose, four different pretreatments were used. The Fe-ZSM-5 catalyst temperature was kept constant at 200 ^oC. Initially, the catalyst was pretreated in the presence of 5% O_2 feed in Ar for 30 min. Then a feed containing 500 ppm NO and 5% O_2 was introduced. The NO_2 concentration increased slowly and reached steady state values. The same experiment was repeated with different pretreatment feed having 1% H_2 in Ar for 30 min after which 500 ppm NO and 5% O_2 were introduced. This resulted in about the same (as observed earlier) transient and steady state response of both NO and NO_2. The next pretreatment exposed the catalyst surface to 500 ppm NH_3 (in Ar) feed after which 500 ppm NO and 5% O_2 were introduced. We reported these particular results with NH_3 pretreatment in Chapter-3 where we recorded a N_2 peak (formed by the standard SCR reaction (8-2) between adsorbed NH_3 and NO/O_2) with the introduction of NO and O_2. The N_2 in the effluent vanishes eventually when the entire surface NH_3 is consumed by reaction (8-2); the NOx (NO and NO_2) concentrations reach the same steady state concentrations as recorded earlier for the above two pretreatments cases. For the next study, 1000 ppm NO_2 in Ar was used as the pretreatment feed. After pretreatment, introduction of 500 ppm NO and 5% O_2 into the reactor resulted in a sharp NO_2 peak which completely disappeared in

about 100 s and the exit NO_2 reached the same steady state concentration as measured for the earlier two cases. The NO_2 peak strongly suggests the presence of nitrates on the catalyst surface which are reduced by NO (reaction 8-3). We carried out an additional experiment similar to case 3 in which the catalyst was initially pretreated with an NO_2 feed. After pretreatment, the catalyst was subjected to NO (in Ar) feed and it resulted in a similar NO_2 peak. After 300 s, the catalyst was flushed with an Ar feed and a temperature ramp of 10 ^oC/min was applied. During the temperature ramp, we did not observe any NO_2 in the outlet. This showed that all the nitrates were initially reduced by NO and catalyst surface was devoid of nitrates by the time the inert Ar was fed. Grossale et al. [32] found that the surface nitrates are reduced in the presence of NO at temperatures as low as 50 ^oC on Fe-zeolite catalysts and this is considered as a key step in the fast SCR reaction (8-7) chemistry [33].

$$2\ NH_3 + NO + NO_2 \rightarrow 2\ N_2 + 3\ H_2O \qquad \Delta H = -\ 3.78 \times 10^5\ J/mol\ NH_3 \qquad (8\text{-}7)$$

We repeated above experiments for different pretreatments cases on Cu-chabazite catalyst where similar behavior was recorded. Collectively, these experiments showed that the nitrates are highly unstable in the presence of NO and that pretreatment by different oxidizing/reducing agents did not appear to have any effect on the steady state NO oxidation reaction. The latter feature is in contrast to a similar study carried out on Pt/Al_2O_3 catalyst by Bhatia et al. [147] who observed different steady state NO conversions for different pretreatments. They observed minimum NO oxidation activity for the NO_2 pretreatment as it was found to poison the catalyst and thus lower its activity. No such NO_2 poisoning effect was observed on the Fe-ZSM-5 catalyst.

8.4.6 Kinetic Modeling and Simulation of Experimental Results

Of interest for catalyst/reactor design and optimization is the development of predictive kinetic and reactor models for NO oxidation and SCR. As discussed earlier, few literature studies have provided global kinetic models for the NO oxidation reaction on Fe- and Cu-zeolite catalysts. Olsson et al. [100] presented a microkinetic model which included three different types of sites for the NOx adsorption and NO oxidation. Here we develop a global kinetic model that comprises a single rate expression based on an assumed rate determining step (RDS). Such a model is more easily used in reactor modeling. In this study, we identify the rate limiting step and present a global kinetic model to predict our experimental results.

The following reaction scheme is described as the basis for the kinetic model. For the sake of simplicity, we assume the existence of a single type of active site (-S) on the catalyst. S may represent a metal-site, O-S a bridging metal oxide, etc. Thus NO_2-S could be considered as nitrate precursor. The kinetic model includes following steps:

S1: $O_2 + S \leftrightarrow O_2\text{-}S$, (8-8)

S2: $O_2\text{-}S + S \leftrightarrow 2\ O\text{-}S$, (8-9)

S3: $NO + O\text{-}S \leftrightarrow NO_2\text{-}S$, (8-10)

S4: $NO_2 + S \leftrightarrow NO_2\text{-}S$. (8-11)

The adsorption of NO is neglected as the TPD data showed negligible adsorption of NO on both the Fe-/Cu-zeolite catalysts. The model assumes reversible adsorption of molecular oxygen (S1) on the catalyst followed by its dissociation in a subsequent step (S2). It also includes an NO oxidation step in which NO in the gas phase reacts with

adsorbed oxygen atom to give NO_2 adspecies on the surface (S3). Finally, the model also accounts for the reversible NO_2 adsorption and desorption (S4).

In addition to these four important steps S1-S4, we include two additional steps S5 and S6 to account for the experimentally observed nitrate (NO_3-S) formation on the catalyst surface:

S5: 2 NO_2-S ←→ NO_3-S + NO + S, (8-12)

S6: NO_2-S + O-S ←→ NO_3-S + S, (8-13)

S5': 3 NO_2-S + O-S ←→ 2 NO_3-S + NO + 2 S. (8-14)

S5 represents the formation of surface nitrate and NO from NO_2 disproportionation. The reverse reaction accounts for the known instability of nitrates in the presence of NO. S6 accounts for the decomposition of nitrates to form NO_2. The overall reaction scheme (S1-S6) is similar to the one used in the microkinetic model derived by Olsson et al. [100]. The sum of steps S5 and S6, given by S5' indicates the formation of 2 moles of nitrates and a mole of NO form 3 moles of NO_2, following equation (8-3). S5' accounts for the rapid evolution NO and nitrates at lower temperatures in the presence of NO_2 and the reverse reaction accounts for the rapid nitrate decomposition in the presence of NO [99]. The rates of all the above reactions are expressed as:

$$R_{v1} = k_{f1} X_{O_2,s} \theta_v - k_{b1} \theta_{O_2}, \quad (8\text{-}15)$$

$$R_{v2} = k_{f2} \theta_{O_2} \theta_v - k_{b2} \theta_O^2, \quad (8\text{-}16)$$

$$R_{v3} = k_{f3} X_{NO,s} \theta_O - k_{b3} \theta_{NO_2}, \quad (8\text{-}17)$$

$$R_{v4} = k_{f4} X_{NO_2,s} \theta_v - k_{b4} \theta_{NO_2}, \quad (8\text{-}18)$$

$$R_{v5'} = k_{f5'} \theta_{NO_2}^3 \theta_O - k_{b5'} \theta_{NO_3}^2 X_{NO,s} \theta_v^2. \quad (8\text{-}19)$$

Here k_{fi} and k_{bi} refer to the forward and backward rate constants of reaction step *i*, respectively and are defined as

$$k_{fi} = A_{fi} e^{-E_{fi}/RT_s}, \tag{8-20}$$

$$k_{bi} = A_{bi} e^{-E_{bi}/RT_s}, \tag{8-21}$$

where A_{fi} and A_{bi} are the pre-exponential factors and E_{fi} and E_{bi} are the activation energies of the forward and backward reaction step *i*, respectively. θ_i refers to the fractional surface coverage of species *i*. The fractional coverage of the various species are defined as follows assuming equilibration of steps S1, S2, S4 and S5':

$$\theta_{O_2} = K_1 X_{O_2,s} \theta_v, \tag{8-22}$$

$$\theta_O = \sqrt{K_1 K_2 X_{O_2,s}}\, \theta_v, \tag{8-23}$$

$$\theta_{NO_2} = K_4 X_{NO_2,s} \theta_v, \tag{8-24}$$

$$\theta_{NO_3} = \sqrt{\frac{K_5' K_4^3 X_{NO_2,s}^3 \sqrt{K_1 K_2 X_{O_2,s}}}{X_{NO,s}}}\ \theta_v. \tag{8-25}$$

Here K_i is the equilibrium constant of the step *i* and is given as $K_i = k_{fi}/k_{bi}$

Our approach in converging on a kinetic model was to assume different rate determining steps and then to check if the resulting rate expression is consistent with the differential data (reaction orders). Amongst the various kinetic models that we tried, we found that the kinetic model with S3 as the RDS was able to best predict the data. The final rate expression is of the form:

$$R_{NO_{oxi}} = k_{f3}\left(X_{NO,s}\sqrt{K_1K_2X_{O_2,s}} - \frac{K_4X_{NO_2,s}}{K_3} \right)\theta_v$$

$$= k_{f3}\sqrt{K_1K_2}\left(X_{NO,s}\sqrt{X_{O_2,s}} - \frac{X_{NO_2,s}}{K_{eq}} \right)\theta_v . \quad (8\text{-}26)$$

Here K_{eq} is the equilibrium constant of the overall NO oxidation reaction and is given by

$$K_{eq} = \frac{K_3\sqrt{K_1K_2}}{K_4}. \quad (8\text{-}27)$$

This model captures the experimentally observed functional form of the NO oxidation reaction rate expression i.e., reaction orders agree well compared to other kinetic models. Moreover, the model was tested for the parametric sensitivity of various pre-exponential factors to confirm the rate limiting step.

We now describe two reaction schemes, keeping with S3 as the RDS, which predict the experimental data equally well. The first one is the four step (S1-S4) scheme where the rate expression is given by equation (8-26) for which the fractional coverage of vacant sites is given by

$$\theta_v = \frac{1}{1 + K_1X_{O_2,s} + \sqrt{K_1K_2X_{O_2,s}} + K_4X_{NO_2,s}}. \quad (8\text{-}28)$$

Thus the final rate expression is given by

$$R_{NO_{oxi}} = \frac{k_{f3}\sqrt{K_1K_2}}{1 + K_1X_{O_2,s} + \sqrt{K_1K_2X_{O_2,s}} + K_4X_{NO_2,s}}\left(X_{NO,s}\sqrt{X_{O_2,s}} - \frac{X_{NO_2,s}}{K_{eq}} \right). \quad (8\text{-}29)$$

This rate expression satisfies the fractional orders with respect to all the participating species as determined by the differential kinetic study. The second reaction scheme adds S5’ to the four step model. We return to this kinetic model later.

In order to estimate various kinetic parameters for the four-step scheme (equation (8-14) – equation (8-29)), we used experimental data from the experiments described in Figures 8-1, 8-7, 8-9 and 8-15. Additional experiments with varied feed NO concentrations (250 ppm, 750 ppm and 1000 ppm) were carried out. The data were fitted using a Levenberg Marquardt algorithm. The initial guess values of activation energies were taken from the literature study by Olsson et al. [100]. The values of resulting parameters estimated for this reaction are summarized in Table 8-5 (Fe-ZSM-5) and Table 8-6 (Cu-chabazite). Using the one dimensional two phase model described in Table 8-1 and various parameters mentioned in Tables 8-2, 8-5 and 8-6, we predicted the steady state NO conversions during the NO oxidation reaction as a function of temperature. Figure 8-1 shows a good agreement between the experimental and model predicted NO conversions obtained on both the catalysts with feeds containing pure NO (500 ppm) and O_2 (5%). Figures 8-7 and 8-9 indicate that the model could predict the low conversion data very satisfactorily. Figure 8-15 compares the experimental results with that predicted by the model for Fe and Cu-zeolite catalysts for various feed NO concentrations over the entire temperature range. For both the cases, the model is able to predict the experimental data satisfactorily.

In spite of the success of the four step model, it does not explicitly account for the formation and decomposition of nitrates. As mentioned earlier, NO_2-S is a surface nitrate precursor. Alternatively, NO_2-S could represent surface NO_2 and nitrate. However, to be more explicit, the five-step model (S1-S4, S5') accounts for the formation of nitrate species on the catalyst surface. The above rate expression (equation 8-26) is slightly modified as vacant site coverage becomes

$$\theta_v = \frac{1}{1 + K_1 X_{O_2,s} + \sqrt{K_1 K_2 X_{O_2,s}} + K_4 X_{NO_2,s} + \sqrt{\frac{K_5' K_4^3 X_{NO_2,s}^3 \sqrt{K_1 K_2 X_{O_2,s}}}{X_{NO,s}}}}. \quad (8\text{-}30)$$

For this case, the final rate expression is given by

$$R_{NO_{oxi}} = \frac{k_{f3}\sqrt{K_1 K_2}}{1 + K_1 X_{O_2,s} + \sqrt{K_1 K_2 X_{O_2,s}} + K_4 X_{NO_2,s} + \sqrt{\frac{K_5' K_4^3 X_{NO_2,s}^3 \sqrt{K_1 K_2 X_{O_2,s}}}{X_{NO,s}}}} \left(X_{NO,s}\sqrt{X_{O_2,s}} - \frac{X_{NO_2,s}}{K_{eq}} \right). \quad (8\text{-}31)$$

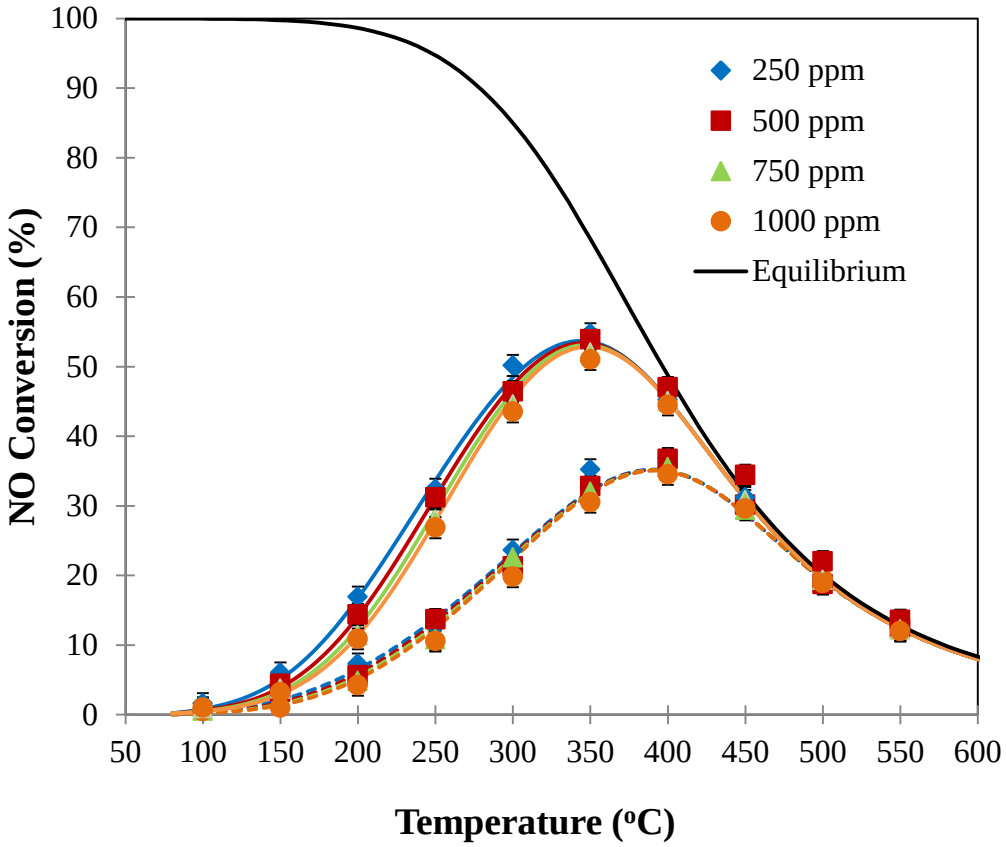

Figure 8-15: Comparison of experimental and model predicted NO conversion on Fe- and Cu-zeolite catalysts. (Symbols: experimental data; Continuous lines: model prediction; solid lines: Fe-ZSM-5, dashed lined Cu-chabazite.).

Table 8-5: Kinetic parameters used in the simulations for Fe-ZSM-5 catalyst.

Parameter	Numerical value (mol/m^3 washcoat s)	Parameter	Numerical value (kJ/mol)
A_{f1}	$1.44 \times 10^8 \pm 0.5 \times 10^8$	E_{f1}	0
A_{b1}	$1.17 \times 10^{14} \pm 0.16 \times 10^{14}$	E_{b1}	48
A_{f2}	5.14×10^{13}	E_{f2}	83.3
A_{b2}	5.12×10^{15}	E_{b2}	161.4
A_{f3}	$7.09 \times 10^5 \pm 0.2 \times 10^5$	E_{f3}	24.66 + 3
A_{b3}	6.38×10^{14}	E_{b3}	160.96 + 3
A_{f4}	$4.71 \times 10^6 \pm 1 \times 10^6$	E_{f4}	0
A_{b4}	5.12×10^{15}	E_{b4}	141.5

Table 8-6: Kinetic parameters used in the simulations for Cu-chabazite catalyst.

Parameter	Numerical value (mol/m^3 washcoat s)	Parameter	Numerical value (kJ/mol)
A_{f1}	$1.82 \times 10^9 \pm 0.8 \times 10^9$	E_{f1}	0
A_{b1}	$9.58 \times 10^{13} \pm 0.16 \times 10^{13}$	E_{b1}	48
A_{f2}	7.7×10^{14}	E_{f2}	83.3
A_{b2}	5.12×10^{15}	E_{b2}	161.4
A_{f3}	$6.41 \times 10^5 \pm 0.6 \times 10^5$	E_{f3}	29.11 + 5
A_{b3}	6.38×10^{14}	E_{b3}	165.41 + 5
A_{f4}	$4.33 \times 10^6 \pm 1 \times 10^6$	E_{f4}	0
A_{b4}	3.41×10^{14}	E_{b4}	141.5

We estimated additional parameters required to predict the data with this second rate expression. Very good agreement was obtained between experimental and model predicted data. For this model, it is found that the reverse reaction in S5', i.e., nitrate decomposition by NO, is much faster than the forward reaction. Hence the equilibrium is

shifted towards the left. The model predicts a fractional coverage of various species (as a function of temperature) participating in the NO oxidation reaction, a typical result of which is shown in Figure 8-16a. The model predicts that the catalyst surface is mainly covered with NO_2 at lower temperatures (< 300 ^oC). As the catalyst temperature increases, the surface coverage of NO_2-S decreases while the coverage of O-S begins to increase until at a high temperature (~ 350 ^oC), at which point adsorbed O starts desorbing from the catalyst. The surface coverage of nitrates and O_2 (not shown) are found to be negligible in the temperature range of interest. These results are in line with our experimental findings in which we observed negligible amount of nitrate present on the catalyst surface in the presence of NO. Few other literature studies also report the instability of nitrates in the presence of NO [32, 94, 99, 100]. They argued that the catalyst surface is mainly covered with nitrates in the absence of NO, such as when the catalyst was exposed to a pure feed of NO_2. We estimated fractional surface coverage of various species for the pure NO_2 feed (Figure 8-16b) and found that the nitrates occupy major active sites at lower temperatures (<300 ^oC) and are decomposed to NO_2 at higher temperatures (> 300 ^oC). These results are in agreement with previous literature findings [99, 100]. Moreover, if nitrates are not reduced by NO (during NO oxidation) immediately, then they will occupy the active NO oxidation sites as a result of which the NO conversion should decrease. With nitrates as the dominant surface species, the rate of forward NO oxidation reaction in equation (8-31) is expressed as

$$R_{NO_{oxi}} = \frac{k_{f3}\sqrt{K_1 K_2}}{K_5 K_4^2}\left(\frac{X_{NO,s}^{1.5} X_{O_2,s}^{0.25}}{X_{NO_2,s}^{1.5}}\right). \qquad (8\text{-}32)$$

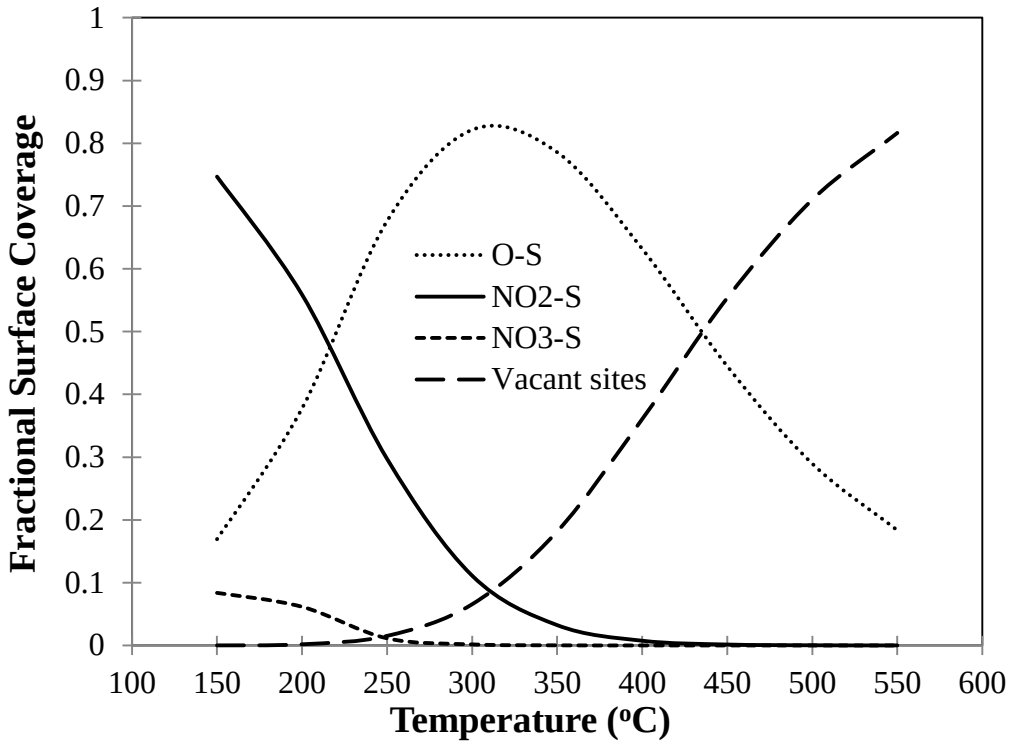

Figure 8-16a: Model predicted change in fractional surface coverage of various species as a function of catalyst temperature for a pure NO feed. Feed: 500 ppm NO, 5% O_2.

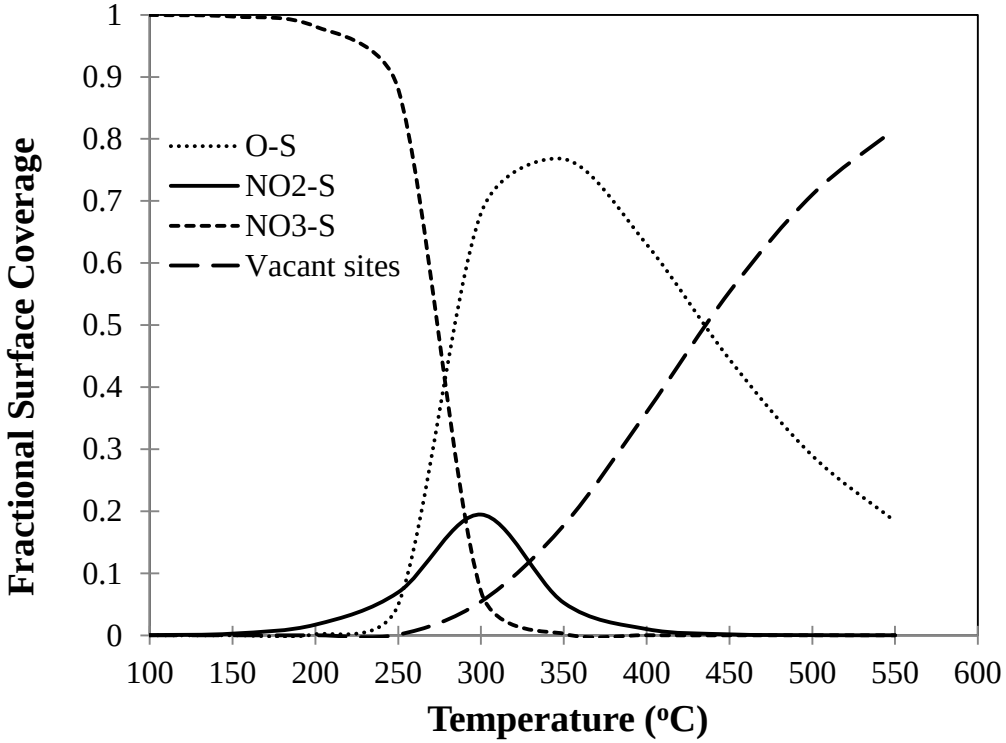

Figure 8-16: Model predicted change in fractional surface coverage of various species as a function of catalyst temperature for NO_2 feed. Feed: 500 ppm NO_2, 5% O_2.

This rate expression shows that the reaction order with respect to NO, O_2 and NO_2 are +1.5, + 0.25 and -1.5, respectively, which are inconsistent with our differential kinetics findings. This analysis, along with the predicted low concentrations of nitrates on the catalyst surface, indicate that the nitrates cannot be a major surface species on the active NO oxidation sites during NO oxidation reaction. The presence of excess NO leads to reverse of S5' which reduces the surface nitrates immediately and this indicates the instability of nitrates in the presence of NO.

Collectively, these findings clearly support the four step (S1-S4) model with S3 as the RDS is sufficient for predicting steady state NO oxidation and that nitrate formation is an equilibrated step that has a negligible effect on the NO_2 formation rate. Moreover, nitrates are important only in the presence of pure feed NO_2.

Apart from nitrate formation on metal sites in zeolite catalysts, few literature studies [100, 220] propose nitrate formation on H-ZSM-5 catalysts. For metal exchanged zeolite catalysts, there are still acid sites [37] present on the catalyst where NO_2 adsorption and nitrate formation can occur, but these sites are not active for NO oxidation. Thus the NO_2/nitrate species adsorbed on metal sites may spillover [37] to an adjacent acid sites which do not participate in NO oxidation. The presence and role of these sites should be considered to predict the transient NOx and NH_3 uptake and SCR data.

The above kinetic rate model applies to NO oxidation in the absence of feed H_2O. As observed and remarked earlier, water inhibits NO oxidation reaction to a great extent. In Chapter 3, we attributed this inhibition to water blocking the active NO oxidation sites

along with formation of nitrous and nitric acids. This adds the following steps to the above proposed kinetic scheme:

S7: $H_2O + S \leftrightarrow H_2O\text{-}S$, (8-33)

S8: $2\ NO_2\text{-}S + H_2O\text{-}S \leftrightarrow HONO\text{-}S + HNO_3\text{-}S + S$, (8-34)

S9: $HNO_3\text{-}S + NO + S \leftrightarrow HONO\text{-}S + NO_2\text{-}S$, (8-35)

S10: $NO + NO_2\text{-}S + H_2O\text{-}S \leftrightarrow HONO\text{-}S + NO_2\text{-}S$. (8-36)

Readers are referred Chapter 3 and [103] for more detail. Clearly, surface spectroscopic evidence is needed to determine the extent of coverage by the acid species and the difference between earlier discussed surface nitrates/nitrites in the absence of water and nitrous/nitric acid species in the presence of water. Ross and DeVore [221] measured the sorption of nitric acid on boehmite and reported the desorption of nitric acid at temperatures as high as 450 K. Water, along with formed nitrous/nitric acids lower the number of active NO oxidation sites (θ_v) by increasing the denominator of equation (8-28) and is given by

$$\theta_v = \frac{1}{1 + K_1 X_{O_2,s} + \sqrt{K_1 K_2 X_{O_2,s}} + K_4 X_{NO_2,s} + K_7 X_{H_2O,s} + \sqrt{K_4 K_{10} K_7 X_{NO_2,s} X_{NO,s} X_{H_2O,s}} + \frac{K_4^2 K_7 K_8 X_{NO_2,s} \sqrt{X_{H_2O,s}}}{\sqrt{K_4 K_7 K_{10} X_{NO_2,s} X_{NO,s}}}} \quad (8\text{-}37)$$

Since water is present in excess and is the key surface species blocking the active NO oxidation reaction sites, the above expression for θ_v can be simplified and final rate expression can be represented by

$$R_{NO_{oxi}} = \frac{k_{f3}\sqrt{K_1 K_2}}{K_7 X_{H_2O,s}} \left(X_{NO,s} \sqrt{X_{O_2,s}} - \frac{X_{NO_2,s}}{K_{eq}} \right). \quad (8\text{-}38)$$

With this simplified rate expression, we predicted the observed inhibition by water (Figure 8-1). Thus the same kinetic model can be used even in the presence of water.

Finally, we verified the robustness of the above kinetic model to predict the experimental data in the presence of feed NO_2 using the parameters estimated above for the NO oxidation reaction in the absence of feed NO_2. Figures 8-2 and 8-3 compare the experimentally observed outlet NO_2/NOx ratios with that of model predictions for NO oxidation reaction studied with feeds containing various NO_2/NOx inlet ratios. The experimental data and model predictions are in very good agreement. In order to predict the experimental data for Cu-chabazite in excess NO_2, activation energies of the forward and backward reactions were increased slightly (~ 5 kJ/mol). Finally, we used the model to predict the NO_2 inhibition effect on the NO oxidation reaction. The concentrations of NO (500 ppm) and O_2 (5%) were kept the same while different feed NO_2 concentrations (50-200 ppm) were used to test the model. Figure 8-17a (Fe) and 8-17b (Cu) show the results obtained with this study where we can see that the model predicts the NO_2 inhibition on Fe-/Cu-zeolite catalysts, and that this inhibition effect is more severe for Cu-chabazite compared to Fe-ZSM-5, in line with experimental findings. Thus the model was robust enough to capture the experimental trends for various feed conditions and it satisfactorily predicts the experimental data.

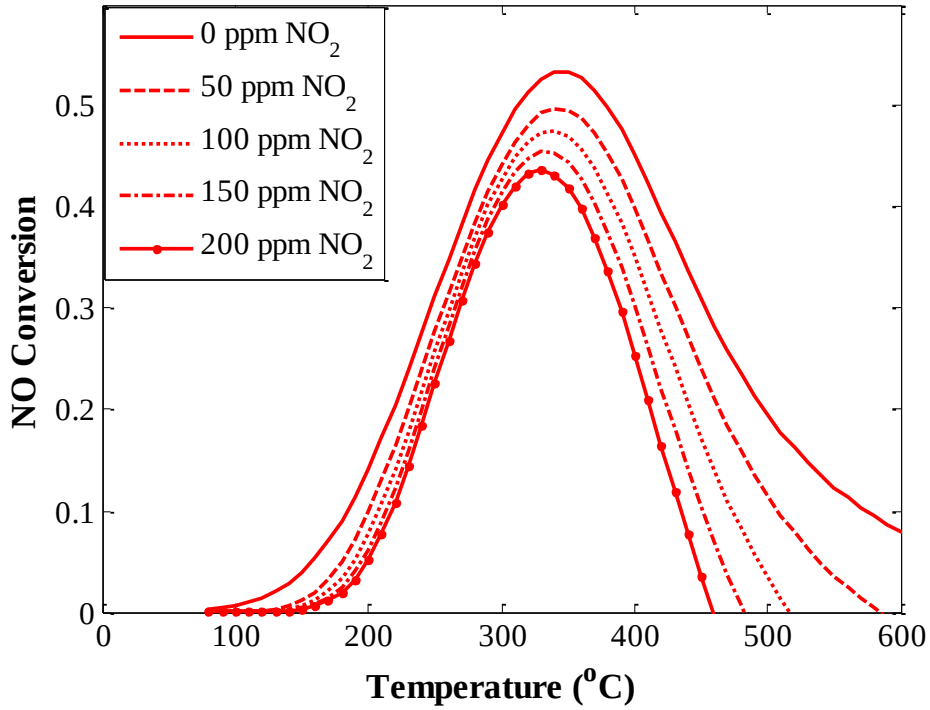

Figure 8-17a: Model predicted NO_2 inhibition effect on NO oxidation reaction on Fe-ZSM-5 catalyst for feeds containing different amounts of NO_2.

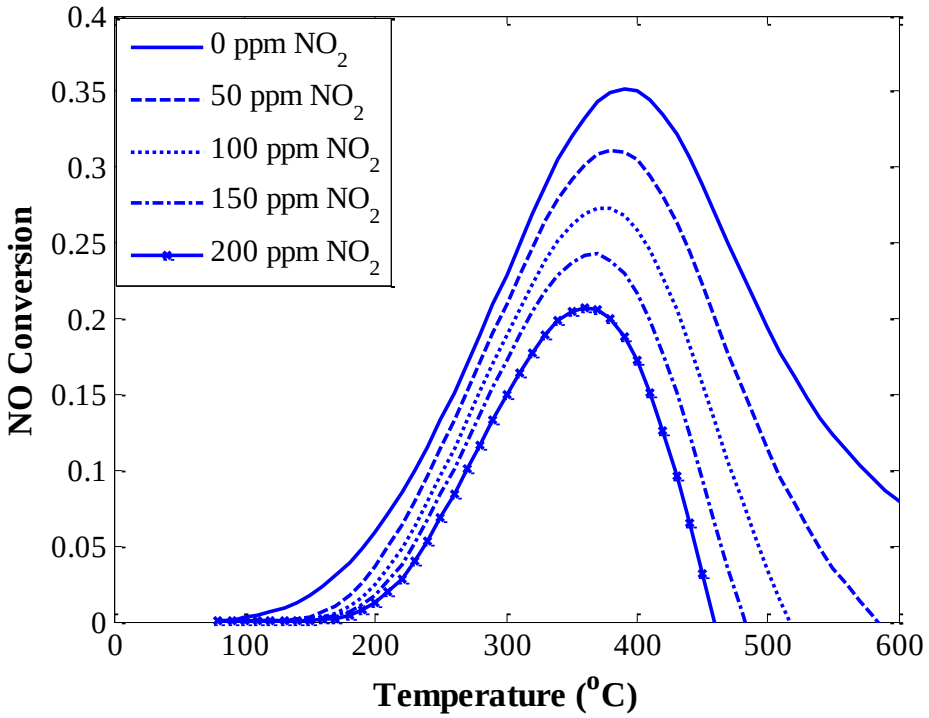

Figure 8-17b: Model predicted NO_2 inhibition effect on NO oxidation reaction on Cu-chabazite catalyst for feeds containing different amounts of NO_2.

8.5 Conclusions

We have carried out a comprehensive experimental and kinetic modeling study of NO oxidation on Fe-ZSM-5 and Cu-zeolite (chabazite and ZSM-5) catalysts. To our knowledge this is a first study focused on the detailed understanding of NO oxidation kinetics on the recently developed small pore Cu-chabazite catalyst and its detailed comparison with Fe-zeolite. This experimental study coupled with kinetic and reactor modeling compares various aspects of NO oxidation reaction kinetics in terms of reaction orders, NO conversions, NO_2 and water inhibition effects, effect of different catalyst pretreatments, mass transfer limitations, NOx uptake, nitrate formation and reverse NO_2 decomposition on both Fe- and Cu-zeolite catalysts.

The steady state data showed that Fe-zeolite is a better NO oxidation catalyst than Cu-zeolite. The NO oxidation reaction is inhibited by NO_2. This inhibition is more pronounced on Cu-chabazite than Fe-ZSM-5, the explanation for Fe being a more active NO oxidation catalyst. The presence of feed water strongly inhibits the NO oxidation on both catalysts. Separate studies of NO_2 decomposition (to NO) reaction showed that the reaction starts at around 300 ^oC on the Fe-ZSM-5 catalyst and at about 350 ^oC on the Cu-chabazite catalyst. The NO_2 uptake experiments showed the formation of surface nitrates on both the Fe- and Cu-zeolite catalysts. The amount of NO_2 released during the TPD experiment was higher on the Cu-chabazite compared to the Fe-ZSM-5 catalyst and was released at higher temperatures. This showed higher stability of surface nitrates (even at higher temperatures) on the Cu-chabazite catalysts. The surface nitrates were found to be unstable in the presence of feed NO and are immediately decomposed to NO_2. Catalyst

pretreatments by different oxidizing/reducing agents did not affect steady state NO oxidation activity.

Steady state experiments carried out on catalysts with the same washcoat volume but different washcoat thicknesses rule out the presence of washcoat diffusion limitations for the forward NO oxidation reaction for temperatures below 350 ^{o}C. This was corroborated by the theoretical analyses of the Weisz-Prater modulus and comparison of characteristic time constants for various processes.

A differential kinetic analysis of the NO oxidation reaction on both the commercial Fe- and Cu-zeolite catalysts shows positive order rate dependence (~ +1) on NO and O_2 (~ +0.5) on both the catalysts, while showing negative order dependence with respect to NO_2, confirming the NO_2 inhibition effect. The reaction order with respect to NO_2 was found to be about -0.5 on the Fe-ZSM-5 and -1 on the Cu-chabazite which confirms the severe inhibitory effect of NO_2 on the Cu-chabazite. The activation energy of the forward NO oxidation reaction was 39 kJ/mol on the Fe-ZSM-5 and 56 kJ/mol on the Cu-chabazite. The presence of feed water did not have any major effect on the reaction orders and activation energies.

Finally we presented a global kinetic model with surface reaction between adsorbed O atoms and gaseous NO as the RDS. This model satisfactorily captures the experimentally observed reaction orders, steady state NO conversions for various feed conditions along with the inhibitory effect of feed NO_2 and water for the entire temperature range. The kinetic model confirms the experimentally observed instability of nitrates in the presence of NO and also shows that the steady state NOx conversions can be estimated even without the inclusion of separate steps for nitrate formation or

decomposition. This analysis also show that nitrates could form on (or be transferred to) adjacent acid sites which should be considered to predict transient NOx and NH_3 uptake and SCR data.

CHAPTER 9 Kinetic Modeling Studies of Selective Catalytic Reduction of NOx with NH_3 on Fe- and Cu-Zeolite Monolithic Catalysts

9.1 Introduction

Selective catalytic reduction (SCR) of NOx with NH_3 has been studied extensively on various catalysts like vanadia-based catalysts [20, 63-65, 160, 161], Cu-zeolites [87, 89, 111, 119, 120] and Fe-zeolites [31-33, 39, 103, 108, 222]. Overall, many experimental studies of ammonia/urea SCR reaction system carried out on these catalysts are available in the literature [29, 30, 43, 98, 116, 149, 155, 167, 168, 223-226]. These experimental studies have provided a clearer picture of the overall NH_3-SCR chemistry occurring on these catalysts. The standard SCR reaction between NO and NH_3 occurs in the presence of oxygen and is given by

$$4\ NH_3 + 4\ NO + O_2 \rightarrow 4\ N_2 + 6\ H_2O \qquad \Delta H = -4.07 \times 10^5\ J/mol\ NH_3. \qquad (9\text{-}1)$$

The NOx reduction activity increases if NO and NO_2 are fed in about equimolecular amounts, compared to the case of only NO being present. The reaction between equimolar amounts of NO and NO_2 with NH_3 is known as the fast SCR reaction and is given by

$$2\ NH_3 + NO + NO_2 \rightarrow 2\ N_2 + 3\ H_2O \qquad \Delta H = -3.78 \times 10^5\ J/mol\ NH_3. \qquad (9\text{-}2)$$

Another reaction which is important in this chemistry is NO_2 SCR reaction and is presented as

$$4\ NH_3 + 3\ NO_2 \rightarrow 3.5\ N_2 + 6\ H_2O \qquad \Delta H = -3.41 \times 10^5\ J/mol\ NH_3. \qquad (9\text{-}3)$$

This reaction is important when the feed consists of NO_2. Apart from these three main important reactions, several side reactions occur in the SCR chemistry and are described in detail in Chapter 1. The presence of NO_2 in the feed accelerates the SCR chemistry on

various catalysts [87, 226]. Also, the SCR chemistry becomes complicated in the presence of feed NO_2. Hence several studies focused on the understanding of NO_2 effect on the SCR chemistry [42]. Many studies proposed that the NO_2 is the reactive species for the SCR of NOx with NH_3 on zeolite catalysts and that the oxidation of NO to NO_2 is the rate-limiting step [211]. Stevenson et al. [113] and Wallin et al. [145] suggest that oxidation of NO is the rate determining step in the reduction of NO by NH_3 on H-ZSM-5. The NO oxidation has been found to be the rate limiting step for the standard SCR reaction on Fe-zeolite catalysts as well [29, 34, 103]. Many other studies focus on the understanding of reaction mechanism in the SCR chemistry. Komatsu et al. [111] suggested a mechanism for the standard SCR reaction on Cu-zeolite catalysts. This mechanism involves the formation of a bridging NO_3. The NO_3 molecule thus formed, further reacts with NO to form NO_2. The NO_2 then reacts with NH_3 to produce N_2 and H_2O. Sun et al. [38] presented a mechanistic model on Fe-MFI catalysts in which they concluded that the preferred path for NOx reduction with ammonia occurs via ammonium nitrite which decomposes to N_2 and H_2O. Many other reaction mechanisms suggested that the reduction of NO and NO_2 by NH_3 involve formation of HNO_2 and HNO_3. Several other reaction mechanisms on different catalysts are presented in various literature studies [90, 115, 138, 227].

Even though there are various experimental studies available on the detailed understanding of reaction mechanism and SCR chemistry, very few studies focused on the kinetic modeling of NH_3-SCR reactions are available in the literature. Few literature studies presented global kinetic models for the standard SCR under steady-state conditions for vanadia-based catalysts [228-230] , Cu-ZSM-5 [116, 117] and Cu-

faujasite. Nova et al. presented a detailed kinetic model for predicting the key features of all the SCR reactions under transient conditions on vanadia-based catalyst [25, 27]. Some other studies also present transient kinetic models for vanadia-based catalysts [231]. Chatterjee et al. [78, 79, 121] presented a global kinetic model for both the vanadia-based and Fe-zeolite based catalysts. Their model can adequately describe the transient and steady-state NOx conversion and the effect of feed NO/NO_2 ratio on the SCR chemistry. Recently, Olsson and co-workers presented both global and detailed kinetic models for NH_3-SCR reactions on Fe-ZSM-5 and Cu-ZSM-5 catalysts [100, 117-120, 213]. Their kinetic models account for the effects of transient conditions and various feed concentrations of NO_2. Few other studies present kinetic models predicting transient behaviors of NH_3-SCR reactions on Fe-zeolite catalysts [118, 124].

The objective of this study is to develop a detailed kinetic model predicting key features of various reactions occurring during the NH_3-SCR chemistry on both the Fe-ZSM-5 and Cu-chabazite catalysts. As discussed earlier, there are various kinetic models available in the literature which predict both the steady state and transient features of NH_3-SCR reactions on Fe- and Cu-zeolite catalysts. Most of these kinetic models do not account for the diffusion limitations in the washcoat. This is because, inclusion of diffusion limitation in the washcoat makes the problem computationally challenging and more time consuming. Hence, many studies neglect the diffusion limitations in the washcoat. Here, we present a detailed two-dimensional, two-phase kinetic model (which accounts for washcoat diffusion limitations) on both the Fe-ZSM-5 and Cu-chabazite catalysts. As mentioned earlier, there are various kinetic model available for the Cu-ZSM-5 and other Cu-zeolites. But there is no kinetic model available for the recently

developed small pore Cu-chabazite catalyst which has been proven to be highly active, efficient and hydrothermally stable catalyst for the NH_3-SCR reactions. Here we present a kinetic model for the Cu-chabazite catalyst. The model considers following reactions: ammonia adsorption and desorption, NH_3 oxidation, NO oxidation, standard SCR, fast SCR, NO_2 SCR, ammonium nitrate formation, N_2O formation, N_2O decomposition to N_2 and N_2O SCR. One of the main objectives of this study is to develop a kinetic model predicting the performance of combined Fe- and Cu-zeolite catalytic systems. Specifically, we considered the sequential brick arrangements and dual-layer configurations of Fe- and Cu-zeolite catalysts. This work is presented as follows.

9.2 Reactor Model

We used a detailed two-dimensional, two-phase model to predict the experimental results of various reactions involved in the NH_3-SCR chemistry. The model accounts for convection (in axial direction), diffusion in the washcoat and reaction. The results obtained during the experimental study are described in detail in earlier Chapters 3-8. We used these results here to develop a detailed kinetic model predicting our experimental data. The model equations used for this study are summarized below. We sued a small reactor of 2 cm length in most of our experiments. Also, the concentrations of the reactants were quite small (about 500 ppm NOx and 500 ppm NH_3) in all the experiments. As a result, the amount of heat generated during the steady-state experimental studies was negligible. This was confirmed by monitoring changes in temperature recoded by thermocouple placed in the middle of reactor. Also, our calculations showed that the estimated adiabatic temperature rise was about 3 K. Overall,

all these findings suggest that the non-isothermal effects could be neglected during the steady-state studies. The model is based on the following assumptions:

i) laminar flow and ii) isothermal operation.

The model incorporates a species balance for the fluid and the solid phases (washcoat). The fluid phase balance accounts for the accumulation, convection and mass transfer of gas species from the bulk fluid to the washcoat. It is given by

$$\frac{\partial X_{jm}}{\partial t} = -\langle u \rangle \frac{\partial X_{jm}}{\partial z} - \frac{k_{c(j,z)}}{R_{\Omega 1}} \left(X_{jm} - X_{jwc}\Big|_{y=0} \right). \qquad (9\text{-}4)$$

The subscript j represents the species (j = NH_3, NO, NO_2, N_2O, N_2, NH_4NO_3), X_{jm} is the dimensionless mixed-cup mole fraction of species j, X_{jwc} is the dimensionless mole fraction of species j in the washcoat, $\langle u \rangle$ the average velocity, $k_{c(j,z)}$ is the position dependent mass transfer coefficient, $R_{\Omega 1}$ is the effective transverse length scale. z represents coordinate of length along axial direction.

Similarly, the solid phase balances describe the accumulation, mass transfer from fluid phase and catalytic reaction occurring within the washcoat,

$$\varepsilon_{wc} \frac{\partial X_{jwc}}{\partial t} = \frac{1}{C_{Tm}} \left(\sum \upsilon_j R_v(T, \theta, X_{jwc}) \right) + De_j \frac{\partial^2 X_{jwc}}{\partial y^2}. \qquad (9\text{-}5)$$

Here ε_{wc} is the washcoat porosity, C_{Tm} is the total molar concentration, R_v is the rate of the reaction, υ_j is the stoichiometric coefficient of species j in a particular reaction and θ is the fractional coverage of adsorbed species on the zeolite catalyst surface. y represents length co-ordinate along radial direction i.e., along the washcoat. The mass transfer coefficient (k_c) of species j was evaluated using the asymptotic Sherwood (Sh) number (3.6) and its axial variation with monolith length was neglected as the flow was found to be fully developed within 5% length of the channel [209].

Fractional coverage of the adsorbed species on the SCR catalyst surface is given by

$$C_s \frac{\partial \theta_{js}}{\partial t} = \sum \upsilon_j R_v(T, \theta, X_{jwc}). \quad (9\text{-}6)$$

Here, C_s is the total concentration of adsorption sites. The above model equations were discretized in both the axial (z) and radial (y) directions. We used following initial and boundary conditions in the above model equations:

$X_{jm}(z) = X_{jm}^{o}(z)$ at $t = 0$, (9-7)

$X_{jm}(t) = X_{jm}^{in}(z)$ at $z = 0$, (9-8)

$$\frac{\partial X_{jwc}}{\partial z} = 0 \text{ at } y = R_{\Omega 2}, \quad (9\text{-}9)$$

$$k_c \left(X_{jm} - X_{jwc}\big|_{y=0} \right) = -De_j \frac{\partial X_{jwc}}{\partial y} \quad \text{at } y = 0. \quad (9\text{-}10)$$

Here, $R_{\Omega 2}$ is the effective washcoat thickness. Table 9-1 shows the values of various parameters used in this study.

Table 9-1: Values of various parameters used in experimental/kinetic modeling study.

L	0.02 m
$R_{\Omega 1}$	2.75×10^{-4} m
$R_{\Omega 2}$	5×10^{-5} m
Q	1000 ml/min
$\langle u \rangle$	0.45 m/s at 300 K
ε_{wc}	0.4

Here, L is the total length of the monolith reactor and Q is the total flow rate. We used a temperature dependent value of linear average velocity. The values of these physical properties were kept the same for both the Fe- and Cu-zeolite catalysts. The values of gas

phase diffusivities were calculated using Lenard-Jones potentials. Table 9-2 gives the correlation for gas phase diffusivities as a function of temperature.

Table 9-2: Temperature dependent diffusivities of gases.

Gas	Diffusivity (m^2/s)
NO	$1.2365\times10^{-9}\,T^{1.7006}$
NO_2	$7.9236\times10^{-10}\,T^{1.7297}$
NH_3	$1.215\times10^{-9}\,T^{1.7389}$
N_2	$1.34\times10^{-9}\,T^{1.6901}$
N_2O	$8.1452\times10^{-10}\,T^{1.7314}$

9.3 Kinetic Model

For the purpose of present study, we have developed a single site global kinetic model for various NOx reduction reactions occurring during the SCR chemistry. As discussed earlier, various global kinetic models are available in the literature on different catalysts [25, 27, 121, 122, 232, 233]. Olsson and co-workers [117, 118] have developed a global kinetic model for Cu-ZSM5 and Fe-ZSM-5 catalysts. Their kinetic model includes various reactions like NH_3 adsorption-desorption, NH_3 oxidation, NO oxidation, selective reduction of NOx by adsorbed NH_3 (mainly standard, fast and NO_2 SCR reactions), N_2O formation, etc. Also, they have developed a detailed kinetic model assuming the existence of three different sites on the catalyst surface. Their model accounts for the effect of feed H_2O separately. A recent study by Colombo et al. [51] proposed a global dual-site kinetic model for the $NO/NO_2/N_2O–NH_3$ SCR reaction system on Fe-zeolite catalyst. Their model considers following additional reactions along with those proposed in earlier studies [117]: N_2O decomposition (to N_2 and O_2), N_2O reduction by NH_3, N_2O reduction by NO, ammonium nitrate formation and

decomposition. The model predicts the effect of NO/NO_2 feed ratios on the NOx conversions and N_2 selectivity. Chatterjee et al. [78] have developed a global kinetic model for commercial zeolite catalysts and vanadium-based catalysts. They used this model to compare the NOx reduction efficiency of both the catalysts. Baik et al. [116] have developed a kinetic model which includes urea decomposition and selective catalytic reduction. Their model includes reaction of NH_3 with NO. The global kinetic model used in this study is described as follows.

The kinetic model assumes the adsorption of ammonia (equation (9-11)) on the catalyst surface. The adsorbed ammonia is desorbed at higher temperature and is presented by the reverse reaction in (9-11). Ammonia can adsorb on both the metal sites and Bronsted acid sites. Few studies propose the adsorption of up to four ammonia molecules on each metal site [111]. Also, the presence of multiple sites has been proposed in some kinetic model. Here, we assume the existence of only single catalytic site (-S) for keeping the model as simple as possible. A coverage dependent activation energy was used for ammonia desorption. This approach has been used in several other models for this step [51, 117].

S1: $NH_3 + S \leftrightarrow NH_3\text{-}S.$ (9-11)

The model includes a global reaction for ammonia oxidation in which ammonia on the catalyst surface reacts with oxygen to produce nitrogen and water,

S2: $2\ NH_3\text{-}S + 1.5\ O_2 \rightarrow N_2 + 3\ H_2O + 2\ S.$ (9-12)

The metal exchanged zeolite catalysts have the ability to oxidize NO to NO_2. Hence a global reaction between NO and O_2 has been included and is given by

S3: $NO + ½\ O_2 \leftrightarrow NO_2.$ (9-13)

The NO oxidation is a reversible reaction and the backward reaction of NO_2 decomposition becomes important at higher temperature. Also, the reaction is kinetically controlled at lower temperatures. But at higher temperatures, it is controlled by the thermodynamic equilibrium.

The selective catalytic reduction of NOx with NH_3 is explained with the help of three reaction steps which depend upon the NO_2/NOx feed ratios. The standard SCR reaction (9-14) involves a reaction between adsorbed NH_3 and gas phase NO and O_2. The fast SCR reaction (9-15) involves the reduction of equimolar amounts of gas phase NO and NO_2 by NH_3 adsorbed on the catalyst surface. The NO_2 SCR reaction (9-16) is described by the reduction of gas phase NO_2 by surface NH_3 species. These reactions are given as follows:

S4: $4\ NH_3\text{-}S + 4\ NO + O_2 \rightarrow 4\ N_2 + 6\ H_2O + 4\ S,$ (9-14)

S5: $2\ NH_3\text{-}S + NO + NO_2 \rightarrow 2\ N_2 + 3\ H_2O + 2\ S,$ (9-15)

S6: $4\ NH_3\text{-}S + 3\ NO_2 \rightarrow 3.5\ N_2 + 6\ H_2O + 4\ S.$ (9-16)

In addition to these important reactions, some side reactions may occur. One important byproduct in the SCR chemistry is ammonium nitrate and it is formed in the presence of excess feed NO_2. The ammonium nitrate formation is particularly important at lower temperatures (< 250 ^oC). Our experiments (Chapters 4,5) showed that the N-balance was not closed at these low temperatures which indicates that some undetected NH_4NO_3 leaves the catalyst reactor in the gaseous form. The NH_4NO_3 species can be assumed to be present on the catalyst surface. In order to simplify the chemistry we assume that the ammonium nitrate is formed and leaves the catalyst in the gaseous form and thus neglect its adsorption on the catalyst surface.

S7: $2\ NH_3\text{-}S + 2\ NO_2 \rightarrow N_2 + NH_4NO_3 + H_2O + 2\ S.$ (9-17)

The NH_4NO_3 can further decompose to N_2O at higher temperatures,

S8: $NH_4NO_3 \rightarrow N_2O + 2\ H_2O.$ (9-18)

Decomposition of N_2O to N_2 and O_2 takes place at higher temperatures [29, 51]. Thus we include this reaction in the current kinetic model,

S9: $2\ N_2O \rightarrow N_2 + O_2.$ (9-19)

The N_2O can also be reduced by NH_3. This reaction is considered as the N_2O SCR reaction [29, 51] and is given by

S10: $2\ NH_3\text{-}S + 3\ N_2O \rightarrow 4\ N_2 + 3\ H_2O + 2\ S.$ (9-20)

All the above reactions were included in the kinetic modeling studies. The rates of all the above reactions are expressed as:

$$R_{v1} = k_{1f} X_{NH_3} \theta_v - k_{1b} \theta_{NH_3}, \quad (9\text{-}21)$$

$$R_{v2} = k_{2f} X_{O_2} \theta_{NH_3}, \quad (9\text{-}22)$$

$$R_{v3} = k_{3f} X_{O_2}^{1/2} X_{NO} - k_{3b} X_{NO_2}, \quad (9\text{-}23)$$

$$R_{v4} = k_{4f} X_{NO} \theta_{NH_3}, \quad (9\text{-}24)$$

$$R_{v5} = k_{5f} X_{NO} X_{NO_2} \theta_{NH_3}, \quad (9\text{-}25)$$

$$R_{v6} = k_{6f} X_{NO_2} \theta_{NH_3}, \quad (9\text{-}26)$$

$$R_{v7} = k_{7f} X_{NO_2} \theta_{NH_3}, \quad (9\text{-}27)$$

$$R_{v8} = k_{8f} X_{NH_4NO_3}, \quad (9\text{-}28)$$

$$R_{v9} = k_{9f} X_{N_2O}, \quad (9\text{-}29)$$

$$R_{v10} = k_{10f} X_{N_2O} \theta_{NH_3}. \quad (9\text{-}30)$$

Here k_{if} and k_{ib} refer to the forward and backward rate constants of reaction step i, respectively and are defined as

$$k_{if} = A_{if} e^{-E_{if}/RT_s}, \tag{9-31}$$

$$k_{ib} = A_{ib} e^{-E_{ib}/RT_s}. \tag{9-32}$$

Here A_{if} and A_{ib} are the pre-exponential factors and E_{if} and E_{ib} are the activation energies of the forward and backward reaction step i, respectively. θ_i refers to the fractional surface coverage of species i and X_j gives the mole fraction of species j. Here, we considered only the adsorption of ammonia on the catalyst surface. Hence the summation of mole fractions of vacant sites (θ_v) and mole fraction of ammonia adsorbed-sites (θ_{NH3}) is 1,

$$\theta_v + \theta_{NH3} = 1. \tag{9-33}$$

The above rate expressions do not include the dependence on O_2 and H_2O concentrations as both were present in excess in the reaction system. The parameters (rate constants and activation energies) in equations (9-21) to (9-33) were estimated by multiresponse nonlinear regression method [100]. The values of resulting parameters estimated for this reaction are summarized in Table 9-3 (Fe-ZSM-5) and Table 9-4 (Cu-chabazite).

Table 9-3: Values of kinetic parameters used in the simulations for Fe-ZSM-5 catalyst.

Parameter	Numerical value (mol/m^3 washcoat s)	Parameter	Numerical value (kJ/mol)
A_{1f}	5.67×10^4	E_{1f}	0
A_{1b}	1.0×10^{10}	E_{1b}	145.9
A_{2f}	2.39×10^4	E_{2f}	90.8
A_{3f}	1×10^7	E_{3f}	48
A_{4f}	5×10^6	E_{4f}	72.4
A_{5f}	1.9×10^{14}	E_{5f}	68.1
A_{6f}	7.1×10^{12}	E_{6f}	140.3
A_{7f}	4.1×10^4	E_{7f}	40
A_{8f}	3.49×10^8	E_{8f}	37
A_{9f}	4.5×10^{11}	E_{9f}	128
A_{10f}	5.5×10^6	E_{10f}	90

Table 9-4: Values of kinetic parameters used in the simulations for Cu-chabazite catalyst.

Parameter	Numerical value (mol/m^3 washcoat s)	Parameter	Numerical value (kJ/mol)
A_{1f}	1.67×10^4	E_{1f}	0
A_{1b}	1.0×10^{12}	E_{1b}	145.9
A_{2f}	1.39×10^{13}	E_{2f}	178.8
A_{3f}	5.1×10^7	E_{3f}	56
A_{4f}	1.77×10^{10}	E_{4f}	89.1
A_{5f}	2.5×10^{14}	E_{5f}	77.1
A_{6f}	4.9×10^{13}	E_{6f}	136.3
A_{7f}	5.7×10^4	E_{7f}	43
A_{8f}	1.25×10^8	E_{8f}	41.5
A_{9f}	3.8×10^{11}	E_{9f}	131.5
A_{10f}	1.8×10^5	E_{10f}	87.5

9.4 Results and Discussion

9.4.1 Ammonia Adsorption-Desorption

Ammonia adsorption is an important step in the NH_3-SCR reaction chemistry. Our experimental study (in Chapters 3,5) shows that sufficient amount of ammonia is adsorbed on both the Fe- and Cu-zeolite catalysts. The model for ammonia adsorption-desorption was fitted to temperature programmed desorption (TPD) studies carried out at 150 ^{o}C on both the catalysts. During the first 3600 s in a TPD experiment, 500 ppm NH_3 (in Ar) was introduced to the reactor. NH_3 uptake occurred during the induction period preceding ammonia breakthrough. After achieving saturation, the NH_3 inlet was shut off and the exit NH_3 concentration decreased monotonically to zero. During the 30 minute post uptake period, some physisorbed ammonia desorbed from the catalyst. A temperature ramp of 10 ^{o}C/min was given at 5400 s. During the temperature ramp, ammonia is desorbed from the catalyst surface. Figure 9-1 (Fe-ZSM-5) and Figure 9-2 (Cu-Chabazite) compare the experimentally observed NH_3 concentration profiles to that predicted by the kinetic model. The thin line shows the model predictions. The model can satisfactorily capture the experimental trends. During the ammonia uptake, experiments reached the inlet NH_3 concentrations in more time. Model predicts the saturation in earlier time. But the overall uptake, which is more important in the SCR model, is the same. For the Cu-chabazite catalyst, two peaks were observed during the NH_3 desorption when the temperature ramp was given. This could be due to the NH_3 adsorption on multiple sites which desorb ammonia at different temperatures. But, the model is simplified with the existence of single site and hence it does not predict the two peaks observed experimentally.

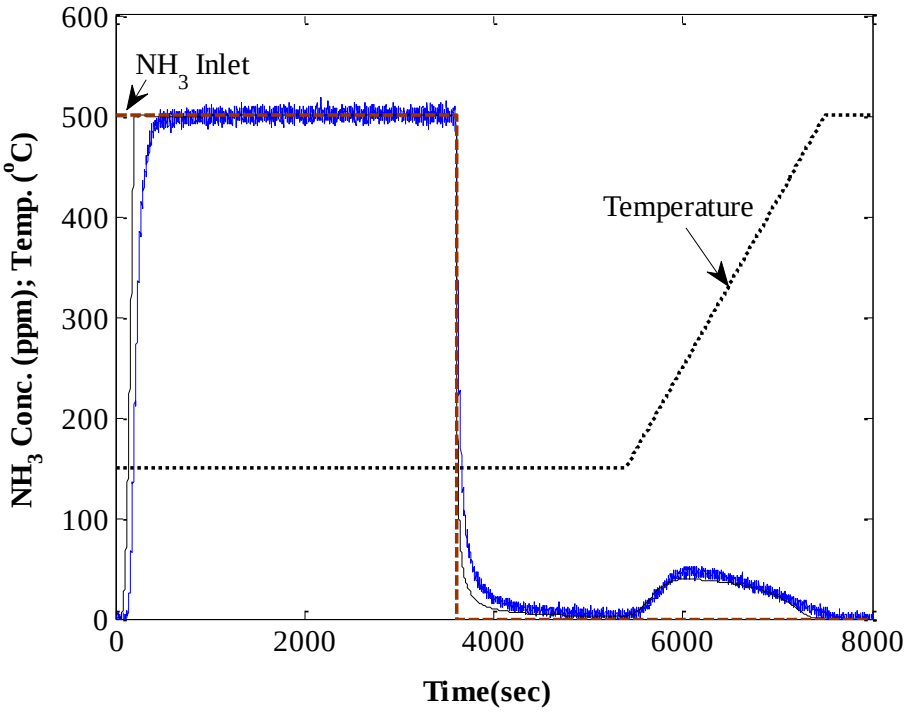

Figure 9-1: Comparison of experimentally measured and model predicted ammonia concentrations during the NH_3 TPD studies carried out on Fe-ZSM-5 catalyst.

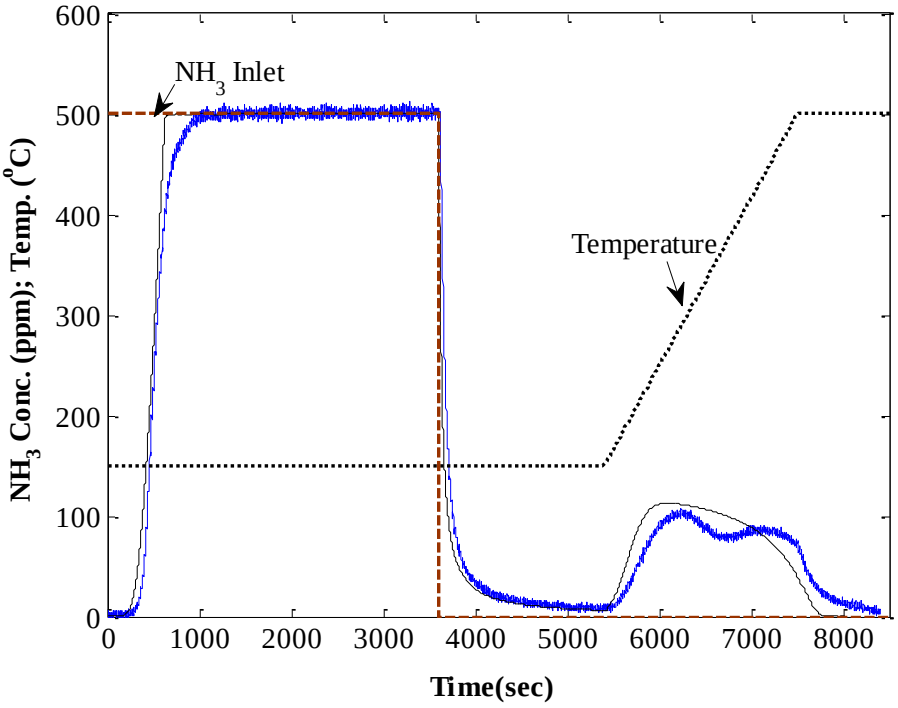

Figure 9-2: Comparison of experimentally measured and model predicted ammonia concentrations during the NH_3 TPD studies carried out on Cu-chabazite catalyst.

9.4.2 Ammonia Oxidation

Ammonia oxidation is an important side reaction in the NH_3-SCR chemistry. Both Fe- and Cu-zeolite catalysts are active ammonia oxidation catalysts. The Cu-chabazite catalyst is found to be a more active NH_3 oxidation catalyst compared to Fe-ZSM-5. We carried out a steady state experiment for NH_3 oxidation on both the Fe- and Cu-zeolite catalysts. The catalyst was exposed to a feed containing 500 ppm NH_3 (in Ar), 5% O_2, 2% H_2O and sufficient time was allotted to reach steady state (about 25 minutes). The reaction was studied in the temperature range of 100-550 ^oC. The experimental data was used to obtain the kinetic parameters. Figure 9-3 compares the experimentally measured concentrations of NH_3 and N_2 with that predicted by model. As shown in Figure 9-3, the model could very well predict the experimental results obtained during the ammonia oxidation studies on both the Fe-ZSM-5 and Cu-chabazite catalysts.

9.4.3 NO Oxidation

Another important side reaction in the SCR chemistry is the oxidation of NO to NO_2. NO oxidation is a reversible reaction which is kinetically controlled at lower temperatures and thermodynamically controlled at higher temperatures. In Chapter 8, we presented a detailed kinetic modeling study of NO oxidation on both the Fe- and Cu-zeolite catalysts. Here, we use a simplified global reaction in our kinetic model to capture the key features of NO oxidation reaction. The experimental study consisted of feeding 500 ppm NO, 5% O_2 and 2% water on the catalyst surface. The steady state NOx concentrations were recorded for both the Fe-ZSM-5 and Cu-chabazite catalysts. The NO_2 concentration in the exit increased with temperature. It reached a maximum at

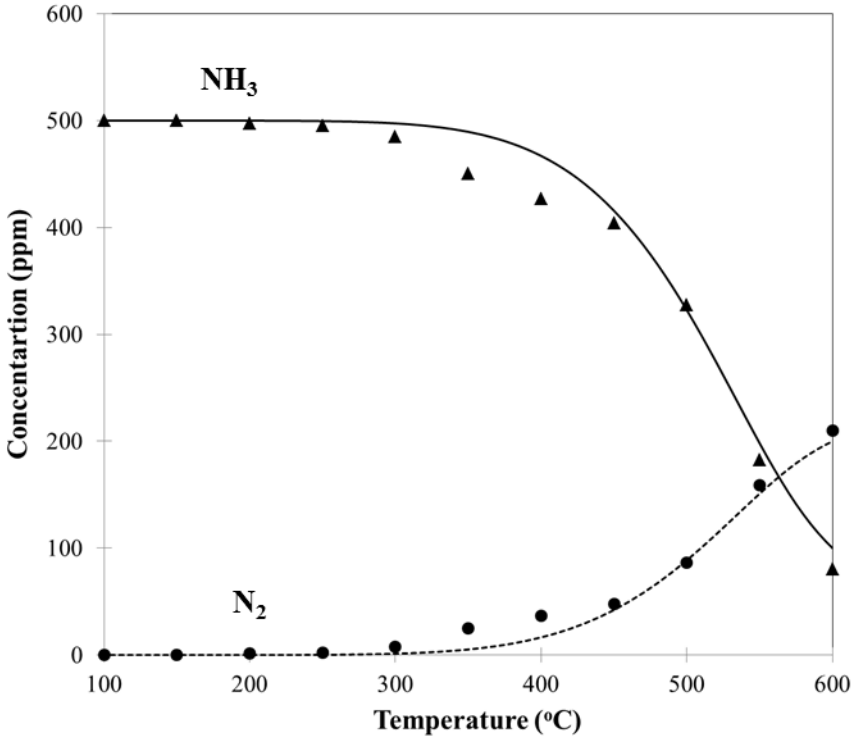

Figure 9-3a: Comparison of experimental (symbols) and model predicted (lines) NH_3 and N_2 concentrations during the NH_3 oxidation studies on Fe-ZSM-5 catalyst.

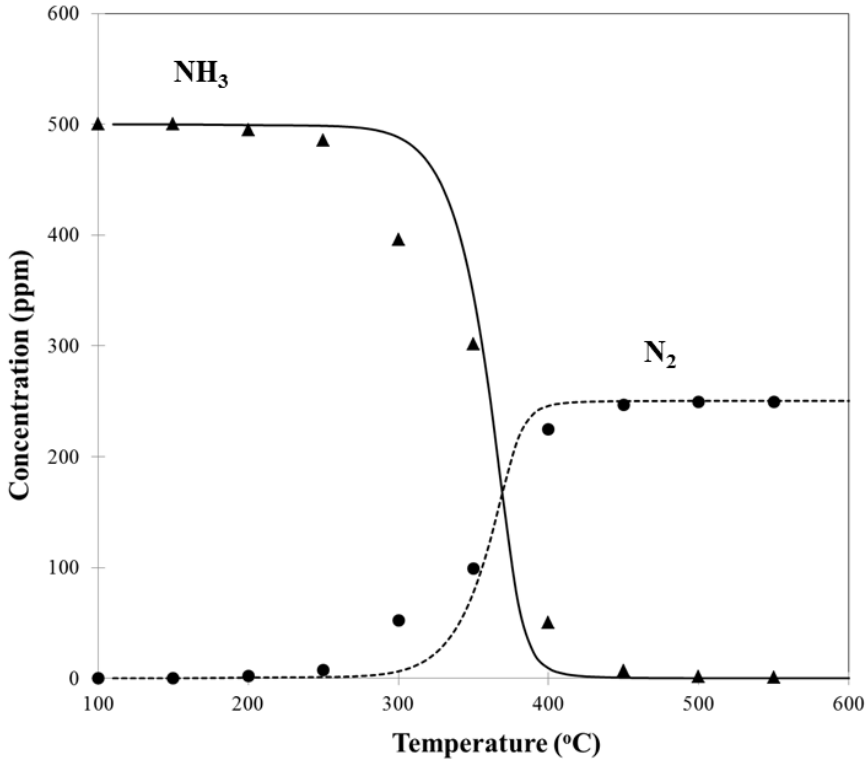

Figure 9-3b: Comparison of experimental (symbols) and model predicted (lines) NH_3 and N_2 concentrations during the NH_3 oxidation studies on Cu-chabazite catalyst.

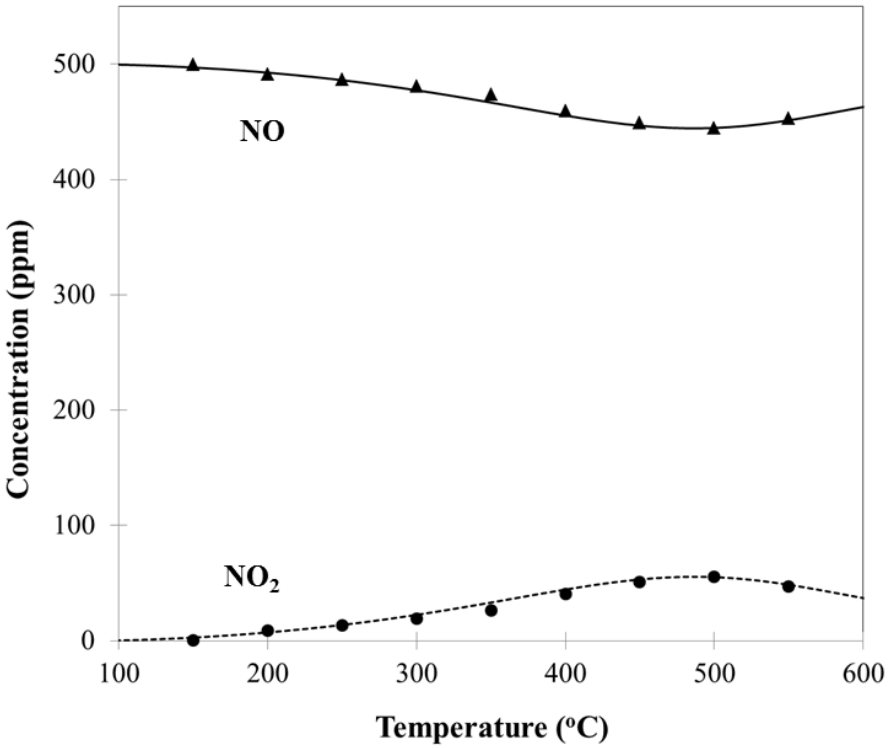

Figure 9-4a: Comparison of experimental (symbols) and model predicted (lines) NO and NO_2 concentrations during the NO oxidation studies on Fe-ZSM-5 catalyst.

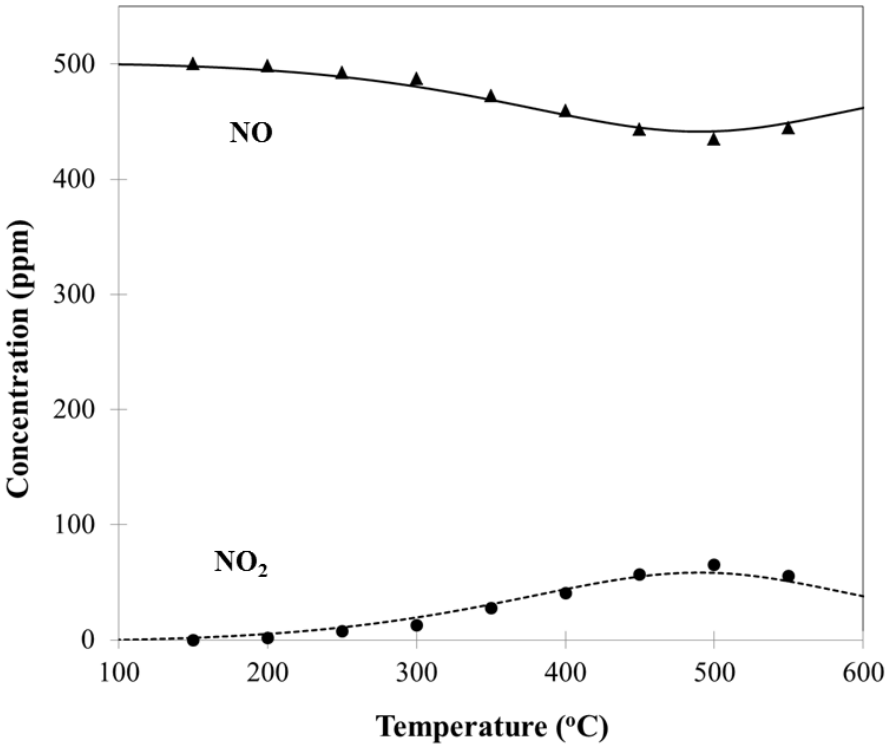

Figure 9-4b: Comparison of experimental (symbols) and model predicted (lines) NO and NO_2 concentrations during NO oxidation studies on Cu-chabazite catalyst.

around 500 ^{o}C and then decreased because the thermodynamic equilibrium favors the backward NO_2 decomposition at higher temperatures. These steady state data were used to estimate the rate parameters. The backward rate constant in equation (9-23) is calculated using thermodynamic constraints for equilibrium. Figure 9-4 shows the comparison of experimental data with that predicted by model. Again, the model captures the experimental data very well.

9.4.4 Standard SCR

We studied the standard SCR reaction (9-1) on both the Fe-ZSM-5 and Cu-chabazite catalysts. The experimental results are reported earlier in Chapters 3 and 5. During the experimental study, a feed containing 500 ppm NO, 500 ppm NH_3, 5% O_2 and 2% water were introduced on the catalyst surface and steady state NO conversions were recorded in the temperature range of 100-600 ^{o}C. The Cu-chabazite catalyst was found to be a more active standard SCR catalyst compared to the Fe-ZSM-5 catalyst. Nearly complete NO conversion activity was observed on the Cu-chabazite catalyst in the temperature range of 250-350 ^{o}C. But at higher temperatures, the NO conversion activity decreased because of the more pronounced ammonia oxidation side reaction which consumed the NH_3 reductant required to reduce NOx. On the other hand, the Fe-ZSM-5 catalyst was not very active for temperatures below 300 ^{o}C. But at higher temperatures, this catalyst gave substantially higher NOx conversions (> 90%). We included the reaction (9-14) given by the rate expression (9-24) to predict the NO conversion activity obtained during the experiments. Figure 9-5 provides the comparison between experimental and model predicted NO conversion activities during the standard SCR

reaction on both the Fe-ZSM-5 and Cu-chabazite catalysts. Our model accurately captures the experimental trends throughout the temperature range.

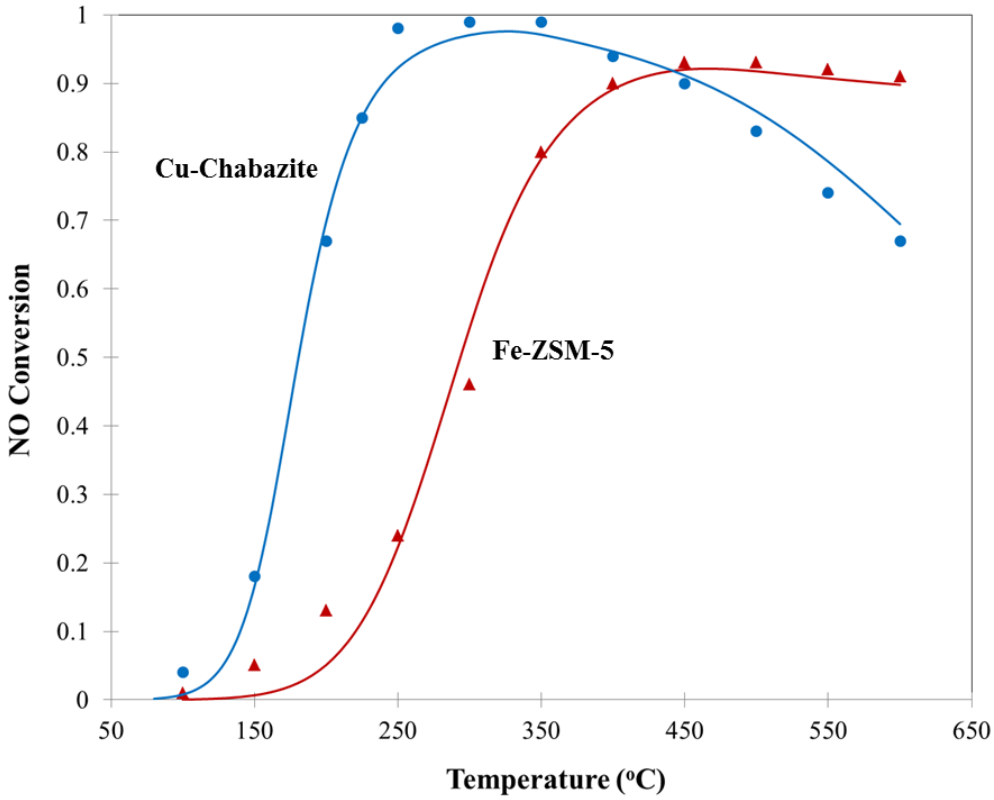

Figure 9-5: Comparison of experimental (symbols) and model predicted (lines) NO conversions during the standard SCR reaction studies carried out on Fe-ZSM-5 and Cu-chabazite catalysts.

9.4.5 Fast SCR

The fast SCR reaction is considered as one of the most important reactions in the SCR chemistry. When NO_2 is present in the reacting system, it accelerates the rate of NOx reduction. Equimolar amounts of NO and NO_2 in the feed has been proposed as an ideal NOx feed ratio for obtaining maximum NOx reduction efficiency and highest selectivity for N_2 in NH_3-SCR systems [29, 39, 51, 63]. In earlier Chapters 4 and 5, we reported the product distributions obtained during the fast SCR reaction studies carried out on Fe-ZSM-5 and Cu-chabazite catalysts. We tried to predict out our experimental

observations with the kinetic model proposed above. Figure 9-6 shows the comparison of experimental and model predicted concentrations of various species during the fast SCR reaction studies on Fe-ZSM-5 catalyst. As shown in Figure 9-6, the kinetic model accurately captures the experimental trends throughout the temperature range. Also, the introduction of NO_2 in the feed substantially increased the NOx reduction rates compared to the standard SCR reaction studies on Fe-ZSM-5 catalyst. There is a negligible N_2O production observed during this reaction.

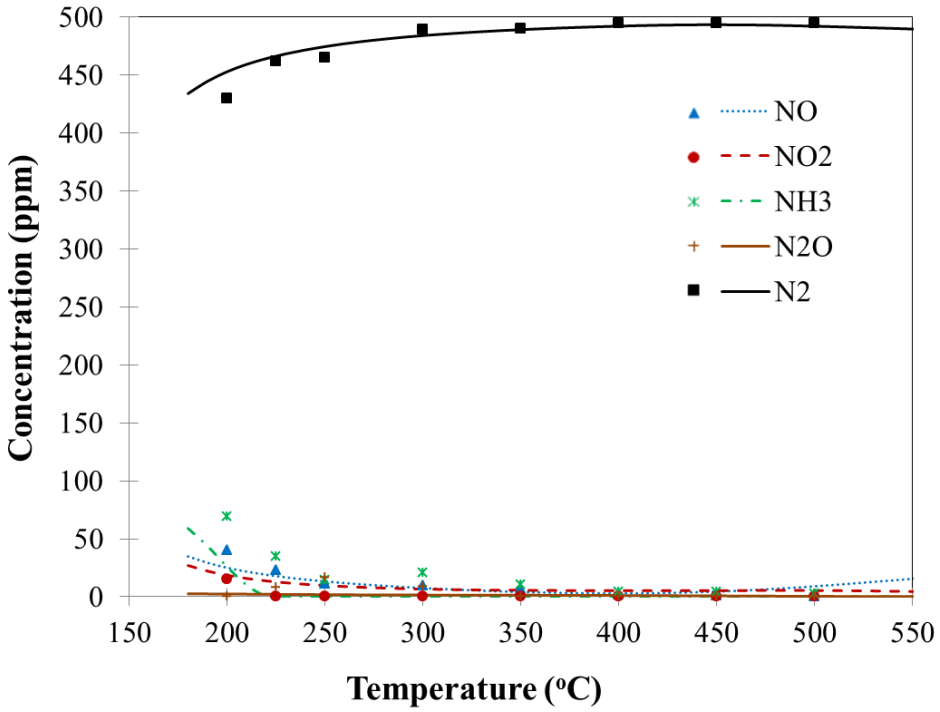

Figure 9-6: Comparison of experimental (symbols) and model predicted (lines) steady state concentrations of various species obtained during the fast SCR reaction studies on Fe-ZSM-5 catalyst. Feed: 250 ppm NO, 250 ppm NO_2, 500 ppm NH_3, 5% O_2, 2% H_2O.

We carried out similar studies on Cu-chabazite catalyst. When the feed consisted of equimolar amounts of NO and NO_2, the NOx conversion increased slightly at lower temperatures (< 200 ^oC) compared to the case of standard SCR reaction. But the increment in conversion was not significant as compared to that observed on the Fe-

ZSM-5 catalyst. Some N_2O was observed at temperatures below 350 ^oC. At higher temperatures, the NOx concentrations increased while NH_3 concentration was nearly zero. Thus NH_3 was completely consumed during this reaction but some NOx remained unconverted. This is explained by the more pronounced ammonia oxidation side reaction which consumes the reductant NH_3 required for NOx reduction. Such feature was not observed on the Fe-ZSM-5 catalyst where the rate of fast SCR reaction was much greater than the NH_3 oxidation side reaction. Our model accurately predicts the experimental data.

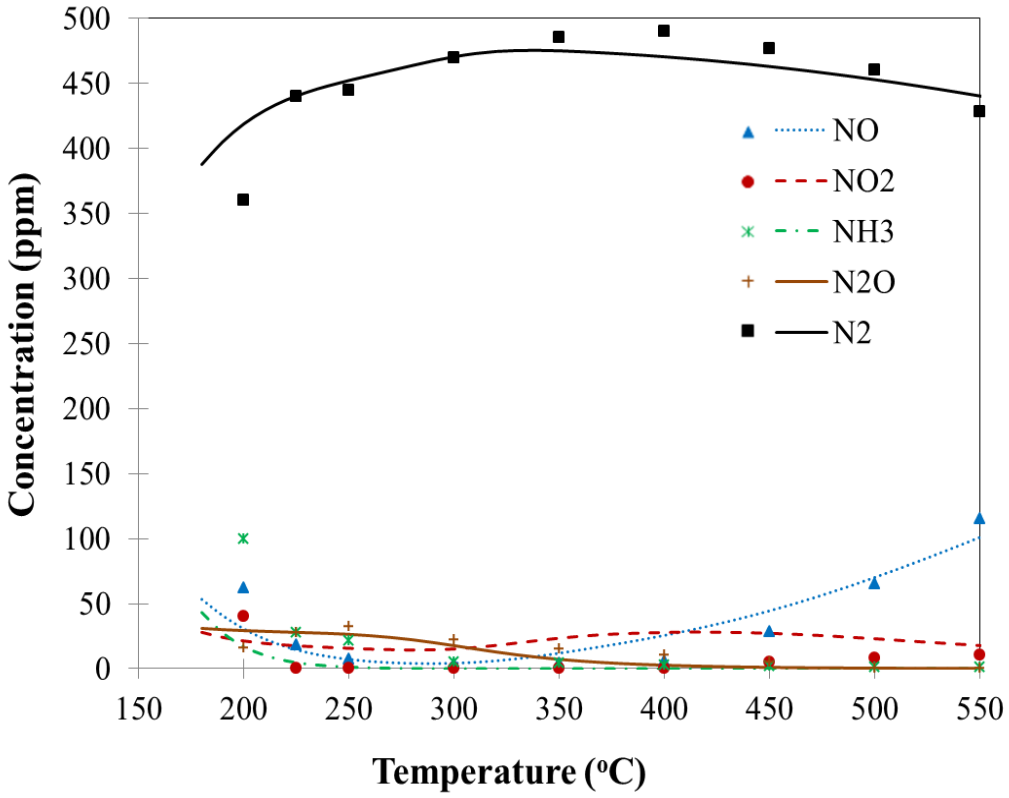

Figure 9-7: Comparison of experimental (symbols) and model predicted (lines) steady state concentrations of various species obtained during the fast SCR reaction studies on Cu-chabazite catalyst. Feed: 250 ppm NO, 250 ppm NO_2, 500 ppm NH_3, 5% O_2, 2% H_2O.

9.4.6 NO_2 SCR

The NO_2 SCR reaction (9-3) occurs when the feed consists of NO_2 and NH_3. The presence of NO_2 in the feed complicates the reaction where a number of byproducts like N_2O and NH_4NO_3 are formed at lower temperatures. At higher temperatures, some NO appeared at the exit even though the feed did not contain any NO. The NO is formed by the NO_2 decomposition reaction. The steady state product distribution obtained during the NO_2 SCR reaction studies carried out on the Fe-ZSM-5 and Cu-chabazite catalysts is shown in Figure 9-8. In order to predict the formation of ammonium nitrate (AN) and N_2O, we included reaction steps (9-17) to (9-21). The model accurately captures the experimental trends showing the formation of ammonium nitrate and N_2O. The NO_2 SCR reaction is active at above 250 ^oC. The amount of N_2 formed during the reaction is accurately captured by the model. At higher temperatures, the amount of NOx converted is higher than that predicted by the model. The stoichiometry of the NO_2 SCR reaction for NH_3/NO_2 is 4/3. Thus the maximum amount of NO_2 that can be reduced is 75% when the feed consists of equal amounts of NO_2 and NH_3. But during the experiments, some side reactions like N_2O/ammonium nitrate formation and decomposition, NO_2 decomposition, fast SCR reactions, etc., take place simultaneously. Even though the model accounts for these reactions, rate parameters need to be tuned further to accurately capture the experimentally observed product distribution and NO_2 conversions. Overall, the model captures the experimental trends very well.

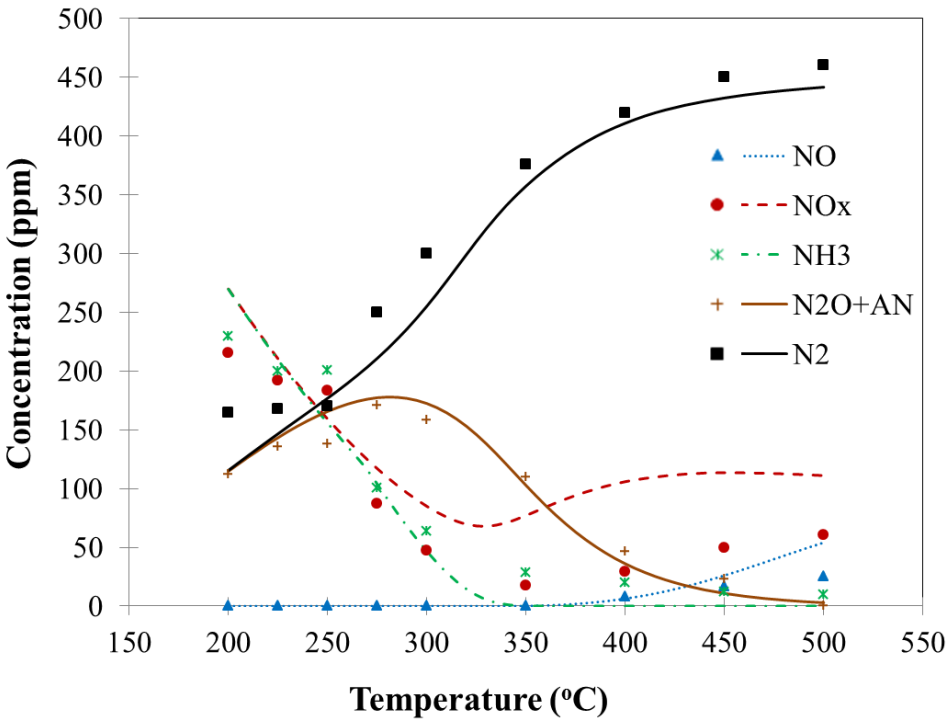

Figure 9-8a: Comparison of experimental (symbols) and model predicted (lines) steady state concentrations of various species obtained during the NO_2 SCR reaction studies on Fe-ZSM-5 catalyst. Feed: 500 ppm NO_2, 500 ppm NH_3, 5% O_2, 2% H_2O.

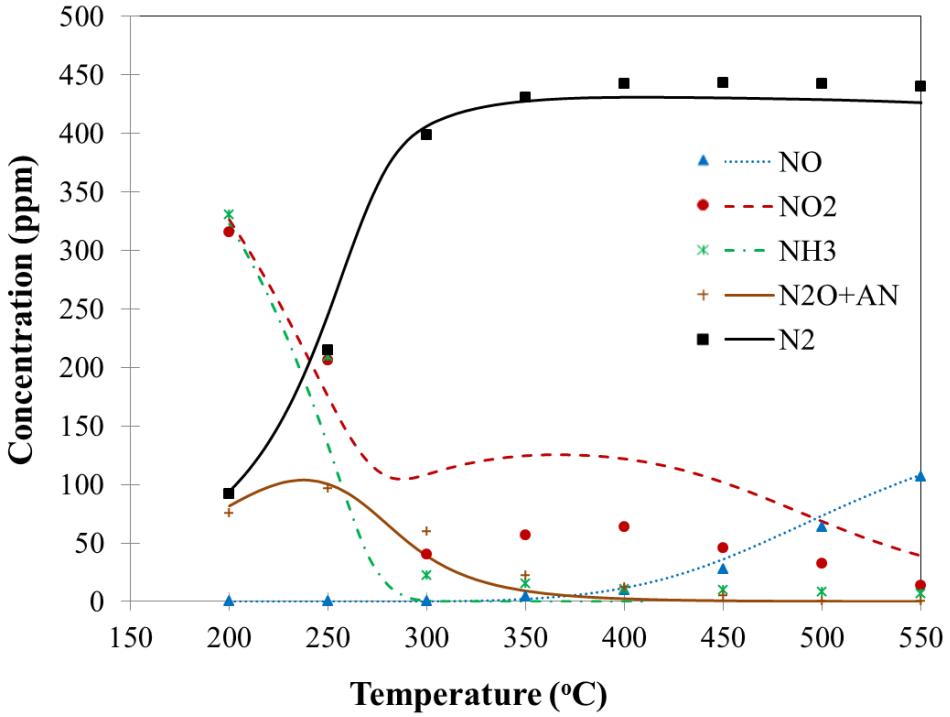

Figure 9-8b: Comparison of experimental (symbols) and model predicted (lines) steady state concentrations of various species obtained during the NO_2 SCR reaction studies on Cu-chabazite catalyst. Feed: 500 ppm NO_2, 500 ppm NH_3, 5% O_2, 2% H_2O.

9.4.7 NO_2/NOx = 0.25, 0.75

The above kinetic model was then validated by predicting the effect of varying NO_2/NOx feed concentrations on product distribution and NOx conversions on both the Fe-ZSM-5 and Cu-chabazite catalysts. We considered two different cases where NO_2/NOx feed ratio was kept constant at 0.25 and 0.75. Figure 9-9 compares the experimental and model predicted concentrations of various species obtained during NH_3-SCR studies carried out on Fe-ZSM-5 and Cu-chabazite catalysts with the NO_2/NOx feed ratio equal to 0.25. For both the catalysts, a negligible amount of N_2O and ammonium nitrate was produced over the entire temperature range. For Fe-ZSM-5, the concentrations of NO and NH_3 decreased at lower temperatures compared to the NO only feed. This shows that the presence of 125 ppm NO_2 enhanced the NOx reduction activity at lower temperatures for Fe-ZSM-5 catalyst. The model accurately captures the experimental data for Fe-ZSM-5. For Cu-chabazite catalyst, the NOx reduction activity enhanced slightly compared to that of NO only feed at lower temperatures. But at higher temperatures, the NOx conversion decreased because of the more pronounced NH_3 oxidation reaction which consumes the reductant NH_3. This feature is similar to that observed earlier for the standard, fast and NO_2 SCR reactions discussed earlier on Cu-chabazite catalyst. The model captures the experimental trends very well even for the Cu-chabazite catalyst.

Figure 9-10 compares the experimental results with that predicted by model for NOx feed with NO_2/NOx inlet ratio of 0.75. For the Fe-ZSM-5 catalyst, large amounts of ammonium nitrate and N_2O were produced in the temperature range of 200-400 ^oC. At temperatures above 400 ^oC, N_2 was the only N-containing product of the reaction. Our

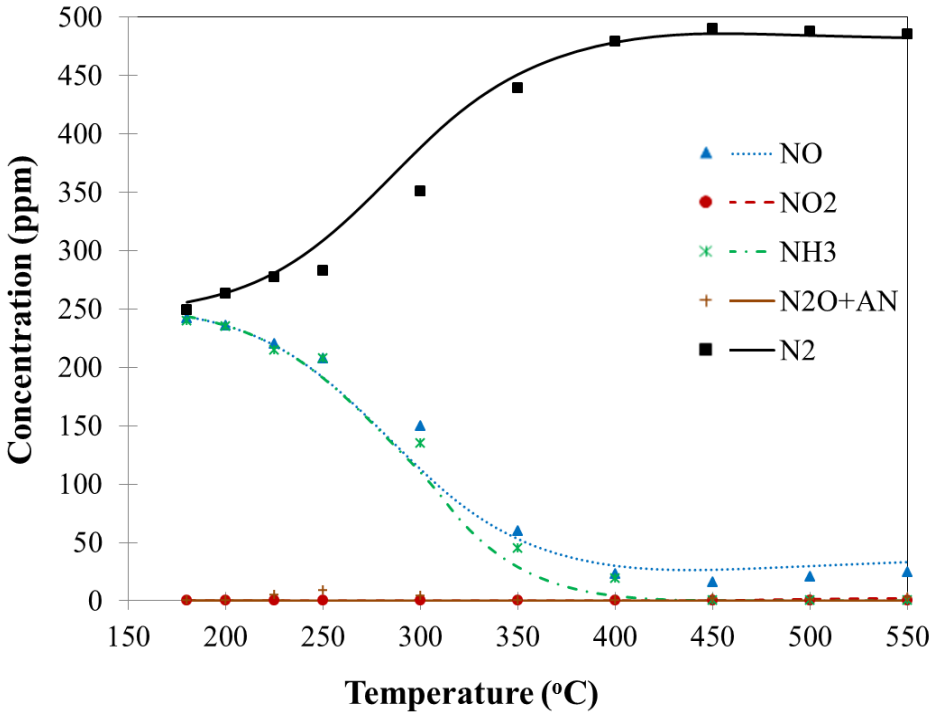

Figure 9-9a: Comparison of experimental (symbols) and model predicted (lines) steady state concentrations of various species obtained during the NOx SCR reaction studies on Fe-ZSM-5 catalyst. Feed: 375 ppm NO, 125 ppm NO_2, 500 ppm NH_3, 5% O_2, 2% H_2O.

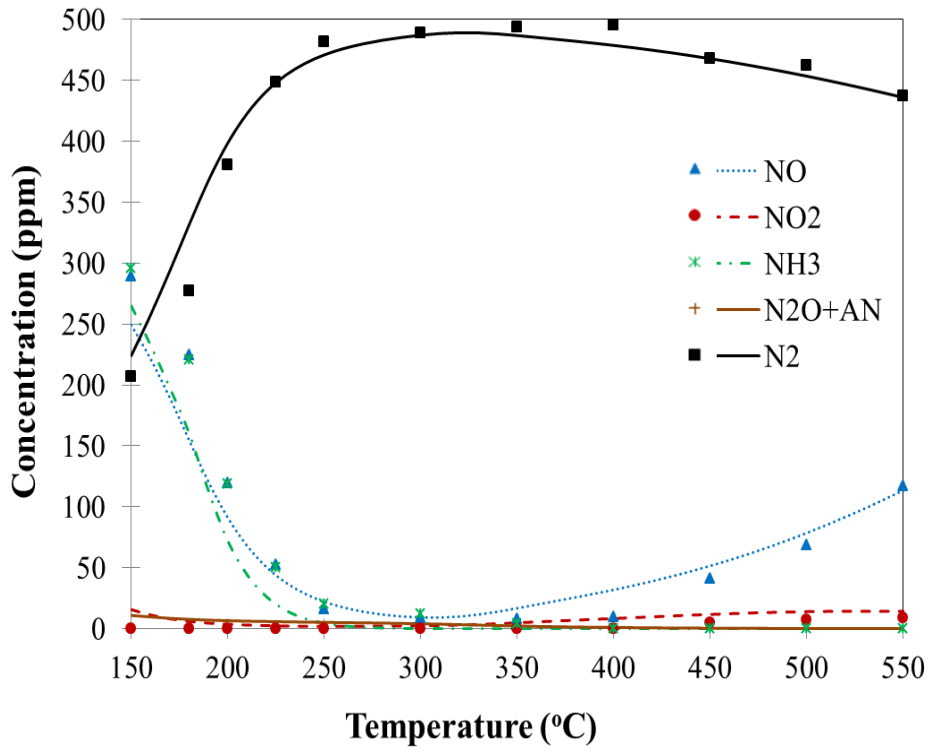

Figure 9-9b: Comparison of experimental (symbols) and model predicted (lines) concentrations of various species obtained during the NOx SCR reaction studies on Cu-chabazite catalyst. Feed: 375 ppm NO, 125 ppm NO_2, 500 ppm NH_3, 5% O_2, 2% H_2O.

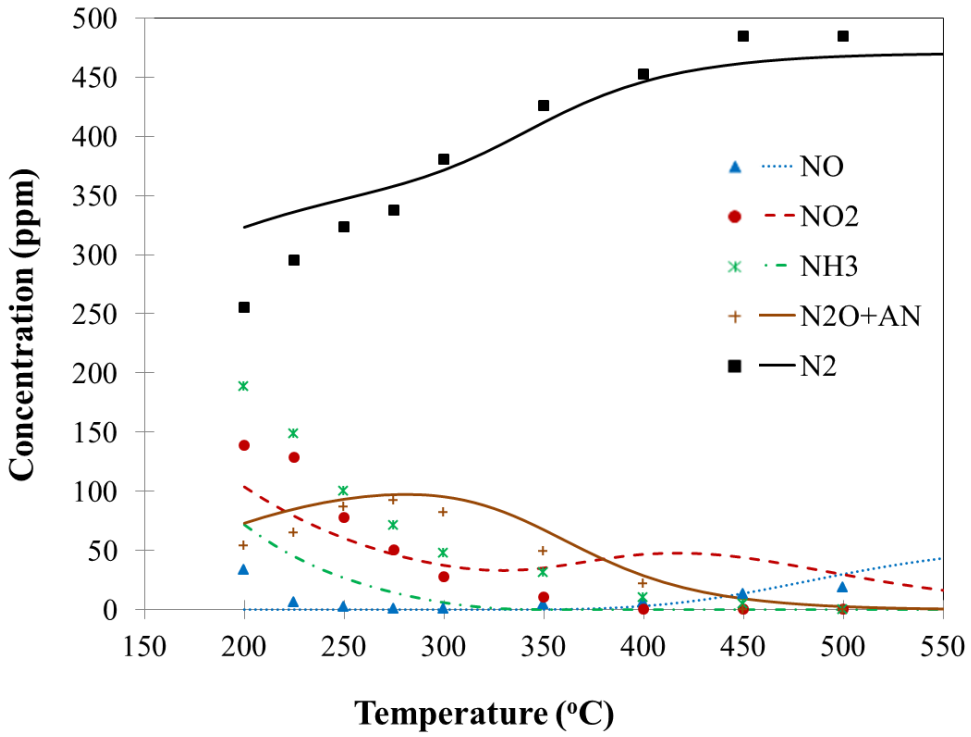

Figure 9-10: Comparison of experimental (symbols) and model predicted (lines) steady state concentrations of various species obtained during the NOx SCR reaction studies on Fe-ZSM-5 catalyst. Feed: 125 ppm NO, 375 ppm NO_2, 500 ppm NH_3, 5% O_2, 2% H_2O.

model could capture the experimental data very well throughout the temperature range except at lower temperatures (< 250 ^oC) where the model predicts higher NOx and NH_3 conversions (and hence lower outlet concentrations). Similar studies on Cu-chabazite catalyst predicted the experimental results very well.

9.4.8 Series Arrangement of Fe- and Cu-Zeolite Bricks

The data presented thus far covered the steady state experimental and kinetic modeling results of various SCR reactions carried out on commercial Fe-ZSM-5 and Cu-chabazite catalysts. These data show that the commercial Cu-chabazite catalyst is an effective NOx reduction catalyst (for standard SCR reaction) at lower temperatures (≤

350 ^{o}C) while the commercial Fe-ZSM-5 is superior at higher temperatures ($\geq$ 400 ^{o}C), in agreement with the literature studies [87, 117]. Also, the NOx conversion activity on Fe-ZSM-5 catalyst was found to be very sensitive to the feed NO_2 concentrations. The presence of NO_2 in the inlet feed greatly enhanced the NOx reduction activity for temperatures below 400 ^{o}C. However, on Cu-chabazite catalyst, the NOx conversion activity was found to be insensitive to the amount of feed NO_2 (up to $NO_2/NOx \leq 0.5$). These conversion versus temperature data for different NOx feeds are utilized in this section in which we examine series combinations of the two catalysts. In Chapter 7, we presented our experimental results on series arrangements of Fe-ZSM-5 and Cu-chabazite catalysts where we studied the sequential brick and dual-layer arrangements of Fe- and Cu-zeolite catalysts. Here we extended that study to consider the effect of various catalyst arrangements on NOx reduction activities. We used the above developed kinetic models on separate Fe-ZSM-5 and Cu-chabazite catalysts to predict the performance of combined Fe- and Cu-zeolite catalyst systems. We present some of the experimental results from Chapter 7 to gain further understanding about the combinations of Fe- and Cu-zeolite catalysts with the help of above developed kinetic model.

The first series monolith configuration considered was a Cu-zeolite followed by a Fe-zeolite. Specifically, a 1 cm long piece of the Cu-chabazite was followed by a 1 cm long piece of Fe-ZSM-5. We studied the standard SCR reaction on this combined system where the feed consisted of 500 ppm NO, 500 ppm NH_3, 5% O_2 and 2% water. The results provided in Figure 9-11a compare the 2 cm long Cu (1 cm)/Fe (1 cm) monolith series combination with the 2 cm long individual Cu-chabazite and Fe-ZSM-5 samples. The sequential configuration exhibited behavior very similar to that of the Cu-chabazite

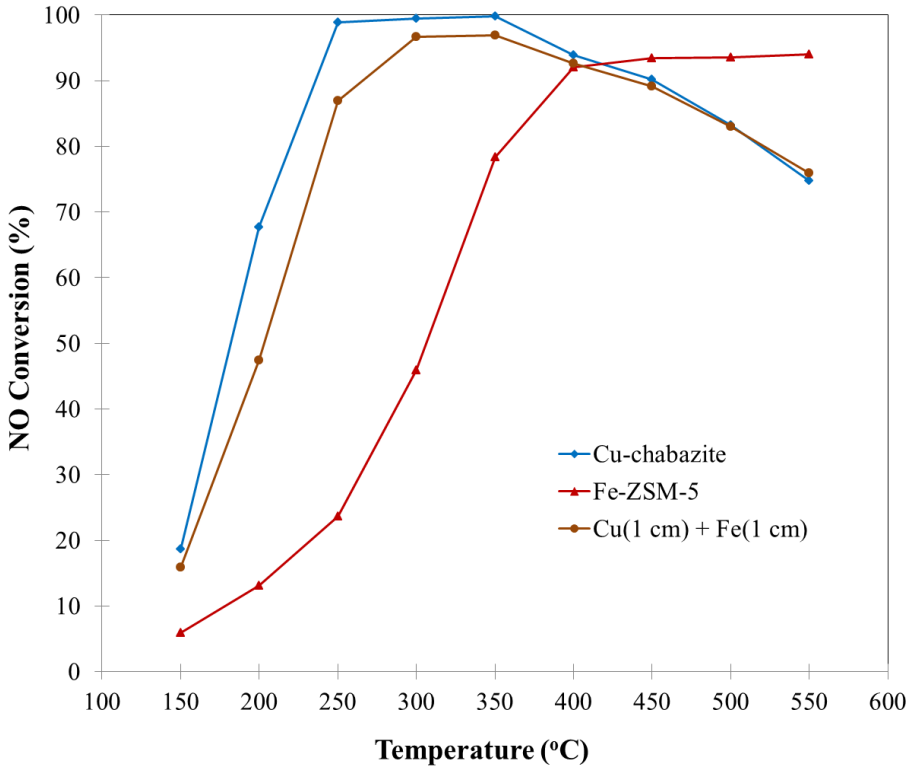

Figure 9-11a: Steady state NOx conversions obtained during the standard SCR reaction studied on Cu-chabazite, Fe-ZSM-5 and a series arrangement of Cu-chabazite (in front) followed by Fe-ZSM-5. Experimental results are shown here.

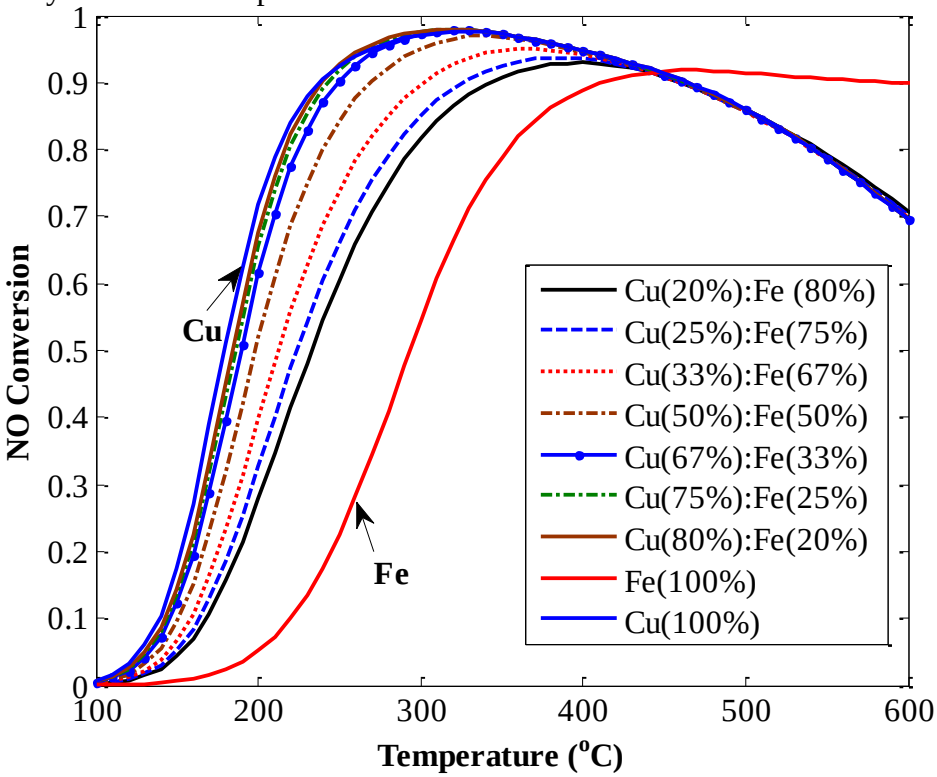

Figure 9-11b: Model predictions of the above experimental data (Figure 9-11a).

catalyst: a sharply increasing NOx conversion at low temperature (< 300 ^{o}C), a maximum NOx conversion exceeding 95% at intermediate temperature (300-350 ^{o}C) and a decreasing conversion at high temperature (> 400 ^{o}C). These data clearly indicate that, at low temperature, most of the NOx reduction occurs in the Cu-chabazite section and that the Fe-ZSM-5 catalyst is not utilized. At higher temperature there is nearly complete overlap of the conversions obtained for the Cu-/Fe- system and the Cu-chabazite monolith. This suggests that the high rate of NH_3 oxidation on the Cu-chabazite prevents the utilization of the Fe-ZSM-5 section for NOx reduction. Thus, in effect, the Fe-ZSM-5 section is not utilized over the entire temperature range. We tried to predict our experimental results with the help of above developed kinetic model. The model predicted results for various combinations of Fe-ZSM-5 and Cu-chabazite catalysts are summarized in Figure 9-11b. The total length was kept the same (2 cm) and lengths of the individual Cu- and Fe- bricks (expressed as % of total length) were varied. The model captures the experimental trends very well. The model predicted results show that the Fe-ZSM-5 only catalyst system functions very well compared to this brick arrangement system at higher temperatures. Overall the experimental and modeling studies show that the series catalyst configuration in which Cu-zeolite is followed by the Fe-zeolite does not improve the NOx reduction performance at high temperatures.

The results are more encouraging when the catalyst arrangement is reversed and the Fe-ZSM-5 catalyst is positioned in front of the Cu-chabazite. For this reason, we studied the standard SCR reaction on three different combinations of Fe-ZSM-5/Cu-chabazite series arrangements. The total catalyst length was fixed at 2 cm while varying

the individual lengths of Fe- and Cu-zeolite sections. Specifically, following three series arrangements were considered:

Series 1: Fe (1.33 cm/ 67% of total length) + Cu (0.67 cm/ 33%)

Series 2: Fe (1 cm/ 50%) + Cu (1 cm/ 50%)

Series 3: Fe (0.67 cm/ 33%) + Cu (1.33 cm/ 67%)

Results obtained with these three series arrangements are shown in Figure 9-12a. For comparison, results obtained with a 2 cm long Cu-chabazite and a 2 cm long Fe-ZSM-5 catalysts are also provided. For Series 1, the NOx conversions exceeded the Fe-only catalyst system conversion at lower temperatures ($\leq$ 350 ^{o}C) although the conversion was still considerably lower than the Cu-chabazite catalyst. At higher temperatures ($\geq$ 400 ^{o}C), the conversion obtained for Series 1 was nearly identical to the Fe-only system. For Series 2, the NOx conversion increased significantly at lower temperatures and remained close to that of the Fe-ZSM-5 only catalyst at higher temperatures. For Series 3, these trends continued. The NOx conversion at low temperature approached that of the Cu-chabazite only catalyst without much loss in conversion at high temperature. We tried to capture these experimental trends with our model described earlier. Several series arrangements of Fe-ZSM-5 (in front) and Cu-chabazite bricks were considered in the model. The total reactor length was kept the same (2 cm) and individual Fe- and Cu-brick lengths (shows here as % of the total length) were varied. Figure 9-12b shows the model predictions for this brick arrangement system. Again, the model could satisfactorily capture the experimental trends. Increasing lengths of Cu-brick at the back improved the NOx reduction activity at lower temperature while lowering the same at higher temperatures. These results show that the series arrangement with a short Fe-brick (33%)

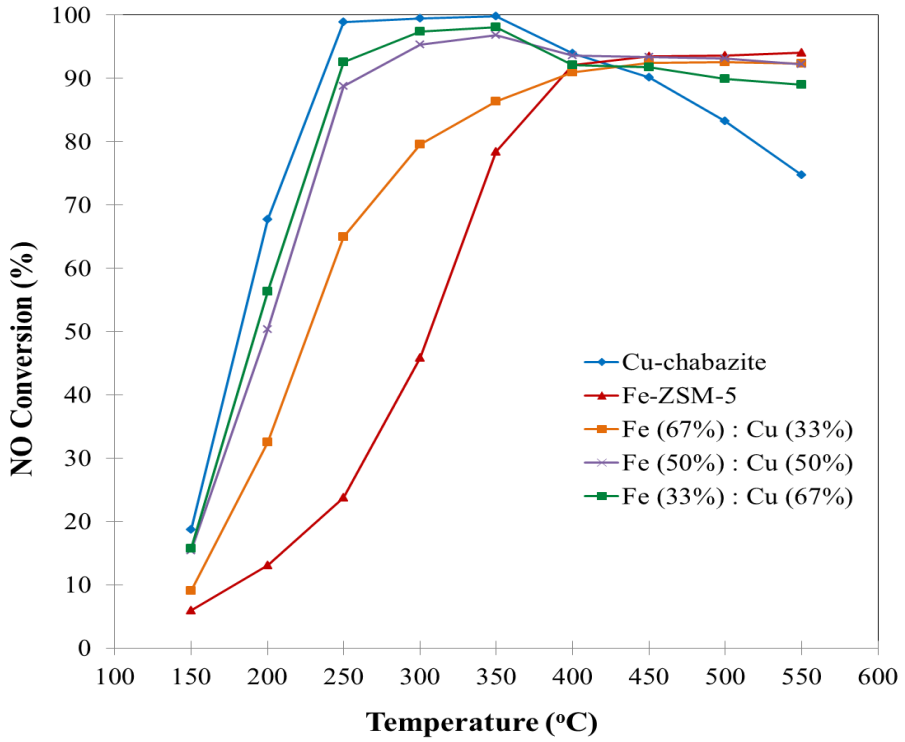

Figure 9-12a: Steady state NO conversions obtained during the standard SCR reaction studied on: Cu-chabazite, Fe-ZSM-5, and series arrangements of Fe-ZSM-5 (in front) followed by Cu-chabazite. Experimental results are shown here.

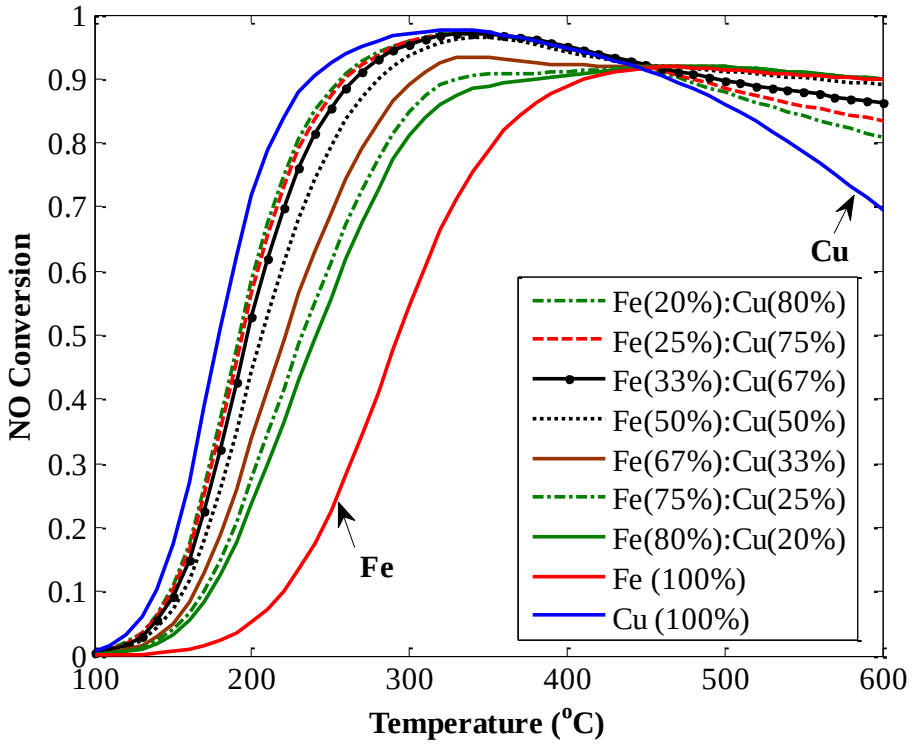

Figure 9-12b: Model predictions of the above experimental data (Figure 9-12a).

followed by a longer Cu-brick (67%) can give an optimal NOx reduction activity throughout the temperature range. Thus the overall NOx conversion can be maintained at a relatively high level over a wide temperature range by utilizing a Fe-ZSM-5/Cu-chabazite series configuration. These experimental and modeling results are in agreement with earlier results of Girard et al. [201] and suggest that there exists an optimal Fe-Z/Cu-Z configuration in terms of NOx conversion for the standard SCR reaction. By positioning Fe-ZSM-5 in front of Cu-chabazite, the high NOx reduction activity of Fe-ZSM-5 is exploited at high temperature while avoiding the detrimental NH_3 oxidation activity of Cu-chabazite. At low temperature the low activity of Fe-ZSM-5 shifts the bulk of the NOx reduction downstream to the Cu-chabazite section.

9.4.9 Dual Layer Catalysts

As discussed earlier, the series combination of Cu-chabazite section followed by Fe-ZSM-5 section (sequential brick arrangement) had similar performance to the Cu-only catalyst and did not show any improvement in the NOx conversion at higher temperatures. These results were confirmed with our modeling studies where we studied different combinations of series arrangements of Cu-chabazite followed by Fe-ZSM-5 catalysts. Here, we carried out an experiment on a monolith with a dual layer catalyst in which Cu-ZSM-5 layer was deposited on top of a commercial Fe-ZSM-5 catalyst.

A dual layer catalyst was prepared by depositing a thin layer (12 wt.%) of Cu-ZSM-5 catalyst on the commercial Fe-ZSM-5 catalyst. The catalyst synthesis procedure (for both the powder and dual layer monolith catalysts) was described earlier in Chapters 2 and 7. The standard SCR reaction was studied on this catalyst under the same

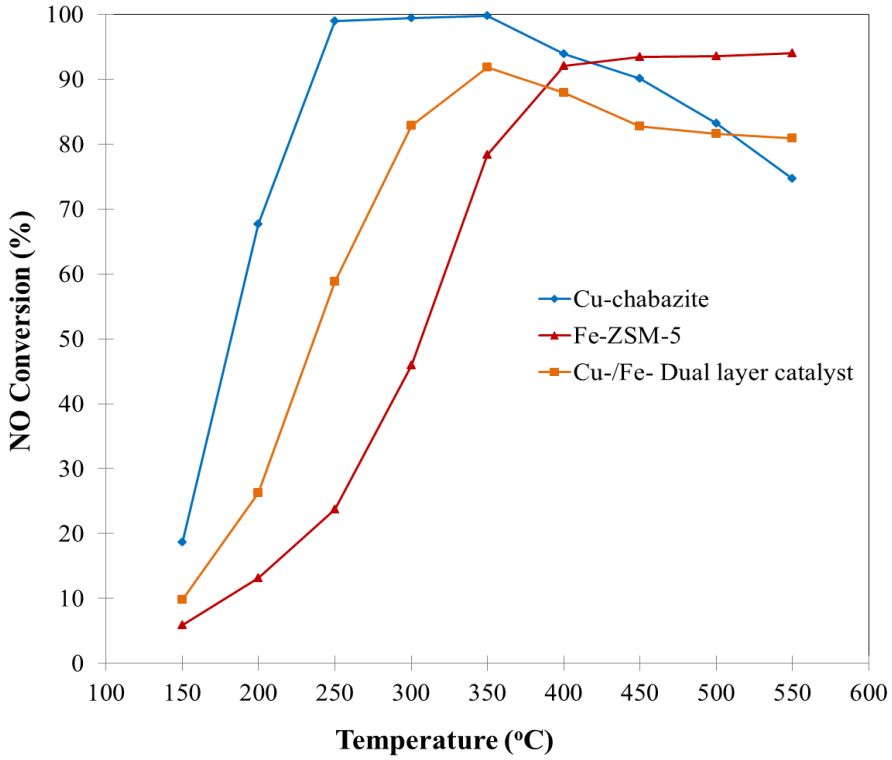

Figure 9-13a: Steady state NO conversions obtained during the standard SCR reaction studied on: Cu-chabazite, Fe-ZSM-5, and dual layer catalysts with Cu-zeolite as top layer and Fe-ZSM-5 as bottom layer. Experimental results are shown here.

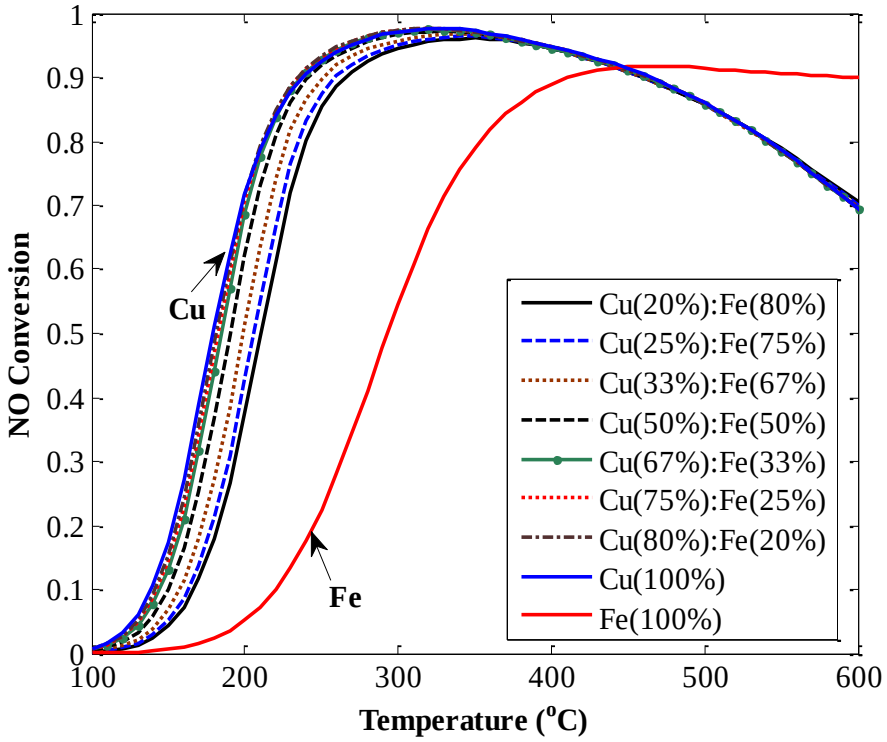

Figure 9-13b: Model predictions of the above experimental data (Figure 9-13a).

conditions as used in previous experiments. The NO conversions obtained on this dual layer catalyst are compared in Figure 9-13a to the unmodified single layer Fe-ZSM-5 and Cu-chabazite catalysts. The trends obtained with this catalyst are similar to those obtained for the Cu-chabazite/Fe-ZSM-5 series configuration (Figure 9-11). The NOx conversion obtained with the dual layer catalyst exceeded that obtained for the Fe-ZSM-5 for temperatures up to 350 ^{o}C. But at higher temperatures (> 350 ^{o}C), the NOx conversion started decreasing and showed similar trends as that for the Cu-chabazite. [Remark: The catalyst used to deposit the Cu-ZSM-5 layer on commercial Fe-ZSM-5 catalyst was different than the commercial Cu-chabazite catalyst. Hence, the catalyst activity cannot match exactly.] With the dual-layer configuration, reactants diffuse into the washcoat, obviously encountering the top layer first. This is comparable but not equivalent to encountering the first section in a series of bricks configuration. Thus, at low temperature, the SCR reaction occurs in the more active Cu-ZSM-5 top layer while the underlying, less active Fe-ZSM-5 layer is essentially not utilized. Similarly, at high temperature, the active Cu-ZSM-5 is encountered first and catalyzes the reaction. But at higher temperatures the ammonia oxidation activity is significant, resulting in the consumption of ammonia in the top layer. This results in a lack of availability of NH_3 for the complete NOx reduction at higher temperatures. We tried to predict the behavior of a dual-layer catalyst with the model developed earlier. We tried different configurations of a dual layer catalyst system with Cu-chabazite as a top layer and Fe-ZSM-5 as a bottom layer. The results obtained with the model are shown in Figure 9-13b. Here the individual Cu-/Fe- layer contribution is shown as the percentage of the total catalyst layer/amount. The total washcoat thickness was kept constant at 50 μm. The model predicts the

experimentally observed trends very well and shows that a dual layer catalyst with Cu-chabazite as a top layer gives NOx conversion activity very similar to that of the Cu-chabazite catalyst system throughout the temperature range. Thus, the experimental and modeling studies show that the dual-layer catalyst system with Cu-zeolite on top of a Fe-zeolite exhibits improved performance (compared to an Fe-only catalyst) at lower temperature but has the drawback of reduced NOx conversions at higher temperatures. Hence this system has very limited practical applications.

We turned our attention to dual-layer catalysts with Fe-ZSM-5 layer on top of a Cu-zeolite layer. A dual layer catalyst with a thin layer (12% by wt.) of Fe-ZSM-5 on top of the Cu-chabazite layer was synthesized. We used Fe-ZSM-5 catalyst provided by Sud-Chemie, Germany for synthesizing this dual layer catalyst. The washcoating procedure for synthesizing this catalyst is described in Chapter 7. The standard SCR reaction was studied on this catalyst under the same conditions as that used in previous experiments. The NO conversions obtained on this dual layer catalyst are compared in Figure 9-14a to the unmodified single layer commercial Fe-ZSM-5 and Cu-chabazite catalysts. The comparison reveals excellent performance for this dual layer catalyst. The NOx conversion exceeds 90% over the 250 to 550 ^{o}C temperature range. The results show that with the simple deposition of a thin layer of the Fe-exchanged zeolite the performance of a commercial Cu-zeolite can be improved significantly. We tried to predict the performance of various dual layer catalyst arrangements (with Fe-ZSM-5 as the top layer and Cu-chabazite as the bottom layer) with the model developed above. We varied the individual layer thicknesses of Fe- and Cu-zeolites keeping the total washcoat thickness

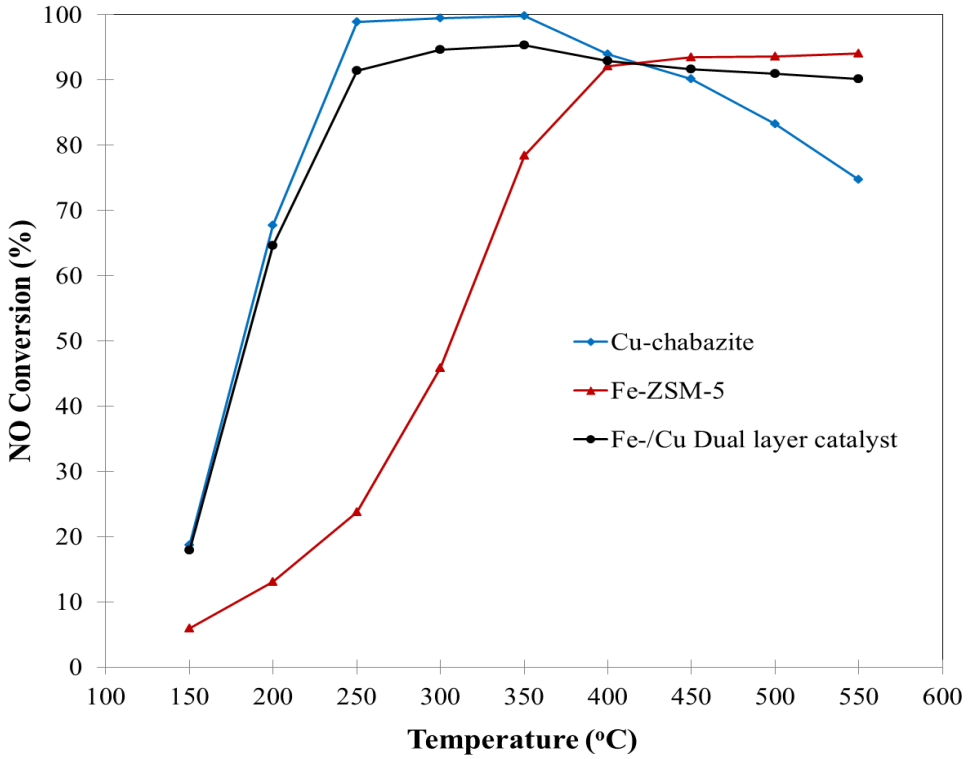

Figure 9-14a: Steady state NO conversions obtained during the standard SCR reaction studied on: Cu-chabazite, Fe-ZSM-5, and dual layer catalysts with Fe-ZSM-5 as top layer and Cu-chabazite as bottom layer. Experimental results are shown here.

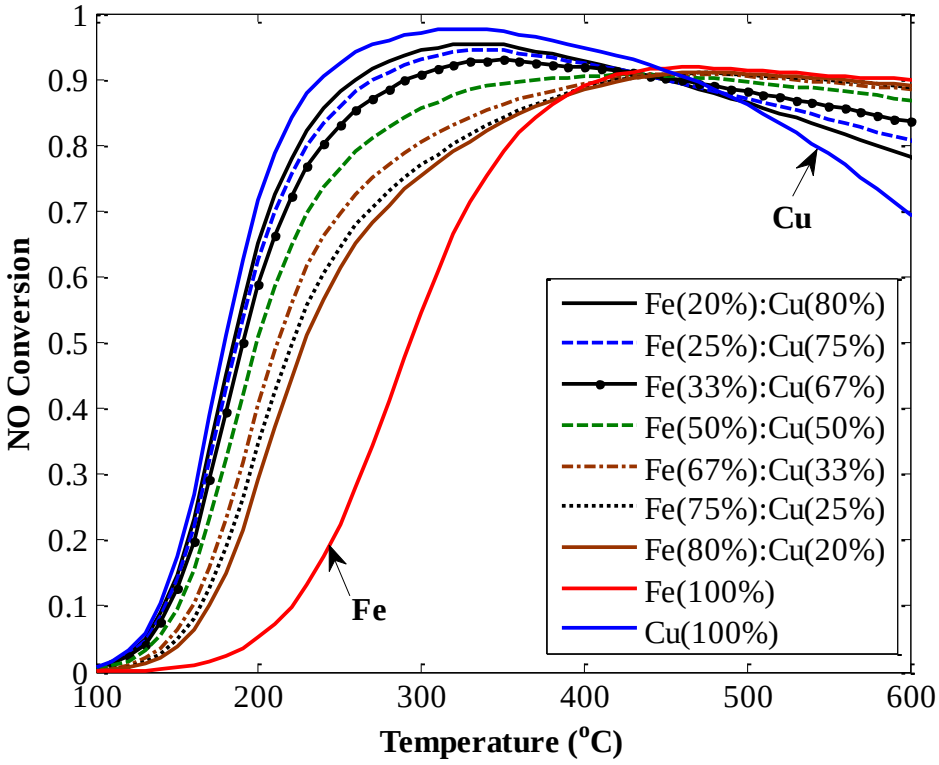

Figure 9-14b: Model predictions of the above experimental data (Figure 9-14a).

constant at 50 μm. The results (Figure 9-14b) show that as the fraction of Fe-ZSM-5 (Cu-chabazite) decreases (increases) there is a progressive increase in the low temperature conversion accompanied by a much less pronounced decrease in high temperature conversion. Following earlier discussion, the reason for this increase at low temperature is clearly a result of the increase in the loading of the underlying Cu-chabazite layer which is a more active NOx reduction catalyst at lower temperatures. At higher temperatures, the Fe-ZSM-5 in the top layer is very active towards NOx reduction during standard SCR reaction and also the ammonia oxidation side reaction is suppressed. The slight decrease in conversion at high temperature for the dual layer catalysts indicates some penetration of reacting species, in particular NH_3, to the underlying Cu-chabazite layer where it is oxidized. Again, the conversions obtained on all these catalysts never reached 100% because of the NH_3 oxidation side reaction.

Overall, these experimental and modeling studies of sequential series (or brick) and dual-layer catalyst arrangements indicate that the NOx reduction efficiency can be maximized over the entire temperature range of practical interests by distributing Fe- and Cu-zeolite along axially (series arrangement) or radially (layer arrangement). Both the arrangements result in significant improvement in the NOx reduction efficiency when Fe-ZSM-5 (layer/brick) is present in the front and Cu-chabazite is present at the back. As discussed earlier, the Cu-chabazite is an effective NOx reduction catalyst at lower temperature whereas Fe-ZSM-5 is relatively inactive. In a dual-layer catalyst, a thick Cu-zeolite layer is needed to achieve high NOx reduction efficiency at lower temperatures. A thinner porous overlayer of Fe-zeolite retains its NOx reduction activity since the Fe-layer behaves essentially as an inactive diffusion barrier. In contrast, at higher

temperatures, the ammonia oxidation reaction proceeds at a much higher rate on Cu-chabazite while NOx reduction is more effective on Fe-ZSM-5. As long as the thickness of the top Fe-zeolite layer is sufficient, most of the desired NOx conversion should occur in the top Fe layer with the underlying Cu layer serving as a spectator. Thus at high temperature, reacting species encounter the SCR-active Fe layer first and reduction proceeds, unlike at lower temperatures in which it served as a comparatively inactive diffusion barrier. The same principle applied for the brick arrangement of these two catalysts. The modeling results indicate that a thin layer (or short brick) of Fe-ZSM-5 followed by a thick layer (or longer brick) of Cu-chabazite catalyst would result in maximum NOx reduction efficiency. Our results indicate that more than 85% NOx reduction efficiency was obtained in the temperature range of 200-600 ^{o}C when we had 33% of Fe-ZSM-5 layer (or brick) followed by 67% Cu-chabazite layer (or brick) in the combined Fe-/Cu system. These results are in agreement with our experimental studies (in Chapter 7) carried out on lab-synthesized dual layer Fe-ZSM-5/Cu-ZSM-5 catalysts.

9.4.10 Dual Layer Catalysts: Application to Fast SCR

In the real exhaust aftertreatment system, the SCR unit is preceded by a diesel oxidation catalyst (DOC) unit (containing a precious metal like Pt) which has the role of catalyzing the oxidation of hydrocarbons, CO and NO. As discussed earlier, the reduction of NOx is enhanced significantly by NO_2 with the optimal feed ratio being $NO/NO_2 = 1$. This is known as the fast SCR reaction system given by reaction (9-2) and it does not require the oxidation of NO to NO_2 in the SCR. It is now well accepted that the rate of SCR reaction increases in the presence of NO_2 (especially at lower temperatures) on both

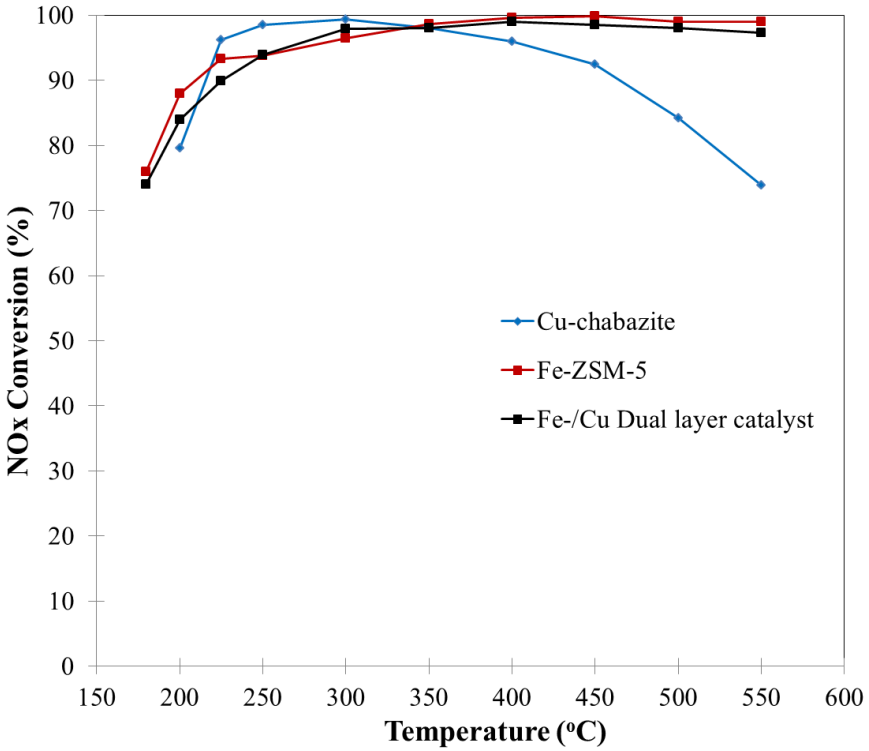

Figure 9-15a: Steady state NOx conversions obtained during the fast SCR reaction studied on: Cu-chabazite, Fe-ZSM-5 and dual layer catalysts with Fe-ZSM-5 as top layer and Cu-chabazite as bottom layer. Experimental results are shown here.

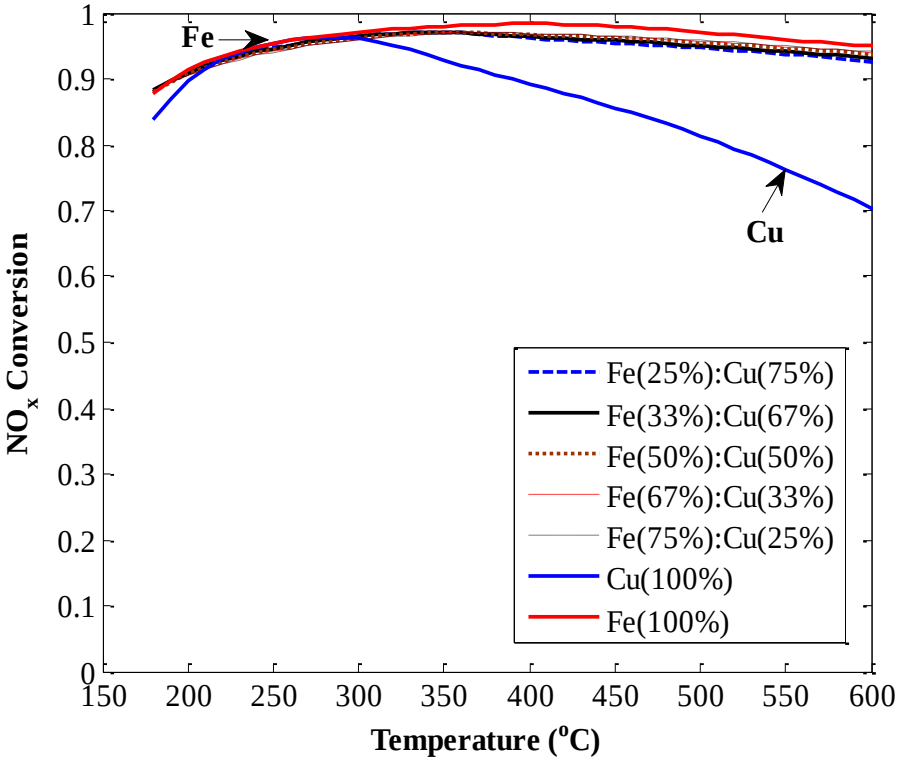

Figure 9-15b: Model predictions of the above experimental data (Figure 9-15a).

the Fe- and Cu-zeolite catalysts [29], although the rate increment is more significant for Fe-zeolite compared to Cu-zeolite catalyst. In the context of the current study, it is of interest to determine the potential for the dual layer catalyst when the feed contains NO_2.

Figure 9-15a summarizes the steady state NOx conversions obtained during the fast SCR reaction on the Fe-ZSM-5, Cu-chabazite and a dual layer catalyst system (8 wt. % Fe-ZSM-5 as top layer, 16 wt.% Cu-ZSM-5 as bottom layer). A feed containing an equimolar mixture (250 ppm each) of NO and NO_2 was introduced in the presence of 500 ppm NH_3, 5% O_2 and 2% water. The results obtained during the fast SCR reaction studies carried out on the separate Fe-ZSM-5 and Cu-chabazite catalysts have been discussed earlier. We obtained very high NOx conversions for the Fe-ZSM-5 catalyst especially at lower temperatures compared to the standard SCR reaction. In the presence of feed NO_2, there was an enhancement in the NOx reduction activity at lower temperatures even for the Cu-chabazite. For the Cu-chabazite catalyst, the NOx conversion decreased at temperatures above 350 ^oC as a result of the consumption of the NH_3 reductant by the NH_3 oxidation side reaction. This behavior is similar to that observed earlier for the standard SCR reaction carried out on the Cu-chabazite catalyst. The dual layer catalyst exhibited remarkably high NOx conversion (> 90%) over the entire temperature range (250-550 ^oC). In fact, the NOx reduction activity of this catalyst was comparable to the Fe-only system even at higher temperatures where it showed very stable NOx reduction efficiency. We used the above developed kinetic model to predict the performance of dual layer catalyst with Fe-ZSM-5 as the top layer and Cu-chabazite as the bottom layer. The layer thickness (shown here as the percentage of the total catalyst amount) of the individual Fe- and Cu-catalysts was varied and different configurations were studied for

the fast SCR reaction. These results (Figure 9-15b) show that the presence of a thin Fe-layer on top gives very high NOx conversions throughout the temperature range. The performance of all the dual-layer catalysts studied was very close to the Fe-only system. These results are in agreement with the experimental observations. Overall, the experimental and modeling studies demonstrate that the dual layer catalyst system with a thinner Fe-zeolite layer on top of a thicker Cu-zeolite layer works well even for the case of fast SCR system which is more representative of an actual diesel exhaust system.

9.5 Conclusions

We have presented a comprehensive experimental study coupled with the detailed kinetic modeling of various reactions occurring in the selective catalytic reduction of NOx with NH_3 on both the commercial Fe-ZSM-5 and Cu-chabazite catalysts. The kinetic model accurately predicts the key features of various reactions studied experimentally. The two-dimensional, two-phase model used in this study accounts for the washcoat diffusion limitations which are of prime importance in any heterogeneous gas-solid reaction systems involving convection, diffusion and reaction. The kinetic model accounts for NH_3 adsorption-desorption, NH_3 oxidation, NO oxidation, standard SCR, fast SCR, NO_2 SCR, N_2O formation and decomposition, NH_4NO_3 formation and decomposition, etc. To our knowledge, this is the first study focused on the detailed understandings of experimental and kinetic modeling aspects of NH_3-SCR reaction system on recently developed small pore Cu-chabazite catalyst.

Both the Fe-ZSM-5 and Cu-chabazite catalysts were found to store NH_3. The ammonia adsorption capacity of Cu-chabazite catalyst was found to be greater than Fe-

ZSM-5 catalysts. The ammonia oxidation side reaction was very active on Cu-chabazite catalysts where complete NH_3 conversions were obtained at temperatures as low as 400-450 ^oC. This reaction was observed on Fe-ZSM-5 catalyst as well, but at much slower rates. Both the catalysts oxidized NO to NO_2. All these features were accurately predicted by the kinetic model.

The effect of NO_2/NOx feed ratio on NOx reduction efficiency and product distribution was considered for the entire temperature range. Cu-chabazite was found to be a very active NOx reduction catalyst at lower temperatures (< 350 ^oC) and about complete NOx conversions were obtained in the temperature range of 250-350 ^oC. Also, the NOx conversions were found to be insensitive to the amount of NO_2 (up to NO_2/NOx $\leq$ 0.5) present in the feed. The Fe-ZSM-5 catalyst was found to be a less active NOx reduction catalyst at lower temperatures when the feed consisted of only NO. But this catalyst resulted in higher NOx reduction efficiency (compared to the Cu-chabazite catalyst) at temperatures above 400 ^oC. This was because the NH_3 oxidation side reaction was less pronounced on this catalyst. Also, the NOx reduction efficiency on Fe-ZSM-5 catalyst was found to be very sensitive to the amount of feed NO_2. For the feeds containing equimolar NO and NO_2 (fast SCR), very high NOx conversions were observed throughout the temperature range. The deNOx performance was found to be worse on both the catalysts for the feeds containing excess NO_2 (NO_2/NOx $\geq$ 0.75). This resulted in the formation of number of byproducts like ammonium nitrate, N_2O, etc. The kinetic model accurately captures the experimentally observed NOx conversions, N_2 selectivity, product distribution, etc. as a function of temperature and various NO_2/NOx feed concentrations.

Based on the fundamental understandings developed about the kinetics and mechanistic aspects of various SCR reactions on separate Fe-ZSM-5 and Cu-chabazite catalyst systems studied in the first part of this work, we carried out a systematic study of standard and fast SCR reaction on combined Fe- and Cu-zeolite catalysts system to determine if a high NOx conversion could be sustained over a wider temperature range than with individual Fe- and Cu-zeolite catalysts. A series combination of Fe-ZSM-5 (in the front) (short brick) followed by Cu-chabazite (longer brick) gave the highest NOx conversion over a wide temperature range. The reverse series catalyst arrangement with the Cu-zeolite in front of the Fe-zeolite catalyst had little if any effect on the NOx reduction efficiencies at higher temperatures. The results indicated that this catalyst system resulted in the deNOx performance very similar to the Cu-only catalysts. The kinetic model corroborates the experimental observations where we studied a wide range of different combinations of series arrangements with Fe-ZSM-5 followed by Cu-chabazite (and vice versa).

Standard and fast SCR experiments were carried out on various dual layer catalysts. Amongst the different combinations of dual-layer catalyst systems with Fe-ZSM-5 catalyst layer on top of a Cu-chabazite catalyst layer, a catalyst with a thinner Fe-ZSM-5 layer on top of a thicker Cu-chabazite layer at bottom gave optimum NOx reduction activities for both the standard and fast SCR reactions. The improvements in the NOx conversion were obtained by exploiting the different reactivities of the two catalysts over the entire temperature range. At low temperatures the Fe-zeolite is less active compared to the Cu-zeolite, whereas at high temperatures the Fe-zeolite top layer is effective in converting most of the NOx while minimizing the consumption of

ammonia via its oxidation on Cu-zeolite. The dual layer catalyst results clearly indicate that an optimal dual-layer catalyst composition would maximize the NOx conversion over a prescribed temperature range. The experimental study was further extended to the modeling of dual layer catalysts where we considered different dual-layer catalyst arrangements of Fe-ZSM-5 as top layer and Cu-chabazite as bottom layer and vice versa. The expansion of the temperature window of high deNOx performance is observed for both the standard SCR and the fast SCR reactions. At high temperatures, the dual layer catalyst utilizes more selective Fe-zeolite top layer. While at lower temperatures, it utilizes highly active Cu-zeolite bottom layer which also reduces the requirements for feed NO_2 for Fe-only catalyst system. The reverse catalyst arrangement (Cu-layer on top, Fe-layer at bottom) was found to be very similar to the Cu-only catalyst system at higher temperatures where the NOx conversions decreased significantly. But there was a slight improvement in the NOx conversion activity because of the more selective Fe-layer at the bottom. All the experimental trends were accurately captured by the model. To our knowledge, this is the first modeling study focused on the in-depth understanding of performance of a dual-layer washcoated monolithic catalyst for widening the overall temperature window of high deNOx efficiency for the standard and fast SCR reactions.

CHAPTER 10 Conclusions and Recommendations for Future Work

10.1 Conclusions

Increasing transportation fuel prices have increased the demand for diesel powered vehicles, which are more fuel efficient than their gasoline counterparts. However, diesel exhaust contains volatile hydrocarbons, particulate matter and NOx, mostly in the form of NO. In response to increasingly stringent EPA standards for NOx, a host of NOx reduction technologies are being developed. Selective catalytic reduction of NOx with NH_3 generated from onboard thermal decomposition of urea has proven to be an effective catalytic process for NOx reduction. Fe- and Cu-zeolite catalysts are considered to be the most promising catalysts for obtaining very high NOx reduction efficiency over the entire temperature range of practical interests. The main objective of this work was to study the kinetics and mechanistic aspects of various reactions on Fe-ZSM-5, Cu-ZSM-5 and recently developed small pore Cu-chabazite catalysts. Overall, this work has presented a comprehensive experimental and kinetic modeling study of NH_3-SCR reaction system on these metal-exchanged zeolite catalysts. The main contributions of this work are: i) steady state and transient kinetics studies of SCR of NOx with NH_3 on Fe-ZSM-5, Cu-ZSM-5 and Cu-chabazite catalysts; ii) the development of fundamental understandings about the importance of mass transfer and washcoat diffusion limitations in metal-exchanged zeolite catalysts used for the NH_3-SCR applications; iii) the development of mechanistic based models explaining the key features of various NH_3-SCR reactions; iv) the introduction of the concept of dual-layer catalysts to widen the temperature window of enhanced deNOx performance and v) the development of global kinetic models predicting the performance of NH_3-SCR reaction

system on Fe-ZSM-5, Cu-chabazite and combined catalyst arrangements of Fe- and Cu-zeolite catalysts which include sequential brick arrangements and dual-layer configurations. The main findings from this work are summarized below.

Cu-ZSM-5 and Fe-ZSM-5 powder catalysts were synthesized in-house by a conventional ion-exchange technique starting with NH_4^+ form of a zeolite powder. The catalyst powder was deposited on blank monolith supports (by dip-coating technique) to obtain washcoated monolithic catalysts. The performance of lab-synthesized Fe-ZSM-5 catalyst was compared to that of the commercial Fe-ZSM-5 catalyst. Very comparable results were obtained on both the catalysts studied proving our catalyst synthesis capabilities. The results obtained with Fe-ZSM-5 catalysts were then compared with the commercial Cu-chabazite catalyst provided by BASF Catalysts LLC.

A comprehensive experimental and kinetic modeling study of NO oxidation was carried out of Fe- and Cu-zeolite catalysts and a comparison is made between Fe-ZSM-5 and Cu-chabazite catalysts. The steady state data showed that Fe-zeolite is a better NO oxidation catalyst than Cu-zeolite. The NO oxidation reaction was inhibited by NO_2. This inhibition was more pronounced on Cu-chabazite than Fe-ZSM-5, the explanation for Fe being a more active NO oxidation catalyst. The presence of feed water strongly inhibited the NO oxidation on both catalysts. Separate studies of NO_2 decomposition (to NO) reaction showed that the reaction started at around 300 ^oC on the Fe-ZSM-5 catalyst and at about 350 ^oC on the Cu-chabazite catalyst. The NO_2 uptake experiments showed the formation of surface nitrates on both the Fe- and Cu-zeolite catalysts. The amount of NO_2 released during the TPD experiment was higher on the Cu-chabazite compared to the Fe-ZSM-5 catalyst and was released at higher temperatures. This showed higher stability of

surface nitrates (even at higher temperatures) on the Cu-chabazite catalysts. The surface nitrates were found to be unstable in the presence of feed NO and were immediately decomposed to NO_2. Catalyst pretreatments by different oxidizing/reducing agents (O_2, NO_2, NH_3, H_2) did not affect steady state NO oxidation activity. Steady state experiments carried out on catalysts with the same washcoat volume but different washcoat thicknesses ruled out the presence of washcoat diffusion limitations for the forward NO oxidation reaction for temperatures below 350 ^oC. A differential kinetic analysis of the NO oxidation reaction on both the commercial Fe- and Cu-zeolite catalysts showed positive order rate dependence (~ +1) on NO and O_2 (~ +0.5) on both the catalysts, while showing negative order dependence with respect to NO_2, confirming the NO_2 inhibition effect. The reaction order with respect to NO_2 was found to be about -0.5 on the Fe-ZSM-5 and -1 on the Cu-chabazite which confirmed the severe inhibitory effect of NO_2 on the Cu-chabazite. The activation energy of the forward NO oxidation reaction was 39 kJ/mol on the Fe-ZSM-5 and 56 kJ/mol on the Cu-chabazite. The presence of feed water did not have any major effect on the reaction orders and activation energies. A global kinetic model was developed to predict the NO oxidation reaction on both the Fe- and Cu-zeolite catalysts. It was based on the surface reaction between adsorbed O atoms and gaseous NO as the RDS. This model satisfactorily captures the experimentally observed reaction orders, steady state NO conversions for various feed conditions along with the inhibitory effect of feed NO_2 and water for the entire temperature range.

Differential kinetics derived on standard SCR reaction studied on both the Fe-ZSM-5 and Cu-chabazite catalysts showed that the reaction was nearly first order with respect to NO, positive (+0.52 to +0.59) order with respect to O_2 and negative (-0.20 to -

0.32) order with respect to ammonia. Ammonia was found to have an inhibiting effect on the standard SCR reaction due to ammonia blocking the active sites required for this reaction at low temperatures. The activation energy of this reaction was found to be 42 kJ/mol on Fe-ZSM-5 and 54 kJ/mol on Cu-chabazite. Agreements in the differential kinetics studies of NO oxidation and standard SCR reaction support the proposed idea in the literature that the NO oxidation is the rate determining step in standard SCR reaction. The presence of water showed negligible inhibition on the standard SCR reaction while the NO and NH_3 oxidation reactions were strongly inhibited by H_2O. NO_2 along with the nitrites and nitrates formed in the presence of water appear to block the active sites for NO oxidation. However, during the standard SCR, NH_3 cleans the catalyst surface by immediately reacting with the surface species to form an unstable intermediate, ammonium nitrite, which decomposes to N_2 and H_2O. The role of NH_3 serves to remove the nitrous and nitric acids, freeing up sites for adsorption of O_2 and NO. A dual-site Langmuir-Hinshelwood kinetic model, which considers the NH_3 adsorption on acidic sites and the NO oxidation on Fe-sites, was proposed in agreement with our experimental observations.

The effect of various feed NO_2 concentrations on the NOx reduction performance was considered for both the Fe-ZSM-5 and Cu-chabazite catalysts. In the absence of feed NO_2, Fe-ZSM-5 catalyst was found to be less active compared to Cu-chabazite catalyst. About complete NO reduction efficiency was obtained on the Cu-chabazite catalyst in the temperature range of 250-350 ^oC. But at higher temperatures, the NO conversions decreased because of the enhanced ammonia oxidation side reaction. The Fe-ZSM-5 catalyst was found to be less active for NH_3 oxidation and it gave a stable and higher

NOx reduction performance at higher temperatures compared to the Cu-chabazite catalyst. In the presence of feed NO_2, the Fe-ZSM-5 catalyst was found to have a promoting effect on the deNOx performance. This effect was more pronounced at lower temperatures (< 400 ^oC). The Cu-chabazite catalyst showed some improvement in the NOx conversion efficiency for the feeds containing NO_2 ($NO_2/NOx \leq 0.5$). But this improvement in the deNOx performance was observed only at very low temperatures $\leq$ 180 ^oC. At higher temperatures ($\geq$ 200 ^oC), very similar deNOx efficiency was observed for all the feeds containing $NO_2/NOx \leq 0.5$. Thus the deNOx efficiency on Cu-chabazite catalyst was rather insensitive to the amount of NO_2 ($NO_2/NOx \leq 0.5$) present in the feed. A feed containing equimolar quantities of NO and NO_2 was found to have maximum selectivity towards N_2 production on both the catalysts. Excess feed NO_2 concentrations ($NO_2/NOx \geq 0.75$) were found to be detrimental for both the catalysts as the NOx conversions and selectivity towards N_2 decreased. Feeds containing NO_2 higher than the equimolar NO/NO_2 ratios led to a number of side reactions at lower temperatures. This led to the formation of byproducts like ammonium nitrate below 250 ^oC. The ammonium nitrate decomposed at higher temperatures and led to the formation of another byproduct N_2O. Maximum N_2O was detected for a feed containing pure NO_2 in the temperature range of 250-300 ^oC. Thus, the presence of NO_2 in the inlet feed complicates the SCR reaction system with number of reactions occurring simultaneously e.g., standard SCR, fast SCR, NO_2 SCR, ammonium nitrate formation and decomposition, ammonia and NO oxidation. The amount of N_2O formed on the Cu-chabazite catalyst was less compared to that formed on the Fe-ZSM-5 catalyst. Steady state and transient experiments confirmed the presence of NH_4NO_3 on the catalyst surface at lower temperatures and the NH_4NO_3

was found to inhibit both the fast and NO_2 SCR reactions at lower temperatures. Increasing amounts of NO in the feed NOx increases the N_2 production by inhibiting the formation of undesirable byproducts like NH_4NO_3 and N_2O. The key role of NO was found to reduce HNO_3 and NH_4NO_3, present on the catalyst, to desired nitrites and thereby increasing N_2 production. Based on the differential kinetics studies, a kinetic rate expression was proposed for the fast SCR reaction which explained key trends obtained during the experiments. Reduction of nitrates by NO appears to be the rate determining step for the fast SCR reaction while reduction of HNO_3 by NH_3 seems to determine the NO_2 SCR reaction mechanism. Water inhibits the NOx reduction for the feeds containing excess NO_2 ($NO_2/NOx > 0.5$) in the temperature range of 200-300 ^oC. This inhibition effect was not observed for the feeds containing $NO_2/NOx \leq 0.5$.

The steady state results with different NO_2/NOx feed ratios were supported by the transient experimental study where NOx feeds containing varied NO/NO_2 ratios were fed to the catalyst surface pre-saturated with NH_3. The transient experiments conveyed the large difference in the SCR chemistry for the standard and fast SCR systems on the Fe-ZSM-5 catalyst. For the equimolar feed corresponding to the fast SCR reaction, the rate of N_2 formation was much higher than for the standard SCR reaction. However, for the Cu-chabazite catalyst, both the standard and fast SCR reactions were observed to have very similar rates for temperatures above 200 ^oC. Also, the amount and the selectivity of N_2 was nearly the same for both these reactions. For the feeds containing only NO_2, N_2O was observed as a byproduct. Thus overall, transient experiments support the steady state findings that the deNOx efficiency is not a strict function of feed NO_2 concentrations on the Cu-chabazite catalyst. Transient experiments performed on the ammonia uptake and

desorption showed that both the Fe- and Cu-zeolite catalysts can adsorb significant amounts of NH_3 and the ammonia adsorption capacity of the Cu-chabazite catalyst was found to be much greater than that of the Fe-ZSM-5 catalyst.

An extensive study carried out on Fe- and Cu-ZSM-5 catalysts of different washcoat loadings, washcoat thicknesses and lengths revealed the importance of washcoat diffusion and mass transfer limitations in various NH_3-SCR reactions. The washcoat diffusion limitations were found to be important in all the NH_3-SCR reactions (except NO oxidation). For the standard SCR reaction, the washcoat diffusion limitations were found to be significant starting at 350 ^oC on Fe-ZSM-5 and 250 ^oC on Cu-ZSM-5. Both the fast and NO_2 SCR reactions, being very fast, showed the presence of washcoat diffusion limitations throughout the temperature range of practical interest. Theoretical calculations of characteristic times for various mass transfer processes and Weisz-Prater modulus supported the experimental findings. A representative case of NO_2 SCR reaction is shown which predicts the effects of washcoat diffusivity and temperatures on the regime transitions (from kinetic to washcoat diffusion to external mass transfer). Fast and NO_2 SCR reactions were found to be mainly in mixed regimes where washcoat diffusion plays a significant role. The understanding of mas transfer processes is important in accurate design of experiments to predict intrinsic kinetics. Also, this knowledge is important in developing intrinsic kinetic models and efficient catalyst designs. The experimental study coupled with theoretical analysis indicate the necessity of inclusion of these mass transfer limitations in SCR modeling. These washcoat diffusion limitations are neglected in the current SCR literature.

We have developed a detailed kinetic model to predict key features of various reactions occurring in the selective catalytic reduction of NOx with NH_3 on both the commercial Fe-ZSM-5 and Cu-chabazite catalysts. We have used a two-dimensional, two-phase model in this study. This model accounts for the washcoat diffusion limitations which are of prime importance in any heterogeneous gas-solid reaction systems involving convection, diffusion and reaction. The kinetic model accounts for the following reactions: NH_3 adsorption-desorption, NH_3 oxidation, NO oxidation, standard SCR, fast SCR, NO_2 SCR, N_2O formation and decomposition, NH_4NO_3 formation and decomposition, etc. This model accurately predicts the steady state experimental findings of NOx conversions, N_2 selectivity, byproduct formations, etc. for various feed conditions (feeds with NO_2/NOx inlet ratio in the range of 0-1) throughout the temperature range.

Based on the fundamental understandings developed about the kinetics and mechanistic aspects of various SCR reactions on separate Fe-ZSM-5, Cu-ZSM-5 and Cu-chabazite catalyst systems, we carried out a systematic study of standard and fast SCR reaction on combined Fe- and Cu-zeolite catalysts system to determine if a high NOx conversion could be sustained over a wider temperature range than with the individual Fe- and Cu-zeolite catalysts. A series combination of Fe-zeolite (in the front) (short brick) followed by Cu-zeolite (longer brick) gave the highest NOx conversion over a wide temperature range. The reverse series catalyst arrangement with the Cu-zeolite in front of the Fe-zeolite catalyst had little if any effect on the NOx reduction efficiencies at higher temperatures. The kinetic model corroborates the experimental observations where

we studied a wide range of different combinations of series arrangements with the Fe-ZSM-5 catalyst followed by the Cu-chabazite (and vice versa).

Standard and fast SCR reaction studies were carried out on various dual layer catalysts where Fe- and Cu-zeolite catalysts were arranged in the form of layers on the same monolithic support. Amongst the various combinations of dual-layer catalyst systems with Fe-ZSM-5 catalyst layer on top of the Cu-chabazite catalyst layer, a catalyst with thinner Fe-ZSM-5 layer on top of a thicker Cu-chabazite layer (at bottom) gave maximum NOx reduction activities for both the standard and fast SCR reactions. The improvements in the NOx conversion were obtained by exploiting the different reactivities of the two catalysts. At low temperatures, the Fe-zeolite was less active compared to the Cu-zeolite, whereas at high temperatures the Fe-zeolite top layer was effective in converting most of the NOx while minimizing the consumption of ammonia via its oxidation on Cu-zeolite. The dual layer catalyst results clearly indicate that an optimal dual-layer catalyst composition would maximize the NOx conversion over a prescribed temperature range. The experimental study was further strengthened with the modeling of dual layer catalysts where we considered different dual-layer catalyst arrangements of Fe-ZSM-5 as top layer and Cu-chabazite as the bottom layer and vice versa. The expansion of the temperature window for high deNOx performance was observed for both the standard SCR and the fast SCR reactions. The reverse catalyst arrangement (Cu-layer on top, Fe-layer at bottom) was found to be very similar to the Cu-only catalyst system at higher temperatures where the NOx conversions decreased significantly. But there was a slight improvement in the NOx conversion activity because of the more selective Fe-zeolite layer at the bottom. All the experimental trends were

accurately captured by the model. To our knowledge, this is the first experimental study coupled with the modeling analysis of dual layer Fe-/Cu-zeolite SCR catalysts used for widening the overall temperature window of high deNOx efficiency for both the standard and fast SCR reactions. The dual layer catalyst seems a promising NH_3-SCR catalyst and offers several advantages over the individual Fe-/Cu-zeolite catalysts.

10.2 Recommendations for Future Work

Based on the insights gained in this study, some recommendations are made for the future work in the area of exhaust aftertreatment systems.

In the current study, we have considered Fe-ZSM-5, Cu-ZSM-5 and Cu-chabazite catalysts for NH_3-SCR reaction studies. The metal loading was kept the same in all the catalysts. It would be interesting to see the effect of metal loading on the NOx and NH_3 conversions and the product distributions for various SCR reactions. The current experimental study was carried out using a flow reactor set up where we could measure the gas phase concentrations only at the exit. The use of other experimental techniques including Diffuse Reflectance Infrared Fourier Transform Spectroscopy (DRIFTS) is recommended to study the species formed on the surface by various surface reactions. This would give further insights into the mechanistic aspects of various SCR reactions. The experimental study showed that various byproducts can be formed in the presence of excess feed NO_2. Also, additional NH_3 was consumed during the standard SCR reaction by parasitic ammonia oxidation reaction. Isotopic labeling studies with $^{14}NH_3$ and/or $^{15}NH_3$ and $^{15}NO(_2)$ and/or $^{14}NO(_2)$ using Temporal Analysis of Products (TAP) is suggested to develop further understanding about the reaction mechanism. In this work,

we used catalysts of different lengths to study the NOx conversion activities along the catalyst lengths. But, it is difficult to cut the catalyst to exact dimensions. Also, decreasing the catalyst lengths leads to more pronounced entrance length effects. A use of spaci-mass spectrometer (MS) can minimize these drawbacks. Also, with the help of spaci-MS, it is possible to study the concentrations of various species at different positions along the catalyst length. The use of spaci-MS is recommended for future studies to spatially resolve SCR reactions on Fe-ZSM-5, Cu-chabazite and dual-layer catalysts. This would give further insights into the optimization of Fe-/Cu-zeolite layer thicknesses in dual-layer SCR catalysts and also brick lengths in sequential Fe-/Cu-zeolite series arrangements.

The current study introduced the concept of dual-layer NH_3-SCR catalysts. In an actual exhaust after-treatment system, NH_3 is generated on-board by thermal decomposition of urea. The unreacted NH_3 leaving the SCR catalytic system is harmful to human beings and hence the NH_3 slip should be minimized. For this purpose, dual layer NH_3 slip catalyst technology is currently under investigation. This technique utilizes Fe-zeolite as top layer and a thin Pt/Al_2O_3 as a bottom layer. Our experimental study showed that the Cu-chabazite is highly active for the NH_3-oxidation compared to the Fe-zeolite catalysts. Also, this catalyst has higher NH_3 and NOx storage capacities than the Fe-zeolite catalysts. The catalyst synthesis technique provided in this study can be used to synthesize dual layer NH_3-slip catalysts with Cu-chabazite as a top layer. The performance of this catalyst can be compared to the existing NH_3-slip catalyst. Also, when Pt is present, NH_3 may be oxidized to harmful N_2O. The N_2O formation was also observed during the NH_3 SCR reactions (carried out on both the Fe-ZSM-5 and Cu-

chabazite catalysts) for the feeds containing excess NO_2. Future experiments should focus on the N_2O decomposition reaction on these catalysts.

In the current work, we proposed the concept of dual-layer catalyst with Fe-ZSM-5 as top layer and Cu-chabazite as the bottom layer. Our experimental findings proved the presence of diffusion limitations in these SCR catalysts. In order to utilize the complete catalyst in the dual-layer, a large pore Fe-zeolite catalyst may be used. This would minimize the diffusion limitations at lower temperatures thus enhancing the deNOx performance. Future work should investigate a hydrothermally stable and sufficiently active large pore Fe-zeolite catalyst that can be used as the top layer in NH_3-SCR catalysts. A recent study by Narula et al. [234] showed the enhancement of NOx reduction activity at lower temperature by including indium in the Cu-zeolite catalyst. The indium doped Cu-chabazite catalyst as a bottom layer in the dual-layer catalyst may further enhance the NOx reduction performance. The present study did not account for the effect of hydrocarbons which are present in actual diesel exhaust. The effect of hydrocarbons should be considered in future work. Along with the proposed dual layer catalyst, several other catalyst combinations including a combination of dual layer and brick systems may be considered in future experimental studies for enhancing the NOx reduction performance over a wide temperature range. Recent research has focused on combinations of lean NOx trap catalysts and SCR catalysts for achieving very high NOx reduction efficiency throughout the temperature range, at the same time minimizing the precious metal (Pt) loading in the LNT catalyst. The concept behind the LNT-SCR combined system is to produce NH_3 from LNT catalyst and store on SCR unit. The stored NH_3 is then used to reduce NOx which remains unreacted in subsequent lean operations.

The use of Cu-chabazite catalyst for the combined LNT-SCR technique may be considered in future as the Cu-chabazite catalyst can store significant amounts of NH_3 and is more effective NOx reduction catalyst compared to Cu-ZSM-5.

While developing the global kinetic model for NO oxidation reaction, we used steady state data. The model could satisfactorily predict the experimental trends for various feed conditions as a function of temperature and space velocities. The transient experimental data showed the formation of nitrates during NOx storage on both the Fe-ZSM-5 and Cu-chabazite catalysts. The SCR operation is considered as more of a steady state operation. Hence the model works very well for the SCR system. But the understanding of transient behavior is also important. The NO oxidation is an important step in the LNT catalysts which work under transient conditions. Many researchers are working on the combined LNT-SCR catalyst systems. In the combined LNT-SCR systems, it is important to know the transient behavior of NO oxidation on both the catalysts. Hence the future modeling effort should be targeted at developing transient kinetic models. Also, the global kinetic model developed to predict the performance of entire SCR reaction system used steady state data. Future work should focus on developing transient SCR models predicting the effect of NO/NO_2 feed ratios on the NOx removal efficiency and N_2 selectivity. The current model was simplified with the assumption of single catalytic site. But, the presence of different catalyst sites has been proposed in various experimental studies. A future kinetic model should incorporate the existence of multiple sites to explain various transient features including NH_3 inhibition on the standard SCR, NH_4NO_3 inhibition on the fast and NO_2 SCR reactions at lower temperatures, etc. The global kinetic model assumed simplified kinetics as discussed in

Chapter 9. This model did not account for nitrous/nitric acid formation steps. A more detailed mechanistic model has been proposed in Chapters 3 and 4. Future kinetic model should incorporate the more detailed reaction chemistry. The effective diffusivities in the washcoat are assumed to be less than gas phase diffusivities by a factor 100. This correlation was derived based on the calculations of Weisz-Prater modulus. Experiments should be targeted at estimating the accurate effective washcoat diffusivities of various molecules. The current SCR model can be extended to study the performance of combined LNT-SCR reaction systems. Also, this model would be useful in predicting the performance of dual layer NH_3-slip catalysts.

References

1. R. M. Heck, R. J. Farrauto, S.T. Gulati, Catalytic Air Pollution Control: Commercial Technology, 2009.
2. C.H. Bartholomew, R.J. Farrauto, Fundamentals of Industrial Catalytic Processes, Second ed., 2005.
3. S. Freni, G. Calogero, S. Cavallaro, "Hydrogen production from methane through catalytic partial oxidation reactions." *Journal of Power Sources*, 87 (2000) 28-38.
4. H. Hwang, R.J. Farrauto, "Process for generating hydrogen-rich gas." U.S. Patent Application No. 2003/0021748A1, 2002.
5. W. Liu, W.P. Addiego, C.M. Sorensen, T. Boger, "Monolith reactor for the dehydrogenation of ethylbenzene to styrene." *Industrial & Engineering Chemistry Research*, 41 (2002) 3131-3138.
6. W.P. Addiego, W. Liu, T. Boger, "Iron oxide-based honeycomb catalysts for the dehydrogenation of ethylbenzene to styrene." *Catalysis Today*, 69 (2001) 25-31.
7. Boger, A.K. Heibel, C.M. Sorensen, "Monolithic catalysts for the chemical industry." *Industrial & Engineering Chemistry Research*, 43 (2004) 4602-4611.
8. http://www.dieselnet.com.
9. Iwamoto, S. Kon, S. Yoshida, T. Inui, "Sharp contrast in thermal stability between MFI-type metallosilicates and metal-ion-exchanged ZSM-5 and their catalytic performances for NO removal." *Studies in Surface Science and Catalysis*, 1997, pp. 1587-1592.
10. Z. Liu, S. Ihl Woo, "Recent advances in catalytic deNOx science and technology." *Catalysis Reviews*, 48 (2006) 43-89.

11. W.S. Epling, L.E. Campbell, A. Yezerets, N.W. Currier, J.E. Parks, "Overview of the fundamental reactions and degradation mechanisms of NOx storage/reduction catalysts." *Catalysis Reviews*, 46 (2004) 163-245.

12. S. Matsumoto, "DeNOx catalyst for automotive lean-burn engine." *Catalysis Today*, 29 (1996) 43-45.

13. S. Matsumoto, K. Yokota, H. Doi, M. Kimura, K. Sekizawa, S. Kasahara, "Research on new deNOx catalysts for automotive engines." *Catalysis Today*, 22 (1994) 127-146.

14. N. Miyoshi, S. Matsumoto, K. Katoh, T. Tanaka, J. Harada, N. Takahashi, K. Yokota, M. Sugiura, K. Kasahara, "Development of new concept three-way catalyst for automotive lean-burn engines." *SAE Technical Paper 950809*, (1995).

15. N. Takahashi, H. Shinjoh, T. Iijima, T. Suzuki, K. Yamazaki, K. Yokota, H. Suzuki, N. Miyoshi, S.-i. Matsumoto, T. Tanizawa, T. Tanaka, S.-s. Tateishi, K. Kasahara, "The new concept 3-way catalyst for automotive lean-burn engine: NOx storage and reduction catalyst." *Catalysis Today*, 27 (1996) 63-69.

16. J.H. Kwak, D.H. Kim, J. Szanyi, C.H.F. Peden, "Excellent sulfur resistance of $Pt/BaO/CeO_2$ lean NOx trap catalysts." *Applied Catalysis B: Environmental*, 84 (2008) 545-551.

17. J. Li, J. Theis, W. Chun, C. Goralski, "Sulfur poisoning and desulfation of the lean NOx trap." *SAE Technical Paper 2001-01-2503*, (2001).

18. J.-S. Choi, W.P. Partridge, C.S. Daw, "Sulfur impact on NOx storage, oxygen storage, and ammonia breakthrough during cyclic lean/rich operation of a

commercial lean NOx trap." *Applied Catalysis B: Environmental*, 77 (2007) 145-156.

19. A. Amberntsson, M. Skoglundh, S. Ljungström, E. Fridell, "Sulfur deactivation of NOx storage catalysts: influence of exposure conditions and noble metal." *Journal of Catalysis*, 217 (2003) 253-263.

20. M. Koebel, M. Elsener, G. Madia, "Reaction pathways in the selective catalytic reduction process with NO and NO_2 at low temperatures." *Industrial & Engineering Chemistry Research*, 40 (2001) 52-59.

21. M. Koebel, G. Madia, M. Elsener, "Selective catalytic reduction of NO and NO_2 at low temperatures." *Catalysis Today*, 73 (2002) 239-247.

22. M. Koebel, G. Madia, F. Raimondi, A. Wokaun, "Enhanced reoxidation of vanadia by NO_2 in the fast SCR reaction." *Journal of Catalysis*, 209 (2002) 159-165.

23. I. Nova, D. Bounechada, R. Maestri, E. Tronconi, A.K. Heibel, T.A. Collins, T. Boger, "Influence of the substrate properties on the performances of NH_3-SCR monolithic catalysts for the aftertreatment of diesel exhaust: An experimental and modeling study." *Industrial & Engineering Chemistry Research*, 50 (2011) 299-309.

24. I. Nova, C. Ciardelli, E. Tronconi, D. Chatterjee, B. Bandl-Konrad, "NH_3-NO/NO_2 chemistry over V-based catalysts and its role in the mechanism of the fast SCR reaction." *Catalysis Today*, 114 (2006) 3-12.

25. I. Nova, C. Ciardelli, E. Tronconi, D. Chatterjee, B. Bandl-Konrad, "NH_3-SCR of NO over a V-based catalyst: Low-T redox kinetics with NH_3 inhibition." *Aiche Journal*, 52 (2006) 3222-3233.

26. I. Nova, C. Ciardelli, E. Tronconi, D. Chatterjee, M. Weibel, "NH_3-NO/NO_2 SCR for diesel exhausts after treatment: mechanism and modeling of a catalytic converter." *Topics in Catalysis*, 42-43 (2007) 43-46.

27. I. Nova, C. Ciardelli, E. Tronconi, D. Chatterjee, M. Weibel, "Unifying redox kinetics for standard and fast NH_3-SCR over a V_2O_5-WO_3/TiO_2 catalyst." *Aiche Journal*, 55 (2009) 1514-1529.

28. I. Nova, A. Grossale, E. Tronconi, "Nitrates and fast SCR reaction in NOx removal from Diesel engine exhausts." *Chimica Oggi-Chemistry Today*, 27 (2009) 17-19.

29. M. Devadas, O. Krocher, M. Elsener, A. Wokaun, N. Soger, M. Pfeifer, Y. Demel, L. Mussmann, "Influence of NO_2 on the selective catalytic reduction of NO with ammonia over Fe-ZSM5." *Applied Catalysis B-Environmental*, 67 (2006) 187-196.

30. M. Devadas, O. Krocher, A. Wokaun, "Catalytic investigation of Fe-ZSM5 in the selective catalytic reduction of NOx with NH_3." *Reaction Kinetics and Catalysis Letters*, 86 (2005) 347-354.

31. A. Grossale, I. Nova, E. Tronconi, "Role of nitrate species in the "NO_2-SCR" mechanism over a commercial Fe-zeolite catalyst for SCR mobile applications." *Catalysis Letters*, 130 (2009) 525-531.

32. A. Grossale, I. Nova, E. Tronconi, “Ammonia blocking of the "Fast SCR" reactivity over a commercial Fe-zeolite catalyst for Diesel exhaust aftertreatment.” *Journal of Catalysis*, 265 (2009) 141-147.

33. A. Grossale, I. Nova, E. Tronconi, D. Chatterjee, M. Weibel, “The chemistry of the NO/NO_2-NH_3 "fast" SCR reaction over Fe-ZSM-5 investigated by transient reaction analysis.” *Journal of Catalysis*, 256 (2008) 312-322.

34. H.Y. Huang, R.Q. Long, R.T. Yang, “Kinetics of selective catalytic reduction of NO with NH_3 on Fe-ZSM-5 catalyst.” *Applied Catalysis a-General*, 235 (2002) 241-251.

35. H.Y. Chen, T. Voskoboinikov, W.M.H. Sachtler, “Reaction intermediates in the selective catalytic reduction of NOx over Fe/ZSM-5.” *Journal of Catalysis*, 186 (1999) 91-99.

36. M. Iwasaki, K. Yamazaki, H. Shinjoh, “Transient reaction analysis and steady-state kinetic study of selective catalytic reduction of NO and NO + NO_2 by NH_3 over Fe/ZSM-5.” *Applied Catalysis a-General*, 366 (2009) 84-92.

37. R.Q. Long, R.T. Yang, “Reaction mechanism of selective catalytic reduction of NO with NH_3 over Fe-ZSM-5 catalyst.” *Journal of Catalysis*, 207 (2002) 224-231.

38. Q. Sun, Z.X. Gao, H.Y. Chen, W.M.H. Sachtler, “Reduction of NOx with ammonia over Fe/MFI: Reaction mechanism based on isotopic labeling.” *Journal of Catalysis*, 201 (2001) 89-99.

39. A. Grossale, I. Nova, E. Tronconi, "Study of a Fe-zeolite-based system as NH_3-SCR catalyst for diesel exhaust aftertreatment." *Catalysis Today*, 136 (2008) 18-27.

40. M. Iwasaki, K. Yamazaki, K. Banno, H. Shinjoh, "Characterization of Fe/ZSM-5 deNOx catalysts prepared by different methods: Relationships between active Fe sites and NH_3-SCR performance." *Journal of Catalysis*, 260 (2008) 205-216.

41. O. Krocher, M. Devadas, M. Elsener, A. Wokaun, N. Soger, M. Pfeifer, Y. Demel, L. Mussmann, "Investigation of the selective catalytic reduction of NO by NH_3 on Fe-ZSM5 monolith catalysts." *Applied Catalysis B-Environmental*, 66 (2006) 208-216.

42. M. Schwidder, S. Heikens, A. De Toni, S. Geisler, M. Berndt, A. Bruckner, W. Grunert, "The role of NO_2 in the selective catalytic reduction of nitrogen oxides over Fe-ZSM-5 catalysts: Active sites for the conversion of NO and of NO/NO_2 mixtures." *Journal of Catalysis*, 259 (2008) 96-103.

43. G. Delahay, D. Valade, A. Guzman-Vargas, B. Coq, "Selective catalytic reduction of nitric oxide with ammonia on Fe-ZSM-5 catalysts prepared by different methods." *Applied Catalysis B-Environmental*, 55 (2005) 149-155.

44. R.Q. Long, R.T. Yang, "Selective catalytic oxidation (SCO) of ammonia to nitrogen over Fe-exchanged zeolites." *Journal of Catalysis*, 201 (2001) 145-152.

45. G.S. Qi, J.E. Gatt, R.T. Yang, "Selective catalytic oxidation (SCO) of ammonia to nitrogen over Fe-exchanged zeolites prepared by sublimation of $FeCl_3$." *Journal of Catalysis*, 226 (2004) 120-128.

46. G.S. Qi, R.T. Yang, "Selective catalytic oxidation (SCO) of ammonia to nitrogen over Fe/ZSM-5 catalysts." *Applied Catalysis a-General*, 287 (2005) 25-33.

47. Y. Yeom, M. Li, A. Savara, W. Sachtler, E. Weitz, "An overview of the mechanisms of NOx reduction with oxygenates over zeolite and gamma-Al_2O_3 catalysts." *Catalysis Today*, 136 (2008) 55-63.

48. Y.H. Yeom, M.J. Li, W.M.H. Sachtler, E. Weitz, "A study of the mechanism for NOx reduction with ethanol on gamma-alumina supported silver." *Journal of Catalysis*, 238 (2006) 100-110.

49. Y.H. Yeom, B. Wen, W.M.H. Sachtler, E. Weitz, "NOx reduction from diesel emissions over a nontransition metal zeolite catalyst: A mechanistic study using FTIR spectroscopy." *Journal of Physical Chemistry B*, 108 (2004) 5386-5404.

50. G. Madia, M. Koebel, M. Elsener, A. Wokaun, "Side reactions in the selective catalytic reduction of NOx with various NO_2 fractions." *Industrial & Engineering Chemistry Research*, 41 (2002) 4008-4015.

51. M. Colombo, I. Nova, E. Tronconi, V. Schmeißer, B. Bandl-Konrad, L. Zimmermann, "$NO/NO_2/N_2O–NH_3$ SCR reactions over a commercial Fe-zeolite catalyst for diesel exhaust aftertreatment: Intrinsic kinetics and monolith converter modeling." *Applied Catalysis B: Environmental*, 111–112 (2012) 106-118.

52. A. Guzmán-Vargas, G. Delahay, B. Coq, "Catalytic decomposition of N_2O and catalytic reduction of N_2O and N_2O + NO by NH_3 in the presence of O_2 over Fe-zeolite." *Applied Catalysis B: Environmental*, 42 (2003) 369-379.

53. D. Kaucký, Z. Sobalík, M. Schwarze, A. Vondrová, B. Wichterlová, "Effect of FeH-zeolite structure and Al-Lewis sites on N_2O decomposition and NO/NO_2-assisted reaction." *Journal of Catalysis*, 238 (2006) 293-300.

54. J. Pérez-Ramírez, F. Kapteijn, G. Mul, J.A. Moulijn, "NO-assisted N_2O decomposition over Fe-Based catalysts: Effects of gas-phase composition and catalyst constitution." *Journal of Catalysis*, 208 (2002) 211-223.

55. P. Forzatti, "Present status and perspectives in de-NOx SCR catalysis." *Applied Catalysis A: General*, 222 (2001) 221-236.

56. J.Girard, C. Montreuil, J.Kim, G. Cavataio, C. Lambert, "Technical advantages of vanadium SCR systems for diesel NOx control in emerging markets." *SAE Technical Paper 2008-01-1029*, (2008).

57. G. Busca, L. Lietti, G. Ramis, F. Berti, "Chemical and mechanistic aspects of the selective catalytic reduction of NOx by ammonia over oxide catalysts: A review." *Applied Catalysis B: Environmental*, 18 (1998) 1-36.

58. V.I. Marshneva, E.M. Slavinskaya, O.V. Kalinkina, G.V. Odegova, E.M. Moroz, G.V. Lavrova, A.N. Salanov, "The influence of support on the activity of monolayer vanadia-titania catalysts for selective catalytic reduction of NO with ammonia." *Journal of Catalysis*, 155 (1995) 171-183.

59. L. Lietti, J.L. Alemany, P. Forzatti, G. Busca, G. Ramis, E. Giamello, F. Bregani, "Reactivity of V_2O_5-WO_3/TiO_2 catalysts in the selective catalytic reduction of nitric oxide by ammonia." *Catalysis Today*, 29 (1996) 143-148.

60. L.J. Alemany, L. Lietti, N. Ferlazzo, P. Forzatti, G. Busca, E. Giamello, F. Bregani, "Reactivity and physicochemical characterization of V_2O_5-WO_3/TiO_2 de-NOx catalysts." *Journal of Catalysis*, 155 (1995) 117-130.

61. B.L. Duffy, H.E. Curry-Hyde, N.W. Cant, P.F. Nelson, "Isotopic labeling studies of the effects of temperature, water, and vanadia loading on the selective catalytic reduction of NO with NH_3 over vanadia-titania catalysts." *The Journal of Physical Chemistry*, 98 (1994) 7153-7161.

62. U.S. Ozkan, Y.P. Cai, M.W. Kumthekar, "Investigation of the mechanism of ammonia oxidation and oxygen exchange over vanadia catalysts using N-15 and O-18 tracer studies." *Journal of Catalysis*, 149 (1994) 375-389.

63. C. Ciardelli, I. Nova, E. Tronconi, D. Chatterjee, B. Bandl-Konrad, M. Weibel, B. Krutzsch, "Reactivity of NO/NO_2-NH_3 SCR system for diesel exhaust aftertreatment: Identification of the reaction network as a function of temperature and NO2 feed content." *Applied Catalysis B-Environmental*, 70 (2007) 80-90.

64. M. Koebel, M. Elsener, "Selective catalytic reduction of NO over commercial DeNO(x)-catalysts: Experimental determination of kinetic and thermodynamic parameters." *Chemical Engineering Science*, 53 (1998) 657-669.

65. M. Koebel, M. Elsener, "Selective catalytic reduction of NO over commercial DeNO(x) catalysts: Comparison of the measured and calculated performance." *Industrial & Engineering Chemistry Research*, 37 (1998) 327-335.

66. M. Koebel, M. Elsener, M. Kleemann, "Urea-SCR: a promising technique to reduce NOx emissions from automotive diesel engines." *Catalysis Today*, 59 (2000) 335-345.

67. G. Madia, M. Elsener, M. Koebel, F. Raimondi, A. Wokaun, "Thermal stability of vanadia-tungsta-titania catalysts in the SCR process." *Applied Catalysis B-Environmental*, 39 (2002) 181-190.

68. G. Madia, M. Koebel, M. Elsener, A. Wokaun, "The effect of an oxidation precatalyst on the NOx reduction by ammonia SCR." *Industrial & Engineering Chemistry Research*, 41 (2002) 3512-3517.

69. M. Inomata, A. Miyamoto, Y. Murakami, "Mechanism of the reaction of NO and NH3 on vanadium oxide catalyst in the presence of oxygen under the dilute gas condition." *Journal of Catalysis*, 62 (1980) 140-148.

70. N.Y. Topsoe, J.A. Dumesic, H. Topsoe, "Vanadia-titania catalysts for selective catalytic reduction of nitric-oxide by ammonia: I.I. Studies of active sites and formulation of catalytic cycles." *Journal of Catalysis*, 151 (1995) 241-252.

71. N.Y. Topsoe, H. Topsoe, J.A. Dumesic, "Vanadia/titania catalysts for selective catalytic reduction (SCR) of nitric-oxide by ammonia: I. Combined temperature-programmed in-situ FTIR and on-line mass-spectroscopy studies." *Journal of Catalysis*, 151 (1995) 226-240.

72. E. Tronconi, I. Nova, M. Colombo, "Dynamic methods in catalytic reaction engineering: Applications to the investigation of the NH_3 selective catalytic reduction reactions for diesel emission control." *Industrial & Engineering Chemistry Research*, 49 (2010) 10374-10385.

73. F.J.J.G. Janssen, F.M.G. Van den Kerkhof, H. Bosch, J.R.H. Ross, "Mechanism of the reaction of nitric oxide, ammonia, and oxygen over vanadia catalysts. I.

The role of oxygen studied by way of isotopic transients under dilute conditions." *The Journal of Physical Chemistry*, 91 (1987) 5921-5927.

74. F.J.J.G. Janssen, F.M.G. Van den Kerkhof, H. Bosch, J.R.H. Ross, "Mechanism of the reaction of nitric oxide, ammonia, and oxygen over vanadia catalysts. 2. Isotopic transient studies with oxygen-18 and nitrogen-15." *The Journal of Physical Chemistry*, 91 (1987) 6633-6638.

75. G. Ramis, G. Busca, F. Bregani, P. Forzatti, "Fourier transform-infrared study of the adsorption and coadsorption of nitric oxide, nitrogen dioxide and ammonia on vanadia-titania and mechanism of selective catalytic reduction." *Applied Catalysis*, 64 (1990) 259-278.

76. G. Ramis, L. Yi, G. Busca, "Ammonia activation over catalysts for the selective catalytic reduction of NOx and the selective catalytic oxidation of NH_3. An FT-IR study." *Catalysis Today*, 28 (1996) 373-380.

77. G. Ramis, L. Yi, G. Busca, M. Turco, E. Kotur, R.J. Willey, "Adsorption, activation, and oxidation of ammonia over SCR catalysts." *Journal of Catalysis*, 157 (1995) 523-535.

78. D. Chatterjee, T. Burkhardt, M. Weibel, I. Nova, A. Grossale, E. Tronconi, "Numerical solution of zeolite- and V-based SCR catalytic converters." *SAE Technical Paper 2007-01-1136* (2007).

79. D. Chatterjee, T. Burkhardt, M. Weibel, E. Tronconi, I. Nova, C. Ciardelli, "Numerical simulation of $NO/NO_2/NH_3$ reactions on SCR catalytic converters: Model development and applications." *SAE Technical Paper 2006-01-0468*, (2006).

80. J. Svachula, L.J. Alemany, N. Ferlazzo, P. Forzatti, E. Tronconi, F. Bregani, "Oxidation of sulfur dioxide to sulfur trioxide over honeycomb DeNoxing catalysts." *Industrial & Engineering Chemistry Research*, 32 (1993) 826-834.

81. L.J. Pinoy, L.H. Hosten, "Experimental and kinetic modelling study of DeNOx on an industrial V_2O_5-WO_3/TiO_2 catalyst." *Catalysis Today*, 17 (1993) 151-158.

82. I.S. Nam, J.W. Eldridge, J.R. Kittrell, "Model of temperature dependence of a vanadia-alumina catalyst for nitric oxide reduction by ammonia: fresh catalyst." *Industrial & Engineering Chemistry Product Research and Development*, 25 (1986) 186-192.

83. H.G. Lintz, T. Turek, "Intrinsic kinetics of nitric oxide reduction by ammonia on a vanadia-titania catalyst." *Applied Catalysis A: General*, 85 (1992) 13-25.

84. M. Turco, L. Lisi, R. Pirone, P. Ciambelli, "Effect of water on the kinetics of nitric oxide reduction over a high-surface-area V_2O_5/TiO_2 catalyst." *Applied Catalysis B: Environmental*, 3 (1994) 133-149.

85. W.C. Wong, K. Nobe, "Kinetics of NO reduction with NH_3 on "chemical mixed" and impregnated V_2O_5-TiO_2 catalysts." *Industrial & Engineering Chemistry Product Research and Development*, 23 (1984) 564-568.

86. A. Grossale, I. Nova, E. Tronconi, D. Chatterjee, M. Weibel, "NH_3-NO/NO_2 SCR for diesel exhausts aftertreatment: Reactivity, mechanism and kinetic modelling of commercial Fe- and Cu-promoted zeolite catalysts." *Topics in Catalysis*, 52 (2009) 1837-1841.

87. M. Colombo, I. Nova, E. Tronconi, "A comparative study of the NH_3-SCR reactions over a Cu-zeolite and a Fe-zeolite catalyst." *Catalysis Today*, 151 (2010) 223-230.

88. M. Colombo, I. Nova, E. Tronconi, "NO_2 adsorption on Fe- and Cu-zeolite catalysts: The effect of the catalyst red–ox state." *Applied Catalysis B: Environmental*, 111–112 (2012) 433-444.

89. H. Sjovall, L. Olsson, E. Fridell, R.J. Blint, "Selective catalytic reduction of NOx with NH3 over Cu-ZSM-5 - The effect of changing the gas composition." *Applied Catalysis B-Environmental*, 64 (2006) 180-188.

90. Y.H. Yeom, J. Henao, M.J. Li, W.M.H. Sachtler, E. Weitz, "The role of NO in the mechanism of NOx reduction with ammonia over a BaNa-Y catalyst." *Journal of Catalysis*, 231 (2005) 181-193.

91. Y.H. Yeom, M. Li, W.M.H. Sachtler, E. Weitz, "NO_2 reduction with nitromethane over Ag/Y: A catalyst with high activity over a wide temperature range." *Catalysis Letters*, 118 (2007) 173-179.

92. A. Savara, A. Danon, W.M.H. Sachtler, E. Weitz, "TPD of nitric acid from BaNa-Y: evidence that a nanoscale environment can alter a reaction mechanism." *Physical Chemistry Chemical Physics*, 11 (2009) 1180-1188.

93. A. Savara, M.J. Li, W.M.H. Sachtler, E. Weitz, "Catalytic reduction of NH_4NO_3 by NO: Effects of solid acids and implications for low temperature DeNO(x) processes." *Applied Catalysis B-Environmental*, 81 (2008) 251-257.

94. A. Savara, W.M.H. Sachtler, E. Weitz, "TPD of NO_2- and NO_3- from Na-Y: The relative stabilities of nitrates and nitrites in low temperature deNOx catalysis." *Applied Catalysis B-Environmental*, 90 (2009) 120-125.

95. M. Iwasaki, H. Shinjoh, "A comparative study of "standard", "fast" and "NO_2" SCR reactions over Fe/zeolite catalyst." *Applied Catalysis A: General*, 390 (2010) 71-77.

96. S. Brandenberger, O. Krocher, A. Tissler, R. Althoff, "The state of the art in selective catalytic reduction of NOx by ammonia using metal-exchanged zeolite catalysts." *Catalysis Reviews-Science and Engineering*, 50 (2008) 492-531.

97. K. Otto, M. Shelef, J.T. Kummer, "Studies of surface reactions of nitric oxide by nitrogen-15 isotope labeling. I. Reaction between nitric oxide and ammonia over supported platinum at 200-250.deg." *The Journal of Physical Chemistry*, 74 (1970) 2690-2698.

98. K. Rahkamaa-Tolonen, T. Maunula, M. Lomma, M. Huuhtanen, R.L. Keiski, "The effect of NO_2 on the activity of fresh and aged zeolite catalysts in the NH_3-SCR reaction." *Catalysis Today*, 100 (2005) 217-222.

99. J. Despres, M. Koebel, O. Krocher, M. Elsener, A. Wokaun, "Adsorption and desorption of NO and NO_2 on Cu-ZSM-5." *Microporous and Mesoporous Materials*, 58 (2003) 175-183.

100. L. Olsson, H. Sjovall, R.J. Blint, "Detailed kinetic modeling of NOx adsorption and NO oxidation over Cu-ZSM-5." *Applied Catalysis B-Environmental*, 87 (2009) 200-210.

101. R. Brosius, D. Habermacher, J.A. Martens, L. Vradman, M. Herskowitz, L. Capek, Z. Sobalik, J. Dedecek, B. Wichterlova, V. Tokarova, O. Gonsiorova, "NO oxidation kinetics on iron zeolites: influence of framework type and iron speciation." *Topics in Catalysis*, 30-1 (2004) 333-339.

102. R. Delahay, S. Kieger, N. Tanchoux, P. Trens, B. Coq, "Kinetics of the selective catalytic reduction of NO by NH_3 on a Cu-faujasite catalyst." *Applied Catalysis B-Environmental*, 52 (2004) 251-257.

103. P.S. Metkar, N. Salazar, R. Muncrief, V. Balakotaiah, M.P. Harold, "Selective catalytic reduction of NO with NH_3 on iron zeolite monolithic catalysts: Steady-state and transient kinetics." *Applied Catalysis B: Environmental*, 104 (2011) 110-126.

104. G. Centi, S. Perathoner, "Role and importance of oxidized nitrogen oxide adspecies on the mechanism and dynamics of reaction over copper-based catalysts." *Catalysis Today*, 29 (1996) 117-122.

105. G.S. Qi, R.T. Yang, "Ultra-active Fe/ZSM-5 catalyst for selective catalytic reduction of nitric oxide with ammonia." *Applied Catalysis B-Environmental*, 60 (2005) 13-22.

106. F. Radtke, R. Köppel, A. Baiker, "Formation of undesired by-products in deNOx catalysis by hydrocarbons." *Catalysis Today*, 26 (1995) 159-167.

107. J.A.Z. Pieterse, S. Booneveld, R.W. van den Brink, "Evaluation of Fe-zeolite catalysts prepared by different methods for the decomposition of N_2O." *Applied Catalysis B: Environmental*, 51 (2004) 215-228.

108. B. Coq, M. Mauvezin, G. Delahay, J.B. Butet, S. Kieger, "The simultaneous catalytic reduction of NO and N_2O by NH_3 using an Fe-zeolite-beta catalyst." *Applied Catalysis B-Environmental*, 27 (2000) 193-198.

109. E.-M. El-Malki, R.A. van Santen, W.M.H. Sachtler, "Active Sites in Fe/MFI Catalysts for NOx Reduction and Oscillating N_2O Decomposition." *Journal of Catalysis*, 196 (2000) 212-223.

110. M. Kögel, V.H. Sandoval, W. Schwieger, A. Tissler, T. Turek, "Catalytic activity and hydrothermal stability of Cu-ZSM-5 used for the decomposition of N_2O." *Chemical Engineering & Technology*, 21 (1998) 655-658.

111. T. Komatsu, M. Nunokawa, I.S. Moon, T. Takahara, S. Namba, T. Yashima, "Kinetic-studies of reduction of nitric-oxide with ammonia on Cu^{2+}-exchanged zeolites." *Journal of Catalysis*, 148 (1994) 427-437.

112. M.D. Amiridis, F. Puglisi, J.A. Dumesic, W.S. Millman, N.Y. Topsoe, "Kinetic and infrared spectroscopic studies of Fe-Y zeolites for the selective catalytic reduction of nitric oxide by ammonia." *Journal of Catalysis*, 142 (1993) 572-584.

113. S.A. Stevenson, J.C. Vartuli, C.F. Brooks, "Kinetics of the selective catalytic reduction of NO over H-ZSM-5." *Journal of Catalysis*, 190 (2000) 228-239.

114. A.A. Battiston, J.H. Bitter, D.C. Koningsberger, "Reactivity of binuclear Fe complexes in over-exchanged Fe/ZSM5, studied by in situ XAFS spectroscopy 2. Selective catalytic reduction of NO with isobutene." *Journal of Catalysis*, 218 (2003) 163-177.

115. E.-Y. Choi, I.-S. Nam, Y.G. Kim, "TPD study of mordenite-type zeolites for selective catalytic reduction of NO by NH_3." *Journal of Catalysis*, 161 (1996) 597-604.

116. J.H. Baik, S.D. Yim, I.S. Nam, Y.S. Mok, J.H. Lee, B.K. Cho, S.H. Oh, "Modeling of monolith reactor washcoated with Cu-ZSM-5 catalyst for removing NO from diesel engine by urea." *Industrial & Engineering Chemistry Research*, 45 (2006) 5258-5267.

117. L. Olsson, H. Sjovall, R.J. Blint, "A kinetic model for ammonia selective catalytic reduction over Cu-ZSM-5." *Applied Catalysis B-Environmental*, 81 (2008) 203-217.

118. H. Sjovall, R.J. Blint, A. Gopinath, L. Olsson, "A Kinetic model for the selective catalytic reduction of NOx with NH_3 over an Fe-zeolite catalyst." *Industrial & Engineering Chemistry Research*, 49 (2010) 39-52.

119. H. Sjovall, R.J. Blint, L. Ollsson, "Detailed kinetic modeling of NH_3 and H_2O adsorption, and NH_3 oxidation over Cu-ZSM-5." *Journal of Physical Chemistry C*, 113 (2009) 1393-1405.

120. H. Sjovall, R.J. Blint, L. Olsson, "Detailed kinetic modeling of NH_3 SCR over Cu-ZSM-5." *Applied Catalysis B-Environmental*, 92 (2009) 138-153.

121. D. Chatterjee, P. Kocí, V. Schmeißer, M. Marek, M. Weibel, B. Krutzsch, "Modeling of a combined NOx storage and NH_3-SCR catalytic system for diesel exhaust gas aftertreatment." *Catalysis Today*, 151 (2010) 395-409.

122. P. Markatou, J. Dai, A. Johansson, W. Klink, M. Castagnola, T.C. Watling, M. Tutuianu, "Fe-zeolite SCR model development, validation and application." *SAE Technical Paper 2011-01-1304*, (2011).

123. T. Watling, M. Tutuianu, M. Desai, J. Dai, P. Markatou, A. Johansson, "Development and validation of a Cu-zeolite SCR catalyst model." *SAE Technical Paper 2011-01-1299*, (2011).

124. S. Malmberg, M. Votsmeier, J. Gieshoff, N. Söger, L. Mußmann, A. Schuler, A. Drochner, "Dynamic phenomena of SCR-catalysts containing Fe-exchanged zeolites – experiments and computer simulations." *Topics in Catalysis*, 42-43 (2007) 33-36.

125. J.H. Kwak, R.G. Tonkyn, D.H. Kim, J. Szanyi, C.H.F. Peden, "Excellent activity and selectivity of Cu-SSZ-13 in the selective catalytic reduction of NOx with NH_3." *Journal of Catalysis*, 275 (2010) 187-190.

126. D.W. Fickel, E. D'Addio, J.A. Lauterbach, R.F. Lobo, "The ammonia selective catalytic reduction activity of copper-exchanged small-pore zeolites." *Applied Catalysis B: Environmental*, 102 (2011) 441-448.

127. I. Bull, W.-M. Xu, P. Burk, S. Boorse, W.M. Jaglowski, G.S. Koermer, A. Moini, J.A. Patchett, J.C. Dettling, M.T. Caudle, US Patent 7,610,662, 2009.

128. N. Salazar, "Selective Catalytic Reduction of NOx by NH_3 over a Fe Zeolite Monolith Catalyst." Chemical Engineering, University of Houston, 2009.

129. A.E.W. Beers, T.A. Nijhuis, N. Aalders, F. Kapteijn, J.A. Moulijn, "BEA coating of structured supports - performance in acylation." *Applied Catalysis a-General*, 243 (2003) 237-250.

130. J.M. Zamaro, M.A. Ulla, E.E. Miro, "Zeolite washcoating onto cordierite honeycomb reactors for environmental applications." *Chemical Engineering Journal*, 106 (2005) 25-33.

131. T.A. Nijhuis, A.E.W. Beers, T. Vergunst, I. Hoek, F. Kapteijn, J.A. Moulijn, "Preparation of monolithic catalysts." *Catalysis Reviews-Science and Engineering*, 43 (2001) 345-380.

132. R.D. Clayton, "Steady State and Cyclic Studies of $Pt/BaO/Al_2O_3$ Lean NOx Traps." Chemical Engineering, University of Houston, 2008.

133. Y. Ren, "Effects of Rh, CeO_2 and Regeneration Conditions on NSR Monolith Catalysts using H_2 as the Reductant." Chemical Engineering, University of Houston, 2011.

134. K. Kamasamudram, N.W. Currier, X. Chen, A. Yezerets, "Overview of the practically important behaviors of zeolite-based urea-SCR catalysts, using compact experimental protocol." *Catalysis Today*, 151 (2010) 212-222.

135. K. Kamasamudram, N.W. Currier, T. Szailer, A. Yezerets, "Why Cu- and Fe-zeolite catalysts behave differently at low temperatures." *SAE Technical Paper 2010-01-1182* (2010).

136. H. Sjovall, R.J. Blint, A. Gopinath, L. Olsson, "A kinetic model for the selective catalytic reduction of NOx with NH_3 over an Fe-zeolite catalyst." *Industrial & Engineering Chemistry Research*, 49 39-52.

137. H.J. Chae, S.T. Choo, H. Choi, I.S. Nam, H.S. Yang, S.L. Song, "Direct use of kinetic parameters for modeling and simulation of a selective catalytic reduction process." *Industrial & Engineering Chemistry Research*, 39 (2000) 1159-1170.

138. J. Eng, C.H. Bartholomew, "Kinetic and mechanistic study of NOx reduction by NH3 over H-form zeolites .1. Kinetic and mechanistic insights into NO reduction over H-ZSM-5." *Journal of Catalysis*, 171 (1997) 14-26.

139. K.S. Kabin, R.L. Muncrief, M.P. Harold, "NOx storage and reduction on a Pt/BaO/alumina monolithic storage catalyst." *Catalysis Today*, 96 (2004) 79-89.

140. K.S. Kabin, R.L. Muncrief, M.P. Harold, Y.J. Li, "Dynamics of storage and reaction in a monolith reactor: lean NOx reduction." *Chemical Engineering Science*, 59 (2004) 5319-5327.

141. R.D. Clayton, M.P. Harold, V. Balakotaiah, "NOx storage and reduction with H-2 on $Pt/BaO/Al_2O_3$ monolith: Spatio-temporal resolution of product distribution." *Applied Catalysis B-Environmental*, 84 (2008) 616-630.

142. R.D. Clayton, M.P. Harold, V. Balakotaiah, C.Z. Wan, "Pt dispersion effects during NOx storage and reduction on $Pt/BaO/Al_2O_3$ catalysts." *Applied Catalysis B-Environmental*, 90 (2009) 662-676.

143. N. Wilken, K. Kamasamudram, N.W. Currier, J.H. Li, A. Yezerets, L. Olsson, "Heat of adsorption for NH_3, NO_2 and NO on Cu-Beta zeolite using microcalorimeter for NH_3 SCR applications." *Catalysis Today*, 151 (2010) 237-243.

144. H.Y. Chen, X. Wang, W.M.H. Sachtler, "Reduction of NOx over various Fe/zeolite catalysts." *Applied Catalysis a-General*, 194 (2000) 159-168.

145. M. Wallin, C.-J. Karlsson, M. Skoglundh, A. Palmqvist, "Selective catalytic reduction of NOx with NH_3 over zeolite H-ZSM-5: influence of transient ammonia supply." *Journal of Catalysis*, 218 (2003) 354-364.

146. S.S. Mulla, N. Chen, W.N. Delgass, W.S. Epling, F.H. Ribeiro, "NO_2 inhibits the catalytic reaction of NO and O_2 over Pt." *Catalysis Letters*, 100 (2005) 267-270.

147. D. Bhatia, R.W. McCabe, M.P. Harold, V. Balakotaiah, "Experimental and kinetic study of NO oxidation on model Pt catalysts." *Journal of Catalysis*, 266 (2009) 106-119.

148. S.S. Mulla, N. Chen, L. Cumaranatunge, W.N. Delgass, W.S. Epling, F.H. Ribeiro, "Effect of potassium and water vapor on the catalytic reaction of nitric oxide and dioxygen over platinum." *Catalysis Today*, 114 (2006) 57-63.

149. G. Delahay, B. Coq, S. Kieger, B. Neveu, "The origin of N_2O formation in the selective catalytic reduction of NOx by NH_3 in O_2 rich atmosphere on Cu-faujasite catalysts." *Catalysis Today*, 54 (1999) 431-438.

150. S.Y. Joshi, M.P. Harold, V. Balakotaiah, "Overall mass transfer coefficients and controlling regimes in catalytic monoliths." *Chemical Engineering Science*, 65 (2010) 1729-1747.

151. D. Bhatia, M.P. Harold, V. Balakotaiah, "Modeling the effect of Pt dispersion and temperature during anaerobic regeneration of a lean NOx trap catalyst." *Catalysis Today*, 151 (2010) 314-329.

152. R.D. Clayton, M.P. Harold, V. Balakotaiah, "Selective catalytic reduction of NO by H_2 in O_2 on $Pt/BaO/Al_2O_3$ monolith NOx storage catalysts." *Applied Catalysis B-Environmental*, 81 (2008) 161-181.

153. J. Xu, R. Clayton, V. Balakotaiah, M.P. Harold, "Experimental and microkinetic modeling of steady-state NO reduction by H_2 on $Pt/BaO/Al_2O_3$ monolith catalysts." *Applied Catalysis B-Environmental*, 77 (2008) 395-408.

154. E. Tronconi, I. Nova, C. Ciardelli, D. Chatterjee, B. Bandl-Konrad, T. Burkhardt, "Modelling of an SCR catalytic converter for diesel exhaust after treatment: Dynamic effects at low temperature." *Catalysis Today*, 105 (2005) 529-536.

155. G. Delahay, B. Coq, L. Broussous, "Selective catalytic reduction of nitrogen monoxide by decane on copper-exchanged beta zeolites." *Applied Catalysis B-Environmental*, 12 (1997) 49-59.

156. S.D. Yim, S.J. Kim, J.H. Baik, I.S. Nam, Y.S. Mok, J.H. Lee, B.K. Cho, S.H. Oh, "Decomposition of urea into NH_3 for the SCR process." *Industrial & Engineering Chemistry Research*, 43 (2004) 4856-4863.

157. Z.M. Wang, T. Arai, M. Kumagai, "Cooperative and competitive adsorption mechanism of NO_2, NO, and H_2O on H-type mordenite." *Industrial & Engineering Chemistry Research*, 40 (2001) 1864-1871.

158. D. Bhatia, R.D. Clayton, M.P. Harold, V. Balakotaiah, "A global kinetic model for NOx storage and reduction on $Pt/BaO/Al_2O_3$ monolithic catalysts." *Catalysis Today*, 147 (2009) S250-S256.

159. J.-Y. Luo, X. Hou, P. Wijayakoon, S.J. Schmieg, W. Li, W.S. Epling, "Spatially resolving SCR reactions over a Fe/zeolite catalyst." *Applied Catalysis B: Environmental*, 102 (2011) 110-119.

160. C. Ciardelli, I. Nova, E. Tronconi, D. Chatterjee, T. Burkhardt, M. Weibel, "NH_3 SCR of NOx for diesel exhausts aftertreatment: Role of NO_2 in catalytic mechanism, unsteady kinetics and monolith converter modelling." *Chemical Engineering Science*, 62 (2007) 5001-5006.

161. C. Ciardelli, I. Nova, E. Tronconi, B. Konrad, D. Chatterjee, K. Ecke, M. Weibel, "SCR-DeNOx for diesel engine exhaust aftertreatment: unsteady-state kinetic study and monolith reactor modeling." *Chemical Engineering Science*, 59 (2004) 5301-5309.

162. M. Iwamoto, H. Furukawa, Y. Mine, F. Uemura, S.-i. Mikuriya, S. Kagawa, "Copper(II) ion-exchanged ZSM-5 zeolites as highly active catalysts for direct and continuous decomposition of nitrogen monoxide." *Journal of the Chemical Society*, Chemical Communications, (1986).

163. M. Iwamoto, H. Yahiro, K. Tanda, N. Mizuno, Y. Mine, S. Kagawa, "Removal of nitrogen monoxide through a novel catalytic process. 1. Decomposition on excessively copper-ion-exchanged ZSM-5 zeolites." *The Journal of Physical Chemistry*, 95 (1991) 3727-3730.

164. W.B. Williamson, J.H. Lunsford, "Nitric oxide reduction with ammonia over copper(II) Y zeolites." *The Journal of Physical Chemistry*, 80 (1976) 2664-2671.

165. M. Mizumoto, N. Yamazoe, T. Seiyama, "Effects of coexisting gases on the catalytic reduction of NO with NH_3 over Cu(II) NaY." *Journal of Catalysis*, 59 (1979) 319-324.

166. S.-W. Ham, H. Choi, I.-S. Nam, Y.G. Kim, "Effect of oxygen on selective catalytic reduction of NO by NH_3 over copper ion exchanged mordenite-type zeolite catalyst." *Catalysis Letters*, 42 (1996) 35-40.

167. S. Kieger, G. Delahay, B. Coq, B. Neveu, "Selective catalytic reduction of nitric oxide by ammonia over Cu-FAU catalysts in oxygen-rich atmosphere." *Journal of Catalysis*, 183 (1999) 267-280.

168. J.H. Park, H.J. Park, J.H. Baik, I.S. Nam, C.H. Shin, J.H. Lee, B.K. Cho, S.H. Oh, "Hydrothermal stability of Cu-ZSM5 catalyst in reducing NO by NH_3 for the urea selective catalytic reduction process." *Journal of Catalysis*, 240 (2006) 47-57.

169. B. Moden, J.M. Donohue, W.E. Cormier, H.X. Li, "Effect of Cu-loading and structure on the activity of Cu-exchanged zeolites for NH_3-SCR." *P.M. Antoine Gédéon, B. Florence (Eds.) Studies in Surface Science and Catalysis, Elsevier*, (2008) 1219-1222.

170. Y. Cheng, J. Hoard, C. Lambert, J.H. Kwak, C.H.F. Peden, "NMR studies of Cu/zeolite SCR catalysts hydrothermally aged with urea." *Catalysis Today*, 136 (2008) 34-39.

171. J.A. Sullivan, J. Cunningham, M.A. Morris, K. Keneavey, "Conditions in which Cu-ZSM-5 outperforms supported vanadia catalysts in SCR of NOx by NH_3." *Applied Catalysis B: Environmental*, 7 (1995) 137-151.

172. G. Moretti, "Turnover frequency for NO decomposition over Cu-ZSM-5 catalysts: insight into the reaction mechanism." *Catalysis Letters*, 28 (1994) 143-152.

173. G. Centi, S. Perathoner, "Nature of active species in copper-based catalysts and their chemistry of transformation of nitrogen oxides." *Applied Catalysis A: General*, 132 (1995) 179-259.

174. V.I. Pârvulescu, P. Grange, B. Delmon, "Catalytic removal of NO." *Catalysis Today*, 46 (1998) 233-316.

175. J. Sárkány, J.L. d'Itri, W.M.H. Sachtler, "Redox chemistry in excessively ion-exchanged Cu/Na-ZSM-5." *Catalysis Letters*, 16 (1992) 241-249.

176. G.D. Lei, B.J. Adelman, J. Sárkány, W.M.H. Sachtler, "Identification of copper(II) and copper(I) and their interconversion in Cu/ZSM-5 De-NOx catalysts." *Applied Catalysis B: Environmental*, 5 (1995) 245-256.

177. D.W. Fickel, R.F. Lobo, "Copper coordination in Cu-SSZ-13 and Cu-SSZ-16 investigated by variable-temperature XRD." *The Journal of Physical Chemistry C*, 114 (2009) 1633-1640.

178. S.T. Korhonen, D.W. Fickel, R.F. Lobo, B.M. Weckhuysen, A.M. Beale, "Isolated Cu^{2+} ions: active sites for selective catalytic reduction of NO." *Chemical Communications*, 47 (2011).

179. R.A. Grinsted, H.W. Jen, C.N. Montreuil, M.J. Rokosz, M. Shelef, "The relation between deactivation of Cu-ZSM-5 in the selective reduction of NO and dealumination of the zeolite." *Zeolites*, 13 (1993) 602-606.

180. K.C.C Kharas, "Performance, selectivity, and mechanism in Cu-ZSM-5 lean-burn catalysts." *Applied Catalysis B: Environmental*, 2 (1993) 207-224.

181. T. Tanabe, T. Iijima, A. Koiwai, J. Mizuno, K. Yokota, A. Isogai, "ESR study of the deactivation of Cu-ZSM-5 in a net oxidizing atmosphere." *Applied Catalysis B: Environmental*, 6 (1995) 145-153.

182. J.Y. Yan, W.M.H. Sachtler, H.H. Kung, "Effect of Cu loading and addition of modifiers on the stability of Cu/ZSM-5 in lean NOx reduction catalysis." *Catalysis Today*, 33 (1997) 279-290.

183. D.W. Fickel, E. D'Addio, J.A. Lauterbach, R.F. Lobo, "The ammonia selective catalytic reduction activity of copper-exchanged small-pore zeolites." *Applied Catalysis B: Environmental*, 102 (2011) 441-448.

184. B. Moden, J. Donohue, W. Cormier, H.-X. Li, "The uses and challenges of zeolites in automotive applications." *Topics in Catalysis*, 53 (2010) 1367-1373.

185. A.V. Kucherov, C.P. Hubbard, M. Shelef, "Rearrangement of cationic sites in Cu-ZSM-5 and reactivity loss upon high-temperature calcination and steam aging." *Journal of Catalysis*, 157 (1995) 603-610.

186. V. Houel, D. James, P. Millington, S. Pollington, S. Poulston, R. Rajaram, R. Torbati, "A comparison of the activity and deactivation of Ag/Al_2O_3 and Cu/ZSM-5 for HC-SCR under simulated diesel exhaust emission conditions." *Journal of Catalysis*, 230 (2005) 150-157.

187. Y. Zhang, M. Flytzani-Stephanopoulos, "Hydrothermal stability of cerium modified Cu-ZSM-5 catalyst for nitric oxide decomposition." *Journal of Catalysis*, 164 (1996) 131-145.

188. S. Brandenberger, O. Kröcher, A. Tissler, R. Althoff, "The state of the art in selective catalytic reduction of NOx by ammonia using metal-exchanged zeolite catalysts." *Catalysis Reviews*, 50 (2008) 492-531.

189. J.H. Kwak, D. Tran, S.D. Burton, J. Szanyi, J.H. Lee, C.H.F. Peden, "Effects of hydrothermal aging on NH_3-SCR reaction over Cu/zeolites." *Journal of Catalysis*, 287 (2012) 203-209.

190. S.P. Felix, C. Savill-Jowitt, D.R. Brown, "Base adsorption calorimetry for characterising surface acidity: a comparison between pulse flow and conventional "static" techniques." *Thermochimica Acta*, 433 (2005) 59-65.

191. V. Balakotaiah, D.H. West, “Shape normalization and analysis of the mass transfer controlled regime in catalytic monoliths.” *Chemical Engineering Science*, 57 (2002) 1269-1286.

192. D.H. West, V. Balakotaiah, Z. Jovanovic, “Experimental and theoretical investigation of the mass transfer controlled regime in catalytic monoliths.” *Catalysis Today*, 88 (2003) 3-16.

193. S.Y. Joshi, Y. Ren, M.P. Harold, V. Balakotaiah, “Determination of kinetics and controlling regimes for H_2 oxidation on Pt/Al_2O_3 monolithic catalyst using high space velocity experiments.” *Applied Catalysis B: Environmental*, 102 (2011) 484-495.

194. K. Ramanathan, V. Balakotaiah, D.H. West, “Light-off criterion and transient analysis of catalytic monoliths.” *Chemical Engineering Science*, 58 (2003) 1381-1405.

195. S.R. Gundlapally, V. Balakotaiah, “Heat and mass transfer correlations and bifurcation analysis of catalytic monoliths with developing flows.” *Chemical Engineering Science*, 66 (2011) 1879-1892.

196. S.Y. Joshi, “Experimental and modeling studies for real time simulations of catalytic monolithic reactor.” Chemical Engineering, University of Houston, 2010.

197. S.Y. Joshi, M.P. Harold, V. Balakotaiah, “On the use of internal mass transfer coefficients in modeling of diffusion and reaction in catalytic monoliths.” *Chemical Engineering Science*, 64 (2009) 4976-4991.

198. S.Y. Joshi, M.P. Harold, V. Balakotaiah, "Low-dimensional models for real time simulations of catalytic monoliths." *Aiche Journal*, 55 (2009) 1771-1783.

199. S.Y. Joshi, Y. Ren, M.P. Harold, V. Balakotaiah, "Experimental and theoretical investigation of controlling regimes during lean oxidation of methane and propylene on Pt/Al_2O_3 monolithic reactors." *Industrial & Engineering Chemistry Research*, (2011).

200. O. Krocher, M. Elsener, "Combination of V_2O_5/WO_3-TiO_2, Fe-ZSM5, and Cu-ZSM5 catalysts for the selective catalytic reduction of nitric oxide with ammonia." *Industrial & Engineering Chemistry Research*, 47 (2008) 8588-8593.

201. J. Girard, C. Cavataio, R. Snow, C. Lambert, "Combined Fe-Cu SCR systems with optimized ammonia to NOx ratio for diesel NOx control." *SAE Technical Paper 2008-01-1185*, (2008).

202. J.R. Theis, R. McCabe, "Selective catalytic reduction (SCR) with urea injection for NOx control on lean-burn gasoline engines." *CLEERS Conference*, (2008).

203. J.R. Theis, M. Dearth, R. McCabe, "LNT+SCR catalyst systems optimized for NOx conversion on diesel applications", *SAE Technical Paper 2011-01-0305* (2011).

204. Q. Xu, D. He, M. Fujiwara, Y. Souma, "Improved activity of Fe-Cu catalysts by physical mixing with zeolites for the hydrogenation of carbon dioxide." *Journal of Molecular Catalysis A: Chemical*, 120 (1997) L23-L26.

205. A. Obuchi, I. Kaneko, J. Uchisawa, A. Ohi, A. Ogata, G.R. Bamwenda, S. Kushiyama, "The effect of layering of functionally different catalysts for the

selective reduction of NOx with hydrocarbons." *Applied Catalysis B: Environmental*, 19 (1998) 127-135.

206. C.-S. Kang, Y.-J. You, K.-J. Kim, T.-h. Kim, S.-J. Ahn, K.-H. Chung, N.-C. Park, S. Kimura, H.-G. Ahn, "Selective catalytic reduction of NOx with propene over double wash-coat monolith catalysts." *Catalysis Today*, 111 (2006) 229-235.

207. S. Akaratiwa, T. Nanba, A. Obuchi, J. Okayasu, J.-O. Uchisawa, S. Kushiyama, "Use of double wash-coatings of platinum and zeolite catalysts to improve selective reduction of NOx by hydrocarbons." *Topics in Catalysis*, 16-17 (2001) 209-216.

208. H.G. Ahn, J.D. Lee, Performance of double wash-coated monolith catalyst in selective catalytic reduction of NOx with propene." *Studies in Surface Science and Catalysis*, 2003, pp. 701-704.

209. P.S. Metkar, V. Balakotaiah, M.P. Harold, "Experimental study of mass transfer limitations in Fe- and Cu-zeolite-based NH_3-SCR monolithic catalysts." *Chemical Engineering Science*, 66 (2011) 5192-5203.

210. G. Cavataio, H. Jen, J. Girard, D.A. Dobson, "Deactivation of zeolite-based SCR catalysts by precious metal and alkali metal contamination." *22nd NAM Meeting*, (2011).

211. J.R. Kiovsky, P.B. Koradia, C.T. Lim, "Evaluation of a new zeolite catalyst for NOx reduction with NH_3." *Industrial & Engineering Chemistry Product Research and Development*, 19 (1980) 218-225.

212. L. Capek, L. Vradman, P. Sazama, M. Herskowitz, B. Wichterlová, R. Zukerman, R. Brosius, J.A. Martens, "Kinetic experiments and modeling of NO oxidation

and SCR of NOx with decane over Cu- and Fe-MFI catalysts." *Applied Catalysis B: Environmental*, 70 (2007) 53-57.

213. L. Olsson, H. Persson, E. Fridell, M. Skoglundh, B. Andersson, "A kinetic study of NO oxidation and NOx storage on Pt/Al_2O_3 and $Pt/BaO/Al_2O_3$." *The Journal of Physical Chemistry B*, 105 (2001) 6895-6906.

214. V. Tomasic, Z. Gomzi, S. Zrncevic, "Catalytic reduction of NOx over Cu/ZSM-5 catalyst." *Applied Catalysis B: Environmental*, 18 (1998) 233-240.

215. P.S. Metkar, M.P. Harold, V. Balakotaiah, "Selective catalytic reduction of NOx on combined Fe- and Cu-zeolite monolithic catalysts: Sequential and dual layer configurations." *Applied Catalysis B: Environmental*, 111-112 (2012) 67-80.

216. D. Bhatia, M.P. Harold, V. Balakotaiah, "Kinetic and bifurcation analysis of the cooxidation of CO and H_2 in catalytic monolith reactors." *Chemical Engineering Science*, 64 (2009) 1544-1558.

217. R.L. Muncrief, P. Khanna, K.S. Kabin, M.P. Harold, "Mechanistic and kinetic studies of NOx storage and reduction on $Pt/BaO/Al_2O_3$." *Catalysis Today*, 98 (2004) 393-402.

218. W.M. Keely, H.W. Maynor, "Thermal studies of Nickel, Cobalt, Iron and Copper oxides and nitrates." *Journal of Chemical & Engineering Data*, 8 (1963) 297-300.

219. K.S. Kabin, P. Khanna, R.L. Muncrief, V. Medhekar, M.P. Harold, "Monolith and TAP reactor studies of NOx storage on $Pt/BaO/Al_2O_3$: Elucidating the mechanistic pathways and roles of Pt." *Catalysis Today*, 114 (2006) 72-85.

220. I. Perdana, D. Creaser, O. Öhrman, J. Hedlund, "A comparison of NOx adsorption on Na, H and BaZSM-5 films." *Applied Catalysis B: Environmental*, 72 (2007) 82-91.

221. M.W. Ross, T.C. DeVore, "Desorption of nitric acid from boehmite and gibbsite." *The Journal of Physical Chemistry A*, 112 (2008) 6609-6620.

222. P.S. Metkar, V. Balakotaiah, M.P. Harold, "Experimental and kinetic modeling study of NO oxidation: Comparison of Fe- and Cu-zeolite catalysts." *Catalysis Today*, 184 (2012) 115-128.

223. E. Tronconi, I. Nova, C. Ciardelli, D. Chatterjee, M. Weibel, "Redox features in the catalytic mechanism of the "standard" and "fast" NH_3-SCR of NOx over a V-based catalyst investigated by dynamic methods." *Journal of Catalysis*, 245 (2007) 1-10.

224. J.H. Baik, S.D. Yim, I.S. Nam, Y.S. Mok, J.H. Lee, B.K. Cho, S.H. Oh, "Control of NOx emissions from diesel engine by selective catalytic reduction (SCR) with urea." *Topics in Catalysis*, 30-1 (2004) 37-41.

225. G. Delahay, A. Guzman-Vargas, D. Valade, B. Coq, "Selective catalytic reduction of NO by NH_3 on Fe-ZSM-5 elaborated from different methods." *Recent Advances in the Science and Technology of Zeolites and Related Materials*, 2004, pp. 2501-2508.

226. M. Devadas, O. Kröcher, M. Elsener, A. Wokaun, G. Mitrikas, N. Söger, M. Pfeifer, Y. Demel, L. Mussmann, "Characterization and catalytic investigation of Fe-ZSM5 for urea-SCR." *Catalysis Today*, 119 (2007) 137-144.

227. M. Richter, R. Eckelt, B. Parlitz, R. Fricke, "Low-temperature conversion of NOx to N_2 by zeolite-fixed ammonium ions." *Applied Catalysis B: Environmental*, 15 (1998) 129-146.

228. J.A. Dumesic, N.Y. Topsøe, H. Topsøe, Y. Chen, T. Slabiak, "Kinetics of selective catalytic reduction of nitric oxide by ammonia over vanadia/titania." *Journal of Catalysis*, 163 (1996) 409-417.

229. B. Roduit, A. Wokaun, A. Baiker, "Global kinetic modeling of reactions occurring during selective catalytic reduction of NO by NH_3 over vanadia/titania-based catalysts." *Industrial & Engineering Chemistry Research*, 37 (1998) 4577-4590.

230. R. Willi, B. Roduit, R.A. Koeppel, A. Wokaun, A. Baiker, "Selective reduction of NO by NH_3 over vanadia-based commercial catalyst: Parametric sensitivity and kinetic modeling." *Chemical Engineering Science*, 51 (1996) 2897-2902.

231. C. Winkler, P. Forchinger, P. Patil, J. Gieshoff, P. Spurk, M. Pfeifer, "Modeling of SCR deNOx catalyst - looking at the impact of substrate attributes." S*AE Paper 2003-01-0845*, (2003).

232. I. Nova, M. Colombo, E. Tronconi, V. Schmeisser, M. Weibel, "The NH_3 inhibition effect in the standard SCR reaction over a commercial Fe-zeolite catalyst for diesel exhaust aftertreatment: An experimental and modeling study." *SAE Technical Paper 2011-01-1319*, (2011).

233. T. Walting, M. Tutuianu, M. Desai, J. Dai, P. Markatou, A. Johansson, "Development and validation of a Cu-zeolite SCR catalyst model." *SAE Technical Paper 2011-01-1299*, (2011).

234. C. Narula, X. Yang, P. Bonnesen, E. Hagaman, "High performance NH_3 SCR zeolite catalysts for treatment of NOx in emissions from off-road diesel engine." *SAE Technical Paper 2011-01-1330*, (2011).